Programming Artificial Antennas through Templated Assembly of Chromophores

Thesis by

Lou ROCARD

Under the supervision of Prof. Davide BONIFAZI

Presented to the School of Chemistry of Cardiff University in Partial

Fulfillment of the Requirements for the degree of Doctor of Philosophy

(Ph.D.) in Chemistry

Cardiff University, 2018

Acknowledgments

I would like to start by thanking my supervisor, *Professor Dr. Davide Bonifazi*. This work would not have been possible without his ideas and his support. It was a pleasure to work with him and in his international working environment. I am very grateful for the trust that he placed in me during this research project. Thanks for being passionate, enthusiastic and encouraging: this gave me the tenacity to achieve this work.

Many thanks go to *Professor Dr. Stefan Matile* and *Dr. Duncan Browne* for accepting the co-examination of this manuscript. I am also very grateful to *Dr. Tanja Miletic* for the proofreading of the thesis.

I would like to express my gratitude to *Professor Dr. Alain Krief* for the time he invested in teaching me and giving me advices.

I sincerely thank all the people who have been involved in this work: *Dr. Andrey Berezin* and *Andrea Sciutto* for their collaboration in the preparation of the chromophores, *Dr. Federica De Leo* for her great work in Molecular Dynamics. Thanks so much to her for being all the time available to help us in this project. Special thanks go to *Lorenzo Luciani*, who did his master thesis under my supervision and prepared with me some target compounds of the thesis: I learnt a lot from this teaching experience. Thanks to *Dr. Andrea Fermi*, who performed photophysical and electrochemical measurements, not only for the measurements but also for teaching me about photochemistry. I want to thank as well *Dr. Olesia Kulyk* for our very fruitful discussions and great collaborative work leading to the design of new antenna systems, unraveling problems in the lab and writing of a review. I also kindly acknowledge *Dr. Stefano Leoni*, *Dr. Darren Wragg* and *Samuel Jobbins* for their collaborative work in metadynamics leading hopefully to an interesting paper very soon. Besides, I would like to sincerely acknowledge the people who help me in the characterization of the compounds: for the mass analyses: the members of the analytical services of Cardiff, in particular, *Thomas Williams*; in Namur, *Marc Dieu*; and special thanks go to *Dr. Julien De Winter* (University of Mons): you have been the best,

Table of Contents

List of abbreviations

aa	Amino acid
A, Ala, A(N$_3$)	Alanine, Azidoalanine
Å	Angstrom
Abs, A$_D$	Absorption, Absorption of the energy donor
Ac	Acetyl
ADIBO	Aza-dibenzocyclooctyne
AE	Antenna effect
AF	Alexa Fluor 647
ATP	Adenosine triphosphate
aq	Aqueous
B	Blue
B$_2$pin$_2$	Bis(pinacolato)diboron
B3LYP	Becke, 3-parameter, Lee-Yang-Parr
BChl	Bacteriochlorophylls
BnBr	Benzyl bromide
Boc	Tert-butyloxycarbonyl
BPh	Bacteriopheophytins
℃	Degree Celsius (0 ℃ = 273.16 K)
C$_{60}$	Fullerene C$_{60}$
calc.	Calculated
CB[7]	Cucurbit[7]uril
CD	Circular dichroism
Chl	Chlorophylls
CuAAC	Copper catalyzed azide-alkyne cycloaddition
CV	Cyclic voltammetry
Cy	Cyanine
d	Day
Dap	2,3-Diaminoproprionic acid
DCC	*N,N'*-Dicyclohexylcarbodiimide
DCC	Dynamic Covalent Chemistry

DCU	*N,N'*-Dicyclohexylurea
DDQ	2,3-Dichloro-5,6-dicyano-1,4-benzoquinone
DFT	Density Functional Theory
DIEA	*N,N*-Diisopropylethylamine
DMA	*N,N*-Dimethylacetamide
DMAP	4-(Dimethylamino)pyridine
DME	Dimethoxyethane
DMF	*N,N*-Dimethylformamide
DMSO	Dimethylsulfoxide
DNA	Deoxyribonucleic acid
DPA	Diphenylanthracene
dppf	1,1'-Bis(diphenylphosphino)ferrocene
EDC.HCl	*N*-(3-Dimethylaminopropyl)-*N'*-ethylcarbodiimide hydrochloride
EDT	1,2-Ethanedithiol
EDTA	Ethylenediaminetetraacetic acid
EET	Excitation energy transfer
EI	Electron ionization
Em	Emission
ESI	Electrospray ionization
ET	Energy transfer
Et$_3$N	Triethylamine
Et$_2$O	Diethyl Ether
EtOAc	Ethyl Acetate
EtOH	Ethanol
eV	Electronvolt (1eV = 1.602 x 10^{-19} J)
Exc, Ex$_D$	Excitation, Excitation of the energy donor
EY	Eosin Y
EYPC	Egg Yolk phosphatidylcholine
F, Phe	Phenylalanine
FFT	Fast Fourier Transform

Fmoc	Fluorenylmethyloxycarbonyl
FRET	Förster resonance energy transfer
Glu	Glutamic acid
Gly	Glycine
GPC	Gel Permeation chromatography
h	Hour
HATU	1-[Bis(dimethylamino)methylene]-1H-1,2,3-triazolo[4,5-b]pyridinium 3-oxid hexafluorophosphate
His	Histidine
HOMO	Highest occupied molecular orbital
HPLC	High-performance liquid chromatography
HR	High resolution
IEDDA	Inverse electron demand Diels-Alder
*i*PrOH	Isopropanol
IR	Infrared (spectroscopy)
$J(\lambda)$	Integral of the normalized spectral overlap
k^2	Transition dipole orientation
K_T	Rate of the energy transfer
L, Leu	Leucine
LHC	Light harvesting complex
LR	Low resolution
LUMO	Lowest unoccupied molecular orbital
Lys	Lysine
M	Molar
MALDI	Matrix-assisted laser desorption/ionisation
MBHA Resin	4-methylbenzhydrylamine Resin
MCH	Methylcyclohexane
m-CPBA	Meta-chloroperoxybenzoic acid
MD	Molecular Dynamic
MeCN	Acetonitrile
MeOH	Methanol

Met	Methionine
min	Minute
M.p.	Melting point
m-PDA	Meta-phenylenediamine
MS	Mass spectrometry
Ms	Mesyl
MW irr	Microwave irradiation
m/z	Mass-to-charge ratio
n	Refractive index
n	Number of unis
(c)NAE	(Core-substituted) Naphtalene-anhydride-ester
NBS	*N*-Bromosuccinimide
(c)NDI	(Core-substituted) Naphtalenediimide
NHS	N-hydroxysuccinimide
Nle, Nle(N$_3$)	Norleucine, Azidonorleucine
NMP	*N*-methyl-2-pyrrolidone
NMI	Naphtalenemonoimides
NIR	Near infrared
nm	Nanometer
NMO	4-methylmorpholine *N*-oxide
NMR	Nuclear magnetic resonance
OFET	Organic field-effect transistor
OPV	Oligo(phenylenevinylene)
PAH	Polycyclic aromatic hydrocarbon
PAMAM	Polyamidoamine
PCDDB	Protein circular dichroism data bank
PDA	Perylene dianhydride
PDI	Perylenediimide
P.E.	Petroleum Ether
PEG	Monomethoxy polyethyleneglycol
Per	Perylene

PG	Protecting group
Ph	Phenyl
pH	Potential of hydrogen
PIDA	Phenyliodine (III) diacetate
PMI	Perylenemonoimide
Pro	Proline
ppm	Parts per million
p-TSA	*p*-Toluenesulfonic acid
Py	Ethynylpyrene
Q	Quinone
Q, Gln	Glutamine
Q-Tof	Quadrupole time-of-flight
QY	Quantum yield
r	Interchromophoric distance
R	Red
RC	Reaction center
RP	Reverse Phase
rt	Room temperature
R_t	Retention time
SCE	Saturated colomel electrode
SCM	Surface-cross linked micelle
SEC	Size exclusion chromatography
S_N2	Bimolecular nucleophilic substitution
SPAAC	Strain promoted azide alkyne cycloaddition
SPPS	Solid Phase Peptide Synthesis
t	Time
T °C	Temperature
*t*Bu	*Tert*-butyl
TCO	*Trans*-cyclooctene
TDI	Terrylenediimide
$TEAPF_6$	Tetraethylammonium hexafluorophosphate

TEG	Monomethoxy triethyleneglycol
TFA	Trifluoroacetic acid
TFE	Trifluoroethanol
THF	Tetrahydrofurane
TIPS	Triisopropylsilyl
TIS	Triisopropylsilane
TLC	Thin layer chromatography
TMPV	Tobacco Mosaic Virus coat Protein
TMS	Trimethylsilyl
Trp	Tryptophan
Trt	Trityl
UV-Vis	Ultraviolet-visible
Val	Valine
vs.	*Versus* (latin)- against
Y	Yellow
X	Modified amino acid
λ	Wavelength
ε	Molar extinction coefficient
Φ_{ET}	Efficiency of the energy transfer
φ, Ψ, ω	Torsion angles in peptidic backbone
τ	Fluorescence lifetimes

X

ABSTRACT

One of the main challenges for the creation of artificial light harvesting systems is to develop high-yielding and easy-to-implement protocols for the assembly of chromophores into spatially organized architectures. The use of a template bearing pre-programmed receptor sites accommodating selectively specific chromophores appears to be a very attractive synthetic approach. In this manuscript, pre-programmed peptides will guide the spatial arrangement of different dyes, acting as energy donors and acceptors and absorbing over the whole visible spectrum. The self-assembly of the chromophores into the scaffold can be achieved through the engineering of orthogonal recognition motifs.

The employed method, described in *Chapter 2*, relies on the development of simultaneous multireaction systems. A triorthogonal system involving three reactions of dynamic covalent chemistry, namely disulfide exchange, boronate and acyl hydrazone formations, is first optimized for the design of triorthogonal recognition motifs. The complexity of the system is then increased by incrementally adding reactions: the strain promoted azide-alkyne cycloaddition and the inverse electron demand Diels-Alder cycloaddition between *s*-tetrazine and *trans*-cyclooctene leading to tetra- and pentaorthogonal recognition motifs.

Chapters 3 and *4* address the creation of a library of multichromophoric architectures with tailored yellow, red and blue chromophores through the three simultaneous reactions of dynamic covalent chemistry. In this respect, the design and synthesis of various α-helix peptides bearing disulfide, diol and hydrazide acting as receptor sites at given positions and chromophoric units with complementary sticky sides are detailed, as well as the dyes assembly leading to excitation energy transfer within the colored structure. Finally, *Chapter 5* focuses on the extension of the absorption range of the colored architectures by selectively incorporating additional dyes following their energy gradient to favor the unidirectionality of the energy transfer. This will be achieved through the introduction of the tetra- and pentaorthogonal recognition motifs within the peptide and the dyes (Figure 1).
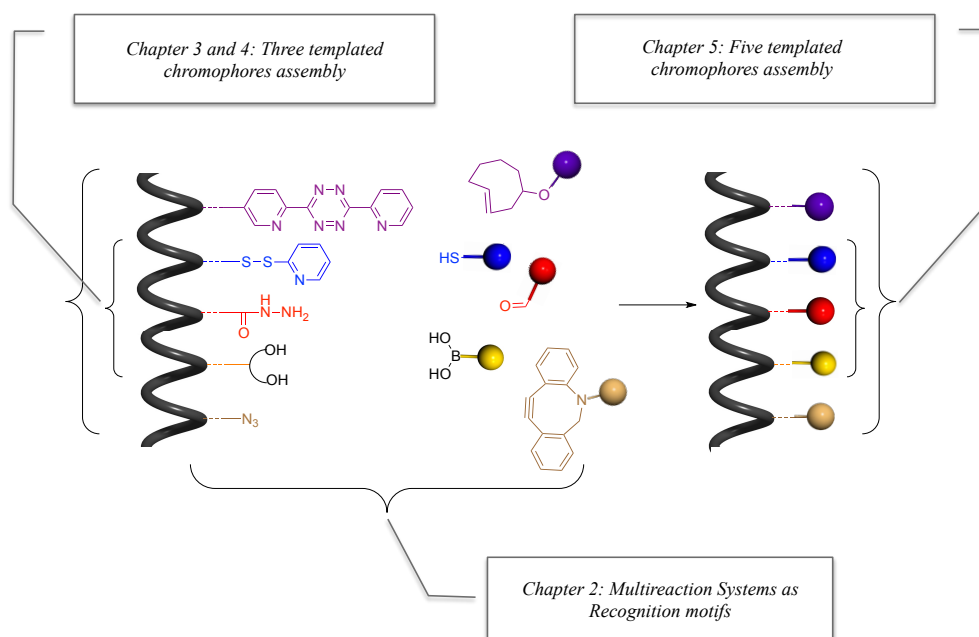
Figure 1 General synthetic strategy for engineering multichromophoric architectures bearing five different dyes.

1. Introduction: From natural to artificial light-harvesting complexes

Energy is the biggest issue of the new century; in their essay, *N. Armaroli* and *V. Balzani* highlighted vital questions for our society: *"Should we stop burning fossil fuels? Can we find an energy source capable of replacing fossil fuels? Will it be possible for all the Earth's inhabitants to reach the standard of living of developed countries without devastating the planet?"*[1] To those fundamental interrogations, solar energy should be the obvious solution. Indeed, sunlight is the most abundant, and besides the most sustainable, source of energy available on Earth. In theory, the amount of sunlight received by the Earth during one day exceeds the worldwide energy requirements for many years.[2] However nowadays, only a tiny fraction of this solar energy is used by thermal collectors and solar panels to generate heat and electricity, in contrast to natural photosystems, such as plants or algae, which are able to collect a much larger fraction. As a chemist, it is our duty to try to solve the energy problem by learning from the nature how to capture, transfer and store the solar energy.[3]

In *Section 1.1*, the natural photosynthetic process will be described and we will particularly focus our attention on the understanding of the natural solar light harvesting: the effective capture, amplification and transfer of photons. *Section 1.2* will be dedicated to the design of artificial light-harvesting systems and examples from the literature will be reviewed.

1.1 Natural light-harvesting complexes

Photosynthesis means literally "synthesis with light" and is the most important biological process in nature, responsible for the development of all life on Earth.[4] It is used by plants and other organisms to capture the sun's energy and convert it into the free energy required to power life. Even though photosynthetic organisms may be quite different, they all use the same basic strategy: The photosynthetic process follows four phases. *i)* It starts with the absorption of sunlight by specialized pigment-protein complexes, so-called light harvesting complexes or antennas. *ii)* This is followed by the funneling of the excitation energy within the antenna assembly to special sites called reaction centers (RCs). *iii)* There, a photochemical reaction takes place, separating a negative and positive charge and generating a primary electron transfer. *iv)* Finally, the primary electron transfer initiates a series of electron transfers and redox reactions, which create an

electrochemical proton gradient used to power the production of adenosine triphosphate (ATP). The last molecule supplies the energy needed for the synthesis of stable high-energy compounds such as sugars.

In the following section, we will focus our attention on two first phases: the light absorption and the excitation energy funneling to the reaction center occurring in the antenna assemblies. Besides, the third phase, in which the charge separation in the reaction center takes place, will be briefly discussed.

1.1.1 Antenna complexes

All photosynthetic organisms contain light harvesting complexes (LHCs or antennas) absorbing sunlight and transferring the energy to a trap, the reaction center, which deactivates the excited state. *R. E. Blankenship* compared light harvesting complexes to *"satellite dish, collecting energy and concentrating it in a receiver"*.[4]

The antenna systems are constituted by a collection of many pigments bound to proteins: chlorophyll, carotenoid, open-chain tetrapyrrole called phycobilin, etc, absorbing light over the whole visible spectrum (Figure 1-1 a and b).
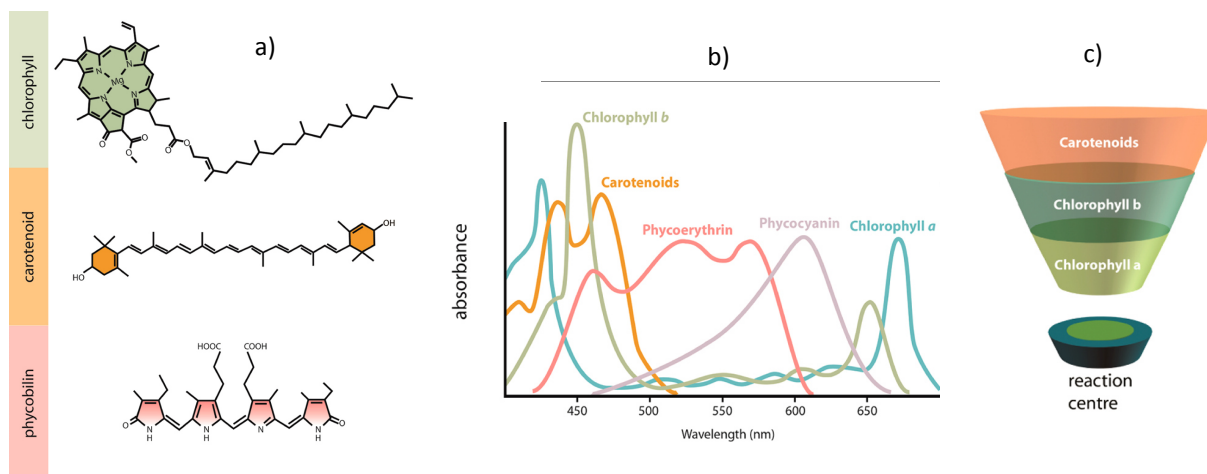
Figure 1-1 a) Structure of pigments present in the light harvesting system: chlorophyll, carotenoid, phycobilin; b) Absorption spectra of photosynthetic pigments; c) Funnel concept in photosynthetic antennas favoring excitation energy transfer from the higher-energy to lower-energy pigments. Adapted with permission from reference 5b. Copyright (2017) American Chemical Society.[5]

This assembly allows the great increasing of the energy absorbed compared with a single pigment. The spatial organization of the pigment within the assembly describes an energy funnel; the pigments at the periphery of the antenna absorb light of high energy (at short wavelength) while the lower-energy pigments (at higher wavelength) are located center. In this respect, the energy funneling is unidirectional minimizing the loss of energy during the excitation transfer (Fig

A large variety of nat... exist, they
chromophore-types (and so optica... chromophores.
focus our attention on one specifi... purple bacteria
organisms, the light harvesting ca... na complexes,
LH2.[6] The LH1 complex is an ... which surrou...
center, and has the role of core co... enna pigment-p...
is not in direct contact with the R(... th LH1 and LH
light absorption and the energy tr... RC through L... as shown in
Figure 1-2.
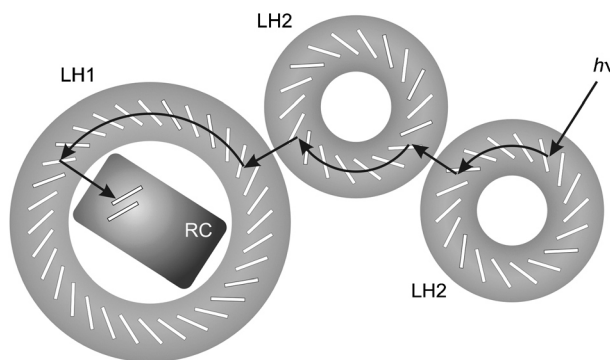
Figure 1-2 Schematic representation of light-harvesting process by LH2 and LH1 antenna complexes in bacterial photosynthesis. Print with permission from reference 7. Copyright (2011) Royal Society of Chemistry.[7]

One of the most studied LH2 is the one from *Rps. acidophila* whose structure has been determined by X-ray diffraction (Figure 1-3) and imaged by atomic force microscopy.[8] It consists of two types of α-helix polypeptides, termed as α and β−apoproteins, repeated in nine copies and forming a cylindrical architecture of diameter around 65 Å. In the two concentric macrocycles formed by the proteins, the pigments: bacteriochlorophylls (BCls, similar to chlorophylls with one more saturated tetrapyrrole re... shift in their absorption spectra... are sandwiched. Two ty... shed and formed two different ... first one, perpendicular ... ler, is composed by 18 BChls "... intensively at 850 nm. ... 0 pigments are coordinated to h... His30 of the β-apoprote... tein. The second ring comprises ... (absorbing at 800 nm) a... e of the cylinder. The Mg^{2+} ions ... axially coordinated to ... he N-terminal of α-apoprotein ... molecules, perpendicular to the plane of the cylindrical membrane, are assembled by van der Waals interactions with hydrophobic residues of the proteins and BChl pigments; they are in close distance to both B800 and B850 BChl (3.4-3.7 Å).
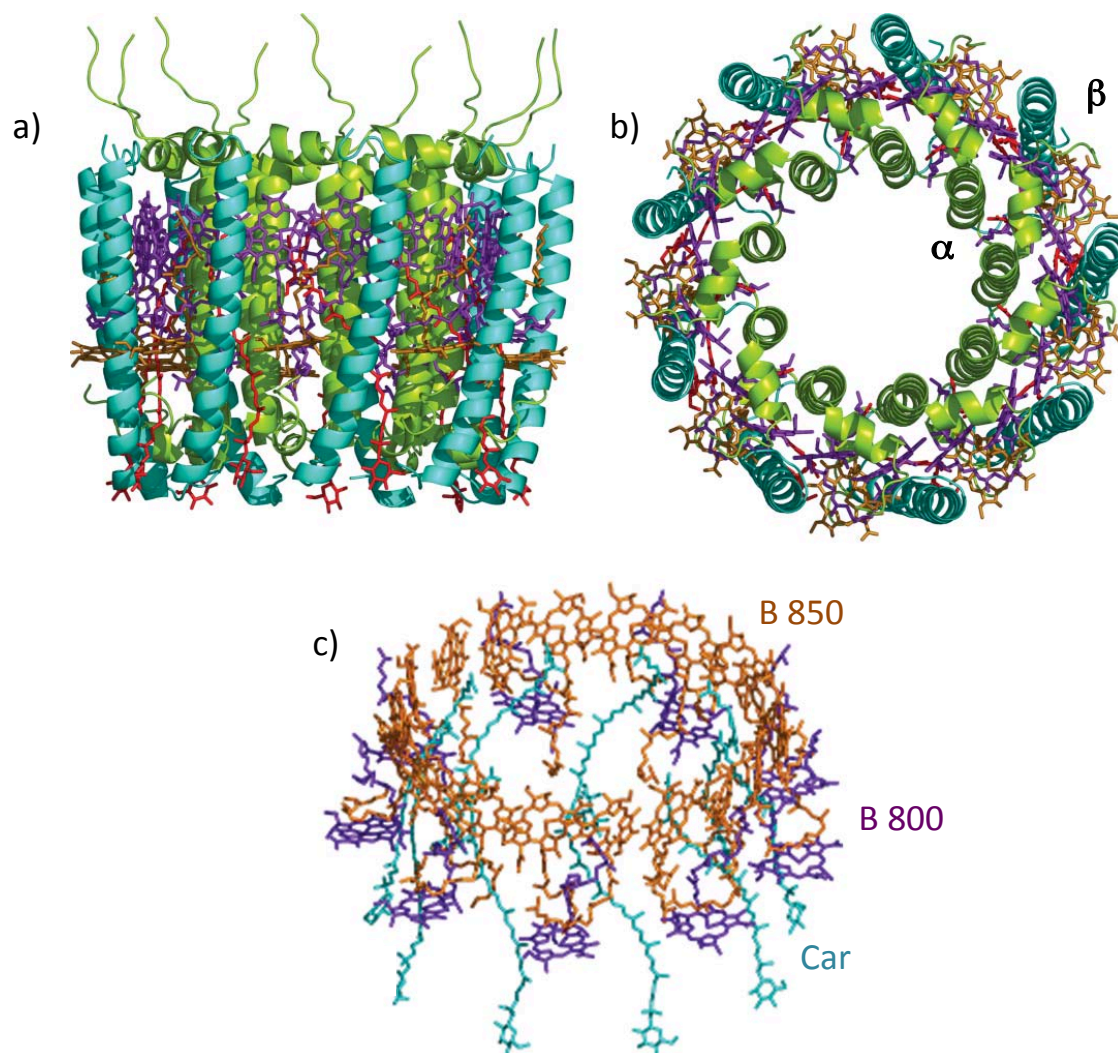
Figure 1-3 Structure of LH2 complex from *Rhodopseudamonas acidophila*. a) Side and b) front view of the complex. The internal α-apoproteins are colored in green and the external β-apoproteins in turquoise. The carotenoid pigments are represented in red, BChl B800 in purple, BChl B850 in brown. c) Spatial arrangement of the pigments in LH2 complex; BChl B800 in orange, BChl B850 in purple, carotenoids in cyan. Adapted with permission from reference 9. Copyright (2008) Royal Society of Chemistry.[9]

LH1 core antenna surrounding the reaction center to form RC-LH1 complex is structurally similar to LH2 (but larger to accommodate RC). The most studied complex is the one from *Rps. Palustris*. LH1 is composed by 15 pairs of α and β apoproteins forming two concentric macrocycles. As in LH2, BChl molecules (called B875 pigments) and carotenoids are sandwiched between the protein rings forming a cylindrical architecture. The structure of RC-LH1 from *Rps. Palustris* has been also identified by X-ray crystallography and is reported in Figure 1-4.[10] The structure of the reaction center will be discussed in *Section 1.1.3*.
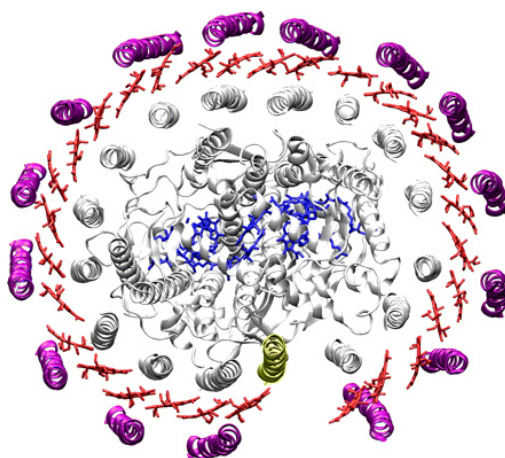
Figure 1-4 Structure of RC-LH1 complex from *Rps. Palustris*. The internal α-apoproteins are colored in gray and the external β-apoproteins in pink. The pigments B875 are represented in red. Copyright from ref 10b (2007) National Academy of Science.[10b]

1.1.2 Excitation energy transfer (EET) within antenna complexes

In the previous part, we highlighted the role of the antenna: the amplification of the absorption of sunlight by various types of pigments, and we discussed the spatial organization of the pigments leading to an efficient transfer of the excitation energy to the reaction center. In this section, we will detail the physical mechanisms for energy transfer within natural antenna complexes.

1.1.2.1 Förster resonance energy transfer

For weak electrostatic interactions between pigments, the Förster mechanism of energy transfer, so-called Förster resonance energy transfer (FRET), proposed first by *T. Förster* in the 1940s, is applicable.[11] This energy transfer mechanism is a non-radiative resonance transfer process. It is based on an electrostatic interaction between the chromophores, in particular a long dipole-dipole interaction between a fluorescent donor in its excited state (D*) and a nearby fluorescent or not acceptor (A). Conceptually, the excited fluorophore can be visualized as an oscillating dipole transferring its energy to a second dipole, the acceptor, having a similar resonance frequency. The mechanism is illustrated in a Jablonski diagram shown in Figure 1-5. The donor D is excited by a photon and then relaxes the lowest excited state S_1. When the electron returns to the ground state, the energy released can simultaneously excite the acceptor A by "resonance". Then, the excited acceptor A* can emit a photon and returns to the ground state S_0 if no other quenching state exists.
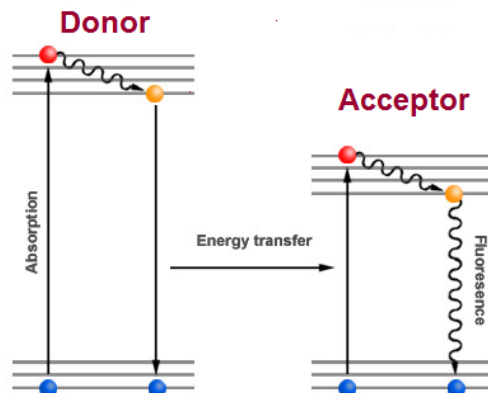
Figure 1-5 Jablonski diagram of FRET.[12]

This phenomenon is highly dependent to the distance r between the donor and the acceptor; according to Förster theory, the rate of the transfer $K_{T(r)}$ is determined by Equation (1).

$$K_{T\,(r)} = \frac{1}{\tau_D}\left(\frac{r_0}{r}\right)^6 \qquad (1)$$

Where τ_D is the fluorescent lifetime of the donor in the absence of the acceptor and r_0 is the "critical distance" between the chromophores (also called Förster distance) for which their energy efficiency is equal to 50%. r_0 is given following Equation (2).

$$r_0 = 9.78 \times 10^3 \left[k^2 n^{-4} Q_D J(\lambda)\right]^{1/6} \text{ (in Å) (2)}$$

Where k^2 described the transition dipole orientation (often estimated to be 2/3 for a random orientation), n is the refractive index of the medium, Q_D is the quantum yield of the donor fluorescence in the absence of the acceptor, and $J(\lambda)$ is the integral of the normalized spectral overlap between the donor emission and the acceptor absorption (Figure 1-6).

a)

$$\kappa^2 = \left(\cos\theta_T - 3\cos\theta_D \cos\theta_A\right)^2$$
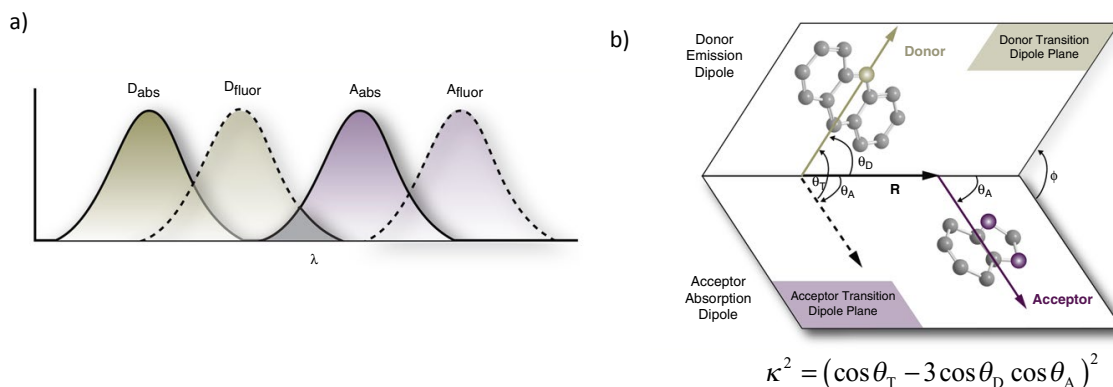
Figure 1-6 a) Representation of the normalized spectral overlap between the donor emission and the acceptor absorption; b) Transition dipole orientation and schematic representation of the angles used to calculate k^2. Adapted with permission from reference 5a. Copyright (2017) American Chemical Society. [5a]

In this respect, few rules resulting from those equations must be satisfied for the mechanism to occur: *i)* the donor fluorescence emission spectrum has to overlap with the absorption spectrum of the acceptor; *ii)* the interchromophoric distance must be in the right magnitude, typically 10-100 Å, *iii)* the dipole orientation of the donor and the acceptor must be approximately parallel, *iv)* the donor lifetime has to be long enough.

In the LH2 complex of the purple bacterial photosynthetic unit described in the previous section, after excitation, ultrafast energy transfer processes take place. The transfer from B800 to B850 can occur according to the FRET mechanism, given the spectral properties and the distance of the pigments. It takes approximately 1 ps. Moreover, it happens as well to transfer the energy from B850 of LH2 to B875 in LH1. Finally, it allows the energetic transfer from B875 in LH1 to BChl in the reaction center (Figure 1-7).

1.1.2.2 Electronic exchange

For an important part of the excitation energy transfer (EET) within antenna complexes, the FRET mechanism is not applicable. This is the case when strong interactions occur between pigments, when they are physically very close (less than 10 Å) leading to the overlap of their orbital.

In this situation, the EET involved is an electronic exchange called Dexter interaction. The mechanism involves the transfer of an electron from the LUMO of the excited donor D* to the LUMO of the acceptor A simultaneously with the movement of an electron between the HOMOs of A to D*. The rate of this transfer K_{Dexter} was proposed by *Dexter* in the 1950s and is given in Equation (3).[13]

$$K_{Dexter} \propto KJ(\lambda) \exp(\frac{-2r}{L}) \qquad (3)$$

Where K is the factor related to specific orbital interaction, $J(\lambda)$ is the integral of the normalized spectral overlap between the donor emission and the acceptor absorption, r is the interchromophoric distance and L the sum of the van der Waals radii of the donor and the acceptor.

This mechanism is not only applicable for EET between distinct chromophores. Indeed, it is mostly involves in the photosynthetic antenna complexes between identical chromophores as an isoenergetic transfer of energy. This phenomenon is called exciton coupling and results in the excitation migration. For instance, in the LH2 and LH1 complexes described previously, the excitation migration occurs within the B850 and B875 rings respectively by this mechanism and is faster than the FRET (around 100 fs).

To summarize, Figure 1-7 illustrates the EETs within the photosynthetic antenna complexes involving the two different mechanisms: the FRET which favors the energy transfer between the different subunits (in LH2: from B800 to B850, from LH2 to LH1: from B850 to

B875 and in RC-LH1: from B875 to P870) and the exciton coupling which allows the excitation migration (within B850 ring in LH2 and B875 in LH1).
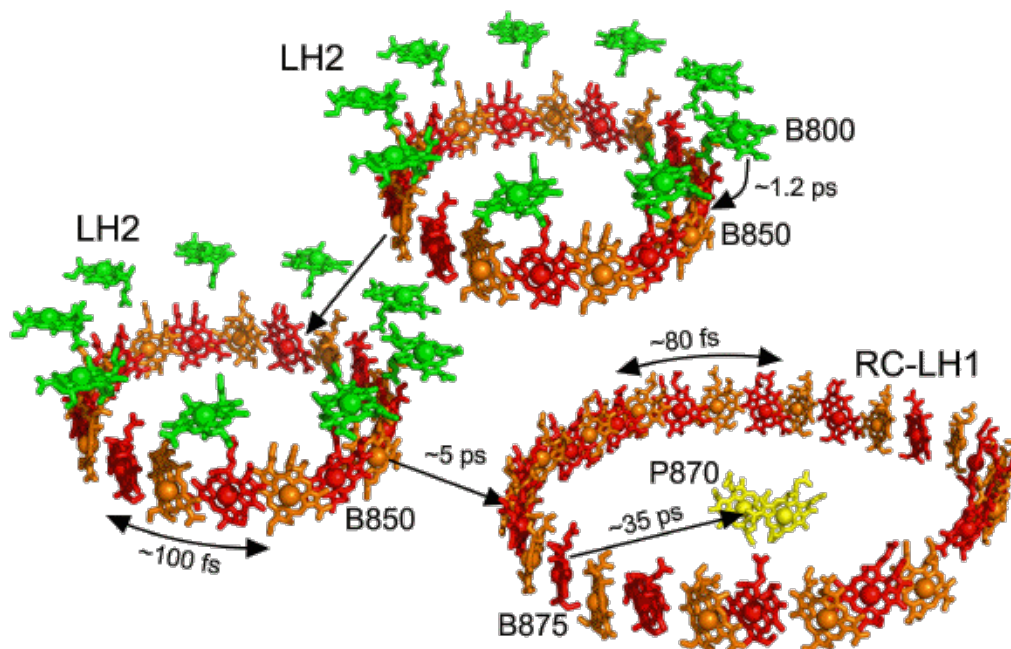
Figure 1-7 Energy transfer pathways and kinetics in the photosynthetic antenna complexes of the purple bacteria.[14]

1.1.3 Charge separation in the reaction center

The reaction center is a pigment-protein complex, which carries out electron transfer reactions leading to a charge separation. In the reaction center of purple bacteria, protein subunits assemble different components including four molecules of BChls, two bacteriopheophytins (BPh, similar to BChl without internal magnesium) and two molecules of quinone. The BChls are very close to each other and are termed as P870 due to their high absorbance at 870 nm. Two first BChl P870 are arranged by pair and this dimer constitute the primary electron donor of the electron transfer cascade since its excited state can easily loose an electron in the presence of a nearby acceptor to become the radical cation $P870\bullet^+$. A nearby BPh can accept the electron to generate the anion radical $BPh\bullet^-$ forming $P870^+BPh^-$ ion-pair. Finally, the electron is transferred to a quinone molecule, acting as a strong acceptor, to form the $P870^+Q^-$ state. This electron transfer cascade allows the efficient separation of the positive and the negative charges by avoiding the recombination process in which the highly reducing $Q\bullet^-$ can simply transfer back its electron to the highly oxidizing $P870\bullet^+$. This is followed by the H^+ transfer leading to the formation of quinol, which is then released from the complex and replaced by a quinone. The proton pump gradient

generated by the electron transfer promotes an electrochemical potential gradient, which is then used to drive the synthesis of ATP.

1.1.4 General conclusion: Lessons from Nature about light-harvesting complexes

In general, an efficient light-harvesting complex requires a good coverage of the solar spectrum in combination with efficient excitation energy transfer (EET). To cover efficiently the solar spectrum, Nature uses various types of chromophore (Chls, carotenoids, tetrapyrroles) with very high molar extinction coefficient, typically 100 000 M^{-1} cm^{-1}. This allows the capture of a maximum of sunlight. Besides, to efficiently transfer the sunlight energy absorbed by the antenna to the reaction center, the spatial organization of the chromophore into the complex is very important. Nature uses the funnel principle: many pigments absorbing light of high-energy placed at the periphery of the antenna transfer their excitation energy to lower-energy pigments until the reaction center, placed at the center. The number of pigments decreases with their energy. This principle allows the amplification of the absorption and the unidirectionality of the energy transfer. Moreover, since the energy transfer process is highly distance-dependent, the chromophores are close to each other. Depending of the interchromophoric distance, different mechanisms of transfer are favored: the FRET for long-distance (from 10 to 100 Å), electronic exchange for short-distance (less than 10 Å). In Nature, FRET is widely used to funnel the energy from the high-energy to the low-energy pigments while the electronic exchange is mostly employed in the excitation migration between isoenergetic pigments.

In the next section, we will review different examples of artificial light-harvesting complex and discover how the scientific community has been inspired by Nature.

1.2 Artificial light-harvesting systems

One of the main challenges in mimicking natural antenna systems is to develop high-yielding and easy-to-implement protocols that can lead to the rational assembly of chromophores into spatially organized architectures. To be efficient, these should feature well-defined distances, orientations, and exact ratio of chromophoric donors to acceptors. In this respect, two approaches are followed: a sequential and a template route as illustrated in Figure 1-8. In the sequential approach, the chromophores are directly assembled together by covalent or non-covalent bindings, while in the template route, the dyes are organized on a programmed scaffold such as in the natural light harvesting complexes.
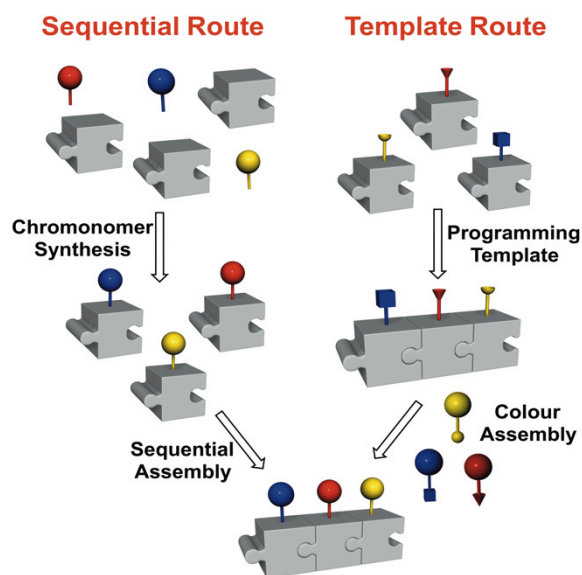
Figure 1-8 The sequential and template routes for engineering multichromophoric architectures.[15]

Following the sequential approach, covalent or non-covalent dendrimers,[7a, 16] macrocycles,[17] supramolecular polymers,[18] nanostructures[19] and functional surfaces[20] have been prepared starting from programmed monomeric chromophores. On the other hand, following the template approach, natural macromolecules like peptides[21] and nucleic acids[22] and artificial polymers[23] have been successfully used as platforms templating the organization of chromophores.

In the following section, we will give an overview of the reported artificial antenna systems following the two different approaches in order to highlight the advantages and drawbacks of the two routes. Besides, strategies used in the literature to evaluate the light harvesting capabilities will be introduced. *Section 1.2.1* will be dedicated to the examples using the sequential assembly while the examples employing the template approach will be described in *Section 1.2.2*.

1.2.1 Sequential assembly of chromophores for artificial antennas

1.2.1.1 Dendrimers

"Dendrimers are tree-like macromolecules, with a high degree of order and the possibility to contain selected chemical units in predetermined sites of their structure."[7a] In this respect, they have attracted a great attention for designing artificial antenna systems containing various chromophores in close proximity.[7a, 16] Because of their proximity, the energy transfer can be easily funneled from the peripheral donors to the acceptor in the core of the dendrimers.

Following this approach, *Müllen* and co-workers reported in 2002 a multichromophoric rigid polyphenylene dendrimer bearing a terrylenediimide (TDI) core, four perylenemonoimides (PMIs) and eight naphtalenemonoimides (NMIs) at the periphery separated by interchromophoric distances of ≈2-3 nm.[24] As shown in Figure 1-9, triad **1-1** absorbs in the whole visible spectrum

and the normalization of the absorption and emission spectra of the chromophores displays a nice overlap between the donor emissions and the acceptor absorptions. Fluorescence measurements were performed to characterize the unidirectional energy transfer from the periphery to the core by FRET mechanism. The emission spectra clearly illustrate the highly efficient energy transfer from NMIs and PMIs to TDI by showing the quenching of the donor fluorescence at 430 and 560 nm and the amplification of the TDI fluorescence at 706 nm upon excitation of the donors (λ_{exc} = 360 and 490 nm). Beside, the FRET efficiency Φ_{ET} from PMIs to TDI within **1-1** was measured to be 99.5% by calculating the ratio of fluorescence lifetimes of the donor in the absence and presence of the acceptor (τ_D and τ_{DA} estimated to be 4.3 and 0.02 ns respectively at λ_{exc} = 490 nm) following Equation (4). The reduction in the lifetime of NMI in the triad (τ_D and τ_{DA} determined to be 0.33 and 0.04 ns respectively at λ_{exc} = 360 nm) highlighted as well the efficient energy transfer within **1-1** from NDIs to TDI by cascade or direct transfer.
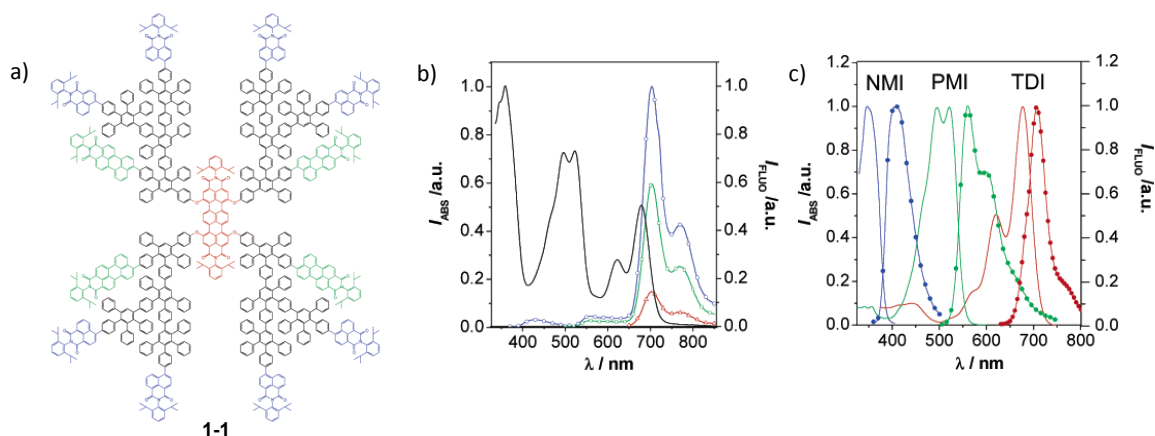
Figure 1-9 Rigid polyphenylene dendrimer **1-1** based on TDI (in red), PMIs (in green), NMIs (in blue); a) structure of the triad; b) Absorption (black line) and emission fluorescence (colored line) upon excitation at 360 nm (blue), 490 nm (green), 640 nm (red) of the triad in toluene; c) Normalized absorption (solid) of fluorescence (solid+symbol) spectra of the distinct chromophores in toluene. Adapted with permission from reference 25. Copyright (2005) American Chemical Society.[25]

$$\Phi_{ET} = 1 - \frac{\tau_{DA}}{\tau_D} \quad (4)$$

Where τ_D and τ_{DA} are fluorescence lifetimes of the donor in the absence and presence of the acceptor respectively.

Efficient light collection and energy transfer have been demonstrated in this example following the sequential approach by employing dendrimers. However, the main drawback of the example, which can be applied to most of the reported light-harvesting dendrimers, is the synthetic accessibility. Indeed, the synthesis of the triad relies on the complex multistep route using repetitive Diels-Alder cycloadditions between ethynyl groups and cyclopentadiones requiring

various steps of protection and deprotection as shown in the retrosynthetic pathway reported in Scheme 1.1.[24]
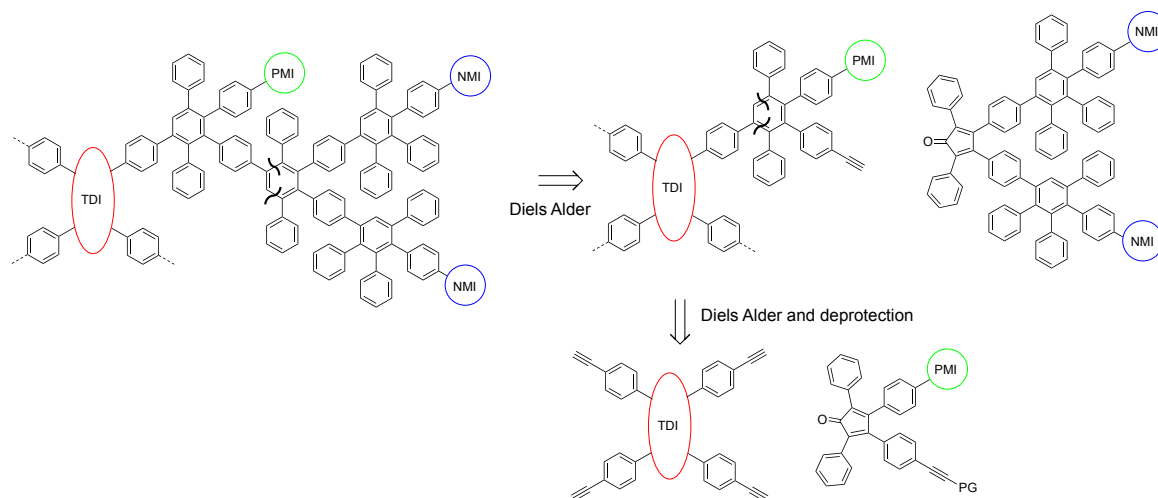
Scheme 1-1 Retrosynthetic pathway for the preparation of triad **1-1**.[24]

1.2.1.2 Porphyrin macrocycles

Another very important class of artificial light-harvesting systems is the array of porphyrins and in particular the porphyrin macrocycle mimicking the natural photosynthetic light-harvestings.[16a] Porphyrins have been widely used for their outstanding photophysical properties including photostability, very high extinction coefficients, and ability to promote fast excitation energy transfer. Their assembly into cyclic architectures has been intensively explored.[26] As an example, we focused our attention on the elegant *"LH2-like supramolecular triple-stranded complexes based upon porphyrin nanorings"* reported by *Anderson* and co-workers.[17b] The synthesis of their complex is based on the self-assembly of two 12-porphyrins nanorings with six free-base porphyrin dimers bearing pyridine substituents coordinating to the zinc metal centers of the porphyrins of the nanorings to form ring-dimer-ring complex **1-2** (Figure 1-10). The free base porphyrin dimers can act as energy donors while the nanorings as energy acceptors. The quantitative energy transfer was highlighted by fluorescence emission titration experiments. When the complex is assembled, the emission spectrum displays one single band at 800-900 nm corresponding to the emission of the nanorings. On the contrary, upon dissociation of complex **1-2** by adding a competing ligand (pyridine), the fluorescence spectra show an intense band for the dimer emission at 716 nm highlighting the loss of the energy transfer. Moreover, the energy transfer rate was estimated to be very fast $(0.65 \text{ ps})^{-1}$ comparable to those observed in the natural light-harvesting systems making the complex an interesting candidate to channel energy in solar-harvesting systems.
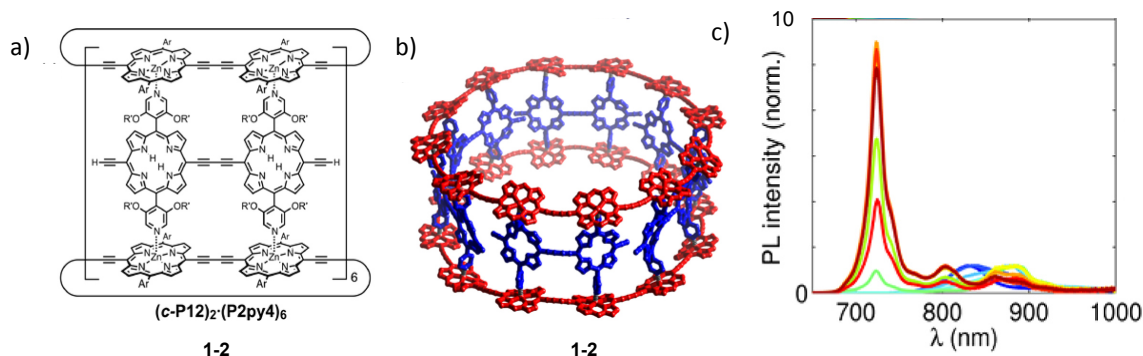
Figure 1-10 a, b) Structure of ring-dimer-ring complex **1-2**, Ar = 3,5-bis(trihexylsilyl)phenyl, R' = dodecyl; c) Steady state emission titrations of the associated complex (spectrum in blue) which is dissociated upon addition of a competing ligand (spectrum of fully dissociated complex in red with 6 equiv. of ligand) *(λ_exc = 450* ce 17b. Copyright (2014) American Chemical Society.[17b]

Her   oach is the synthetic accessibility. In particular, the last

step   templated macrocyclization, is achieved through Pd-

cata   ow yield (14%). Moreover, despite the addition of

solu   orphyrin derivatives limits the expansion of the system.

Anc   arrays in general is their narrow absorption windows,

whi   of light.

1.2.1.3 Supramolecular architectures

To bypass the synthetic limitations of a covalent approach described in the previous sections, nanostructures assembled by supramolecular methodologies such as H-bonding,[18, 27] π stacking,[19a, 19c] van der Waals interactions,[28] metal coordination etc,[29] have been as well widely developed to create light-harvesting complexes.[30] Among all the supramolecular architectures, gels formed by non-covalent interactions containing chromophores have been used for light harvesting since they can facilitate energy transfer processes. In this respect, *Ajayaghosh* and co-workers used organogelator oligo(phenylenevinylene) **1-3** (OPV) as an energy donor to promote energy transfer to Rhodamine B **1-4** (in 2:1 mol ratio) encapsulated into the gel.[19e] The energy transfer was illustrated by the amplification of the acceptor emission at 620 nm with the concomitant quenching of OPV emission between 500-650 nm in the organogel (λ_exc = 470 nm) as shown in Figure 1-11 b. Its efficiency was determined to be 90% from the quenching of OPV fluorescence profile following Equation 5. Interestingly, the authors reported the thermocontrol of energy transfer by the reversible gelation of the OPV gel upon heating or cooling.

$$\Phi_{ET} = 1 - \frac{I_{DA}}{A_{DA}} \frac{A_D}{I_D} \qquad (5)$$

13

Where I_{DA} and I_D are the integrated area of donor fluorescence emission upon excitation of the donor with and without acceptors and A_{DA} and A_D are the absorbance of the donor at the excitation wavelength with and without acceptors.

Later, the same group reported the encapsulation of less than 2 mol% of a new acceptor called PYPV **1-5** reported in Figure 1-11 c.[19c] This results in a highly efficient energy transfer quenching 95% of the OPV emission. Fluorescence microscopy images of gel fibers before and after encapsulation of the acceptor illustrate the energy transfer since the yellow emission of the gel before encapsulation turns to red in presence of PYPV upon excitation of OPV (Figure 1-11 d).
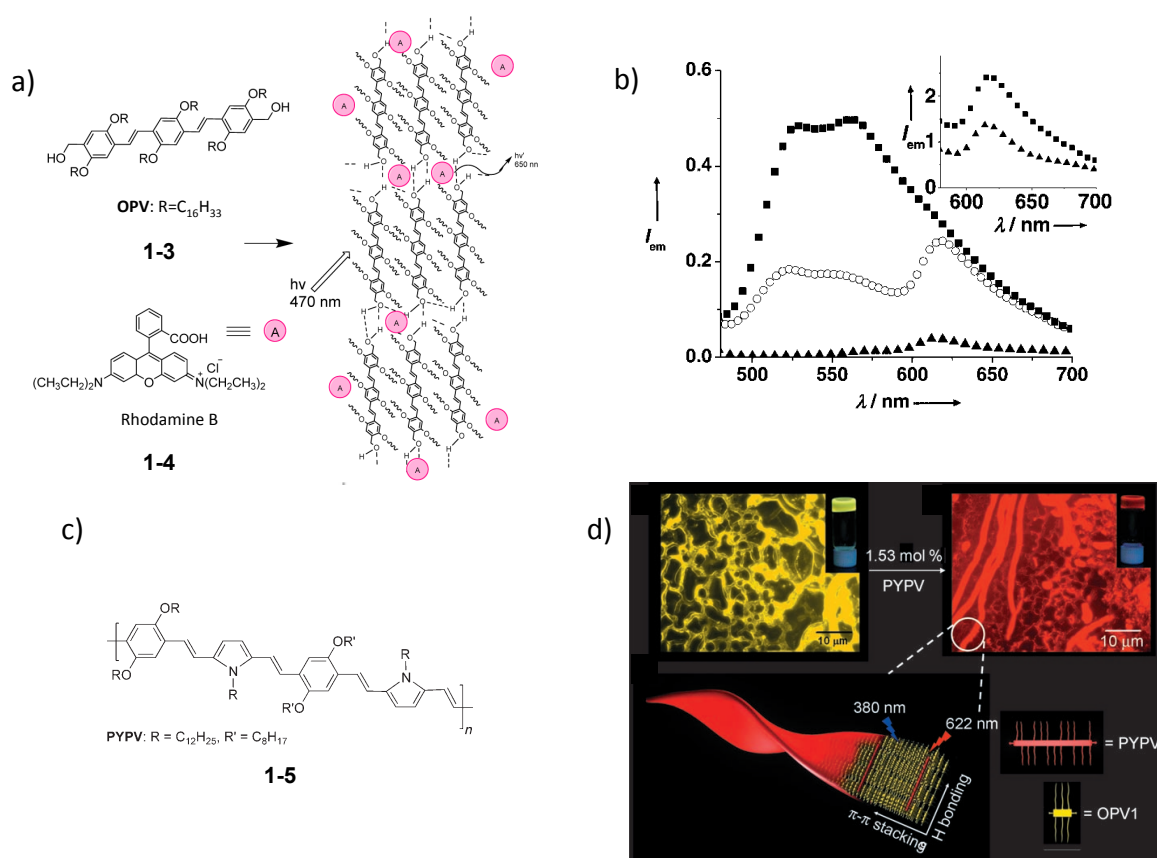
Figure 1-11 a) Structures of energy donor OPV **1-3** and energy acceptor Rhodamine B **1-4** used to form light-harvesting gel and probable self-assembly of Rhodamine B dispersed OPV gel; b) Fluorescence emission spectra in cyclohexane/chloroform (16:1) of OPV (black square), OPV+Rhodamine B (white circle), Rhodamine B (black triangle) at λ_{exc} = 470 nm. Adapted with permission from references 19e and 30. Copyright (2003) John Wiley and Sons;[19e] c) Structure of energy acceptor PYPV **1-5**; d) Fluorescence microscopy images of OPV cyclohexane gel before and after encapsulation of PYPV upon illumination at 365 nm and schematic representation of PYPV-encapsulated OPV tape. Adapted with permission from reference 19c. Copyright (2007) John Wiley and Sons.[19c]

On the other hand, supramolecular polymers have been as well successfully used to assemble chromophores.[18] For instance in 2014, *Yang* and co-workers reported nanoparticles of H-bonded supramolecular polymers to mimic the natural light-harvesting systems (Figure 1-12).[18b] The

nanospheres, containing energy donor **1-6** and acceptor **1-7** in different ratio, exhibit an efficient energy transfer, which was clearly visualized by steady-state and time-resolved fluorescence measurements. As shown in Figure 1-12c, quenching of the donor emission at 430 nm and amplification of the acceptor emission at 496 nm were observed by adding the acceptor in the nanospheres when the donor was selectively excited (λ_{exc} = 375 nm). To evaluate the light harvesting capability of the system, the authors determined the "antenna effect" (AE), a parameter particularly used in systems in which high donor-to-acceptor ratio is found.[31] This value estimates the degree of the amplification of acceptor emission by donor excitation and was calculated following Equation (6). In the best case (D/A ratio: 3 ... ...tor emission was observed.

$$AE = \frac{I_{A(D)}}{I_{A(A)}}$$

Where $I_{A(D)}$ is the emission intensity of the acceptor u... ...m) and $I_{A(A)}$ the emission intensity of the acceptor upon dir...
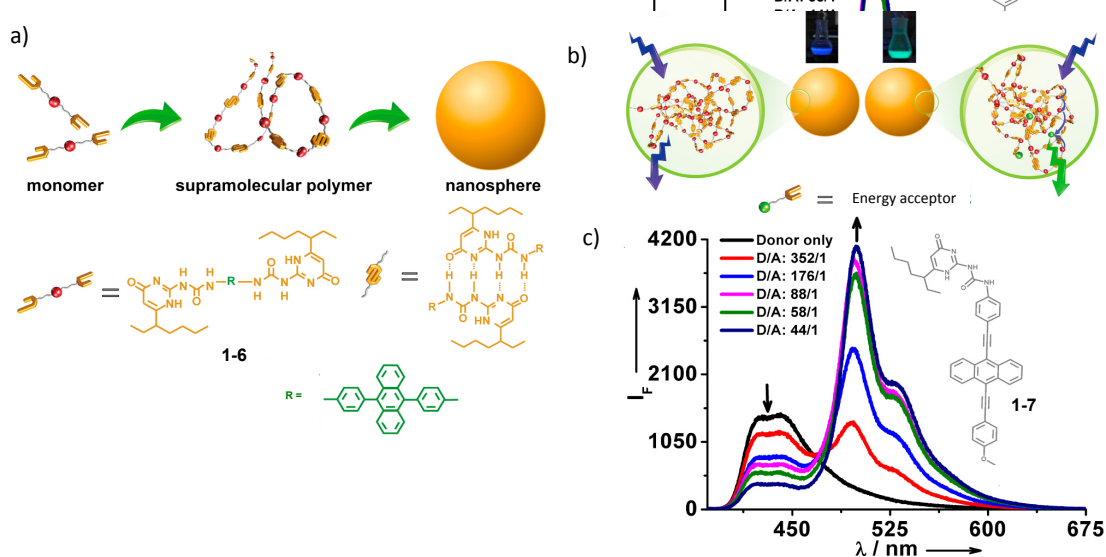
Figure 1-12 a) Schematic representation of preparation of energy donor (**1-6**) containing nanosphere of hydrogen-bonded supramolecular polymer; b) Comparison of chromophoric organization within energy donor (**1-6**) containing nanosphere and energy donor (**1-6**) and acceptor (**1-7**) containing nanosphere; c) Fluorescence emission spectra of light-harvesting nanospheres dispersed in water with different molar donor-to-acceptor ratio at λ_{exc} = 375 nm. Adapted with permission from reference 18b. Copyright (2013) Royal Society of Chemistry.[18b]

The use of non-covalent interactions for the preparation of light harvesting systems, for example in the formation of gel or supramolecular polymer, have been demonstrated to be an excellent strategy: very simple and promoting in certain cases good energy transfer. Even though those light-harvesting supramolecular architectures follow the sequential route since their synthetic

pathway consists to assembly "chromonomers" between themselves, the approach is very similar to the template one in the sense that the supramolecular architecture, gel or polymer in those specific cases, can be consider as a platform used to guide the spatial arrangement of the dyes. In this respect, the advantages and drawbacks resulting from those methodologies are very similar to those which will be discussed in the next section: the materials are synthetically very accessible; nevertheless, the positioning of the chromophores into the superstructure is difficult to predict and control. This general disadvantage can result in the loss of energy transfer in certain case favored by other mechanism of quenching such as self-quenching or excimer formation.

1.2.2 Templated assembly of chromophores for artificial antennas

Different strategies following a sequential approach to spatially organize various chromophores favoring energy transfer have been discussed. Complex architectures requiring difficult synthesis have been described with very well controlled unidirectional energy transfer, in contrast to much more simple systems leading to a more-difficult-to-predict arrangement of the chromophores. In this section, the use of a template to spatially guide the organization of the chromophores, in the same manner than the natural light harvesting complexes, will be exposed.

1.2.2.1 Biomaterials as templates

Biomaterials, including proteins and DNA, have been widely used for the creation of artificial antennas to control the spatial arrangement of pigments and favor the energy transfer between them.[21-22] In 2007, *Francis* and co-worker reported the assembly of different chromophoric units **1-8**, **1-9** and **1-10**, acting as donors and acceptor, on cysteine-containing protein called tobacco mosaic virus coat protein (TMVP) by thiol-maleimide "click" reaction to form different chromophore-protein conjugates (Figure 1-13a, b).[21a] The authors investigated the self-assembly of those conjugates forming disks or rods depending on the pH and optimized the ratio between donor and acceptor (Figure 1-13b). They highlighted the energy transfer in the resulting systems by steady-state fluorescence measurements. The excitation spectra of the self-assembled architecture built with the highest donor-to-acceptor ratio (**1-8/1-9/1-10** 8:4:1) monitored at 650 nm and proved the major contribution of the donors in the acceptor emission (Figure 1-13c Left). Besides, the overall efficiency Φ_{ET} of the energy transfer in this system was measured by comparison of the excitation spectrum of the complex with its absorption spectrum both normalized on the maximum absorption of the acceptor at 597 nm. The value is given by the ratio of absorbance and excitation intensities of the primary donor following Equation (7) and was estimated to be over 90% (Figure 1-13c Left). Moreover, the amplification of the acceptor emission (at 612 nm) in the same ratio was illustrated in the emission spectra (Figure 1-13c Right)

16

and the factor of enhancement of the acceptor emission upon excitation of the primary donor at 495 nm, the antenna effect, was calculated to be 4.6.

$$\text{Overall efficiency: } \Phi_{ET} = \frac{Ex_D}{A_D} \qquad (7)$$

Where Ex_D and A_D are excitation and absorption intensities of the donor in the normalized excitation and absorption spectra, respectively.
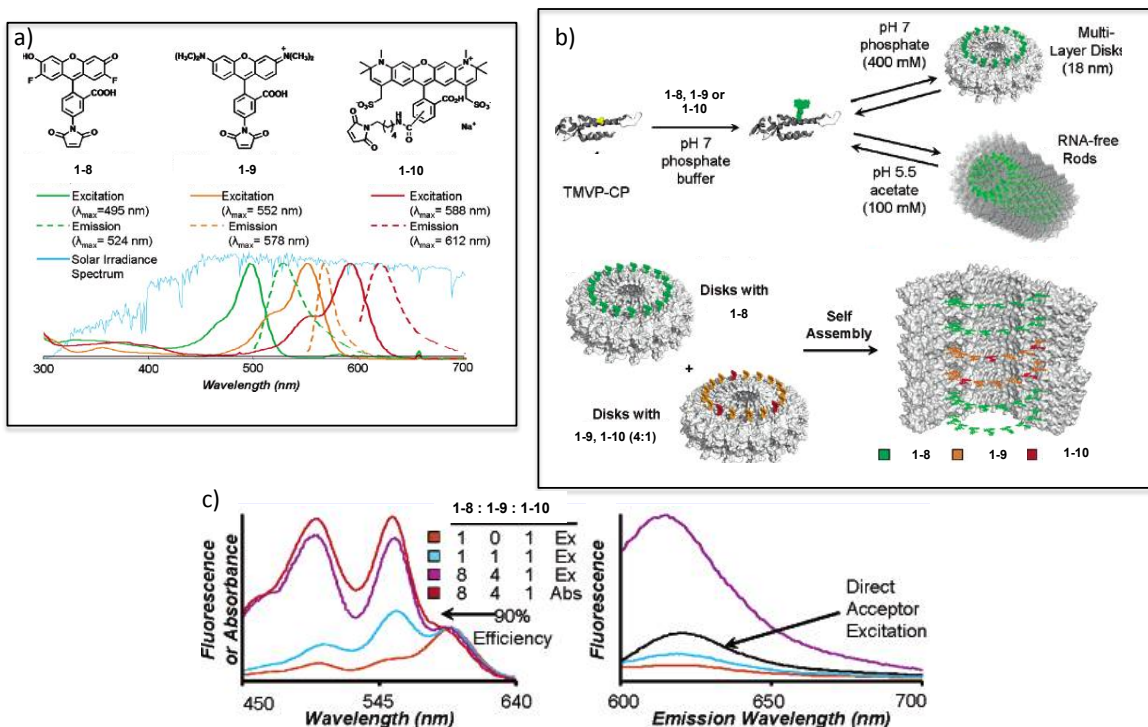
Figure 1-13 a) Structures of the chromophores **1-8**, **1-9**, **1-10** and their normalized fluorescence excitation and emission spectra plotted against the solar spectrum; b) Self-assembly of the chromophore-protein conjugates into rods or disks and spatial distribution of the chromophores in antenna complex built with optimized ratio donor **1-8**:donor **1-9**:acceptor **1-10** (8:4:1); c) Left: excitation spectra (Ex) of antenna complexes built with different ratio donor **1-8**:donor **1-9**:acceptor **1-10** and absorption spectrum (Abs) for the 8:4:1 system in red (normalized with the excitation spectra at the acceptor absorption 597 nm); Right: emission spectra upon excitation of the donor (λ_{exc} = 495 nm) compared with emission spectra (in black) upon direct excitation of the acceptor unit (λ_{exc} = 588 nm). Adapted with permission from reference 21a. Copyright (2007) American Chemical Society.[21a]

If the approach appears to be synthetically accessible and displays an efficient energy transfer, it is however noteworthy to indicate that the only controllable parameter in this example is the ratio between donor and acceptor; the spatial arrangement of the chromophoric units being dictated by the self-assembly of the protein was difficult to predict and not really optimizable.

On the other hand, *Liu* and co-workers used DNA nanotechnology to spatially organize chromophores and constructed *"DNA-directed artificial Light-Harvesting Antenna"*.[22a] In a similar manner than the natural light-harvesting complexes, different chromophores (donors and

acceptor) were incorporated into DNA nanoscaffolds at selected positions to form multiple arrays of chromophores, so-called triads. Different triads, containing different dyes ratio (primary donor ethynylpyrene **Py**/ intermediate donor cyanine **Cy3**/ acceptor Alexa Fluor 647 **AF**), were prepared (Figure 1-14). In the case of the triad **T1**, with a ratio of 6:6:1, the energy transfer was illustrated in the fluorescence emission spectra of the material by the quenching of the primary donor emission. The FRET efficiency was calculated from this quenching following Equation (5) and was estimated to be around 90%. Moreover, the amplification of the acceptor emission was here again evaluated by calculating the antenna effect (AE). The overall AE was determined to be 85%.
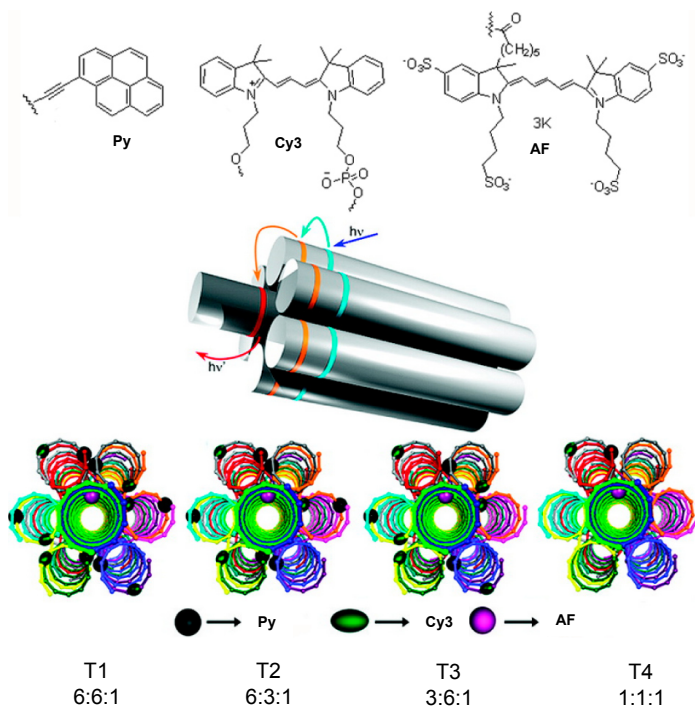
Figure 1-14 Structures of the chromophoric units incorporated into DNA strands; schematic representation of self-assembled DNA nanoscaffolds called triads, containing different ratios (Py/Cy3/AF) of chromophores. Adapted with permission from reference 22a. Copyright (2011) American Chemical Society.[22a]

In contrast to the previous example, this use of DNA nanoscaffolds to organize the dyes, is a mixture between the sequential and the template approach. Indeed, the dyes were incorporated into the DNA scaffold by synthesizing DNA strands using chromophore-modified nucleotides. Consequently, the positioning of the dyes was well-controlled by the authors but, each different antennas required new DNA strands synthesis which highlight problems of synthetic accessibility and lack of versatility of the used methodology.

1.2.2.2 Other scaffolds

Non-biomaterials were also applied as scaffolds to spatially organize dyes for light harvesting applications. Multichromophoric dendrimers have been already discussed in the previous secti dedicated to the sequential assembly of the "chromonomers", but it is worth mentioning that n chromophoric dendrimers have been also used as scaffolds to template chromophores. I instance, in 2009, *Li* and co-worker reported a water-soluble polyamidoamine (PAMA dendrimer decorated with naphtyl chromophores at the periphery with an anthracene derivat AN encapsulated as energy acceptor.[32] Due to the strong interactions between the naph moieties resulting in excimer formation and self-quenching (which is often the case in flexi light-harvesting dendritic systems), the intensity of the emission of AN within the light-harvesti complex upon excitation of the donor (λ_{exc} = 276 nm) is relatively low and is dominated by excimer emission (broad band around 400 nm). Nevertheless, by adding cucurbit[7]uril (CB[forming a host-guest complex with naphtyl chromophores, interactions between peripheral naphtyl were restrained and the improvement of the energy transfer from naphtyl to anthracene was observed by the amplification of the acceptor AN emission than in the emission spectra (Figure 1-15).
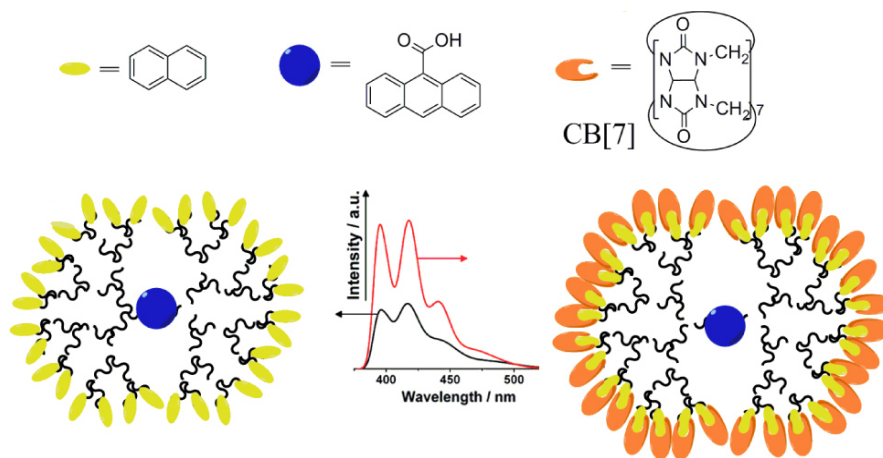
Figure 1-15 Expression of the energy transfer by amplification of the acceptor AN emission in fluorescen emission spectra *(λ_{exc} = 276 nm)* within two dendritic systems: left: PAMAM decorated with naphtyl – A complex, right: PAMAM decorated with naphtyl•CB[7] – AN complex. Adapted with permission fro reference 30. Copyright (2015) American Chemical Society.[30, 32]

Yang and co-workers followed a similar approach.[33] Nevertheless, to overcome the synthet difficulties of the dendrimers, they reported the use of surface-cross linked micelle (SCM) scaffold. Micelles were formed with 4-(dodecyloxy)benzyltripropargylammonium bromide **1-1** and cross-linked by copper catalyzed azide alkyne cycloaddition (CuAAC) using **1-12**. TI surface functionalization by the energy donor diphenylanthracene **DPA** was performed through tl same reaction (Figure 1-16). In contrast with the previous example, the micelle-bound DP

system displayed a high quantum yield which was estimated to be 80% and so neither self-quenching or excimer formation occurred in the system possibly due to the non-planarity of the donor, the rigidity of the system and the electrostatic repulsion between the positively charged SCM. The energy acceptor Eosin Y **EY** was spontaneously assembled on the surface of the micelle by electrostatic interactions. The energy transfer was observed by steady-state fluorescence titration experiments leading to the quenching of [...] the increasing of the acceptor emission at 550 nm upon additio[...] (λ_{exc} = 375 nm). The study suggested that for one molecule of [...] excited **DPA** units were completely quenched through Förste[...] pathways.
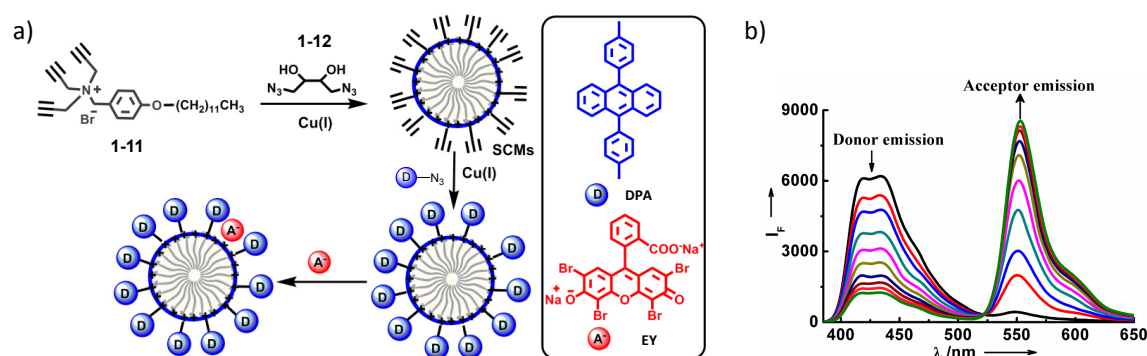
Figure 1-16 a) Preparation of the artificial antenna based on surface-cross-linked micelles (SCM); b) Fluorescence emission spectra *(λ $_{exc}$ = 375 nm)* of DPA-SCM in black (C$_D$ = 23 μM) upon addition of the acceptor EY (C$_A$ = 0, 0.08, 0.17, 0.33, 0.5, 0.67, 0.84, 1, 1.17, 1.34 μM) in green for highest C$_A$ in THF. Adapted with permission from reference 30. Copyright (2015) American Chemical Society.[33]

Tho[...] [...]rs and micelles are in many aspects com[...] in *Section 1.2.1.3*: in all those cases, a sup[...] the dyes. The energy transfers in the disc[...] nstruction of the materials very simple. Hov[...] donor and one energy acceptor for the fabr[...] mall window of the solar spectrum and cons[...] But, this considerably simplifies the opti[...] r that the authors needed to control was the [...] of the energy transfer is intrinsic to the use[...] ores would require the control of their posi[...]

1.3 Aim and outline of the dissertation

To summarize, various types of material have been used as scaffolds to organize the spatial arrangement of dyes and favor the energy transfer between them. The synthesis of artificial antennas following the template approach appears to be very simple and versatile. However, contrary to the template route presented in Figure 1-8, in which receptor sites are pre-programmed in the scaffold to control the spatial organization of the dyes, the reported examples do not follow this strategy. In this respect, the main limitation of the template approach as it is used in those examples, is the lack of control of the incorporation of the different dyes necessary to maximize the energy transfer.

Taking into consideration the advantages and drawbacks of the sequential and the template approaches for the creation of light harvesting systems, the general aim of the dissertation is to create a library of artificial antenna systems following a template approach which will allow the controlled incorporation of dyes into a scaffold. The controlled self-assembly of the chromophore can be achieved by pre-programming periodic receptor sites on the scaffold to selectively accommodate a specific chromophore. In this respect, starting from one pre-programmed scaffold, an unlimited number of antennas exhibiting any desired absorbed color can be obtained; besides, the efficiency of the energy transfer can be modulated by tuning the dyes and their spatial arrangement. In this manuscript, methodologies for the incorporation of three, four and then five different chromophores will be targeted. To develop this methodology, the different objectives of the thesis are:

Chromophores and Scaffold bearing pre-programmed complementary recognition motifs

Self-assembly

Artificial antenna system with optimized interchromophoric spatial arrangement
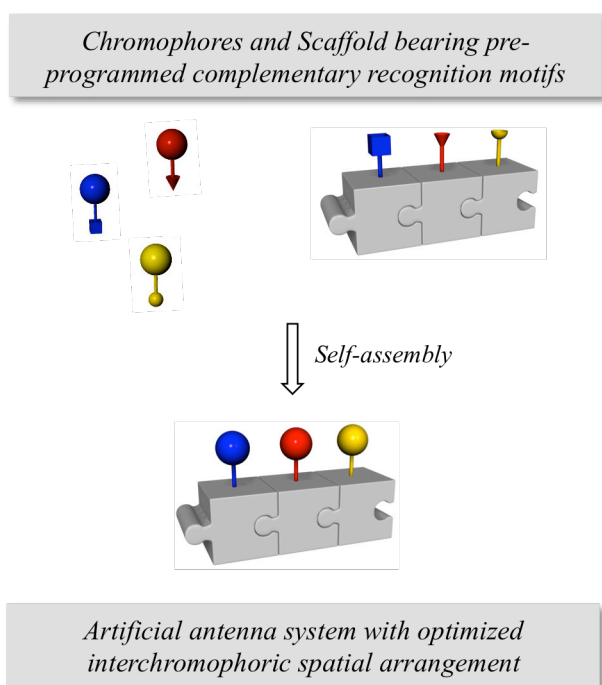
i) the engineering of recognition motifs between the template and the dyes and the evaluation of their orthogonality

ii) the design, the synthesis and the optimization of a pre-programmed scaffold bearing receptor sites to selectively incorporate dyes

iii) the development and the optimization of luminophores absorbing and emitting efficiently in the different regions of the visible spectrum and bearing complementary sticky side to be assembled on the scaffold

iv) the optimization of the molecular assembly between the scaffold and the dyes and the evaluation of the photophysical properties of the artificial antenna systems

Following this, the manuscript will be divided in four parts. *Chapter 2* will focus on the engineering of the recognition motifs between the scaffold and the dyes. For this purpose, simultaneous tri-, tetra- and pentaorthogonal multireaction systems will be developed involving dynamic and non-dynamic covalent reactions. *Chapter 3* and *Chapter 4* will be dedicated to selectively template three different chromophores into a peptidic scaffold by the simultaneous use of three dynamic covalent bonds. The chapters will address the preparation of a pre-programmed scaffolds bearing receptor sites, the synthesis of the chromophores with complementary sticky side, the self-assembly of the components and the investigation of the light harvesting capabilities of the antenna systems. Finally, *Chapter 5* will focus on the assembly of additional chromophores on the scaffold (up to five) by simultaneously applying the dynamic and non-dynamic reactions to the decoration of the peptidic scaffold.
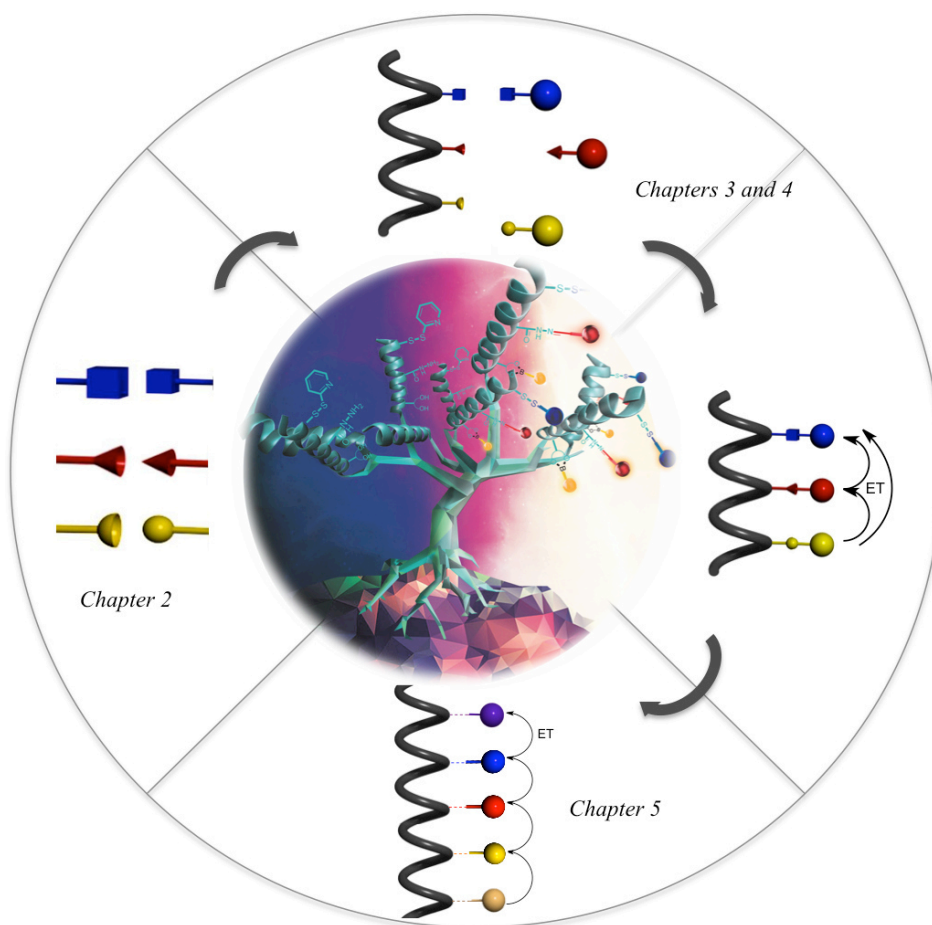
Figure 1-17 Schematic representation of the outline of this dissertation.

1.4 References

[1]   N. Armaroli, V. Balzani, *Angew. Chem. Int. Ed.* **2007**, *46*, 52-66.

[2]   R. E. Blankenship, D. M. Tiede, J. Barber, G. W. Brudvig, G. Fleming, M. Ghirardi, M. R. Gunner, W. Junge, D. M. Kramer, A. Melis, T. A. Moore, C. C. Moser, D. G. Nocera, A. J. Nozik, D. R. Ort, W. W. Parson, R. C. Prince, R. T. Sayre, *Science* **2011**, *332*, 805-809.

[3]   G. D. Scholes, G. R. Fleming, A. Olaya-Castro, R. Van Grondelle, *Nat. Chem.* **2011**, *3*, 763-774.

[4]   R. E. Blankenship, *Molecular Mechanisms of Photosynthesis, 2nd Edition*, Wiley-Backwell, **2014**.

[5]   a) T. Mirkovic, G. D. Scholes, in *Photobiology: The Science of Light and Life, Third Edition*, Springer, New York, **2015**, pp. 231-241; b) T. Mirkovic, E. E. Ostroumov, J. M. Anna, R. Van Grondelle, Govindjee, G. D. Scholes, *Chem. Rev.* **2017**, *117*, 249-293.

[6]   R. J. Cogdell, A. Gall, J. Köhler, *Q. Rev. Biophys.* **2006**, *39*, 227-324.

[7]   a) V. Balzani, G. Bergamini, P. Ceroni, E. Marchi, *New J. Chem.* **2011**, *35*, 1944-1954; b) V. Balzani, A. Credi, M. Venturi, *Molecular Devices and Machines: Concepts and Perspectives for the Nanoworld: Second Edition*, Wiley-VCH, Weinheim, **2008**.

[8]   a) G. McDermott, S. M. Prince, A. A. Freer, A. M. Hawthornthwaite-Lawless, M. Z. Papiz, R. J. Cogdell, N. W. Isaacs, *Nature* **1995**, *374*, 517-521; b) S. Bahatyrova, R. N. Frese, C. A. Siebert, J. D. Olsen, K. O. van der Werf, R. van Grondelle, R. A. Niederman, P. A. Bullough, C. Otto, C. N. Hunter, *Nature* **2004**, *430*, 1058-1062.

[9]   R. J. Cogdell, A. T. Gardiner, H. Hashimoto, T. H. P. Brotosudarmo, *Photochem. Photobiol. Sci.* **2008**, *7*, 1150-1158.

[10]   a) A. W. Roszak, T. D. Howard, J. Southall, A. T. Gardiner, C. J. Law, N. W. Isaacs, R. J. Cogdell, *Science* **2003**, *302*, 1969-1972; b) M. F. Richter, J. Baier, J. Southall, R. J. Cogdell, S. Oellerich, J. Köhler, *Proc. Natl. Acad. Sci. U. S. A.* **2007**, *104*, 20280-20284.

[11]   T. Forster, *Discuss. Faraday Soc.* **1959**, *27*, 7-17.

[12]   S. A. Hussain, *arXiv.org, e-Print Arch., Phys.* **2009**, 1-4, arXiv:0908.1815v0901 [physics.gen-ph].

[13]   D. L. Dexter, *J. Chem. Phys.* **1953**, *21*, 836-850.

[14]   a) V. Sundström, T. Pullerits, R. Van Grondelle, *J. Phys. Chem. B* **1999**, *103*, 2327-2346; b) http://photobiology.info/Jones.html.

[15]   L. Rocard, A. Berezin, F. De Leo, D. Bonifazi, *Angew. Chem. Int. Ed.* **2015**, *54*, 15739-15743.

[16]   a) M. S. Choi, T. Yamazaki, I. Yamazaki, T. Aida, *Angew. Chem. Int. Ed.* **2004**, *43*, 150-158; b) S. Hecht, J. M. J. Fréchet, *Angew. Chem. Int. Ed.* **2001**, *40*, 74-91; c) U. Hahn, M. Gorka, F. Vogtle, V. Vicinelli, P. Ceroni, M. Maestri, V. Balzani, *Angew. Chem. Int. Ed.* **2002**, *41*, 3595-3598.

[17]   a) R. Takahashi, Y. Kobuke, *J. Am. Chem. Soc.* **2003**, *125*, 2372-2373; b) P. Parkinson, C. E. I. Knappke, N. Kamonsutthipaijit, K. Sirithip, J. D. Matichak, H. L. Anderson, L. M. Herz, *J. Am. Chem. Soc.* **2014**, *136*, 8217-8220.

[18]   a) R. Abbel, C. Grenier, M. J. Pouderoijen, J. W. Stouwdam, P. E. L. G. Leclere, R. P. Sijbesma, E. W. Meijer, A. P. H. J. Schenning, *J. Am. Chem. Soc.* **2009**, *131*, 833-843; b) H. Q. Peng, J. F. Xu, Y. Z. Chen, L. Z. Wu, C. H. Tung, Q. Z. Yang, *Chem. Commun.* **2014**, *50*, 1334-1337.

[19]   a) T. E. Kaiser, H. Wang, V. Stepanenko, F. Würthner, *Angew. Chem. Int. Ed.* **2007**, *46*, 5541-5544; b) A. Lohr, F. Würthner, *Angew. Chem. Int. Ed.* **2008**, *47*, 1232-1236; c) A. Ajayaghosh, V. K. Praveen, C. Vijayakumar, S. J. George, *Angew. Chem. Int. Ed.* **2007**, *46*, 6260-6265; d) A. Ajayaghosh, C. Vijayakumar, V. K. Praveen, S. S. Babu, R. Varghese, *J. Am. Chem. Soc.* **2006**, *128*, 7174-7175; e) A. Ajayaghosh, S. J. George, V. K. Praveen, *Angew. Chem. Int. Ed.* **2003**, *42*, 332-335.

[20]   a) N. Sakai, M. Lista, O. Kel, S. I. Sakurai, D. Emery, J. Mareda, E. Vauthey, S. Matile, *J. Am. Chem. Soc.* **2011**, *133*, 15224-15227; b) G. Sforazzini, E. Orentas, A. Bolag, N. Sakai, S. Matile, *J. Am. Chem. Soc.* **2013**, *135*, 12082-12090.

[21]   a) R. A. Miller, A. D. Presley, M. B. Francis, *J. Am. Chem. Soc.* **2007**, *129*, 3104-3109; b) M. Endo, M. Fujitsuka, T. Majima, *Chem. Eur. J.* **2007**, *13*, 8660-8666.

[22]   a) P. K. Dutta, R. Varghese, J. Nangreave, S. Lin, H. Yan, Y. Liu, *J. Am. Chem. Soc.* **2011**, *133*, 11985-11993; b) J. G. Woller, J. K. Hannestad, B. Albinsson, *J. Am. Chem. Soc.* **2013**, *135*, 2759-2768; c) A. Ruiz-Carretero, P. G. A. Janssen, A. Kaeser, A. P. H. J. Schenning, *Chem. Commun.* **2011**, *47*, 4340-4347.

[23]   Z. M. Hudson, D. J. Lunn, M. A. Winnik, I. Manners, *Nat. Commun.* **2014**, *5*, 3372.

[24]   T. Weil, E. Reuther, K. Müllen, *Angew. Chem. Int. Ed.* **2002**, *41*, 1900-1904.

[25]   M. Cotlet, T. Vosch, S. Habuchi, T. Weil, K. Müllen, J. Hofkens, F. De Schryver, *J. Am. Chem. Soc.* **2005**, *127*, 9760-9768.

[26]   a) Y. Nakamura, N. Aratani, A. Osuka, *Chem. Soc. Rev.* **2007**, *36*, 831-845; b) J. Yang, M. C. Yoon, H. Yoo, P. Kim, D. Kim, *Chem. Soc. Rev.* **2012**, *41*, 4808-4826.

[27]   T. S. Balaban, N. Berova, C. M. Drain, R. Hauschild, X. Huang, H. Kalt, S. Lebedkin, J. M. Lehn, F. Nifaitis, G. Pescitelli, V. I. Prokhorenko, G. Riedel, G. Smeureanu, J. Zeller, *Chem. Eur. J.* **2007**, *13*, 8411-8427.

[28] K. Sugiyasu, N. Fujita, S. Shinkai, *Angew. Chem. Int. Ed.* **2004**, *43*, 1229-1233.

[29] I. W. Hwang, T. Kamada, K. A. Tae, M. K. Dah, T. Nakamura, A. Tsuda, A. Osuka, D. Kim, *J. Am. Chem. Soc.* **2004**, *126*, 16187-16198.

[30] H. Q. Peng, L. Y. Niu, Y. Z. Chen, L. Z. Wu, C. H. Tung, Q. Z. Yang, *Chem. Rev.* **2015**, *115*, 7502-7542.

[31] D. W. Brousmiche, J. M. Serin, J. M. J. Fréchet, G. S. He, T. C. Lin, S. J. Chung, P. N. Prasad, R. Kannan, L. S. Tan, *J. Phys. Chem. B* **2004**, *108*, 8592-8600.

[32] Y. Zeng, Y. Li, M. Li, G. Yang, Y. Li, *J. Am. Chem. Soc.* **2009**, *131*, 9100-9106.

[33] H. Q. Peng, Y. Z. Chen, Y. Zhao, Q. Z. Yang, L. Z. Wu, C. H. Tung, L. P. Zhang, Q. X. Tong, *Angew. Chem. Int. Ed.* **2012**, *51*, 2088-2092.

2. Simultaneous dynamic and non-dynamic covalent reactions

In *Chapter 1*, the creation of artificial antenna systems following a template approach has been reported in detail, and this approach appeared to be very convenient in term of synthesis. Therefore, the aim of this thesis is to explore the self-assembly of chromophores into a scaffold for artificial antenna. To achieve this, periodic receptor sites on the scaffold have to be programmed to selectively anchor a specific molecular chromophore. This chapter will focus on the design and the fundamental understanding of the interactions between the receptor sites and the self-assembled molecular guests. This will be performed through the development of simultaneous multireaction systems based on dynamic and non-dynamic covalent reactions.

The chapter will be divided in two main sections: *i) Section 2.2.1* will address the design and the synthesis of receptor sites to undergo simultaneously the anchoring reactions namely disulfide exchange, boronate formation, acyl hydrazone formation, strain promoted azide-alkyne cycloaddition and the inverse electron demand Diels-Alder cycloaddition between *s*-tetrazine and *trans*-cyclooctene. *ii)* In *Section 2.2.2*, the anchoring reactions will be independently and simultaneously optimized to develop tri-, tetra- and pentaorthogonal multireaction systems.

The X-ray analyses shown in this chapter have been performed by *Bernadette Norberg* (*University of Namur*) and *Benson Kariuki* (*Cardiff University*). Furthermore, I want to kindly acknowledge *Nicolas Biot* (*Cardiff University)* for his Density Functional Theory (DFT) calculations in the second section.

2.1 Simultaneous Multireaction Systems

The creation of complex architectures such as artificial antennas following a template approach, *i.e.* the self-assembly of the components of interest (dyes in the case of the antenna) on the scaffold in a one-pot reaction, has been demonstrated to be synthetically very efficient and versatile. However, the control of the spatial organization of the components following this approach, which is particularly important in the case of the antenna systems to control the energy

transfer, appeared to be rarely used in the literature as described in *Chapter 1*. This might be due to the major hurdle to achieve the selective incorporation of the components into the scaffold consisting in designing orthogonal recognition motifs between the scaffold and the molecular guests.

Orthogonal recognition motifs can be engineered by the use of covalent or non-covalent interactions. In order to build robust systems, which can be purified and isolated, we focused our attention on recognition motifs based on covalent interactions. In this respect, orthogonal multireaction systems, which refer to simultaneous reactions where the components react in very high yield, fast and selectively in the presence of many other functional groups, can be developed to engineer covalent orthogonal recognition motifs.[1] So, chemoselective reactions have to be used to design such a system; they can be split into two different classes: dynamic covalent reactions *vs.* non-dynamic (Figure 2-1).

The big advantage of the dynamic covalent reactions, as it will be described more into details in *Section 2.1.1*, is their possibility to be robust and quantitative under certain conditions or reversible under other conditions. For the eventual possibility to take advantage of this dual nature, bi- or triorthogonal multireaction systems can be developed by using Orthogonal Dynamic Covalent Chemistry as introduced in *Section 2.1.1*. Moreover, in order to increase the complexity of the multireaction system and introduce more orthogonal recognition motifs (up to five), non-dynamic reactions can also be added to the system for the construction of non-reversible architectures. Indeed, the non-dynamic orthogonal covalent reactions being more various, their use considerably expands the choice of functional groups involved the multireaction system and so potentially the chemoselectivity between the reactions. In *Section 2.1.2*, non-dynamic reactions of interest developed for bioconjugation will be introduced.
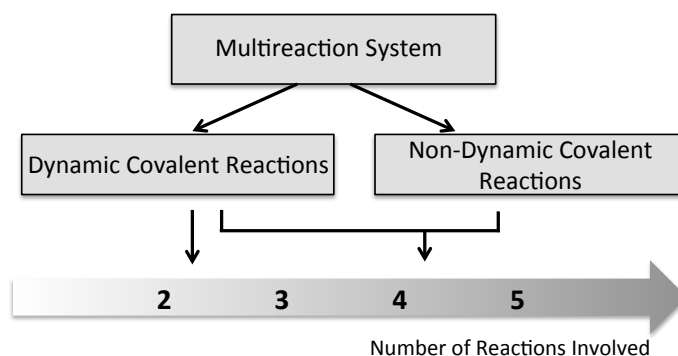
Figure 2-1 Strategy for the creation of multireaction systems for engineering covalent orthogonal recognition motifs.

2.1.1 General introduction on Orthogonal Dynamic Covalent Chemistry

The construction of complex molecular and supramolecular architectures have been extremely attractive in the last decades leading to Nobel Prizes in Chemistry;[2] especially last year, being awarded to *J.-P. Sauvage*, *Sir J. F. Stoddart* and *B. L. Feringa "for the design and the synthesis of molecular machines"*.[3] For the creation of such architectures, covalent, non-covalent and dynamic covalent bonds are available tools (Table 2-1). Dynamic covalent chemistry (DCC), which relies on reversible covalent bond-forming reactions leading to thermodynamically most favored species, combines both the advantages of the covalent (by its robustness) and the non-covalent chemistry (by its reversibility) and in this respect, has seen its interest growing in the last decades.[4] Various types of reactions have been reviewed as dynamic covalent reactions. They can be classified following the functional group involved. One of the most important class of reactions involves the exchange of a carbonyl group: the acyl transfer (C(O)-X) within transesterification, transamidation, transthioesterification. Exchange reactions can also concern imine and derivatives (hydrazone and oxime), acetal and thioacetal, disulfide, or boronate ester. Less common reactions have been also described as dynamic covalent reactions such as reversible Diels-Alder or alkene and alkyne metathesis.

Table 2-1 Most promising toolbox for creation of complex matter. Adapted from reference 7.

Non-covalent	Dynamic covalent	Covalent
Hydrogen bonds	Disulfides	C-C
Ion pairs	Hydrazones, imines, oximes	C-N
Hydrophobic	Boronic esters	B-O
π–π	Thioesters	C-S
Cation-π	Hemi-/acetals	C-O
Anion-π	Hemiaminals	O-N
Halogen bonds…	Dithianes…	O-S…

Thanks to the reversible nature of the DCC allowing the self-organization of the system, very sophisticated molecular systems were reported and, contrary to supramolecular systems assembled by non-covalent interactions, can be purified and isolated.[5] In this respect, DCC became an essential tool, especially in polymer, macrocycle, and macro-cage chemistry.[6]

In supramolecular architectures, different non-covalent interactions are routinely used simultaneously. For instance, the self-assembly of DNA combines hydrogen bonding, π–π interactions, hydrophobic interactions and charge repulsions. Those interactions can be defined as orthogonal since they occur simultaneously without interfering with each other.[1] Applying the concept of orthogonality to dynamic covalent bonds to increase the capability of the tool for complex functional system is surprisingly quite new and not very well developed.[7] One of the first examples of orthogonal dynamic covalent bonds has been reported in 2005. The authors used simultaneously the disulfide and thioester exchange to obtain a diverse library of cyclic and acyclic compounds (Figure 2-2 a).[8] Three years later, the orthogonality between disulfide and hydrazone exchange was reported by *Otto* and co-workers.[9] The study focused on the possibility to selectively activate or desactivate one of the exchange by changing the pH. This methodology has been used for the development of the molecular "walkers" by *Leigh* and co-workers, which allows the directional moving of a component along a molecular track.[10] The first example describing three covalent reversible reactions used similarly the exchange of disulfide and hydrazone but in combination with the thioester exchange.[11] Here again, the authors played with the pH to selectively activate the reactions. Besides, the combination of orthogonal imine and disulfide bonds with metal coordination for construction of multicomponent architectures has been reported (Figure 2-1 b).[12] Finally, the creation of macrocycles by using simultaneously the imine and the boronic ester formation[13] or imine formation and olefin metathesis[14] opens new horizons for the field of orthogonal dynamic covalent chemistry (Figure 2-2 c, d, e).
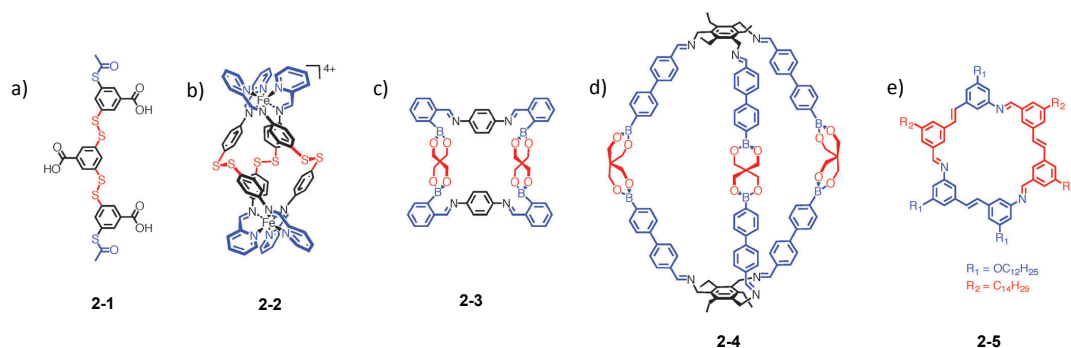
Figure 2-2 Advanced architectures built by bi-orthogonal dynamic covalent reactions. Adapted from reference 7.[7]

With the aim to create versatile multichromophoric architectures following a template approach, orthogonal dynamic covalent bonds appear to be good candidates to achieve the selective recognition between a pre-programmed scaffold bearing receptor sites and the different molecular guests, the chromophores. In this respect, three dynamic covalent reactions: the disulfide

exchange, the formation of boronic ester and acyl hydrazone, were selected among all the reactions of DCC. It is noteworthy to mention that during the progression of this work, those three reactions have been reported for the creation of multicomponent surface architectures.[15] *Matile* and co-workers published a series of studies in which they used sequentially disulfide exchange in basic conditions, hydrazone exchange under acidic conditions, and boronic ester exchange under neutral conditions. However, the simultaneous exploitation of the reactions was remaining unknown. Hence, the first aim of the chapter is to design model compounds and find conditions capable to undergo simultaneously the reactions and to prove their mutual orthogonality (Scheme 2-1).
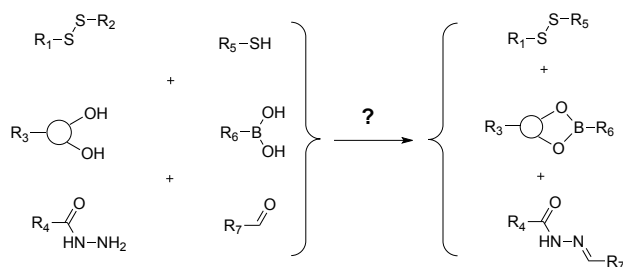
Scheme 2-1 General representation of the triorthogonal multireaction system selected for this study.

Presently, the interest for the field of orthogonal dynamic covalent bonds extensively increases.[7, 15-16] For instance, after publishing our work,[17] *Anslyn* and co-workers reported the first system involving four simultaneously dynamic covalent reactions, namely the boronic ester exchange, the thiol addition to a conjugate acceptor, the hydrazone exchange and the terpyridine-zinc complexation (Figure 2-3).[16b]
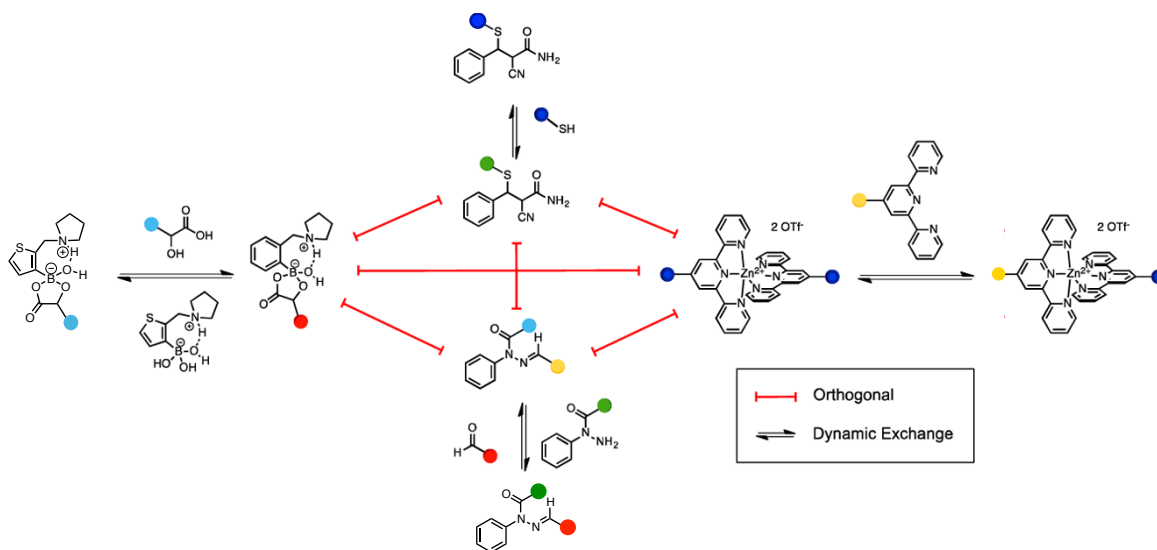
Figure 2-3 "Four simultaneously dynamic covalent reactions." Adapted with permission from reference 17. Copyright (2016) American Chemical Society.[16b]

2.1.2 Non-dynamic Orthogonal Covalent Reactions

On the other hand, chemoselective non-dynamic covalent reactions, so-called bioorthogonal or "click" reactions, have been extensively studied and developed to selectively modify biomolecules.[18] These reactions, whose components must react in very high yield, fast and selectively to each other, appear to be as well interesting candidates for engineering additional covalent orthogonal recognition motifs for the construction of more complex molecular architectures.

During the past century, the chemical modifications of biomolecules involved classic residue protein modifications, such as cysteine which can undergo disulfide exchange or lysine which can be used in reductive amination reactions with aldehydes or amide bond formation for example.[19] Nevertheless, in 1996, the first site-specific modification of protein using unnatural functional group was reported involving the incorporation of keto amino acid by biosynthetic machinery.[20] The possibility to introduce new functionalities for unique and selective functionalization considerably expanded the field and various bioorthogonal reactions involving aldehyde, azide, nitrone, nitrile oxide, tetrazine, alkene, etc., were developed.[18] We focused our attention on reactions involving azide and tetrazine, two functional groups potentially inert in the presence of the functions involved in the selected reactions of dynamic covalent chemistry: thiol-disulfide, diol-boronic acid, hydrazide-aldehyde.

Azides have been widely used in bioconjugation since their introduction into biomolecules is very well reported *via* diazo-transfer into amine or non-natural amino acid incorporation.[21] In this respect, many reactions involving azide have been developed. First of all, in 2000, *Bertozzi* and co-worker reported the Staudinger ligation between azide and triarylphosphine derivative leading to the formation of an amide bond as described in Scheme 2-2.[22] However, the major drawback of the reaction is its low kinetic (k = 2.1 10^{-3} M^{-1} s^{-1} in CD_3CN). Besides, the components of the reaction can potentially cross-react with those of the disulfide exchange; the phosphine having a reducing power toward disulfide.

R_1, R_2 = biomolecule or tag
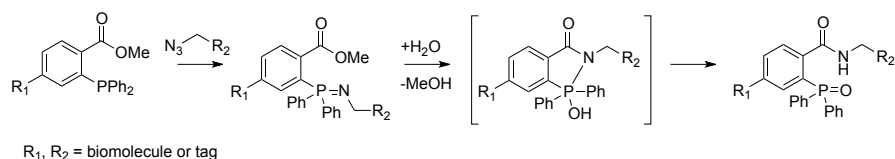
Scheme 2-2 Staudinger ligation between triarylphosphine derivative and azide.

On the other hand, reactions between azide and alkyne have been widely developed. The famous "click reaction" copper-catalyzed azide-alkyne cycloaddition[23] (CuAAC) has been applied to biomolecule modifications.[24] However, the required Cu(I)-catalyst can possibly interact with other functional groups so, metal-free alkyne-azide cycloaddition methods appeared to be more

suitable for our system. In 2004, *Bertozzi* and co-workers explored the spontaneous reaction between cyclooctyne and azide, so-called Strain-Promoted Azide Alkyne Cycloaddition (SPAAC), for cell-surface labeling (Figure 2-4).[25]
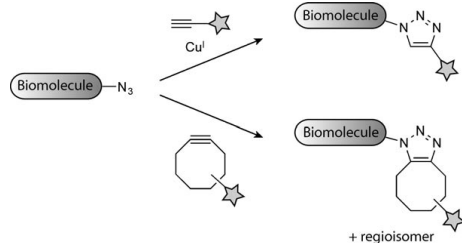
Figure 2-4 Bioorthogonal cycloaddition of azides and alkynes catalyzed by Cu[I] or promoted by strain.[18a]

Alkenes have been also used with azides in 1,3-dipolar cycloaddition. The product from azide-alkene cycloaddition, the triazoline, being unstable compared to triazole, oxanorbornadiene, containing electron-deficient olefin was used as dipolarophile to undergo cycloaddition with azide and extruding furan by Diels-Alder reaction to yield triazole products (Scheme 2-3 A).[26] Alternative strategies to the 1,3-dipolar cycloadditions with azide or other less stable 1,3-dipoles such as nitrile oxide or nitrone as well used in bioconjugation,[27] are the *s*-tetrazine (1,2,4,5-tetrazine or *sym*-tetrazine) based cycloadditions.[28] Those cycloadditions occur *via* inverse-electron demand Diels-Alder (IEDDA) in the presence of a strained alkene: for example with *trans*-cyclooctene or norbornene as reported in Scheme 2-3 B and C respectively.[29]
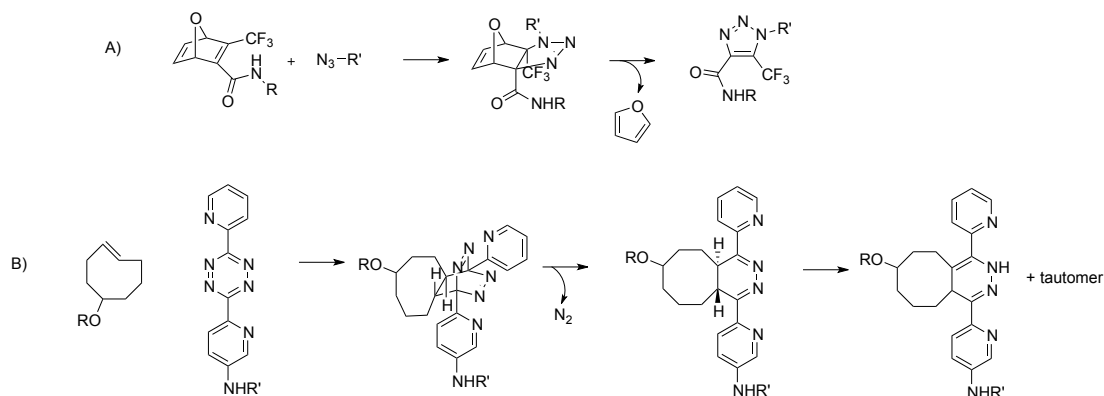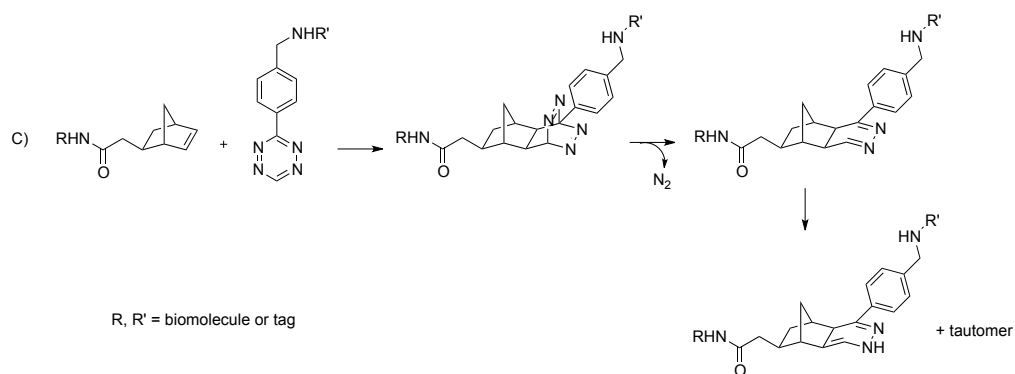
Scheme 2-3 Bioorthogonal reactions with alkenes; A) 3+2 cycloaddition between oxanornadiene and azide; B) Inverse electron demand Diels-Alder (IEDDA) between *trans*-cyclooctene and dipyridyl-*s*-tetrazine; C) IEDDA between norbornene and *s*-tetrazine.

For the design of the tetra- and pentaorthogonal multireaction system, two of those reactions were selected: the strain-promoted azide alkyne cycloaddition (SPAAC) and the IEDDA between *trans*-cyclooctene and dipyridyl-*s*-tetrazine. Herein, model compounds undergoing click cycloadditions SPAAC and IEDDA will be prepared in order to perform the four and five reactions simultaneously and examine if they take place selectively and efficiently (Scheme 2-4).
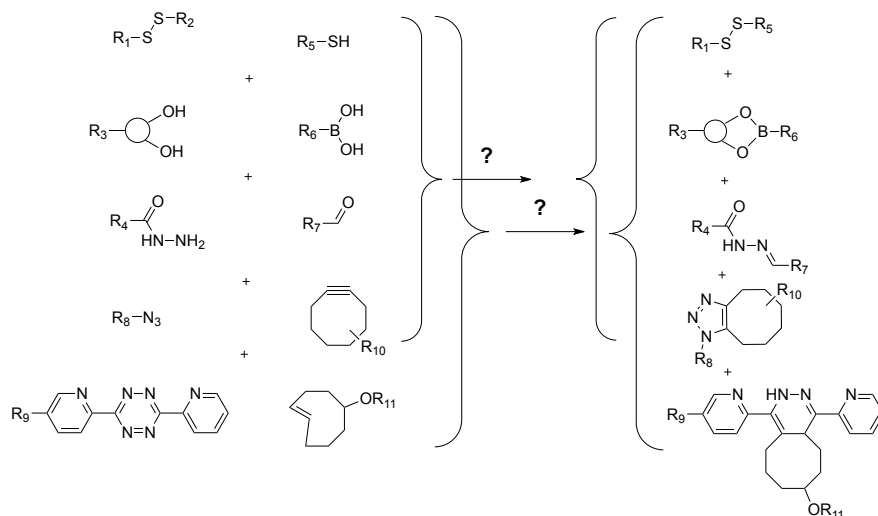
Scheme 2-4 General representation of the tetra- and pentaorthogonal multireaction system selected for this study.

2.2 Results and discussion

2.2.1   Design and Synthesis of the model compounds

2.2.1.1 Disulfide exchange

The first selected reaction was the disulfide exchange, which is a reaction between a thiol (R_1SH) and a disulfide (R_2SSR_3) leading to the formation of a new disulfide (R_1SSR_2) and a thiol derived from the original disulfide (R_3SH) (Equation 1).[30]

$$R_1SH \quad + \quad R_2SSR_3 \quad \rightleftharpoons \quad R_1SSR_2 \quad + \quad R_3SH \qquad (1)$$

This reaction is an S_N2 type reaction, with the thiolate anion (RS^-) acting as the active nucleophile (Equation 2, 3, 4).

$$R_1SH \quad \rightleftharpoons \quad R_1S^- \quad + \quad H^+ \qquad (pk_a\,R_1SH) \quad (2)$$

$$R_1S^- \quad + \quad R_2SSR_3 \quad \rightleftharpoons \quad R_1SSR_2 \quad + \quad R_3S^- \qquad (3)$$

$$H^+ \quad + \quad R_3S^- \quad \rightleftharpoons \quad R_3SH \qquad (pk_a\,R_3SH) \quad (4)$$
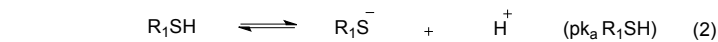
Thiol-disulfide exchange involves multiple equilibria (equation 1, 5, 6 etc.): the reaction products include all possible thiols (R_1SH, R_2SH, R_3H), symmetrical disulfides (R_1SSR_1, R_2SSR_2, R_3SSR_3), and mixed disulfides (R_2SSR_3, R_1SSR_2, R_2SSR_3 etc.)

$$R_1SH \quad + \quad R_2SSR_3 \quad \rightleftharpoons \quad R_1SSR_2 \quad + \quad R_3SH \qquad (1)$$

$$R_1SH \quad + \quad R_1SSR_2 \quad \rightleftharpoons \quad R_1SSR_1 \quad + \quad R_2SH \qquad (5)$$

$$R_2SH \quad + \quad R_2SSR_3 \quad \rightleftharpoons \quad R_2SSR_2 \quad + \quad R_3SH \qquad (6) \quad \text{etc.}$$

Suitable substituents can be designed in order to displace equilibria and favor one of the possible products. Among all the reported disulfides, 2-pyridyl-disulfide is perhaps the most popular functional group used for thiol-disulfide exchange, since it undergoes a single interchange reaction with a free thiol to yield a single mixed disulfide product.[31] This is due to the fact that the pyridyl disulfide contains a leaving group, which is easily transformed into a non-reactive compound, pyridinethione, not capable of participating in further mixed disulfide formation (Scheme 2-5). Therefore, this moiety was selected for our target disulfide.

Pyridine
2-thione
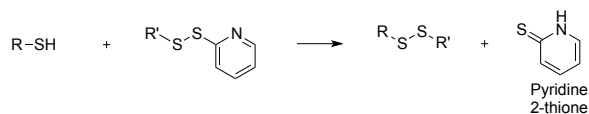
Scheme 2-5 Disulfide exchange between pyridyl disulfide and thiol.

For the design of our model compounds, a triazole moiety will be introduced, since the functionalities used as receptor sites, will be implemented later on the scaffold by Cu-catalyzed cycloaddition (CuAAC).[23] Moreover, due to the tendency of the pyridyl moiety to complex copper, its introduction will be performed at the last step. In this respect, model disulfide **2-6** will be prepared from protected intermediate thiol **2-7,** which can be synthesized from mercaptoethanol **2-8** after introduction of the trityl protecting group, its conversion into azide, and CuAAC (Scheme 2-6).
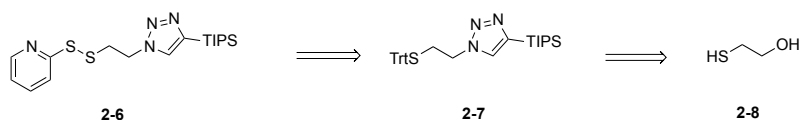
Scheme 2-6 Retrosynthetic pathway for the desired disulfide **2-6**.

The synthesis, described in Scheme 2-7, commenced with the protection of commercially available mercaptoethanol **2-8** into trityl thiol **2-9** with trityl chloride. Mesylation of this alcohol in the presence of mesyl chloride was directly followed by the substitution of the mesylate group into azide affording compound **2-11** in 85% yield over two steps. Then, the CuAAC was performed with TIPS acetylene in the presence of $CuSO_4.5H_2O$ and sodium ascorbate to give triazole **2-7** in 90% yield. Finally, trityl protecting group was removed using trifluoroacetic acid and triisopropylsilane as a scavenger and without isolate the intermediate thiol, the pyridine-disulfide moiety was introduced by disulfide exchange with 2,2'-dipyridyl disulfide to afford **2-6** in 75% yield.
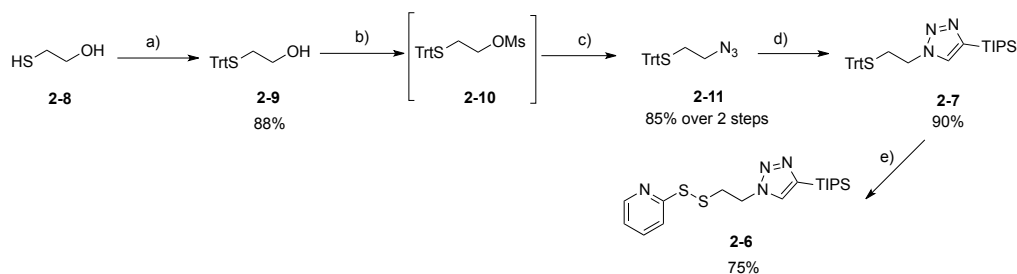
Scheme 2-7 Synthesis of pyridine disulfide **2-6**; a) TrtCl, THF, 50 °C, 4 h; b) MsCl, Et₃N, CH₂Cl₂, 0 °C to rt, 2 h; c) NaN₃, DMF, 70 °C, 3 h; d) TIPS acetylene, CuSO₄·5H₂O, Na ascorbate, DMF/H₂O (4:1), rt, 16 h; e) *i)* TFA, TIS, CH₂Cl₂, rt, 1 h, *ii)* 2,2'-dipyridyl disulfide, DIEA, CH₂Cl₂, rt, 1 h.

2.2.1.2 Boronic ester formation

The second DCC reaction selected was the boronic ester formation. Indeed, boronic acids are known to bind with compounds containing diol moieties with high affinity through reversible ester formation (Scheme 2-8).[32]

Scheme 2-8 General scheme of boronic ester formation.

However, the equilibrium can be displaced depending on the structure of the diol. For our purpose, a diol reacting fast with boronic acid and forming stable boronic ester was required. In the literature, *Roy et al.* studied boronic ester transesterification to understand their relative stability.[33] Some of their results are summarized in Table 2-2. It was found that the introduction of methyl substituents on ethyleneglycol increases the thermodynamic stability of the boronic

ester. Nevertheless, the introduction of very bulky groups on the diol, such as in pinacol **2-13(II)** or cyclic diol **2-13 (VIII)**, formed very stable boronic ester but considerably slowed down the transesterification. The introduction of electron-withdrawing group substituents such as in diol **2-13(III)** decreases the thermodynamic stability of the boronic ester. Moreover, the investigation of cyclic 1,2-diols showed that the *cis*-stereochemistry of diols **2-13(V)**, **(VII)**, **(VIII)** favors the displacement of the equilibrium while *trans*-1,2-cyclopentanediol **2-13(VI)** was found to be inert.

Table 2-2 Transesterification of 2-(phenyl)-1,2,3-dioxoborolane with various diols.[33]

Diol **2-13**	Time (h)	Transesterification (%)
1,2-Propanediol **I**	0.1	68.6
Pinacol **II**	94	87.8
(+)-Diisopropyl Tartrate **III**	0.1	4.5
Catechol **IV**	5	28
Cis-1,2-cyclopentanediol **V**	0.1	99
Trans-1,2-cyclopentanediol **VI**	47	0
Exo,exo-2,3-Norbornanediol **VII**	0.1	99.5
Cis-1,2-dimethyl-1,2-cylopentanediol **VIII**	258	99

Finally, increasing the ring strain of the cycle by adding a bicycle appears to favor the formation of stable boronic ester and accelerate the reaction rate. Indeed*,* the transesterification of 2-(phenyl)-1,2,3-dioxaborolane boronate ester **2-12** with exo,exo-2-norbornanediol **2-13(VII)** into corresponding boronate **2-14(VII)** has been described at room temperature in CDCl₃ in only 0.1 h in 99.5% yield. Taking this into consideration, this compound appears to be a suitable candidate for our targeted diol. Its functionalization can be performed on the bridged carbon; and can be easily achieved by replacing the carbon atom by nitrogen.

For this reason, model diol **2-16** has been designed. The compound can be synthesized following the retrosynthetic pathway described in Scheme 2-9. The triazole moiety can be introduced by CuAAC from the corresponding azide at the last step, while the *cis*-diol can be obtained from azabicycloalkene **2-17**. The functionalization of the bridged nitrogen will be achieved by amide formation from azabicycloalkene **2-18** after Boc removal. Compound **2-18** can be obtained *via* Diels-Alder cycloaddition from Boc-pyrrole **2-19** following the literature.[34] It is noteworthy to indicate that the phenyl ring has been introduced on the bicyclic diol for the Diels-Alder reaction to occur, the dienophile requiring an electron-withdrawing substituent.
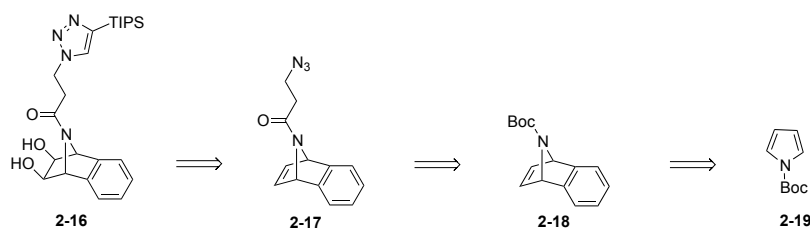
Scheme 2-9 Retrosynthetic pathway for desired diol **2-16**.

The synthesis of **2-16** started with the *N*-Boc protection of pyrrole **2-23**. Then, 7-Azabicloalkene **2-18** was synthesized following the literature procedure *via* Diels-Alder cycloaddition between *N*-Boc pyrrole **2-19** and benzyne generated in situ from anthranilic acid and isoamyl nitrite in 50% yield.[34] 7-Azabicloalkene **2-18** was then deprotected with HCl formed *in situ* by the addition of acetyl chloride in methanol to give unstable compound **2-24**. This last compound was directly acylated with 3-azido propanoic acyl chloride **2-22** (prepared over two steps from commercially available **2-20**) to give unstable azide **2-17**. The *cis*-dihydroxylation of olefins, which is one of the most widely used reactions for the synthesis of vicinal diol,[35] was performed in the presence of OsO$_4$ and NMO as co-oxidant, to obtain the azido-diol derivative **2-25** in 36% yield over three steps. Finally, the CuAAC between **2-25** and TIPS acetylene afforded **2-16** in 70% yield (Scheme 2-10). All intermediates and target diol **2-16** were fully characterized by melting points, infrared, ^{1}H and ^{13}C NMR spectroscopy, high-resolution mass spectrometry and the data are reported in *Chapter 6*. Moreover, crystals of **2-25,** suitable for single-crystal X-ray analysis, were grown by slow evaporation from THF solution. The crystal structure, reported in Figure 2-5, will be discussed in *Chapter 4*.
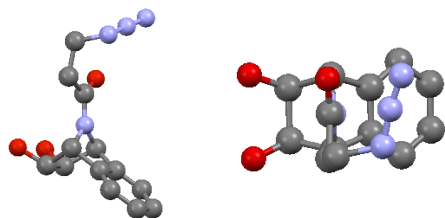
Figure 2-5 Side-view and top-view of the crystal structure of **2-25**. Solvent for crystallization: THF (space group: P21/c, hydrogen atoms hidden). Color code: grey: C, red: O and blue: N.
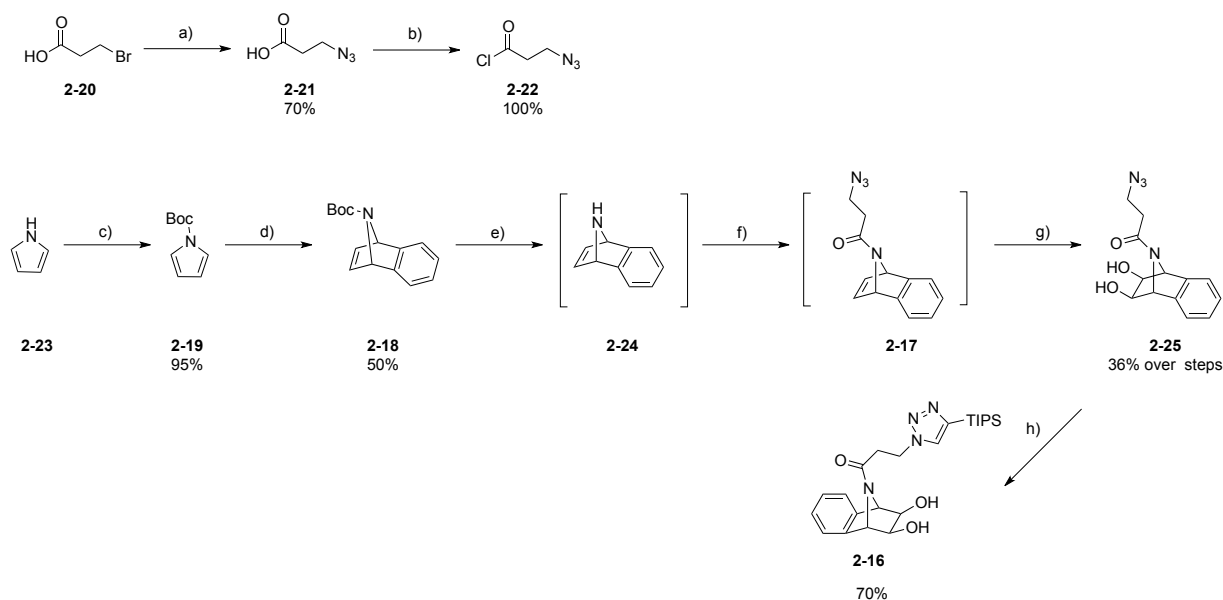
Scheme 2-10 Synthesis of target diol **2-16**; a) NaN$_3$, CH$_3$CN, 85 $^{\circ}$C, 4 h; b) (COCl)$_2$, DMF (cat), CH$_2$Cl$_2$, 0 $^{\circ}$C to rt, 20 h; c) Boc$_2$O, DMAP, CH$_3$CN, rt, 4 h; d) anthranilic acid, isoamyl nitrite, DME, 50 $^{\circ}$C, 30 min; e) AcCl, MeOH, 0 $^{\circ}$C to rt, 2 h; f) **2-22**, Et$_3$N, CH$_2$Cl$_2$, rt, 2 h; g) OsO$_4$ (4 mol%), NMO, acetone/H$_2$O 9:1, rt 16 h; h) TIPS acetylene, CuSO$_4$·5H$_2$O, Na ascorbate, DMF/H$_2$O (4:1), rt, 16 h.

2.2.1.3 Acyl hydrazone formation

The third reaction of DCC selected for our system was the acyl hydrazone bond formation between hydrazide and aldehyde (Scheme 2-11).

Scheme 2-11 General scheme of acyl hydrazone formation.

This reaction has been found to be very useful in bioconjugation due to its high stability compared to imine or hydrazone bond formation.[52] Indeed, hydrazones and acyl hydrazones possess better stability than imines due to the presence of the resonance forms **II** and **IV** respectively, as shown in Scheme 2-12, which increase the negative-charge on C1. This results in the reduction of its electrophilicity and hence the resistance of hydrazone derivatives toward hydrolysis.[53]
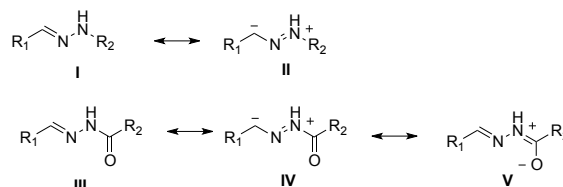
Scheme 2-12 Mesomeric form of hydrazone and acyl hydrazone.

Moreover, acyl hydrazones are known to be more stable compared to the hydrazones due to their resistance to protonation. In both cases, during the hydrolysis reaction the rate determining step is the protonation of the N1 atom. This results in the enhancement of the electrophilicity of the C1

atom and hence the attack of the water on it. However, in the case of acyl hydrazone, the protonation is discouraged by the mesomeric form **V**, which can occur due to the presence of the additional carbonyl group (Scheme 2-13). [53]

Scheme 2-13 Putative mechanism for the hydrolysis of acyl hydrazone.

If the good stability of the acyl hydrazone is well appreciated, its impact has been tempered by the slow equilibration kinetics of the reaction. Moreover, in our case, the use of acid, known to catalyze the reaction, was ruled out, being incompatible with the other reactions. Thus, with the aim to accelerate the reaction, various reaction conditions have been screened with simple analogues. The most relevant results are reported in Table 2-3. The presence of electron withdrawing substituents in ortho positions of benzaldehyde **2-26**, in particular fluorine atoms, increases the rate of the reaction. In the case of the reaction between 2,6-difluorobenzaldehyde **2-26d** and benzyl hydrazine **2-27** in the presence of a catalytic amount of *m*-phenylenediamine (*m*-PDA), being reported as an efficient nucleophilic catalyst for hydrazone and oxime reactions,[36] the acyl hydrazone has been obtained quantitatively in 1 h (Entry 6, Table 2-3). Hence, these optimized reaction conditions have been selected for our system.

Table 2-3 Reaction conditions for the optimization of the kinetic rate of acyl hydrazone formation.

Entry	Aldehydes	R	Conditions	Yield
1	**2-26a**	-	CHCl₃, rt, 24 h	90%
2	**2-26b**	2-nitro	CHCl₃, rt, 20 h	Quant.
3	**2-26b**	2-nitro	THF, rt, 2 h	22%
4	**2-26c**	2-fluoro	THF, rt, 2 h	53%
5	**2-26d**	2,6-difluoro	THF, rt, 2 h	90%
6	**2-26d**	2,6-difluoro	*m*-phenylene diamine, THF, rt, 1 h	Quant.

Model hydrazide **2-29** was designed accordingly and can be easily obtained from the commercially available 4-(bromomethyl)benzoic acid **2-31**. The retrosynthetic approach adopted for the preparation of **2-29** is described in Scheme 2-14. The triazole moiety can be introduced by CuAAC from azide **2-30** which can be obtained from bromo derivative **2-31** after substitution into azide and hydrazide formation.
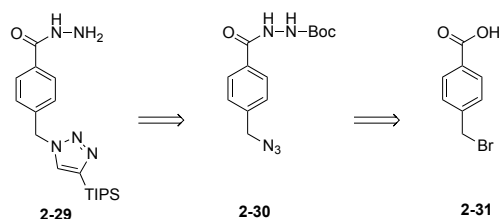
Scheme 2-14 Retrosynthetic pathway for the desired hydrazide.

The synthesis of compound **2-29** commenced with the substitution of bromo derivative **2-31** into azide **2-32** with sodium azide. This was followed by the introduction of the Boc-hydrazine moiety in the presence of *tert*-butyl carbazate and EDC.HCl as coupling agent. Then, the CuAAC was performed with TIPS acetylene affording triazole **2-33** in 86% yield. The Boc protecting group was finally removed to give third model compound **2-29** using trifluoroacetic acid (Scheme 2-15).
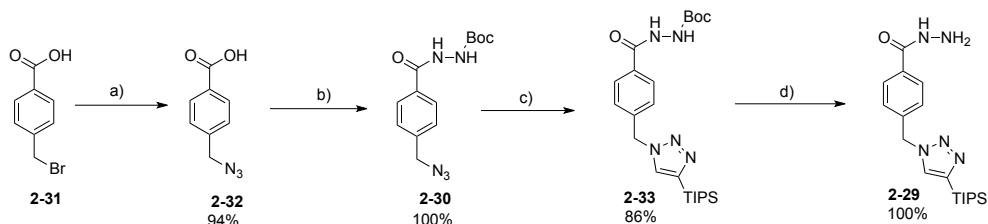
Scheme 2-15 Synthesis of hydrazide **2-29**; a) NaN$_3$, DMF, 50 °C, 15 h; b) *tert*-butyl carbazate, EDC.HCl, CH$_2$Cl$_2$, rt, 16 h; c) TIPS acetylene, CuSO$_4$·5H$_2$O, Na ascorbate, DMF/H$_2$O 4:1, rt, 16 h; d) TFA/CH$_2$Cl$_2$ (1:4), rt, 1 h.

2.2.1.4 Strain Promoted Azide-Alkyne Cycloaddition (SPAAC)

As a fourth reaction, the cycloaddition between cyclooctyne and azide, well known to react without a catalyst under ambient conditions, was selected (Scheme 2-16).[37]
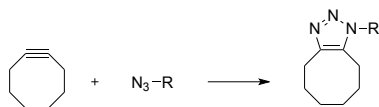
Scheme 2-16 General scheme of strain-promoted azide-alkyne cycloaddition (SPAAC).

The major limitation of the reaction is the relatively low rate. In this respect, the choice of the cyclooctyne reagent is extremely important and has been widely investigated.[25, 38] Some of the reactive cyclooctyne derivatives known in the literature are reported in Table 2-4 with their overall yield highlighting their synthetic accessibility and their rate constant for the cycloaddition with

benzyl azide. The first generation of cyclooctyne (Entry 1) promotes SPAAC with a low rate comparable to the Staudinger ligation discussed in *Section 2.1.2*.[25] To improve the kinetic of the process, fluorine atoms were introduced at the propargylic position enhancing the rate particularly for the difluorinated cyclooctyne (Entry 2 and 3).[38a, 38b] Another interesting strategy to improve the kinetic of the reaction is the introduction of two fused phenyl rings increasing the ring strain and the conjugation of the cyclooctyne system (Entry 4).[38c] The substitution of one of the saturated carbon on the cyclooctyne ring into a nitrogen atom improves its reactivity and moreover, aza-dibenzocyclooctyne (ADIBO) appears to be synthetically more accessible (Entry 5).[38d] So, following the literature, ADIBO derivative was prepared and used in this study.[39] The synthetic pathway adopted for the preparation of ADIBO **2-40** is reported in Scheme 2-17.

Table 2-4 Functionalizable cyclooctynes used for SPAAC; overall yield for their preparation; rate constant of SPAAC with benzyl azide in mentioned solvent.

Entry	Cyclooctyne	Overall yield / %	k / × 10^{-3} M^{-1} s^{-1}	Solvent	Ref.
1		52	2.4	CD_3CN	[25]
2		15	4.3	CD_3CN	[38a]
3		27	42	CD_3CN	[38b]
4		10	57	CH_3OH	[38c]
5		41	310	CD_3CN	[38d]
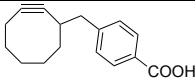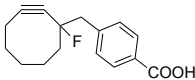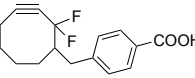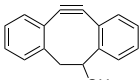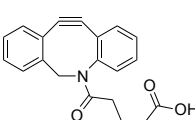
Commercially available dibenzosuberone **2-34** reacted with hydroxylamine to give dibensuberone oxime **2-35** followed by the polyphosphoric acid-catalyzed Beckman rearrangement to afford lactam **2-36**. Subsequently, lactam was reduced with lithium aluminium hydride to give **2-37**. The secondary amine was converted into amide **2-38** by addition of acyl chloride in the presence of pyridine. The olefin was converted into acetylene moiety *via* a bromination-dehydrobromination procedure to give **2-40** in 76% yield over the two steps. All the intermediates and the final product were characterized in agreement with the data reported in the literature.
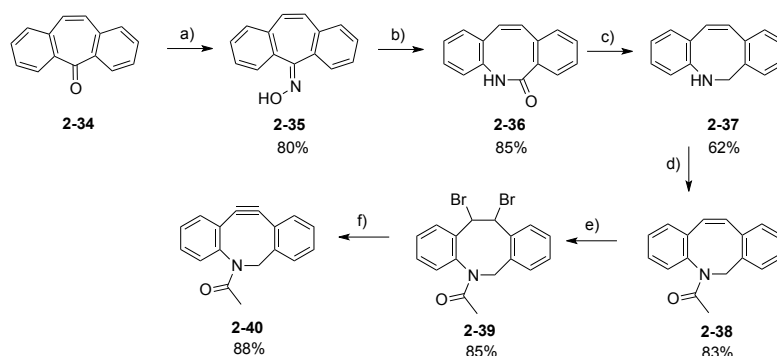
Scheme 2-17 Synthesis of ADIBO **2-40**; a) hydroxylamine.HCl, pyridine, 120 °C, 20 h; b) polyphosphoric acid, 125 °C, 1 h; c) LiAlH$_4$, Et$_2$O, 40 °C, 18 h; d) AcCl, pyridine, CH$_2$Cl$_2$, rt, 1 h; e) pyridinium tribromide, CH$_2$Cl$_2$, rt, 18 h; f) *t*BuOK, THF, rt, 1 h.[39]

2.2.1.5 Inverse electron demand Diels-Alder (IEDDA) between *trans*-cyclooctene and *s*-tetrazine

The fifth reaction selected is the extremely fast reaction between *s*-tetrazines (1,2,4,5-tetrazines or *sym*-tetrazines) and strained alkenes reported by *Fox* and co-workers. The authors described the IEDDA between *trans*-cyclooctene derivatives (TCO) and dipyridyl-*s*-tetrazines (k = 400 M^{-1} s^{-1} in THF).[29a] In contrast to a normal Diels Alder, the electron rich dienophile (TCO) reacts with electron poor diene (tetrazine) forming a six membered ring in a [4+2] fashion.[40] The reaction proceeds *via* intermediate **I**, which rapidly loses N$_2$ and undergoes a retro-Diels-Alder to yield intermediate **II**, which isomerizes to the corresponding 1,4-dihydropyridazine product as reported in Scheme 2-18.
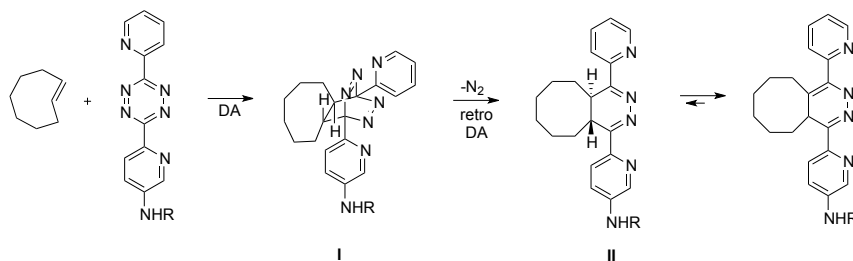
Scheme 2-18 General representation of IEDDA reaction of *trans*-cyclooctene with dipyridyl-s-tetrazine.[29a]

According to this work, it has been decided to perform the reaction between TCO **2-43** and dipyridyl-*s*-tetrazine **2-45** (whose syntheses were already reported in the literature) and to investigate its orthogonality with the SPAAC. Nevertheless, for studying the penta-reaction system with the dynamic covalent reactions, the preparation of acetyl-protected TCO **2-44** was targeted in order to prevent possible cross-reactions with the free alcohol of **2-43** (Scheme 2-19).
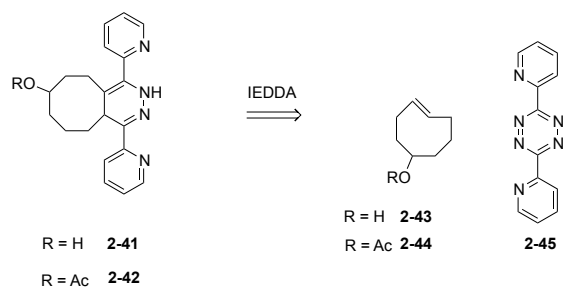
Scheme 2-19 Target TCO **2-43, 2-44** and tetrazine **2-45** for IEDDA.

The synthetic pathway of *trans*-cyclooctene **2-43** and **2-44**, described in Scheme 2-20, commenced by the synthesis of *cis*-cyclooctenol **2-48**, according to the literature.[41] Cyclooctadiene **2-46** was first oxidized into epoxide **2-47** with *m*-CPBA and subsequently reduced in the presence of LiAlH$_4$ into cyclooctenol **2-48**. Then, *trans*-cyclooctenol **2-43** was obtained from *cis*-cyclooctene **2-48** by a photochemical protocol described in the literature.[42] The compound was irradiated at 254 nm with an equimolar amount of methyl benzoate as photosensitizer and *trans*-isomer was produced. After the photoirradiation, the reaction mixture was passed through AgNO$_3$ impregnated silica. The *trans*-cyclooctene was selectively retained by the AgNO$_3$ impregnated silica, while the *cis*-isomer eluted back to the reaction flask, where it was re-photoisomerized. After 10 cycles of 30 min, the desorption of the AgNO$_3$ impregnated silica afforded *trans*-cyclooctenol **2-43** in 50% yield as a mixture of two diastereoisomers (**2-43a/2-43b** dr: 1:3) easily separable by silica gel column chromatography. On the other hand, to prepare TCO **2-44**, *cis*-cyclooctenol **2-48** was acetylated in the presence of acetic anhydride. It is noteworthy to mention that the protection step was not performed directly with TCO **2-43** due to the low stability of the *trans*-alkene, which tends to re-isomerize in *cis*-alkene even at rt. The *cis-trans* isomerization was performed as previously by irradiating **2-49** with methyl benzoate at 254 nm. The *trans*-isomer **2-44** was selectively retained by the AgNO$_3$ impregnated silica and isolated after desorption of the silica in 53% yield as a mixture of two diastereoisomers (dr: 1.6:1; ratio determined from the ^{1}H NMR spectrum), which was not separable by normal silica gel column chromatography.

In parallel, *s*-tetrazine derivative **2-45** was synthesized following the well-established method consisting in condensation reactions between hydrazine and aryl nitriles.[43] **2-50** was treated with hydrazine hydrate at 90 °C for 12 h to afford dihydro-*s*-tetrazine **2-51** in 60% yield. The latter was subsequently oxidized in the presence of DDQ into *s*-tetrazine **2-45** (Scheme 2-21). The target compounds and their intermediates were characterized in accordance with the data reported in the literature.
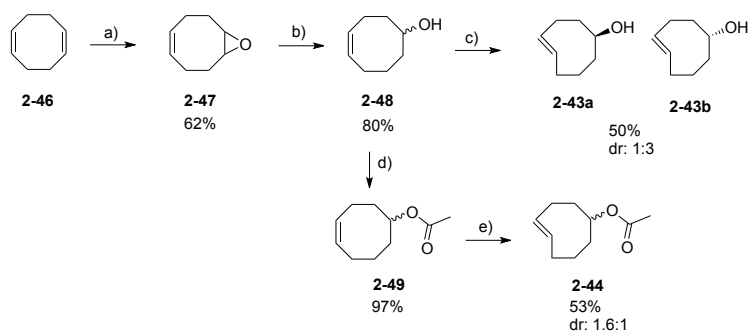
Scheme 2-20 Synthesis of *trans*-cyclooctene **2-43** and **2-44**; a) *m*-CPBA, CHCl$_3$, 0 °C to rt, 12 h; b) LiAlH$_4$, THF, 0 °C to 70 °C, 4 h; c) methyl benzoate, *hv* 254 nm, Et$_2$O/hexane (9:1), AgNO$_3$/SiO$_2$, 10 × 30 min; d) acetic anhydride, pyridine, CH$_2$Cl$_2$, 20 h, 40 °C, e) methyl benzoate, *hv* 254 nm, Et$_2$O/hexane (1:9), AgNO$_3$/SiO$_2$, 10 × 30 min.
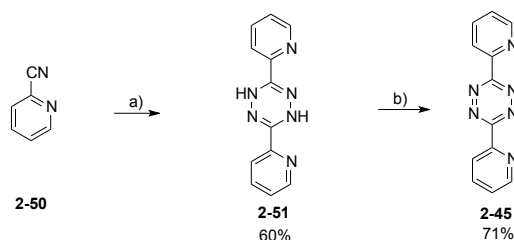
Scheme 2-21 Synthesis of dipyridyl-*s*-tetrazine **2-45**; a) hydrazine hydrate, 90 °C, 12 h; b) DDQ, toluene, 110 °C, 12 h.

2.2.2 Simultaneous multireaction systems

Having the model compounds in hands, each anchoring reaction was optimized under the same conditions and their mutual orthogonality investigated to sequentially develop a tri-, tetra- and pentaorthogonal multireaction systems.

2.2.2.1 Triorthogonal Multireaction System involving Dynamic Covalent Reactions

For the triorthogonal multireaction system, model compounds disulfide **2-6**, diol **2-16** and hydrazide **2-29** were used first to independently performed the three dynamic covalent reactions with commercially available partners under similar conditions, typically in THF at rt for 1 h. Disulfide-pyridine **2-6** undergoes the disulfide exchange reaction with 2-naphtalene thiol **2-52** to yield only mixed disulfide **2-54**. It is worth noting that, under those neutral conditions, only aryl thiol, having a lower pka than alkyl thiol, can afford quantitatively the product. Besides, 1,2-cis bicyclodiol **2-16** gave the corresponding boronate **2-56** quantitatively with 4-tert butyl phenyl boronic acid **2-53**. Finally, hydrazide **2-29** was converted into acyl hydrazone **2-57** with electron-poor 2,6-difluorobenzaldehyde **2-26d**, in the presence of a catalytic amount of *m*-phenylenediamine (*m*-PDA) increasing the rate of the reaction (Scheme 2-22). The products were fully characterized by melting points, infrared, ^{1}H and ^{13}C NMR spectroscopy, high-resolution mass spectrometry and the data are reported in *Chapter 6*.
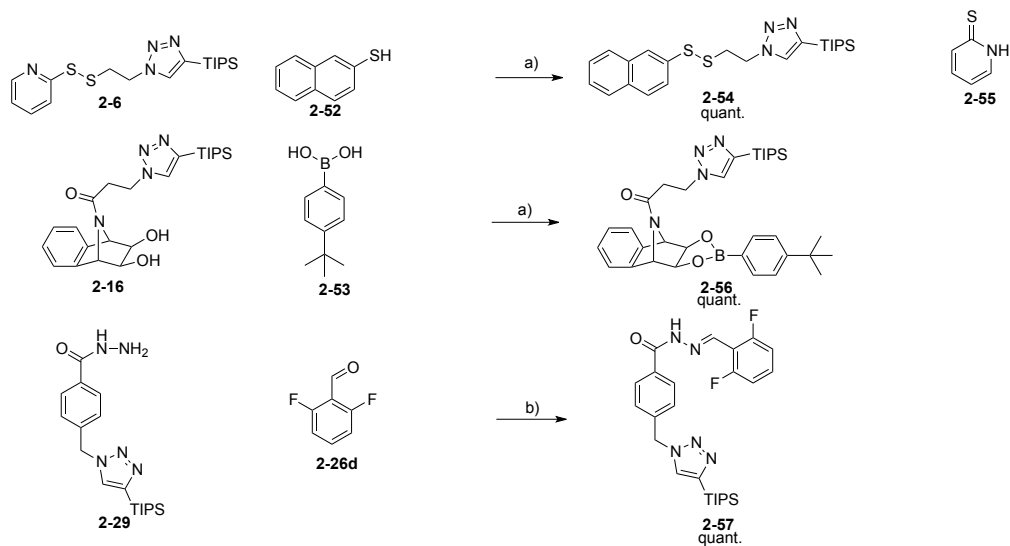
Scheme 2-22 Disulfide interchange, boronate and acyl hydrazone formation; a) THF, rt, 1 h; b) *m*-phenylene diamine, THF, rt, 1 h.

Operating the three reactions simultaneously, as shown in Scheme 2-23, full conversion of 1,2-*cis* bicyclodiol **2-16** into *^t*butyl-phenyl boronate **2-56**, disulfide pyridine **2-6** into disulfide naphthalene **2-54** and hydrazide **2-29** into acyl hydrazone **2-57** was achieved in the presence of a catalytic amount of *m*-PDA.
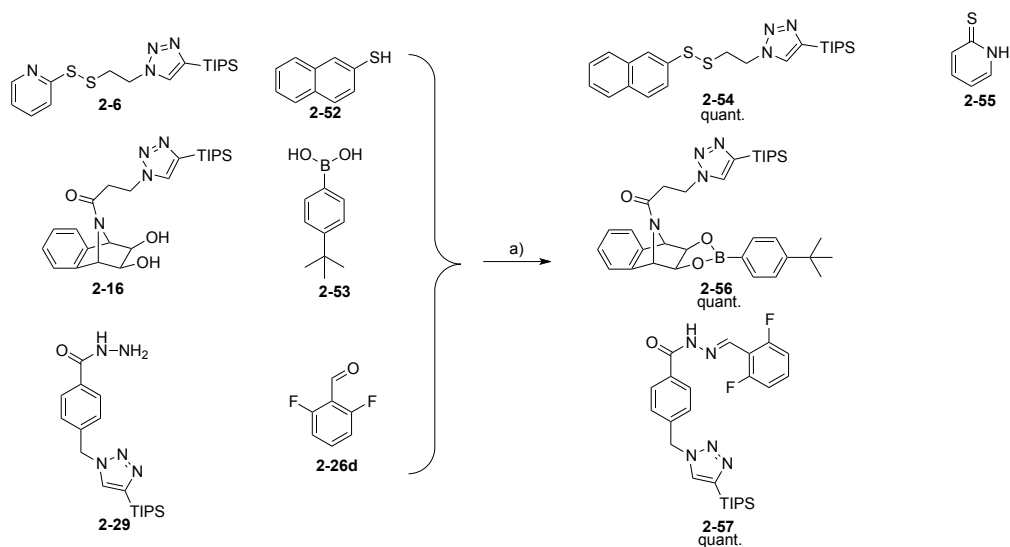
Scheme 2-23 Simultaneous disulfide interchange, boronate and acyl hydrazone formation; a) *m*-PDA, THF, rt, 1 h.

To prove the quantitative formation of the three expected products, the physical mixture of the three starting materials and the crude material after the reaction were analyzed by ¹H NMR and compared. Figure 2-6 shows 100% conversion of diol **2-16** (light green) into boronate **2-56** (dark green), as it can be seen by the change of chemical shift of the signals corresponding to the

bridged protons (from 5.05 and 5.45 to 5.15 and 5.7 ppm) or the protons on the carbons bearing the hydroxyl groups (from 3.9 to 4.6 ppm). It shows as well 100% conversion of disulfide pyridine **2-6** (light blue) into disulfide naphthalene **2-54** (dark blue) by the shift of the signals of protons in α-position of the disulfide (from 3.3 to 3.25 ppm) and the one in α-position of the triazole (from 4.75 to 4.7 ppm). However, it is difficult to see the conversion of hydrazide **2-29** (beige) into hydrazone **2-57** (red), due to the small shift of the signal of the protons in α-position of the triazole (around 5.6 ppm). Besides, the crude material has been also analyzed by MS(ES+)-TOF showing the presence of the monocharged ion peaks of the three expected products **2-54** (proton adduct at m/z = 444.2 and sodium adduct at m/z = 466.2), **2-56** (proton adduct at m/z = 599.4 and sodium adduct at m/z = 621.4), **2-57** (proton adduct at m/z = 498.3 and sodium adduct at m/z = 520.3) but also of disulfide **2-6** (proton adduct at m/z = 394.2) and diol **2-16** (sodium adduct at m/z = 479.3) being re-formed during the ionization process. Purification of the crude material by silica gel column chromatography allowed the isolation of the expected products, ultimately confirming their quantitative conversion.

Figure 2-6 Top) Zoom of ^{1}H NMR between 2.5 and 6.5 ppm in CDCl$_3$ at 25 °C of 1) physical mixture of disulfide-pyridine **2-6** (light blue), diol **2-16** (light green) and hydrazide **2-29** (beige), 2) one-pot reaction, 3) disulfide naphtalene **2-54** (dark blue), 4) boronate **2-56** (dark green), 5) acyl hydrazone **2-57** (red); bottom) Mass Analysis ESI-MS (Q-Tof) of one-pot reaction.

2.2.2.2 Tetraorthogonal multireaction system involving SPAAC

The SPAAC was performed under the conditions of the triorthogonal multireaction system, *ie* stirring in THF for 1 h at rt. The reaction was carried out with azide **2-48**, which was synthesized by substitution of bromo derivative **2-58** with sodium azide in quantitative yield. The cycloaddition reaction between cyclooctyne **2-40** and **2-48** in THF at rt for 1 h afforded two different regioisomers **2-60a** and **b** separable by silica gel column chromatography (Scheme 2-24). The two triazoles were fully characterized by infrared, ^{1}H, ^{13}C NMR spectroscopy and high-resolution mass spectrometry. It is noteworthy to mention that the ^{1}H and ^{13}C NMR spectra of **2-60a** revealed the presence of more than the expected number of signals (See Chapter 6 and Appendix) due to the presence of two conformers for this regioisomer. Indeed, for similar triazoles, it has been reported that conformational isomery can be observed by NMR spectroscopy, particularly for **a**-type regioisomer, caused by the rotation of the aliphatic part of the triazole substituent.[44] Crystals of **2-60a** suitable for single-crystal X-ray analysis were grown by slow evaporation from EtOAc, and the crystal structure shows one of the conformer and allows assigning the yield of the two different regioisomers difficult to differentiate by ^{1}H NMR and (Figure 2-7).
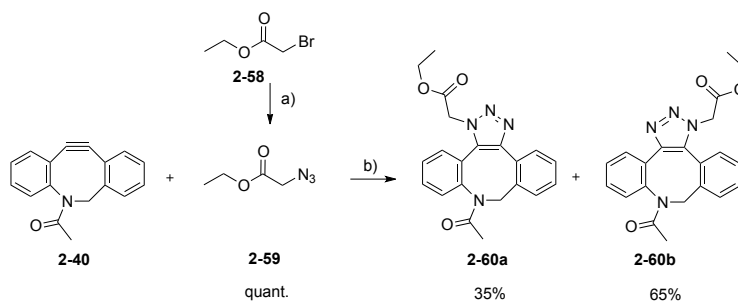
Scheme 2-24 Strain promoted azide-alkyne cycloaddition; a) NaN$_3$, H$_2$O/acetone (1:3), 60 °C, 4 h; b) THF, rt, 1 h.
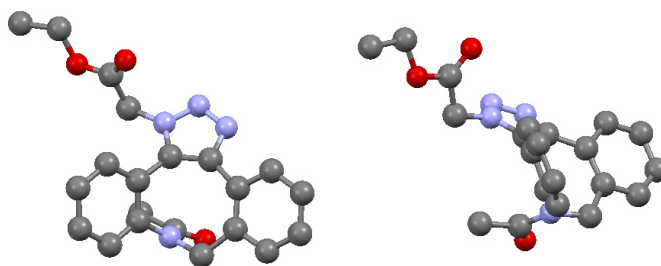
Figure 2-7 Front-view and side-view of crystal structure of **2-60a**; solvent for crystallization: EtOAc. (Space group: P2$_1$/n, hydrogen atoms hidden) Color code: grey: C, red: O, blue: N.

Having successfully performed the cycloaddition reaction independently under the conditions of the multireaction system, the reaction was simultaneously carried out with the dynamic covalent reactions as shown in Scheme 2-25. Disulfide-pyridine **2-6**, diol **2-16**, hydrazide **2-29** and

cyclooctyne **2-40** were mixed together and model partners, naphthalene-thiol **2-52**, tBu-phenyl boronic acid **2-53**, 2,6-difluorobenzaldehyde **2-26d** and azide **2-59**, were added. The reaction was stirred in the presence of *m*-PDA as catalyst in THF at rt for 1 h.
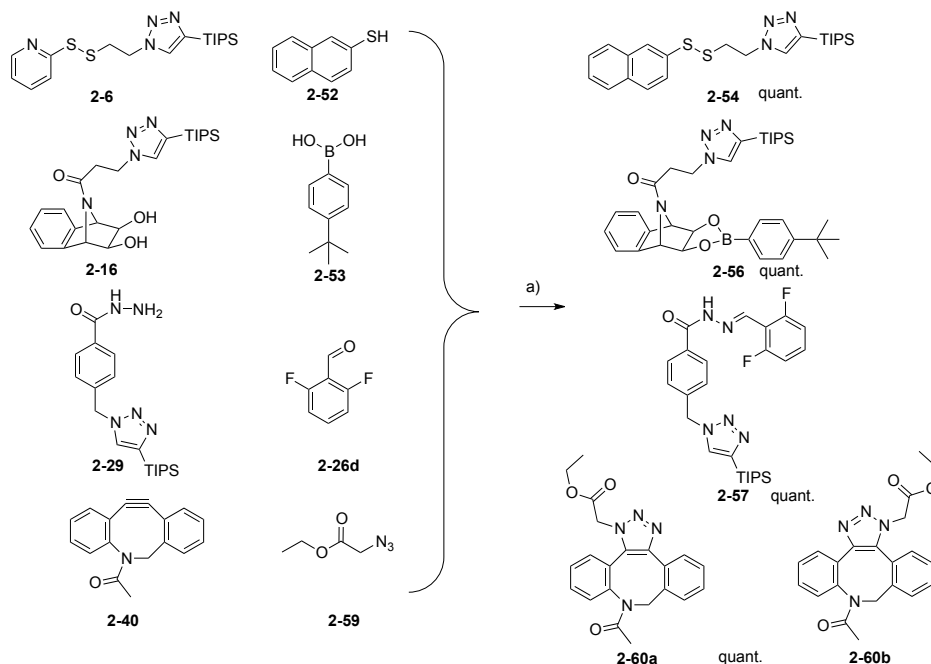
Scheme 2-25 Simultaneous disulfide interchange, boronate, acyl hydrazone formation and SPAAC; a) *m*-PDA, THF, rt, 1 h.

The crude material was analyzed by ^{1}H NMR and ESI-TOF mass spectrometry. The data reported in Figure 2-8, highlight full conversions of disulfide-pyridine **2-6** into naphthalene disulfide **2-54**, of diol **2-16** into boronate **2-56**, of hydrazide **2-29** into acyl hydrazone **2-57**, of cyclooctyne **2-40** into triazoles **2-60**. As in the previous section, the full conversion of the disulfide exchange was observed by the change of chemical shift of the two triplets (in blue) while the quantitative boronate formation was confirmed by the shift of the signal corresponding to the bridged protons and the protons in α-position of oxygen atoms (in green). Here again, the full conversion of hydrazide **2-29** into acyl hydrazone **2-57** was difficult to distinguish by ^{1}H NMR but confirmed by mass spectrometry. For the SPAAC, the characteristic signal of **2-40** (two doublets at 5.15 and 3.65 ppm, in light purple) corresponding to the protons in α-position of the nitrogen atom split and shifted at 6.15 and 4.4 ppm for **2-60b** and 5.95, 5.3, 4.85 and 4.45 ppm for **2-60a** due to the presence of the two different conformers. The MS spectrum shows the peaks of all the expected products: **2-60** (m/z: 377.16), **2-54** (m/z: 444.20), **2-57** (m/z: 498.26), **2-56** (m/z: 598.38) (Figure 2-8). Purification of the crude by silica gel column chromatography allows the isolation of the expected products, confirming their quantitative conversion.
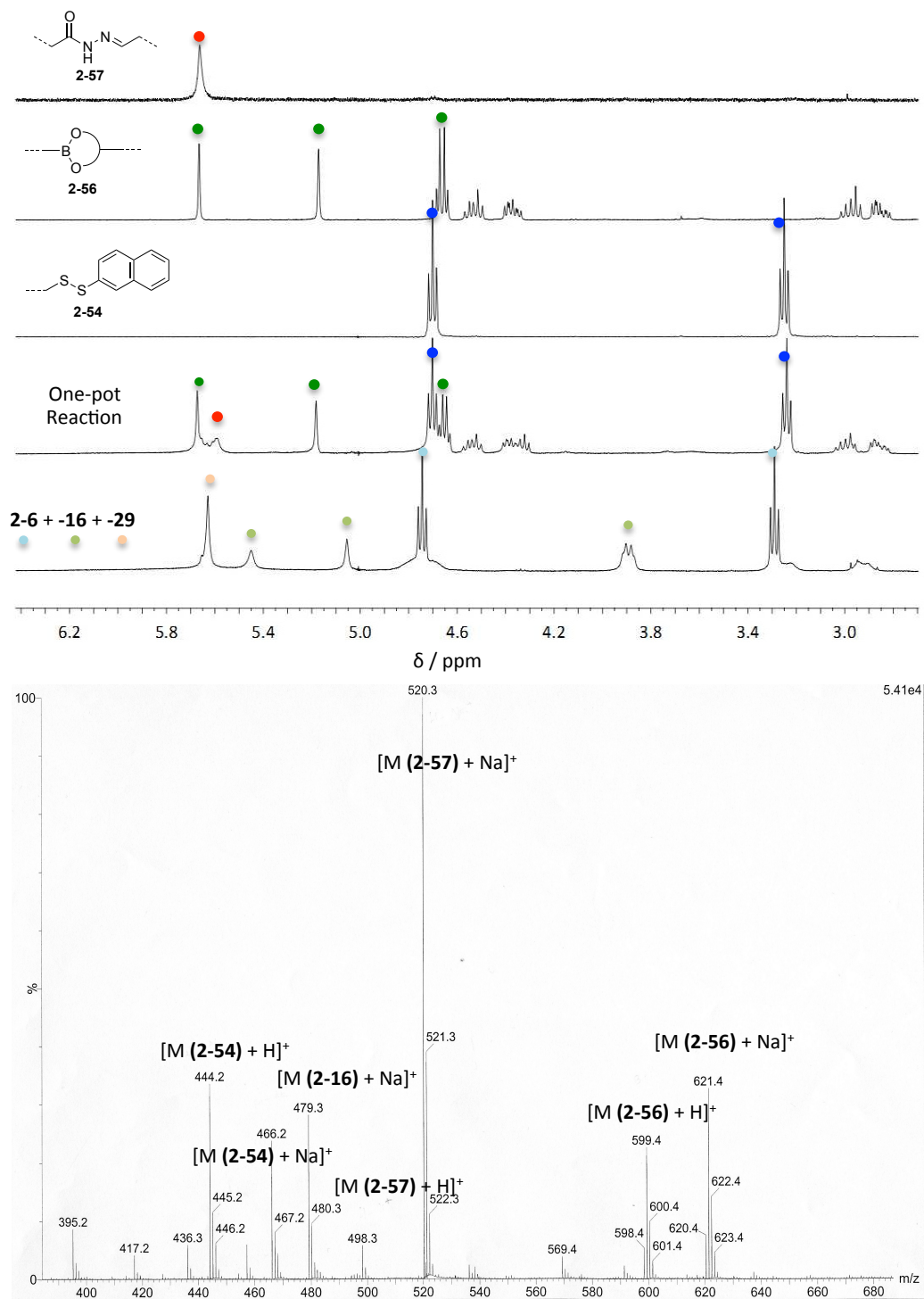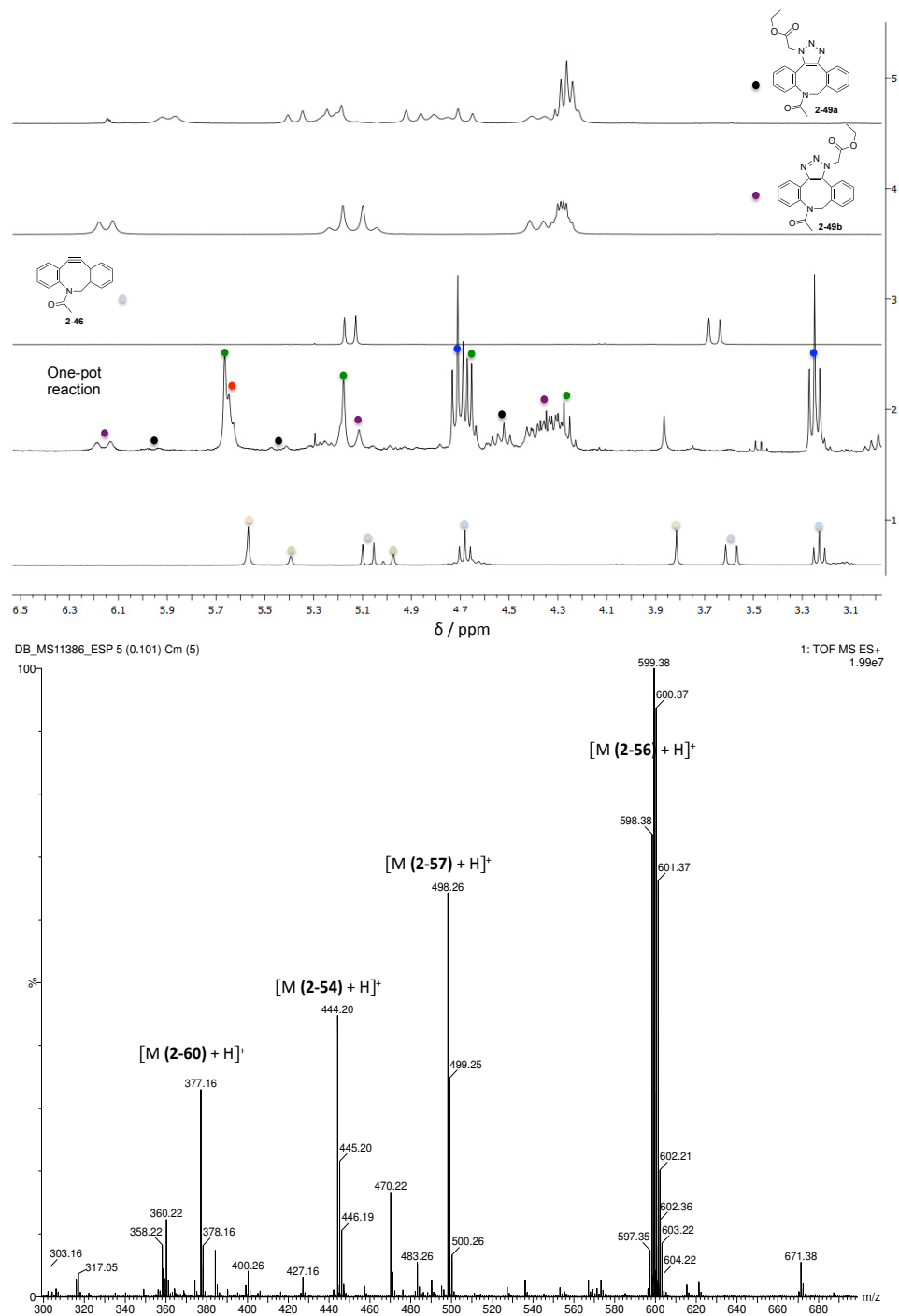
Figure 2-8 Top) Zoom of ^{1}H NMR between 3.1 and 6.3 ppm in CDCl$_3$ at 25 °C of 1) physical mixture of disulfide-pyridine **2-6**, diol **2-16**, hydrazide **2-29** and cyclooctyne **2-40**; 2) one-pot reaction, 3) cyclooctyne **2-40**, 4) triazole **2-60b**, 5) triazole **2-60a**; bottom) Mass Analysis ESI-MS (Q-Tof) of one-pot reaction.

2.2.2.3 Pentaorthogonal multireaction system involving IEDDA

The IEDDA cycloadditions between TCO **2-43a** as a single diastereoisomer or **2-44** as mixture of diastereoisomers with dipyridyl-*s*-tetrazine **2-45** were carried out in THF for 1 h. Upon addition of the *trans*-cyclooctene derivative, the pink solution of tetrazine **2-45** turned immediately yellow indicating that the reaction had gone to completion. As reported in the literature, when the cycloaddition was performed with **2-43a** (with the hydroxyl in axial position), ligation product **2-41** was obtained as a single diastereoisomer of 1,4-dihydropyridazine.[45] However, the product was not isolated due to its tendency to be oxidized into pyridazine. The IEDDA with **2-44** afforded **2-42** as a mixture of isomers, which were not separated (Scheme 2-26). Indeed, the equatorially functionalized diastereoisomer of **2-44**, being less reactive, gave the corresponding two tautomers.[45]
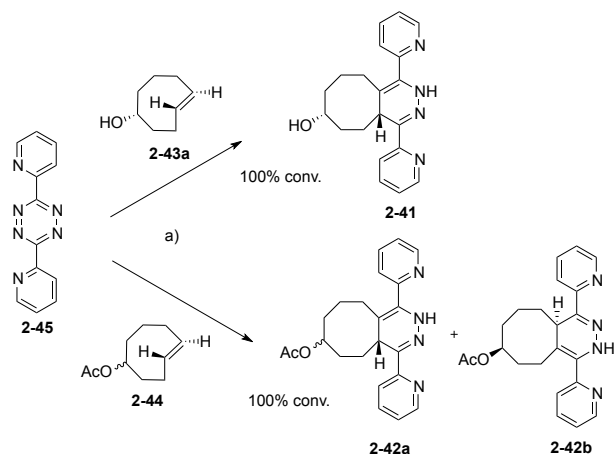
Scheme 2-26 IEDDA reaction between TCO **2-43** and **2-44** and dipyridyl-*s*-tetrazine **2-45**; a) THF, rt, 1 h.

In order to investigate the pentaorthogonal multireaction system, *i.e.* the mutual orthogonality between the IEDDA reaction, the SPAAC, the disulfide exchange, the boronate formation, and the acyl hydrazone formation, the two cycloadditions were first simultaneously investigated. First, Density Functional Theory (DFT) calculations at B3LYP/6-31G** level of theory were performed to optimize geometries, examine the HOMO/LUMO levels of the components of the two cycloadditions and so highlight the potential cross-reactions between them. Accordingly, the cross-reactions were tested as reported in Figure 2-9 b. The computational results support that ADIBO **2-40** (HOMO level: -113.6 kcal/mol) can act as dipolarophile and react with azide **2-59** (LUMO level: -20.4 kcal/mol) but also as a dienophile and react with tetrazine **2-45** (LUMO level: -60.4 kcal/mol). Indeed, *s*-tetrazine are known to react with cyclooctyne derivatives,[46] in particular, it has been reported that cycloaddition between dipyridyl *s*-tetrazine and cyclooctyne occurs with a rate constant of 2 $M^{-1} s^{-1}$.[47] However, to an appreciable degree, ADIBO **2-40** did not react with dipyridyl-*s*-tetrazine **2-45** at rt for 1 h, which might be due to steric hindrance. The other

possible cross-reaction highlighted by the calculations was between azide **2-59** and TCO **2-43** (HOMO level: -145.1 kcal/mol). By performing the test reaction between the components, it was found that they slowly reacted together to form corresponding unstable triazoline **2-62**, leading to decomposition.
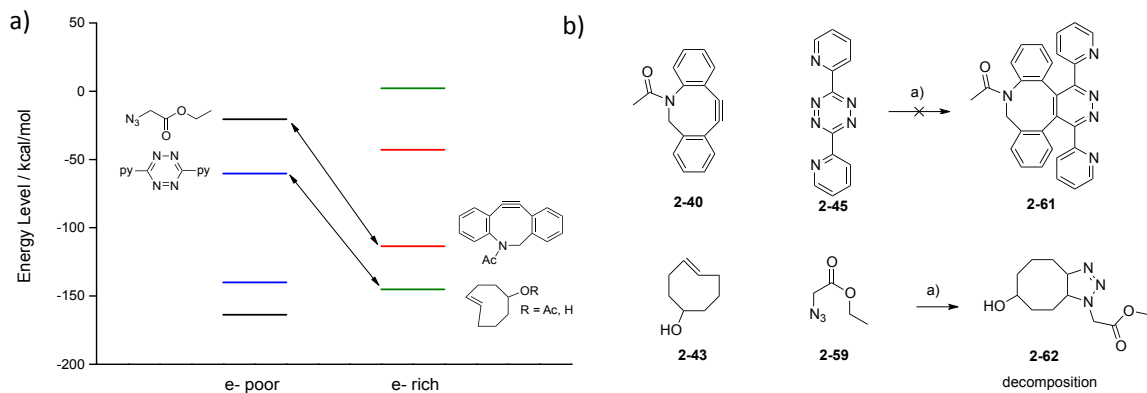
Figure 2-9 a) Orbital energy levels of the four components of the two cycloadditions computed by DFT (B3LYP/6-31G**); b) Test reactions of the two potential cross-reactions; a) THF, rt, 1 h.

Nevertheless, by performing the IEDDA and the SPAAC reactions simultaneously, the expected products **2-41** and **2-60** were formed quantitatively (Scheme 2-27). Those results were fully in agreement with the data reported in the literature.[48]
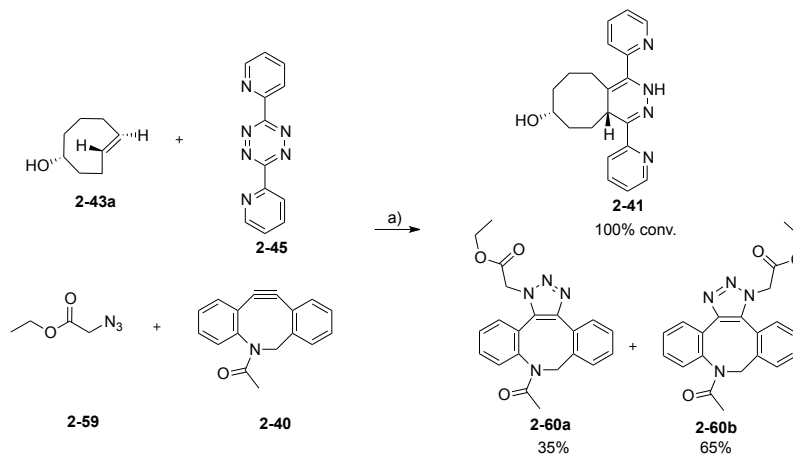
Scheme 2-27 Simultaneous IEDDA and SPAAC reactions; a) THF, rt, 1 h.

With the mutual orthogonality of the two cycloadditions being proven, the IEDDA cycloaddition was simultaneously performed with the tetraorthogonal multireaction system involving the disulfide exchange, the boronate and acyl hydrazone formations, and the SPAAC reactions. The one-pot reaction was carried out under the standard conditions: in THF at rt for 1 h with a catalytic amount of *m*-PDA (Scheme 2-28). For this reaction, protected TCO **2-44** was used to prevent any cross-reactions between the free alcohol and for instance the boronic ester.
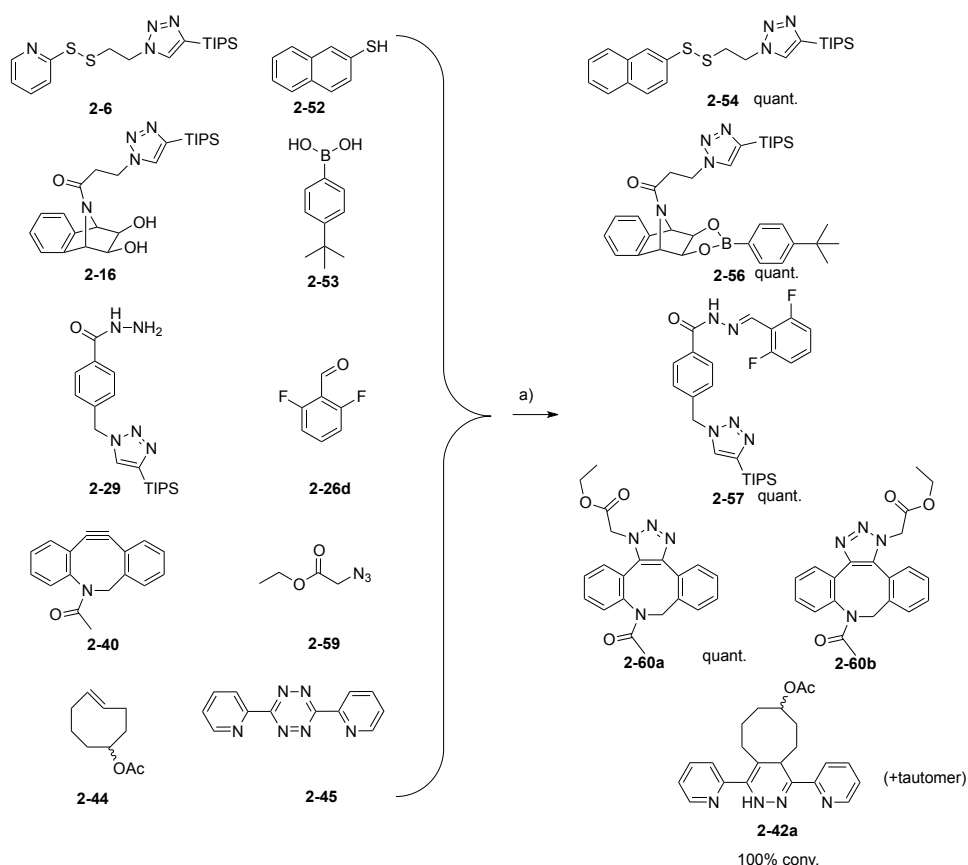
Scheme 2-28 Simultaneous disulfide interchange, boronate, hydrazone formation, SPAAC, IEDDA; a) *m*-PDA, THF, rt, 1 h.

After the reaction, the crude material was analyzed by ^{1}H NMR and ESI-TOF mass spectrometry, the data are reported in Figure 2-10. The ^{1}H NMR spectrum highlights unambiguously the full conversions of disulfide-pyridine **2-6** into naphthalene disulfide **2-54** (tagged in blue), diol **2-16** into boronate **2-56** (in green), and hydrazide **2-29** into acyl hydrazone **2-39** (in red). Similarly to *Section 2.2.2.2*, the signals corresponding to cyclooctyne **2-40** (doublets at 5.15 and 3.65) were not observed in the crude proving the full conversion of **2-40**; and despite the complexity of the spectrum, some characteristic signals of triazoles **2-60a** and **2-60b** were noticed (in purple and black respectively). Notably, since an excess of reactants was used, characteristic signals of azide **2-59** were observed. Finally, the signals of tetrazine ligation products **2-42** (in yellow) are difficult to distinguish among all the other peaks but can be guessed. The MS spectrum displays intense peaks corresponding to cycloadducted product **2-42**, disulfide **2-54,** boronic ester **2-56** and acyl hydrazone **2-57** while the peak for triazoles **2-60** is weaker. After purification through silica gel column chromatography, all the expected products were isolated ultimately proving the mutual orthogonality of the five reactions.
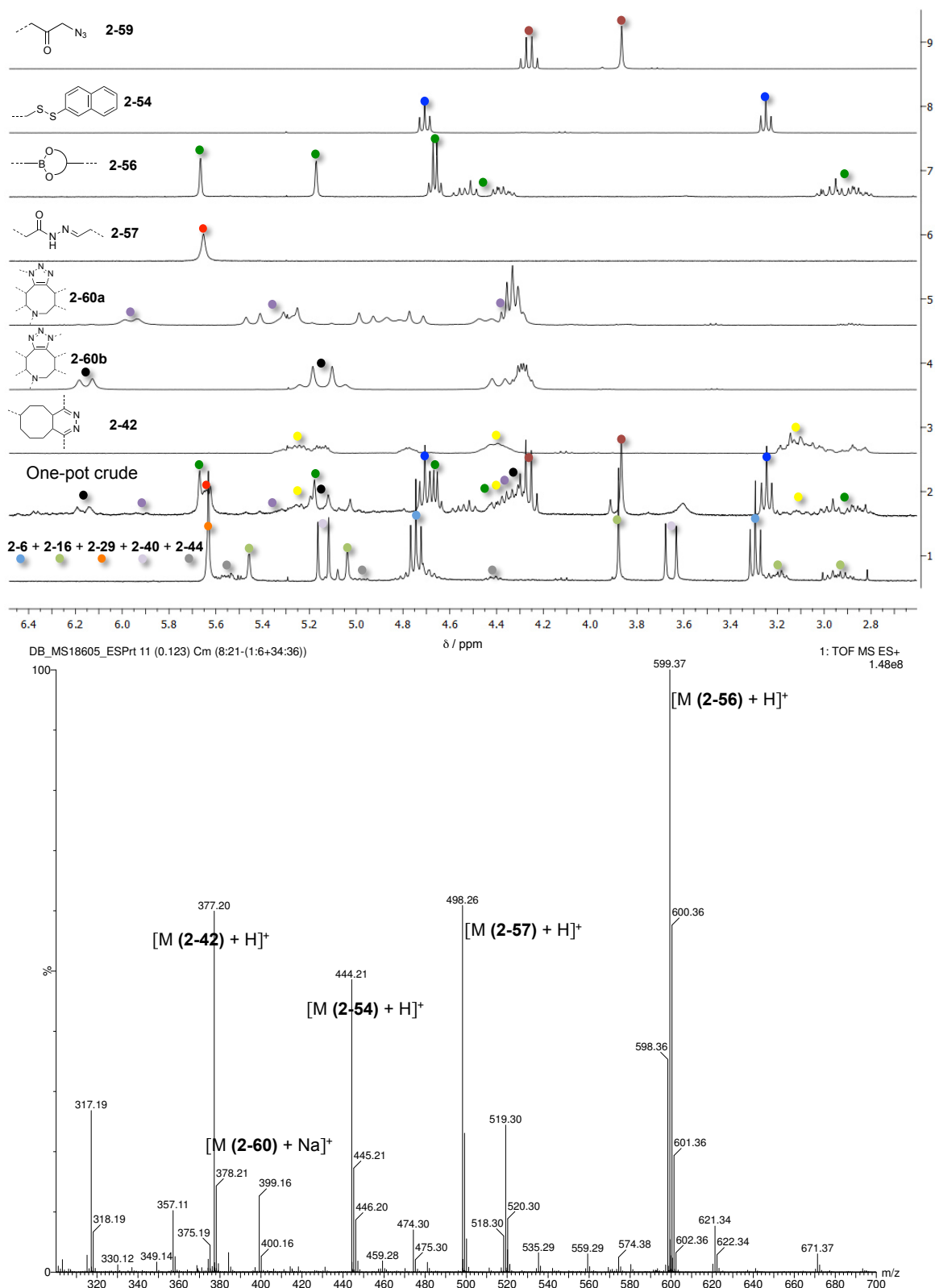
Figure 2-10 Top) Zoom of ¹H NMR between 2.7 and 6.5 ppm in CDCl₃ at 25 °C of 1) physical mixture of starting materials **2-6**, **2-16**, **2-29**, **2-40**, **2-44**, 2) crude material of one-pot reaction, 3) tetrazine ligation product **2-42**, 4) triazole **2-60a**, 5) triazole **2-60a**, 6) acyl hydrazone **2-57,** 7) boronic ester **2-56**, 8) disulfide-naphtalene **2-54**; 9) azide **2-59**; bottom) Mass Analysis ESI-MS (Q-Tof) of one-pot reaction.

2.3 Conclusions

In summary, five anchoring reactions have been selected and optimized under the same conditions to engineer orthogonal recognition motifs. The first major achievement concerns the development of a triorthogonal multireaction system based on dynamic covalent chemistry. In this respect, we reported for the first time the fast and simultaneous disulfide exchange, boronic ester formation and acyl hydrazone formation leading quantitatively to the formation of the expected products without any cross-reaction.[17] The simultaneous process was performed thanks to the use of a nucleophilic catalyst increasing the kinetic rate of the acyl hydrazone formation in neutral conditions and as well the design of the model compounds accelerating the reactions and stabilizing the products formed. Those conditions allow the robust recognition process; nevertheless it is noteworthy to indicate that thanks to the use of dynamic covalent bonds, the system is potentially reversible under other conditions or at least versatile, the disulfide, acyl hydrazone and boronate exchange being possible.

Besides, the complexity of the triorthogonal system was increased and two non-dynamic reactions were introduced to the multireaction system, namely strain promoted azide-alkyne cycloaddition between ADIBO derivative and azide and, inverse electron demand Diels-Alder between dipyridyl *s*-tetrazine and *trans*-cyclooctene. The mutual orthogonality of the anchoring reactions was proven to engineer new tetra- and pentaorthogonal multireaction systems as recognition motifs. The choice of the cyclooctyne ADIBO is one of the key of those systems allowing the increasing of the kinetic rate for the SPAAC and preventing the cross-reaction between the two cycloadditions.

2.4 References

[1]   C. H. Wong, S. C. Zimmerman, *Chem. Commun.* **2013**, *49*, 1679-1695.

[2]   "The Nobel Prize in Chemistry 1987". Nobelprize.org. Nobel Media AB 2014. Web. 17 May 2017. <http://www.nobelprize.org/nobel_prizes/chemistry/laureates/1987/%3E.

[3]   "The Nobel Prize in Chemistry 2016". Nobelprize.org. Nobel Media AB 2014. Web. 21 Dec 2016. <http://www.nobelprize.org/nobel_prizes/chemistry/laureates/2016/%3E.

[4]   a) S. J. Rowan, S. J. Cantrill, G. R. L. Cousins, J. K. M. Sanders, J. F. Stoddart, *Angew. Chem. Int. Ed.* **2002**, *41*, 899-952; b) P. T. Corbett, J. Leclaire, L. Vial, K. R. West, J. L. Wietor, J. K. M. Sanders, S. Otto, *Chem. Rev.* **2006**, *106*, 3652-3711.

[5]   a) J. Li, P. Nowak, S. Otto, *J. Am. Chem. Soc.* **2013**, *135*, 9222-9239; b) F. B. L. Cougnon, J. K. M. Sanders, *Acc. Chem. Res.* **2012**, *45*, 2211-2221.

[6]   a) M. Mastalerz, *Angew. Chem. Int. Ed.* **2010**, *49*, 5042-5053; b) T. Maeda, H. Otsuka, A. Takahara, *Prog. Polym. Sci.* **2009**, *34*, 581-604; c) Y. Jin, Q. Wang, P. Taynton, W. Zhang, *Acc. Chem. Res.* **2014**, *47*, 1575-1586.

[7]   A. Wilson, G. Gasparini, S. Matile, *Chem. Soc. Rev.* **2014**, *43*, 1948-1962.

[8]   J. Leclaire, L. Vial, S. Otto, J. K. M. Sanders, *Chem. Commun.* **2005**, 1959-1961.

[9]   Z. Rodriguez-Docampo, S. Otto, *Chem. Commun.* **2008**, 5301-5303.

[10]   M. J. Barrell, A. G. Campana, M. von Delius, E. M. Geertsema, D. A. Leigh, *Angew. Chem. Int. Ed.* **2011**, *50*, 285-290.

[11]   A. M. Escalante, A. G. Orrillo, R. L. E. Furlan, *J. Comb. Chem.* **2010**, *12*, 410-413.

[12]   R. J. Sarma, S. Otto, J. R. Nitschke, *Chem. - Eur. J.* **2007**, *13*, 9542-9546.

[13]   a) M. Hutin, G. Bernardinelli, J. R. Nitschke, *Chem. - Eur. J.* **2008**, *14*, 4585-4593; b) N. Christinat, R. Scopelliti, K. Severin, *Angew. Chem. Int. Ed.* **2008**, *47*, 1848-1852.

[14]   K. D. Okochi, Y. Jin, W. Zhang, *Chem. Commun.* **2013**, *49*, 4418-4420.

[15]   a) K.-D. Zhang, S. Matile, *Angew. Chem. Int. Ed.* **2015**, *54*, 8980-8983; b) K.-D. Zhang, N. Sakai, S. Matile, *Org. Biomol. Chem.* **2015**, *13*, 8687-8694.

[16]   a) S. Lascano, K. D. Zhang, R. Wehlauch, K. Gademann, N. Sakai, S. Matile, *Chem. Sci.* **2016**, *7*, 4720-4724; b) H. M. Seifert, K. Ramirez Trejo, E. V. Anslyn, *J. Am. Chem. Soc.* **2016**, *138*, 10916-10924; c) B. M. Matysiak, P. Nowak, I. Cvrtila, C. G. Pappas, B. Liu, D. Komáromy, S. Otto, *J. Am. Chem. Soc.* **2017**, *139*, 6744-6751.

[17]   L. Rocard, A. Berezin, F. De Leo, D. Bonifazi, *Angew. Chem. Int. Ed.* **2015**, *54*, 15739-15743.

[18]   a) E. M. Sletten, C. R. Bertozzi, *Angew. Chem. Int. Ed.* **2009**, *48*, 6974-6998; b) M. F. Debets, J. C. M. Van Hest, F. P. J. T. Rutjes, *Org. Biomol. Chem.* **2013**, *11*, 6439-6455; c) C. S. McKay, M. G. Finn, *Chem. Biol.* **2014**, *21*, 1075-1101.

[19]   A. N. Glazer, *Annu. Rev. Biochem.* **1970**, *39*, 101-130.

[20]   V. W. Cornish, K. M. Hahn, P. G. Schultz, *J. Am. Chem. Soc.* **1996**, *118*, 8150-8151.

[21]   a) S. F. M. Van Dongen, R. L. M. Teeuwen, M. Nallani, S. S. Van Berkel, J. J. L. M. Cornelissen, R. J. M. Nolte, J. C. M. Van Hest, *Bioconjugate Chem.* **2009**, *20*, 20-23; b) S. A. Slavoff, I. Chen, Y. A. Choi, A. Y. Ting, *J. Am. Chem. Soc.* **2008**, *130*, 1160-1162.

[22]   E. Saxon, C. R. Bertozzi, *Science* **2000**, *287*, 2007-2010.

[23]   V. V. Rostovtsev, L. G. Green, V. V. Fokin, K. B. Sharpless, *Angew. Chem. Int. Ed.* **2002**, *41*, 2596-2599.

[24]   a) P. C. Lin, S. H. Ueng, M. C. Tseng, J. L. Ko, K. T. Huang, S. C. Yu, A. K. Adak, Y. J. Chen, C. C. Lin, *Angew. Chem. Int. Ed.* **2006**, *45*, 4286-4290; b) A. H. El-Sagheer, T. Brown, *Acc. Chem. Res.* **2012**, *45*, 1258-1267.

[25]   N. J. Agard, J. A. Prescher, C. R. Bertozzi, *J. Am. Chem. Soc.* **2004**, *126*, 15046-15047.

[26]   B. S. S. van, A. T. J. Dirks, M. F. Debets, D. F. L. van, J. J. L. M. Cornelissen, R. J. M. Nolte, F. P. J. T. Rutjes, *Chembiochem* **2007**, *8*, 1504-1508.

[27]   K. Gutsmiedl, C. T. Wirges, V. Ehmke, T. Carell, *Org. Lett.* **2009**, *11*, 2405-2408.

[28]   S. Mayer, K. Lang, *Synthesis* **2017**, *49*, 830-848.

[29]   a) M. L. Blackman, M. Royzen, J. M. Fox, *J. Am. Chem. Soc.* **2008**, *130*, 13518-13519; b) N. K. Devaraj, R. Weissleder, S. A. Hilderbrand, *Bioconjugate Chem.* **2008**, *19*, 2297-2299.

[30]   S. P. Black, J. K. M. Sanders, A. R. Stefankiewicz, *Chem. Soc. Rev.* **2014**, *43*, 1861-1872.

[31]   G. T. Hermanson, in *Bioconjugate Techniques (Third edition)*, Academic Press, Boston, **2013**.

[32]   D. G. Hall, *Boronic Acids: Preparation and Applications in Organic Synthesis, Medicine and Materials, 2nd Revised Edition* Wiley-VCH, Weinheim, **2011**.

[33]   C. D. Roy, H. C. Brown, *J. Organomet. Chem.* **2007**, *692*, 784-790.

[34]   M. Lautens, K. Fagnou, V. Zunic, *Org. Lett.* **2002**, *4*, 3465-3468.

[35]   M. Schröder, *Chem. Rev.* **1980**, *80*, 187-213.

[36]   M. Rashidian, M. M. Mahmoodi, R. Shah, J. K. Dozier, C. R. Wagner, M. D. Distefano, *Bioconjugate Chem.* **2013**, *24*, 333-342.

[37]   J. Dommerholt, F. P. J. T. Rutjes, D. F. L. van, *Top. Curr. Chem.* **2016**, *374*, 16.

[38]   a) N. J. Agard, J. M. Baskin, J. A. Prescher, A. Lo, C. R. Bertozzi, *ACS Chem. Biol.* **2006**, *1*, 644-648; b) J. A. Codelli, J. M. Baskin, N. J. Agard, C. R. Bertozzi, *J. Am. Chem. Soc.* **2008**, *130*, 11486-11493; c) X. Ning, J. Guo, M. A. Wolfert, G. J. Boons, *Angew. Chem. Int. Ed.* **2008**, *47*, 2253-2255; d) M. F. Debets, S. S. Van Berkel, S. Schoffelen, F. P. J. T. Rutjes, J. C. M. Van Hest, F. L. Van Delft, *Chem. Commun.* **2010**, *46*, 97-99.

[39]   A. Kuzmin, A. Poloukhtine, M. A. Wolfert, V. V. Popik, *Bioconjugate Chem.* **2010**, *21*, 2076-2085.

[40]   a) B. L. Oliveira, Z. Guo, G. J. L. Bernardes, *Chem. Soc. Rev.* **2017**, *46*, 4895-4950; b) Z. M. Png, H. Zeng, Q. Ye, J. Xu, *Chem. Asian J.* **2017**, *12*, 2142-2159; c) A. C. Knall, C. Slugovc, *Chem. Soc. Rev.* **2013**, *42*, 5131-5142; d) S. Mayer, K. Lang, *Synthesis* **2017**, *49*, 830-848.

[41]   P. G. Clark, E. N. Guidry, W. Y. Chan, W. E. Steinmetz, R. H. Grubbs, *J. Am. Chem. Soc.* **2010**, *132*, 3405-3412.

[42]   C. J. Zhang, C. Y. J. Tan, J. Ge, Z. Na, G. Y. J. Chen, M. Uttamchandani, H. Sun, S. Q. Yao, *Angew. Chem. Int. Ed.* **2013**, *52*, 14060-14064.

[43]   G. Clavier, P. Audebert, *Chem. Rev.* **2010**, *110*, 3299-3314.

[44]   P. Smyslova, I. Popa, A. Lyčka, G. Tejral, J. Hlavac, *PLoS ONE* **2015**, *10*.

[45]   A. Vázquez, R. Dzijak, M. Dračínský, R. Rampmaier, S. J. Siegl, M. Vrabel, *Angew. Chem. Int. Ed.* **2017**, *56*, 1334-1337.

[46]   J. Sauer, D. K. Heldmann, J. Hetzenegger, J. Krauthan, H. Sichert, J. Schuster, *Eur. J. Org. Chem.* **1998**, 2885-2896.

[47]   W. Chen, D. Wang, C. Dai, D. Hamelberg, B. Wang, *Chem. Commun.* **2012**, *48*, 1736-1738.

[48]   M. R. Karver, R. Weissleder, S. A. Hilderbrand, *Angew. Chem. Int. Ed.* **2012**, *51*, 920-922.

3. Templated chromophore assembly by simultaneous dynamic covalent bonds

In *Chapter 2*, a methodology of triorthogonal dynamic covalent reactions, involving disulfide exchange, boronic ester and acyl hydrazone formation, was developed. This chapter will focus on the creation of artificial antenna systems following the template approach using this methodology. To accomplish this, chromophoric units bearing suitable functional groups will be selectively attached on a peptidic scaffold bearing receptor sites. The design and the synthesis of the peptidic scaffold, the chromophores and the chromophoric assembly will be detailed in the chapter.

The chapter will be divided in three main sections: *i)* in *Section 3.2.1*, the design and the synthesis of the peptidic scaffold bearing the receptor sites will be presented. *ii)* Subsequently, in *Section 3.2.2*, the first generation of molecular chromophoric units, including synthesis and photophysical characterization, will be exposed. *iii)* Finally, in *Section 3.2.3*, the self-assembly between scaffold and chromophores will be examined. Besides, for a better understanding the design of the peptidic scaffold, a general introduction on peptides will open the chapter.

The X-ray analysis of **3-7b** was carried out by *Bernadette Norberg* (*University of Namur*). The synthesis of B-NDI **3-11,** and its intermediates, presented in *Section 3.2.2*, was performed by *Dr Andrey Berezin (University of Namur)*. The modelisation of peptide Ac-(QLAFQLA)$_3$-NH$_2$ presented in *Section 3.2.1*, and Molecular Dynamics simulations of the final architecture, described in *Section 3.2.3*, were carried out by *Dr Federica De Leo (University of Namur).* For their contributions in this work, I want to kindly acknowledge them.

3.1 General introduction on peptides

Peptides and proteins are polymers of amino acids (aa) connected by amide bonds, also called peptide bonds.[1] The twenty natural aa possess an amino group (-NH$_3^+$), a carboxylate (-COO$^-$) and differ from their side chain R. R can be hydrophobic, aromatic, polar, positively and negatively charged, cyclic, which allows classifying the aa (Figure 3-1). According to the

nomenclature rules, peptides composed of fewer than 15 aa are called "oligopeptides", those containing 15-50 aa "polypeptides" and the expression "protein" is used for more than 50 aa.
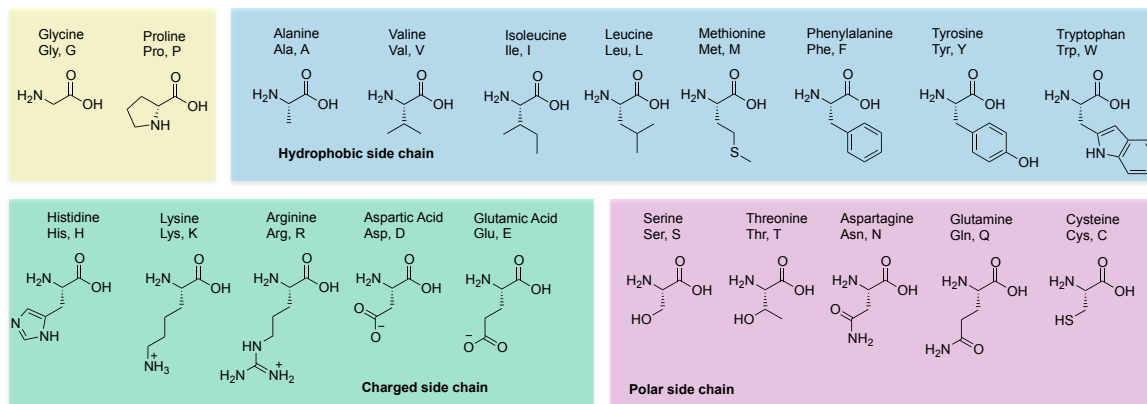
Figure 3-1 Structures of the twenty natural α-amino acids (aa) classified according to the nature of their side chains R: hydrophobic, charged or polar. Full names, three and single letter codes are reported.[1a]

The structural description of the polypeptides and proteins can be considered at four levels of organization. *(i)* The first level, the primary structure, comprises the number and the sequence of aa connected by peptide bonds within the peptide chain (Figure 3-2a). *(ii)* The secondary structure describes the three-dimensional arrangement, also called conformation, of the peptide backbone resulting from hydrogen bonds between amide hydrogen's and carbonyl oxygen's of the backbone. The most common conformations that peptides can adopt are helices, β-sheets or random coils, when no specific conformation is adopted, especially for short peptides (Figure 3-2b). Those are determined by the energetically favoured torsion angles φ, ψ, ω, which are defined by the rotation around the bonds of the backbone atoms of each aa, namely N-Cα (φ) Cα-C(=O) (ψ) and (C=O)-N (ω) as shown in Figure 3-2a. Due to the partial double bound character of the peptide bond, the rotation around it is hindered and so, most of the conformation can be determined by φ and ψ. The accessible regions of φ and ψ torsion angles are displayed in a Ramachandran plot indicating the secondary structure adopted (Figure 3-2b right).[2] *(iii)* The tertiary structure concerns long polypeptides and proteins and takes place when intramolecular interactions, such as disulfide bond, H-bonding, ionic bonds or hydrophobic interactions occur between secondary structures within the long chain (Figure 3-2c). *(iv)* Finally, the quaternary structure refers to the spatial arrangement of two or more polypeptide chains associated by intermolecular interactions (Figure 3-2d).
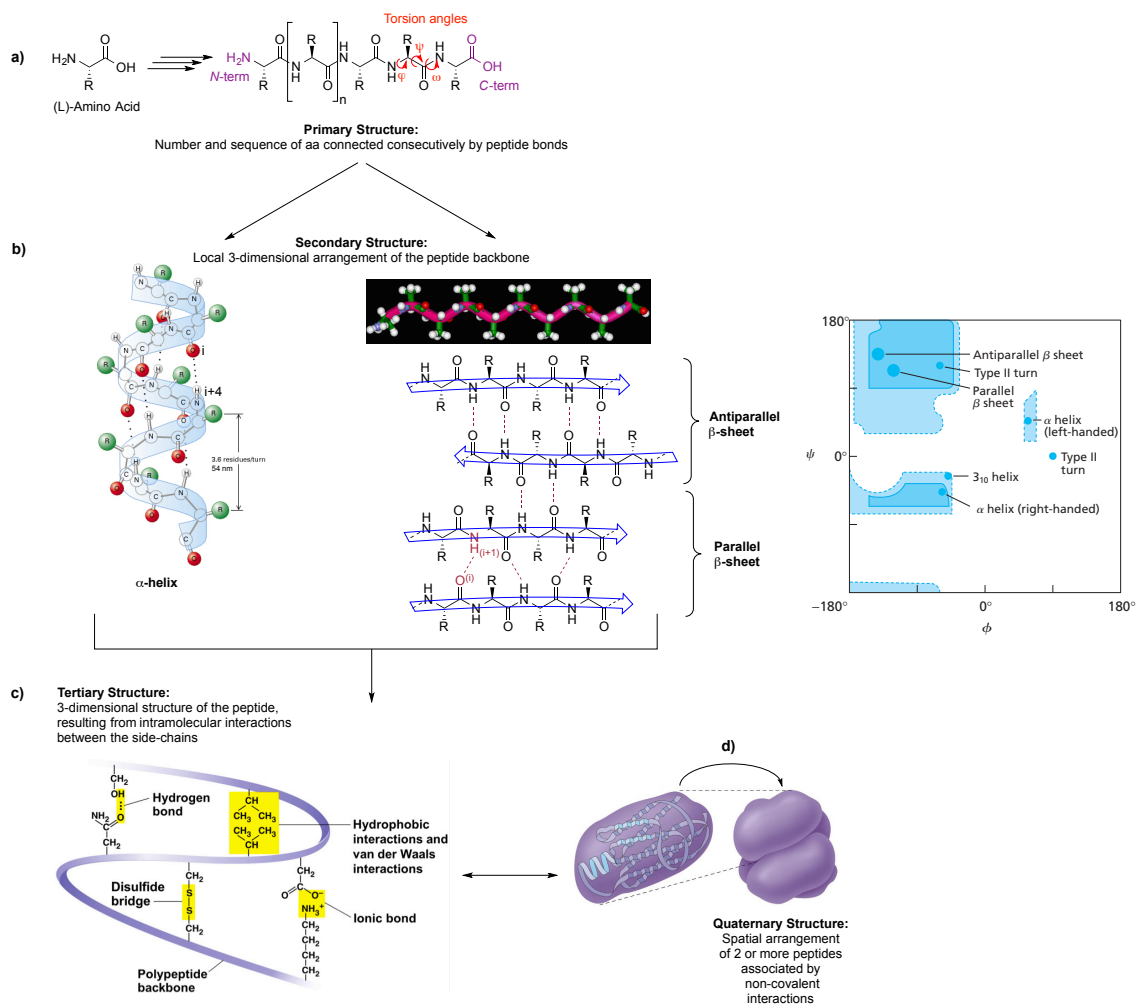
Figure 3-2 a) Primary structure of peptides obtained from (L)-aa. Torsion angles φ, ψ, ω around the backbone bounds N-Cα, Cα-C(=O), and (C=O)-N are highlight. b) The two most common types of secondary structure: α-helix and β-sheets are represented. The Ramachandran plot indicates the range of permissible φ, ψ values based on the molecular models. c) Tertiary structure formed by intramolecular interactions. d) Quaternary structure, association of two or more polypeptides. Adapted from reference 1b. Copyright (2012) Pearson.[1b, 3]

For oligopeptides or short polypeptides, which will be the molecules of interest for this study, the secondary structure is enough to understand the three dimensional arrangement of the structure. A brief overview of the two most common conformations, α-helix and β-sheet, is given.

3.1.1 Helix

The α-helix, the most common form of helix, was proposed by *Linus Pauling* and *Robert Corey* in 1950.[4] The α-helix constitutes a spiral arrangement of the peptide backbone with 3.6 amino acid residues per turn (n = 3.6), a helix pitch (h) of 0.54 nm, and the torsion angles φ= -57°, ψ= -47° (Figure 3-2b). It can be right- ("P" (plus) for clockwise) or left-handed ("M" (minus) for anti-

clockwise) depending if the peptide contains exclusively natural (L-) or unnatural (D-) amino acid; so, it is almost always right-handed in protein. Within a α-helix, each carbonyl oxygen of a residue *i* in the peptide backbone is hydrogen-bonded to the backbone amide hydrogen of the fourth residue *i+4* further toward the C-terminus forming a 13-membered "ring" as shown in Figure 3-2b and 3-3. Therefore, the full nomenclature of an α-helix composed of L-aa is 3.6_{13}-P-helix. Other less prominent helix types are 3_{10}-helix, π-helix (4.4_{16}-P-helix) and γ-helix (5.1_{17}-helix) (Figure 3-3).

The nature of the aa is crucial for the helix stability. For instance, Ala, Val, Leu, Phe, Trp, Met, His, Gln are highly compatible with helical structures while Pro, as an N-alkylated aa, can not act as hydrogen donor and so displays high helix-breaking properties. The general criteria for helix stabilization are: *(i)* the steric requirements of the aa side chain, *(ii)* the electrostatic interactions between the charged aa side chains, *(iii)* the interactions between the distant aa side chains (of residue *i* and *i+3* or *i* and *i+4*) such as H-bonding and van der Waals, *(iv)* the presence of proline and *(v)* the interactions between the aa at the helix termini and the dipole moment of the helix. Regarding the last point, the presence of an acetyl group on the *N*-terminal and an amide on the *C*-terminal stabilizes the helical conformation, the first and the last units forming hydrogen bonds.[5]
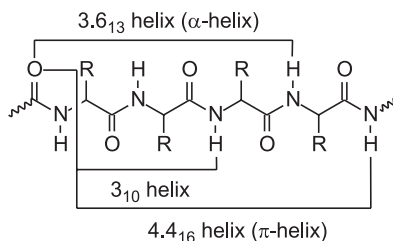
Figure 3-3 Schematic view of the hydrogen bonding pattern in different helices.[1a]

3.1.2 β-Sheets

In β-sheets, the hydrogen bonds are formed between two neighbouring peptidic chains. Two different β-sheet structures are known: *(i)* the parallel β-sheet, where the two chains are aligned in a parallel manner, *(ii)* the antiparallel β-sheet, where the chains are aligned in an antiparallel way (Figure 3-3b). In a β-strand, the fully extended portion of β-sheets, each residue corresponds to about 0.33 nm of an overall length while in α-helix 0.15 nm. An ideal β-sheet is characterized by the torsion angles φ, ψ=+/-180° respectively. Studies of proteins of known structure revealed that β-branched and aromatic aa most frequently occur in β-sheet, while Gly and Pro tend to be poor β-sheet-forming residues.

3.1.3 General approach: Peptidic scaffold to template chromophores

Biomaterials, such as proteins or DNA, have been widely used as platforms templating covalently or electrostatically pigments,[7] as detailed in *Chapter 1*. Indeed, their self-assembly, *i.e.* their conformation in the case of proteins, was used to control the distribution and orientation of the chromophore to achieve efficiently light harvesting.

The general aim of the project is to engineer various multichromophoric architectures covering efficiently the solar spectrum and displaying efficient unidirectional energy transfer from primary energy donor to acceptor. The creation of those architectures can be achieved by following the versatile template approach and so exploiting the self-assembly of chromophores on a scaffold. In this study, polypeptides have been selected to act as scaffold for their great advantages: easy to prepare on solid phase, very good stability, solubility, easy to functionalize, etc.[1a]

To control the incorporation of the dyes into the template, periodic receptor sites can be introduced on the peptidic scaffold forming dynamic covalent bonds with the chromophoric units by applying the triorthogonal multireaction system developed in *Chapter 2*. The design and the synthesis of a peptidic scaffold bearing disulfide-pyridine moiety, hydrazide and diol will be described in *Section 3.2.1 and 3.2.2* (Figure 3-4 *i)*. It is worth noting that a unique conformation of the polypeptide has to be stabilized and used to control the distribution and orientation of the chromophores to achieve efficiently energy transfer within the multichromophoric structure; here α-helix peptide is targeted. Moreover, for the creation of the multicolored architecture, three chromophores (blue naphthalene-diimide, red perylene diimide and yellow ethylnylpyrene), displaying complementary spectral properties and bearing suitable functional groups to be recognized by the peptide, *i.e.* thiol, aldehyde and boronic acid, have to be prepared (Figure 3-4 *ii)*. The synthesis and the photophysical characterization of the dyes will be discussed in *Section 3.2.3*. Finally, the chromophoric assembly on the peptide by simultaneous dynamic covalent reactions must be performed for creating the artificial antenna (Figure 3-4 *iii*). The assembly and the properties of the antenna will be investigated in *Section 3.2.4*.

ii) Preparation of Yellow, Red, Blue Dyes bearing Complementary Sticky Side

i) Design and Synthesis of Programmed Peptidic Scaffold

iii) Chromophoric Assembly
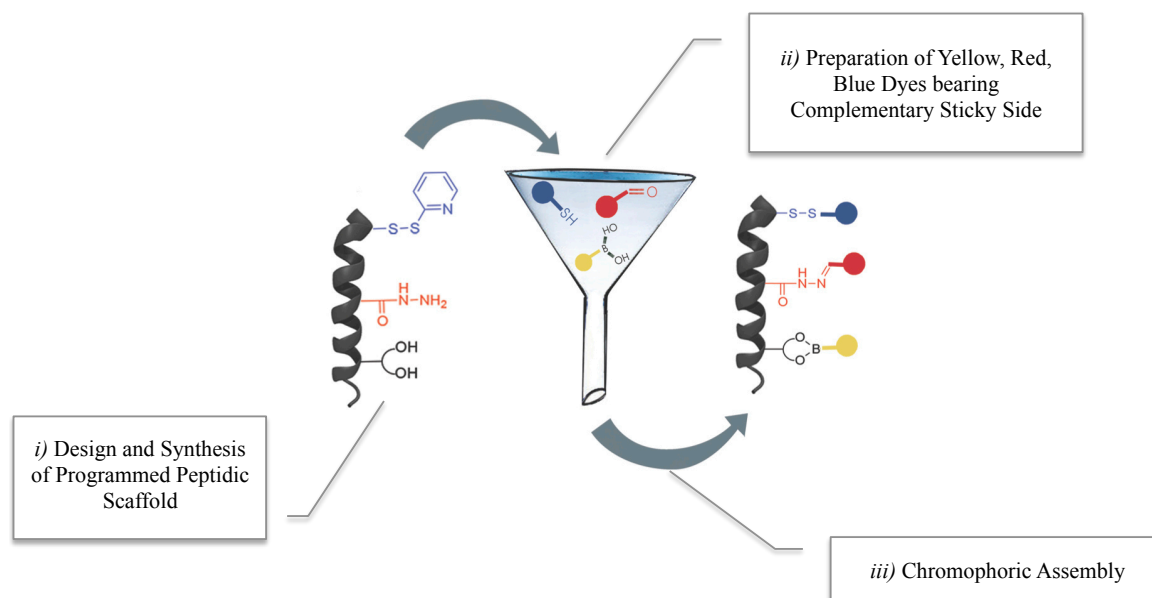
Figure 3-4 Templated chromophore Assembly by Dynamic Covalent Chemistry.[8]

3.2 Results and discussion

3.2.1 Design of the α-helix peptidic scaffold

To template the chromophoric units, peptides appear to be suitable candidates as they can easily be functionalized by receptor sites at given position to spatially organize chromophores. However, polypeptides are very flexible since they can adopt different conformations. So, the distance and the orientation between the chromophores in the final architecture, two highly important parameters for the energy transfer, can be difficult to control. Therefore, stabilizing one unique conformation with optimized chromophoric distances and orientations to control the positions of the dyes in the final architecture seems to be crucial; and so, α-helix peptide was selected.

For the energy transfer to occur according to Förster theory, the chromophoric units have to be in close distance (typically 1 to 3 nm) and their dipole orientation approximately parallel. By introducing them each (*i, i+7*) residue in an ideal α-helix peptide, they should overlap since α-helix has 3.6 residues per turn and, and be separated by a distance of 1.08 nm, an α-helix having a pitch of 0.54 nm. In order to force this conformation, an amphiphilic peptide has been selected.[5] The amphiphilicity has the double advantage to bring aqueous solubility by the introduction of hydrophilic residues to the structure and to stabilize the helicity. Thus, the peptide will contain one face based on alanine (A), the most helix-stabilizing amino acid;[9] one hydrophobic face based on leucine (L) and one hydrophilic face based on a hydrophilic residue: glutamine (Q). This residue has been selected since it will not react with one of the functionalities involved in the three covalent reactions, and moreover, placed each (*i, i+3*) or (*i, i+4*), it is known to stabilize the

helicity of peptide by H-bonding.[10] Besides, the *N*-terminal acetylation and the *C*-terminal amidation should also favor the helical conformation as described in *Section 3.1.1*. The peptide Ac-(QLAFQLA)$_3$-NH$_2$, in which phenylalanine (F) residues were used to mimic the chromophoric units, has been modeled to visualize: *(i)* the overlapping between side chains of F, *(ii)* the short distance between the *(i, i+7)* residues, and *(ii)* the helical conformation stabilized by the interactions between the distant aa side chains (*i, i+4*) of the repeated trimeric sequence QLA (Figure 3-5).
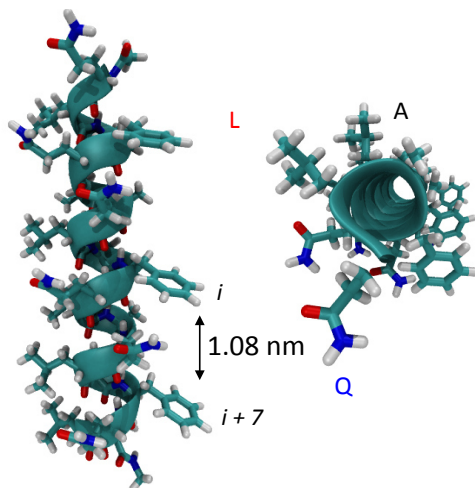
Figure 3-5 Side and Top view of Model peptide Ac-(QLAFQLA)$_3$-NH$_2$ showing the overlapping and the close distance of the (*i, i+7*) residues and the helical conformation of the designed peptide.

The model peptide shows good distance and overlapping between the F residues confirming the design of the structure and the possibility to promote the energy transfer by stabilizing the helical conformation of the peptide. The substitution of the F residues by three modified residues **X** bearing the receptor sites (disulfide-pyridine, hydrazide and diol) afforded the sequence of the peptidic scaffold **3-1** Ac-QLA-**X(disulfide)**-QLAQLA-**X(hydrazide)**-QLAQLA-**X(diol)**-QLA-NH$_2$.

3.2.2 Synthetic strategy for modified amino acids and peptidic scaffold

The synthesis of the peptidic scaffold Ac-QLA-**X(disulfide)**-QLAQLA-**X(hydrazide)**-QLAQLA-**X(diol)**-QLA-NH$_2$ **3-1** commenced with the design and the synthesis of the unnatural aa bearing the protected receptor sites **3-2**, **3-3**, **3-4**. The peptide will be prepared by solid phase peptide synthesis (SPPS) in Fmoc/*t*Bu strategy (Fmoc/*t*Bu-SPPS), the most common strategy for peptide synthesis.[11] This strategy combines orthogonal Fmoc protecting group, removed in nucleophilic-basic conditions, for the lateral chain, and acid-labile protecting groups, such as *t*Bu, for the side

chains. Accordingly, modified aa **3-2, 3-3, 3-4** were *N*-Fmoc protected and the receptor sites, which can be introduced by Cu-catalyzed azide-alkyne cycloaddition (CuAAC) from **3-5** as shown in Scheme 3-1, were protected by acid-labile protecting groups: trityl, *p*-methoxybenzylidene, Boc respectively. Regarding the pyridine-disulfide moiety, it has been decided to perform the SPPS with the protected thiol and to introduce it later in solution to avoid its exposure to the SPPS conditions (in particular those used for Fmoc deprotection).
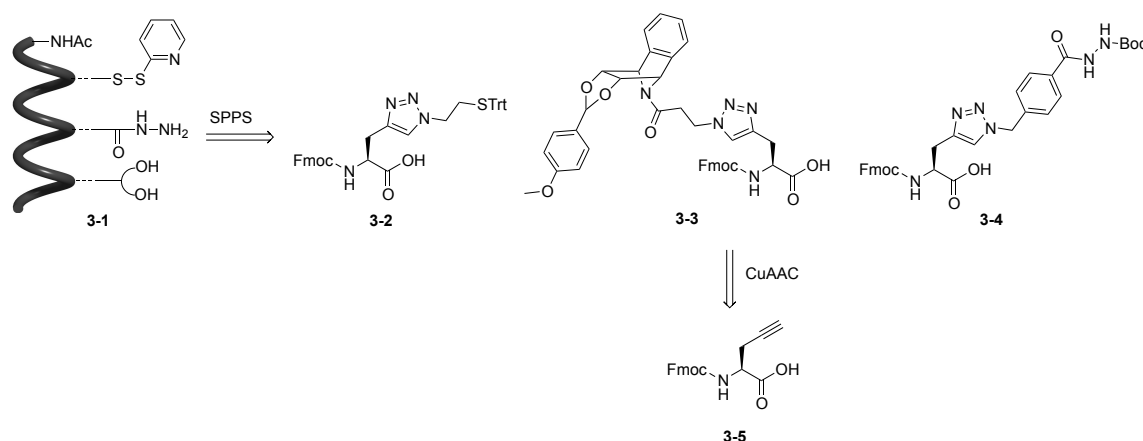
Scheme 3-1 Retrosynthetic pathway for the preparation of the peptidic scaffold bearing the three receptor sites.

3.2.2.1 Synthesis of modified amino acids

Following the retrosynthetic pathway described in Scheme 3-1, the three modified aa **3-2, 3-3, 3-4** can be prepared from commercially available aa Fmoc-Gly(Propargyl)-OH **3-5** and the corresponding azide.

3.2.2.1.1 Synthesis of amino acid 3-2

For the synthesis of aa **3-2** bearing the protected thiol**,** CuAAC was performed between aa **3-5** and azide **2-11** in the presence of $CuSO_4.5H_2O$ and sodium ascorbate in a mixture of DMF and water (Scheme 3-2). This aa will be used for the SPPS. Nevertheless, to prove the synthetic strategy chosen for peptide **3-1** and described in Scheme 3-1 (consisting in introducing the disulfide-pyridine moiety after the SPPS), the thiol deprotection was carried out under resin cleavage conditions to afford thiol **3-6**. Without isolating this intermediate, the disulfide exchange was directly performed between **3-6** and 2,2'-dipyridyl disulfide to give aa **3-7** in 97% yield over two steps validating the strategy.
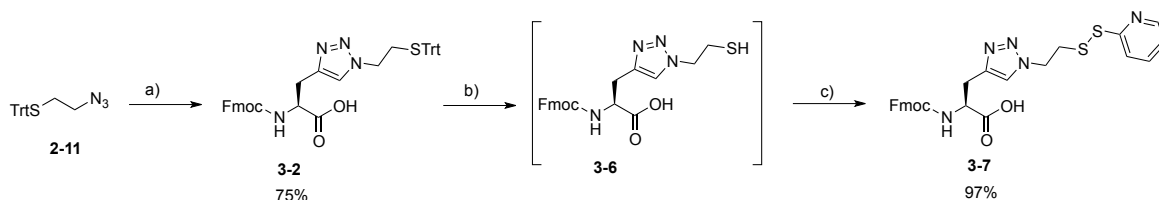
Scheme 3-2 Synthesis of amino acid bearing protected thiol **3-2** followed by trityl deprotection under resin cleavage conditions and disulfide exchange; a) Fmoc-Gly(Propargyl)-OH **3-5**, CuSO$_4$·5H$_2$O, Na ascorbate, DMF/H$_2$O 4:1, rt, 3 h; b) TFA/TIS/H$_2$O 95:2.5:2.5, rt, 2 h; c) 2,2'-dipyridyl disulfide, DIEA, MeOH, rt, 1 h.

3.2.2.1.2 Synthesis of amino acid 3-3

Before preparing aa **3-3** bearing the protected diol, a preliminary study was performed to select the appropriate protecting group (PG). Different PGs: dimethylacetal, *p*-methoxybenzylidene and *p,m*-dimethoxybenzylidene, have been introduced and removed under resin cleavage conditions from diol **2-25** to find the best balance between ability to be introduced and cleaved. The results are gathered in Table 3-1 and 3-2. In the case of the dimethylacetal PG (Entry 1), its introduction was achieved quantitatively in the presence of a catalytic amount of *p*-toluenesulfonic acid, however, its removal under resin cleavage conditions afforded diol **2-25** in only 50% yield. On the other hand, the cleavage of *p,m*-dimethoxybenzylidene gave **2-25** in very high yield, but its introduction was achieved in only 55% yield (Entry 3). This study showed that *p*-methoxybenzylidene possesses the best balance between ability to be introduced and removal under resin cleavage conditions (Entry 2) and so, was selected as PG for the SPPS. Crystals of **3-8b** suitable for single-crystal X-ray analysis, grown by slow evaporation from EtOAc, were obtained and the crystal structure is presented in Figure 3-6 and will be discussed in *Chapter 4*.

Table 3-1 Introduction of three different protecting groups; a) *p*TSA.H$_2$O, THF, rt, 7 h.

Entry	Product	R$_1$	R$_2$	Yield
1	**3-8a**	Me	Me	Quant.
2	**3-8b**	*p*-methoxybenzene	H	75%
3	**3-8c**	*p,m*-dimethoxybenzene	H	55%

Table 3-2 Removal of three different protecting groups; a) TFA/TIS/H$_2$O (95:2.5:2.5), rt, 2 h.
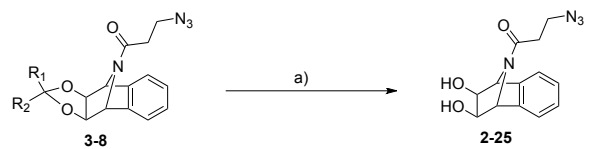
Entry	Starting material	R$_1$	R$_2$	2-25 (^{1}H NMR yield)	3-8 (^{1}H NMR yield)
1	**3-8a**	Me	Me	50%	50%
2	**3-8b**	*p*-methoxybenzene	H	91%	9%
3	**3-8c**	*p,m*-dimethoxybenzene	H	97%	3%
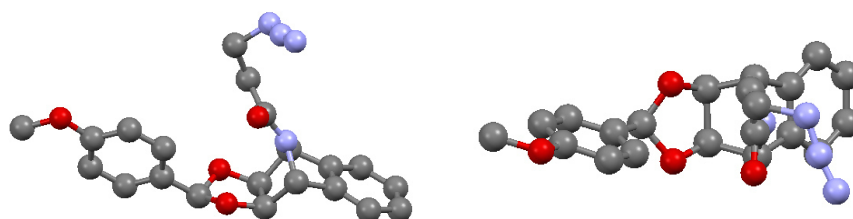
Figure 3-6 Side- and top-view the crystal structure of **3-8b**. Solvent for crystallization: EtOAc (space group: P21/c, H hidden). Color code: grey: C, red: O and blue: N.

After the introduction of the *p*-methoxybenzylidene on diol **2-25** using anisaldehyde dimethylacetal in acidic conditions, the CuAAC was performed affording amino acid **3-3** in 89% yield available for the peptide synthesis as reported in Scheme 3-3. Finally, the deprotection of *p*-methoxybenzylidene on **3-3** under resin cleavage conditions gave quantitatively amino acid **3-9**.
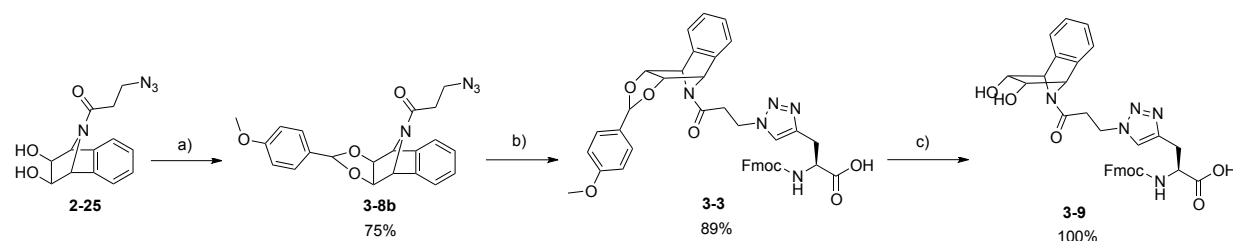
Scheme 3-3 Synthesis of amino acid bearing protected diol **3-3** followed by deprotection of PG under resin cleavage conditions; a) anisaldehyde dimethylacetal, *p*TSA.H$_2$O, THF, rt, 6 h; b) Fmoc-Gly(Propargyl)-OH **3-5**, CuSO$_4$·5H$_2$O, Na ascorbate, DMF/H$_2$O 4:1, rt, 3 h; c) TFA/TIS/H$_2$O 95:2.5:2.5, rt, 2 h.

3.2.2.1.2 Synthesis of amino acid *3-4*

Finally, amino acid **3-4** bearing protected hydrazide was synthesized as reported in Scheme 3-4. The Cu-catalyzed cycloaddition was performed between aa **3-5** and azide **2-30** in the presence of CuSO$_4$.5H$_2$O and sodium ascorbate in a mixture of DMF and water, affording amino acid **3-4** in 86% yield, which will be used for the peptide synthesis. Finally, the deprotection of Boc-PG on **3-4** was carried out under resin cleavage conditions giving quantitatively free hydrazide **3-10**.
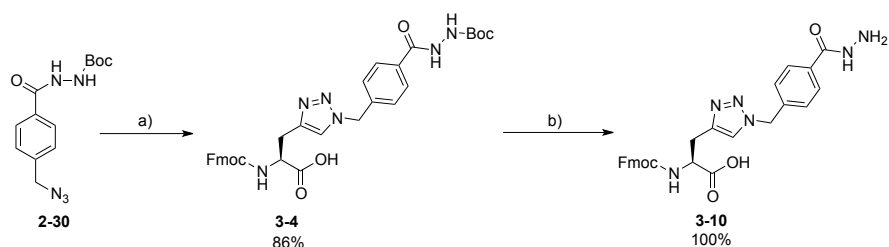
Scheme 3-4 Synthesis of amino acid bearing protected hydrazide **3-4** followed by deprotection of PG under resin cleavage conditions; a) Fmoc-Gly(Propargyl)-OH **3-5**, CuSO$_4$·5H$_2$O, Na ascorbate, DMF/H$_2$O 4:1, rt, 3 h; b) TFA/TIS/H$_2$O 95:2.5:2.5, rt, 2 h.

3.2.2.2 Synthesis of the peptidic scaffold

Having in hands the three modified amino acids: **3-2**, **3-3** and **3-4**; the peptidic scaffold bearing the three receptor sites: the disulfide pyridine, the hydrazide and the diol, was prepared by SPPS. The peptide was grown on a polymeric support, Rink Amide MBHA resin affording peptide-amide, using the natural and modified amino acids following the general procedure described in Scheme 3-5.
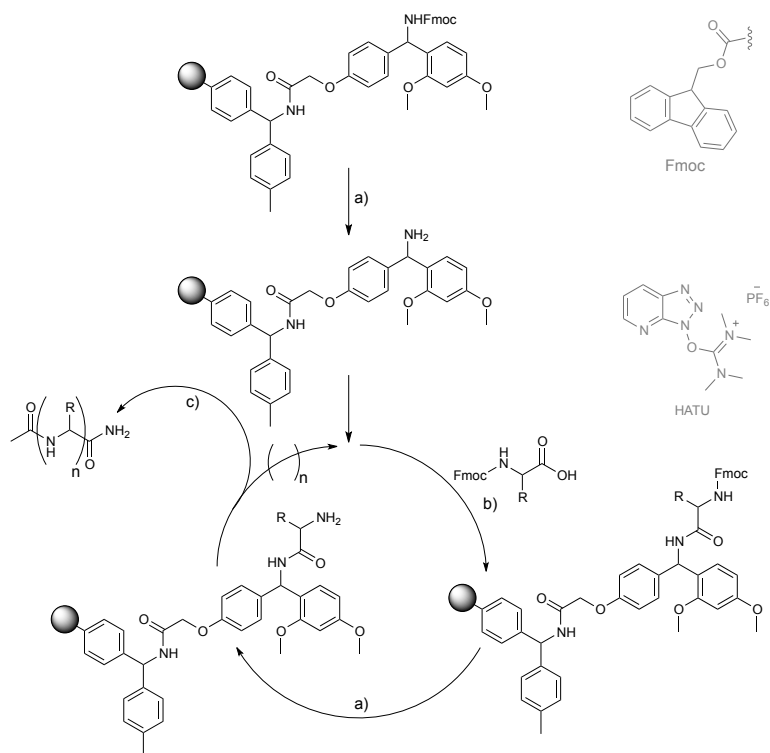
Scheme 3-5 General procedure of Solid Phase Peptide Synthesis in Fmoc/*t*Bu strategy (Fmoc/*t*Bu-SPPS); a) *i)* Fmoc deprotection: 20% piperidine in DMF, 3 × 4 min, *ii)* DMF washing; b) *i)* HATU, DIEA, DMF, NMP, 25 min, *ii)* DMF washing c) *i)* Ac$_2$O/pyridine/NMP (1:2:2), 2 × 15 min; *ii)* TFA/TIS/H$_2$O/EDT, 94:1:2.5:2.5, 2 h.

This procedure consists in repeating cycles between *(i)* Fmoc deprotection with piperidine, *(ii)* washing of the resin, *(iii)* coupling with the aa in the presence of a coupling agent, here HATU, *(iv)* and washing. Once the solid-phase attached peptide was entirely synthesized, the last Fmoc-deprotection was performed followed by the acetylation of the free *N*-terminal amine with acetic anhydride. Subsequently, the simultaneous resin cleavage and side chains deprotection affording crude peptide **3-11** bearing a free thiol was carried out in the presence of TFA/TIS/H$_2$O/EDT, (94:1:2.5:2.5). The disulfide pyridine moiety was then introduced in solution by disulfide exchange between peptide **3-11** and 2,2'-dipyridyl disulfide in the presence of DIEA affording the peptidic scaffold **3-1** (Scheme 3-6).
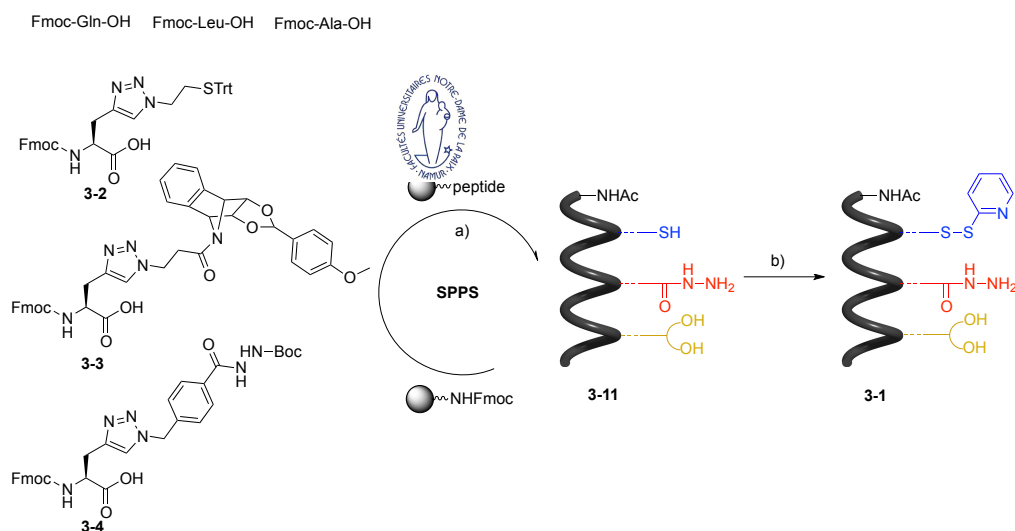
Scheme 3-6 Synthesis of peptidic scaffold **3-1**; a) SPPS see Scheme 3-5; b) 2,2'-dipyridyl disulfide, DIEA, DMF, rt, 1 h.

Component	Molecular Mass	Molecule	Abundance	Absolute Abundance	Relative Abundance
	2894.4401	2896.2907	Mr	1586171	100.00
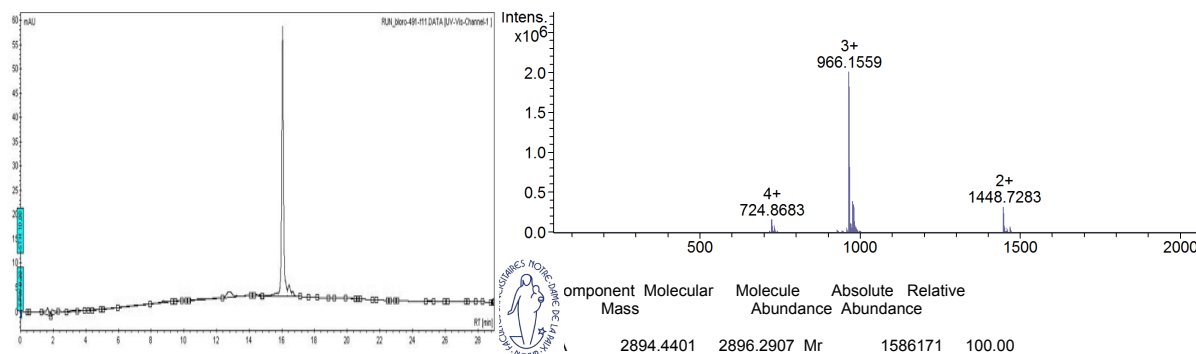
Figure 3-7 HPLC chromatogram and ESI-MS(QTof) analysis of purified peptide **3-1**.

Peptidic scaffold **3-1** has been characterized by RP-HPLC on column C$_8$ and mass analysis after purification by preparative RP-HPLC (Figure 3-7). ESI-MS(Q-Tof) showed M^{4+}, M^{3+}, M^{2+}; after deconvolution of multicharged ions, the monoisotopic mass was found: 2894.4401 (calculated mass: 2894.4333 for C$_{129}$H$_{195}$N$_{41}$O$_{32}$S$_2$).

3.2.3 Preparation of the first generation of the color emitters

For the creation of the final multichromophoric architecture, three dyes have been selected for their complementary UV-Vis absorption and fluorescence emission profiles: a core-substituted naphthalene diimide (cNDI), a perylene diimide (PDI), and an ethynyl pyrene (Py) covering the red, yellow and blue regions respectively. To be assembled on the peptidic scaffold previously prepared, the three dyes have to be functionalized with complementary sticky sides: phenyl thiol, 2,6-difluorobenzaldehyde, and phenyl boronic acid. Besides, a solubilizing moiety, 3,5-O(triethyleneglycol monomethoxy)benzyl imide, can be introduced on poorly soluble cNDI and PDI derivatives. In this respect, the three colored emitters blue NDI **3-12** (B-NDI), red PDI **3-13** (R-PDI), and yellow Py **3-14** (Y-Py) were targeted as the first generation of chromophores (Figure 3-8).
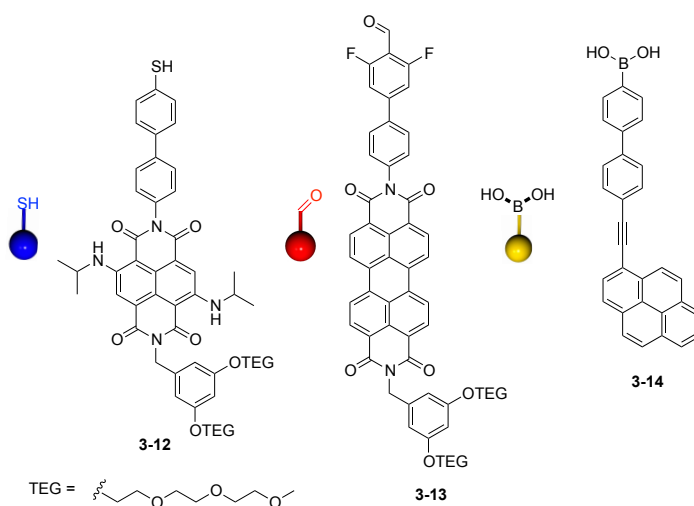
Figure 3-8 Color emitters selected for the study: B-NDI **3-12,** R-PDI **3-13** and Y-Py **3-14**.

3.2.3.1 Synthesis and photophysical characterization of B-NDI (3-12)

Core-substituted naphtalenediimides (cNDI) are a very attractive class of chromophore since they have impressively tunable properties (Figure 3-9).[12] In particular, their ability to change color and redox properties, resulting from the decreasing of HOMO-LUMO bandgap while increasing the push-pull character by changing the electron donating groups on the core, make them good candidates for the preparation of various materials such as organic field-effect transistors (OFETs),[13] emissive devices,[14] artificial photosynthetic systems,[15] n-type semiconductors.[15b]
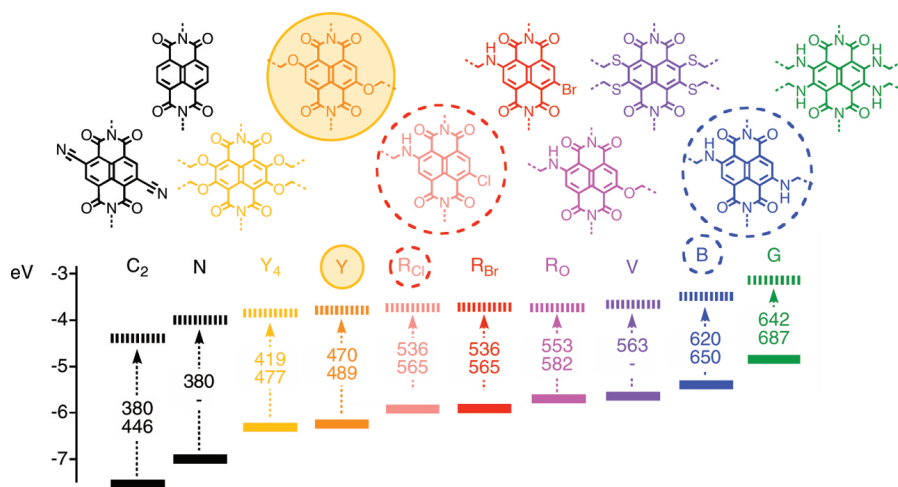
Figure 3-9 Core substituted naphtalenediimides: "A rainbow collection" with indication of HOMO (bold) and LUMO (dashed) energies in eV against vacuum and maximal absorption (top) and emission wavelength (bottom) in nm. Reprinted from reference 15b with permission. Copyright (2009) American Chemical Society.[15b]

In our group, a methodology for the preparation of unsymmetrical cNDI was developed consisting in a four steps high yielding synthesis of a broad range of heterocyclic, aromatic and aliphatic hetero-N-substituted cNDI (Scheme 3-7).[16] The acid mediated transformation of the tetra-ester affords the "magic" intermediate core-substituted naphthalene-anhydride-ester (cNAE) in quantitative yield, which allows achieving the sequential condensation into unsymmetrical cNDI.
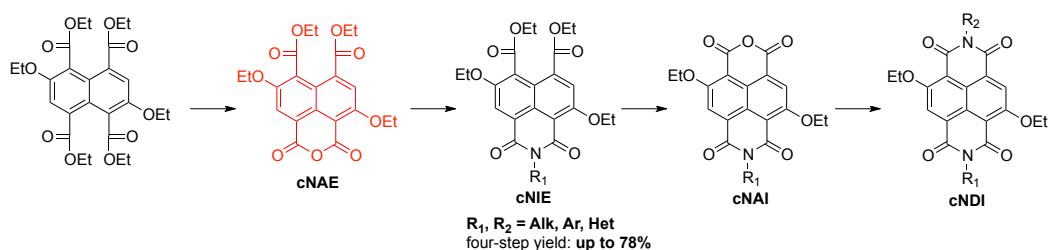
Scheme 3-7 Sequential methodology for the preparation of unsymmetrical cNDI.[16]

Following this methodology, the synthesis commenced with the selective condensation of solubilizing benzylamine **3-17**, prepared from **3-16** by Pd-catalyzed hydrogenation, and "magic" cNAE **3-15** in the presence of DIEA in dioxane at 100 °C for 2 h yielding **3-18** in 92%. This was followed by the high yielding acid-mediated formation of monoanhydride **3-19,** and its condensation with amine **3-22,** previously synthesized by Suzuki coupling, affording **3-23** in 72% yield. The substitution of the diethylether chains of **3-23** into isopropylamine gave blue cNDI **3-24** in 91% yield. Finally the Hg^{II}-assisted *t*Bu deprotection giving the free thiol was carried out leading to B-NDI **3-12** in 72% yield (Scheme 3-8).
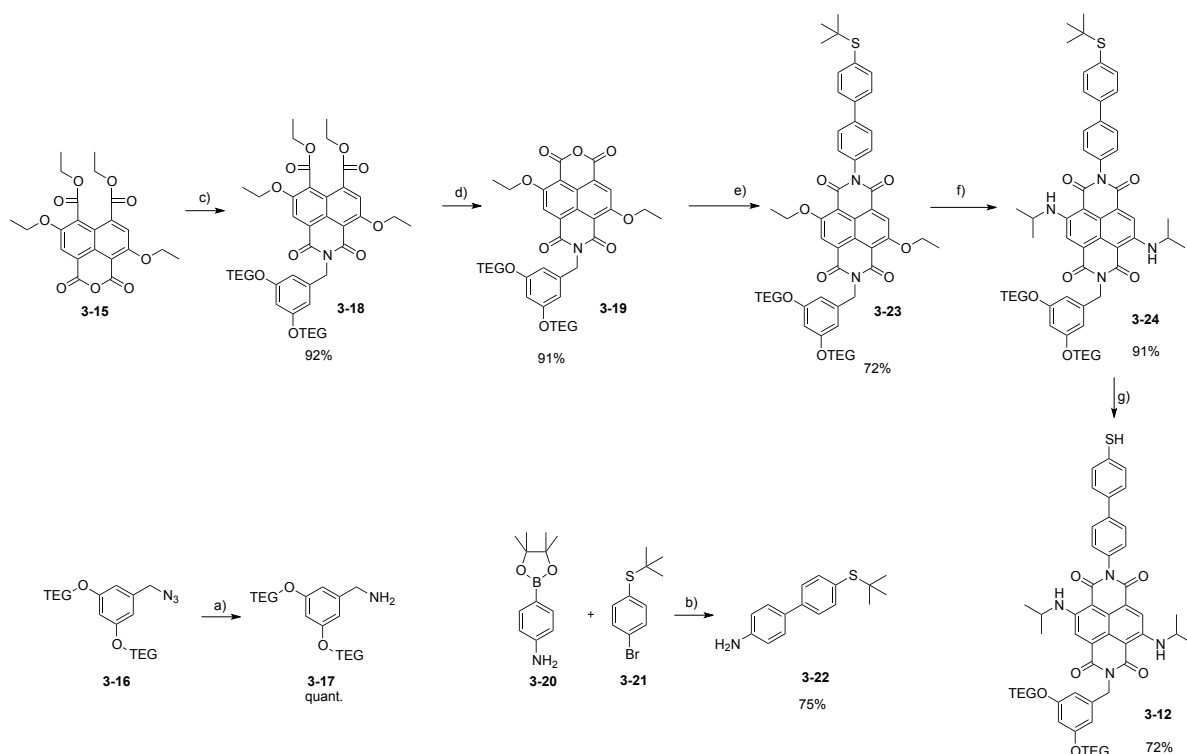
Scheme 3-8 Synthesis of B-NDI **3-12**; a) H$_2$, Pd(OH)$_2$/C, MeOH, rt, 20 h; b) Cs$_2$CO$_3$, [Pd(PPh$_3$)$_4$], toluene, reflux, 12 h; c) **3-17**, DIEA, dioxane, 101 °C, 2 h; d) TFA, 73 °C, 24 h; e) **3-22**, NEt$_3$, benzoic acid, DMF, 110 °C, 6 h; f) iPrNH$_2$, 110 °C, 48 h; g) *i)* Hg(ClO$_4$)$_2$, MeOH/CH$_2$Cl$_2$ (1:5), 30 min, rt, *ii)* H$_2$S, rt, 10 min.

B-NDI **3-12** and intermediates were fully characterized by melting points, infrared, ^{1}H and ^{13}C NMR spectroscopy, high-resolution mass spectrometry and the data are reported in *Chapter 6*. Moreover, the UV-Vis absorption spectrum of B-NDI **3-12** was recorded in DMF and is in agreement with the data reported in the literature for similar *N*-substituted cNDI.[12] The π−π* transition, not sensitive to the core-substitution, is characterized by the two bands at 345 (ε = 14700 L mol^{-1} c^{-1}) and 362 nm (ε = 15900 L mol^{-1} cm^{-1}), while the broad band with a maximum at 612 nm (ε = 23500 L mol^{-1} cm^{-1}) is due to a charge-transfer from the electron donating core substituents (Figure 3-10). The emission fluorescence spectrum (λ_{exc} = 609 nm) shows the mirror image of the absorption spectrum with a maximum at 641 nm. The quantum yield (determined from *N,N'*-di(2,6-diisopropylphenyl)-1,6,7,12-tetraphenoxyperylene- 3,4 :9,10-tetracarboxylic acid bisimide (QY= 96% in CHCl$_3$))[17] was estimated to be 33% using Equation (1).

$$QY_X = QY_S \times (A_S I_X / A_X I_S) \times (n_x/n_s)^2 \qquad (1)$$

Where *QY* is the fluorescence quantum yield, *A* is the absorbance at the excitation wavelength, *I* is the integrated area of fluorescence emission, and *n* is the refractive index of the solvent used. Subscripts s and x refer to the standard and to the unknown, respectively.
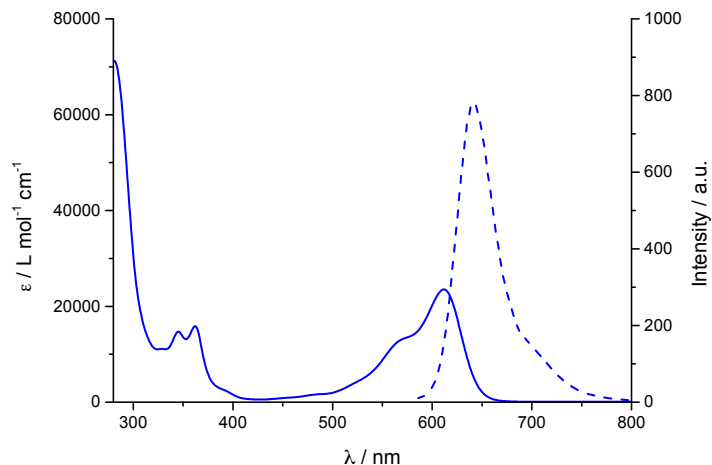
Figure 3-10 Absorption (solid line) and fluorescence emission (dashed line) spectra (λ_{exc} = 580 nm) of B-NDI **3-12** in DMF.

3.2.3.2 Synthesis and photophysical characterization of R-PDI (3-13)

The second chromophore selected was a perylene diimide (PDI) derivative.[18] Originally developed as an industrial pigment,[19] PDIs are now extensively used in (multi)chromophoric system,[20] supramolecular architecture[21] and organic electronic and photovoltaic devices.[13b, 13c] Indeed, their great properties such as photochemical stability, high fluorescence quantum yields, ability to self-assemble, and to accept electron, make this class of dyes one of the most explored. Those outstanding properties are due to the strong conjugation within the molecular structure, an electron rich rigid polycyclic aromatic core (perylene) substituted with two electron withdrawing imide groups. The preparation of unsymmetrical PDI, from the corresponding di-anhydride PDA, can be performed using either simultaneous or sequential addition of two different amines. The one-step procedure is usually unsuccessful due to the difference of reactivity of amines. Typically, the desired product is obtained in low yield (around 10%), the symmetrical products being the dominant species.[22] In this respect, a stepwise approach was followed for the synthesis of R-PDI **3-13** bearing the electron-poor aldehyde.

The synthesis, described in Scheme 3-9, commenced with the preparation of symmetrical PDI **3-26** following the literature protocol.[23] The employed method relies on partial saponification of symmetrical dicyclohexyl PDI **3-26** in the presence of 50 equivalents of KOH in a iPrOH/H$_2$O mixture, affording perylene monoimide monoanyhydride **3-27** according to the literature procedure.[24] This compound was not isolated due to its very low solubility and was subsequently condensed with amine **3-17** in the presence of imidazole in a toluene/DMF mixture at 110 °C for 16 h, to give unsymmetrical PDI **3-28** in 30% yield over two steps. The selective hydrolysis of the cyclohexyl imide was then performed to give **3-29** under the same saponification

conditions than previously, the benzyl imide being stable under those conditions. This was followed by the condensation of iodo aniline to yield **3-30** in 78% yield over two steps. Finally, a Pd-catalyzed Suzuki cross-coupling was exploited to introduce the 2,6-difluorobenzaldehyde moiety affording R-PDI **3-13** in 95% yield.
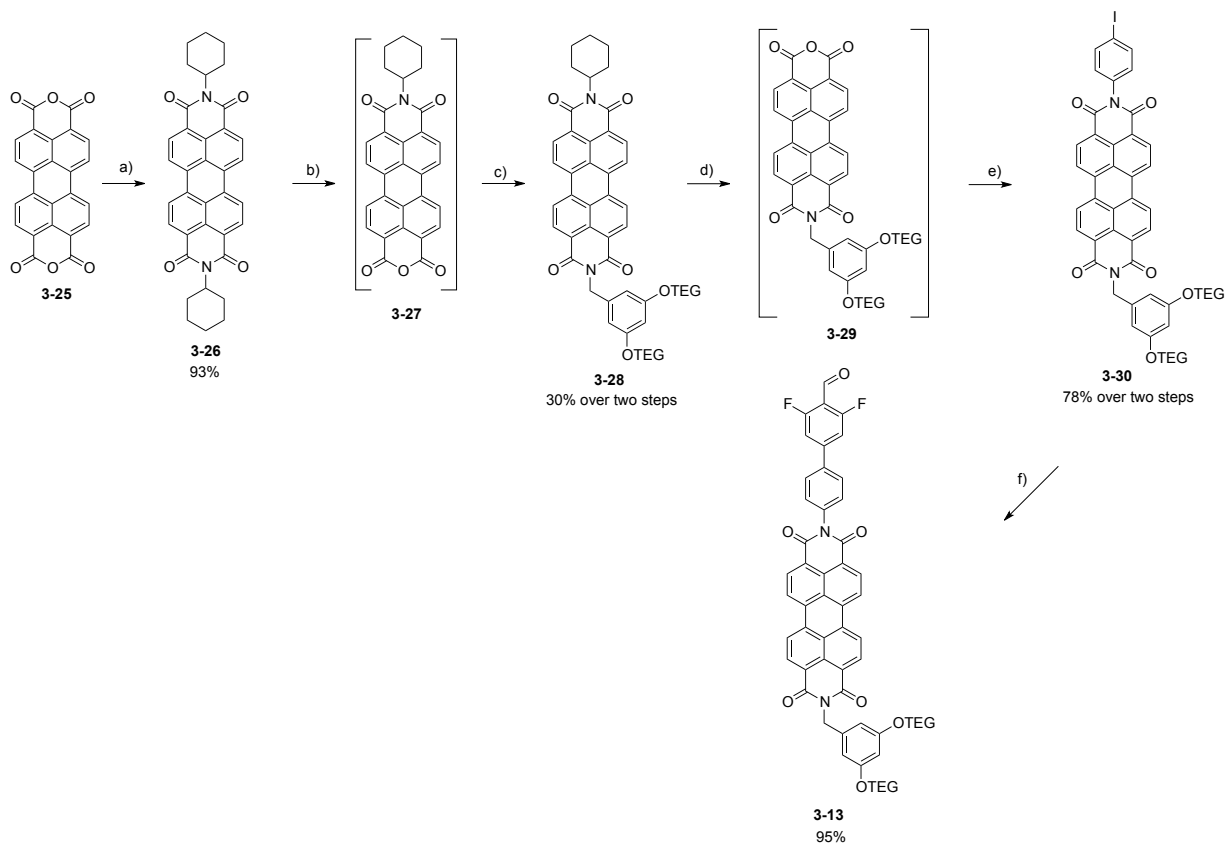
Scheme 3-9 Synthesis of R-PDI **3-13**; a) cyclohexylamine, 140 °C, 15 h; b) *i)* KOH, iPrOH/H$_2$O (6:1), 80 °C, 3 h, *ii)* AcOH, rt, 15 min; c) **3-17**, imidazole, toluene/DMF (6:1), 110 °C, 16 h; d) *i)* KOH, iPrOH/H$_2$O (6:1), 80 °C, 3 h, *ii)* AcOH, rt, 15 min; e) iodo-aniline, imidazole, toluene/DMF (6:1), 110 °C, 16 h; f) 2,6-difluoro-4-formylphenylboronic acid, K$_2$CO$_3$, [Pd(PPh$_3$)$_4$], dioxane/H$_2$O (7:1).

R-PDI **3-13** and intermediates were fully characterized by melting points, infrared, ^{1}H and ^{13}C NMR spectroscopy, high-resolution mass spectrometry and the data are reported in *Chapter 6*. Moreover, the UV-Vis absorption spectrum of R-PDI **3-13,** recorded in DMF and reported in Figure 3-11, shows the three typical maxima of absorption bands at 527 ($\varepsilon = 85500$ L mol^{-1} cm^{-1}), 491 ($\varepsilon = 54500$ L mol^{-1} cm^{-1}) and 460 ($\varepsilon = 20300$ L mol^{-1} cm^{-1}) corresponding to the π–π* electronic transition (comprising three vibronic transitions: 0→0, 0→1, 0→2). The fluorescence emission spectrum of **3-13** displays the mirror image of its absorption profile in agreement with PDI derivatives reported in the literature (Figure 3-14).[21] However, the quantum yield (determined from *N,N'*-di(2,6-diisopropylphenyl)-1,6,7,12-tetraphenoxyperylene- 3,4 :9,10-

tetracarboxylic acid bisimide (QY= 96% in $CHCl_3$))[17] was estimated to be 4% while high fluorescence quantum yields (>90%) are usually observed for PDI derivatives. This might be due to the presence of the electron-rich benzyl amine leading to a photoinduced electron transfer to the electron-deficient PDI,[18] and will be more detailed in *Chapter 4*.
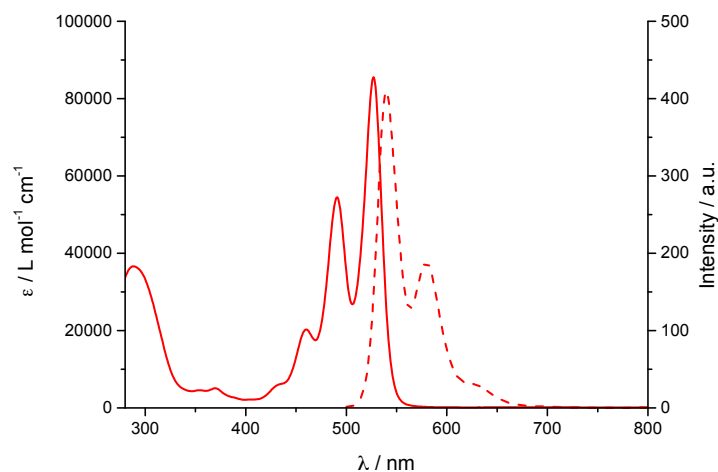

Figure 3-11 Absorption (solid line) and fluorescence emission (dashed line) spectra (λ_{exc} = 495 nm) of R-PDI **3-13** in DMF.

3.2.3.3 Synthesis and photophysical characterization of Y-Py (3-14)

Ethynylpyrene was chosen as the third chromophore. Pyrene is a blue-emitting chromophore belonging to the family of polycyclic aromatic hydrocarbon (PAH). As the previous dyes, it has been widely used for the fabrication of optoelectronic materials.[25]
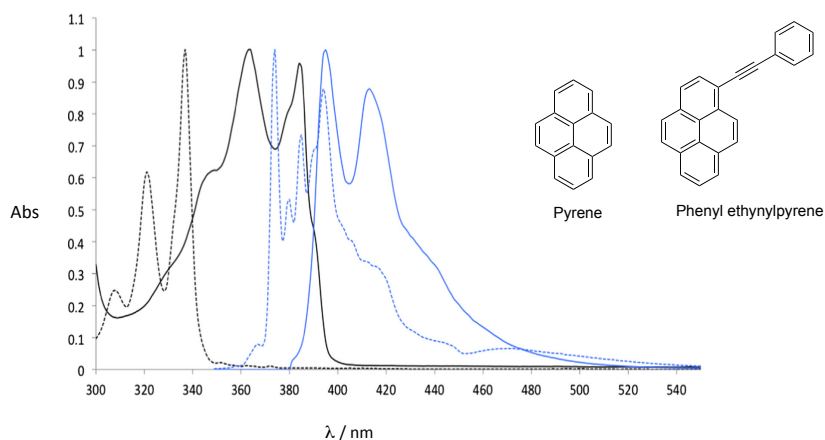
Figure 3-12 Normalized absorption (in black) and emission (in blue) spectra of pyrene (dashed line) and phenyl-ethynylpyrene (solid line). Adapted from reference 26.[26]

Compared to pyrene, ethynylpyrene derivatives show a bathochromic shift in their UV-Vis absorption and fluorescence emission spectra resulting from the extended π-conjugation,[26] as

depicted in Figure 3-12, allowing a better spectral complementarity with the other selected dyes.

The synthesis of Y-Py **3-14** commenced with commercially available 1-bromo-pyrene **3-31**, which was quantitatively converted into 1-ethynylpyrene **3-32** by Sonogashira cross-coupling with TMS-acetylene. This was followed by the deprotection of the TMS group with potassium carbonate in a mixture of MeOH/THF to yield **3-33** quantitatively. In parallel, 4,4'-iodo-1,1'-biphenylpinacol boronate **3-35** was prepared by *Miyaura* borylation starting from derivative **3-34** and affording statistical amount of starting material, mono- and bis-borylated compound. A Pd-catalyzed Sonogashira cross-coupling between ethynylpyrene **3-33** and 4'-iodo-[1,1'-biphenyl]-4-(pinacol borate) **3-35** yielded compound **3-36**, which was subsequently treated with a 2M aqueous solution of HCl in THF to obtain the desired boronic acid **3-14** in 85% yield (Scheme 3-10).
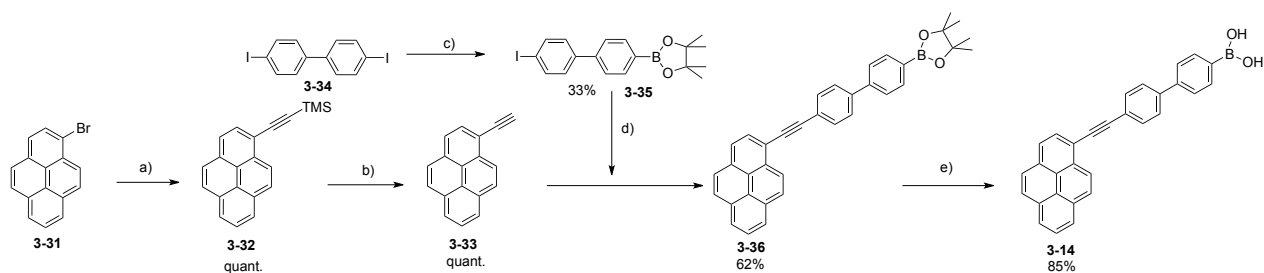
Scheme 3-10 Synthesis of Y-Py **3-14**; a) TMS-acetylene, [Pd(PPh$_3$)$_2$Cl$_2$], CuI, NEt$_3$, 70 °C, 20 h; b) K$_2$CO$_3$, MeOH/THF (1:1), rt, 20 h; c) KOAc, B$_2$Pin$_2$, [PdCl$_2$(dppf)], DMSO, 80 °C, 20 h; d) [Pd(PPh$_3$)$_2$Cl$_2$], CuI, NEt$_3$, THF, 40 °C, 6 h; e) HCl (aq, 2M)/THF (1:2), rt, 40 h.

Y-Py **3-14** and intermediates were fully characterized by melting points, infrared, ^{1}H and ^{13}C NMR spectroscopy, high-resolution mass spectrometry and the data are reported in Chapter 6. The UV-Vis absorption spectrum, reported in Figure 3-13, was recorded in DMF.
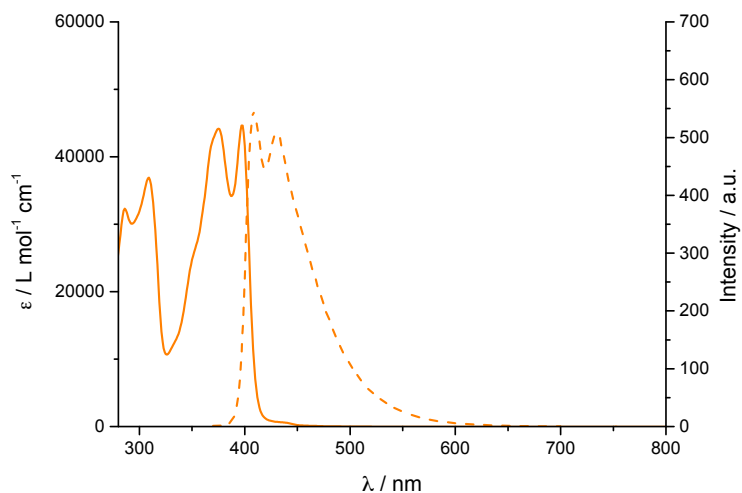
Figure 3-13 Absorption and fluorescence emission spectra (λ_{exc} = 398 nm) of Y-Py **3-14** in DMF.

It shows maxima of absorption at 398 nm (ε = 44600 L mol^{-1} cm^{-1}) and 375 (ε = 44200 L mol^{-1} cm^{-1}) nm. Besides, the fluorescence emission spectrum (λ_{exc} = 375 nm) recorded in DMF as well, shows the mirror image of the absorption spectrum. The quantum yield (determined from quinine hemisulfate salt monohydrate (QY=54.6% in 0.5 M H$_2$SO$_4$))[27] was estimated to be 68%.

Finally, the absorption and the fluorescence emission spectra of B-NDI **3-12**, R-PDI **3-13**, Y-Py **3-14** were normalized and overlapped to evaluate the complementary spectral properties of the chromophores (Figure 3-14).
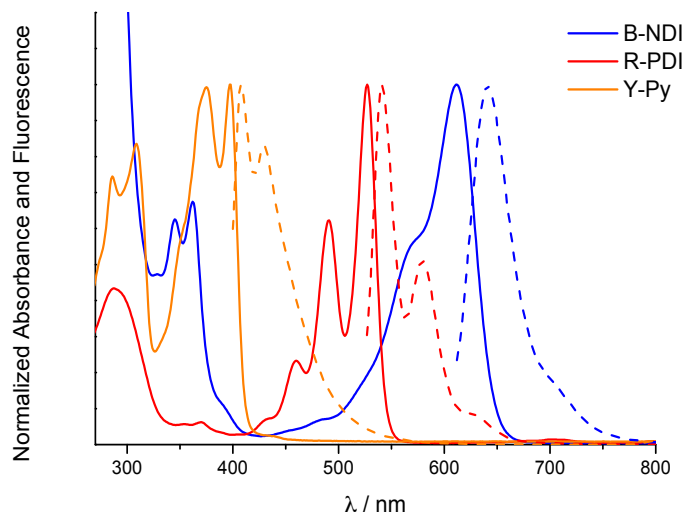
Figure 3-14 Normalized absorption (solid) and fluorescence (dashed) spectra of colored dyes Y-Py **3-14**, R-PDI **3-13**, B-NDI **3-12** in DMF.

To conclude this part, the three dyes of first generation bearing the suitable functional groups to be recognized by the peptidic scaffold were designed and successfully synthesized. They have complementary spectral properties to each other, *i.e.* the normalized fluorescence spectra of the donors (Y-Py and R-PDI) overlap with the normalized absorption spectra of the acceptors (R-PDI and B-NDI), one of the crucial prerequisites for the energy transfer to occur. So, they can be exploited in the creation of antenna systems.

3.2.4 Chromophore assembly on the peptidic scaffold

Having in hands the peptidic scaffold **3-1** bearing the different receptor sites and the three dyes with the suitable functionalities to be selectively recognized by the peptide; the objective of this section is to investigate the recognition capabilities between the chromophores and the functionalized peptide.

3.2.4.1 Chromophore assembly

The three chromophores were simultaneously assembled into peptide **3-1** by simply mixing the dyes Y-Py **3-14**, R-PDI **3-13** and B-NDI **3-12** with **3-1** at rt in the presence of *m*-PDA in anhydrous DMF, as presented in Scheme 3-11. Separation by gel permeation chromatography (GPC), also called size exclusion chromatography (SEC) (Figure 3-15 Left), afforded colored YRB-peptide **3-37** as pure material, whose structure was confirmed by mass spectrometry. The HR-MALDI-TOF analysis, reported in Figure 3-16, shows $[M+Na]^+$ peak at m/z = 5173.2615 in accordance with the calculated mass for $[C_{265}H_{315}BN_{46}O_{56}F_2NaS_2]^+$: 5173.2261. Moreover, other peaks have been identified corresponding to the product after hydrolysis of the boronate ester or/and cleavage of the disulfide occuring during the ionization process; the presumable products are summarized in Table 3-3.
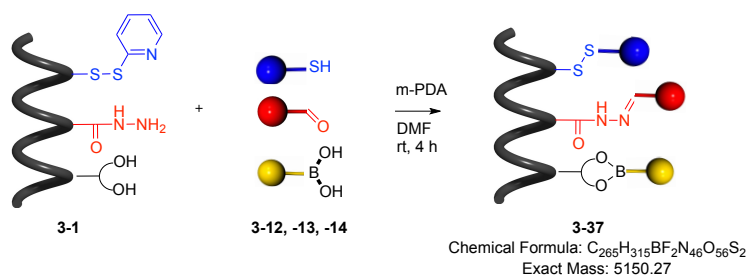
Scheme 3-11 Synthesis of peptide **3-37** by one-pot reaction.
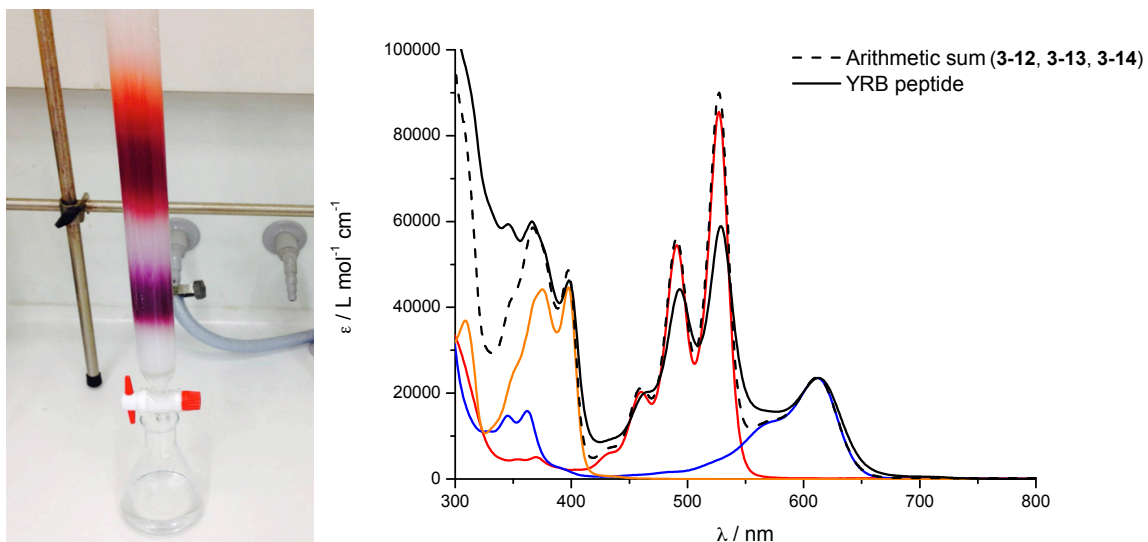
Figure 3-15 Left) Purification of peptide **3-37** by Gel Permeation Chromatography; Right) Normalized absorption spectra of peptide **3-37** with arithmetic sum of dyes **3-12, 3-13** and **3-14** absorption on B-NDI (612 nm) in DMF.

Table 3-3 Peaks found in MALDI/Tof analysis of **3-37.**

Entry	m/z	Formula $[M + Na]^+$	Comments
1	5173.2	$[C_{265}H_{315}BF_2N_{46}NaO_{56}S_2]^+$	Expected product
2	4787.1	$[C_{235}H_{300}F_2N_{46}NaO_{56}S_2]^+$	Boronate ester hydrolysis
3	4196.8	$[C_{212}H_{255}BF_2N_{42}NaO_{44}S]^+$	Disulfide cleavage
4	3810.6	$[C_{182}H_{240}F_2N_{42}NaO_{44}S]^+$	Disulfide cleavage and boronate hydrolysis

Figure 3-16 MALDI-Tof analysis of peptide **3-37**; Inset: zoom of $[M + Na]^+$ peak (bottom-right) compared with the calculated mass (top-right).

The positive outcome of the reaction was also confirmed by UV-Vis measurement in DMF (Figure 3-15 Right). The triad **3-37** absorbs throughout the entire visible spectrum with distinct peaks at 376, 398, 495, 527, 612 nm, characteristic of the Y-Py, R-PDI and B-NDI chromophoric units, respectively (Figure 3-15 Right). By normalizing the absorption spectrum of YRB-peptide and the arithmetic sum of the three dyes absorption on B-NDI (at 612 nm), a good correlation of the spectra was observed. Notably, a significant hypochromism of the R-PDI bands was noticed, which is possibly due to the formation of H-type complexes. Indeed, the stacking of planar π-systems of PDI is well known in the literature particularly in the crystal structure, but also in solution. *Würthner* and coworkers described that upon aggregation of a flat PDI, by increasing the concentration of a solution (from 10^{-7} to 10^{-5} M in methylcyclohexane), strong hypochromism is

observed in the UV-Vis absorption spectra until almost complete loss of fine structure as shown in Figure 3-17.[18, 28]
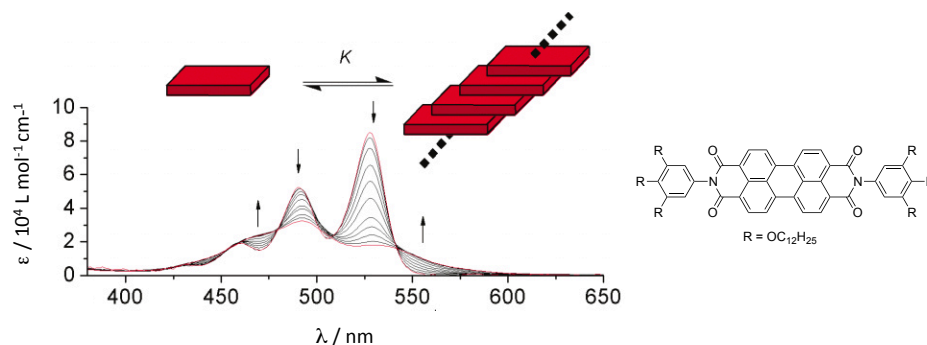
Figure 3-17 Concentration-dependent UV-Vis spectra of PDI derivative recorded in MCH (methylcyclohexane): arrows indicate changes upon increasing concentration. Concentration range 10^{-7} – 10^{-5} M. Adapted from reference 18 with permission. Copyright (2004) Royal Society of Chemistry.[18]

In our case, the reported absorption spectrum was recorded in DMF at 5.1 µM, which could explain that YRB-peptide is sensitive of aggregation phenomena. By decreasing the concentration, no effect in the ratio of absorbance at the maximum of absorption of the different chromophoric units ($Abs_{529\ nm}$/ $Abs_{613,\ 493\ or\ 398}$) was observed (Figure 3-18).
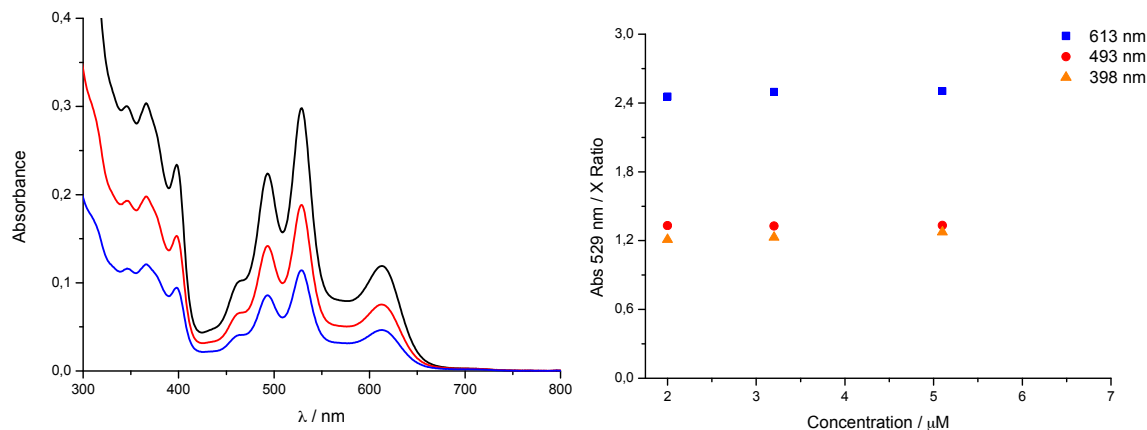
Figure 3-18 Left: Absorption spectra of **3-36** (C = 5.1 µM, 3.2 µM and 2 µM in DMF); Right: Ratio of absorbance at 529 nm and 613 nm (blue square), 493 nm (red round), 398 nm (orange triangle) at different concentrations in DMF.

Moreover, in order to study possible aggregation phenomena, variable temperature experiments were carried out in DMF. The solution was heated gradually from 25 to 95 °C (spectrum was recorded each 10 °C); subsequently cooled at 25 °C and gradually cooled from 25 °C to 5 °C (spectrum was recorded each 10 °C), but no significant change was observed for the PDI absorption bands. Only the maximum absorption bands attributed to the ethynylpyrene unit around 376 and 398 nm showed a hypochromic shift by increasing the temperature (Figure 3-19).
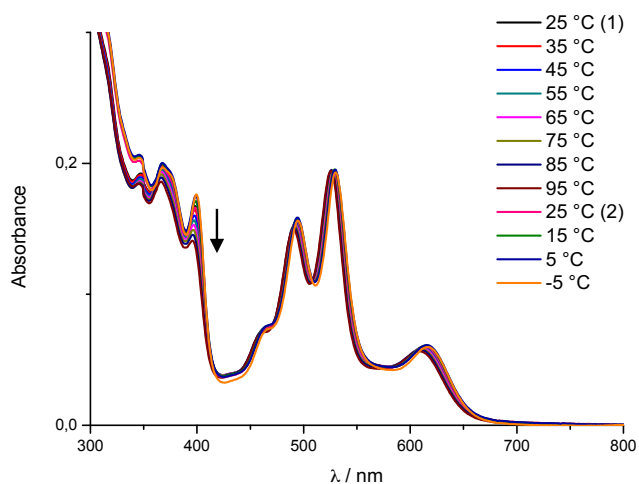
Figure 3-19 Absorption spectra of peptide **3-37** in DMF (3.2 μM) at different temperatures. The arrow indicates changes upon increasing temperature.

3.2.4.2 Estimation of the energy transfer efficiency by fluorescence spectroscopy

The energy transfer (ET) process for the triad was investigated using steady-state fluorescence spectroscopy. Excitation measurements indicated that all dyes contribute to the emission of the lowest-energy acceptor unit, B-NDI (λ_{em} = 640 nm), confirming the ET from R-PDI to B-NDI and from Y-Py to B-NDI either by direct or stepwise ET cascade (Figure 3-20). The quantum yield of the acceptor unit B-NDI (QY$_{B\text{-}NDI}$) within YRB peptide by direct excitation (λ_{exc} = 609 nm) was determined to be 27%. Upon selective excitation of the donor units R-PDI (λ_{exc} = 495 nm) and Y-Py (λ_{exc} = 398 nm), QY$_{B\text{-}NDI}$ were evaluated to be 1.5% and 1.4%, respectively (Figure 3-21 a). By calculating the ratio of the QY$_{B\text{-}NDI}$ upon indirect and direct excitation, the energy transfer efficiency Φ_{ET} from the donor to the acceptor was estimated to be 5% and 5.6% for the Y-Py→B-NDI and R-PDI→B-NDI sensitization, respectively. The *QY* of B-NDI unit were determined using *N,N'*-di(2,6-diisopropylphenyl)-1,6,7,12-tetraphenoxyperylene-3,4:9,10-tetracarboxylic acid bisimide (QY = 96% in CHCl$_3$) as a reference.[17]
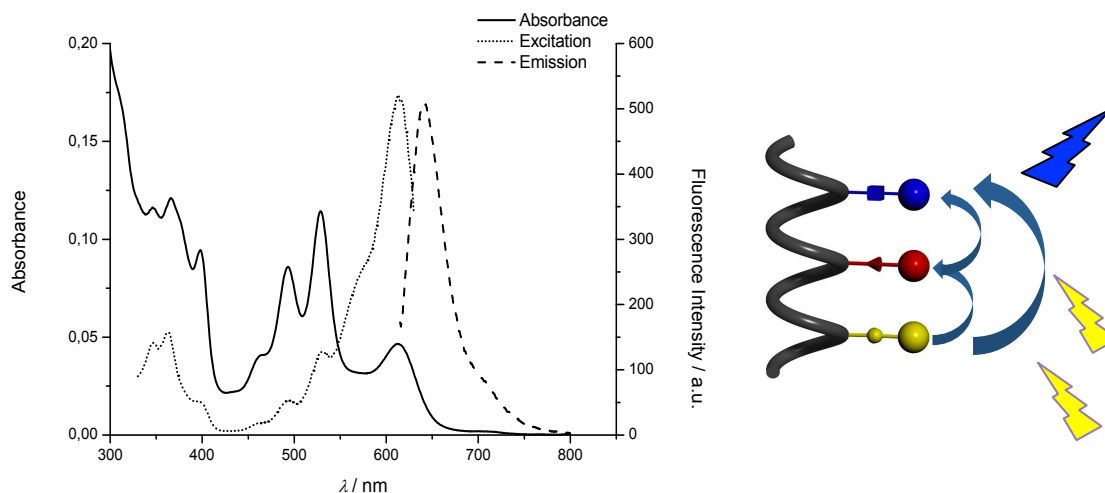
Figure 3-20 Left: Absorption (solid line), emission (long-dashed line, λ_{exc} =609 nm), and excitation profiles (short-dashed line, λ_{em} = 640 nm) for peptide **3-37** in DMF, C = 2 μM. Right: Schematic representation of ET from R-PDI to B-NDI and from Y-Py to B-NDI either by direct or stepwise ET cascade.
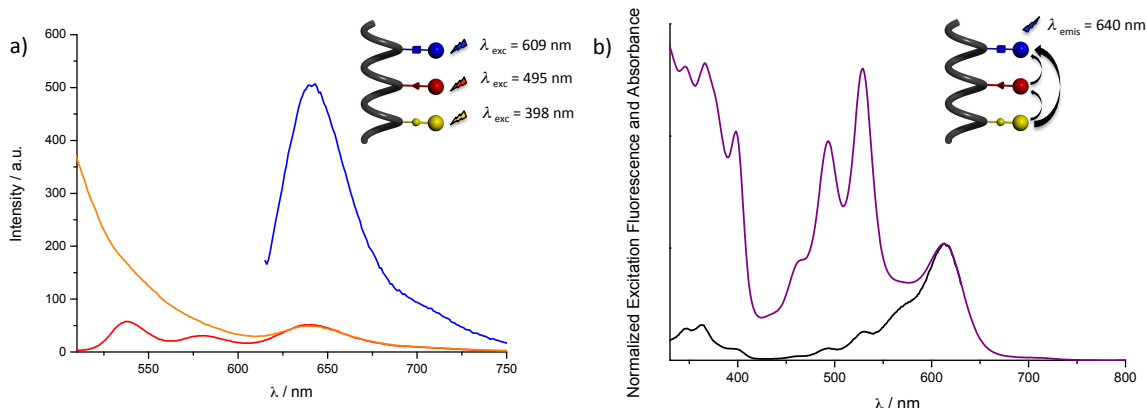
Figure 3-21 a) Fluorescence emission spectra of **3-37** at (λ_{exc}) 398 nm, 495 nm, 609 nm in DMF (C = 2 μM). b) Normalized absorption (in purple) and fluorescence excitation (in black) spectra (λ_{emis} = 640 nm) of YRB peptide **3-37** in DMF.

To validate our hypothesis, Φ_{ET} was determined upon comparison of the absorption and excitation spectra, both normalized at the maximum absorption wavelength of blue chromophore unit B-NDI (λ_{max} = 612 nm), by using the equation $\Phi_{ET} = Ex_D/A_D$, where Ex_D and A_D are fluorescence intensity and absorption of the donor in the normalized excitation and absorption spectra, respectively. The efficiencies were estimated to be 5% and 5.4% for Y-Py→B-NDI and R-PDI→B-NDI, respectively, in agreement with the previous experimental measurements (Figure 3-21 b).

Considering the low energy transfer efficiencies, the secondary structure of the peptide before and after the chromophoric assembly was investigated. Among all the methods for structural analysis of polypeptides allowing the determination of their secondary structure, (including infrared, NMR spectroscopy, X-ray crystallography), circular dichroism (CD) is the most used.

3.2.4.3 Circular Dichroism

Linear polarized light consists of two circularly polarized components of equal intensity by opposite sense of rotation (left and right-handed). When it passed through an optically active medium, the speed of light differs from the left and the right circular components and so the optical rotatory dispersion of an enriched optically active compound can be measured. However, not only this parameter changes but also the extinction of chiral chromophores. Circular dichroism (CD) spectroscopy detects the difference of absorption of the left- and right-circular polarized components, also called ellipticity, depending of the wavelength. CD is widely used to determine the secondary structure of a polypeptide since when circular polarized light is passed through it, the electronic transitions of its chromophores, especially the amide groups, give rise to characteristic bands in specific region of the CD spectra. Two electronic transitions of the amide chromophore are characteristic: *(i)* the n-π* transition occurring as a negative band around 220 nm, and *(ii)* the π–π* transition, stronger, observed as a positive band around 192 nm and a negative band around 210 nm (Figure 3-8). The α-helix conformation is characterized by two negative bands at 222 nm and 208 nm, and a positive band at 192 nm. β-sheets display a negative band at 216 nm and a positive at 195 nm, while the random coil conformation is characterized only by a negative CD band just below 200 nm.[1a, 6] An example is reported in Figure 3-22, showing the CD curves of three proteins: myoglobin, β-lactoglobulin and ferredoxin, whose X-ray crystallographic structures have shown high proportion of α-helix, β-sheet and random coil form respectively.[6]
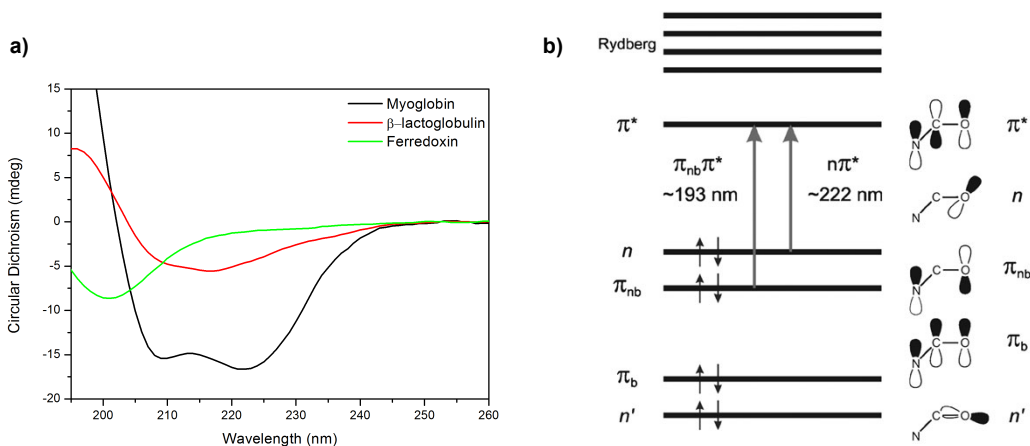
Figure 3-22 a) Characteristic CD curves of the secondary structure elements. Myoglobin (PCDDBID: CD0000047000) contains high proportion of α-helix; β-lactoglobulin (PCDDBID: CD000001100) contains a high proportion of β-sheet; ferredoxin (PCDDBID: CD0000032000) is in random coil form; b) electronic transitions of the amide group in the far-UV region. The molecular orbitals shown are the bonding, non-bonding and anti-bonding π orbitals (π$_{bo}$, π$_{nb}$ and π*), and the lone pairs of the O atom (n and n'). Adapted from reference 6 with permission. Copyright (2007) Royal Society of Chemistry.[6]

Taking this into consideration, peptidic scaffold **3-1** was analyzed by circular dichroism in water/CH$_3$CN (3:1, C = 51 μM). The recorded spectrum, reported in Figure 3-23 in black, shows that the peptidic scaffold adopts a α-helix conformation, proven by the presence of the positive band at 192 nm and two negative ones at 208 and 222 nm. Its α-helix content was estimated to be 87% after deconvolution of the spectrum by the algorithm CONTINLL (Table 3-4 Entry 1).[29] Moreover, when water was partially replaced by the helix inducing solvent trifluoroethanol (TFE),[30] the helicity of the peptide was not improved, proving the high inherent helicity of **3-1** (Figure 3-23 and Table 3-4).
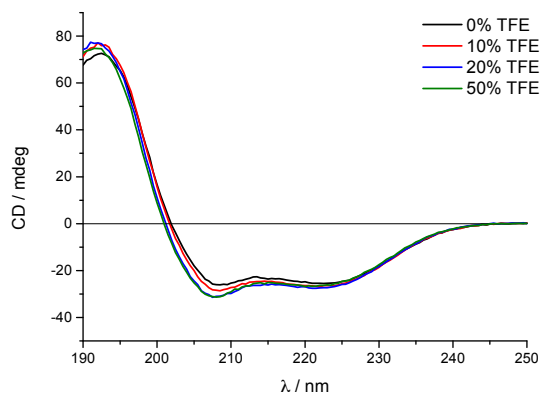
Figure 3-23 Circular Dichroism analysis of peptide **3-1** in CH$_3$CN/H$_2$O (1:1, C$_0$ = 102 μM) dissolved in water and/or TFE (C$_1$ = 51 μM).

Table 3-4 Content of secondary structure elements for **3-1** determined by CONTINLL

Entry	Conditions	% α-helix	% β-sheet	% random coil
1	0% TFE	87	1	12
2	10% TFE	89	1	10
3	20% TFE	89	1	10
4	50% TFE	87	1	12

Furthermore, the secondary structure of peptide **3-37** was investigated in order to know if the helical structure was maintained after the incorporation of the dyes. In this respect, circular dichroism spectra were recorded in TFE/milli-Q water. These solvents have been chosen for their low cut-off (190 nm), which allow seeing the transitions of the secondary structure, and their ability to solubilize the peptide. The CD spectra, reported in Figure 3-24, shows that peptide YRB **3-37** adopts an helical structure, indicated by the positive band at 192 nm and the two negative one at 208 and 222 nm. By reducing the concentration of TFE up to the limit of solubility, no significant changes have been observed in the helical profile: α-helix content was estimated to be 78% in pure TFE and in TFE/water 33/66 (Table 3-5). Additionally, the spectra were recorded

over the wavelength range 190-700 nm, in order to see if the chirality was induced to the chromophoric region. No any or negligible Cotton Effect was observed, probably due to the important distance between the chromophores and the stereogenic centers (Figure 3-24).
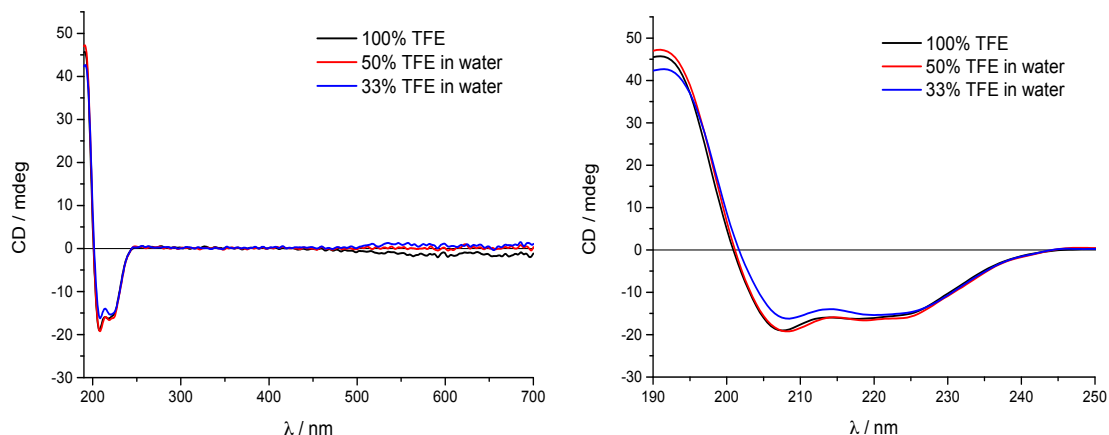
Figure 3-24 Circular dichroism analysis of peptide **3-37**.

Table 3-5 Content of secondary structure elements for **3-37** determined by CONTINLL.

Entry	Conditions	% α-helix	% β-sheet	% random coil
1	100% TFE	78	4	18
2	50% TFE in water	82	2	16
3	33% TFE in water	78	4	18

3.2.4.5 Molecular Dynamic simulation of colored peptide

Molecular Dynamic (MD) simulations (55 ns) of YRB peptide **3-37** were performed in order to deeply understand the arrangement of the three chromophores attached to the peptidic scaffold.[8] Simplified structures of the chromophores were modelled without the polyethyleneglycol chains assuming the negligible effect of the solubilizing substituents. Figure 3-25 shows that the chromophoric units are confined in defined conformational spaces in which red, blue and yellow regions are easily discerned. Notably, in the most stable conformation, the red and blue units are facing to each other through H type complexes, supporting the hypochromism observed for the R-PDI bands in the UV-Vis absorption spectrum (Figure 3-26 b).
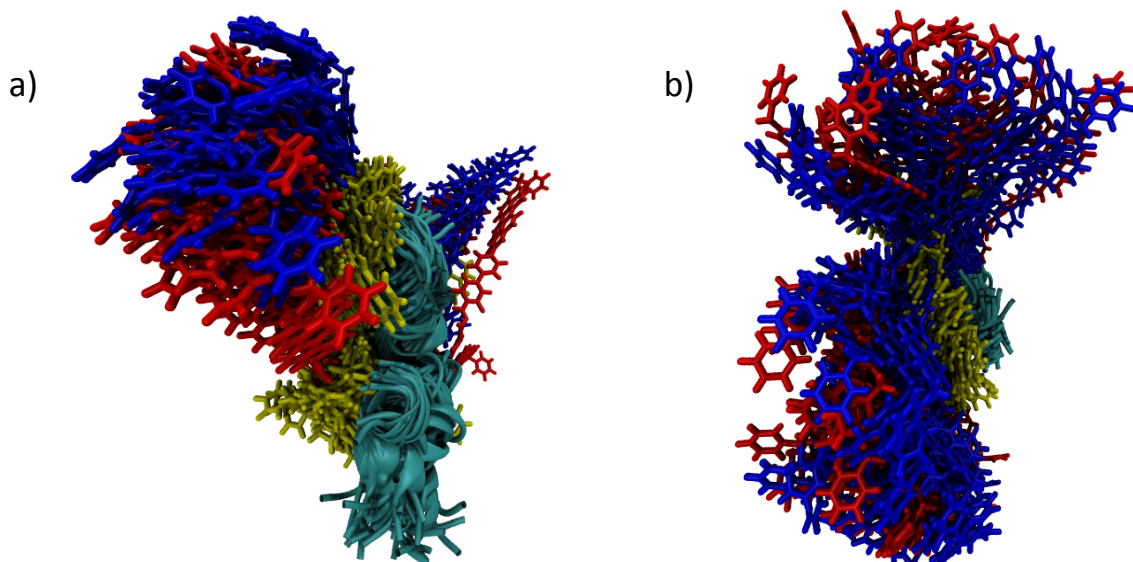
Figure 3-25 MD simulations (55 ns) of YRB peptide. a) side and b) top view of 500 overlaid frames.

The most stable conformation (at the 53 ns) and the conformation from the last snapshot at 55 ns of the MD trajectory were characterized by visualizing its torsion angles φ, ψ in the Ramachandran plots (Figure 3-27). It results that the most stable conformation unveils 84.2% of residues in the favoured α-helix region (bottom left square within the sky blue region marked with black dots), significantly higher than the 73.7% observed for the last snapshot of the simulation. This nicely demonstrates that the most stable conformation corresponds to the one with higher number of residues in the α-helix region.
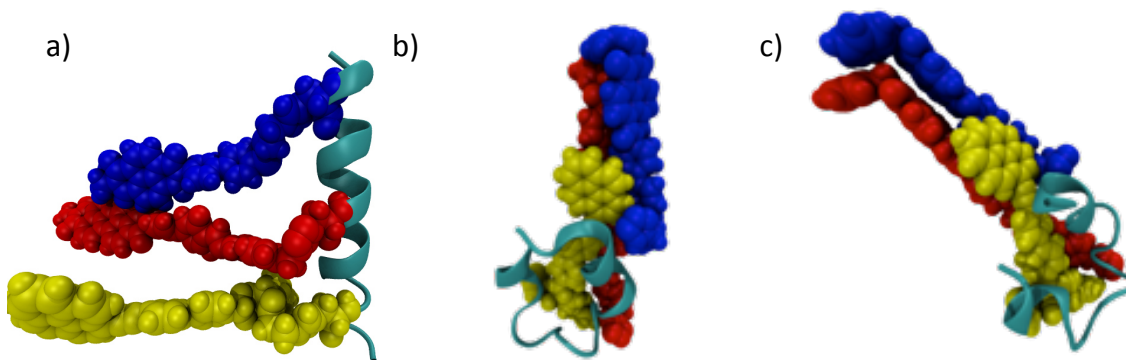
Figure 3-26 Side views of YRB peptide at a) t = 0 ns; b) t = 53 ns, most stable conformation (E_{tot} = -1001 kcal/mol); c) t = 55 ns, in the last snapshot of the simulation.
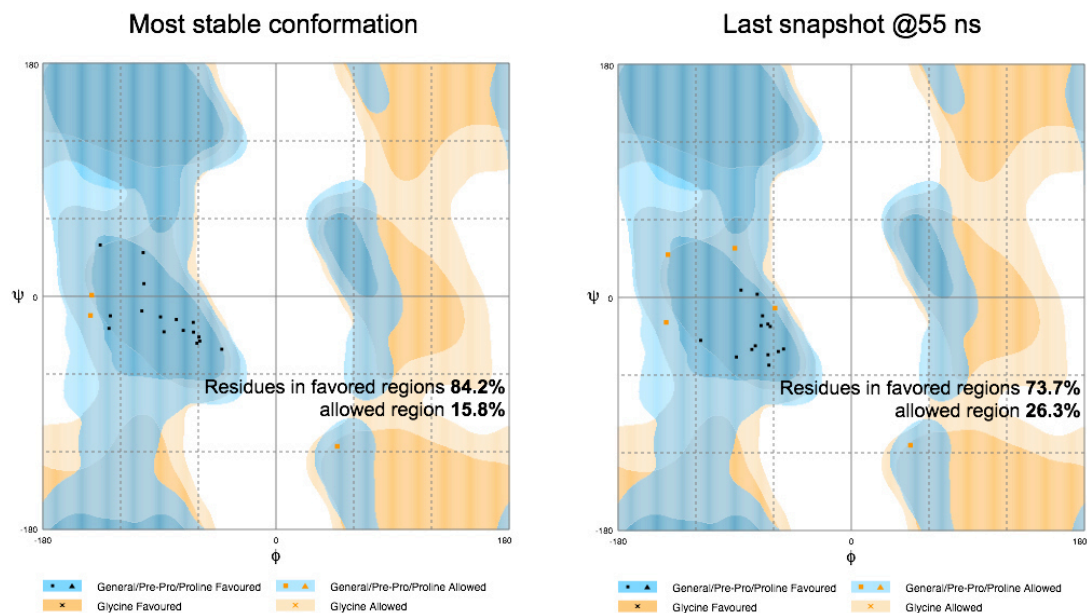
Figure 3-27 Ramachandran plots with the % of residues in favored (black dots) and allowed (orange dots) region for the most stable conformation (left) and the last snapshot of the 55 ns trajectory (right).

3.3 Conclusions

In summary, we have engineered the first orthogonal multireaction system consisting of simultaneous disulfide exchange, boronate and acyl hydrazone formation. The exploitation of this methodology allowed the simultaneous organization of tailored blue, red and yellow chromophores on a pre-programmed α-helix peptide. The energy transfer efficiencies Φ_{ET} within the multichromophoric structure from the primary donor Y-Py to the acceptor B-NDI and from the intermediate donor R-PDI to B-NDI were estimated to be 5% and 5.5% respectively by steady-state fluorescence measurements as recapitulated in Figure 3-28. The low Φ_{ET} are possibly due to the chromophores by themselves exhibiting moderate to low quantum yields and not ideal spectral overlap, or their spatial arrangement which might favor mechanism of fluorescence quenching other than energy transfer such as contact quenching. The proof-of-concept put forward in this chapter, and published, allows the bottom-up approach of multichromophoric architectures exhibiting any desired absorbed or emitted colors, enabling unlimited surfing through the color coordinate diagram (Figure 3-29). In this respect, the versatility of the approach will be exploited in *Chapter 4* allowing the creation of various new multichromophoric architectures with better light harvesting capabilities.
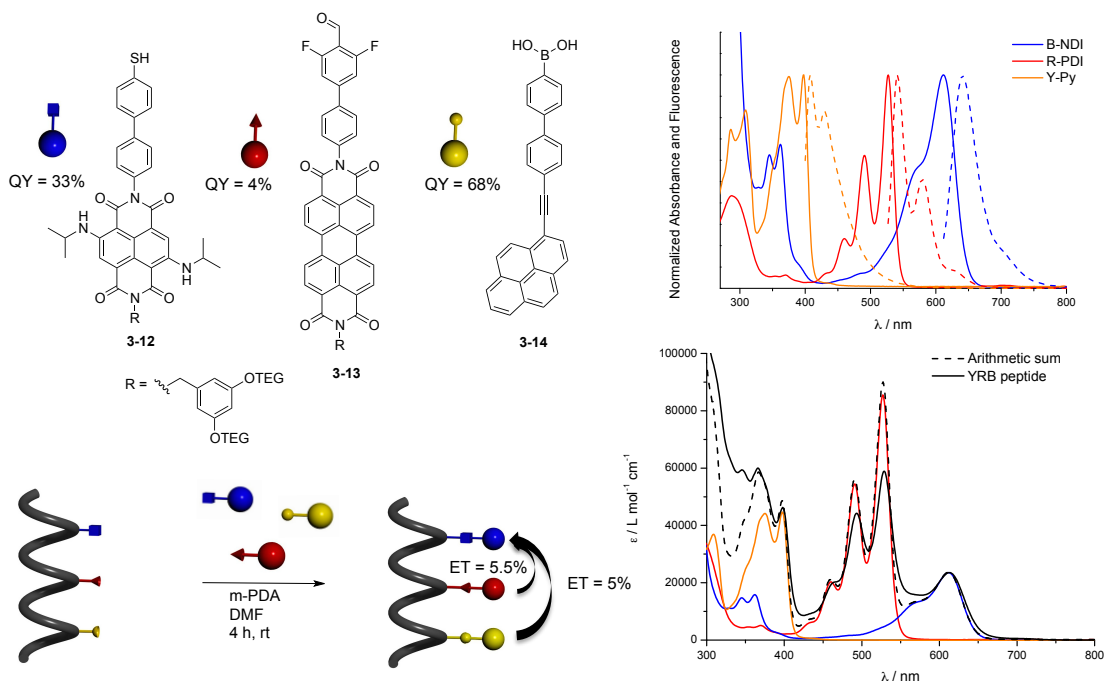
Figure 3-28 Top left: three color emitters: B-NDI **3-12**, R-PDI **3-13**, Y-Py **3-14**; top right: normalized absorption (solid) and fluorescence (dashed) spectra of the 3 color emitters; bottom left: colored assembly on the scaffold giving YRB peptide; bottom right: absorption spectrum of YRB peptide **3-37** normalized with arithmetic sum of the absorption spectra of color emitters **3-12**, **3-13**, **3-14** on B-NDI.

A Journal of the Gesellschaft Deutscher Chemiker

Angewandte

GDCh

International Edition

Chemie

www.angewandte.org

2015–54/52

WILEY-VCH
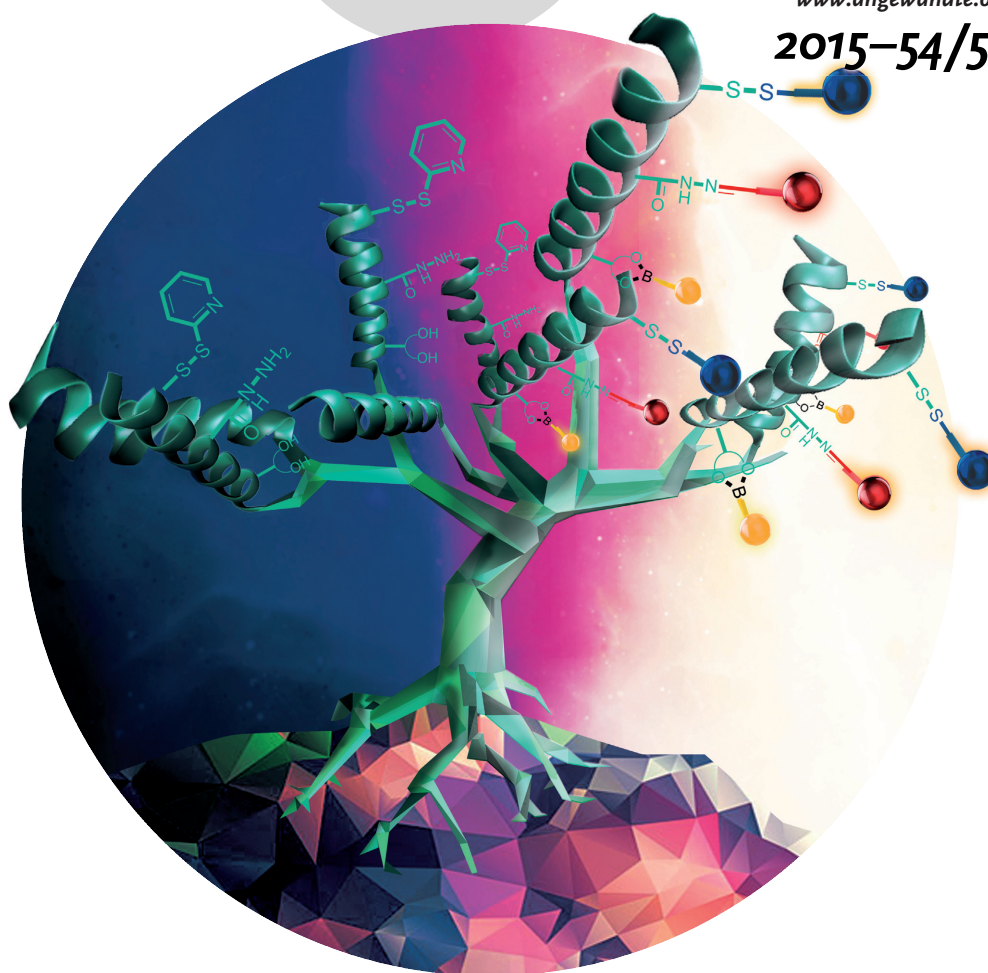
The development of ...

… easy-to-implement protocols to spatially organize chromophores for mimicking natural antennae is a challenging task. In their Communication on page 15739 ff., D. Bonifazi et al. report on the organization of chromophores through the simultaneous use of three orthogonal dynamic covalent reactions: disulfide exchange, and boronate and acyl hydrazone formation. This methodology enables the creation of multichromophoric architectures with tailored absorption or emission wavelengths.

Figure 3-29 Inside Cover: Templated Chromophore Assembly by Dynamic Covalent Bonds (Angew. Chem. Int. Ed. 52/2015). Reprinted from reference 8. Copyright (2015) John Wiley and Sons.

3.4 References

[1] a) N. Sewald, H. D. Jakubke, *Peptides: Chemistry and Biology: Second Edition*, **2009**; b) L. A. Moran, R. A. Horton, G. Scrimgeour, M. Perry, *Principles of Biochemistry (5th Edition)*, Pearson, **2012**.

[2] G. N. Ramachandran, V. Sasisekharan, *Adv. Protein Chem.* **1968**, *23*, 283-438.

[3] **"**http://www.nslc.wustl.edu/**, 2015**.

[4] L. Pauling, R. B. Corey, *Proc. Natl. Acad. Sci. U. S. A.* **1951**, *37*, 241-250.

[5] J. M. Scholtz, R. L. Baldwin, *Annu. Rev. Biophys. Biomol. Struct.* **1992**, *21*, 95-118.

[6] B. M. Bulheller, A. Rodger, J. D. Hirst, *Phys. Chem. Chem. Phys.* **2007**, *9*, 2020-2035.

[7] H. Q. Peng, L. Y. Niu, Y. Z. Chen, L. Z. Wu, C. H. Tung, Q. Z. Yang, *Chem. Rev.* **2015**, *115*, 7502-7542.

[8] L. Rocard, A. Berezin, F. De Leo, D. Bonifazi, *Angew. Chem. Int. Ed.* **2015**, *54*, 15739-15743.

[9] S. Marqusee, V. H. Robbins, R. L. Baldwin, *Proc. Natl. Acad. Sci. U. S. A.* **1989**, *86*, 5286-5290.

[10] J. M. Scholtz, E. J. York, J. M. Stewart, R. L. Baldwin, *J. Am. Chem. Soc.* **1991**, *113*, 5102-5104.

[11] E. Atherton, H. Fox, D. Harkiss, C. J. Logan, R. C. Sheppard, B. J. Williams, *J. Chem. Soc., Chem. Commun.* **1978**, 537-539.

[12] N. Sakai, J. Mareda, E. Vauthey, S. Matile, *Chem. Commun.* **2010**, *46*, 4225-4237.

[13] a) B. A. Jones, A. Facchetti, M. R. Wasielewski, T. J. Marks, *Adv. Funct. Mater.* **2008**, *18*, 1329-1339; b) F. Würthner, M. Stolte, *Chem. Commun.* **2011**, *47*, 5109-5115; c) X. Zhan, A. Facchetti, S. Barlow, T. J. Marks, M. A. Ratner, M. R. Wasielewski, S. R. Marder, *Adv. Mater.* **2011**, *23*, 268-284.

[14] C. W. Marquardt, S. Grunder, A. Blaszczyk, S. Dehm, F. Hennrich, H. von Loehneysen, M. Mayor, R. Krupke, *Nat. Nanotechnol.* **2010**, *5*, 863-867.

[15] a) S. Bhosale, A. L. Sisson, P. Talukdar, A. Fuerstenberg, N. Banerji, E. Vauthey, G. Bollot, J. Mareda, C. Roeger, F. Würthner, N. Sakai, S. Matile, *Science* **2006**, *313*, 84-86; b) R. S. K. Kishore, O. Kel, N. Banerji, D. Emery, G. Bollot, J. Mareda, A. Gomez-Casado, P. Jonkheijm, J. Huskens, P. Maroni, M. Borkovec, E. Vauthey, N. Sakai, S. Matile, *J. Am. Chem. Soc.* **2009**, *131*, 11106-11116.

[16] A. A. Berezin, A. Sciutto, N. Demitri, D. Bonifazi, *Org. Lett.* **2015**, *17*, 1870-1873.

[17] G. Seybold, G. Wagenblast, *Dyes Pigm.* **1989**, *11*, 303-317.

[18] F. Würthner, *Chem. Commun.* **2004**, 1564-1579.

[19]   W. Herbst, K. Hunger, *Industrial Organic Pigments, 2nd completely revised ed.*, Wiley-VCH, Weinheim, **1997**.

[20]   M. Cotlet, T. Vosch, S. Habuchi, T. Weil, K. Müllen, J. Hofkens, F. De Schryver, *J. Am. Chem. Soc.* **2005**, *127*, 9760-9768.

[21]   F. Würthner, C. R. Saha-Moeller, B. Fimmel, S. Ogi, P. Leowanawat, D. Schmidt, *Chem. Rev.* **2016**, *116*, 962-1052.

[22]   a) X. Zhang, Z. Chen, F. Würthner, *J. Am. Chem. Soc.* **2007**, *129*, 4886-4887; b) R. F. Kelley, M. J. Tauber, M. R. Wasielewski, *J. Am. Chem. Soc.* **2006**, *128*, 4779-4791.

[23]   Z. J. Chen, L. M. Wang, G. Zou, L. Zhang, G. J. Zhang, X. F. Cai, M. S. Teng, *Dyes Pigm.* **2012**, *94*, 410-415.

[24]   F. Würthner, V. Stepanenko, Z. Chen, C. R. Saha-Möller, N. Kocher, D. Stalke, *J. Org. Chem.* **2004**, *69*, 7933-7939.

[25]   T. M. Figueira-Duarte, K. Müllen, *Chem. Rev.* **2011**, *111*, 7260-7314.

[26]   P. E. Gama, R. J. Corrêa, S. J. Garden, *J. Lumin.* **2015**, *161*, 37-46.

[27]   A. M. Brouwer, *Pure Appl. Chem.* **2011**, *83*, 2213-2228.

[28]   F. Würthner, C. Thalacker, S. Diele, C. Tschierske, *Chem. Eur. J.* **2001**, *7*, 2245-2253.

[29]   S. W. Provencher, J. Glöckner, *Biochemistry* **1981**, *20*, 33-37.

[30]   J. W. Nelson, N. R. Kallenbach, *Proteins: Struct., Funct., Genet.* **1986**, *1*, 211-217.

4. Structural evolution of the antenna: Toward efficient energy transfer

In *Chapter 3*, the preparation of a pre-programmed α-helix peptide Ac-QLA-**X(disulfide)**-QLAQLA-**X(hydrazide)**-QLAQLA-**X(diol)**-QLA-CONH$_2$ **3-1** bearing receptor sites on a modified glycine each (*i, i+7*) residues, and the synthesis of color emitters (ethynyl pyrene Y-Py, perylene diimide R-PDI, naphthalene diimide B-NDI) with suitable functional groups were reported.[1] The assembly of the dyes on the peptidic scaffold afforded a multichromophoric architecture, called YRB peptide, showing energy transfer efficiencies (Φ_{ET}), which have been estimated to be 5% and 5.6% for the Y-Py→B-NDI and R-PDI→B-NDI sensitization, respectively. This chapter will focus on the improvement of the energy transfer within the colored peptide. To achieve this, different approaches can be followed consisting in modifying the chromophores or changing the scaffold to play with the spatial organization of the dyes.

The chapter will be divided in three parts: *i)* in *Section 4.1.1*, a second generation of dyes will be developed and its assembly into the peptide will be investigated; *ii)* in *Section 4.1.2*, modifications on the peptidic scaffold will be made and their effect on the energy transfer will be studied; *iii)* finally, *Section 4.1.3* will focus on a effect of the solvent on the energy transfer.

For his help in the preparation of R-PDI **4-2** and peptidic scaffolds **4-17** and **4-18**, described in *Section 4.1.1* and *4.1.2*, *Lorenzo Luciani (University of Perugia, Italy)* who did his Master thesis under my supervision, is kindly acknowledged. Moreover, I would like to thank *Dr Andrea Fermi (Cardiff University)* for the cyclovoltametric and fluorescent lifetime measurements of dyes reported in *Section 4.2.1*.

Considering the low energy transfer efficiencies determined in *Chapter 3* within the multichromophoric peptide **3-37**, the general aim of this chapter is to exploit the versatility of the synthetic template approach to build new antenna systems with better light-harvesting capabilities. Indeed, an unlimited number of multichromophoric architectures can be easily obtained by performing the self-assembly with new dyes from the same scaffold. On the other hand,

modifications can be as well applied to the scaffold to change the spatial organization of the dyes and so the emitting profiles of the multichromophoric structure.

Hence, to improve the energy transfer within the peptidic antenna, different parameters can be optimized. Indeed, as introduced in the first chapter, the rate of energy transfer K_T according to the Förster theory (FRET) is defined by Equation (1).

$$K_{T\,(r)} = \frac{1}{\tau_D} \left(\frac{r_0}{r}\right)^6 \qquad (1)$$

Where τ_D is the fluorescent lifetime of the donor in the absence of the acceptor, r is the interchromophoric distance and r_0 is the critical distance between the chromophores for which their energy transfer efficiency is equal to 50%. r_0 is calculated following Equation (2).

$$r_0 = 9.78 \text{ x } 10^3 \left[k^2 n^{-4} Q_D J(\lambda)\right]^{1/6} \text{ (in Å) (2)}$$

Where k^2 described the transition dipole orientation, n is the refractive index of the medium, Q_D is the quantum yield of the donor fluorescence in the absence of the acceptor, and $J(\lambda)$ is the integral of the normalized spectral overlap between the donor emission and the acceptor absorption.

Accordingly, first of all, the chromophores have to be optimized. In *Section 4.1.1*, a new generation of dyes will be designed and synthesized with improved normalized spectral overlap $J(\lambda)$ between donor emission and acceptor absorption and optimized donor quantum yields Q_D and will be introduced into the peptide.

i) Second generation of dyes: optimization of Q_D and $J(\lambda)$

ii) Scaffold modification: position and structure of receptor sites

iii) Assembly: improvement of the conditions
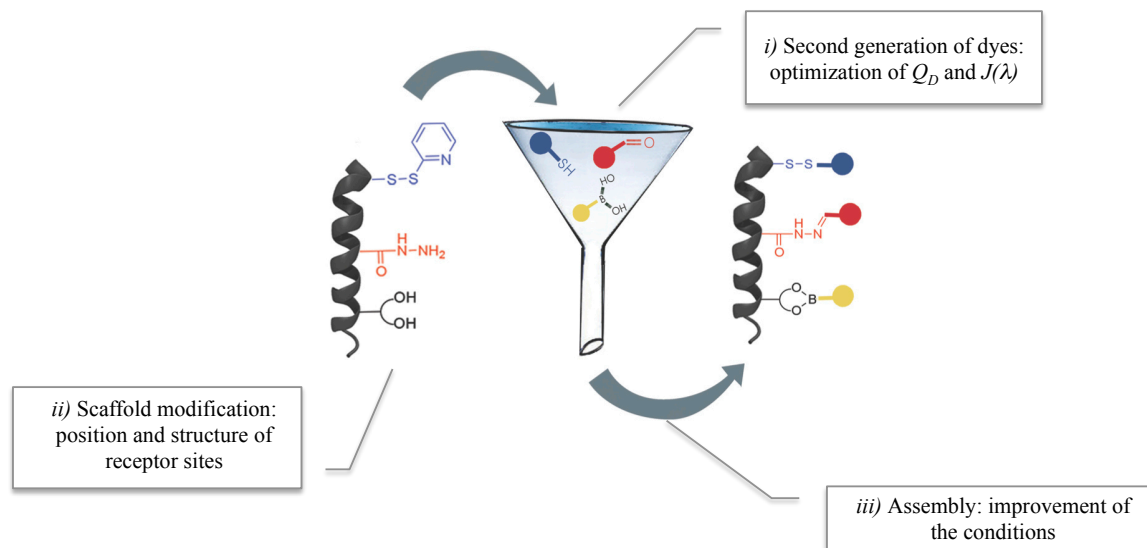
Figure 4-1 Strategies for energy transfer improvement: optimization of *i)* chromophores, *ii)* position and structure of receptor sites on the peptidic backbone, *ii)* assembly conditions.

Moreover, in *Section 4.1.2,* the scaffold will be modified to optimize the spatial arrangement of the dyes. In this respect, the effect on the energy transfer of the distance r between the chromophores,

their order and their dipole orientation will be investigated (Figure 4-1). Finally, the effect of the solvent of the reaction and analyses on the energy transfer will be studied in *Section 4.2.3*.

4.1 Results and discussion

4.1.1 Development of a new generation of chromophores and colored assembly

The low energy transfer between the chromophores can result in the small-normalized spectral overlap between the fluorescence emission of Y-Py **3-14** and R-PDI **3-13** absorption, as it can be observed in Figure 4-2.
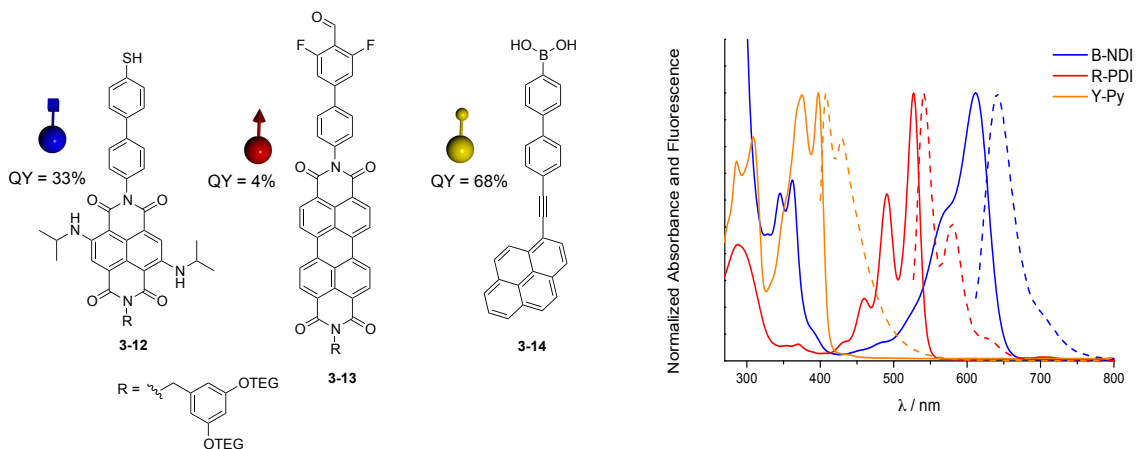
Figure 4-2 Left: First generation of color emitters: B-NDI **3-12**, R-PDI **3-13**, Y-Py **3-14**; right: normalized absorption (solid) and fluorescence (dashed) spectra of the 3 color emitters.

Accordingly, another yellow dye red-shifted compared to the previous ethynylpyrene was targeted: a perylene derivative, so-called Y-Per **4-1**. Perylene is a polycyclic aromatic hydrocarbon (PAH) and has been widely applied for organic electronics and photovoltaics for its great chemical, thermal and photochemical stability.[2] The optical properties of the perylene make it a suitable candidate for our system since it absorbs strongly in the blue region with a molar extinction coefficient of $\varepsilon = 38500$ L mol^{-1} cm^{-1} at 434 nm, and is highly fluorescent with a small Stokes shift and a high quantum yield (QY=98%).[3] Regarding the design of Y-Per **4-1** (reported in Figure 4-3), as in R-PDI and B-NDI, biphenyl chain will be introduced as a linker between the chromophoric unit and the functional group used to recognize the peptide, *i.e.* the boronic acid. This should induce a slight red-shifted absorption and emission maximum, making the targeted molecule ideal for our purpose.[4]

On the other hand, for the improvement of the Φ_{ET}, a second strategy can be envisaged consisting in re-designing R-PDI **3-13**. Indeed, the previously reported R-PDI, in which a benzyl group bearing monomethoxy triethyleneglycol (TEG) chains was introduced to increase the solubility, was poorly soluble and its quantum yield was estimated to be 4%. Perylene bisimides are known to be highly fluorescent (>90%), however, it has been reported that the quantum yield

of PDI bearing electron-rich alkoxyphenyl substituents at the imide nitrogens drops to < 5%.[5] This has been attributed to a photoinduced electron transfer from the electron-rich aromatic to the electron-deficient perylene bisimide unit. This issue can be bypassed with the design of a new PDI. In PDI **4-2**, linear TEG chains improving the solubility can be introduced to avoid the quenching of fluorescence (Figure 4-3). Moreover, 2,6-diisopropylphenyl substituents will be introduced in order to prevent π-π stacking within the multichromophoric peptide. Indeed, PDI with those substituents arranged perpendicularly to the planar PBI core, effectively inhibiting intermolecular π-π stacking of the PBI dyes.[6] The synthesis of PDI **4-2** will be described in *Section 4.2.1.2*.

Figure 4-3 Second generation of chromophores; modifications applied to the new generation of dyes are highlighted in red.

4.1.1.1 Synthesis of Y-Per 4-1

The synthesis of Y-Per **4-1**, described in Scheme 4-1, started by the conversion of commercially available perylene **4-3** into bromo-perylene **4-4** using *N*-Bromo succinimide in very high yield following the literature.[7] A Pd-catalyzed Suzuki cross-coupling was subsequently carried out in the presence of 4,4'-biphenyldiboronic acid (bis)pinacol ester in 72% yield to afford **4-5**. This was followed by the pinacol removal by oxidative cleavage with sodium periodate and treatment with a 1M aqueous solution of HCl to obtain the desired boronic acid Y-Per **4-1** in 90% yield.[8]

Scheme 4-1 Synthesis of Y-Per **4-1**; a) NBS, THF, rt, 24 h; b) 4,4'-biphenyldiboronic acid bis(pinacol)ester, K_2CO_3, $[Pd(PPh_3)_4]$, dioxane/H_2O, 85 °C, 3 h; c) *i)* $NaIO_4$, THF/H_2O (4 :1), rt, 1 h 30, *ii)* HCl (1M), rt, 20 h.

Y-Per **4-1** and intermediates were fully characterized by melting points, infrared, ^{1}H and ^{13}C NMR spectroscopy, and HR mass spectrometry. Moreover, UV-Vis absorption spectrum of **4-1**, recorded in DMF, shows two maxima at 423 (ε = 28700 L mol^{-1} cm^{-1}) and 450 nm (ε = 34800 L mol^{-1} cm^{-1}); and its fluorescence emission (λ_{exc} = 423 nm) displays the mirror image of the absorption (λ_{max} = 470 and 500 nm). The quantum yield of the compound (determined from perylene QY=94% in cyclohexane)[3] was estimated to be 70%. The absorption and emission spectra of **4-1** were normalized and overlapped with those of B-NDI **3-11** and R-PDI **3-12,** as reported in Figure 4-4b; and the spectral overlap indicates that compound **4-1** shows better complementarity spectral properties with R-PDI than Y-Py **3-11** (Figure 4-4a). Besides, the new generation of dyes shows a better coverage of the solar spectrum than the previous one indicating promising capabilities of the system to collect light.

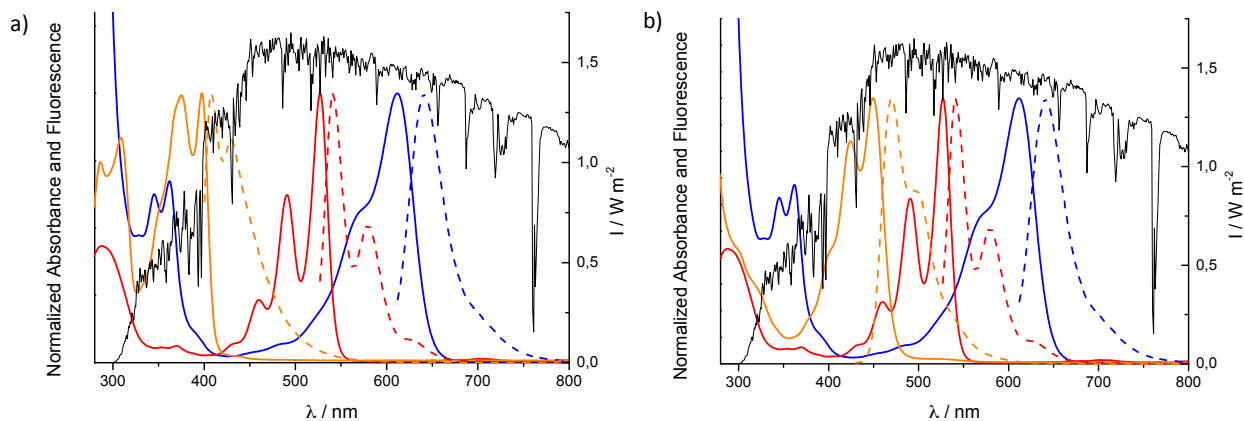**Figure 4-4** Normalized absorption (solid) and fluorescence (dashed) spectra of colored dyes a) Y-Py **3-13** (yellow), R-PDI **3-12** (red), B-NDI **3-11** (blue) and b) Y-Per **4-1** (yellow), R-PDI **3-12** (red), B-NDI **3-11** (blue) in DMF plotted against the solar spectrum.

4.1.1.2 Synthesis of R-PDI 4-2

The synthesis of R-PDI **4-2** follows a stepwise approach as in *Chapter 3*, and so started with the

99

preparation of monoanhydride **4-11**, being the key intermediate of the synthesis, following the literature.[9] In this respect, the TEG swallowtail amine **4-10** was prepared by *N,N*-dibenzyl protection of serinol **4-7** with benzyl bromide and subsequent double Williamson alkylation of *N,N*-dibenzyl-protected serinol **4-8** with triethyleneglycol monomethyl ether tosylate (TEG-OTs) in the presence of NaH as base. This was followed by Pd-catalyzed hydrogenation of the benzyl protecting group affording compound **4-10** in 81% yield. A mono-condensation reaction was subsequently performed with perylene dianhydride (PDA) in a water/isopropanol mixture at 120 °C for ten days to give key monoanhydride **4-11**. The compound was not isolated due to its low solubility. In order to obtain compound **4-12**, a second condensation reaction with 4-bromo-2,6-diisopropylaniline was carried out in propionic acid at 140 °C for 7 h under microwave irradiation affording **4-12** in 38% over two steps. The moderate yield results from the low reactivity of the aniline derivative due to the presence of sterically hindered substituents. Finally, a Pd-catalyzed Suzuki cross-coupling in the presence of Pd tetrakis and K_2CO_3 was exploited to introduce the electron poor aldehyde derivative affording final R-PDI **4-2** (Scheme 4-2).
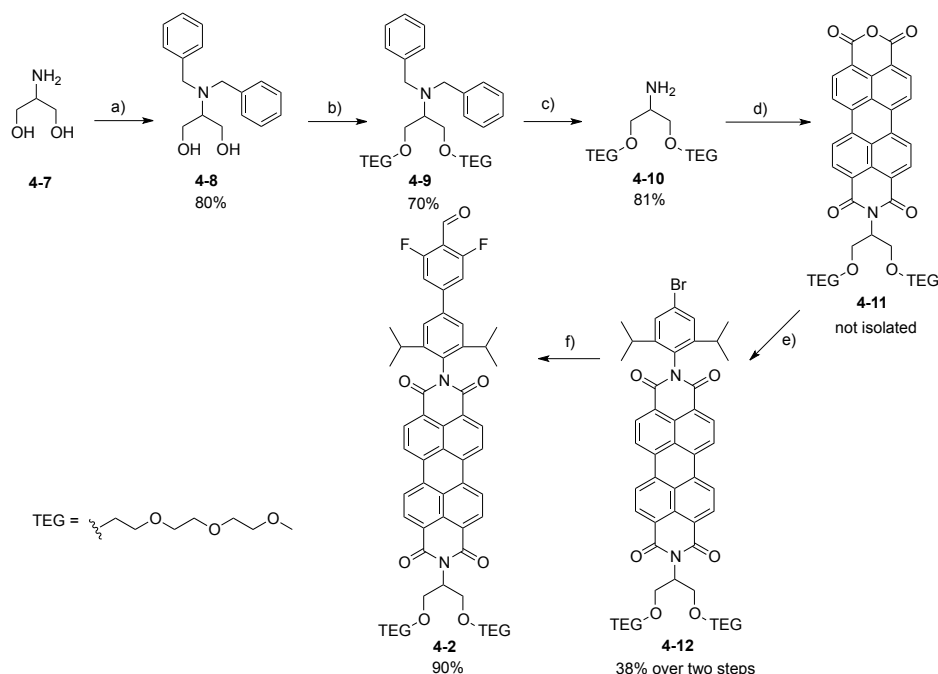
Scheme 4-2 Synthesis of new R-PDI **4-2**; a) BnBr, K_2CO_3, EtOH, reflux, 3 h; b) NaH, TEG-OTs, THF, reflux, 20 h; c) H_2, Pd/C 10%wt, MeOH, rt, 20 h; d) *i)* PDA, Et_3N, iPrOH/H_2O, 120 °C, 10 d, *ii)* 5% HCl (aq), 120 °C, 10 min; e) 4-bromo-2,6-diisopropylaniline, propionic acid, MW irr, 140 °C, 7 h; f) 3,5-difluoro-4-formylphenyl boronic acid, K_2CO_3, [Pd(PPh$_3$)$_4$], dioxane/H_2O, 80 °C, 20 h.

It is noteworthy to indicate that final PDI **4-2** is very well soluble in Et_2O compared to PDI **3-13**, which will simplify the purification of the multichromophoric architecture after the chromophoric assembly. PDI **4-2** and intermediates were fully characterized by melting points, infrared, ^{1}H and

^{13}C NMR spectroscopy, and HR mass spectrometry. Furthermore, the absorption spectrum of **4-2** shows the π–π* electronic transition bands (λ_{max} = 528, 492, 461 nm; ε_{528} = 77200 L mol^{-1} cm^{-1}, ε_{492} = 48000 L mol^{-1} cm^{-1}, ε_{461} = 18000 L mol^{-1} cm^{-1}). The fluorescence emission displays the mirror image of the absorption with two maxima at 540 and 579 nm (Figure 4-5). The compound is highly fluorescent; its quantum yield was estimated to be 94% in DMF using Rhodamine 6G as standard (QY=94% in EtOH).[10]
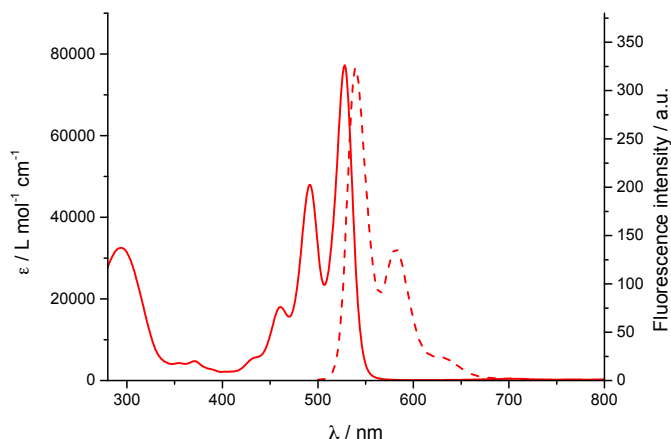
Figure 4-5 Absorption (solid line) and fluorescence emission (dashed line) *(λ_{exc}=495 nm)* spectra of R-PDI **4-2** recorded in DMF.

4.1.1.3 Optoelectronic properties of the second generation of dyes

The photophysical properties recorded in DMF, including lifetime measurements, of the new generation of chromophores B-NDI **3-12**, R-PDI **4-2**, Y-Per **4-1** are summarized in Table 4-1. In general, all compounds show high molar absorption coefficient (up to 7.7 10^4 M^{-1} cm^{-1}) spanning from the blue to the red region of the visible spectrum with luminescence lifetimes in the same order of magnitude (τ = 2-9 ns) and possess good to remarkably high quantum yield. Moreover, the energy levels of the LUMOs of B-NDI **3-24**, R-PDI **4-2**, and Y-Per **4-5** were determined by cyclic voltammetry (CV, reported in *Chapter 6*) while the energy levels of the HOMOs of the same compounds were calculated using the optical values obtained by absorption spectroscopy, and are also reported in Table 4-1 and Figure 4-6.

Table 4-1 Optoelectronic properties of chromophores B-NDI **3-12** and **3-24**, R-PDI **4-2**, Y-Per **4-1** and **4-5** recorded in DMF.

Entry	Compounds	Abs (λ_{max})	ε / L mol^{-1} cm^{-1}	Em (λ_{max})	QY / %	τ / ns	E_{red}[d] (E_{LUMO}[f])	E_{ox}[d] (E_{HOMO}[f])
1	B-NDI **3-12**	612	23500	641	33[a]	9.2	-	-
2	B-NDI **3-24**	612	-	-	-	-	-0.79 (-3.85[g])	1.07[e] (-5.87[h])
3	R-PDI **4-2**	460, 491, 527	18000, 48000, 77200	540, 579	94[b]	3.8	-0.44 (-4.2[g])	nd (-6.55[h])
4	Y-Per **4-1**	423, 450	28600, 34700	472	70[c]	2.6	-	-
5	Y-Per **4-5**	450	-	-	-	-	-1.58 (-3.06[g])	1.05[e] (-5.82[h])

*QY determined from [a]N,N'-di(2,6-diisopropylphenyl)-1,6,7,12-tetraphenoxyperylene- 3,4 :9,10-tetracarboxylic acid bisimide (QY=96% in CHCl$_3$);[11] [b]Rhodamine 6G (QY=94% in EtOH);[10] [c]perylene (QY=94% in cyclohexane).[3] [d]First oxidation and reduction potential in V vs. SCE; [e]Peak potentials (irreversible process); [f]LUMO and HOMO energies in eV vs. vacuum determined by CV following equation [g]$E_{HOMO/LUMO}$ = -(5.1 eV + $E_{red/ox}$ vs. Fc$^+$/Fc) or [h]E_{HOMO}= E_{LUMO} -$\Delta E_{HOMO/LUMO}^{opt}$ for not detectable or irreversible oxidation process. All the measurements were performed in DMF. Fc$^+$/Fc = 0.46 V vs. SCE = -5.1 eV vs. vacuum. $\Delta E_{HOMO/LUMO}^{opt}$ = 1240/λ_{abs}.
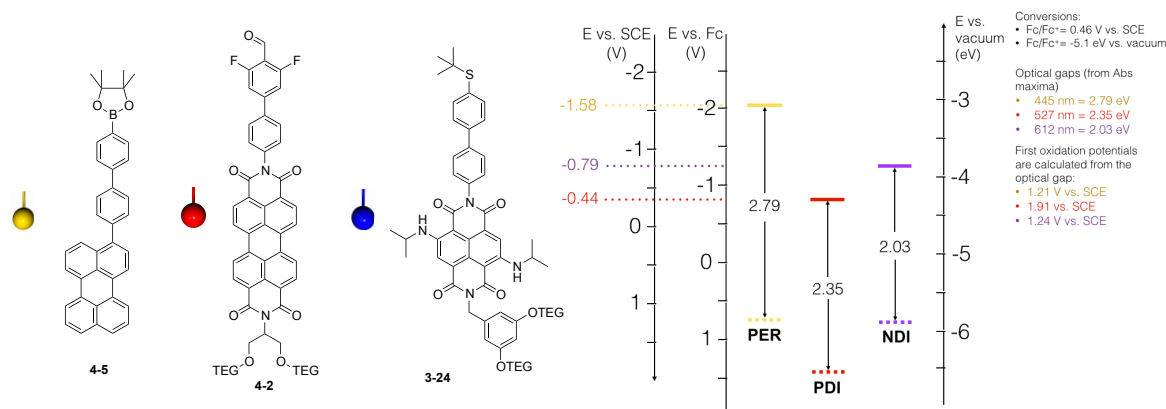
Figure 4-6 Left: Structure of the dyes used to determine HOMO/LUMO energy levels by CV and absorption spectroscopy; Right: Frontier orbital potentials determined by cyclic voltammetry in DMF.

4.1.1.4 Assembly of the second generation of dyes

Having in hands the newly synthesized dyes Y-Per **4-1** and R-PDI **4-2**, the chromophoric assemblies on peptidic scaffold **3-1** were tested: first, with Y-Per **4-1**, R-PDI **3-13**, and B-NDI **3-12,** and then, with Y-Per **4-1**, R-PDI **4-2**, and B-NDI **3-12**. The reactions were performed as in *Chapter 3* by mixing the four components in anhydrous DMF for 4 h in the presence of a catalytic amount of *m*-PDA affording colored peptides **4-13** and **4-14** respectively (Scheme 4-3). When R-

PDI **3-13** was used, peptide **4-13** was purified by GPC using anhydrous DMF as eluent while in the second case, due to the well-appreciated solubility of R-PDI **4-2**, colored peptide **4-14** was isolated by simple precipitation in Et$_2$O and washing with THF as mentioned in *Chapter 6*.

Scheme 4-3 Colored assembly with B-NDI **3-12**, R-PDI **3-13** or **4-2** and Y-Per **4-1** on peptidic scaffold **3-1**; a) *m*-PDA, DMF, rt, 4 h.

The chemical identity of desired peptides **4-13** and **4-14** were confirmed by MALDI-TOF analyses, reported in Figure 4-8 and 4-9. The analysis of **4-13** shows $[M+Na]^+$ as a small peak (m/z = 5199.3). Due to the complexity of the spectrum, the assignment of the other peaks is challenging. Except $[M+Na]^+$ peak, the spectrum displays three different regions which seem to correlate with the loss of one, two and three chromophores respectively. The peak corresponding to the product after hydrolysis of the boronic ester $[M(-Per)+Na]^+$ was unambiguously identified (at m/z = 4787.1) (Figure 4-7).

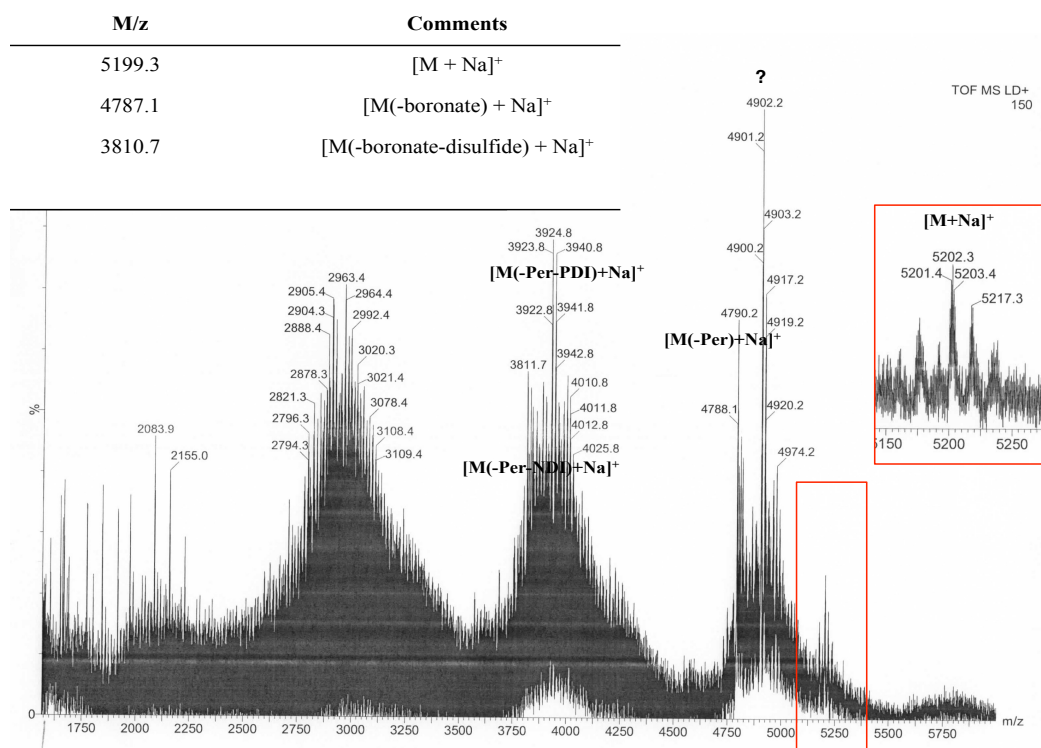| M/z	Comments
5199.3	$[M + Na]^+$
4787.1	$[M(\text{-boronate}) + Na]^+$
3810.7	$[M(\text{-boronate-disulfide}) + Na]^+$

Figure 4-7 MALDI-TOF analysis of purified peptide **4-13**; Inset: Zoom of $[M+Na]^+$ peak.

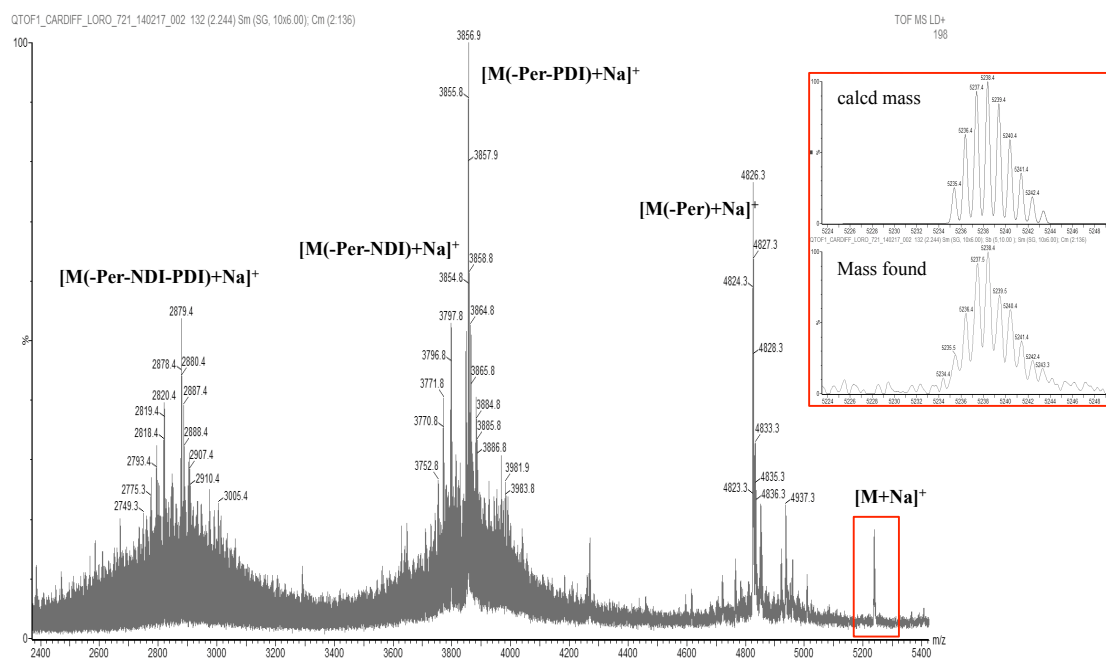**Figure 4-8** MALDI-TOF analysis of purified peptide **4-14**; Inset: Zoom of $[M+Na]^+$ peak (bottom) compared with calculated mass (top).

The MALDI-TOF analysis of **4-14** displays a small peak for $[M+Na]^+$ (m/z = 5235.4) in accordance with the calculated mass. Peak corresponding to the hydrolyzed boronic ester product ($[M(\text{-Per})+Na]^+$ at m/z = 4823.3) was also found (Figure 4-8). Besides, the main peak at m/z =

3854.8 seems to correspond to the peptide bearing only the NDI unit ([M(-Per-PDI)+Na]$^+$), in which the hydrazide moiety did not react with R-PDI and formed an adduct from a secondary reaction with DMF possibly during the ionization process.

Peptides **4-13** and **4-14** were analyzed by UV-Vis absorption spectroscopy in DMF solution. As in the *Chapter 3*, the spectra were compared with the arithmetic sum of the three independent dyes after normalization on B-NDI maximum (at 612 nm) (Figure 4-9). In the absorption spectra, hypochromism of the R-PDI bands is observed in both cases (compared to the arithmetic sum of the 3 dyes). According to the MALDI-TOF spectra, the acyl hydrazone formation were not quantitative in both cases, possibly due to π–π interactions between the chromophores preventing the full introduction of the PDI moiety, sandwiched between the two other dyes.
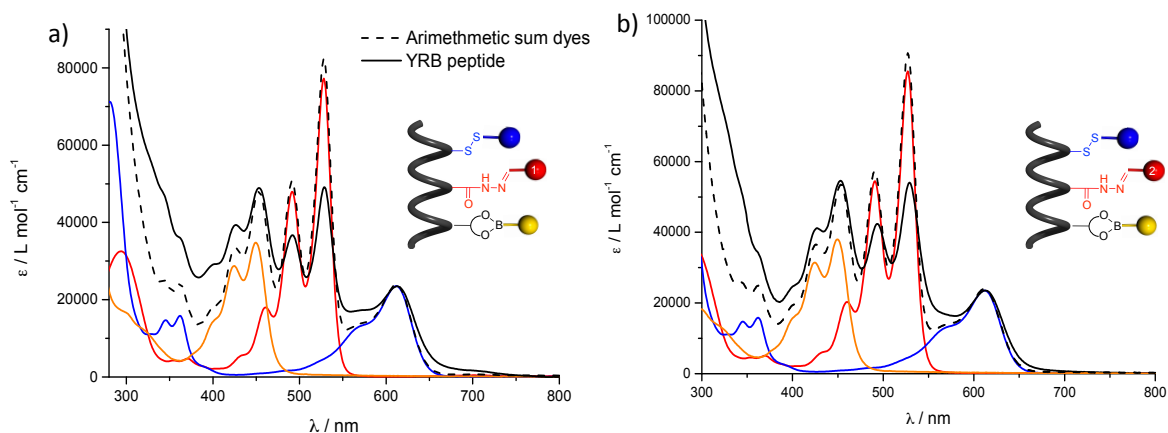

Figure 4-9 Absorption spectra of a) YRB peptide **4-13** (solid black line) and b) YRB peptide **4-14 (**solid black line) normalized with arithmetic sum (dashed line) of absorption of dyes B-NDI **3-11**, R-PDI **3-12** or **4-2**, Y-Per **4-1** in DMF on B-NDI unit.

Steady-state fluorescence measurements were performed in DMF to characterize the energy transfers within the colored peptides. For YRB **4-13**, the excitation spectrum, recorded at the emission of B-NDI (λ_{em} = 640 nm), indicates the contribution of the three chromophoric units and so the existence of the ETs Y-Per→B-NDI and R-PDI→B-NDI (Figure 4-10). The ET efficiencies Φ_{ET} were measured using the methods described in the previous chapter: *i)* quantum yield of B-NDI within YRB peptide (QY$_{B-NDI}$) upon selective excitation of the donor units R-PDI (λ_{exc} = 495 nm) or Y-Per (λ_{exc} = 423 nm) divided by QY$_{B-NDI}$ upon direct excitation (λ_{max} = 609 nm); *ii)* comparison of the absorption and excitation spectra, both normalized at the maximum absorption wavelength of blue chromophore unit B-NDI (λ_{max} = 612 nm), by using the equation $\Phi_{ET} = Ex_D/A_D$, where Ex_D and A_D are fluorescence and absorption intensities of the donor in the normalized excitation and absorption spectra, respectively. ET efficiencies Φ_{ET} within peptide **4-13** were estimated to be 7.7% and 7.7% by the first method and 7% and 7.2% with method 2 for

Y-Per→B-NDI and R-PDI→B-NDI, respectively. Following the same strategies for peptide **4-14**, Φ_{ET} were estimated to be 3.7% and 19% for Y-Per→B-NDI and R-PDI→B-NDI respectively by method 1; while by normalization of the absorption and excitation spectra Φ_{ET} were measured to be 3.2% and 17.9% for Y-Per→B-NDI and R-PDI→B-NDI (Figure 4-11).
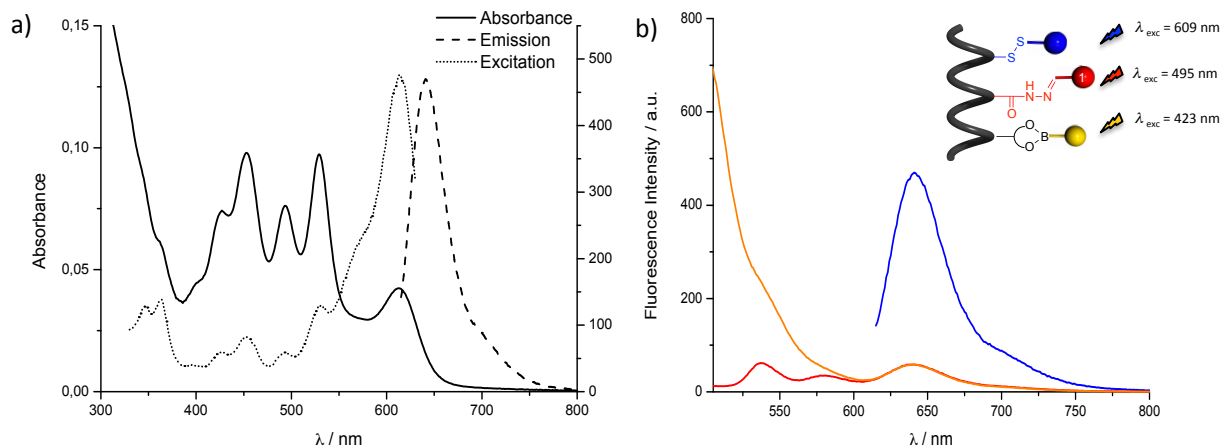

Figure 4-10 a) Absorption (solid line), Emission (λ_{exc} = 609 nm) (long-dashed line), Excitation (λ_{em} = 640 nm) (short dashed line) spectra of YRB peptide **4-13**; b) Fluorescence emission spectra of YRB peptide upon selective excitation of B-NDI (λ_{exc} = 609 nm), R-PDI (λ_{exc} = 495 nm), Y-Per (λ_{exc} = 423 nm) in DMF.
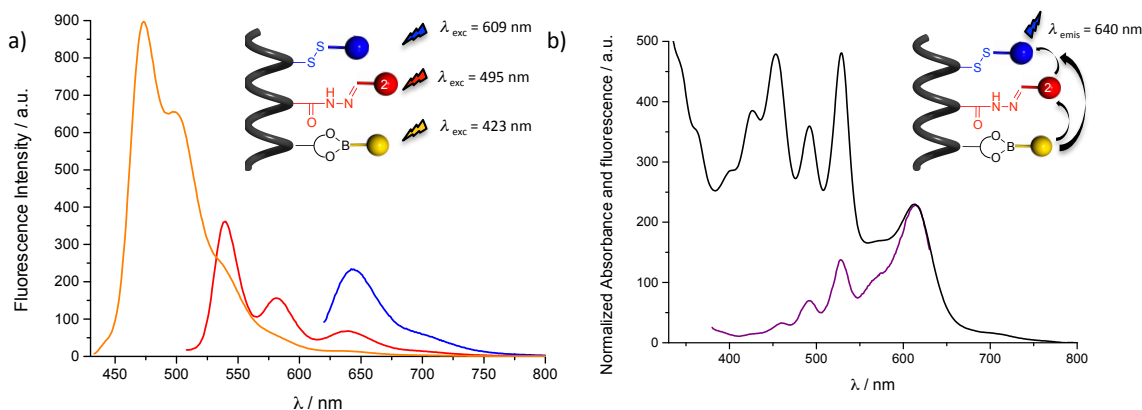

Figure 4-11 a) Fluorescence emission spectra of YRB peptide **4-14** at (λ_{exc}) 423 nm (yellow), 495 nm (red), 609 nm (blue) in DMF to determine ET efficiency following the first method: Φ_{ET} = QY*$_{B-NDI}$/QY$_{B-NDI}$; b) Normalized absorption and excitation spectra $(\lambda_{em}$=640 nm) in DMF for the second method: Φ_{ET} = Ex$_D$/A$_D$.

In conclusion, the Φ_{ET} (Y-Per→B-NDI) was not really improved by the introduction of the perylene derivative **4-1** despite the good normalized spectral overlap between Y-Per fluorescence and R-PDI absorption. Indeed, if a slight enhancement (7.7% within **4-13**) compared to the ethynylpyrene (5.5% within **3-37**) unit has been observed in the first assembly, the second one in which Φ_{ET} (Y-Per→B-NDI) decreased to 3.7%, has counterbalanced it. However a significant improvement for Φ_{ET} (R-PDI→B-NDI) was noticed by using newly synthesized R-PDI **4-2,** due to its high quantum yield, from 5.5% in peptide **3-37** and 7.7% in **4-13** to 19% in **4-14**.

4.1.2 Modification of the peptidic scaffold

In order to improve the energy transfer of our system, we decided to investigate the effect of different scaffold modifications (Figure 4-12).

i) First, the effect of the interchromophoric distance on the energy transfer efficiencies will be studied in *Section 4.1.2.1*.

ii) Section 4.1.2.2 will be dedicated to understand the effect of the order of the dyes on the energy transfer.

iii) Finally, *Section 4.1.2.3* will explore the introduction of a new diol moiety to enhance the parallel dipole orientation between the dyes required for the energy transfer.
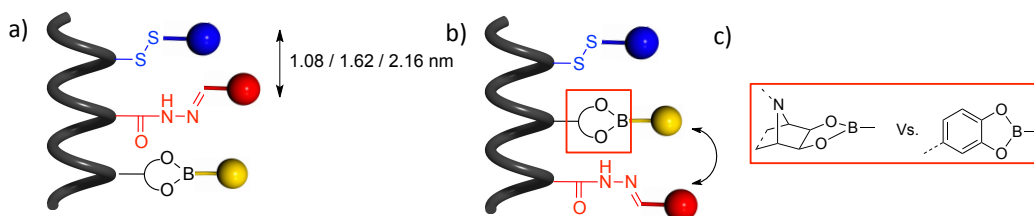

Figure 4-12 Different scaffold modifications to improve the energy transfer: a) increasing the distance between dyes; b) changing their order; c) optimizing their dipole orientation.

4.1.2.1 Effect of the interchromophoric distance on the energy transfer

Taking into consideration the helical conformation of the original designed peptide Ac-QLA-X(disulfide)-QLAQLA-X(hydrazide)-QLAQLA-X(diol)-QLA-NH$_2$ **3-1** (detailed in *Chapter 3*), the receptor sites, introduced each (*i, i+7*) residue in the pre-programmed peptide, are positioned at 1.08 nm from each other. We hypothesized that this short interchromophoric distance might prevent the quantitative introduction of the PDI moiety and favor mechanisms of quenching of fluorescence other than energy transfers such as contact quenching; so, we decided to increase it. By introducing the receptor sites each (*i, i+10*) and (*i, i+14*) residues, corresponding respectively to three and four turns of α-helix, they should be separated by 1.62 nm and 2.16 nm (pitch of α-helix=0.54 nm).[12] The increased distance might lead to an improvement of the ET efficiencies as it is known that maximum FRET efficiencies are observed for interchromophoric distances between 1 and 3 nm.[13]

Hence, two newly designed pre-programmed peptides presented in Figure 4-13, the 27-mer Ac-QLA-X(disulfide)-QLAQLAQLA-X(hydrazide)-QLAQLAQLA-X(diol)-QLA-NH$_2$ **4-17** and the 35-mer Ac-QLA-X(disulfide)-QLAQLAQLAQLAQ-X(hydrazide)-QLAQLAQLAQLAQ-X(diol)-QLA-NH$_2$ **4-18**, were synthesized according to the general procedure by SPPS described in *Chapter 3*. The peptide was grown on Rink Amide MBHA resin using modified amino acids **3-2**, **3-3**, **3-4** following the general procedure consisting in cycles between Fmoc deprotection with piperidine and coupling the activated amino acid with HATU in the presence of DIEA to the resin.
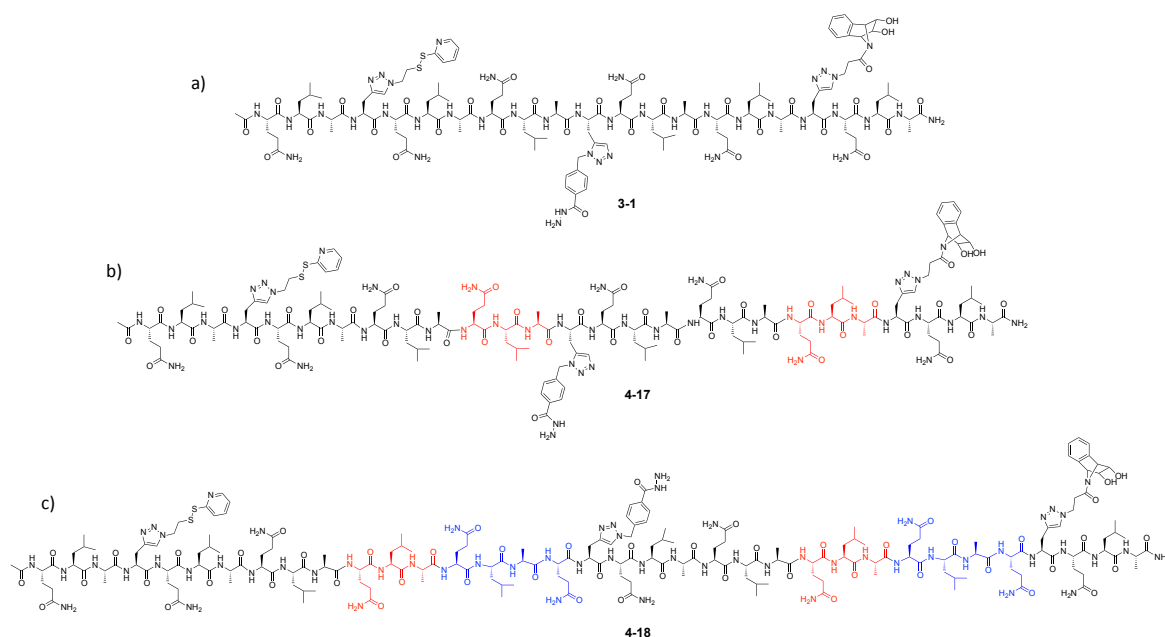
Figure 4-13 Structures of peptides a) **3-1**, b) **4-17**, c) **4-18** in which receptor sites are separated by 1.08 nm, 1.62 nm and 2.16 nm respectively.

After acidic treatment, in which peptides were cleaved from the resin and the side chains were deprotected, disulfide pyridine moieties were introduced by disulfide exchange in solution between peptides **4-15** and **4-16** and 2,2'-disulfide pyridine affording peptidic scaffolds **4-17** and **4-18** (Scheme 4-3).
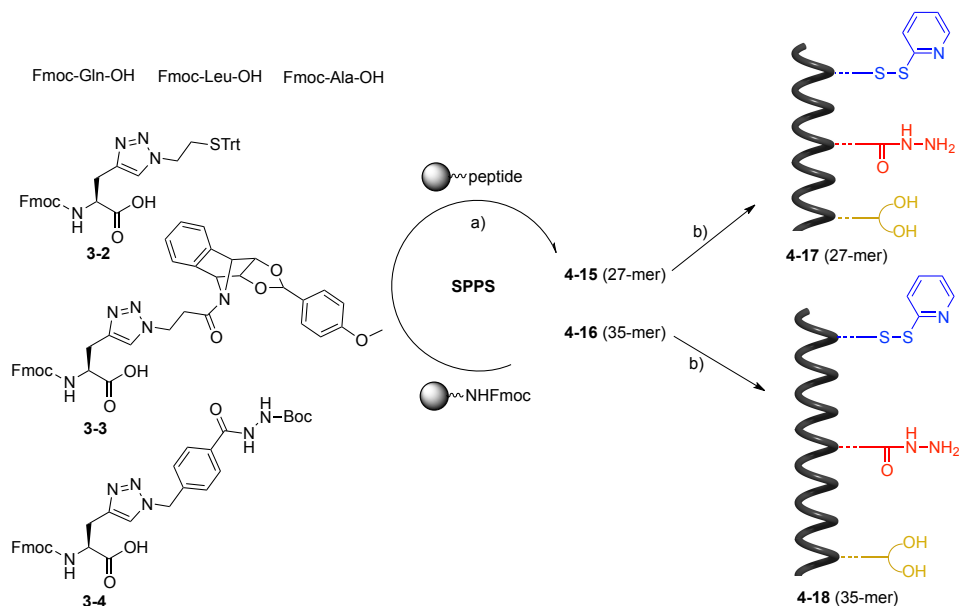
Scheme 4-3 Peptidic scaffold **4-17** and **4-18** synthesis; a) SPPS: *i)* Fmoc deprotection: 20% piperidine in DMF, rt, 3 × 6 min; *ii)* AA coupling: Fmoc-AA-OH, HATU, DIEA, DMF/NMP, rt, 25 min; *iii)* Ac₂O/pyridine/NMP (1:2:2), 2 × 15 min; *iv)* TFA/TIS/H₂O/EDT (94:1:2.5:2.5), rt, 2 h; b) 2,2'-dipyridyl disulfide, DIEA, DMF, 1 h.

Figure 4-14 ESI-MS(Q-TOF) analysis of purified peptide **4-17** showing M^{4+}, M^{3+}, M^{2+} multicharged ions.

Figure 4-15 ESI-MS(Q-TOF) analysis of purified peptide **4-18** showing M^{5+}, M^{4+}, M^{3+} multicharged ions.
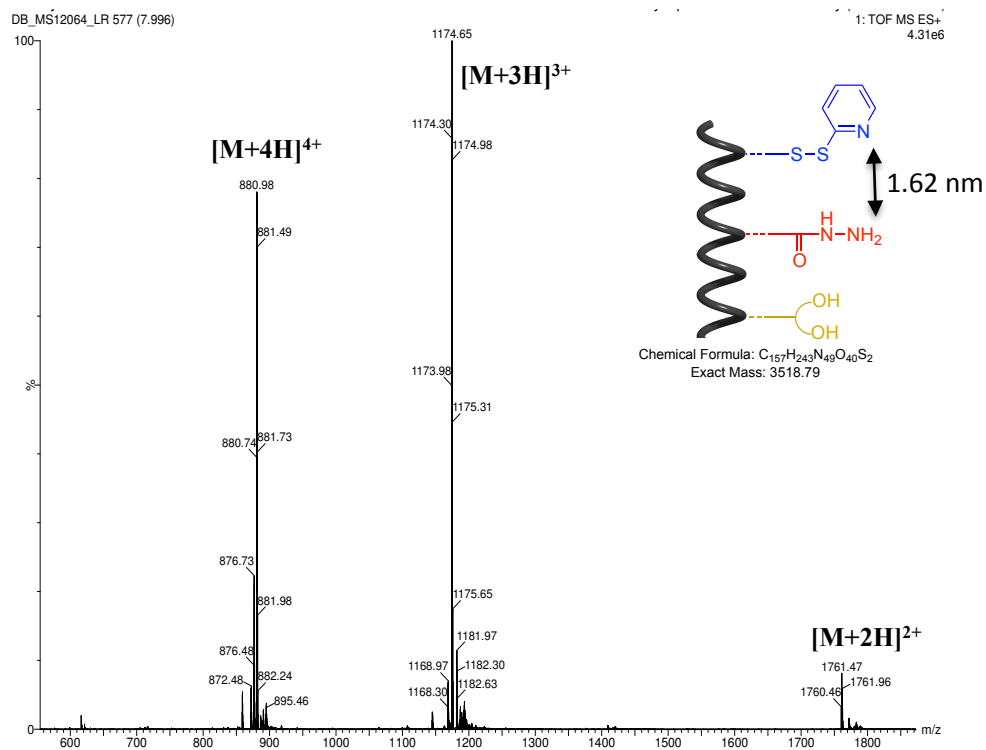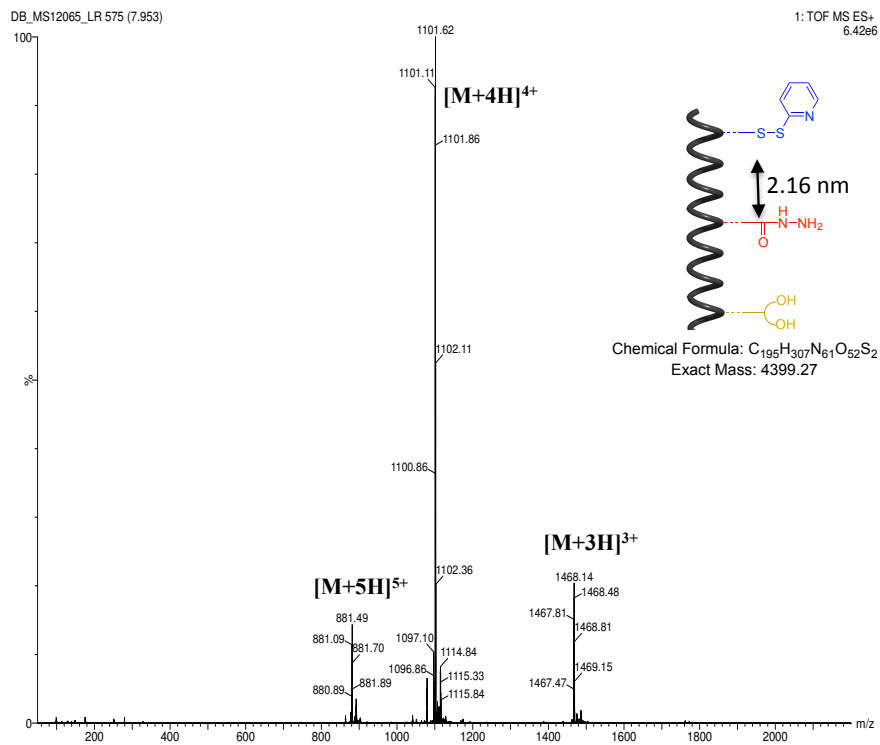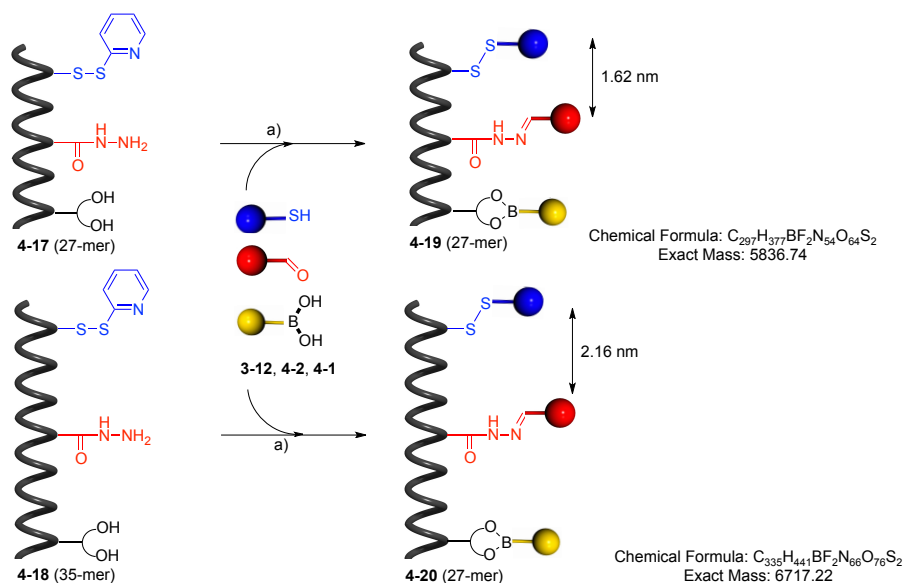
The peptides were purified by RP-HLPC and analyzed by ESI-MS(Q-TOF). The spectra show the multicharged ions $[M+5H]^{5+}$, $[M+4H]^{4+}$, $[M+3H]^{3+}$, $[M+2H]^{2+}$, which after deconvolution gave the expected monoisotopic mass: 3518.79 and 4399.27 for peptides **4-17** and **4-18** respectively (Figure 4-14 and 4-15).

Scheme 4-4 Colored assembly with B-NDI **3-12**, R-PDI **4-2** and Y-Per **4-1** on peptidic scaffold **4-17** and **4-18**; a) *m*-PDA, DMF, 4 h, rt.

Having in hands the new peptidic scaffolds **4-17** and **4-18**, the assembly of the second generation of dyes B-NDI **3-11**, R-PDI **4-6** and Y-Per **4-4** was performed on them using the general protocol affording respectively YRB peptides **4-19** and **4-20** (Scheme 4-4). After purification by precipitation in Et₂O and THF, the peptides were characterized by MALDI-TOF mass spectrometry, UV-Vis and fluorescence spectroscopy. MALDI-TOF analyses of the compounds, reported in Figure 4-16 and 4-17, show the peaks corresponding to the products after hydrolysis of the boronate ester $[M(-Per)+Na]^{+}$ (m/z: 5447.7 for **4-19** and m/z: 6328.1 for **4-20**); $[M+Na]^{+}$ peaks are not observed. Moreover, hydrolysis of the other dynamic covalent bonds was observed. In particular, for peptide **4-20**, peaks (at m/z= 5362.7 and 4386.3 after disulfide cleavage) highlight the non-quantitative acyl hydrazone formation; while for peptide **4-19**, less peaks were found, the main one corresponding to the product after hydrolysis of the boronic ester and cleavage of the disulfide (m/z = 4471.2) occurring during the ionization process.

Figure 4-16 MALDI-TOF analysis of purified peptide **4-19**; Inset: Zoom of [M(-boronate)+Na]⁺ peak (bottom) compared with calculated mass [M+Na]⁺ (top).

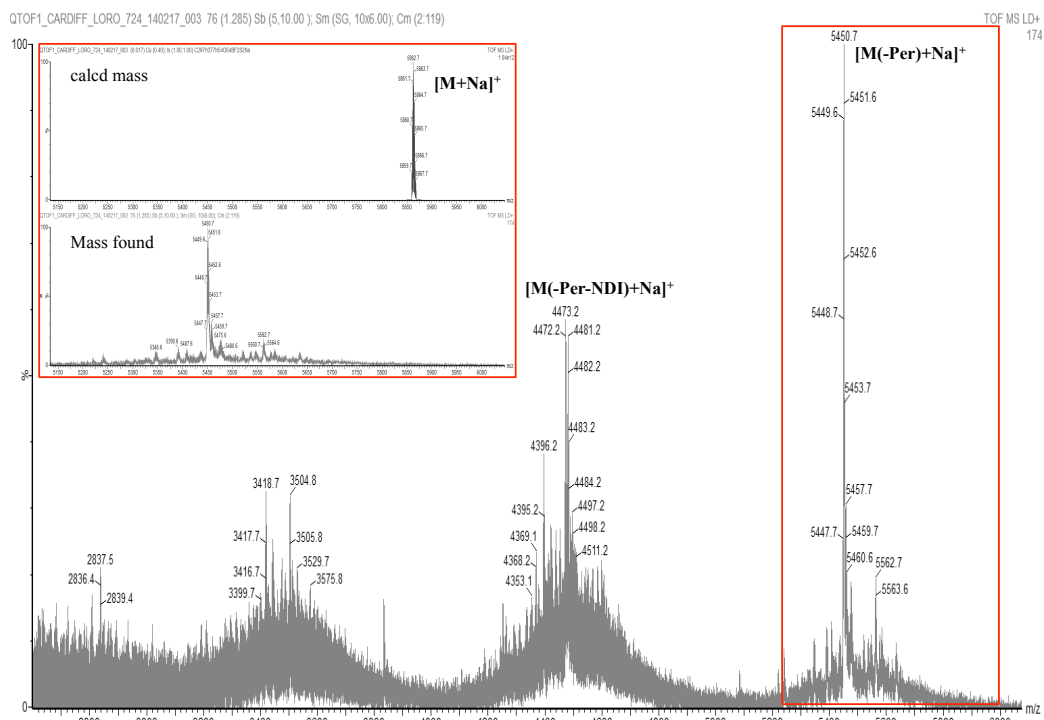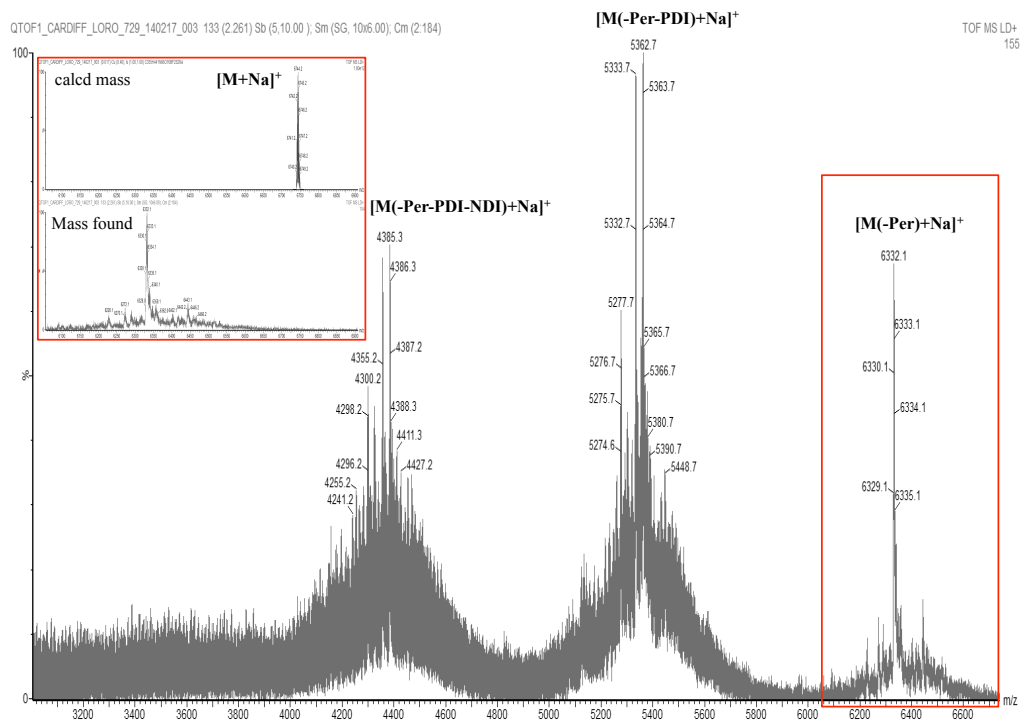**Figure 4-17** MALDI-TOF analysis of purified peptide **4-20**; Inset: Zoom of [M(-boronate)+Na]⁺ peak (bottom) compared with calculated mass [M+Na]⁺ (top).

The absorption spectrum of colored peptide **4-19** was normalized with the arithmetic sum of the absorption spectra of the three free dyes on B-NDI unit and is reported in Figure 4-18 a. The good

correlation between the two spectra indicates the introduction of the three dyes in ratio close to 1:1:1. However, within peptide **4-20**, in which the receptor sites are arranged at a distance of 2.16 nm, the significant hypochromism for R-PDI bands (compared to the arithmetic sum of dyes) is observed similarly to peptide **4-14** (Figure 4-18 b).
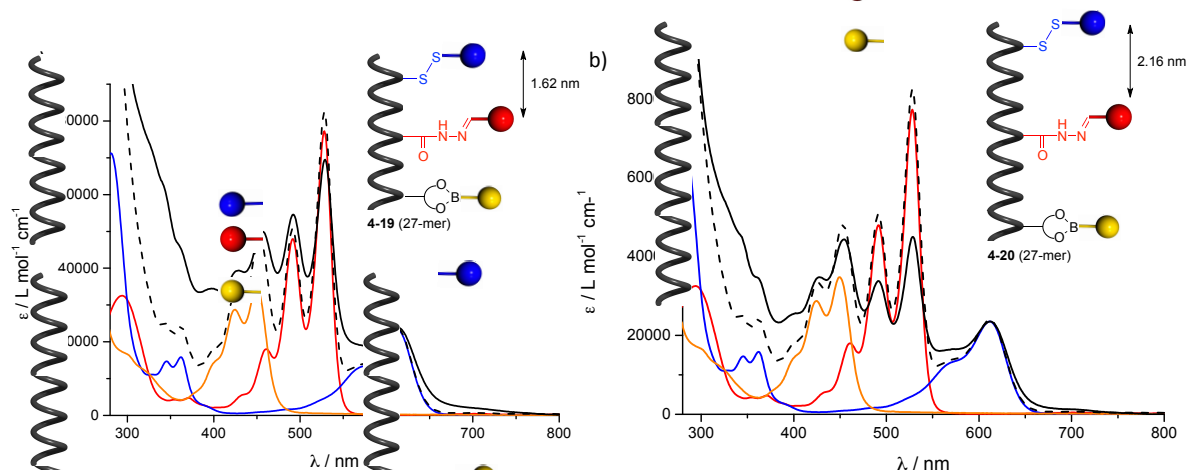
Figure 4-18 Absorption spectra of YRB peptides (solid black line) a) **4-19** and b) **4-20** normalized with the arithmetic sum of dyes (dashed blue line) B-NDI **3-12**, R-PDI **4-2**, Y-Per **4-1** on B-NDI in DMF.

The emission and excitation measurements were performed to determine the ET efficiencies Φ_{ET} by using the two usual methods (Figures 4-19 and 4-20). The efficiencies are gathered in Table 4-2 and compared with those estimated into the original peptide **4-14**. The change of the distance did not show a significant effect on Φ_{ET}: Φ_{ET} (Y-Per→B-NDI) was determined around 3% while Φ_{ET} (R-PDI→B-NDI) was around 18% in the three cases.
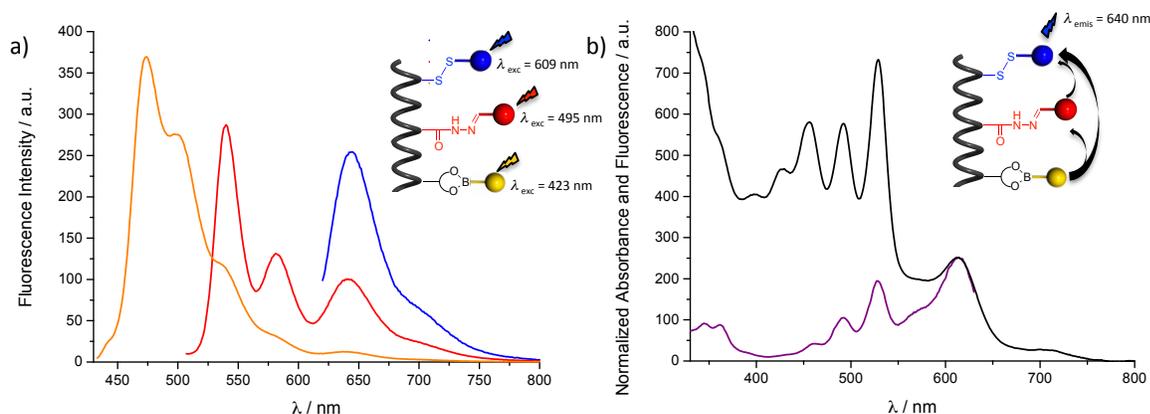
Figure 4-19 a) Fluorescence emission spectra of YRB peptide **4-19** at *(λ_{exc})* 423 nm (yellow), 495 nm (red), 609 nm (blue) to determine ET efficiencies following the first method: $\Phi_{ET} = QY^*_{B-NDI}/QY_{B-NDI}$; b) Normalized absorption (black) and fluorescence excitation (purple) spectra of YRB peptide **4-19** *(λ_{em}=640 nm)* for the second method: $\Phi_{ET} = Ex_D/A_D$.
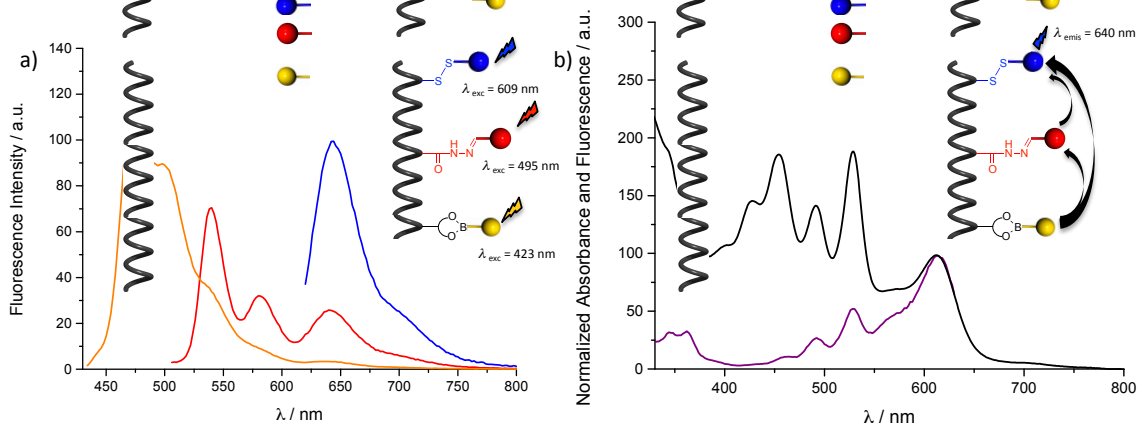
Figure 4-20 a) Fluorescence emission spectra of YRB peptide **4-20** at *(λexc)* 423 nm (yellow), 495 nm (red), 609 nm (blue) to determine ET efficiencies following the first method: $\Phi_{ET} = QY^*_{B-NDI}/QY_{B-NDI}$; b) Normalized absorption (black) and fluorescence excitation (purple) spectra of YRB peptide **4-20** *(λem*=640 nm) for the second method: $\Phi_{ET} = Ex_D/A_D$.

Table 4-2 Energy transfer efficiencies within **4-14, 4-19, 4-20** calculated following methods 1 and 2.

Entry	Peptides	Dyes Distance	Methods	Φ_{ET} (Y-Per→B-NDI) %	Φ_{ET} (R-PDI→B-NDI) %
1	YRB **4-14**	1.08 nm	1: $\Phi_{ET} = QY^*_{B-NDI}/QY_{B-NDI}$	3.7	17.9
			2: $\Phi_{ET} = Ex_D/A_D$	3.2	19
2	YRB **4-19**	1.62 nm	1	2.7	17
			2	2.9	17
3	YRB **4-20**	2.16 nm	1	2.5	19.1
			2	2.5	18.5

To summarize, new peptidic scaffolds **4-17** and **4-18** bearing the receptor sites separated by largest distance, 1.62 and 2.16 nm respectively (compared to 1.08 nm in the original peptidic scaffold), were successively prepared. After the assembly of the chromophores on those new peptides, the absorption spectra of the colored architectures highlight the introduction of the three chromophores in different ratio. When the chromophores were separated by 1.62 nm, the dyes were almost quantitatively introduced. However, by increasing the distance to 2.16 nm, the same hypochromism for R-PDI bands (compared to the arithmetic sum of the dyes) than in the original peptide was noticed. This is due to the non-quantitative introduction of R-PDI by acyl hydrazone formation possibly caused by the steric hindrance within the original peptide and self-aggregation phenomenon for the less soluble longest peptide. In any case, the change of the distance between the chromophores did not improve the ET efficiencies Φ_{ET}. So, the shortest sequence of the

original peptidic backbone was kept for the rest of the study simplifying and reducing the cost of the synthesis.

4.1.2.2 Effect of the order of the dyes on the energy transfer

In the previous section, we observed than the increased distance (1.62 nm) between the chromophores allows the quantitative introduction of the three dyes; while in the original scaffold, in which the dyes were separated by 1.08 nm, the acyl hydrazone formation was not completed. However, the strategy did not improve the energy transfer within the multichromophoric structure, on the contrary, the increasing of the distance led to a slight decreasing of the ET.

Another strategy envisaged in order to favor the quantitative introduction of R-PDI was to change the order of the chromophores. Indeed, the quasi-superimposable absorption spectra of peptides **4-13**, **4-14** and **4-20** possibly indicate that after introduction of 50-60% of R-PDI, the $\pi-\pi$ stacking between the dyes prevents the quantitative acyl hydrazone formation, the reaction being slower than the others. Therefore, placing R-PDI unit at one extremity of the structure and not sandwiched between B-NDI and Y-Per might lead to the full introduction of R-PDI unit. Besides, we were interested in studying the effect of the order of the chromophores on the scaffold on the ET. This was as well driven by the non-cascaded reported values of the LUMO energy levels of the different chromophores for similar structures found in the literature and confirmed by CV in the previous section ($LUMO_{Y\text{-}Per} > LUMO_{R\text{-}PDI} < LUMO_{B\text{-}NDI}$).[5a, 14] Indeed, those values might support an electron transfer from the electron rich Y-Per to the electron-deficient R-PDI possibly blocking the cascaded energy transfer Y-Per→B-NDI. Hence, we decided to change the order of the chromophores within the colored peptide in order to study the effect on the energy transfer (ET). By introducing Y-Per unit between R-PDI and B-NDI, ET Y-Per→B-NDI might be improved, and moreover, R-PDI moiety should be quantitatively introduced.

Consequently, the pre-programmed peptide Ac-QLA-X(disulfide)-QLAQLA-X(diol)-QLAQLA-X(hydrazide)-NH$_2$ **4-22** was prepared by SPPS according to the general procedure (Figure 4-21 and Scheme 4-5).
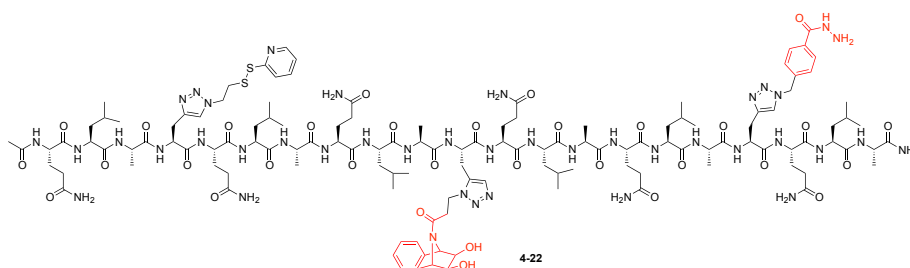
Figure 4-21 Structures of peptides **4-22** in which the order of the receptor sites has been changed.

Scheme 4-5 Synthesis of peptidic scaffold **4-22**; a) SPPS: *i)* Fmoc deprotection: 20% piperidine in DMF, rt, 3 × 6 min; *ii)* AA coupling: Fmoc-AA-OH, HATU, DIEA, DMF/NMP, rt, 25 min; *iii)* Ac$_2$O/pyridine/NMP (1:2:2), 2 × 15 min; *iv)* TFA/TIS/H$_2$O/EDT (94:1:2.5:2.5), rt, 2 h; b) 2,2'-dipyridyl disulfide, DIEA, DMF, 1 h.

Figure 4-22 ESI-MS(Q-TOF) analysis of purified peptide **4-22** showing M^{4+}, M^{3+}, M^{2+} multicharged ions.

The peptide was analyzed by ESI-MS(Q-TOF) and the spectrum showed the multicharged ions [M+4H]$^{4+}$, [M+3H]$^{3+}$, [M+2H]$^{2+}$, which after deconvolution, gave the expected monoisotopic mass: 2894.43 (Figure 4-22). The assembly of the dyes was performed on scaffold **4-22** according to the general procedure (stirring in DMF in the presence of a catalytic amount of *m*-PDA) to give

colored peptide **4-23** (Scheme 4-6). After purifying it, the chemical identity of the compound was confirmed by MALDI-TOF analysis.

4-22   **3-12**, **4-1**, **4-2**   **4-23**

Chemical Formula: $C_{269}H_{329}BF_2N_{46}O_{56}S_2$
Exact Mass: 5212.38
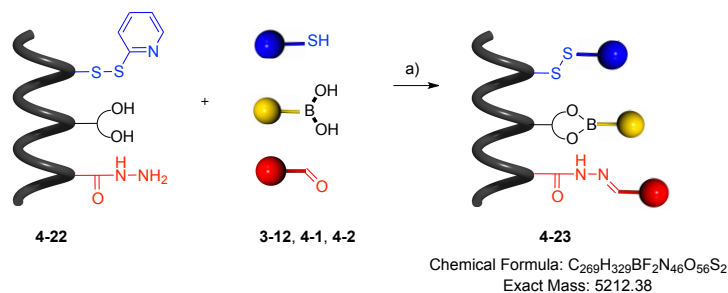
Scheme 4-6 Colored assembly with B-NDI **3-11**, R-PDI **4-2** and Y-Per **4-1** on peptidic scaffold **4-22**; a) *m*-PDA, DMF, 4 h, rt.

The mass spectrum of **4-23**, reported in Figure 4-23, nicely shows the $[M+Na]^+$ peak in accordance with the calculated mass (m/z: 5235.4). Peaks corresponding to the product after hydrolysis/cleavage of the boronate ester $[M(-Per)+Na]^+$ (m/z: 4823.2), disulfide $[M(-NDI)+Na]^+$ (m/z: 4259), boronate and disulfide $[M(-Per-NDI)+Na]^+$ (m/z: 3846.8), occurring during the ionization, were also found.

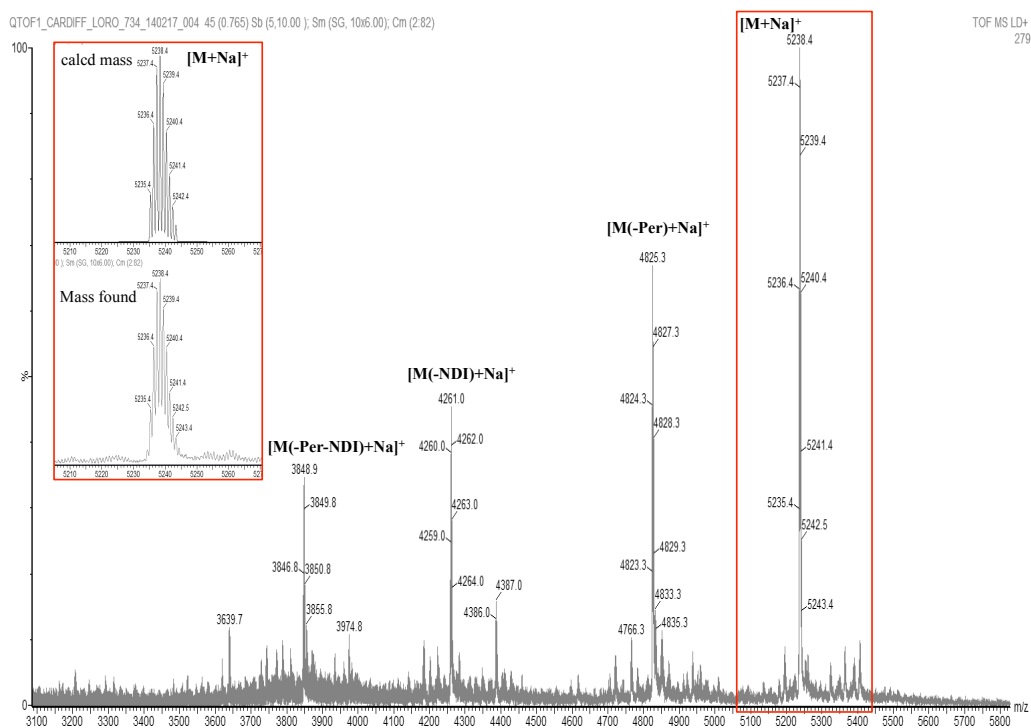**Figure 4-23** MALDI-TOF analysis of purified peptide **4-23**; Inset: Zoom of $[M+Na]^+$ peak (bottom) compared with calculated mass $[M+Na]^+$ (top).

The photophysical properties of peptide **4-23** were analyzed. The normalized UV-Vis absorption spectrum shows a great correlation with the arithmetic sum of the absorption of the three dyes (Figure 4-24a) confirming the quantitative introduction of the three dyes. Indeed, the

116

hypochromism of R-PDI bands observed when R-PDI unit was sandwiched between B-NDI and Y-Per (shown in Figure 4-24b) is considerably reduced with the new order proving the quantitative acyl hydrazone formation. The ET efficiencies Φ_{ET} were estimated to be 7.7% and 21.9% for Y-Per→B-NDI and R-PDI→B-NDI, respectively with method 1; and 7.4% and 21.8% with method 2 (Figure 4-25). Hence, the new order of the chromophore surprisingly slightly improved ET efficiencies Φ_{ET} Y-Per→B-NDI and R-PDI→B-NDI determined to be around 3% and 18% respectively for the previous order (YRB peptide **4-14)** despite the possible bidirectional ET. In this respect, this order will be kept (RYB) in the next section.
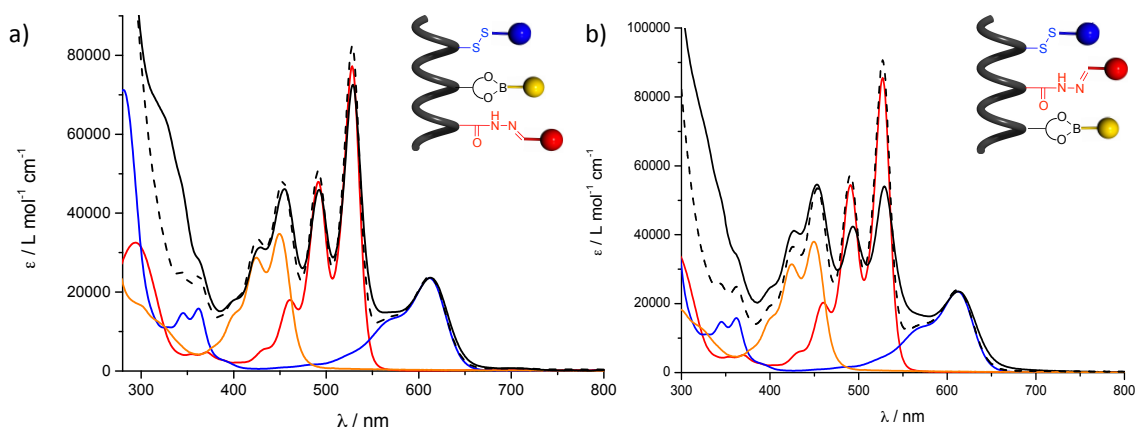
Figure 4-24 Absorption spectrum of a) RYB peptide **4-23** (black solid line) and b) YRB peptide **4-14** (black solid line) normalized on B-NDI with arithmetic sum (dashed line) of absorption of dyes B-NDI (in blue), R-PDI (in red), Y-Per (in yellow) in DMF.
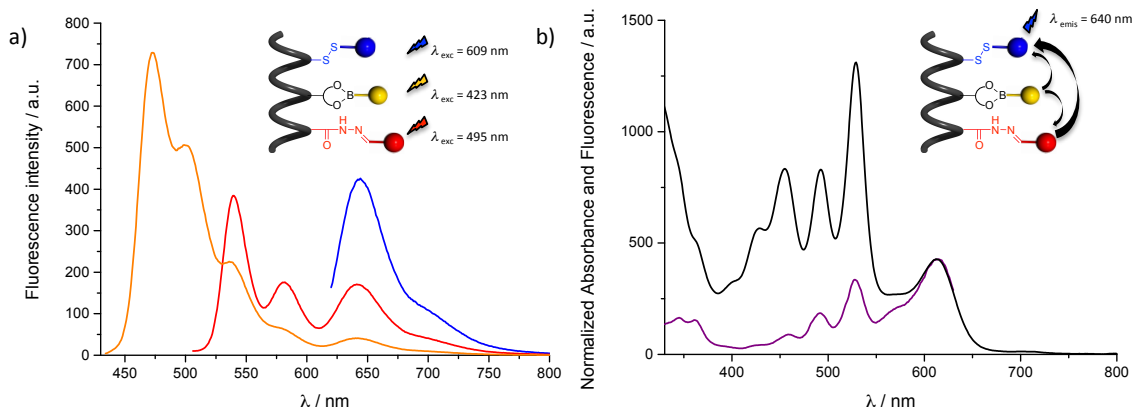
Figure 4-25 a) Fluorescence emission spectra of RYB peptide **4-23** at (λ_{exc}) 423 nm (yellow), 495 nm (red), 609 nm (blue) to determine ET efficiencies following the method 1: $\Phi_{ET} = QY^*_{B\text{-}NDI}/QY_{B\text{-}NDI}$; b) Normalized absorption (black) and fluorescence excitation (purple) spectra of RYB peptide **4-23** $(\lambda_{em}=640$ nm) for the method 2: $\Phi_{ET} = Ex_D/A_D$.

4.1.2.3 Effect of the dipole orientation of the dyes on the energy transfer

Another strategy envisaged to improve the energy transfer was to optimize the dipole orientation of the dyes. In the MD simulations detailed in *Chapter 3*, the spatial occupancy of the three

chromophores clearly indicated that R-PDI and B-NDI units faced to each other but Y-Per/Y-Py is pointing in another direction (Figure 4-26 c). This is probably due to the conformation of the bicyclic diol bearing the yellow chromophore. Indeed the crystal structures of diol **2-25** and **3-8b** show that the diol receptor site belongs to a different plan than the linker contrary to the other receptor sites leading to the non-overlapping of the three dyes in the colored peptides (Figure 4-26 a and b).
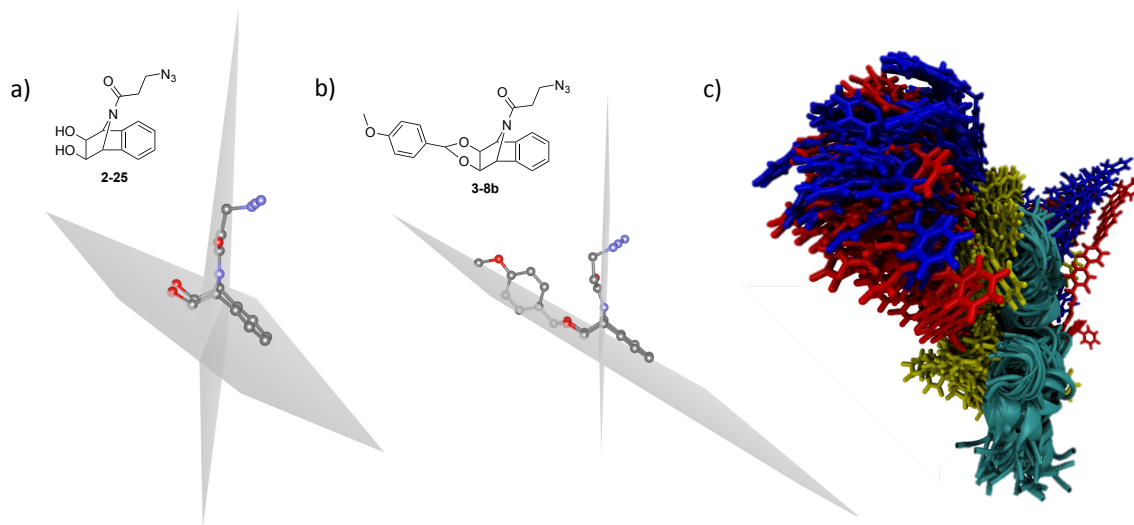

Figure 4-26 Side view of the crystal structures of a) diol **2-25** and b) protected diol **3-8b**. c) Side view of 500 overlaid frames of MD simulations (55 ns) of YRB peptide **3-36**.

In this respect, catechol derivatives, forming boronic ester quantitatively in organic solvent, can be introduced into the scaffold instead of the bicyclic diol to improve the overlapping of Y-Per with the other dyes. Two catechols will be tested in this study: one more rigid, with only one sp^3 carbon between the catechol and the triazole, and a second one, more flexible, with three sp^3 carbons as linker. Accordingly, two modified amino acids **4-24** and **4-25** bearing the protected catechol with different length chains were designed and synthesized. Their structure is presented in Figure 4-27.
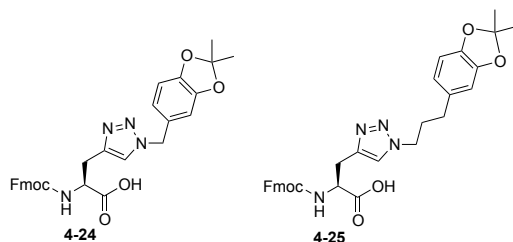

Figure 4-27 Structure of the two amino acids bearing the protected catechol.

The synthesis of **4-24**, reported in Scheme 4-7, commenced with the introduction of the dimethyl acetal protecting group on commercially available diol **4-26** with acetone in the presence of phosphorus trichloride.[15] The obtained ester **4-27** was subsequently reduced into alcohol **4-28**

using LiAlH$_4$. Mesylation of alcohol with mesyl chloride was directly followed by the substitution of the mesylate group into azide in the presence of sodium azide affording compound **4-30** in 55% yield over two steps. Finally, Cu-catalyzed cycloaddition was performed with commercially available amino acid Fmoc-Gly(Propargyl)-OH in the presence of CuSO$_4$.5H$_2$O and sodium ascorbate to afford amino acid **4-24** in 87% yield.
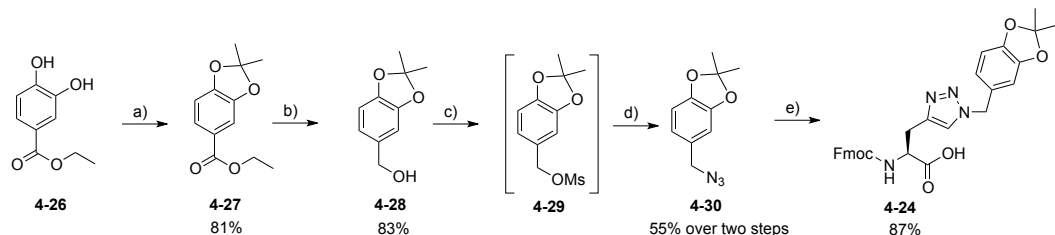
Scheme 4-7 Synthesis of amino acid **4-24**; a) acetone, PCl$_3$, benzene, rt, 16 h; b) LiAlH$_4$, THF, 0 °C to rt, 3 h; c) MsCl, NEt$_3$, CH$_2$Cl$_2$, 0 °C to rt, 1 h; d) NaN$_3$, DMF, rt, 16 h; e) Fmoc-Gly(Propargyl)-OH, CuSO$_4$·5H$_2$O, Na ascorbate, DMF/H$_2$O, rt, 16 h.

For the second amino acid **4-25**, the flexible linker was introduced following a six steps synthetic pathway described in Scheme 4-8. First, inexpensive catechol **4-31** was protected into dimethyl acetal **4-32** using the same conditions as described for **4-27**. Compound **4-32** was then reacted with iodine in the presence of Ag$_2$SO$_4$ to give **4-33**.[16] A Sonogashira cross-coupling reaction between iodo derivative **4-33** and propargyl alcohol in the presence of [Pd(PPh$_3$)$_2$Cl$_2$] was exploited for the preparation of **4-34**. Finally, the carbon-carbon triple bond was reduced into hydrocarbon linker by catalytic hydrogenation using of Pd/C yielding derivative **4-35**. Alcohol **4-35** was subsequently converted into azide **4-37** as previously, and the CuAAC was performed with Fmoc-Gly(Propargyl)-OH affording amino acid **4-25** in 94% yield.
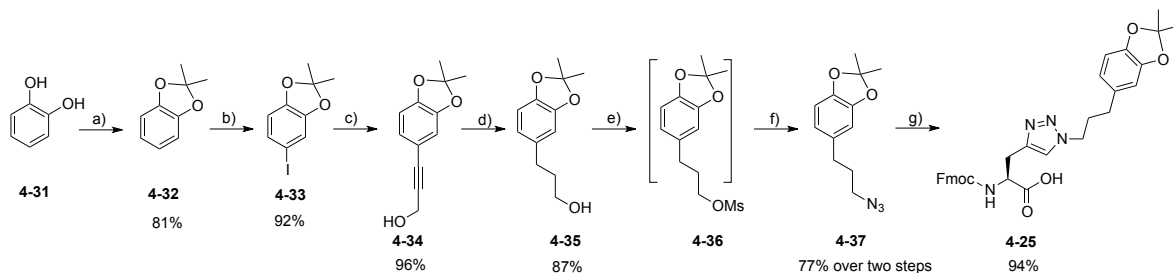
Scheme 4-8 Synthesis of amino acid **4-25**; a) acetone, PCl$_3$, benzene, rt, 1 h; b) I$_2$, Ag$_2$SO$_4$, EtOH, rt, 2 h; c) Propargyl alcohol, NEt$_3$, CuI, [Pd(PPh$_3$)$_2$Cl$_2$], -10 °C to rt, 17 h; d) H$_2$, Pd/C 10% wt, MeOH, rt, 18 h; e) MsCl, NEt$_3$, CH$_2$Cl$_2$, 0 °C to rt, 1 h; f) NaN$_3$, DMF, rt, 16 h; d) Fmoc-Gly(Propargyl)-OH, CuSO$_4$·5H$_2$O, Na ascorbate, DMF/H$_2$O, rt, 16 h.
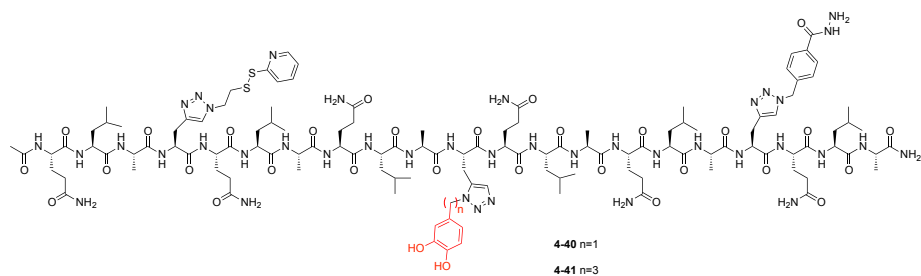
Figure 4-28 Structures of peptides **4-40** and **4-41** bearing catechol derivative as diol.

Having in hands the two protected catechol amino acids, the peptidic scaffolds Ac-QLA-X(disulfide)-QLAQLA-X(catechol)-QLAQLA-X(hydrazide)-NH$_2$ **4-40** and **4-41**, presented in Figure 4-28, were prepared by SPPS according to the general method (Scheme 4-9).
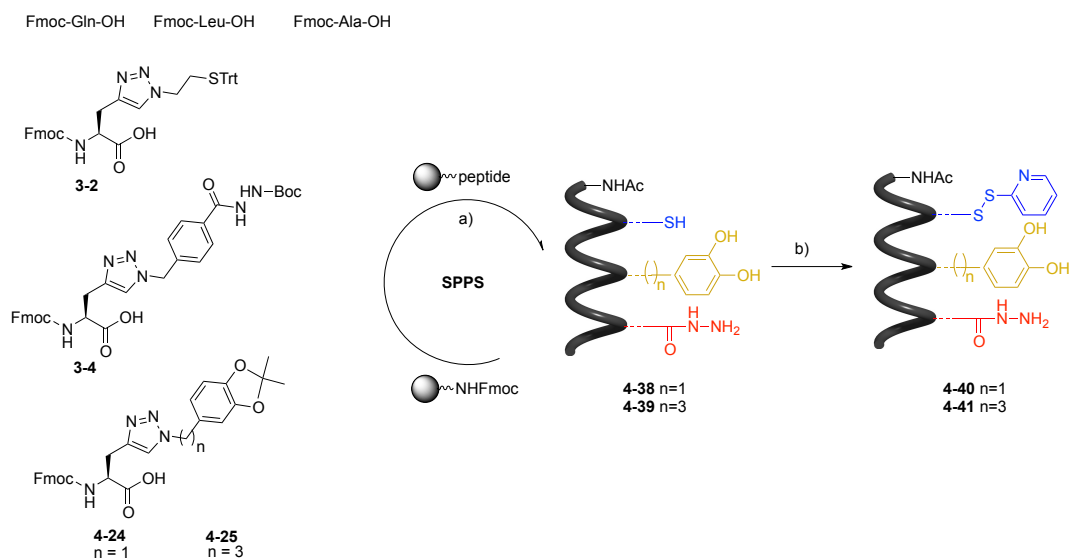
Scheme 4-9 Peptidic scaffold synthesis; a) SPPS: i) Fmoc deprotection: 20% piperidine in DMF, rt, 3 × 6 min; ii) AA coupling: Fmoc-AA-OH, HATU, DIEA, DMF/NMP, rt, 25 min; iii) Ac$_2$O/pyridine/NMP (1:2:2), 2 × 15 min; iv) TFA/TIS/H$_2$O/EDT (94:1:2.5:2.5), rt, 2 h; b) 2,2'-dipyridyl disulfide, DIEA, DMF, 1 h.
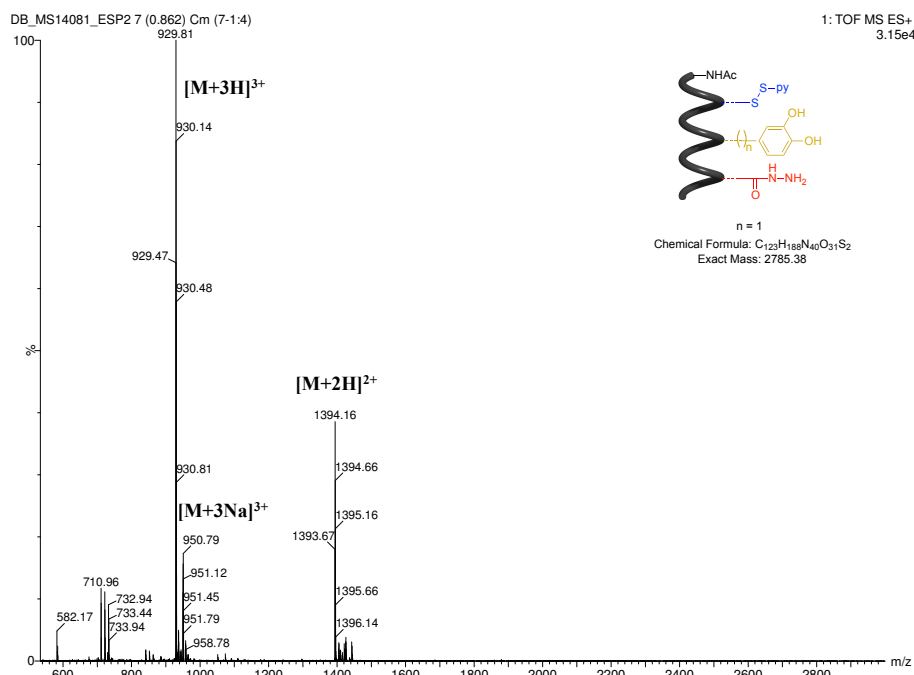
Figure 4-29 ESI-MS(Q-TOF) analysis of purified peptide **4-40** showing M^{3+}, M^{2+} multicharged ions.
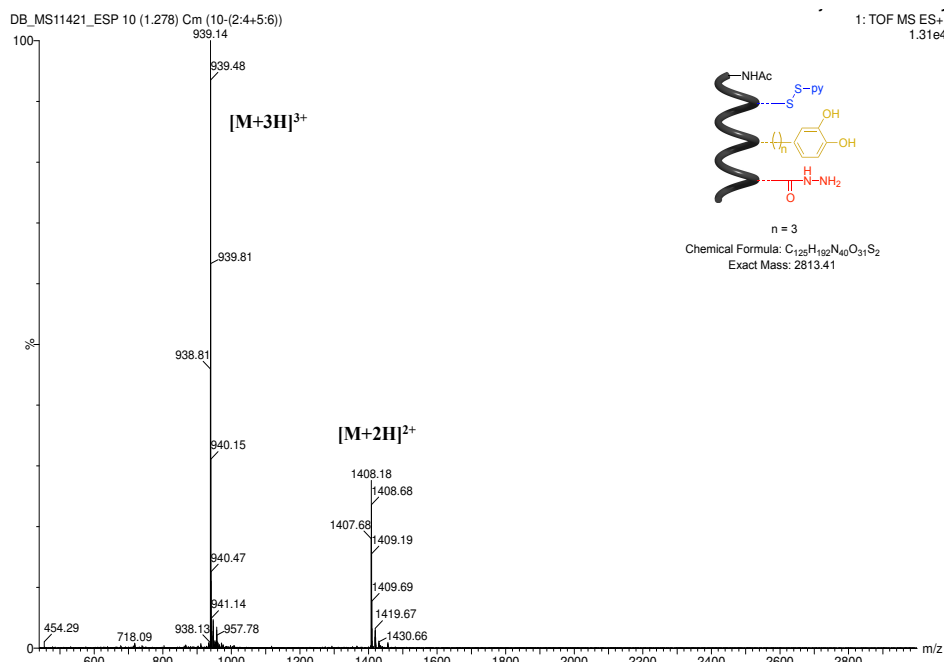
Figure 4-30 ESI-MS(Q-TOF) analysis of purified peptide **4-41** showing M^{3+}, M^{2+} multicharged ions.

Peptides **4-40** and **4-41** were analyzed by ESI-MS(Q-TOF) and the spectra, reported in Figure 4-29 and 4-30, showed the multicharged ions $[M+3H]^{3+}$, $[M+2H]^{2+}$, which after deconvolution, gave the expected monoisotopic mass: 2785.38 and 2813.41 for the rigid (n=1) and flexible (n=3) catechols respectively. Using the standard protocol, the chromophore assembly on scaffolds **4-40** and **4-41** was performed affording respectively **4-42** and **4-43** (Scheme 4-10). After purification,

121

the colored peptides were characterized by mass spectrometry and absorption and fluorescence spectroscopy.
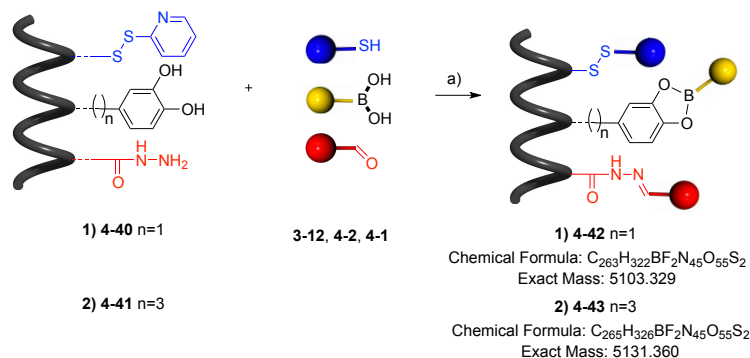
Scheme 4-10 Colored assembly with B-NDI **3-12**, R-PDI **4-2** and Y-Per **4-1** on peptidic scaffold **4-40** and **4-41**; a) *m*-PDA, DMF, 4 h, rt.

The MALDI-TOF analyses of the compounds, reported in Figure 4-31 and 4-32, display peaks corresponding to the products after hydrolysis of the boronate ester (at m/z = 4714.2 and 4742.2 for **4-42** and **4-43** respectively) and the cleavage of disulfide (at m/z = 3737.8 and 3765.8 for **4-42** and **4-43** respectively) occurring during the ionization process. No peaks corresponding to the peptide without R-PDI were found. Furthermore, it is noteworthy to indicate that $[M+Na]^+$ peaks were not observed highlighting the sensitivity of the catechol boronate moiety toward the presence of water.
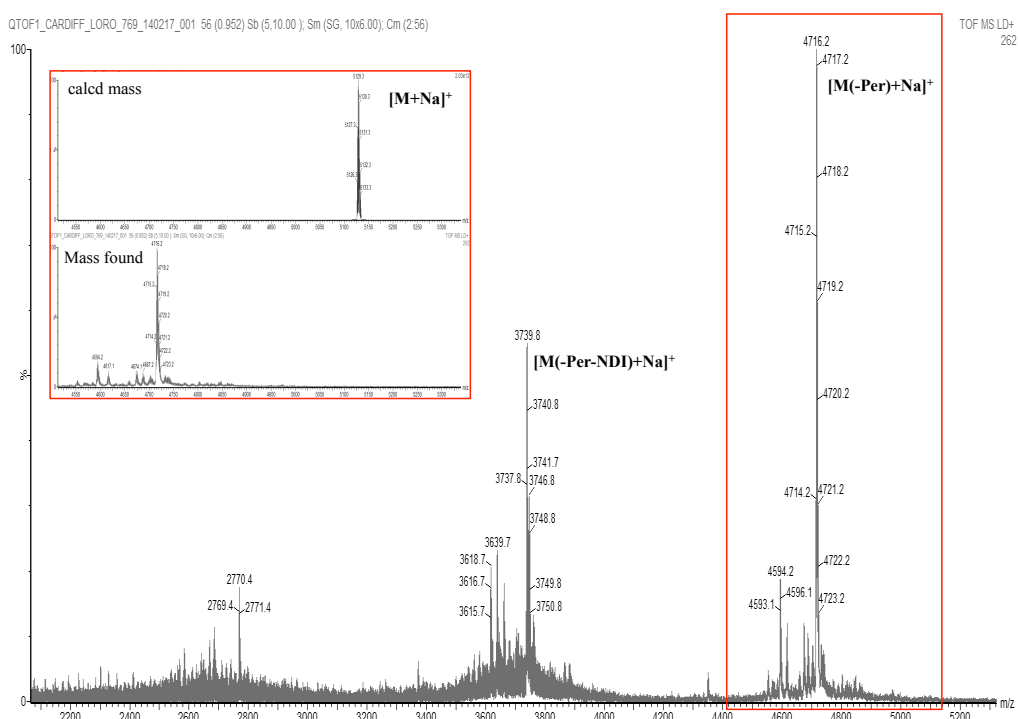
Figure 4-31 MALDI-TOF analysis of purified peptide **4-42**; Inset: Zoom of $[M(\text{-boronate})+Na]^+$ peak (bottom) compared with calculated mass $[M+Na]^+$ (top).
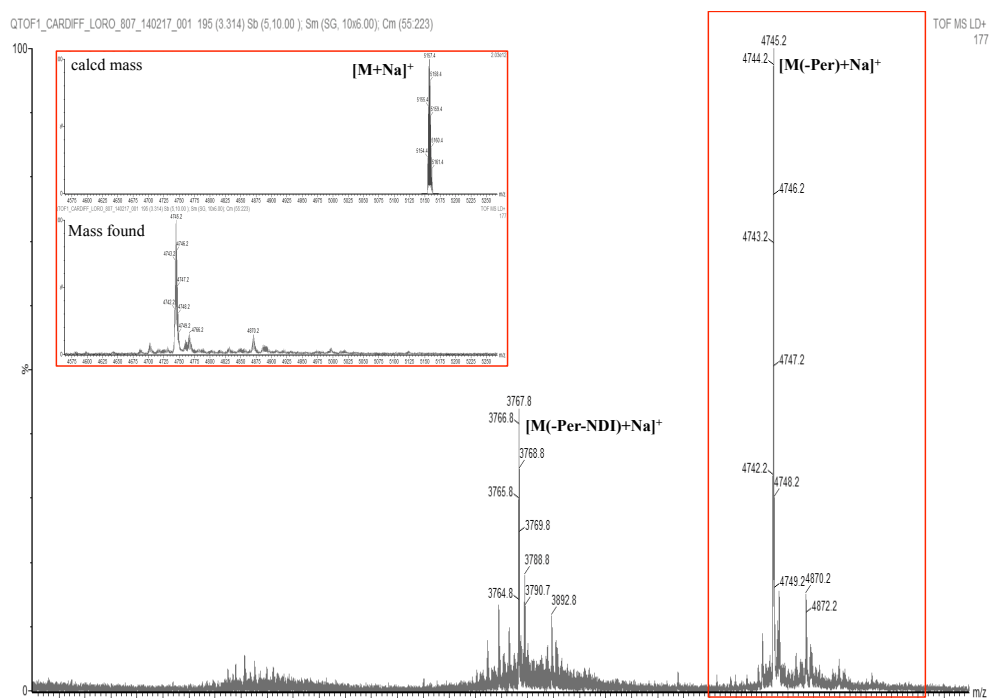
Figure 4-32 MALDI-TOF analysis of purified peptide **4-43**; Inset: Zoom of $[M(\text{-boronate})+Na]^+$ peak (bottom) compared with calculated mass $[M+Na]^+$ (top).

The absorption spectra of **4-42** and **4-43** normalized with the arithmetic sum of the absorption of the dyes on B-NDI show a good correlation in both cases (Figure 4-33).
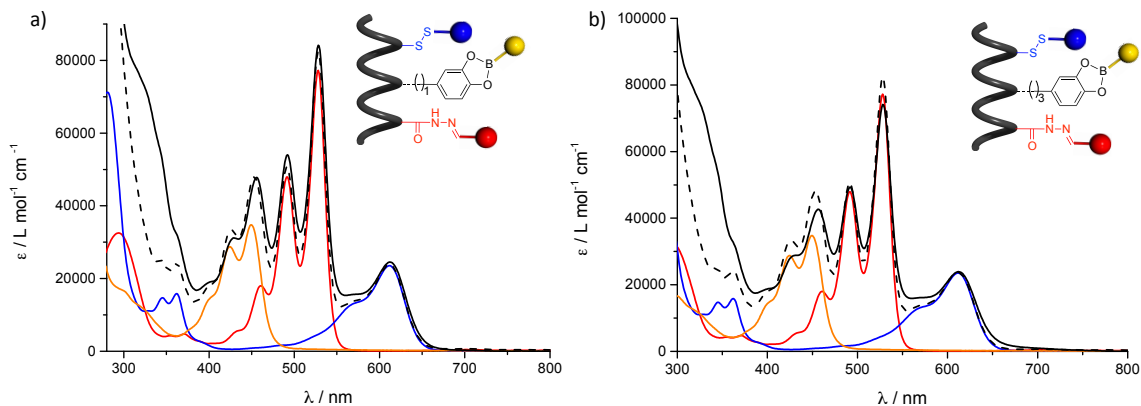
Figure 4-33 Absorption spectra of RYB peptides a) **4-42** (solid black line) with rigid catechol and b) **4-43** (solid black line) with flexible catechol normalized on B-NDI with arithmetic sum (dashed line) of absorption of dyes B-NDI, R-PDI, Y-Per in DMF.

The fluorescence measurements were performed to determine the ET efficiencies Φ_{ET} (Figures 4-34, 4-35) and those results are gathered in Table 4-3. In comparison with RYB peptide **4-23** bearing the bicyclic diol, the calculated Φ_{ET} for catechol peptides **4-42** and **4-43** are slightly lower: Φ_{ET} (R-PDI→B-NDI) around 18% for **4-42** and 16% for **4-43**, Φ_{ET} (Y-Per→B-NDI) around 4% for **4-42** and 5% for **4-43**.

123
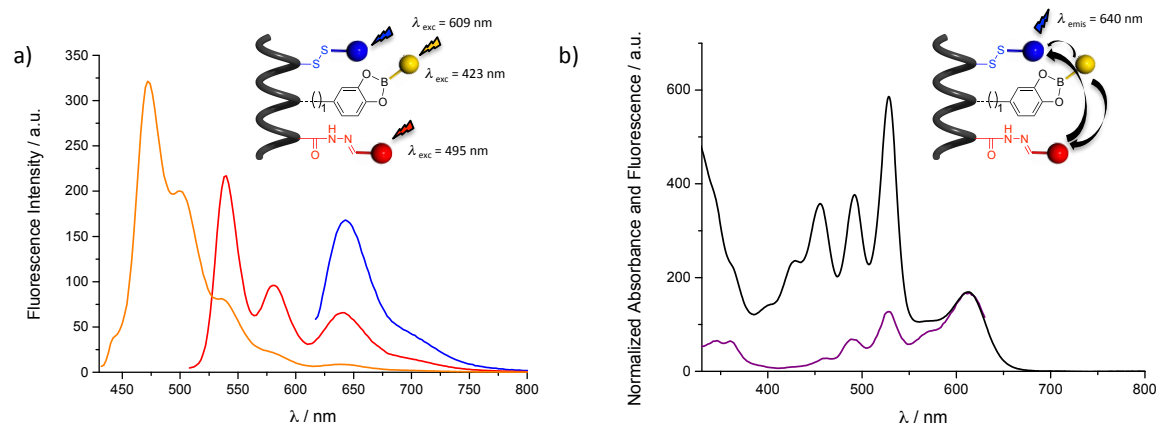
Figure 4-34 a) Fluorescence emission spectra of YRB peptide **4-42** at *(λ_exc)* 423 nm (yellow), 495 nm (red), 609 nm (blue) to determine ET efficiencies following the method 1: $\Phi_{ET} = QY^*_{B\text{-}NDI}/QY_{B\text{-}NDI}$; b) Normalized absorption (black) and fluorescence excitation (purple) spectra of YRB peptide **4-42** (λ_{em}=640 nm) for the method 2: $\Phi_{ET} = Ex_D/A_D$.
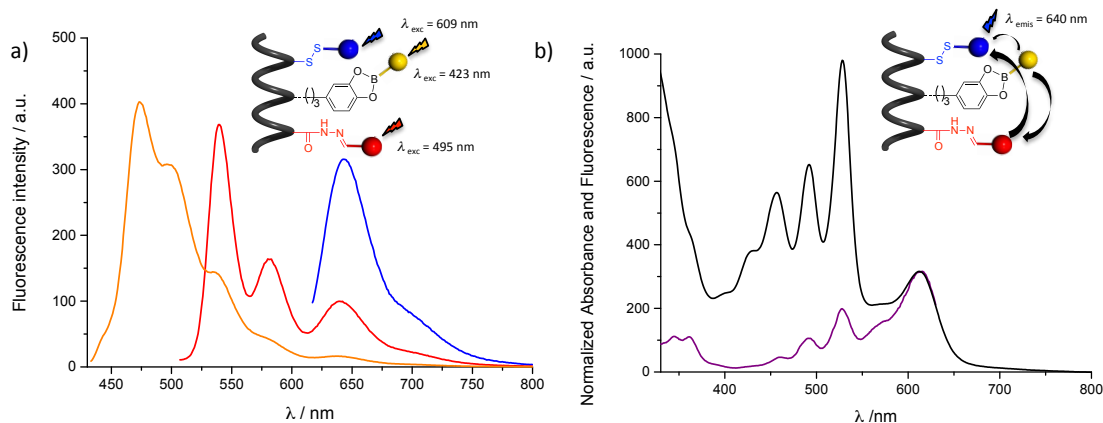
Figure 4-35 a) Fluorescence emission spectra of YRB peptide **4-43** at (λ_{exc}) 423 nm (yellow), 495 nm (red), 609 nm (blue) to determine ET efficiencies following the method 1: $\Phi_{ET} = QY^*_{B\text{-}NDI}/QY_{B\text{-}NDI}$; b) Normalized absorption (black) and fluorescence excitation (purple) spectra of YRB peptide **4-43** (λ_{em}=640 nm) for the method 2: $\Phi_{ET} = Ex_D/A_D$.

Table 4-3 Energy transfer efficiencies within **4-42, 4-43** and **4-23** calculated following methods 1 and 2.

Entry	Peptides	Methods	Φ_{ET} (R-PDI→B-NDI) %	Φ_{ET} (Y-Per→B-NDI) %
1	RYB **4-42** (n=1)	1: $\Phi_{ET} = QY^*_{B\text{-}NDI}/QY_{B\text{-}NDI}$	18	4.2
		2: $\Phi_{ET} = Ex_D/A_D$	17.4	4
2	RYB **4-43** (n = 3)	1	16.6	4.7
		2	16.2	4.6
3	RYB **4-23**	1	21.9	7.7
		2	21.8	7.4

To summarize, the bicyclic diol receptor site into the peptidic scaffold has been successfully replaced by planar catechol derivatives in order to enhance the spatial overlap of the dyes favoring

the ET. Nevertheless, the ET efficiencies obtained in the new colored peptides **4-42** and **4-43** (with catechol) have been found to be lower than those calculated for peptide RYB **4-23** (with bicyclic diol) as reported in Table 4-3. The boronic ester linkage into catechol-based peptides appeared to be less stable than the one obtained from the bicyclic diol, as illustrated in the MALDI-Tof analyses, in which $[M+Na]^+$ peaks were not observed. Indeed, the conjugation of the catechol moiety makes those derivatives more Lewis acidic and so more sensitive toward hydrolysis. Hence, we can imagine that the partial hydrolysis of the boronic ester linkage within **4-42** and **4-43** occurred at low concentration (during the fluorescence measurements) resulting in the ET efficiencies decreasing. Based on this hypothesis: the potential partial hydrolysis of the boronate linkage at low concentration in DMF, we were finally interested to study the effect of the solvent of the assembly on the ET efficiencies.

4.1.3 Effect of the solvent

N,N'-dimethyformamide (DMF) is a widely used solvent, however its thermal degradation favored by the extrusion of carbon monoxide can easily occur in the presence of water producing dimethylamine. The presence of traces of dimethylamine and water, especially under very diluted conditions (for the fluorescence measurements), might catalyze the hydrolysis of the boronic ester linkage, explaining the low ET efficiencies between Y-Per and B-NDI.

In this respect, we were interested to investigate the effect of the solvent of the assembly and photophysical analyses on the energy transfer. However, after the chromophoric assembly, the triad is difficult to solubilize in usual solvents due to its amphiphilic nature coming from the protic peptidic backbone and the very hydrophobic chromophores. So, only few polar aprotic solvents have been found to be suitable to solubilize the triad such as DMF or dimethylacetamide (DMA). DMA is very similar to DMF in term of structure and properties, but its highest stability makes it a good candidate for the chromophoric assembly. Accordingly, the assembly of the dyes was performed on Ac-QLA-X(disulfide)-QLAQLA-X(diol)-QLAQLA-X(hydrazide)-NH$_2$ **4-22** in distillated DMA for 4 h at rt as shown in Scheme 4-11. After purification by GPC, the material was analyzed by mass spectrometry, absorption and fluorescence spectroscopy.
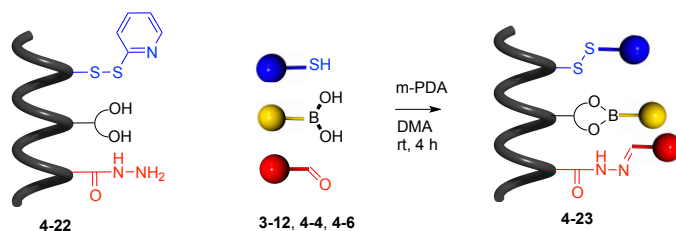
Scheme 4-11 Chromophore assembly on peptide **4-22** with B-NDI, R-PDI, Y-Per in DMA.

After performing the reaction in DMA, MALDI-TOF analysis of **4-23**, reported in Figure 4-36, displays $[M+Na]^+$ (m/z: 5235.4) as the main peak. Peaks corresponding to the product after hydrolysis of the boronate ester (m/z: 4823.2; m/z: 3846.8) and cleavage of disulfide (m/z: 4259.0; m/z: 3846.8) occurring during the ionization were found.
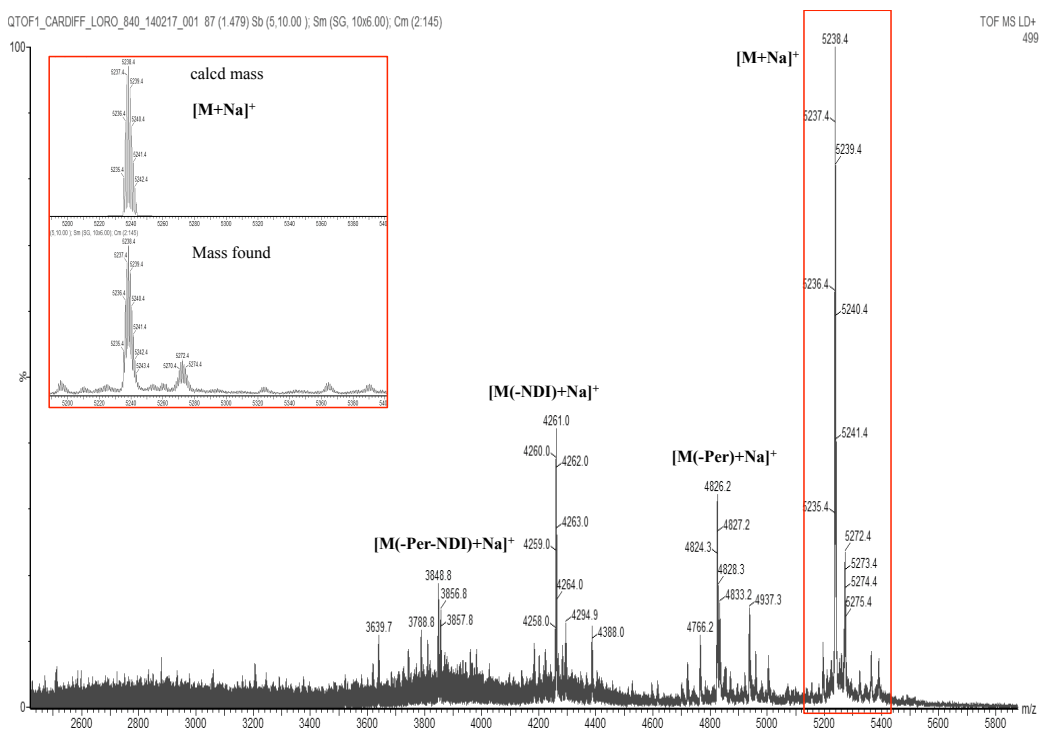
Figure 4-36 MALDI-TOF analysis of purified peptide **4-23**; Inset: Zoom of $[M+Na]^+$ peak (bottom) compared with calculated mass $[M+Na]^+$ (top).

The normalization of the absorption spectrum of **4-23** in DMA with the arithmetic sum of the dyes shows a good correlation confirming the quantitative introduction of the chromophores as in DMF (Figure 4-37).
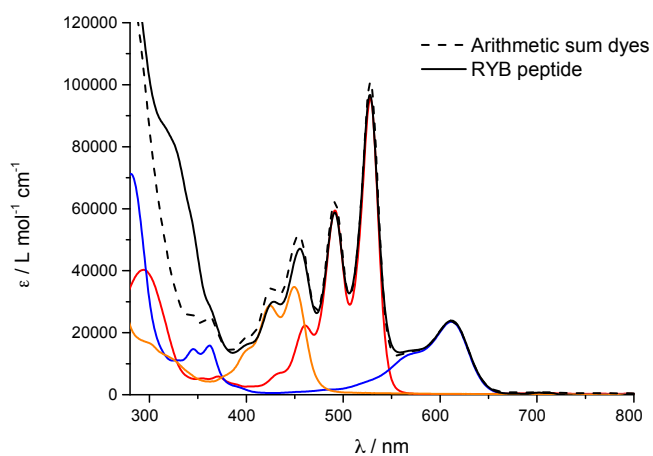
Figure 4-37 Absorption spectra of RYB peptide **4-23** in DMA normalized on B-NDI with arithmetic sum of absorption of dyes B-NDI, R-PDI, Y-Per in DMA.

Finally, the fluorescence measurements were monitored in DMA and compared with those obtained in DMF to evaluate the ET efficiencies (Figure 4-38). Φ_{ET} (R-PDI→B-NDI) was estimated to be 22% in both solvent while Φ_{ET} (Y-Per→B-NDI) was significantly improved in DMA, being determined to be around 15% possibly due to the less favored hydrolysis of the boronate ester in this solvent at low concentration (Table 4-5).
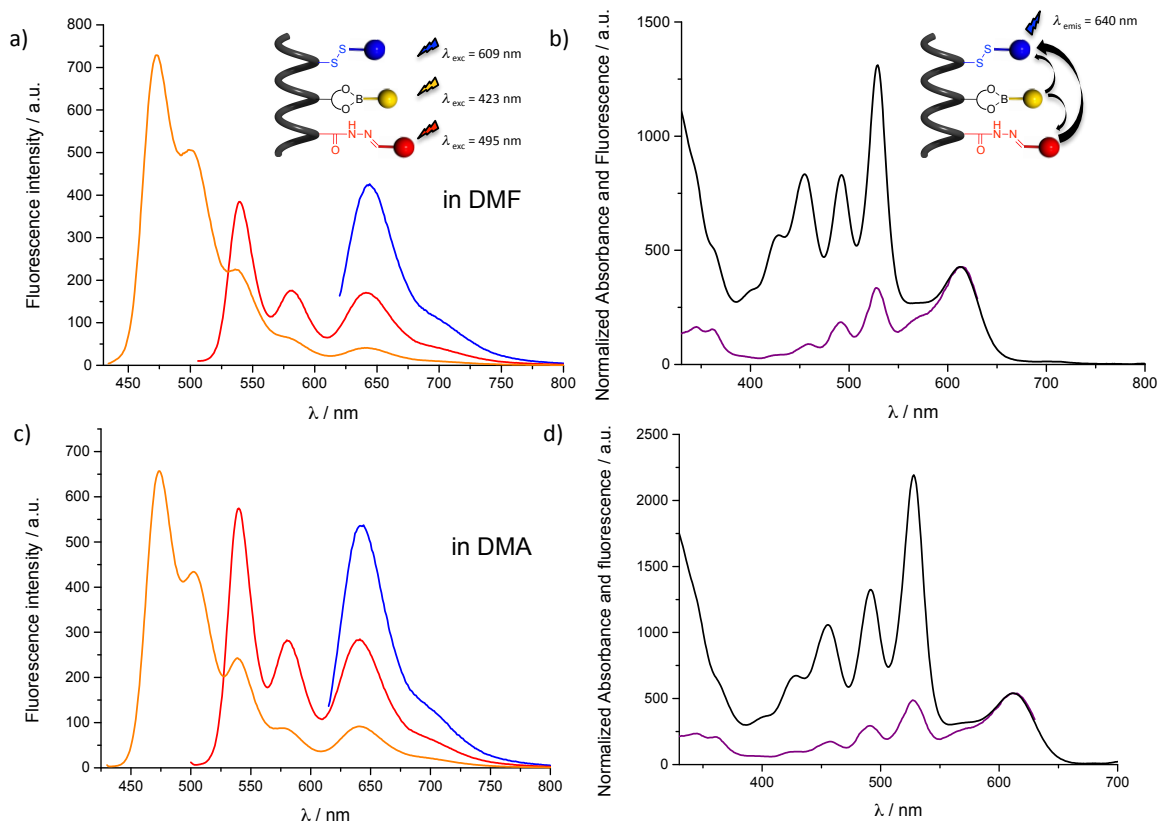
Figure 4-38 Fluorescence emission spectra of YRB peptide **4-23** at (λ_{exc}) 423 nm (yellow), 495 nm (red), 609 nm (blue) to determine ET efficiency following the method 1: $\Phi_{ET} = QY^*_{B\text{-}NDI}/QY_{B\text{-}NDI}$ in a) DMF and c) DMA; Normalized absorption and fluorescence excitation spectra of YRB peptide **4-23** ($\lambda_{em} = 640$ nm) for the method 2: $\Phi_{ET} = Ex_D/A_D$ in b) DMF and d) DMA.

Table 4-5 Energy transfer efficiencies within **4-23** calculated following methods 1 and 2.

Entry	Peptide	Solvent	Methods	Φ_{ET} (R-PDI→B-NDI) %	Φ_{ET} (Y-Per→B-NDI) %
1	RYB **4-23**	DMF	1: $\Phi_{ET} = QY^*_{B\text{-}NDI}/QY_{B\text{-}NDI}$	21.9	7.7
			2: $\Phi_{ET} = Ex_D/A_D$	21.8	7.4
2	RYB **4-23**	DMA	1	22	14
			2	22	15

4.2 Conclusion

To conclude, the versatility of the system has been widely explored in this chapter with the aim to improve the ET efficiencies. The system has been deeply understood and the major problems, leading to the low Φ_{ET}, have been highlighted and solved. In order to simplify the description of the results obtained in this chapter, Figure 4-39 recapitulates its major achievements. In the first part, a new generation of chromophores was prepared with better spectral overlaps between the fluorescence of the donor units and the acceptor absorption, and higher donor quantum yields. In particular, new R-PDI **4-2** exhibits a very high quantum yield (QY=94% compared to 4% for **3-13**) thanks to the substitution of the electron rich benzyl amine into linear TEG chains. This allowed obtaining new multichromophoric architectures with tailored absorbed and emitted colors with a significant improvement of the ET efficiency for R-PDI→B-NDI (Φ_{ET} from 5 to 19%). The second part of the chapter focused on the modifications of the peptidic scaffold and their effect on the ET efficiencies Φ_{ET}. In this respect, the distance between the chromophoric units, their order and dipole orientation were changed. By increasing the interchromophoric distance from 1.08 nm to 1.62 and 2.16 nm, no effect was noticed on the Φ_{ET}. Placing the primary yellow donor between R-PDI and B-NDI surprisingly increased the Φ_{ET} despite the bidirectional ET. Finally, the replacement of bicyclic diol by planar catechol derivatives to enhance the spatial overlap of the dyes did not improve the Φ_{ET}; in fact, Φ_{ET} decreased. This is due to the low stability of the catechol based boronate ester, very sensitive toward the presence of water. The hydrolysis of the boronate favors the release of the free yellow dye in solution not capable to participate further in the ET processes. The latter study has led to investigate the effect of the solvent on Φ_{ET}; in this respect, DMA has been found to significantly improve of the Φ_{ET} for Y-Per→B-NDI (from 5 to 15%). This is possibly due to the less favored hydrolysis of boronate linker in this solvent containing a negligible amount of dimethylamine compared to DMF.

4.2.1 Effect of the chromophores

Peptides	Dyes	Φ_{ET} (Y→B)	Φ_{ET} (R→B)
3-37	3-12, -13, -14	5%	5.6%
4-13	3-12, -13, 4-1	7.5%	7.5%
4-14	3-12, 4-2, 4-1	3.5%	18.5%

4.2.2.1 Effect of distance between dyes

Dyes involved: **3-12, 4-2, 4-1**

1.08, 1.62, 2.16 nm

Peptides	Distance	Φ_{ET} (Y→B)	Φ_{ET} (R→B)
4-14	1.08 nm	3.5%	18.5%
4-19	1.62 nm	2.8%	17%
4-20	2.16 nm	2.5%	18.7%

4.2.2.2 Effect of order of dyes

Dyes involved: **3-12**, **4-2**, **4-1**

Peptides	Order	Φ_{ET} (Y→B)	Φ_{ET} (R→B)
4-14	Y-R-B	3.5%	18.5%
4-23	R-Y-B	7.5%	21.9%

4.2.2.3 Effect of dipole orientation of Y-Per unit

Dyes involved: **3-12**, **4-2**, **4-1**

Peptides	Amino acid	Φ_{ET} (Y→B)	Φ_{ET} (R→B)
4-23	3-3	7.5%	21.9%
4-42	4-24	4.1%	17.7%
4-43	4-25	4.7%	16.6%

Assembly and analyses in DMF for 4.2.1 and 4.2.2

4.2.3 Effect of solvent

Assembly and Analyses in DMA

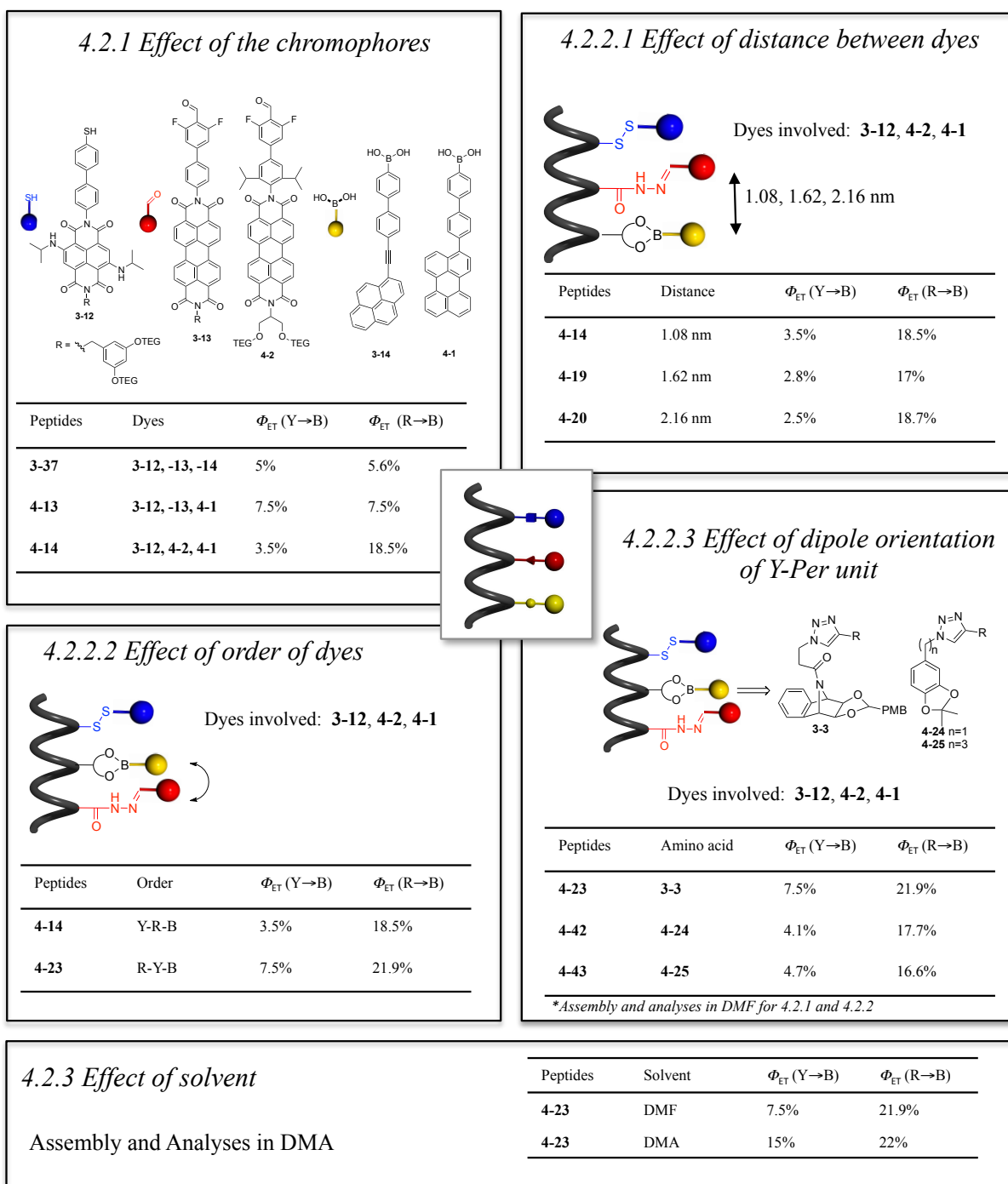| Peptides	Solvent	Φ_{ET} (Y→B)	Φ_{ET} (R→B)
4-23	DMF	7.5%	21.9%
4-23	DMA	15%	22%

Figure 4-39 Summary of the chapter.

4.3 References

[1]   L. Rocard, A. Berezin, F. De Leo, D. Bonifazi, *Angew. Chem. Int. Ed.* **2015**, *54*, 15739-15743.

[2]   a) Z. Sun, Q. Ye, C. Chi, J. Wu, *Chem. Soc. Rev.* **2012**, *41*, 7857-7889; b) J. T. Markiewicz, F. Wudl, *ACS Appl. Mater. Interfaces* **2015**, *7*, 28063-28085.

[3]   I. B. Berlman, *Handbook of fluorescence spectra of aromatic molecules*, Academic Press: New York, **1971**.

[4]   K. Kawasumi, K. Mochida, Y. Segawa, K. Itami, *Tetrahedron* **2013**, *69*, 4371-4374.

[5]   a) F. Würthner, *Chem. Commun.* **2004**, 1564-1579; b) F. Würthner, C. Thalacker, S. Diele, C. Tschierske, *Chem. Eur. J.* **2001**, *7*, 2245-2253.

[6]   P. D. Frischmann, F. Würthner, *Org. Lett.* **2013**, *15*, 4674-4677.

[7]   É. Torres, M. N. Berberan-Santos, M. J. Brites, *Dyes Pigm.* **2015**, *112*, 298-304.

[8]   S. J. Coutts, J. Adams, D. Krolikowski, R. J. Snow, *Tetrahedron Lett.* **1994**, *35*, 5109-5112.

[9]   R. Kota, R. Samudrala, D. L. Mattern, *J. Org. Chem.* **2012**, *77*, 9641-9651.

[10]   M. Fischer, J. Georges, *Chem. Phys. Lett.* **1996**, *260*, 115-118.

[11]   G. Seybold, G. Wagenblast, *Dyes Pigm.* **1989**, *11*, 303-317.

[12]   N. Sewald, H. D. Jakubke, *Peptides: Chemistry and Biology: Second Edition*, Wiley-VCH, Weinheim, **2009**.

[13]   a) J. R. Lakowicz, *Principles of fluorescence spectroscopy 3rd Edition*, Springer, Singapore, **2006**; b) I. B. Berlman, *Energy Transfer Parameters of Aromatic Compounds*, Academic Press, New York, **1973**.

[14]   a) W. B. Davis, M. A. Ratner, M. R. Wasielewski, *Chem. Phys.* **2002**, *281*, 333-346; b) C. Thalacker, C. Röger, F. Würthner, *J. Org. Chem.* **2006**, *71*, 8098-8105.

[15]   R. R. Bikbulatov, T. V. Timofeeva, L. N. Zorina, O. G. Safiev, V. V. Zorin, D. L. Rakhmankulov, *Zh. Obshch. Khim.* **1996**, *66*, 1854-1855.

[16]   W. W. Sy, *Synth. Commun.* **1992**, *22*, 3215-3219.

5. Templated chromophore assembly by dynamic and non-dynamic covalent bonds

In the two previous chapters, we described the creation of multichromophoric architectures using pre-programmed peptides bearing receptor sites in which three chromophoric units were assembled by dynamic covalent bonds. This chapter will focus on the extension of the absorption range of the multichromophoric system by introducing additional chromophores. This will be achieved by using simultaneously to the dynamic covalent reactions, non-dynamic reactions: the strain-promoted azide alkyne and the inverse electron demand Diels-Alder cycloadditions.

The chapter will be divided in two sections: *i)* in *Section 5.2.1*, new chromophoric units bearing suitable functional groups (ADIBO and TCO involved in non-dynamic reactions) will be developed; while *ii)* Section *5.2.2* will be dedicated to the creation multichromophoric systems involving the cycloadditions. In the latter, the synthesis of new modified amino acids, peptidic scaffolds, and the chromophoric assembly will be described.

For her help in the preparation of the tripeptide reported in *Section 5.2.2.1.3*, I want to kindly acknowledge *Dr Olesia Kulyk*. Besides, for their outstanding work regarding the photophysical characterization of complex multichromophoric structures (tetrad **5-56** and pentad **5-64**) and the determination of optoelectronic properties of dyes (in *Section 5.2.1.3*), I greatly thank *Dr. Andrea Fermi* and *Dr. Nicola Armaroli* (ISOF Bologna).

5.1 Context and aim of the chapter

In *Chapters 3 and 4*, various multichromophoric architectures have been prepared by templating dyes on a pre-programmed peptide. The controlled self-assembly was achieved by using orthogonal recognition motifs based on three dynamic covalent reactions: the disulfide exchange between the activated disulfide-pyridine and thiol, the acyl hydrazone formation between an hydrazide and an electron poor aldehyde in the presence of a nucleophilic catalyst (*m*-PDA) and the boronate ester formation between a bicyclic diol and a boronic acid.

The aim of this chapter is to extend the absorption range of the multichromophoric system, and consequently the efficiency of the artificial antenna. In this respect, the introduction of additional chromophores (four and later five) in the architecture is targeted. To selectively achieve the incorporation of new dyes in the system, two non-dynamic covalent reactions have been explored in *Chapter 2*: the strain-promoted azide alkyne cycloaddition (SPAAC) with aza-dibenzocyclooctyne (ADIBO) and the inverse electron demand Diels-Alder (IEDDA) reaction between dipyridyl-*s*-tetrazine and *trans*-cyclooctene (TCO). The orthogonality of those reactions with the dynamic covalent bonds has been proven by performing simultaneously the five reactions leading to the quantitative formation of the expected products (Scheme 5-1). Hence, those non-dynamic covalent reactions can be used as new orthogonal recognition motifs in the multichromophoric structure.
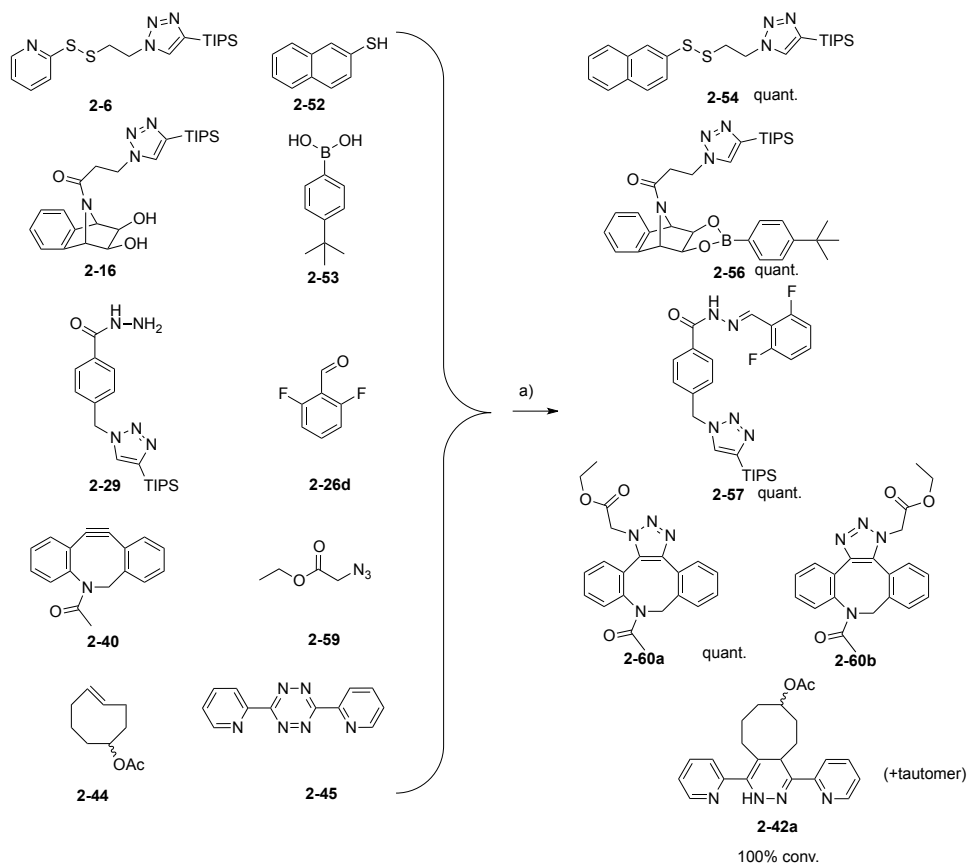
Scheme 5-1 Simultaneous disulfide interchange, boronate, acyl hydrazone formation, ADIBO-azide cycloaddition, tetrazine ligation; a) *m*-PDA, THF, rt, 1 h.

The chapter will address the design and synthesis of new peptidic scaffolds and chromophoric units bearing the new involved functional groups: azide, tetrazine, ADIBO, TCO; and so, the creation of tetra- and pentachromophoric architectures. In this respect, ethynylpyrene, perylene,

PDI, NDI and cyanine (with complementary spectral properties) will be selectively assembled into the scaffold to give a material absorbing over the whole visible spectrum; and the controlled incorporation of the dyes following their energy gradient will favor the unidirectional energy transfer within the structure (Figure 5-1).
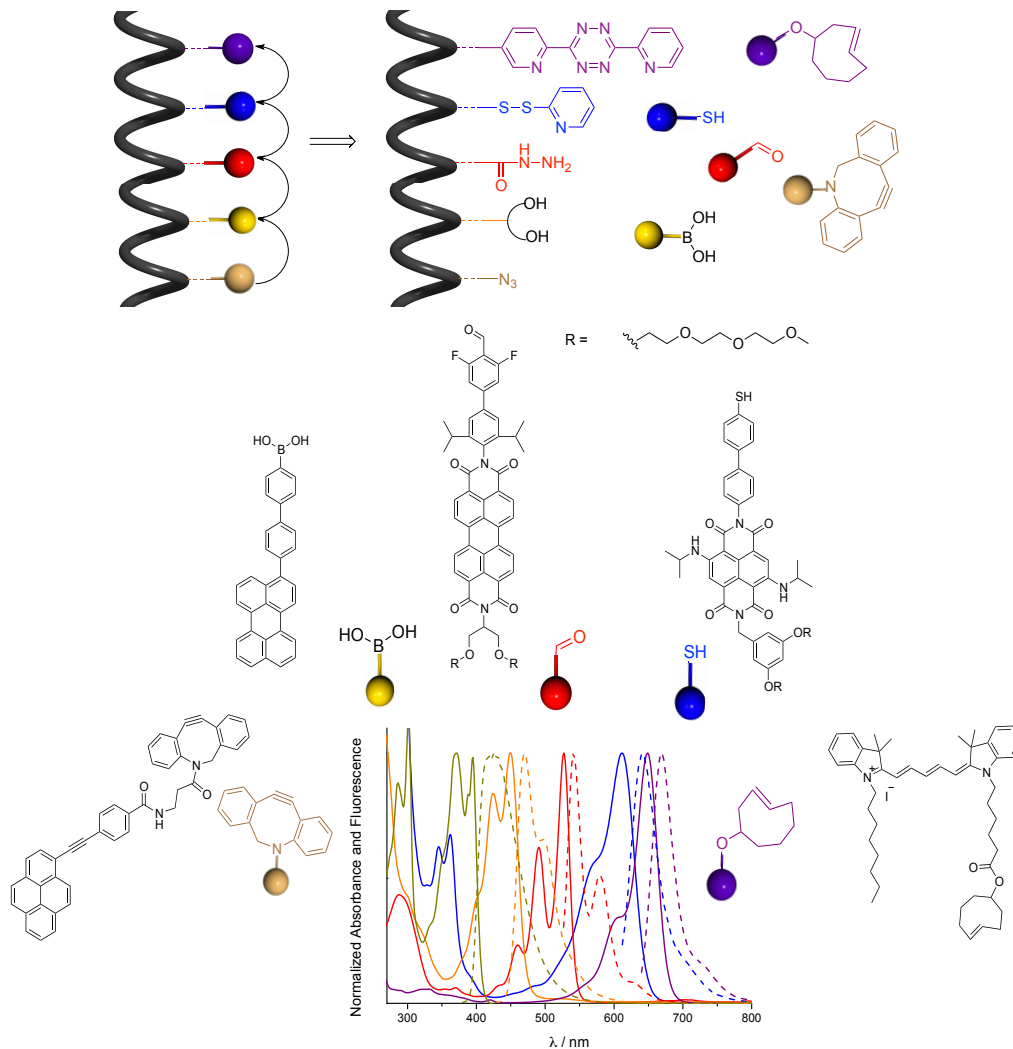
Figure 5-1 Top: Schematic representation of the creation of the fully extended absorption range multichromophoric peptide; Bottom: Structure and normalized absorbance (solid line) and fluorescence emission (dashed line) of ADIBO-ethynylpyrene (green), Y-Per (orange), R-PDI (red), B-NDI (blue), B-Cy (purple) in DMF.

5.2 Results and discussion

For the preparation of an extended absorption range multichromophoric system bearing 5 dyes, the same synthetic approach developed in the previous chapters will be applied. Hence, the preparation of new chromophores and peptidic scaffolds functionalized by recognition motifs followed by their assembly is described in the following sections.

133

5.2.1 Development of ADIBO and TCO-chromophores

As shown in Figure 5-1, to apply the SPAAC and the IEDDA to the chromophoric decoration of the peptide, it has been decided to introduce the most reactive functional groups on the dyes and the others on the peptidic scaffold. In this respect, TCO and ADIBO moieties can be anchored to the chromophoric motif to avoid their exposure to the conditions of the SPPS. Two different ADIBO-dyes have been targeted: first, a perylene derivative **5-1,** will be introduced in trichromophoric architectures with PDI and NDI moieties in order to compare the ET efficiencies with those obtained in *Chapter 4*. The second, **5-2**, an ethynylpyrene derivative, will be introduced in tetra- and pentachromophoric systems allowing the extension of the absorption to lower wavelength (Figure 5-2). For the TCO-dye, pentamethylcyanine **5-3,** absorbing and emitting light at higher wavelengths than B-NDI (λ_{abs}>612 nm; λ_{em}>640 nm), has been selected as final energy acceptor in the pentachromophoric system. The preparation of those three compounds is presented in this section.
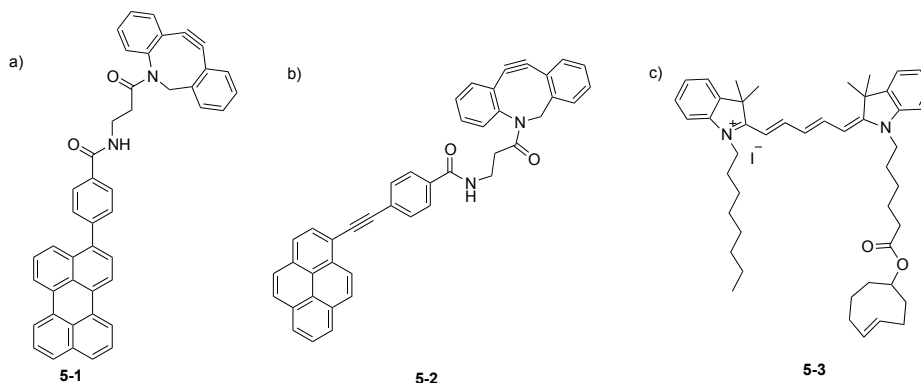

Figure 5-2 Targeted ADIBO- and TCO-chromophores: a) ADIBO-perylene **5-1**; b) ADIBO-ethynylpyrene **5-2**; c) TCO-pentamethylcyanine **5-3**.

5.2.1.1 Synthesis and characterization of ADIBO-chromophoric units

For the preparation of ABIDO-chromophores **5-1** and **5-2**, the retrosynthetic pathway is based on the amide coupling between cyclooctyne-amine **5-10** and the chromophoric moiety bearing a carboxylic acid. The synthesis of amine-ADIBO **5-10**, described in Scheme 5-2, follows the literature procedure.[1] β-Alanine **5-4** was protected with trifluoroacetyl group using ethyltrifluoroacetate and the carboxylic acid **5-5** was subsequently activated into acyl chloride **5-6** by using oxalyl chloride and a catalytic amount of DMF. Afterwards, acyl chloride **5-6** was coupled with dibenzocycloctene **2-37** (prepared in *Chapter 2*) to afford **5-7** in 77% yield. The olefin was converted into acetylene moiety *via* a bromination-dehydrobromination procedure to give **5-9** in 87% yield over two steps. Finally, the amine deprotection was performed in the

presence of K_2CO_3 in MeOH affording **5-10**. The latter was not isolated due to its low stability and tendency to polymerize, and was directly introduced into the chromophoric coupling.
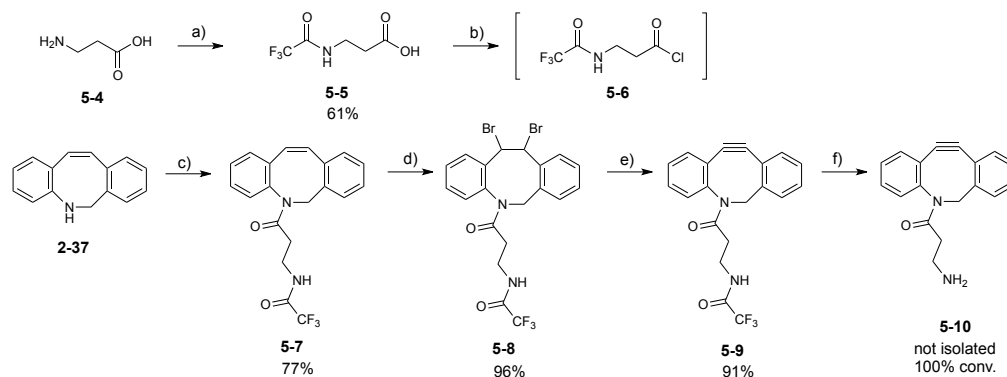
Scheme 5-2 Synthesis of ADIBO-amine **5-10**; a) ethyltrifluoroacetate, NEt₃, MeOH, rt, 24 h; b) oxalyl chloride, DMF (cat), CH_2Cl_2, rt, 2 h; c) **5-6**, pyridine, CH_2Cl_2, rt, 1 h; d) pyridinium tribromide, CH_2Cl_2, rt, 18 h; e) *t*BuOK, THF, rt, 1 h; f) K_2CO_3, MeOH/H_2O, rt, 18 h.[1b]

All intermediates were characterized in accordance with the literature.[1b] Having in hands ADIBO-amine **5-10**, a large variety of ADIBO-chromophores can be easily obtained by amide bond formation.

The synthesis of ADIBO-perylene **5-1** commenced with a Pd-catalyzed Suzuki cross-coupling between 3-bromoperylene **4-4** and 4-methoxycarbonylphenylboronic acid in the presence of Pd tetrakis and K_2CO_3 affording **5-11** in 75% yield. The methyl ester was subsequently hydrolyzed under basic conditions and the amide bond was formed between acid **5-12** and amine **5-10** in 66% yield using EDC·HCl as coupling agent and a catalytic amount of DMAP (Scheme 5-3).
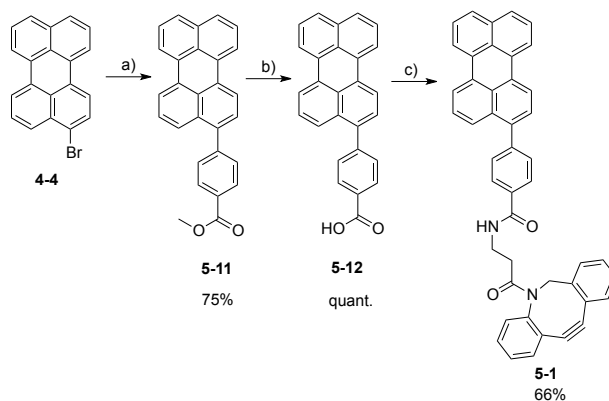
Scheme 5-3 Synthesis of ADIBO-perylene **5-1**; a) 4-Methoxycarbonylphenylboronic acid, [Pd(PPh₃)₄], K_2CO_3, dioxane/H_2O (7:1), 80 °C, 16 h; b) NaOH 2M (aq), THF/EtOH, rt, 16 h; c) ADIBO-amine **5-10**, EDC.HCl, DMAP, CH_2Cl_2, rt, 20 h.

For ADIBO-ethynylpyrene **5-2**, a similar strategy was adopted. Ethynylpyrene **3-32** was first coupled with methyl-4-bromo-benzoate by Pd-catalyzed Sonogashira cross-coupling affording **5-**

13 in 55% yield. The hydrolysis of the methyl ester was performed and the amide bond formation was carried out under the same conditions as before with amine **5-10** yielding **5-2** (Scheme 5-4).
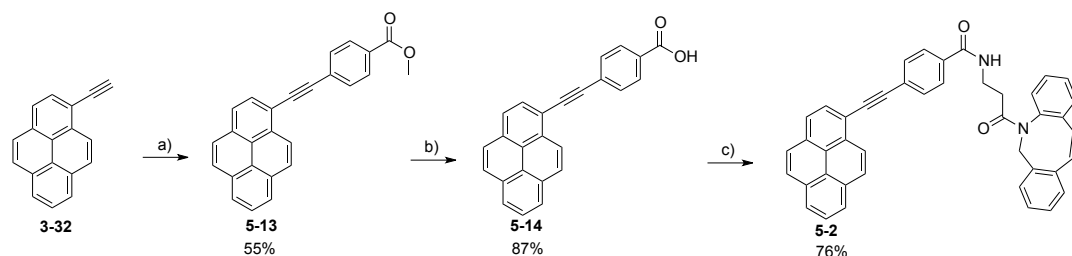
Scheme 5-4 Synthesis of ADIBO-ethynylpyrene **5-2**; a) methyl-4-bromo-benzoate, $[Pd(PPh_3)_2Cl_2]$, CuI, NEt_3, THF, 40 °C, 16 h; b) NaOH 2M (aq), THF/EtOH, rt, 3 h; c) ADIBO-amine **5-10**, EDC.HCl, DMAP, CH_2Cl_2, rt, 20 h.

ADIBO-chromophores **5-1** and **5-2** and intermediates were fully characterized by melting points, infrared, ^{1}H and ^{13}C NMR spectroscopy, and HR mass spectrometry. Furthermore, UV-Vis absorption and fluorescence emission spectra of the perylene and ethynylpyrene derivatives show similar profiles than chromophores Y-Py **3-11** and Y-Per **4-1** previously prepared in *Chapter 3* and *4* (Figure 5-3). The photophysical properties of the two compounds are detailed in Table 5-1.
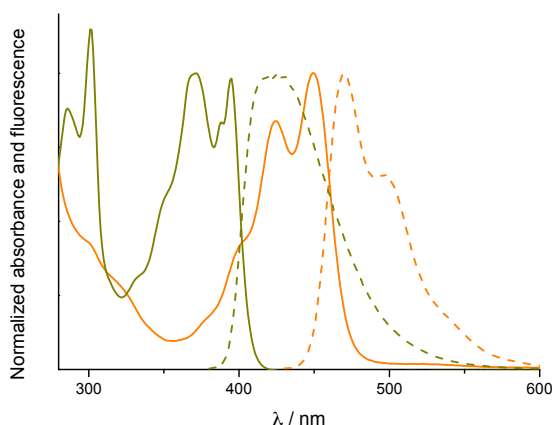
Figure 5-3 Normalized absorbance (solid line) and fluorescence emission (dashed line) of ADIBO-perylene **5-1** (λ_{exc} = 423 nm, orange) and ADIBO-ethynylpyrene **5-2** (λ_{exc} = 371 nm, green) in DMF.

Table 5-1 Photophysical characterization of ADIBO-perylene and ADIBO-ethynylpyrene in DMF.

Entry	Dyes	$\lambda_{max\ abs}$ / nm	ε / L mol^{-1} cm^{-1}	$\lambda_{max\ em}$ / nm	QY/%
1	ADIBO-Per **5-1**	450, 424	45000, 37000	470, 496	96[a]
2	ADIBO-Py **5-2**	395, 371	39000, 39600	426	48[b]

QY determined from [a]perylene (QY=94% in cyclohexane),[2] [b]quinine hemisulfate (QY=54.6% in 0.5 M H_2SO_4)[3]

5.2.1.2 Development and characterization of TCO-cyanine

For the extension of the absorption range of the multichromophoric architecture at higher wavelength than 620 nm, the introduction of a new dye through IEDDA cycloaddition was investigated. In this respect, our attention focused on the well-developed cyanine dyes widely used as fluorescence probes in bioconjugation or in optoelectronic applications,[4] and employed as FRET acceptors.[5] The structure of cyanine is composed of two quaternized nitrogen-containing heterocycles which are bridged by a polymethine chain.[6] Depending on the number of carbon in the polymethine chain, cyanine (Cy) can absorb from the visible to the near-IR. For instance, classic Cy3 fluoresces in the green region; while Cy5 emits in the near-IR. Indolium-based pentamethine cyanine Cy5 was selected, its absorption band maxima being located at around 650 nm (ε around 10^5 L mol^{-1} cm^{-1}).[7]
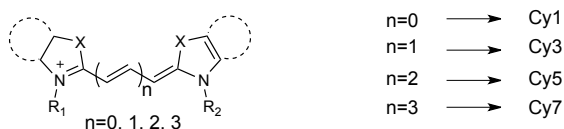

Figure 5-4 Schematic representation of classic cyanines.

The synthesis of TCO-pentamethylcyanine **5-3** required unsymmetrical cyanine **5-19**, bearing on one of the indolium, an anchoring chain with a carboxylic acid and, on the other, a solubilizing n-octyl chain, which was obtained following the literature procedure.[7] Accordingly, two cyanine precursors **5-16** and **5-17**, containing an activated methyl group, were prepared by quaternization of 2,3,3-trimethylindolenine **5-15** with 1-iodooctane and 6-bromohexanoic acid in 75% and 61% yields respectively. Then, activated intermediate **5-18** was synthesized by a condensation reaction between **5-16** and malondialdehyde dianil, as a chain cyanine agent, under reflux in Ac$_2$O for 2 h. The compound was not isolated and directly used in a following condensensation reaction, affording desired cyanine **5-19** in 51% yield over two steps, in the presence of **5-17** and NaOAc. Finally, the introduction of *trans*-cyclooctenol **2-43** was carried out by esterification in the presence of EDC·HCl and DMAP to yield final cyanine **5-3** (Scheme 5-5). TCO-cyanine **5-3** and intermediates were fully characterized by infrared, ^{1}H and ^{13}C NMR spectroscopy, and HR mass spectrometry. ESI-HRMS(Q-Tof) analysis in positive mode of TCO-cyanine **5-3,** shown in Figure 5-5 a), displays an intense peak due to the ionic structure of the compound perfectly in accordance with the calculated mass ([M-I]$^+$ calcd for calcd for [C$_{47}$H$_{65}$N$_2$O$_2$]$^+$: 689.5046, found: 689.5046).

The tetrazine ligation between TCO-cyanine **5-3** and tetrazine **2-45** was tested; the ^{1}H NMR of the crude material, reported in *Chapter 6* (Figure 6-20), shows a quantitative conversion into dihydropyridazine **5-20** as a mixture of isomers. Furthermore, ESI-HRMS(Q-Tof) analysis of the isolated products displays peaks corresponding to the mono- and the bis-charged ions in

accordance with the calculated mass ([M-I]$^+$ calcd for [C$_{59}$H$_{73}$N$_6$O$_2$]$^+$: 897.5795, found: 897.5825); and notably peaks corresponding to the oxidation of the dihydropyridazine were also found ([M(-2H)-I]$^+$ calcd for [C$_{59}$H$_{71}$N$_6$O$_2$]$^+$: 895.5638, found: 895.5673) such as for **2-42** (see appendix) (Figure 5-5).
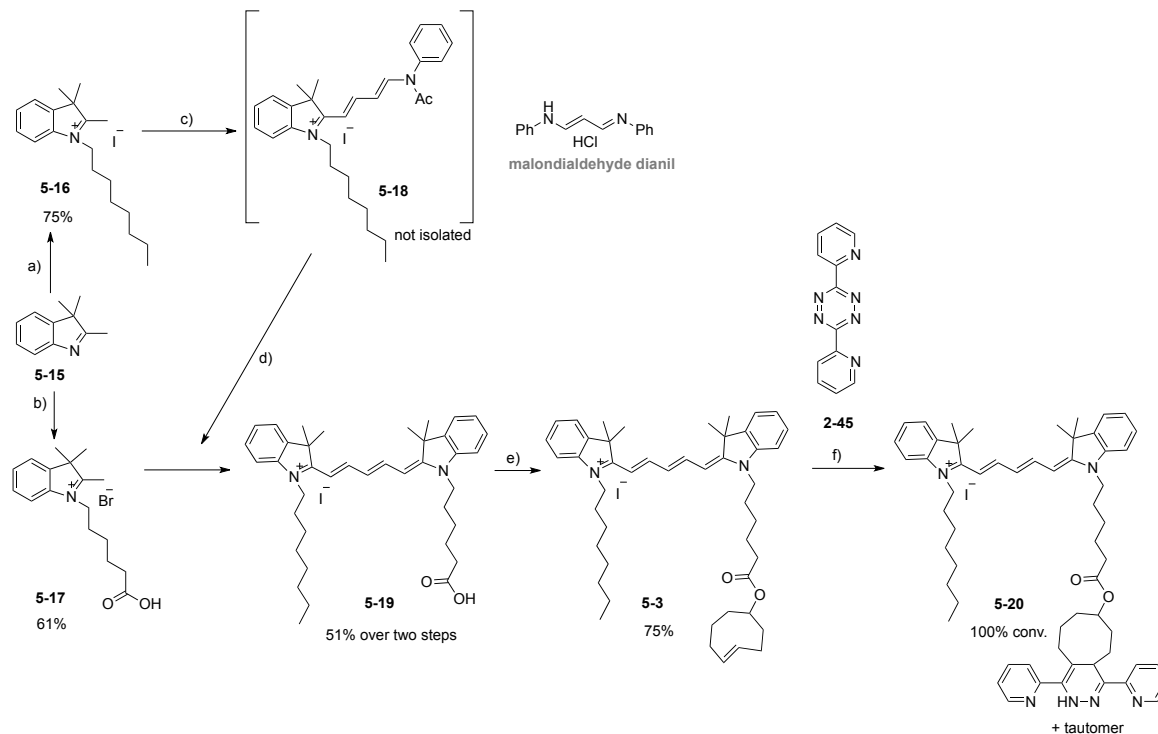
Scheme 5-5 a) Synthesis of TCO-cyanine **5-3**; a) 1-iodooctane, 145 °C, 3 h; b) 6-bromohexanoic acid, o-dichlorobenzene, 120 °C, 24 h; c) malondialdehyde dianil HCl, Ac$_2$O, 140 °C, 2 h; d) NaOAc, EtOH, 90 °C, 3 h; e) *trans*-cyclooctenol **2-43**, EDC.HCl, DMAP, CH$_2$Cl$_2$, rt, 20 h; f) **2-52**, THF, rt, 1 h.

The photophysical characterization of **5-20** was performed in DMF and is in agreement with the data reported in the literature for similar structures (Figure 5-6).[7] The maximum of absorption in the UV-Vis spectrum is located around 649 nm with a high molar absorption coefficient (ε = 148300 L mol^{-1} cm^{-1}) corresponding to the π–π* transition. The fluorescence emission spectrum (λ_{exc}=630 nm) displays a maximum at around 670 nm, with a Stokes shift of 21 nm. The quantum yield was estimated to be 61% determined from Nile Blue A (QY=27% in EtOH).[8] The normalization of the absorption and emission fluorescence spectra of the five different chromophores, which will be used for the creation of the fully extended absorption range multichromophoric architecture: ADIBO-ethynylpyrene **5-2**, Y-Per **4-1**, R-PDI **4-2**, B-NDI **3-11**, Cy **5-20,** displays great overlaps between the donor absorption and the acceptor fluorescence (Figure 5-1).
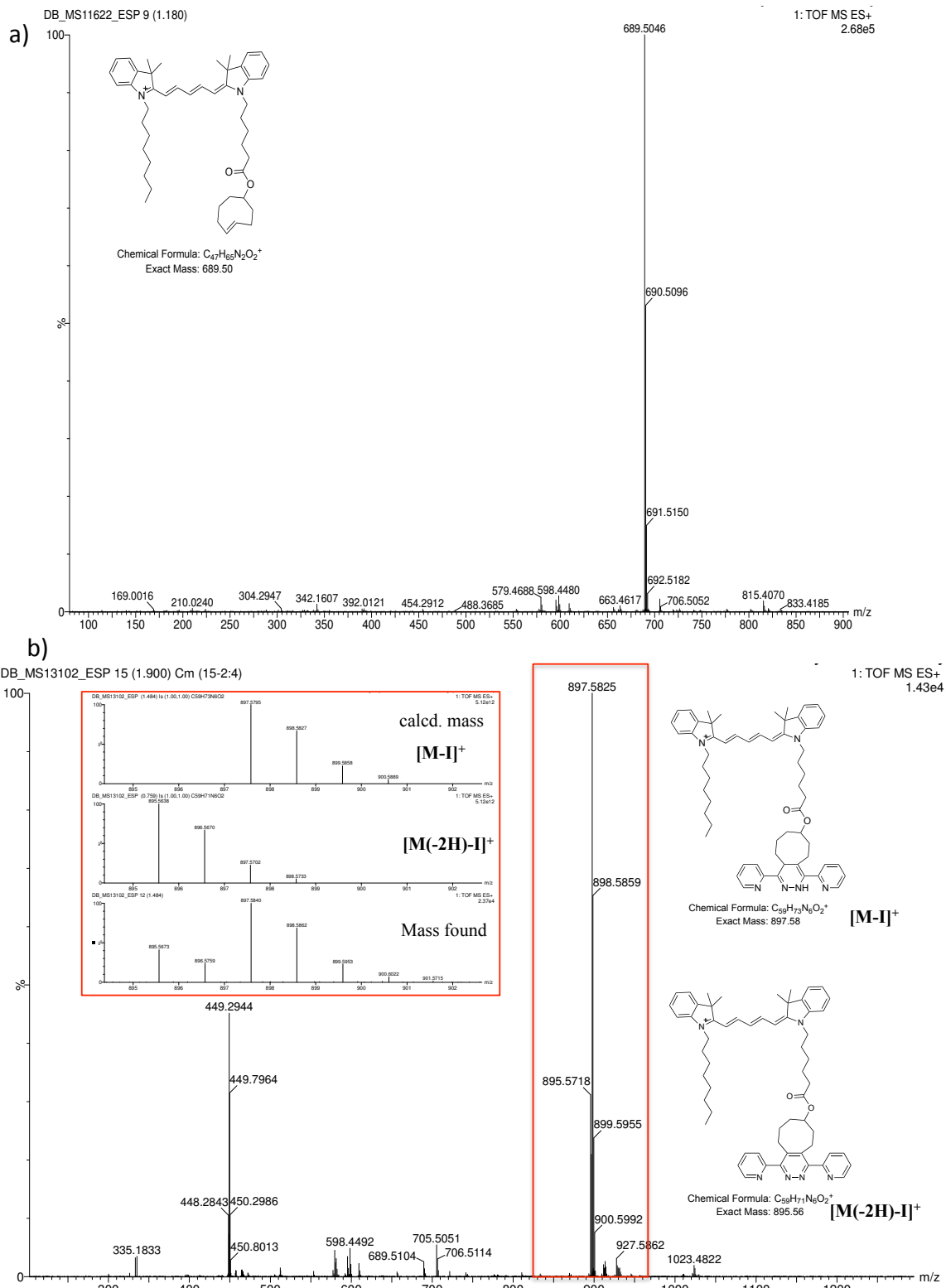
Figure 5-5 ESI-HRMS(Q-Tof) analyses of a) TCO-cyanine **5-3**; b) cyanine tetrazine ligation product **5-20;** inset: zoom of monocharged peak showing mixture between [M-I]$^+$ and [M(-2H)-I]$^+$.
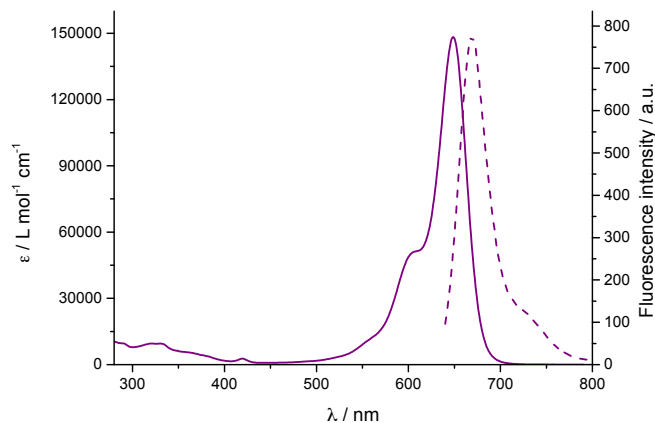
Figure 5-6 Absorption and fluorescence emission *(λ_{exc} = 630 nm)* spectra of tetrazine ligation product **5-20** in DMF.

5.2.1.3 Optoelectronic properties of dyes

The photophysical properties of chromophores TCO-Cy **5-3**, B-NDI **3-12**, R-PDI **4-2**, Y-Per **4-1**, ADIBO-Py **5-2**, including lifetime measurements, were also recorded in CHCl$_3$ and are summarized in Table 5-2. In general, all compounds show high molar absorption coefficients, spanning from the violet to the red region of the visible spectrum with luminescence lifetimes in the same order of magnitude (τ = 1.5 - 9.5 ns) and possess high quantum yields (46 – 97%). Moreover, the energy levels of the frontier molecular orbitals (FMO) of B-NDI **3-24**, R-PDI **4-2**, and Y-Per **4-5** were estimated by cyclic voltammetry (CV; recorded in CH$_2$Cl$_2$, see *Chapter 6*) and are reported in Table 5-2 and Figure 5-7.

Table 5-2 Optoelectronic properties of chromophores TCO-Cy **5-3** and Cy **5-19**, B-NDI **3-12** and **3-24**, R-PDI **4-2**, Y-Per **4-5**, ADIBO-Py **5-2** recorded in CHCl$_3$.

Entry	Compounds	Abs *(λ_{max})*	ε / L mol^{-1} cm^{-1}	Em *(λ_{max})*	QY / %	τ / ns	E_{red}[f] / V (E_{LUMO}[h] / eV)	E_{ox}[f] / V (E_{HOMO}[h] / eV)
1	TCO-Cy **5-3**	657	122000	678	46[a]	1.69	-	-
2	Cy **5-19**	657	122000	-	-	-	-0.84[g] (-3.5)	0.79[g] (-5.13)
3	B-NDI **3-12**	623	23000	641	49[b]	9.54	-	-
4	B-NDI **3-24**	623	-	-	-	-	-0.96 (-3.38)	1.01 (-5.35)
5	R-PDI **4-2**	460, 490, 527	20200, 54300, 90000	537, 577	97[c]	3.55	-0.53 (-3.81)	1.82 (-6.16)

6	Y-Per **4-5**	449, 423	38500, 32000	470, 500	85[d]	2.39	-1.68 (-2.66)	1.00 (-5.34)
7	ADIBO-Py **5-2**	395, 370	43000, 46500	420, 438	69[e]	1.45	~ -2.0[g]	~0.6[g]

*QY determined from [a]Nile Blue (QY=27% in EtOH);[8] [b]Rhodamine 101 (QY=100% in MeOH);[9] [c]Rhodamine 6G (QY=94% in EtOH);[10] [d]Ru(bpy)$_3^{2+}$ (QY=1.8% in H$_2$O);[11] [e]Quinine sulfate (QY=54.6% in 0.5 M H$_2$SO$_4$).[3] [f]First oxidation and reduction potential in V vs. SCE; [g]Peak potentials (irreversible process); [h]LUMO and HOMO energies in eV vs. vacuum determined by CV following equation [g]$E_{HOMO/LUMO}$ = -(4.8 eV + $E_{red/ox}$ vs. Fc$^+$/Fc). Fc$^+$/Fc = 0.46 V vs. SCE = -4.8 eV vs. vacuum. CV were recorded in CH$_2$Cl$_2$.
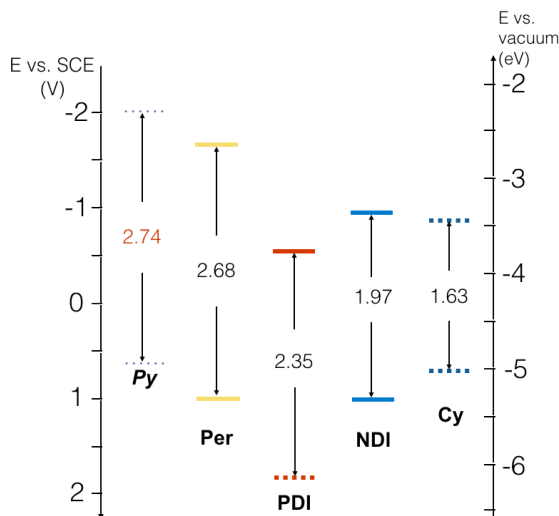

Figure 5-7 Frontier orbital potentials determined by cyclic voltammetry in CH$_2$Cl$_2$. Data for Py were taken from literature for a similar molecule.[12]

5.2.2 Development of multichromophoric architectures

The following section is dedicated to the creation of new multichromophoric architectures involving the SPAAC and the IEDDA as additional recognition motifs. Following the retrosynthetic pathway depicted in Figure 5-8, the work comprises the design and synthesis of modified amino acids, of the peptidic scaffolds and the chromophoric assembly.

Two different types of peptidic scaffold will be used in this section: QLA-based α-helix peptides (HP), and short tri-, tetra-, and pentatopic peptides (SP) bearing only the anchoring modified aa. This new type was developed in order to bypass the solubility difficulties of the amphiliphic HPs. New triads assembling R-PDI **4-2**, B-NDI **3-12** and ADIBO-Per **5-1,** will be targeted in order to: *i)* optimize the conditions of the assembly when the SPAAC is involved and, *ii)* compare the ET efficiencies within triads with those obtained in *Chapter 4* and definitely unravel the effect of the scaffold on them. Subsequently, the widening of the absorption window towards the creation of tetrads and pentads will be investigated.
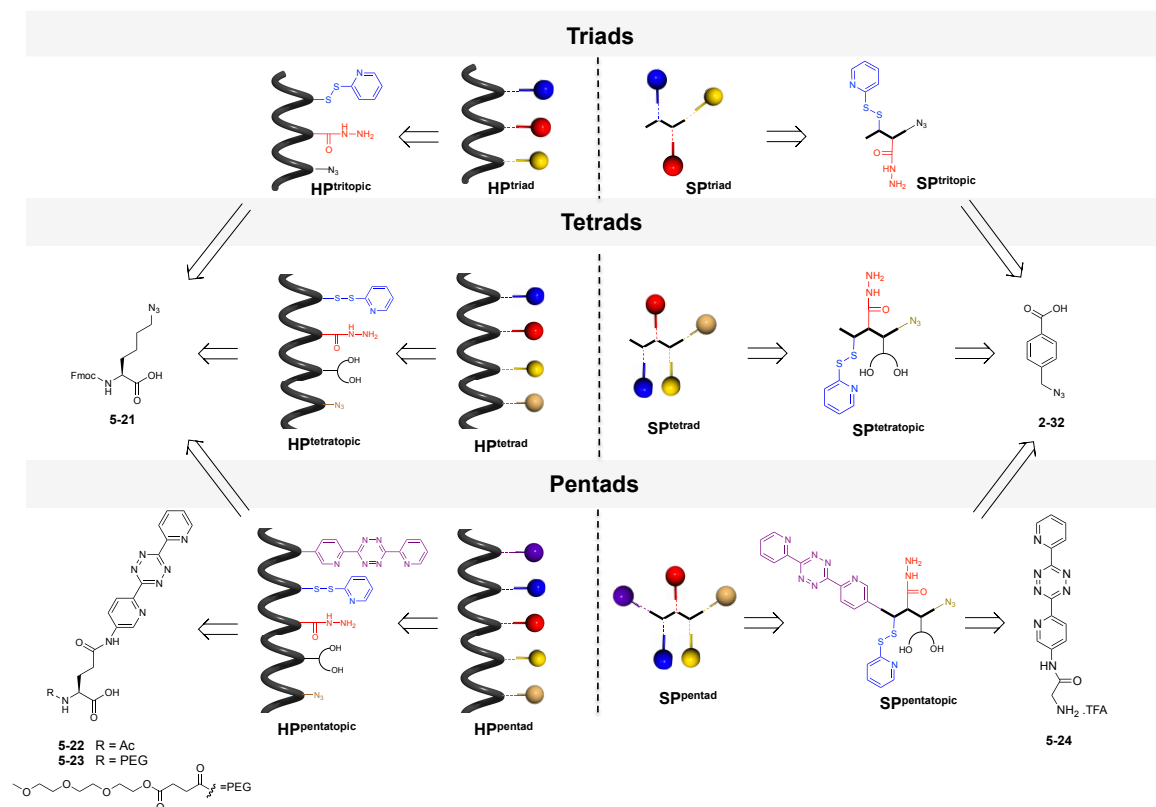
Figure 5-8 Schematic representation and retrosynthetic pathways of targeted triads, tetrads, and pentads.

5.2.2.1 Synthesis of modified amino acids

The design and the synthesis of azide and tetrazine containing aa, depicted in Figure 5-8, are reported in this section. It is noteworthy to indicate that the functionalities were targeted on the side chains of the aa (**5-21**, **5-22**, **5-23**) for the HP scaffolds in order to do not affect their helical conformation; while they can be introduced with simple derivatives (such as **2-32** prepared in *Chapter 2* or **5-24**) for SP-type scaffold as no particular conformation is adopted in such a small peptides (Figure 5-9).
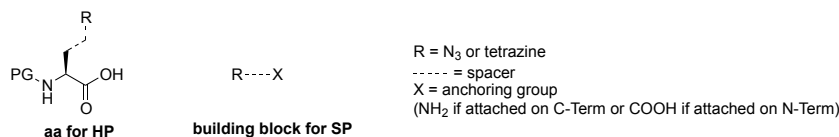
Figure 5-9 General design of azido and tetrazine containing amino acids.

5.2.2.1.1 Azido containing amino acid

Azide-containing peptides have been widely developed in bioconjugation due to the success of the copper-catalyzed azide-alkyne cycloaddition (CuAAC), SPAAC reactions, or Staudinger ligation, for site-specifically modifying peptides and proteins.[13] In this respect, many amino acids with azide group in the side chain have been reported for their use in the SPPS such as *N*-Fmoc

protected azidonorleucine (n=4), azidonorvaline (n=3), azidohomoalanine (n=2), and azidoalanine (n=1) (Figure 5-10).[14]

Figure 5-10 Amino acids with azide group.

Amino acids bearing azido functional group can be synthesized from the cheap amine analogue by the copper(II)-catalyzed diazo transfer method.[15] Accordingly, *N*-Fmoc protected azidonorleucine **5-21** was prepared following the literature procedure.[16] First, diazo transfer reagent triflic azide **5-26** was synthe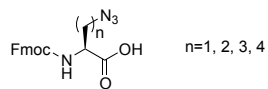sized *in situ* by mixing triflic anhydride **5-25** and sodium azide in a biphasic mixture of H_2O/CH_2Cl_2. It is noteworthy to indicate that the compound cannot be isolated due to its high explosive character. The copper(II)-catalyzed diazo transfer was then performed in the presence of a catalytic amount of $CuSO_4.5H_2O$ to convert the amino group into azide in quantitative yield. As reported, $NaHCO_3$ was used as the base instead of the generally employed K_2CO_3,[17] to avoid the cleavage of the Fmoc group (Scheme 5-6).
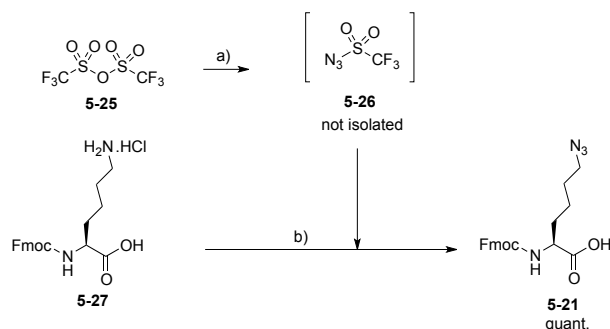
Scheme 5-6 Synthesis of Fmoc-Nle(N₃)-OH **5-21**; a) NaN_3, H_2O/CH_2Cl_2, rt, 2 h; b) $NaHCO_3$, $CuSO_4.5H_2O$, $H_2O/CH_2Cl_2/MeOH$, rt, 18 h.

5.2.2.1.2 Tetrazine containing amino acids

The IEDDA cycloaddition between tetrazine and TCO derivative is a very attractive reaction in bioconjugation thanks to its rate constant highly faster than other bioorthogonal reactions, and has been widely used to label proteins.[18] However, only a few tetrazine-containing amino acids have been reported, the moiety being usually incorporated by functionalization of protein using tetrazine containing a unique reactive group.[19] In 2012, the first tetrazine unprotected amino acid was reported but its incorporation into protein was performed by site-specifically encoding using most likely phosphate buffer saline (PBS).[20] Recently, the first *N*-Fmoc- and *N*-Boc-protected tetrazine-containing amino acids were synthesized to investigate their stability toward the conditions of the SPPS: 20% piperidine in DMF for the Fmoc deprotection, 50%TFA in CH_2Cl_2 for the resin cleavage or the Boc deprotection and the coupling conditions in DIEA/DMF.[21] The

143

amino acids showed good stability toward the TFA and coupling conditions, however, the tetrazine entirely decomposed within 60 seconds in the presence of 20% piperidine in DMF. So, in this study, the authors used the *N*-Boc-protected tetrazine-containing amino acid for their SPPS.

In our case, the use of *N*-Boc protecting group (within tetrazine-containing aa for **HP^pentatopic**) was not an option, the lateral chains of the other modified amino acids being already protected by acido-labile groups. In this respect, it has been decided to target *N*-cap tetrazine-containing amino acid and to introduce it at the N-terminus of the peptide. Two synthetic strategies have been envisaged: preparing acetyl peptide and, pegylated one considering the low solubility of **HP^pentatopic**. For this reason, *N*-acetyl **5-22** and *N*-PEG **5-23** tetrazine-containing aa, whose structures are presented in Scheme 5-7, were synthesized.

For *N*-acetyl tetrazine-containing aa **5-22**, the synthesis, reported in Scheme 5-7, started with the preparation of unsymmetrical dihydrotetrazine **5-29** from the statistical condensation between hydrazine hydrate, 5-amino-2-cyanopyridine **5-28** and 2-cyanopyridine **2-50** following the literature.[22] The amino group of dihydrotetrazine **5-29** was then coupled to the unprotected side chain of *N*-acetyl-L-glutamic acid gamma *t*Bu-ester (Ac-Glu-O*t*Bu) in the presence of EDC·HCl as coupling agent and a catalytic amount of DMAP to afford **5-30** in 68% yield. The compound was subsequently oxidized into tetrazine **5-31** in 97% yield by using phenyliodine (III) diacetate (PIDA), a milder oxidant than the previously used DDQ.[23] Finally, the deprotection of the tert-butyl ester with 50%TFA in CH$_2$Cl$_2$ afforded quantitatively desired tetrazine-containing amino acid **5-22** available for the SPPS.

Scheme 5-7 Syntheses of tetrazine containing aa **5-22** and **5-23**; a) hydrazine hydrate, 90 °C, 12 h; b) R$_1$(CO)-Glu-O*t*Bu, EDC·HCl, DMAP, CH$_2$Cl$_2$, rt, 20 h; c) PIDA, CH$_2$Cl$_2$, rt, 1.5 h; d) TFA, CH$_2$Cl$_2$, rt, 2 h;

e) succinic anhydride, DMAP, CH$_2$Cl$_2$, rt, 20 h; f) *N*-hydroxysuccinimide, EDC.HCl, DMAP, CH$_2$Cl$_2$, rt, 20 h; g) H-Glu-O*t*Bu, DIEA, DMF, rt, 16 h.

For the preparation of PEG *N*-protected tetrazine-containing aa **5-23**, the introduction of the PEG chain on the unprotected L-glutamic acid gamma *t*Bu-ester (H-Glu-O*t*Bu) required the pre-activation of PEG-acid **5-33** into NHS-ester **5-34**. The latter was prepared treating **5-33** with *N*-hydroxysuccinimide (NHS) in the presence of EDC.HCl as coupling agent. Afterwards, activated ester **5-34** was coupled with H-Glu-O*t*Bu by stirring the components in DMF in the presence of DIEA affording **5-35** in 85% yield**.** The compound was subsequently coupled with the amine group of dihydrotetrazine **5-29** in the presence of EDC·HCl and DMAP to yield **5-36**. Then, the same strategy described for **5-22** was applied consisting in oxidizing the dihydrotetrazine core of **5-36** into tetrazine **5-37** with PIDA**,** and removing the *t*Bu protecting group with TFA (Scheme 5-18). Amino acids **5-22** and **5-23**, and intermediates were fully characterized by melting point, infrared, ^{1}H and ^{13}C NMR spectroscopy, and HR mass spectrometry (see *Chapter 6*).

Finally, the synthesis of tetrazine containing glycine **5-24** required for **SP^{pentatopic}** is described in Scheme 5-8 and follows the same procedure. Dihydrotetrazine **5-29** was coupled with Boc-Gly-OH in the presence of EDC·HCl and DMAP and was subsequently oxidized with PIDA to afford **5-39**. Finally, Boc protecting group was removed with TFA to give salt **5-24**.[24]
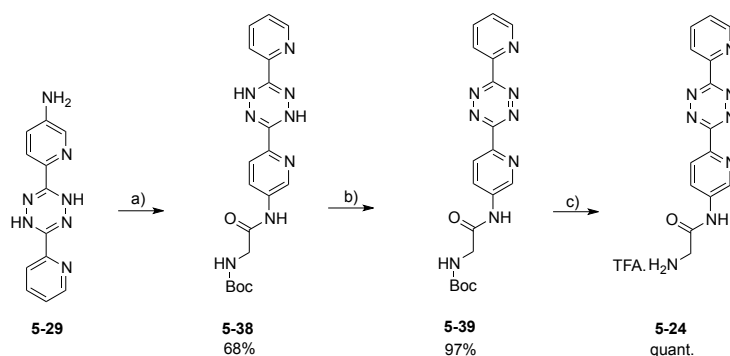

Scheme 5-8 Synthesis of H-Gly-tetrazine **5-24**; a) Boc-Gly-OH, EDC.HCl, DMAP, CH$_2$Cl$_2$, rt, 20 h; b) PIDA, CH$_2$Cl$_2$, rt, 16 h; c) TFA, CH$_2$Cl$_2$, rt, 1 h.

5.2.2.2 Trichromophoric structures involving SPAAC

5.2.2.2.1 Triad assembly templated by helical peptide

Having in hands Fmoc-Nle(N$_3$)-OH **5-21**, peptidic scaffolds Ac-QLAQLA-X(disulfide)-QLAQLA-**Nle(N$_3$)**-QLAQLA-X(hydrazide)-QLA-NH$_2$ **5-42** and Ac-QLAQLA-X(disulfide)-QLAQLA-X(hydrazide)-QLAQLA-**Nle(N$_3$)**-QLA-NH$_2$ **5-43** were prepared to fully unravel the effect of the order of the chromophores on the energy transfer and compare ET efficiencies with those obtained in the previous chapter. The syntheses were performed according to the general procedure by SPPS; however, the cleavage of peptides from the resin was carried out in the TFA

cocktail cleavage without 1,2-ethanedithiol (EDT) for 1.5 h (Scheme 5-9). Indeed, it has been reported that 20% of azide was converted into amine within 2 h when 1,2-ethanedithiol (EDT) was used in the cocktail cleavage due to the reducing ability of the thiol compound.[16] The peptides were characterized by ESI-MS (Q-Tof) and RP-HPLC. ESI-MS spectra of peptides **5-42** and **5-43** display peaks for the tri- and bischarged ions (Na and H adducts), which after deconvolution gave the expected monoisotopic mass: 2679.38 (Figures 5-11 and 5-12).
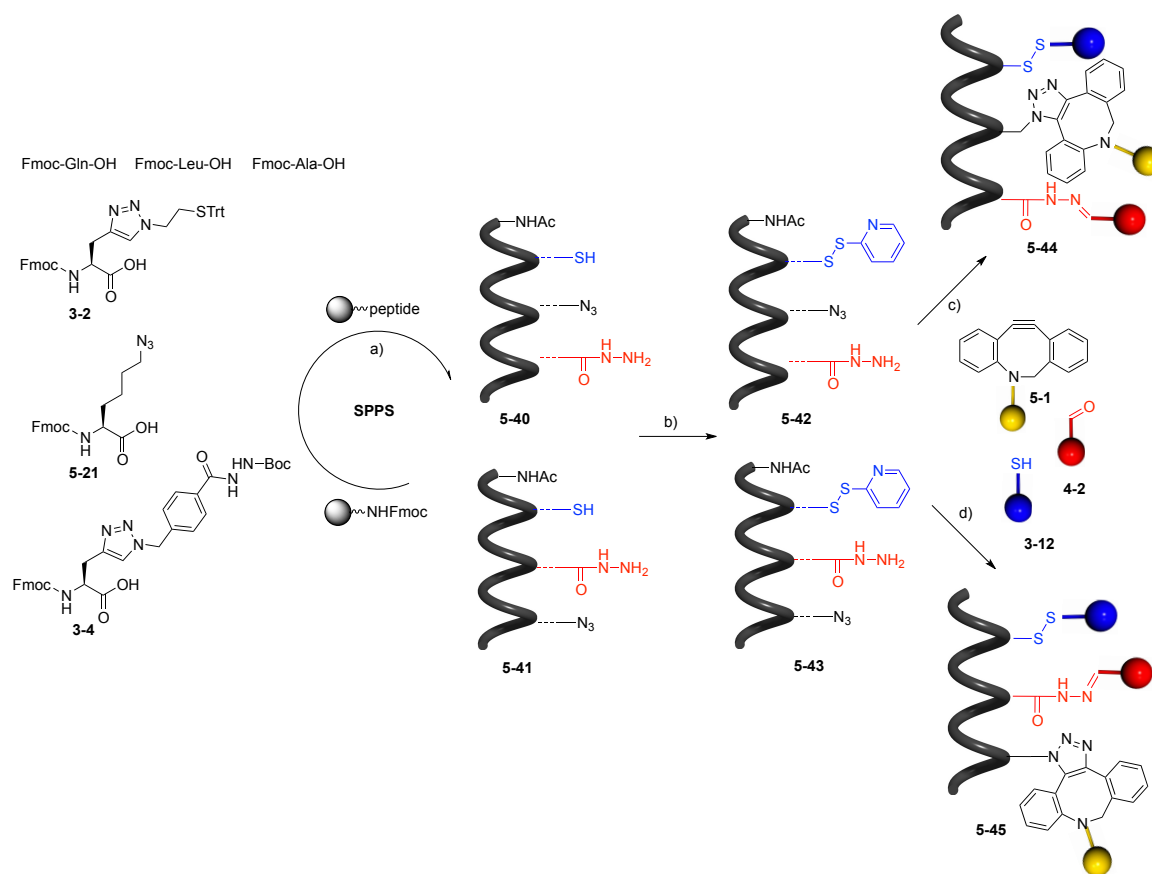
Scheme 5-9 Preparation of triads **5-44**, **5-45**; a) SPPS: *i)* Fmoc deprotection: 20% piperidine in DMF, rt, 3 × 6 min; *ii)* AA coupling: Fmoc-AA-OH, HATU, DIEA, DMF/NMP, rt, 25 min; *iii)* Ac$_2$O/pyridine/NMP (1:2:2), 2 × 15 min; *iv)* TFA/TIS/H$_2$O (95:2.5:2.5), rt, 2 h; b) 2,2'-dipyridyl disulfide, DIEA, DMF, 1 h; c) *m*-PDA, DMA, 4 h at rt and 2 h at 40 °C; d) *m*-PDA, DMA, 2 h at rt and 2 h at 40 °C.
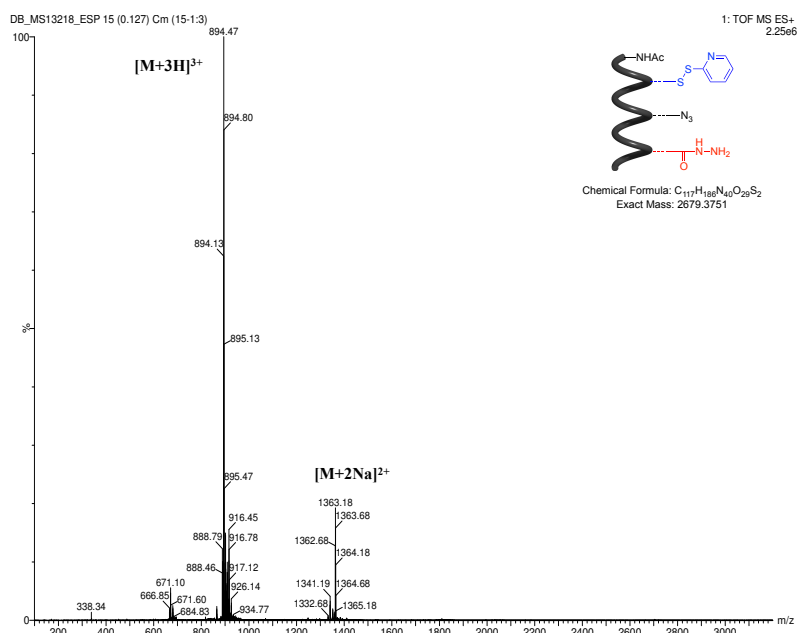
Figure 5-11 ESI-MS(Q-Tof) analysis of purified peptide **5-42** showing $[M+3H]^{3+}$, $[M+2Na]^{2+}$.
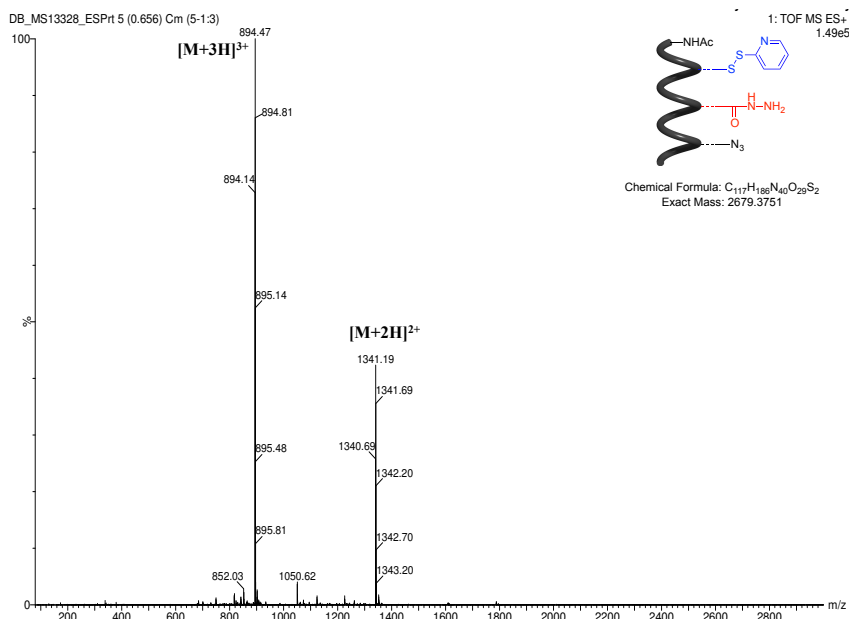

Figure 5-12 ESI-MS(Q-Tof) analysis of purified peptide **5-43** showing $[M+3H]^{3+}$, $[M+2H]^{2+}$.

The chromophoric assembly was performed treating peptide **5-42** with dyes **3-12**, **4-2**, **5-1** in DMA to afford **5-44** (Scheme 5-9). The completion of the reaction was followed by UV-Vis: after 4 h at rt, the absorption spectrum of the purified peptide by GPC does not show quantitative introduction of ADIBO-Per unit (Figure 5-13a, grey line). When the mixture was heated at 40 °C for additional 2 h and purified through GPC, the absorption spectrum indicates the quantitative SPAAC (Figure 5-13a, black line).
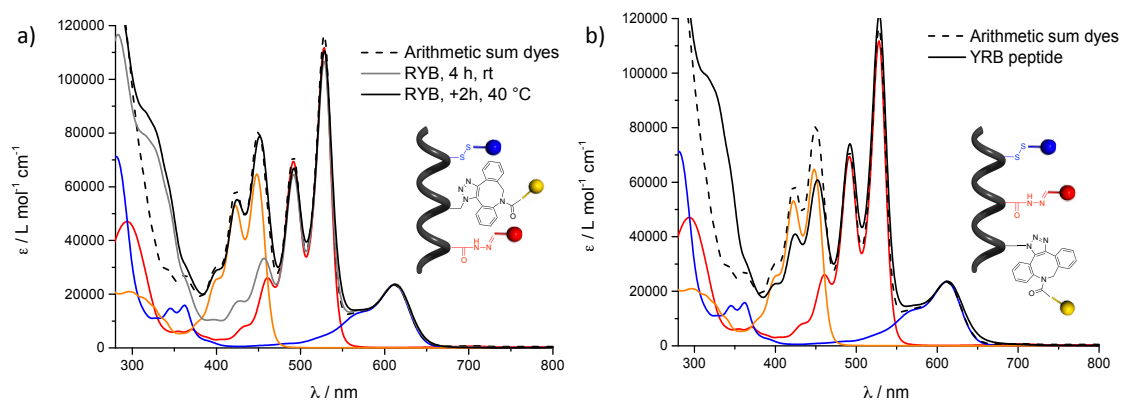
Figure 5-13 Absorption spectra of a) RYB peptide **5-44** after 4 h of reaction at rt (in grey) and additional 2 h at 40°C (in black) and b) YRB **5-45,** normalized with arithmetic sum of dyes ADIBO-Per **5-1**, R-PDI **4-2** and B-NDI **3-12** on B-NDI in DMA.

The chromophore assembly was then performed with peptide **5-43**. The components were mixed in DMA at rt for 2 h and 40 °C for additional 2 h to give peptide **5-45**. After purification through GPC, the absorption spectrum of the material shows the introduction of the three dyes but not quantitative for ADIBO-Per (Figure 5-13b). It is noteworthy to indicate that the assembly was also tested on another synthesized peptide: Ac-QLAQLA-X(disulfide)-QLAQLA-**A**(N$_3$)-QLAQLA-X(hydrazide)-QLA-NH$_2$ bearing an azidoalanine residue. However, in that case, the SPAAC did not work at all probably due to the steric hindrance around the azido moiety.

The chemical identity of desired peptides **5-44** and **5-45** was confirmed by MALDI-TOF analysis, reported in Figure 5-14 and 5-15 respectively. The analyses display intense peaks for [M+Na]$^+$ (at m/z = 5238.4) in accordance with the calculated mass; and peaks corresponding to the products after cleavage of the disulfide possibly occurring during the ionization are also found (m/z = 4262.0). Furthermore, in the spectrum of **5-45,** peaks highlighting the non-quantitative SPAAC (at m/z = 4608.2 with free azide and 4580.2 after loss of N$_2$) are observed. Finally, it is worth indicating that the two spectra show an unexpected peak at m/z=4893.2. After investigation, it was found that this mass corresponds to a side product in which peptides bearing free thiol (traces of **5-40** and **5-41** possibly in mixture with the peptidic scaffolds) reacted with **5-1** by thiol-yne addition.
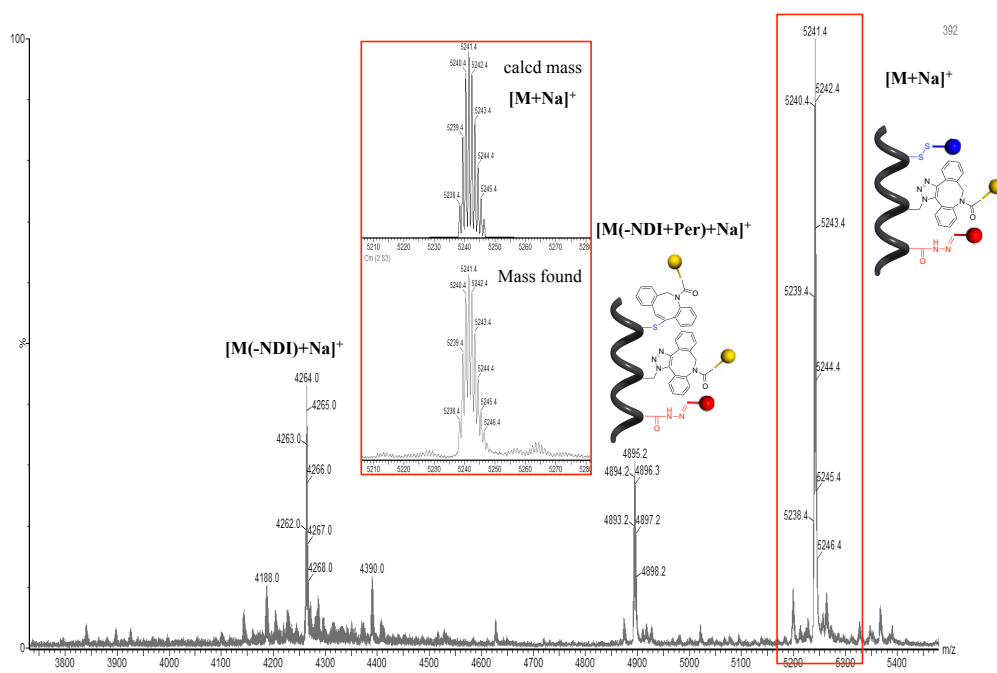
Figure 5-14 MALDI-Tof analysis of purified peptide **5-44**; inset: Zoom of $[M+Na]^+$ peak (bottom) compared with calculated mass (top).
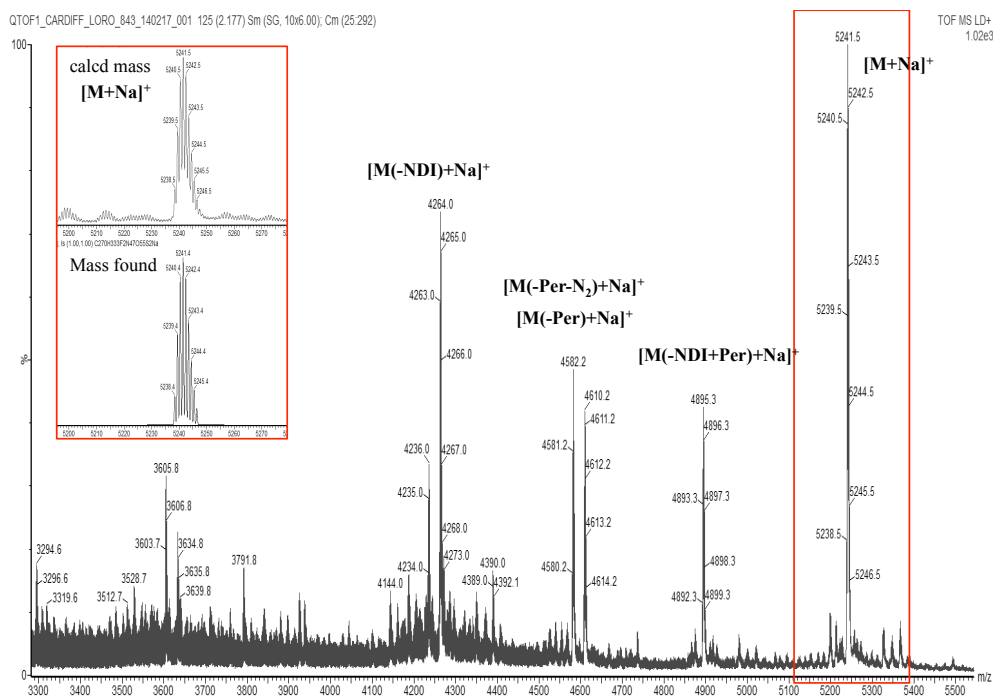

Figure 5-15 MALDI-Tof analysis of purified peptide **5-45**; inset: Zoom of $[M+Na]^+$ peak (top) compared with calculated mass (bottom).

Despite the traces of the side products, peptides **5-44** and **5-45** were analyzed by fluorescence spectroscopy (Figure 5-16 and 5-17). The ET efficiencies Φ_{ET} between donors and acceptor were determined by method 1 and 2 (see *Chapters 3* and *4*): 1) $\Phi_{ET} = QY*_{B-NDI}/QY_{B-NDI}$; 2) $\Phi_{ET} =$

Ex_D/A_D. The efficiencies are summarized in Table 5-3 and compared with those obtained in the previous chapter for **4-23** when DMA was used as solvent. For peptide **5-44**, Φ_{ET} have been estimated to be around 16.5% and 17.8% for Y-Per→B-NDI and R-PDI→B-NDI, respectively, while for peptide **5-45**, around 13.6% and 20%.
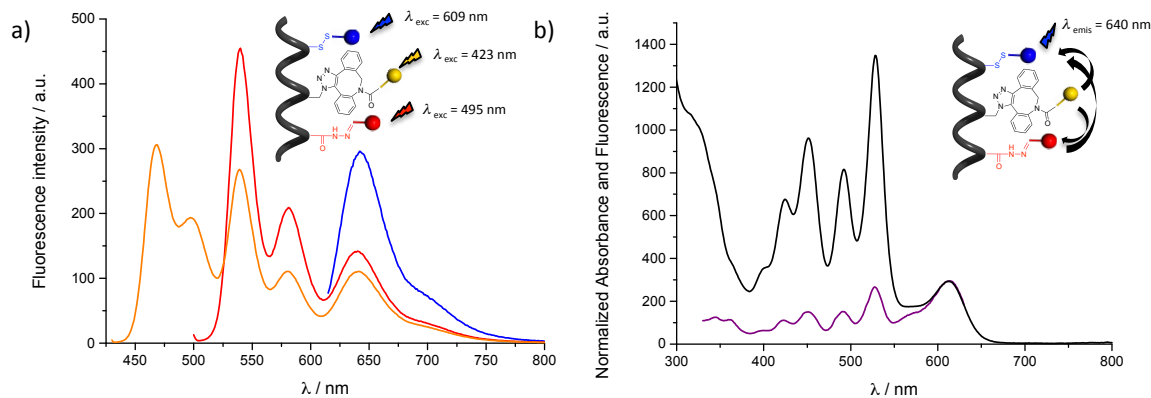

Figure 5-16 a) Fluorescence emission spectra of RYB peptide **5-44** at (λ_{exc}) 423 nm (yellow), 495 nm (red), 609 nm (blue) in DMA to determine ET efficiencies following method 1: $\Phi_{ET} = QY^*_{B\text{-}NDI}/QY_{B\text{-}NDI}$; b) Normalized absorption (black) and fluorescence excitation (purple) spectra of YRB peptide **5-44** (λ_{em}=640 nm) in DMA for method 2: $\Phi_{ET} = Ex_D/A_D$.
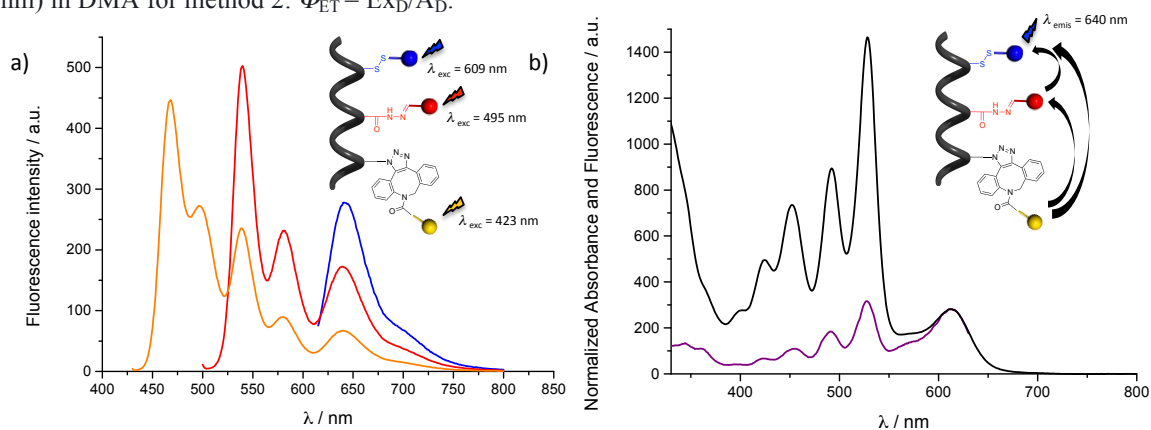

Figure 5-17 a) Fluorescence emission spectra of RYB peptide **5-45** at *(λ_{exc})* 423 nm (yellow), 495 nm (red), 609 nm (blue) in DMA to determine ET efficiencies following method 1: $\Phi_{ET} = QY^*_{B\text{-}NDI}/QY_{B\text{-}NDI}$; b) Normalized absorption (black) and fluorescence excitation (purple) spectra of YRB peptide **5-45** *(λ_{em}=640 nm)* in DMA for method 2: $\Phi_{ET} = Ex_D/A_D$.

Table 5-3 Energy transfer efficiencies within **5-44**, **5-45**, **4-23** calculated following methods 1 and 2.

Entry	Peptides	Methods	Φ_{ET} (R-PDI→B-NDI) %	Φ_{ET} (Y-Per→B-NDI) %
1	RYB **5-44**	1: $\Phi_{ET} = QY^*_{B\text{-}NDI}/QY_{B\text{-}NDI}$	17.6	16.1
		2: $\Phi_{ET} = Ex_D/A_D$	18	16.6
2	YRB **5-45**	1	20	13.5
		2	20	13.7
3	RYB **4-23**	1	22	14
		2	22	15

The energy transfer efficiencies within **5-44** and **5-45** confirm the results of the previous chapter when the assembly was performed in DMA, the ET efficiencies Φ_{ET} within **4-23** being determined around 20% for R-PDI→B-NDI and around 15% for Y-Per→B-NDI. As similar efficiencies were obtained when the perylene moiety was introduced through the boronate formation and the SPAAC, this proves the stability of the boronate ester within the triad in DMA, and further supports its partial hydrolysis in DMF leading to the poor Φ_{ET} for Y-Per→B-NDI (around 5%) in all the previous studies. Moreover, those results confirm the small effect of the order of the chromophores on the energy transfer. Indeed, Φ_{ET} (R-PDI→B-NDI) is slightly improved when the PDI and NDI are close to each other (20% *vs.* 18% when the units are separated by Per) and the same observation is done for Φ_{ET} (Y-Per→B-NDI), being estimated to be 16% when the units are in close distance *vs.* 14% when they are separated by PDI.

5.2.2.2.2 Triad assembly templated by tritopic short peptide

In *Chapter 4*, we have reported that the increasing of the interchromophoric distance did not lead to an improvement of the ET efficiencies. The opposite approach is explored in this section to simplify the scaffold. Hence, we decided to design and synthesize a short tritopic peptide, in which the chromophoric units will be positioned in a new arrangement, and study the effect of this scaffold on the ET. Regarding the design of scaffold **SP**^tritopic, namely **5-47** (depicted in Scheme 5-10), if the disulfide-pyridine and the hydrazide moieties remain unchanged, it was decided to introduce the azide through tolyl-benzamide linker to limit the flexibility of the scaffold and hopefully prevent the stacking between the dyes within triad **5-48**. Moreover, the free carboxylic acid on the C-terminal brings versatility to the system, as we envisage to further functionalize the triad with other photoactive species.

The synthesis of the peptidic scaffold was performed by SPPS using amino acids **3-2**, **3-4** and azide **2-32** on Fmoc-Ala Wang resin. The growing of the peptide on the resin was conducted in the same way using piperidine for Fmoc-deprotection and HATU in the presence of DIEA for the coupling steps; after the resin cleavage, the pyridine-disulfide was introduced in solution (Scheme 5-10).
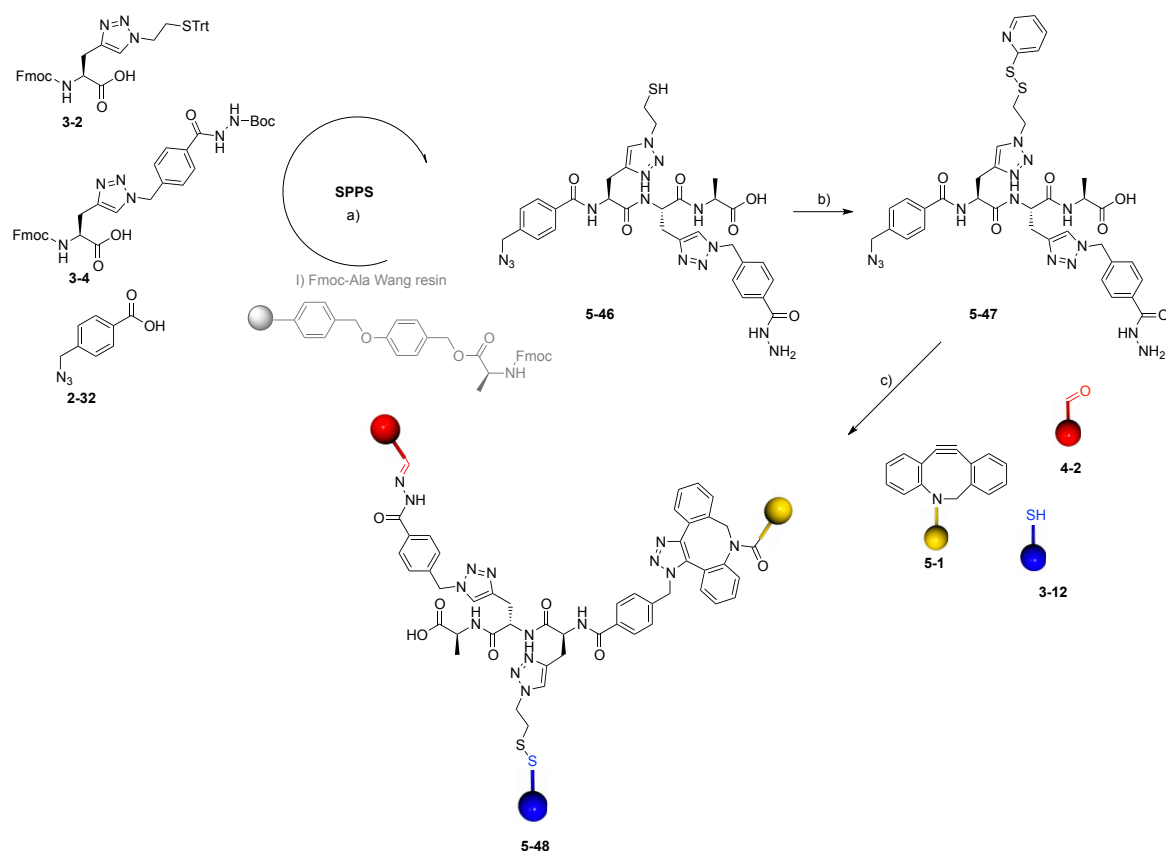
Scheme 5-10 Synthesis of tripeptide **5-47**; a) SPPS on Fmoc-Ala Wang resin: *i)* Fmoc deprotection: 20% piperidine in DMF, rt, 3 × 6 min; *ii)* AA coupling: Fmoc-AA-OH, HATU, DIEA, DMF/NMP, rt, 1 h; b) *i)* TFA/TIS/H₂O (95:2.5:2.5), rt, 2 h, *ii)* 2,2'-dipyridyl disulfide, DIEA, DMF, 1 h; Chromophoric assembly on tripeptide **5-47**; c) B-NDI **3-12**, ADIBO-Per **5-1**, R-PDI **4-2**, *m*-PDA, DMA, rt, 17 h.
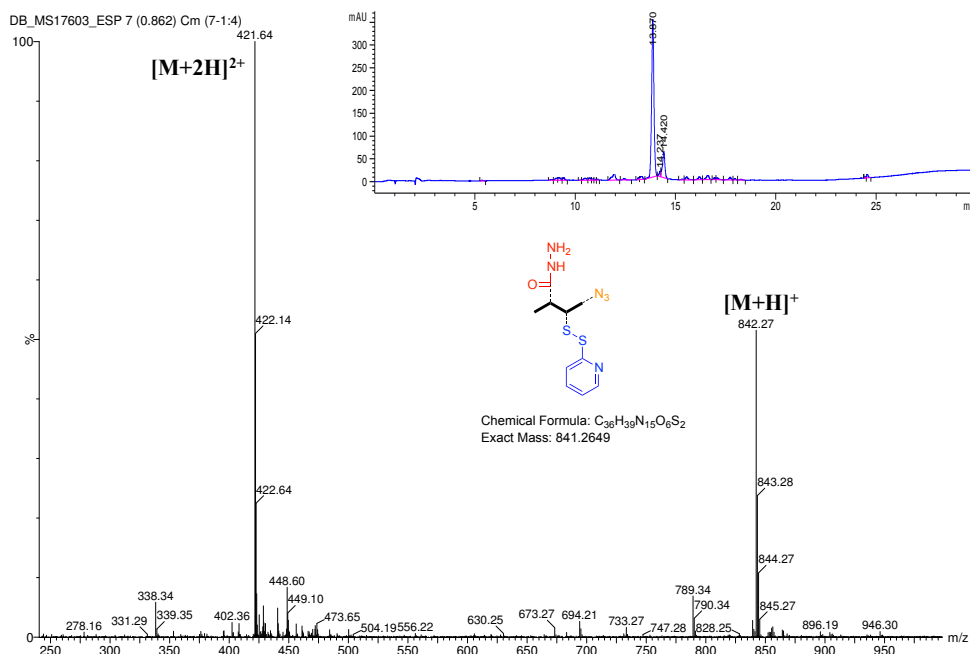

Figure 5-18 ESI-MS (Q-Tof) analysis of peptide **5-47** showing [M+2H]²⁺, [M+H]⁺; Inset: HPLC chromatogram of crude material **5-47**.

It is noteworthy to indicate that peptide **5-47** cannot be purified by RP-HPLC since the purification process, in aqueous media, promoted disulfide metathesis leading to the formation of the dimer, possibly due to the small size of the peptide. However, the HPLC chromatogram and the ESI-MS spectrum of the peptide highlight the good purity of **5-47** (Figure 5-18). The assembly of chromophores ADIBO-Per **5-1**, R-PDI **4-2**, B-NDI **3-12** was then performed on peptide **5-47** by mixing the components in the presence of *m*-PDA in DMA at rt for 17 h (Scheme 5-10). After purification through GPC, the absorption spectrum of **5-48** shows a perfect correspondence with the linear combination of the absorption of the three dyes (Figure 5-19).
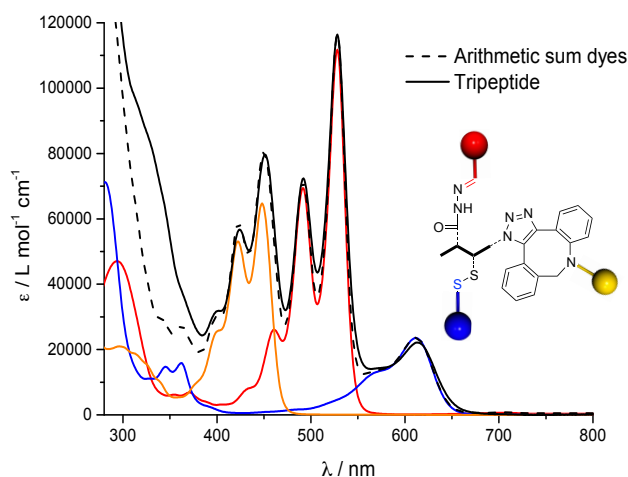

Figure 5-19 Absorption spectrum of triad **5-48** normalized with arithmetic sum of dyes ADIBO-Per **5-1**, R-PDI **4-2** and B-NDI **3-12** on B-NDI in DMA.

The chemical structure of triad **5-48** was confirmed by MALDI-TOF analysis, reported in Figure 5-20. The spectrum displays peaks for $[M+H]^+$ and $[M+Na]^+$ (at m/z = 3378.4 and 3400.1) in accordance with the calculated mass (calc. for $[C_{189}H_{187}F_2N_{22}O_{32}S_2]^+$: 3378.3). Peak corresponding to the product after loss of R-PDI unit and cyclization with carboxylic acid in C-terminal $[M(-PDI-H_2O)+H]^+$ probably occurring during the ionization process was also detected (m/z = 2321.9).

Steady-state fluorescence measurements were performed in DMA directly after the purification, and the energy transfer efficiencies Φ_{ET} within **5-48** have been estimated to be around 16% and 20% for Y-Per→B-NDI and R-PDI→B-NDI, respectively (Figure 5-21 and Table 5-3). Φ_{ET} (Y-Per→R-PDI) was also evaluated to be 54% by taking the excitation spectra at λ_{emis}=580 nm.
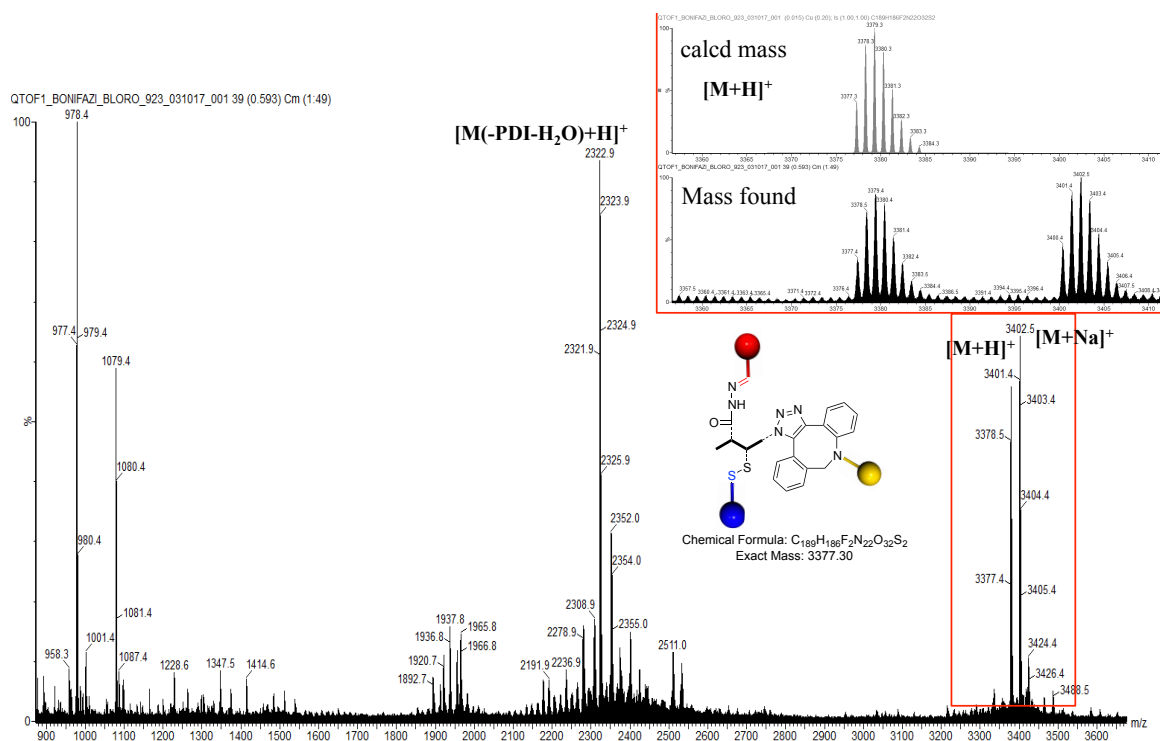
153

Figure 5-20 MALDI-Tof analysis of peptide **5-48**; Inset: Zoom of $[M+H]^+$ and $[M+Na]^+$ peak (bottom) compared with calculated mass $[M+H]^+$ (top).
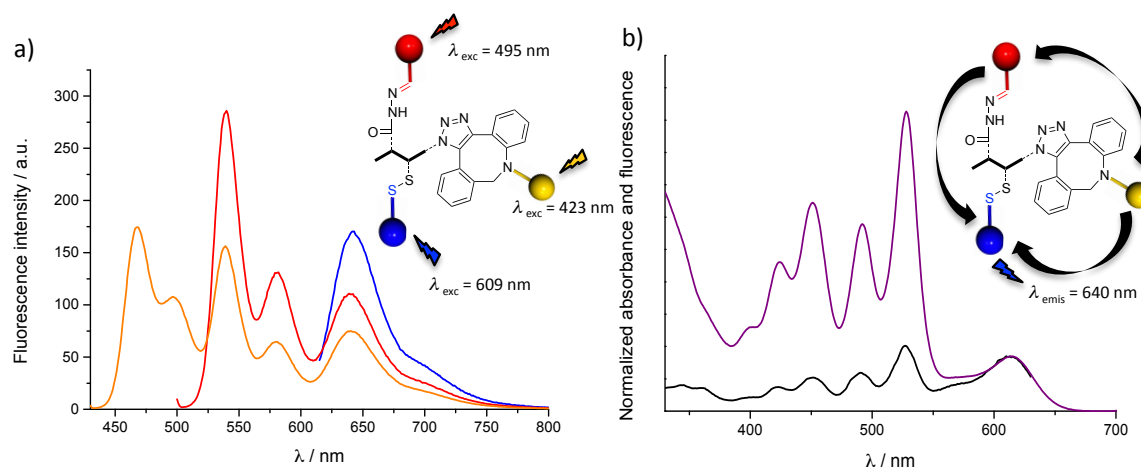

Figure 5-21 a) Fluorescence emission spectra of YRB peptide **5-48** in DMA at (λ_{exc}) 423 nm (yellow), 495 nm (red), 609 nm (blue) to determine ET efficiencies following method 1: $\Phi_{ET} = QY^*_{\text{B-NDI}}/QY_{\text{B-NDI}}$; b) Normalized absorption (black) and fluorescence excitation (purple) spectra of **5-48** in DMA $(\lambda_{em}=640$ nm) for method 2: $\Phi_{ET} = Ex_D/A_D$.

Table 5-4 Energy transfer efficiencies within **5-48** calculated following methods 1 and 2 in DMA.

Peptide	Methods	Φ_{ET} (R-PDI→B-NDI) %	Φ_{ET} (Y-Per→B-NDI) %	Φ_{ET} (Y-Per→R-PDI) %
YRB **5-48**	1: $\Phi_{ET} = QY^*_{\text{B-NDI}}/QY_{\text{B-NDI}}$	19.4	15.8	-
	2: $\Phi_{ET} = Ex_D/A_D$	20	16	54

These efficiencies, being very close to those obtained with the long helical peptide, highlight the weak influence of the scaffold on the ET. After drying the colored tripeptide and re-dissolving it in new media (taking advantage of the good solubility of the material in chlorinated solvents), Φ_{ET} were determined and are reported in Table 5-5. In $CHCl_3$, CH_2Cl_2 and DMA, similar results were obtained for Φ_{ET} (R-PDI→B-NDI) determined around 20%; however, for Φ_{ET} (Y-Per→B-NDI) and (Y-Per→R-PDI), smaller efficiencies were observed in particular in chlorinated solvents, in which stacking between Y-Per and R-PDI seems to occur.

Table 5-5 Energy transfer efficiencies within **5-48** calculated following methods 1 and 2 after drying the compound and re-dissolving in different media.

Media	Methods	Φ_{ET} (R-PDI→B-NDI) %	Φ_{ET} (Y-Per→B-NDI) %	Φ_{ET} (Y-Per→R-PDI) %
$CHCl_3$	1: $\Phi_{ET} = QY^*_{B-NDI}/QY_{B-NDI}$	21.7	12.7	-
	2: $\Phi_{ET} = Ex_D/A_D$	24.3	14.7	29.6
CH_2Cl_2	1	19.2	8.2	-
	2	16.7	9.5	26.2
DMA	1	18.1	15.9	-
	2	19.1	15.8	36.6
DMA + EYPC	1	17.6	15.2	-
	2	18.5	15.2	35.4
$CHCl_3$/DMA (1:1) + EYPC	1	19.2	14.4	-
	2	20.5	14.4	34.3
$CHCl_3$ + EYPC	**1**	**29**	**22.3**	**-**
	2	**28.7**	**19.6**	**46.7**

Besides, several attempts to complex the triad within cationic lipid nanostructures in aqueous media following the literature were tried unsuccessfully (insoluble material was obtained scattering light).[25] Nevertheless, the simple addition of 80 equivalents of egg yolk phosphatidylcholine (EYPC) in $CHCl_3$ allows the improvement of Φ_{ET} (Y-Per→B-NDI) and (Y-Per→R-PDI) estimated to be 29% and 20% respectively; preventing aggregation phenomena possibly through the formation of reverse lipidic bilayer (Figure 5-22).[26] Further measurements have to be carried out to unravel the self-assembly between the lipid and the triad. The loss of the ground state interactions by adding the lipid is highlighted in the absorption spectra (hypochromism observed for ABIBO-Per bands) while the improvement of the ET is illustrated in the excitation spectra (Figure 5-23).
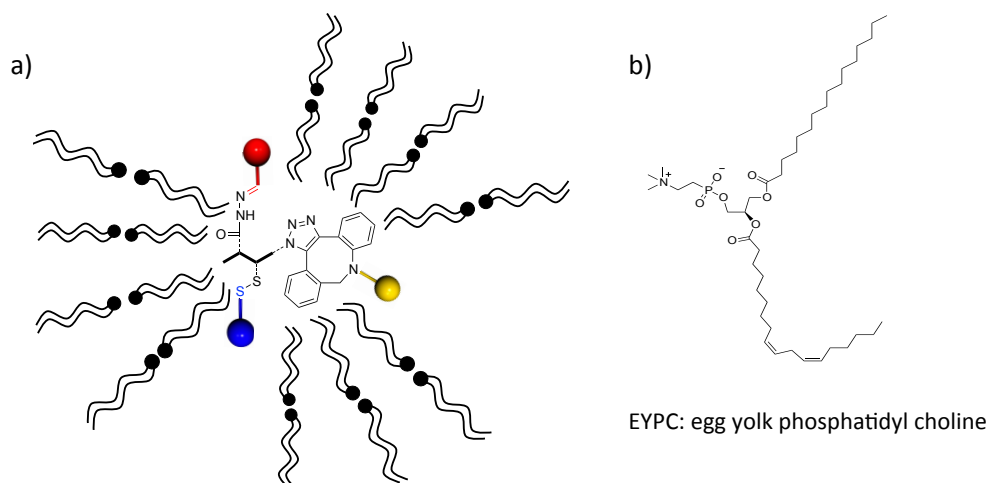
EYPC: egg yolk phosphatidyl choline

Figure 5-22 a) Schematic representation of possible self-assembly between EYPC (reverse lipidic bilayer) and triad **5-48** in CHCl$_3$ b) Chemical structure of EYPC.
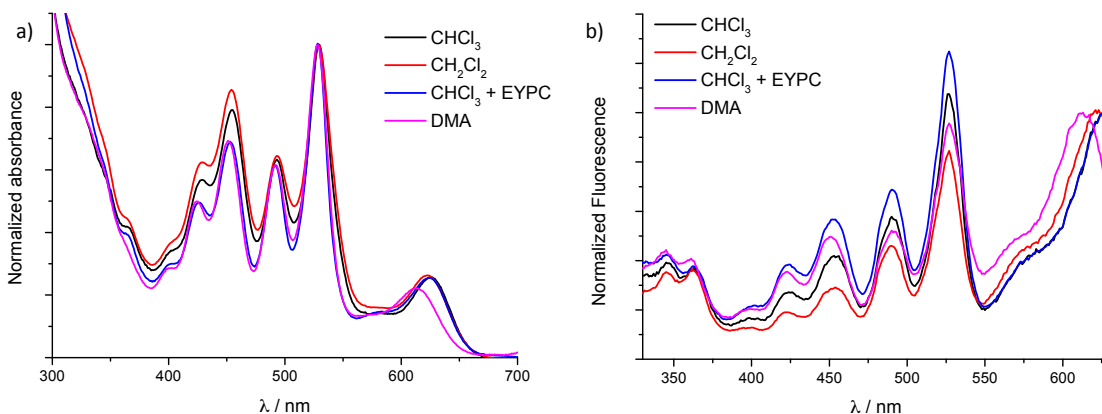

Figure 5-23 a) Normalized absorption spectra (at 527 nm) of triad **5-48** in different media; b) excitation spectra of **5-48** normalized at the excitation maximum of B-NDI unit *(λ_{em}=*640 nm) in different media.

5.2.2.3 Tetrachromophoric architectures

5.2.2.3.1 Tetrad assembly templated by helical scaffold

For the preparation of the first extended absorption range multichromophoric peptide bearing four dyes, the synthesis of peptide Ac-QLA-X(disulfide)-QLAQLA-X(hydrazide)-QLAQLA-X(diol)-QLAQLA-Nle(N$_3$)-QLA-NH$_2$ **5-50** bearing as well the bicyclic diol receptor site was performed by SPPS according to the general method used for the helical scaffold (Scheme 5-11).
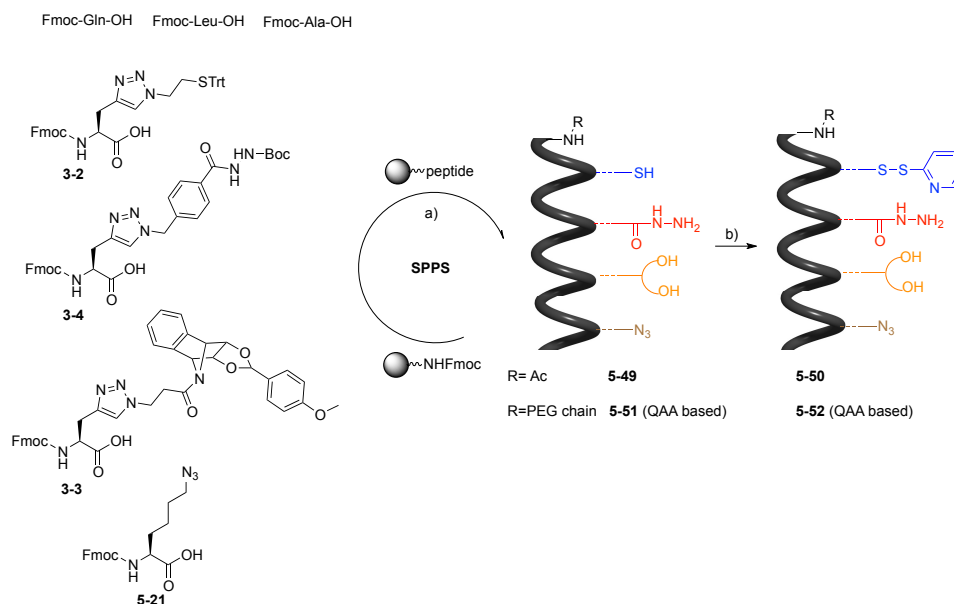
Scheme 5-11 Synthesis of peptidic scaffolds **5-50** and **5-52**; a) SPPS: *i)* Fmoc deprotection: 20% piperidine in DMF, rt, 3 × 6 min; *ii)* AA coupling: Fmoc-AA-OH, HATU, DIEA, DMF/NMP, rt, 25 min; *iii)* Capping: Ac$_2$O/pyridine/NMP (1:2:2), 2 × 15 min for **5-49** or **5-33**, HATU, DIEA, DMF/NMP, rt, 2 × 25 min for **5-51**; *iv)* Cleavage: TFA/TIS/H$_2$O (95:2.5:2.5), rt, 2 h; b) 2,2'-dipyridyl disulfide, DIEA, DMF, 1 h.

However, due to the high hydrophobicity of the peptide (elutes from the analytical column with 68% CH$_3$CN in H$_2$O), the purification through preparative RP-HPLC using C$_3$ column or cyano-bonded phase column was not successively achieved (**5-50** does not elute from the preparative column, see *Chapter 6*). Purification of the material was tested with different organic solvents (CH$_3$CN, THF, *i*PrOH) or by heating the column; in all cases, the peptide stacked to the stationary phase. To reduce the hydrophobicity of the material, hydrophobic leucine residues were substituted by alanine. In this respect, PEG-QAA-X(disulfide)-QAAQAA-X(hydrazide)-QAAQAA-X(diol)-QAAQAA-Nle(N$_3$)-NH$_2$ **5-52** was synthesized using PEG-acid **5-33** as a capping agent to improve the solubility of the polyalanine derivative. The hydrophobicity of peptide **5-52** was considerably reduced (elutes from the analytical column with 36% CH$_3$CN in H$_2$O, see *Chapter 6*), and the material was purified through preparative RP-HPLC using C$_3$ column. However, only a small amount of **5-52** was isolated after the purification process, possibly due to aggregation on the column, not allowing the assembly. ESI-MS(Q-Tof) spectrum of peptide **5-52** displays peaks for the multicharged ions [M+2H]$^{2+}$, [M+3H]$^{3+}$, [M+4H]$^{4+}$ which after deconvolution gave the monoisotopic mass: 3540.6 corresponding to the expected mass (Figure 5-24).
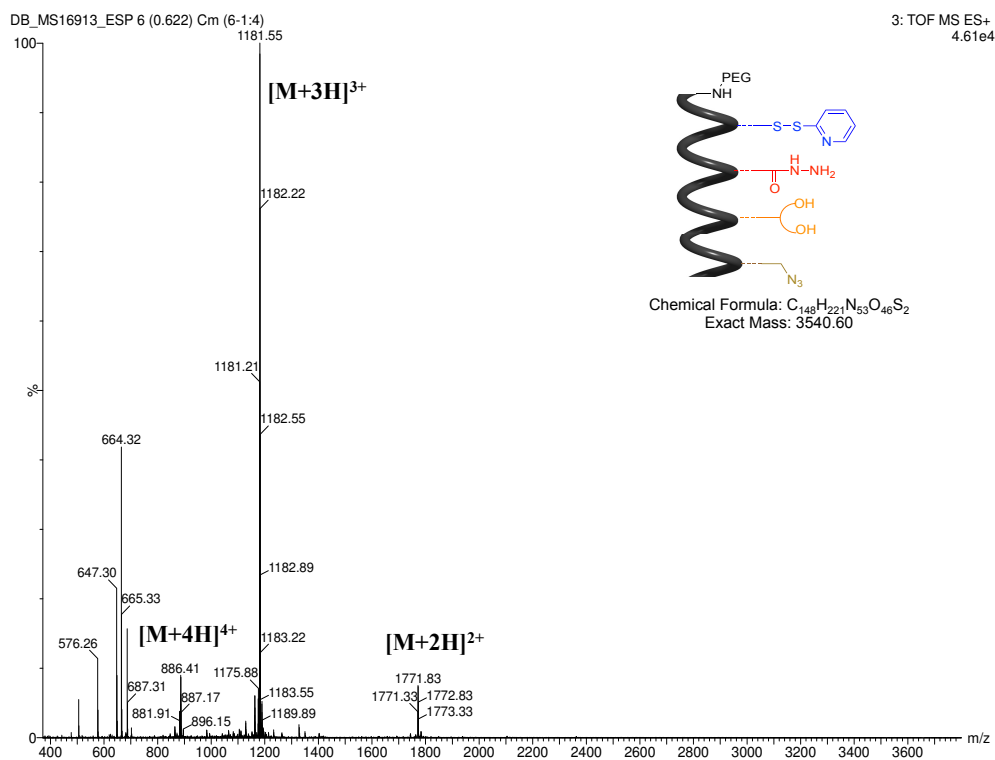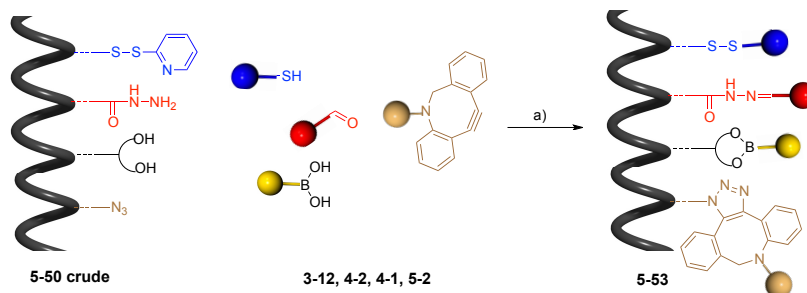
Figure 5-24 ESI-MS(Q-Tof) analysis of purified peptide **5-52** showing $[M+2H]^{2+}$, $[M+3H]^{3+}$, $[M+4H]^{4+}$.

Scheme 5-12 Chromophoric assembly of ADIBO-Py **5-2**, R-PDI **4-2**, Y-Per **4-1**, B-NDI **3-12** within crude peptide **5-50**; a) *m*-PDA, DMA, 3 h, rt, 2 h, 40 °C.

The chromophoric assembly was performed on non-purified peptide **5-50** by applying the optimized conditions described in *Section 5.2.2.1.2, i.e.* by mixing the components in a one-pot reaction for 3 h at rt and 2 h at 40 °C in the presence of a catalytic amount of *m*-PDA (Scheme 5-12). B-NDI **3-12**, R-PDI **4-2**, Y-Per **4-1** bearing the boronic acid, ADIBO-ethynylpyrene **5-2**, were used for the assembly of tetrad **5-53** for their complementary spectral properties. The excess of chromophores was removed through GPC, and the material was analyzed by UV-Vis spectroscopy. The absorption spectrum of **5-53** normalized with the linear combination of the dyes on B-NDI maximum shows the presence of the four chromophores. However, in a similar way to *Chapter 3 and 4*, R-PDI was not introduced quantitatively due to the positioning of the dye on the scaffold being sandwiched between Y-Per and B-NDI units (Figure 5-25).
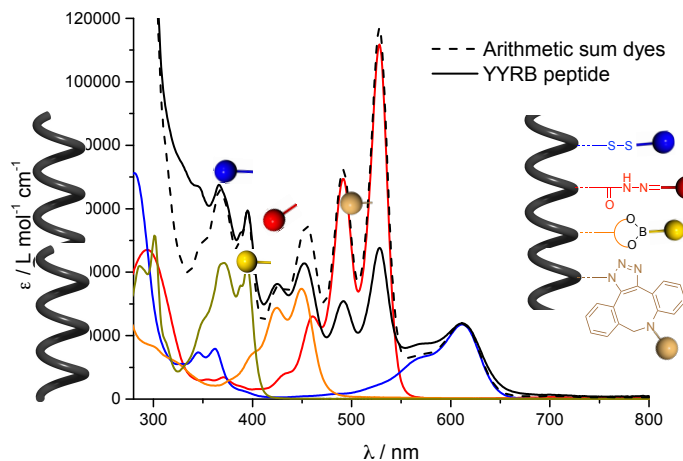
Figure 5-25 Absorption spectra of YYRB tetrad **5-53** normalized with arithmetic sum of chromophores on B-NDI in DMA.
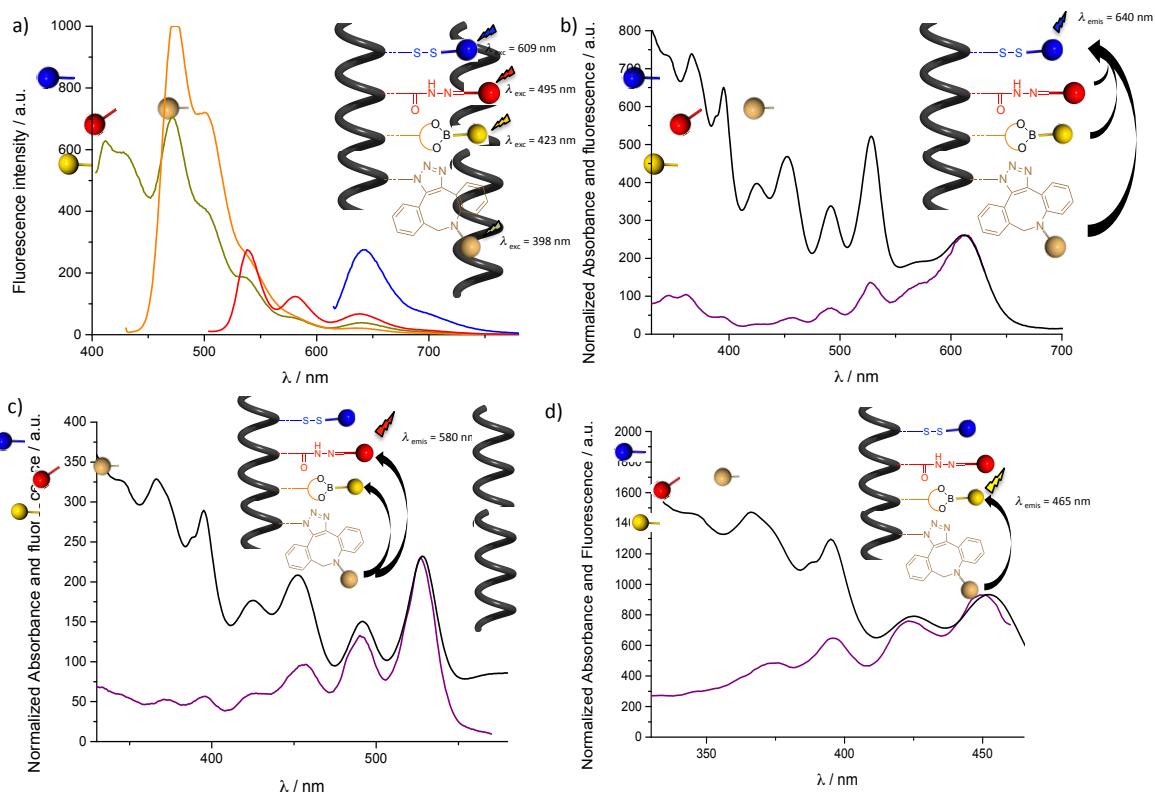

Figure 5-26 a) Fluorescence emission spectra of YYRB peptide **5-53** at *(λ$_{exc}$)* 398 nm (green), 423 nm (yellow), 495 nm (red), 609 nm (blue) to determine ET efficiencies following method 1: $\Phi_{ET} = QY*_{B\text{-}NDI}/QY_{B\text{-}NDI}$; b, c, d) Normalized absorption (in black) and fluorescence excitation (in purple) spectra of YYRB peptide 2 *(λ$_{em}$=640, 580, 465 nm respectively)* for method 2: $\Phi_{ET} = Ex_D/A_D$.

Fluorescence measurements were carried out in DMA to evaluate the efficiencies of the energy transfers Φ_{ET} within tetrad **5-53**. Notably, the selective excitation of the primary donor unit Py (at 398 nm) led to an overall energy transfer determined to be around 6-7% (Figure 5-26 and Table 5-

4). Considering the strong emission of Y-Per, we assume the low efficiency of ET (Y-Per→R-PDI) or the possible hydrolysis of the boronate ester during the measurements. For a better understanding of the process, the intermediate Φ_{ET} (Y-Per→R-PDI), (Y-Py→R-PDI), (Y-Py→R-PDI) were also evaluated according to the second method: by normalizing the excitation (at the emission of acceptor R-PDI and Y-Per, 580 and 465 nm respectively) and the absorption spectrum on acceptor maximum and comparing the intensities of the donor on the two spectra. However, those values, reported in Table 5-6 (Entries 4-6), are only qualitative as it is not possible to target selectively the emission of the intermediate acceptors due to the important fluorescence overlap of the dyes.

Table 5-6 Energy transfer efficiencies within **5-53** calculated following methods 1 and 2.

Entry	Φ_{ET} (donor → acceptor) %	1: $\Phi_{ET} = QY^*_{B\text{-}NDI}/QY_{B\text{-}NDI}$	2: $\Phi_{ET} = Ex_D/A_D$
1	R-PDI→B-NDI	19.3	20.1
2	Y-Per→B-NDI	9.5	8.9
3	Y-Py→B-NDI	6.3	6.9
4	Y-Per→R-PDI	-	33.5
5	Y-Py→R-PDI	-	20.5
6	Y-Py→Y-Per	-	53

5.2.2.3.2 Tetrad assembly templated by tetratopic short peptide

Inspired by the results obtained from the triad templated by the short scaffold in *Section 5.2.2.2.2*, a short tetratopic peptide was targeted in order to bypass the problem of hydrophobicity of the helical scaffold. The synthetic approach for tetratopic peptide **5-55** was slightly modified. Indeed, in Section *5.2.2.2.2,* it was observed that short peptidic sequence bearing the pyridyl-disulfide moiety led very easily to the disulfide metathesis (formation of the dimer), in particular in aqueous media, preventing the purification of the peptide through RP-HPLC. In this respect, the tetrapeptide was grown on H-Ala 2-Cl-Trt resin using the general procedure and fully protected peptide **5-54** was cleaved from the resin using mild acidic conditions (AcOH/TFE/CH$_2$Cl$_2$ (1:1:8), rt, 30 min) (Scheme 5-13). After purification through RP-HPLC, side chains deprotection and subsequent disulfide exchange to introduce the disulfide-pyridine moiety were performed to afford **5-55**. The chemical identity of the product was confirmed by ESI-MS(Q-Tof); the spectrum displays peaks for mono and bischarged ions (H and Na adducts) (Figure 5-27).
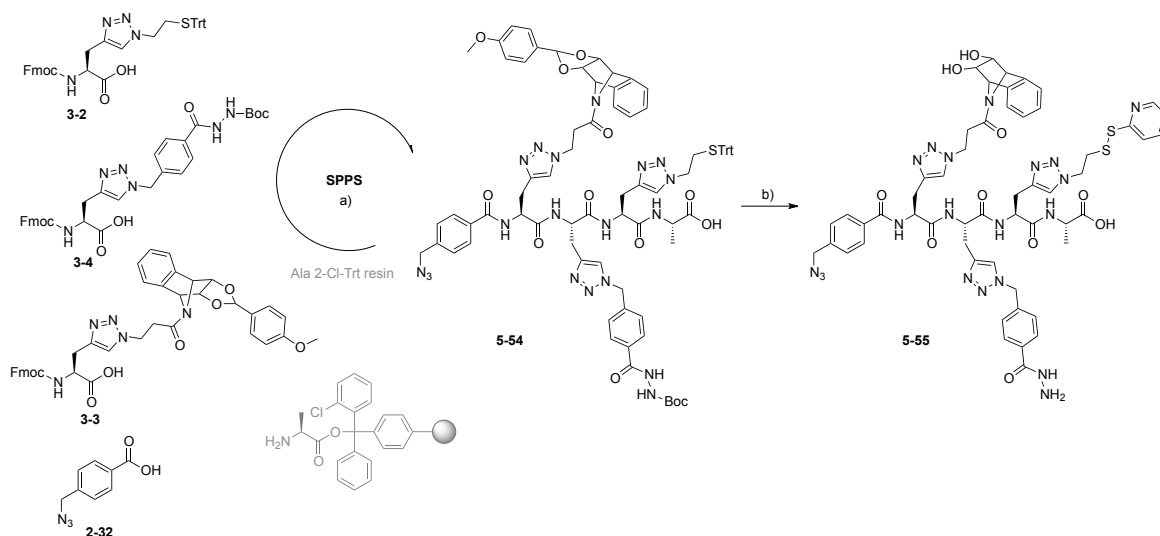
Scheme 5-13 Synthesis of peptidic scaffold **5-55**; a) SPPS: *i)* AA coupling: Fmoc-AA-OH, HATU, DIEA, DMF/NMP, rt, 1 h; *ii)* Fmoc deprotection: 20% piperidine in DMF, rt, 3 × 6 min; *iii)* capping with **2-32**: HATU, DIEA, DMF/NMP, rt, 1h30; *iv)* Resin cleavage: AcOH/TFE/CH$_2$Cl$_2$ (1:1:8), rt, 30 min; b) *i)* TFA/TIS/H$_2$O (95:2.5:2.5), rt, 2 h; *ii)* 2,2'-dipyridyl disulfide, DIEA, DMF, 30 min.
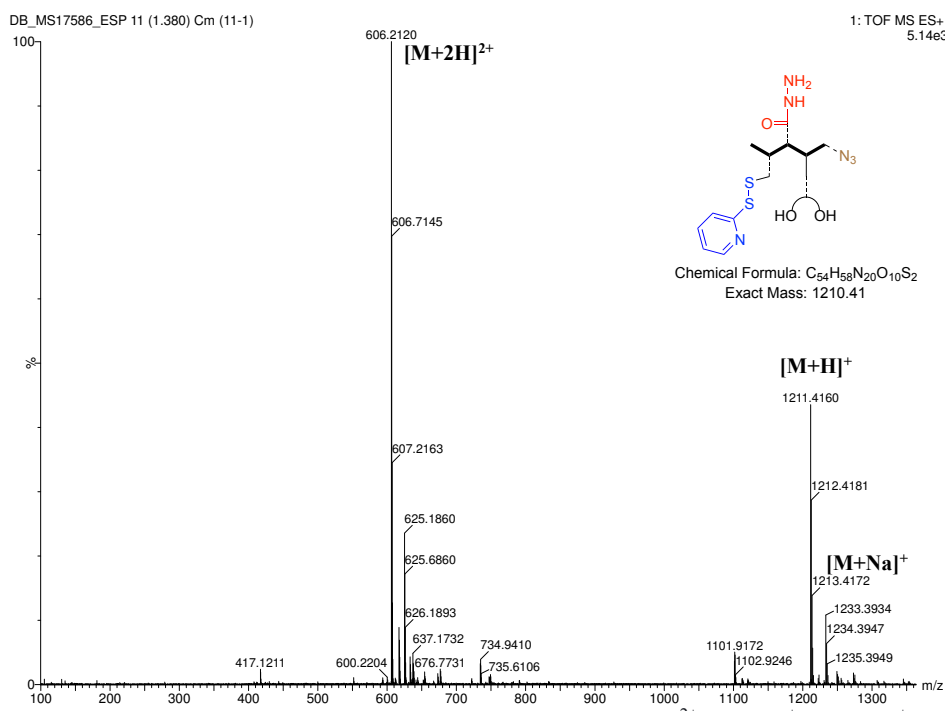

Figure 5-27 ESI-MS(Q-Tof) analysis of peptide **5-55** showing [M+2H]$^{2+}$, [M+H]$^+$, [M+Na]$^+$.

Tetrad **5-56** was assembled on peptide **5-55** in a one-pot fashion. As a first trial, similar conditions than those employed for the helical scaffold (2 h at rt and 2 h at 40 °C) were employed (Scheme 5-14; one-pot approach). After purification by GPC to remove the excess of chromophores, **5-56** was analyzed by UV-Vis spectroscopy.
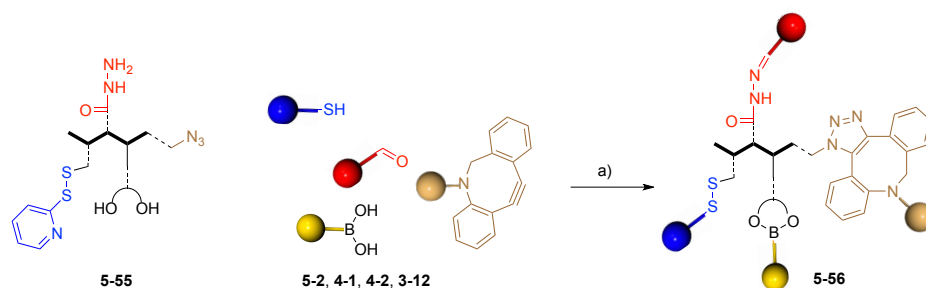
Scheme 5-14 Chromophoric assembly of ADIBO-Py **5-2**, R-PDI **4-2**, Y-Per **4-1**, B-NDI **3-12** within peptide **5-55**; a) One-pot approach: *i) m*-PDA, DMA, 2 h, rt, 2 h, 40 °C; *ii)* +16 h, rt; Stepwise approach: *i)* R-PDI, *m*-PDA, DMA, 17 h, rt, *ii)* B-NDI, Y-Per, 2 h, rt, *iii)* ADIBO-Py, 40 °C, 2 h.

The absorption spectrum of the tetrad normalized (on B-NDI) with the linear combination of the 4 dyes shows that R-PDI and Y-Per units were not quantitatively introduced while the intensity of ADIBO-Py bands overcomes the arithmetic sum of the dyes (Figure 5-28 a, grey line). This could suggest either the excess of ADIBO-Py with respect to the other dyes or the existence of ground state interactions in this region possibly due to aggregation phenomena. Increasing the reaction time to additional 16 h slightly improved the incorporation of R-PDI unit (Figure 5-28 a, black line). In order to unravel the reactivity of the dyes within this short scaffold, in which the chromophores are in very close proximity possibly preventing their simultaneous quantitative introduction, the assembly was performed by adding the dyes stepwisely (from the center to the extremities of the scaffold). In this respect, R-PDI **4-2** was first mixed with the scaffold in the presence of the catalyst (at rt for 17 h), then B-NDI **3-12** and Y-Per **4-1** were added and mixed for two additional hours. Finally, ADIBO-Py **5-2** was introduced to the mixture, which was stirred at 40 °C for 2 h more (Scheme 5-14; stepwise approach). After purification of tetrad **5-56**, the absorption spectrum shows the same profile than the one obtained with the one-pot approach (Figure 5-28 b) indicating that the steric hindrance within the tetrad prevents the quantitative incorporation of those two dyes in both one-pot and stepwise approaches. After drying the material and re-dissolving it in CHCl$_3$, its absorption spectrum normalized with the linear combination of the dyes absorption spectra (in CHCl$_3$) shows a good correlation for ADIBO-Py unit bands (below 400 nm, Figure 5-28 c). This supports the presence of ground state interactions in DMA leading to the exceed intensity of the ethynylpyrene moiety.

The MALDI-TOF spectrum of tetrad **5-56** displays peaks for $[M+H]^+$ and $[M+Na]^+$ (at m/z = 4133.6 and 4155.6) in accordance with the calculated mass (Figure 5-29). Moreover, as for triad **5-48**, peak corresponding to the product after loss of R-PDI unit and cyclization with carboxylic acid in C-terminal $[M(-PDI-H_2O)+H]^+$ probably occurring during the ionization process was also detected (m/z = 3077.1).
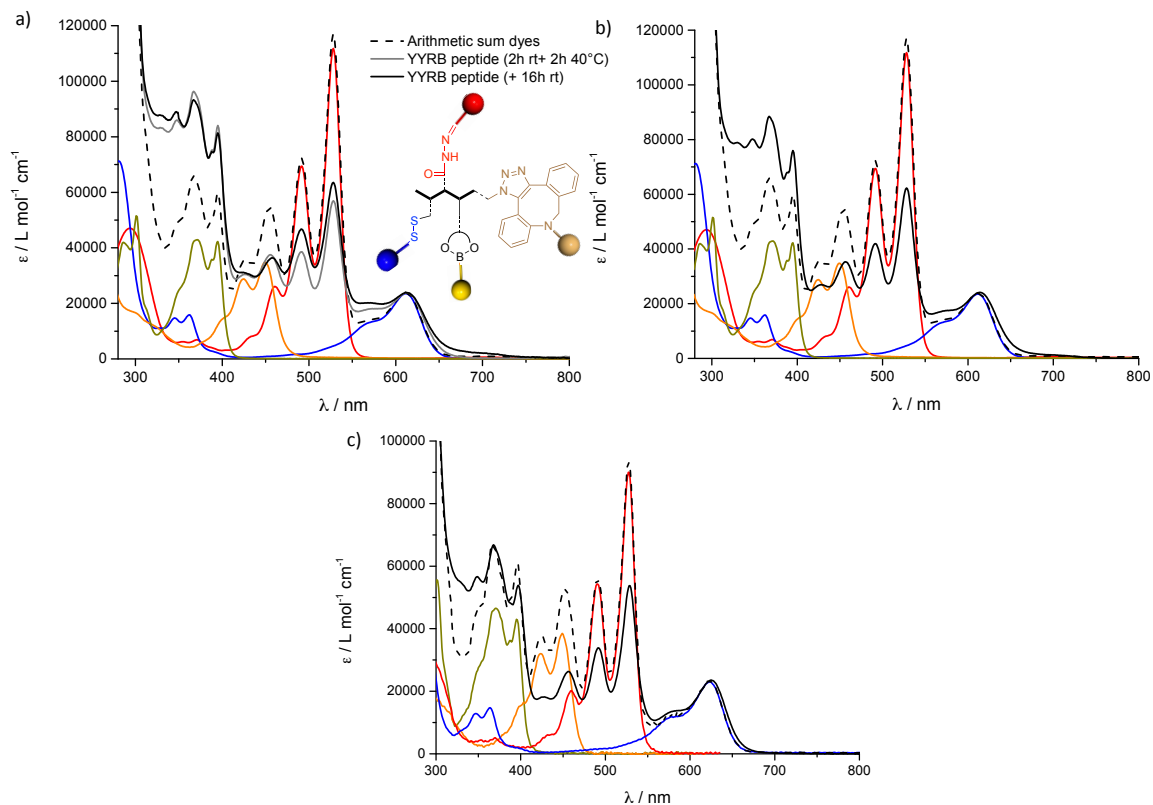
Figure 5-28 Absorption spectra of YYRB tetrad **5-56** normalized with arithmetic sum of chromophores ADIBO-Py **5-2**, Y-Per **4-1**, R-PDI **4-2**, B-NDI **3-12** on B-NDI following a) one-pot approach in DMA; b) stepwise approach in DMA; c) in CHCl₃.
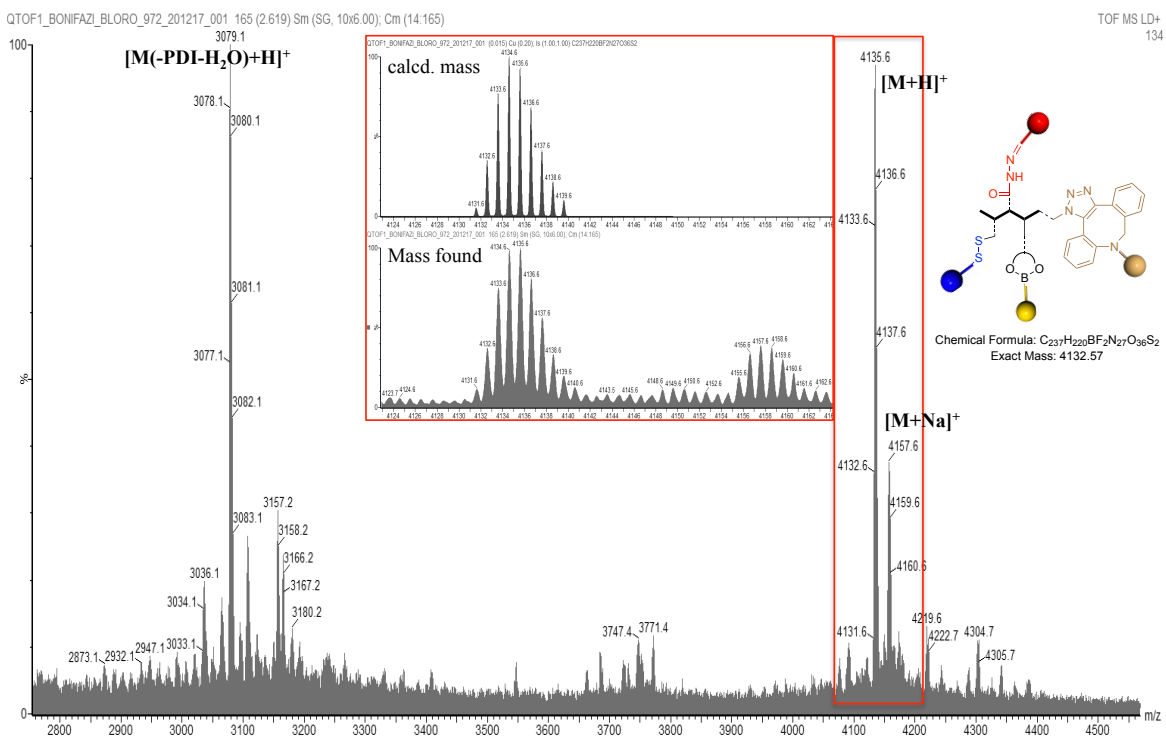

Figure 5-29 MALDI-Tof analysis of peptide **5-56**; Inset: Zoom of $[M+H]^+$ and $[M+Na]^+$ peaks (bottom) compared with calculated mass $[M+H]^+$ (top).

163

Preliminary ET studies were performed by steady-state fluorescence spectroscopy in DMA and CHCl$_3$ (with and without EYPC) in order to select the best medium. In this respect, CHCl$_3$ appeared to improve both Φ_{ET} (R-PDI→B-NDI) and Φ_{ET} (Y-Per→B-NDI) as highlighted in the excitation spectra (Figure 5-30). This is explained by the better stability of the boronate ester within the tetrad in this medium while the presence of hygroscopic lipid favored its hydrolysis.
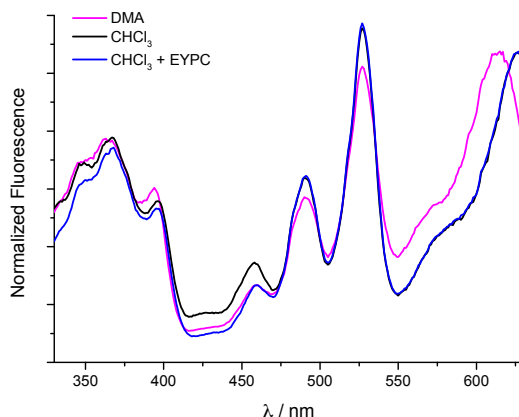

Figure 5-30 Excitation spectra of tetrad **5-56** *(λ_{em}=640 nm)* normalized at the excitation maximum of B-NDI unit in different media.
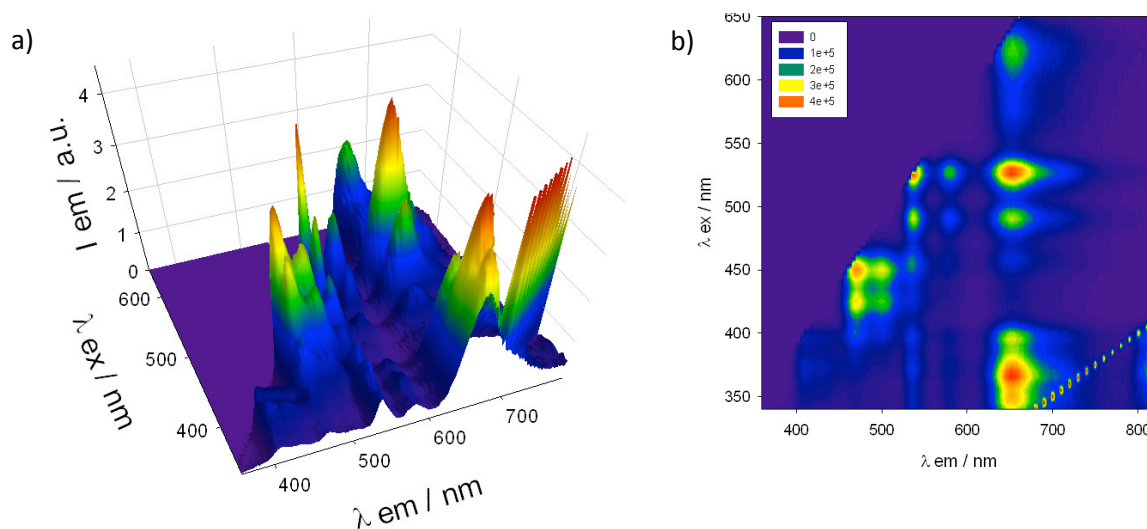

Figure 5-31 a) Emission map for **5-56** in CHCl$_3$ at $340 < \lambda_{exc} < 650$ nm. b) Emission contour map for **5-56**.

The energy transfer within tetrad **5-56** was investigated in-depth. The emission fluorescence mapped against the excitation wavelengths shows the B-NDI acceptor emission almost at any excitation and particularly upon excitation of Py and PDI units (Figure 5-31). The energy transfer efficiencies were determined by method 2, *i.e.* by superposition of the absorption and excitation spectra (Figure 5-32), and are reported in Table 5-7. Besides, the fluorescence quenching yields of the dyes in **5-56** were also estimated with respect to the corresponding free chromophores and are reported in the same table (see *Chapter 6* for data). Notably, if most of the quenching of the donor

units can be explained by energy transfer, 56% of B-NDI acceptor emission was also quenched highlighting the presence of deactivation pathways other than energy transfers such as electron transfers. This hypothesis is in accordance with the frontier molecular orbital levels (Figure 5-7) supporting the possible oxidative electron transfer to the electron poor PDI: B-NDI* + R-PDI → B-NDI$^{\bullet+}$ + R-PDI$^{\bullet-}$ or the reductive one from the pyrene moiety: B-NDI* + Y-Py → B-NDI$^{\bullet-}$ + Y-Py$^{\bullet+}$. Further transient absorption spectroscopy measurements will be carried out to confirm the presence of radical species.

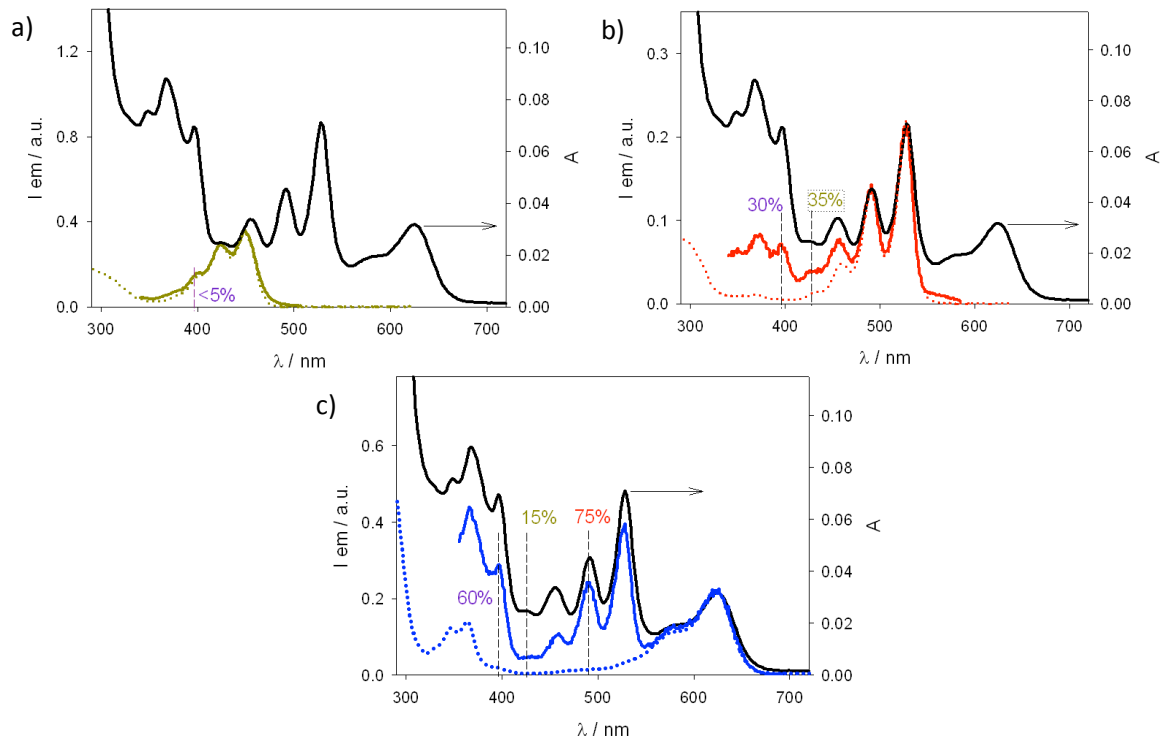**Figure 5-32** Normalized absorption (solid black) and fluorescence excitation (solid colored) spectra of YYRB peptide **5-56** *(λ_{em}=510, 590, 700 nm for a) b) and c) respectively)* in CHCl$_3$ for method 2: $\Phi_{ET} = Ex_D/A_D$ and normalized absorption (dotted colored) of free chromophores.

**Table 5-7** Fluorescence quenching yield and energy transfer efficiencies within **5-56** calculated following method 2 CHCl$_3$.

Entry	Dyes in **5-56**	Φ_{quench} / 1 dye %	$\Phi_{ET} = Ex_D/A_D$ %
1	Y-Py	96	→Y-Per: <5 →R-PDI: 30 →B-NDI: 60
2	Y-Per	62	→ R-PDI: 35 →B-NDI: 15
3	R-PDI	88	→ B-NDI: 75
4	B-NDI	56	-

165

5.2.2.4 Pentachromophoric architectures: introduction of the inverse electron demand Diels-Alder (IEDDA) in the system

5.2.2.4.1 Pentad assembly templated by helical scaffold

The synthesis of peptidic scaffold Ac-E(tetrazine)-QLAQLA-X(disulfide)-QLAQLA-X(hydrazide)-QLAQLA-X(diol)-QLAQLA-Nle(N$_3$)-QLA-NH$_2$ **5-58** was carried out by elongating on solid phase Fmoc-QLA-X(STrt)-QLAQLA-X(hydrazide-Boc)-QLAQLA-X(diol-PMB)-QLAQLA-Nle(N$_3$)-QLA-NH-resin prepared in *Section 5.2.2.3.1* (Scheme 5-15). Tetrazine-containing amino acid **5-22** was introduced as last residue to avoid its exposure was. However, the purification of peptide **5-58** was not successfully performed on RP-HPLC due to its high hydrophobic nature. The same strategy as before was applied consisting in substituting leucine L residue by alanine A. In this respect, peptide PEG-E(tetrazine)-QAAQAA-X(disulfide)-QAAQAA-X(hydrazide)-QAAQAA-X(diol)-QAAQAA-Nle(N$_3$)-QAA-NH$_2$ **5-60** was synthesized following the same synthetic strategy from Fmoc-QAA-X(STrt)-QAAQAA-X(hydrazide-Boc)-QAAQAA-X(diol-PMB)-QAAQAA-Nle(N$_3$)-QAA-NH-resin and aa **5-23** (Scheme 5-15). Here again, purification of the material through RP-HPLC was not successively achieved possibly due to the increased hydrophobicity of the peptide when tetrazine-containing aa was introduced.
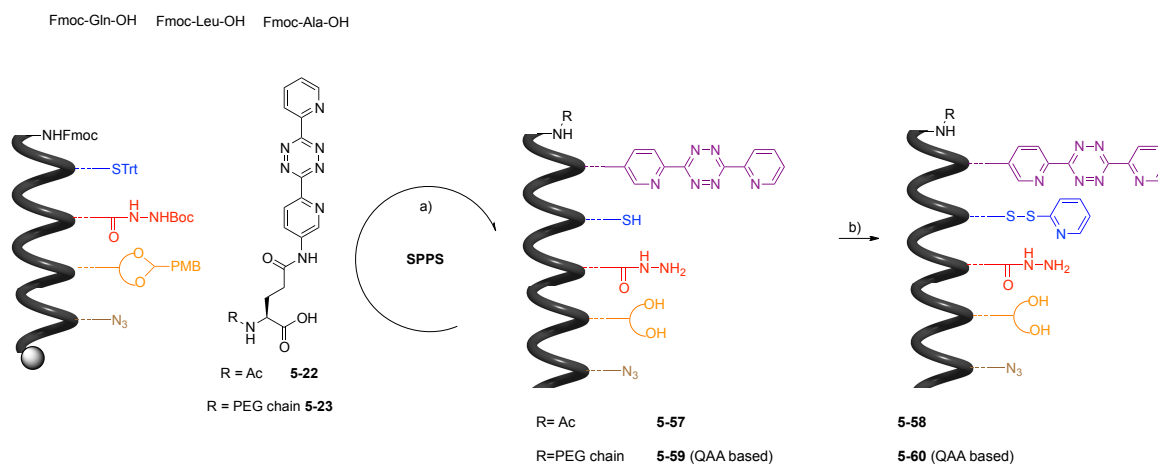
Scheme 5-15 Synthesis of peptidic scaffolds **5-58** and **5-60**; a) SPPS: *i)* Fmoc deprotection: 20% piperidine in DMF, rt, 3 × 6 min; *ii)* AA coupling: Fmoc-AA-OH, HATU, DIEA, DMF/NMP, rt, 25 min or 1 h for last coupling with tetrazine containing aa; *iii)* TFA/TIS/H$_2$O (95:2.5:2.5), rt, 2 h; b) 2,2'-dipyridyl disulfide, DIEA, DMF, 1 h.
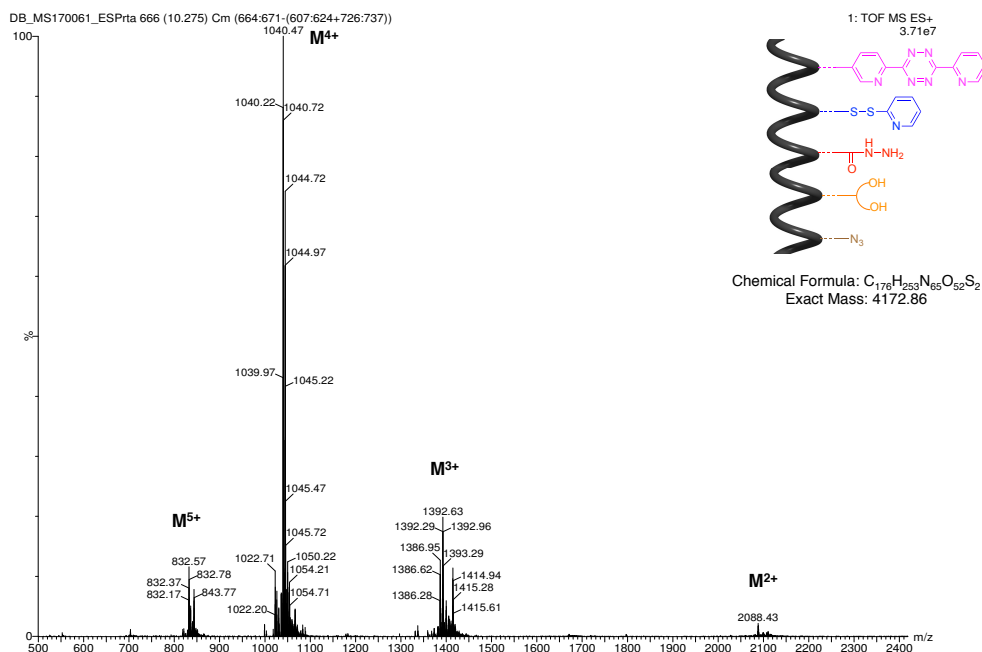
Figure 5-33 LC-ESI-MS(Q-Tof) analysis of crude peptide **5-60** showing $[(M+2)+2H]^{2+}$, $[(M+2)+3H]^{3+}$, $[(M+2)+4H]^{4+}$.

Nevertheless, in this case, thanks to the decreased hydrophobicity of the material, the analysis of the crude material by LC-MS (C_4 column) shows the peaks for multicharged ions M^{4+}, M^{3+}, M^{2+}, which after deconvolution gave mainly the monoisotopic mass 4174.86 (Figure 5-33). This corresponds to ($M_{peptide}+2$) possibly due to the reduction of the tetrazine core into dihydrotetrazine during the peptide cleavage from the resin in the presence of an excess of triisopropylsilane in TFA.
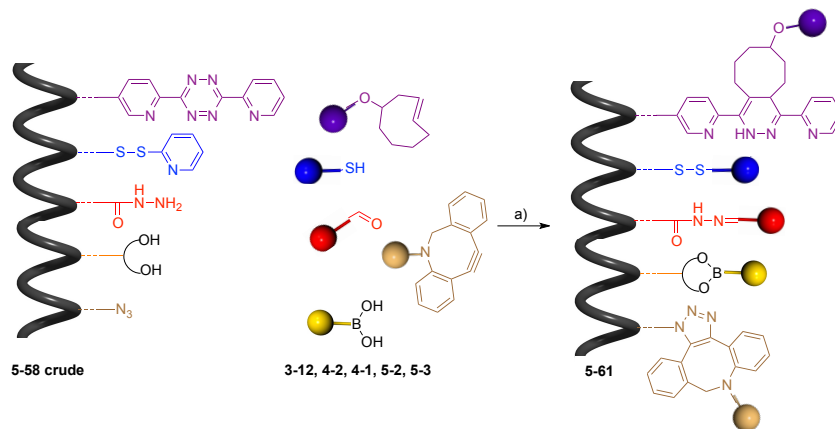
Scheme 5-16 Chromophoric assembly of ADIBO-Py **5-2**, R-PDI **4-2**, Y-Per **4-1**, B-NDI **3-12**, TCO-Cy **5-3** within crude peptide **5-58**; a) *m*-PDA, DMA, 4 h, rt, 3 h, 40 °C.

To confirm this result, pentad **5-61** was assembled on crude **5-58**. The reaction was performed according to the optimized procedure with the SPAAC on the helical scaffold, *i.e.* stirring at rt for 3 h and two additional hours at 40 °C in DMA in the presence of *m*-PDA as catalyst (Scheme 5-

167

16). After purification by GPC, the absorption spectrum of **5-61** shows the characteristic bands of the five chromophores (Figure 5-34).
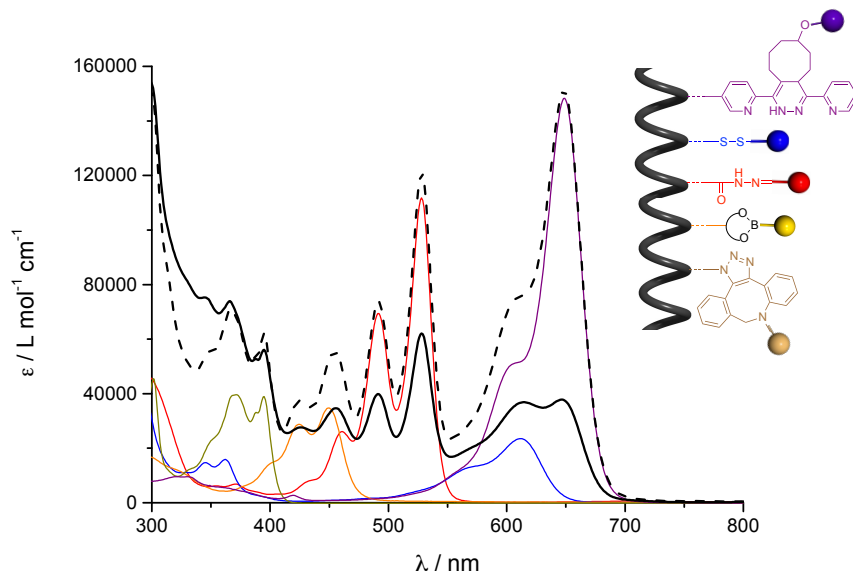

Figure 5-34 Absorption spectrum (in black) of peptide **5-61** bearing 5 dyes normalized with arithmetic sum of absorption spectra of dyes (dashed black) ADIBO-Py **5-2**, Y-Per **4-1**, R-PDI **4-2**, B-NDI **3-12**, B-Cy **5-20** on ADIBO-Py (398 nm) in DMA.

The normalization of the spectrum with the linear combination of the five chromophores on the ethynylpyrene unit (at 398 nm) indicates the low introduction of the cyanine moiety with respect to the others, possibly due to the partial reduction of the tetrazine core and/or, the presence of truncation side products in the crude material. The fluorescence emission spectra confirmed as well the introduction of the five chromophores and the cascade energy transfer (Figure 5-35). In particular, by exciting the primary donor Y-Py unit at 398 nm, all the characteristic emission maxima corresponding to the 5 dyes were observed. However, due to the absorption and fluorescence overlapping of the five chromophores, it was not possible to determine precisely the ET efficiencies. Nevertheless, the excitation fluorescence spectra of **5-61**, recorded at the emission of acceptor B-Cy *(λ_{em} = 670 nm)* and B-NDI (λ_{em} = 640 nm) and normalized on the maximum of absorption of **5-20** and **3-12** respectively, allow the approximate estimation of ET efficiencies (Figure 5-36, Table 5-8). It is noteworthy to indicate that Φ_{ET}(donor→B-NDI) are overestimated due to the overlapping of the absorption of B-NDI and B-Cy units, while obviously Φ_{ET}(donor→B-Cy) are underestimated as a direct consequence.
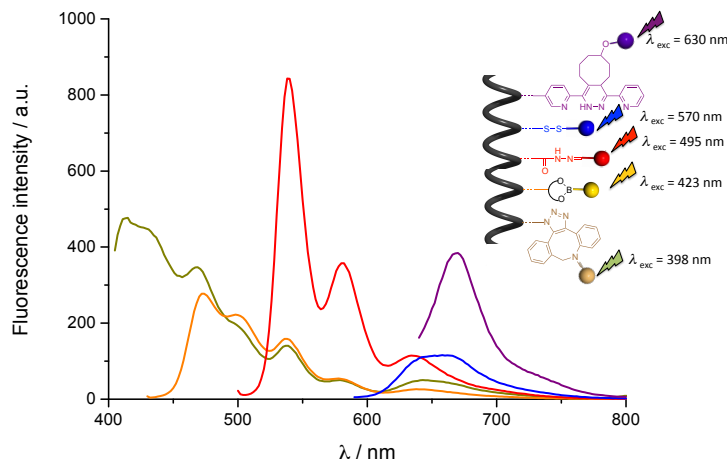
Figure 5-35 Fluorescence emission spectra of **5-61** at (λ_{exc}) 398 nm (green), 495 nm (red), 570 nm (blue), 630 nm (purple) in DMA.

Table 5-8 Energy transfer efficiencies within peptide **5-61** calculated following method 2 in DMA.

Entry	Φ_{ET} (donor → acceptor)	$\Phi_{ET} = Ex_D/A_D$
1	Y-Py→B-Cy	4
2	Y-Per→B-Cy	3.1
3	R-PDI→B-Cy	7
4	Y-Py→B-NDI	15.6
5	Y-Per→B-NDI	15.7
6	R-PDI→B-NDI	47
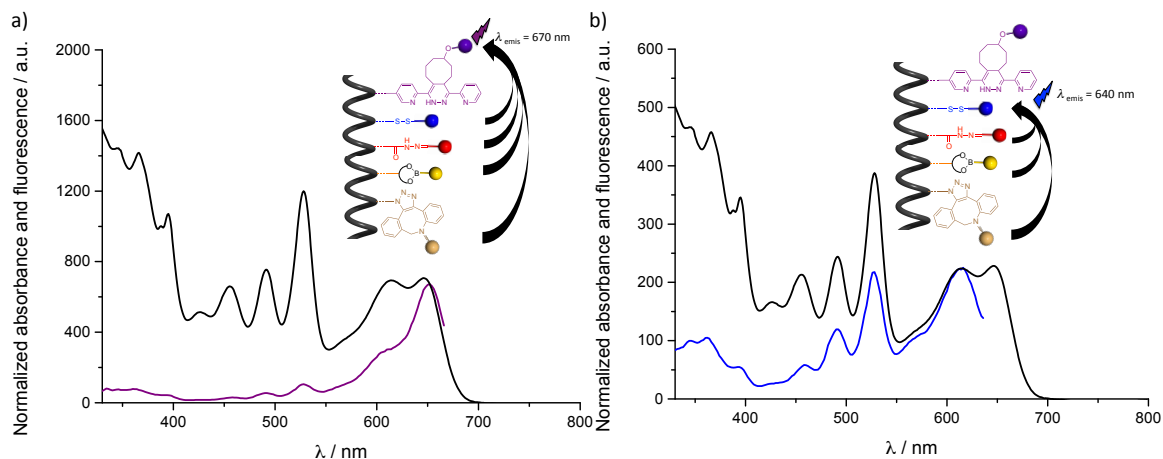
Figure 5-36 Normalized absorption (black) and fluorescence excitation (purple for a, blue for b) spectra of colored peptide **5-61** at a) λ_{emis} = 640 nm; b) 670 nm in DMA.

5.2.2.4.2 Pentad assembly template by pentatopic short peptide

In the same way as for *Section 5.2.2.3.2*, a short oligopeptide can be used to assembly 5 dyes. Having in hands fully protected peptide **5-54** and amine **5-24**, the tetrazine moiety can be easily introduced through an amide bond formation as described in Scheme 5-17.
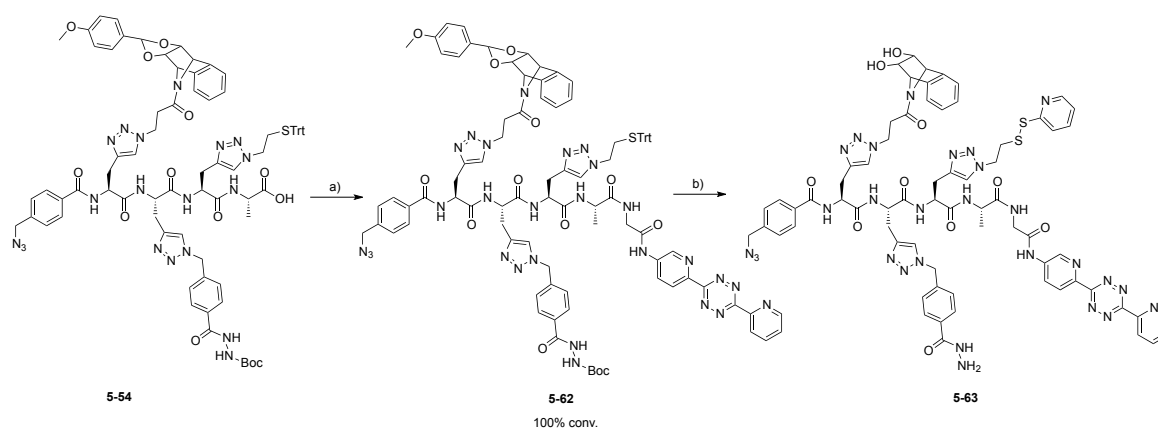
Scheme 5-17 Synthesis of pentapeptide **5-63**; a) **5-24**, HATU, DIEA, DMF/NMP, rt, 1h30; b) *i)* TFA/TIS (5 equiv) /H_2O, rt, 2 h; *ii)* 2,2'-dipyridyl disulfide, DIEA, DMF, 30 min.

Peptidic coupling was carried out in solution between H-Gly-tetrazine **5-24** and fully protected tetrapeptide **5-54** in the presence of HATU and DIEA. The ESI-MS(Tof) spectrum of protected peptide **5-62** displays peaks for mono- and bischarged ions corresponding to the mass of the expected product and after loss of -Trt and -Boc protecting groups during the ionization process Figure 5-37).
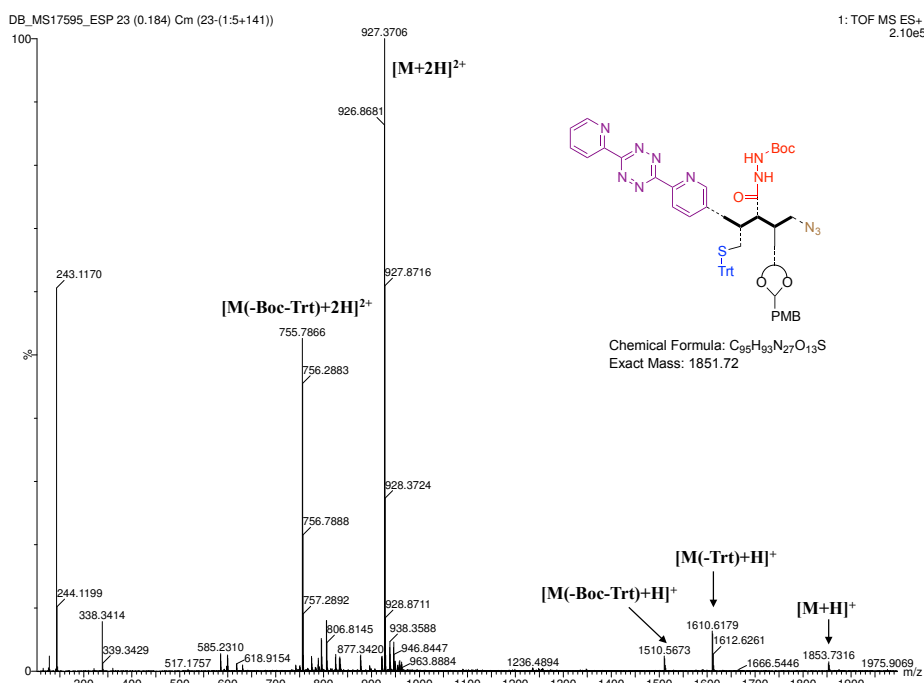

Figure 5-37 ESI-HRMS(Q-Tof) analysis of peptide **5-62** showing $[M+2H]^{2+}$, $[M+H]^{+}$ and fragmented ions.
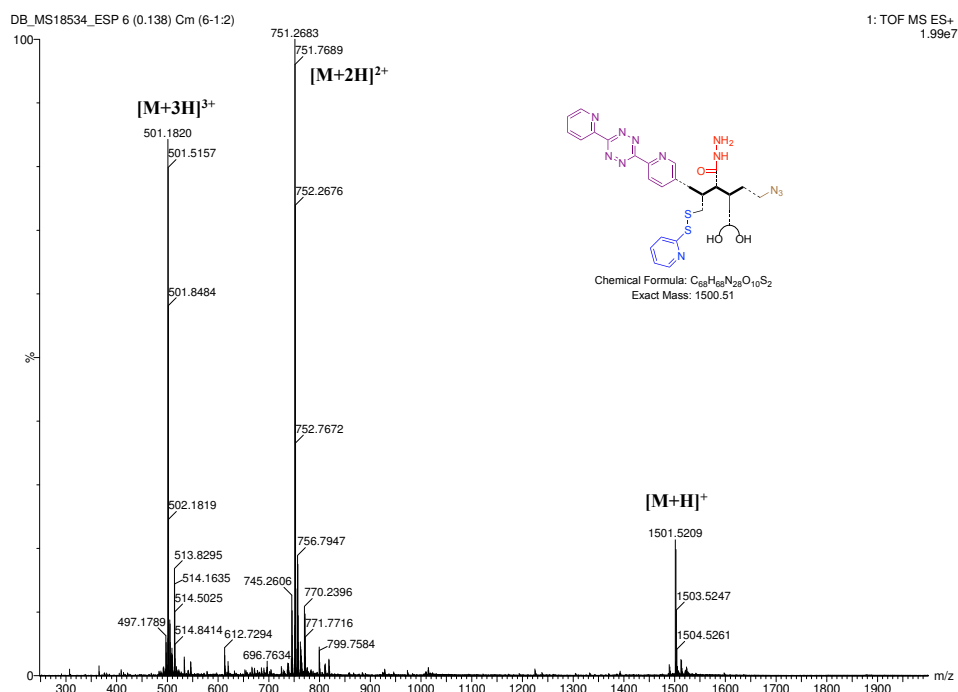
Figure 5-38 ESI-HRMS(Q-Tof) analysis of peptide **5-63** showing $[M+3H]^{3+}$, $[M+2H]^{2+}$, $[M+H]^{+}$.

Then, side chains were deprotected with TFA/TIS/H$_2$O cocktail and the disulfide pyridine moiety was introduced as in the general procedure. Nevertheless, it is noteworthy to indicate that when TFA/TIS/H$_2$O was used in ratio 95:2.5:2.5 (corresponding to 80 equiv. of TIS with respect to the peptide), the targeted product was in mixture with a by-product (in 1:1 ratio) remaining unidentified ((M$_{peptide}$+40) possibly induced by the reduction of the tetrazine core into dihydrotetrazine by the large excess of TIS in TFA). In contrast, when 5 equiv. of TIS and H$_2$O were added to scavenge cationic species, the product was formed as the main product. The ESI-MS(Q-Tof) spectrum of **5-63** displays $[M+3H]^{3+}$, $[M+2H]^{2+}$ and $[M+H]^{+}$ peaks (Figure 5-38). Pentad **5-64** was assembled on pentatopic peptide **5-63** in a one-pot reaction according to the procedure developed in *Section 5.2.2.3.2*, *i.e.* by mixing the components at rt for 2 h and at 40 °C for two additional hours (Scheme 5-18 a). Pentad **5-64** was purified by GPC and the product was analyzed by UV-Vis and fluorescence spectroscopy in CHCl$_3$. The absorption spectrum of the pentad (grey line) normalized with the arithmetic sum of the dye absorptions (at 612 nm) highlights the introduction of the 5 dyes (Figure 5-39).
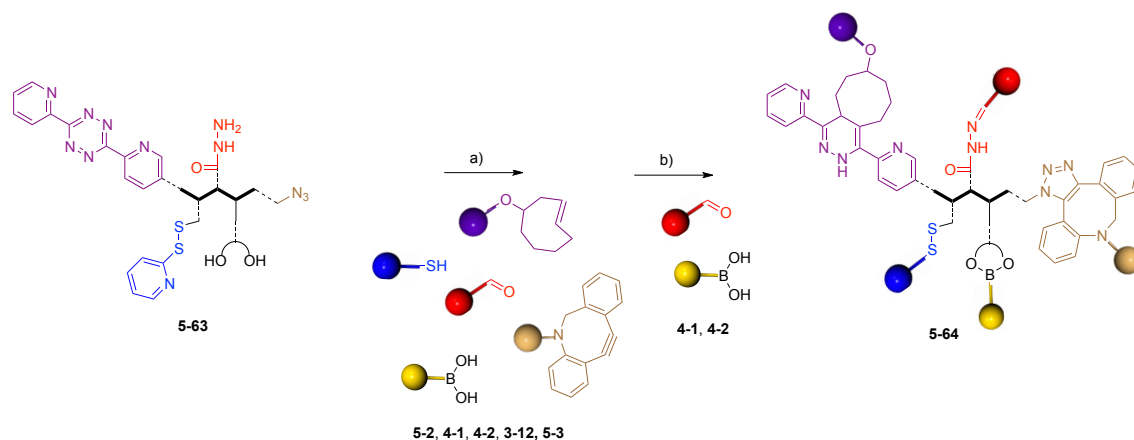
Scheme 5-18 Chromophoric assembly of ADIBO-Py **5-2**, R-PDI **4-2**, Y-Per **4-1**, B-NDI **3-12**, B-Cy **5-3** within peptide **5-63**; a) *m*-PDA, DMA, 2 h, rt, 2 h, 40 °C; b) *m*-PDA, CHCl₃, 16 h, rt.

Notably, the tetrazine moiety was much more introduced than on the helical scaffold. Similarly to the tetrad, R-PDI and Y-Per were not incorporated quantitatively due to the steric hindrance within the pentad. By re-introducing the isolated material in reaction with Y-Per **4-1** and R-PDI **4-2** in CHCl₃ for 17 h at rt (Scheme 5-18 b), the absorption spectrum (black line, Figure 5-39) of the purified pentad shows the quantitative incorporation of R-PDI and Y-Per units. Nevertheless, an hypochromism for B-Cy band was observed presumably due to the low photochemical stability of B-Cy unit. The MALDI-Tof spectrum of the isolated material displays an intense peak for $[M(-2H)-I]^+$ corresponding to the product with one additional insaturation: due to the oxidation of the dihydropyridazine ring into pyridazine as for **5-20** and **2-42** (Figure 5-40). The other peaks at m/z=4070.7 and 4029.7 remain unidentified.
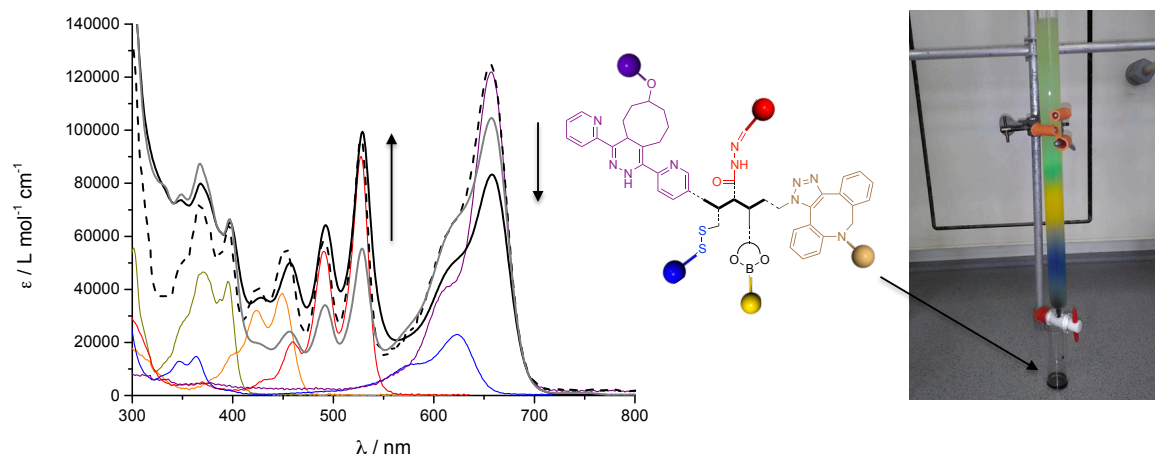

Figure 5-39 Left: Absorption spectra (in grey after 4 h of reaction in DMA; black after 16 h in CHCl₃) of pentad **5-64** normalized with arithmetic sum of dyes (dashed black) ADIBO-Py **5-2**, Y-Per **4-1**, R-PDI **4-2**, B-NDI **3-12**, B-Cy **5-20** on Y-Py unit (396 nm) in CHCl₃; Right: Purification of **5-64** by GPC.
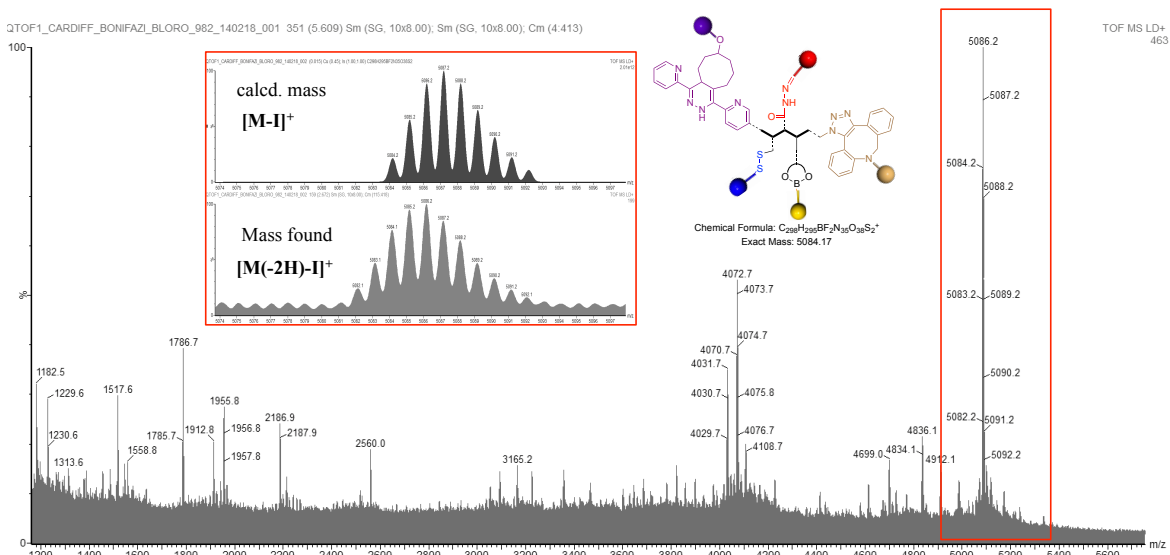
Figure 5-40 MALDI-Tof analysis of peptide **5-64**; Inset: Zoom of $[M(-2H)-I]^+$ peak (bottom) compared with calculated mass $[M-I]^+$ (top).

The behavior of pentad **5-64** was studied by steady-state fluorescence spectroscopy in CHCl$_3$ and compared with that of an isoabsorbing solution of free dyes Y-Py **5-2**, Y-Per **4-1**, R-PDI **4-2**, B-NDI **3-12** and **5-3** B-Cy, present either as a mixture or as single dyes. Notably, significant quenching of the fluorescence of the dyes within **5-64** was observed with respect to the free dyes in solution (single or in mixture, see *Chapter 6* Figure 6-48 and 6-49 respectively), from 66 to 99%, confirming the intramolecular deactivation pathway (Table 5-9). Besides, the emission of final acceptor B-Cy upon almost any excitation wavelength within the pentad (except for the selective excitation of Y-Per) supports an efficient energy transfer (Figure 5-41). The energy transfer efficiencies were determined by method 2 (Figure 5-42) and are reported in Table 5-9. The overall Φ_{ET} (Y-Py→B-Cy) was estimated to be around 50%. However, it is noteworthy to indicate that, despite the spectral overlap (Figure 5-1) of the five dyes supporting a cascaded energy transfer, the mechanism is not straightforward. For instance, the Y-Py moiety passed most of its energy directly to B-NDI and B-Cy while Y-Per transferred it only to R-PDI. Here again, if most of the fluorescence quenching of the donor moieties can be explained by energy transfer, 85% of the acceptor B-Cy fluorescence was quenched possibly due to photoinduced electron transfer. Indeed, according to the FMO levels reported in Figure 5-6, the deactivation of the excited state B-Cy* can occur via oxidative electron transfer to R-PDI leading to the formation of the radical pair R-PDI$^{•-}$/B-Cy$^{•+}$ or reductive mechanism from Y-Py affording B-Cy$^{•-}$/Y-Py$^{•+}$ (transient absorption spectroscopy measurements in progress).
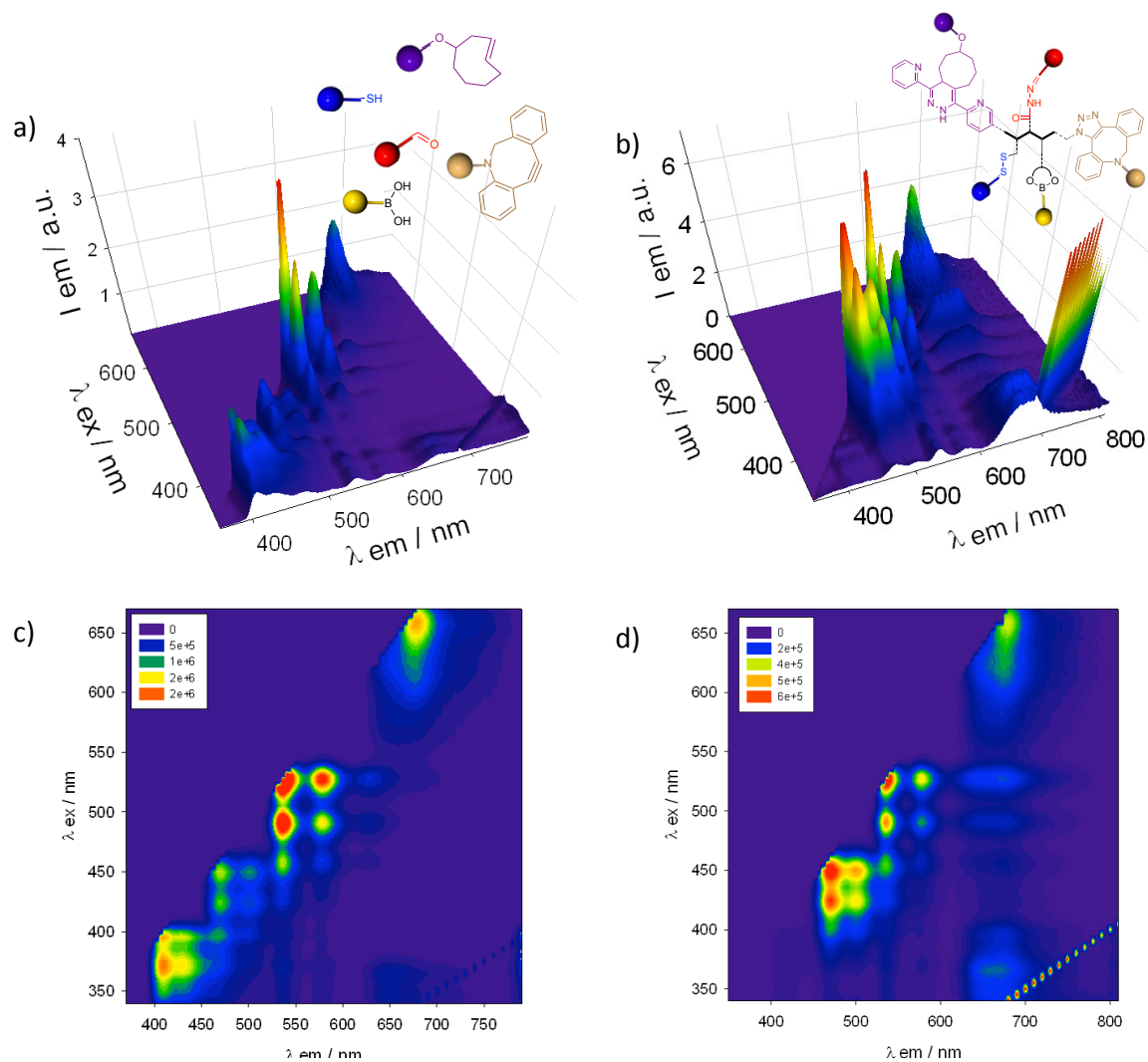
Figure 5-41 Comparison between emission map (a,b) and contour map (c,d) of isoabsorbing solutions of a, c) mixture of 5 chromophores **5-2, 4-1, 4-2, 3-12, 5-3** and b, d) peptide **5-64** in anhydrous CHCl$_3$; 340<λ_{exc}<670 nm.

Table 5-9 Energy transfer efficiencies within peptide **5-64** in anhydrous CHCl$_3$.

Entry	Dyes in **5-64**	Φ_{quench} / 1 dye %	Φ_{quench} / 5 dye mixture %	$\Phi_{ET} = Ex_D/A_D$ %
1	Y-Py	>99	>99	→Y-Per ≈ 0 →R-PDI <10 →B-NDI ≈ 40 →B-Cy ≈ 50
2	Y-Per	78	66	→ R-PDI ≈ 40 →B-NDI < 5 →B-Cy < 5
3	R-PDI	93	91	→ B-NDI ≈ 25 →B-Cy ≈ 45
4	B-NDI	87	81	→B-Cy ≈ 90
5	B-Cy	85	84	-
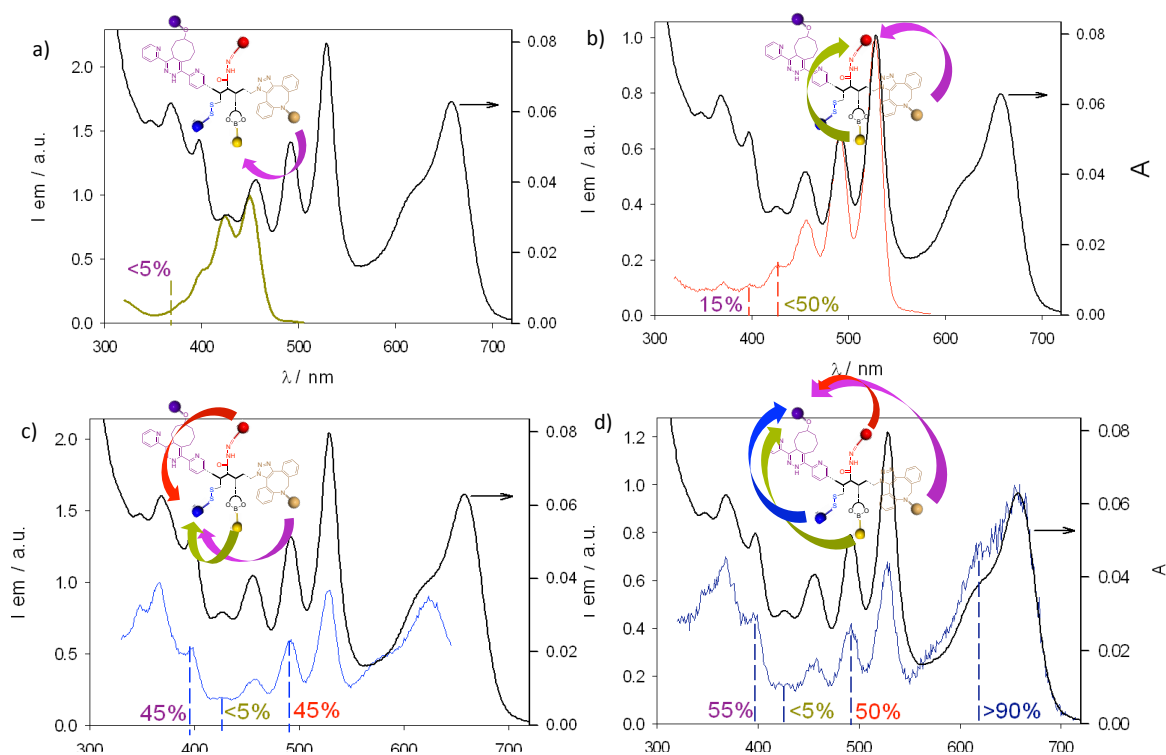
Figure 5-42 a, b, c, d) Normalized absorption (black) and fluorescence excitation (colored) spectra of peptide **5-64** *(λ_{em}=510, 590, 650 and 775 nm respectively)* in CHCl$_3$ for the method 2: $\Phi_{ET} = Ex_D/A_D$.

5.3 Conclusions

In summary, the pentaorthogonal reaction system, developed in *Chapter 2,* was successfully applied to program the chromophoric decoration of a peptidic scaffold. In this respect, multichromophoric architectures exhibiting any desired absorbed and emitted colors were obtained (Figure 5-44). In this chapter, we have reported new templated multichromophoric architectures on two different types of peptidic scaffold: helical polypeptides and short oligopeptides through dynamic and non-dynamic bonds. When Y-Per, R-PDI and B-NDI units were assembled within helical triad **5-45,** Φ_{ET} (Y-Per→B-NDI) and (R-PDI→B-NDI) were determined to be 13.7 and 20% respectively in DMA. Extending this system to 4 and 5 chromophores appeared to be synthetically challenging due to the high hydrophobicity of the corresponding helical templates. Hence, helical tetrad **5-53** and pentad **5-61** were obtained as non-pure materials and overall ET efficiencies Φ_{ET} (Y-Py→B-NDI) and Φ_{ET} (Y-Py→B-Cy) were evaluated around 7 and 4% respectively. For the short peptide based multichromophoric systems, similar efficiencies as for **5-45** were obtained for triad **5-48** in DMA. Nevertheless, the good solubility of the triad in chlorinated solvents allows their notable improvement in CHCl$_3$ in the presence of lipids (EYPC; estimated to be 19.6 and 28.7%), possibly preventing aggregation phenomena. The introduction of

175

primary donor Y-Py within tetrad **5-56** significantly enhances the efficiencies up to 75% for (R-PDI→B-NDI) with an overall efficiency Φ_{ET} (Y-Py→B-NDI) determined around 60% in CHCl$_3$. For this structure, the presence of hygroscopic lipids does not improve the efficiencies, on the contrary; they tend to decrease due to the partial hydrolysis of the boronate ester. Finally, pentad **5-64** was assembled by incorporating a cyanine moiety as final acceptor through IEDDA tetrazine ligation. In this case, overall energy transfer efficiency Φ_{ET} (Y-Py→B-Cy) was estimated to be around 50%. Those systems capture efficiently the sunlight energy by absorbing over the whole visible spectrum, and transfer the absorbed photon from primary donor until final acceptor in a unidirectional pathway. Finally, they seem to promote a charge separated state via photoinduced electron transfer, possibly due to the presence of electron deficient R-PDI moiety. Taking advantage of the versatility of the synthetic approach, the properties of the materials can be easily tuned by changing any of the photoactive moiety/ies.
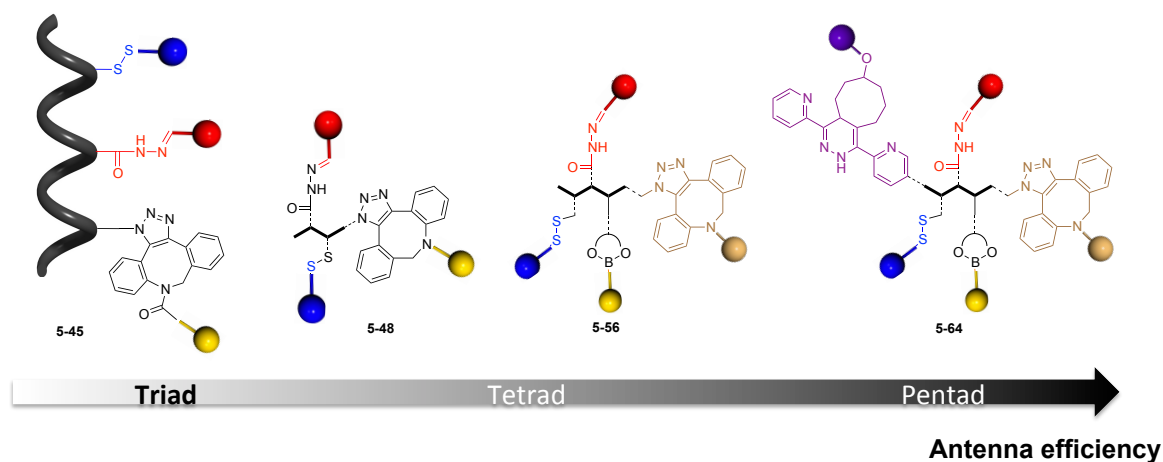
Figure 5-43 Major achievements of *Chapter 5*.

Table 5-10 Energy transfer efficiencies within peptide **5-45**, **5-48**, **5-56** and **5-64** estimated in [a]DMA, [b]CHCl$_3$ (80 equiv. of EYPC), [c]CHCl$_3$, by method 2 ($\Phi_{ET} = Ex_D/A_D$).

Entry	Φ_{ET} (donor → acceptor) %	**5-45**[a]	**5-48**[b]	**5-56**[c]	**5-64**[c]
1	Y-Per→B-NDI	13.7	19.6	15	<5
2	R-PDI→B-NDI	20	28.7	75	25
4	Y-Py→B-NDI	-	-	60	40
5	Y-Py→B-Cy	-	-	-	50
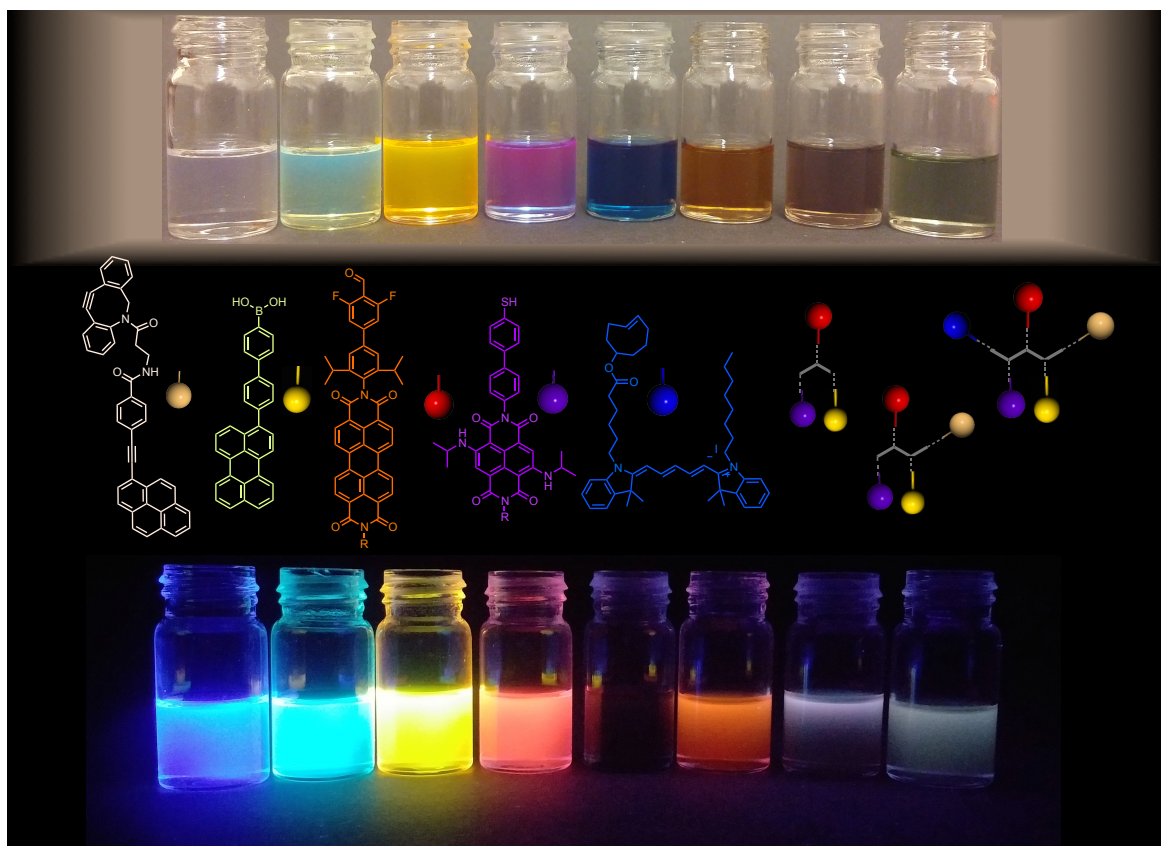
Figure 5-44 Pictures of solutions of (from left to right) free dyes Y-Py **5-2**, Y-Per **4-1**, R-PDI **4-2**, B-NDI **3-12**, B-Cy **5-3**, triad **5-48**, tetrad **5-56**, pentad **5-64** under visible (top), UV light (λ_{exc} = 254 nm) (bottom).

5.4 References

[1]   a) A. Kuzmin, A. Poloukhtine, M. A. Wolfert, V. V. Popik, *Bioconjugate Chem.* **2010**, *21*, 2076-2085; b) Z. Cheng, D. R. Elias, N. P. Kamat, E. D. Johnston, A. Poloukhtine, V. Popik, D. A. Hammer, A. Tsourkas, *Bioconjugate Chem.* **2011**, *22*, 2021-2029.

[2]   I. B. Berlman, *Handbook of fluorescence spectra of aromatic molecules*, Academic Press: New York, **1971**.

[3]   A. M. Brouwer, *Pure Appl. Chem.* **2011**, *83*, 2213-2228.

[4]   a) M. S. T. Goncalves, *Chem. Rev.* **2009**, *109*, 190-212; b) S. Luo, E. Zhang, Y. Su, T. Cheng, C. Shi, *Biomaterials* **2011**, *32*, 7127-7138; c) A. Samanta, M. Vendrell, R. Das, Y.-T. Chang, *Chem. Commun.* **2010**, *46*, 7406-7408.

[5]   a) P. K. Dutta, R. Varghese, J. Nangreave, S. Lin, H. Yan, Y. Liu, *J. Am. Chem. Soc.* **2011**, *133*, 11985-11993; b) A. Ruiz-Carretero, P. G. A. Janssen, A. L. Stevens, M. Surin,

L. M. Herz, A. P. H. J. Schenning, *Chem. Commun.* **2011**, *47*, 884-886; c) A. Wagh, F. Jyoti, S. Mallik, S. Qian, E. Leclerc, B. Law, *Small* **2013**, *9*, 2129-2139; d) W. Sun, S. Guo, C. Hu, J. Fan, X. Peng, *Chem. Rev.* **2016**, *116*, 7768-7817.

[6]   A. Mishra, R. K. Behera, P. K. Behera, B. K. Mishra, G. B. Behera, *Chem. Rev.* **2000**, *100*, 1973-2011.

[7]   D. S. Pisoni, L. Todeschini, A. C. A. Borges, C. L. Petzhold, F. S. Rodembusch, L. F. Campo, *J. Org. Chem.* **2014**, *79*, 5511-5520.

[8]   R. Sens, K. H. Drexhage, *J. Lumin.* **1981**, *24-25*, 709-712.

[9]   K. H. Drexhage, *J. Res. Natl. Bur. Stand., Sect. A* **1976**, *80A*, 421-428.

[10]   M. Fischer, J. Georges, *Chem. Phys. Lett.* **1996**, *260*, 115-118.

[11]   K. Suzuki, A. Kobayashi, S. Kaneko, K. Takehira, T. Yoshihara, H. Ishida, Y. Shiina, S. Oishi, S. Tobita, *Phys. Chem. Chem. Phys.* **2009**, *11*, 9850-9860.

[12]   D. Wang, Z. Jin, J. Tang, P. Liang, Y. Mi, Z. Miao, Y. Zhang, H. Yang, *Tetrahedron* **2012**, *68*, 6338-6342.

[13]   W. Tang, M. L. Becker, *Chem. Soc. Rev.* **2014**, *43*, 7013-7039.

[14]   H. Johansson, D. S. Pedersen, *Eur. J. Org. Chem.* **2012**, 4267-4281.

[15]   a) P. B. Alper, S. C. Hung, C. H. Wong, *Tetrahedron Lett.* **1996**, *37*, 6029-6032; b) A. K. Pandiakumar, S. P. Sarma, A. G. Samuelson, *Tetrahedron Lett.* **2014**, *55*, 2917-2920.

[16]   H. Katayama, H. Hojo, T. Ohira, Y. Nakahara, *Tetrahedron Lett.* **2008**, *49*, 5492-5494.

[17]   a) J. T. Lundquist Iv, J. C. Pelletier, *Org. Lett.* **2001**, *3*, 781-783; b) J. T. Lundquist Iv, J. C. Pelletier, *Org. Lett.* **2002**, *4*, 3219-3221.

[18]   a) B. L. Oliveira, Z. Guo, G. J. L. Bernardes, *Chem. Soc. Rev.* **2017**, *46*, 4895-4950; b) Z. M. Png, H. Zeng, Q. Ye, J. Xu, *Chem. Asian J.* **2017**, *12*, 2142-2159; c) A. C. Knall, C. Slugovc, *Chem. Soc. Rev.* **2013**, *42*, 5131-5142; d) S. Mayer, K. Lang, *Synthesis* **2017**, *49*, 830-848.

[19]   K. Lang, L. Davis, S. Wallace, M. Mahesh, D. J. Cox, M. L. Blackman, J. M. Fox, J. W. Chin, *J. Am. Chem. Soc.* **2012**, *134*, 10317-10320.

[20]   J. L. Seitchik, J. C. Peeler, M. T. Taylor, M. L. Blackman, T. W. Rhoads, R. B. Cooley, C. Refakis, J. M. Fox, R. A. Mehl, *J. Am. Chem. Soc.* **2012**, *134*, 2898-2901.

[21]   Z. Ni, L. Zhou, X. Li, J. Zhang, S. Dong, *PLoS ONE* **2015**, *10*.

[22]   M. L. Blackman, M. Royzen, J. M. Fox, *J. Am. Chem. Soc.* **2008**, *130*, 13518-13519.

[23]   R. Selvaraj, J. M. Fox, *Tetrahedron Lett.* **2014**, 4795-4797.

[24]   K. Lang, L. Davis, J. Torres-Kolbus, C. Chou, A. Deiters, J. W. Chin, *Nat. Chem.* **2012**, *4*, 298-304.

[25]   a) S. D. Jo, J. S. Kim, I. Kim, J. S. Yun, J. C. Park, B. I. Koo, E. Lee, Y. S. Nam, *Adv. Funct. Mater.* **2017**, *27*; b) S. Bhosale, A. L. Sisson, P. Talukdar, A. Fürstanberg, N. Banetji, E. Vauthey, G. Bollot, J. Mareda, C. Röger, F. Würthner, N. Sakai, S. Matile, *Science* **2006**, *313*, 84-86; c) J. C. Meillon, N. Voyer, *Angew. Chem. Int. Ed. Engl.* **1997**, *36*, 967-969.

[26]   S. H. Tung, H. Y. Lee, S. R. Raghavan, *J. Am. Chem. Soc.* **2008**, *130*, 8813-8817.

6. Experimental Part

6.1 General Remarks

6.1.1 Instrumentation

Thin layer chromatography (TLC) was conducted on pre-coated aluminum sheets with 0.20 mm *Machevery-Nagel* Alugram SIL G/UV254 with fluorescent indicator UV254. *Column chromatography* was carried out using *Merck Gerduran* silica gel 60 (particle size 63-200 μm). ***Microwave reactions*** were performed on a *Biotage AB Initiator microwave instrument* producing controlled irradiation at 2.450 GHz. ***Solid Phase Peptide Syntheses*** were carried out on a semi-automatic *FOCUS XC peptide synthesizer* from *aapptec* with a control system. ***HPLC*** analyses and purifications were performed on the following systems: Analytical and Preparative HPLC: *Varian 940-LC* liquid chromatography or *Agilent 1260 Infinity*. The analytical columns used were: *Agilent Zorbax SB-C$_8$* (5 μm, 4.6 × 150 mm), *Agilent Zorbax SB-C$_3$* (5 μm, 4.6 × 150 mm); the preparative columns: *Varian Pursuit XRs C18* (5 μm, 21.2 × 250 mm), *Agilent Zorbax PrepHT 300SB-C$_3$* (7 μm, 21.2 × 150 mm). ***Lyophilisation*** was performed on a *Christ Freeze Dryer ALPHA 2-4 LD$_{plus}$*, connected to a *Vaccumbrand Chemistry-HYBRID-pump*. The ice condenser was approx. -85 °C and the vacuum around 2.10^{-3} mbar. ***Circular Dichroism*** spectroscopic analysis were carried out with a Jasco Model J-810 using a quartz cell with a pathlength of 0.1 cm. ***UV-Vis absorptions*** were recorded on a *Varian Cary 5000 Bio* or *Agilent Cary 5000* UV-Vis spectrophotometer using quartz cell (pathlength of 1 cm). ***Fluorescence*** was measured on a *Cary Eclipse Fluoresence* Spectrophotometer using quartz cell (pathlength of 1 cm). Emission lifetime measurements were performed on a *JobinYvon-Horiba FluoroHub* single photon counting module, using Nano-LED pulsed sources at 372 nm. ***Cyclic voltammetry*** experiments were carried out at room temperature in nitrogen-purged dry DMF with a *Model 800 potentiostat* (CH Instruments). ***Melting points*** (M.p.) were measured on *i)* a *Büchi Melting Point* B-545 or on *ii)* a *Gallenkamp* apparatus in open capillary tubes. ***Nuclear magnetic resonance*** (NMR) ^{1}H, ^{13}C and ^{19}F spectra were obtained on a 270 MHz (*Jeol JNM EX-270*), 300 MHz (*Brüker*), 400 MHz (*Jeol JNM EX-400 or Brüker* AVANCE III HD), 500 MHz (*Jeol JNM EX-500 or Brüker)* or 600 MHz (*Brüker*) NMR at rt otherwise stated. Chemical shifts were reported in ppm according to tetramethylsilane using the solvent residual signal as an internal reference (CDCl$_3$: δ_H = 7.26 ppm, δ_C = 77.16 ppm; DMSO-d_6: δ_H = 2.50 ppm, δ_C = 39.52 ppm; methanol-d_4: δ_H = *3.31* ppm, δ_C = 49 ppm; acetone-d_6: δ_H = 2.05 ppm, δ_C = 29.84 ppm; DMF-d_7: δ_H = 8.03 ppm, δ_C = 163.15 ppm). Coupling constants

(*J*) were given in Hz. Resonance multiplicity was described as *s* (singlet), *d* (doublet), *t* (triplet), *dd* (doublet of doublets), *dt* (doublet of triplets), *td* (triplet of doublets), *q* (quartet), *m* (multiplet) and *br* (broad signal). Carbon spectra were acquired with a complete decoupling for the proton. ***Infrared spectra*** (IR) were recorded on a *i) Perkin-Elmer Spectrum II FT-IR System* with *Specac* Silver Gate Evolution single-reflection ATR mounted with a diamond mono-crystal or *ii)* on a *Shimadzu IR Affinity 1S FTIR* spectrometer in ATR mode with a diamond mono-crystal. ***Mass spectrometry*** were performed by *i)* the *Centre de spectrométrie de masse at the Université de Mons in Belgium*. ESI-MS measurements were performed on a *Waters QToF2 mass spectrometer* operating in positive mode. The analyte solutions were delivered to the ESI source by a *Harvard Apparatus* syringe pump at a flow rate of 5 μL/min. Typical ESI conditions were, capillary voltage 3.1 kV; cone voltage 20-50 V; source temperature 80 °C; desolvation temperature 120°C. Dry nitrogen was used as the ESI gas. For the recording of the single-stage ESI-MS spectra, the quadrupole (rf-only mode) was set to pass ions from 50 to 1000 Th, and all ions were transmitted into the pusher region of the time-of-flight analyzer where they were mass analyzed with 1 s integration time. MALDI-MS were recorded using a *Waters QToF Premier mass spectrometer* equipped with a nitrogen laser, operating at 337 nm with a maximum output of 500 mW delivered to the sample in 4 ns pulses at 20 Hz repeating rate. Time-of-flight analyses were performed in the reflectron mode at a resolution of about 10,000. The matrix solution (1 μL) was applied to a stainless steel target and air-dried. Analyte samples were dissolved in a suitable solvent to obtain 1 mg/mL solutions. 1 μL aliquots of those solutions were applied onto the target area already bearing the matrix crystals, and air-dried. For the recording of the single-stage MS spectra, the quadrupole (rf-only mode) was set to pass ions from 100 to 1000 Th, and all ions were transmitted into the pusher region of the time-of-flight analyzer where they were analyzed with 1 s integration time. *ii)* The "Fédération de Recherche" ICOA/CBM (FR2708) platform of Orléans in France. High-resolution ESI mass spectra (HRMS) were performed on a Bruker maXis Q-TOF in the positive ion mode. The analytes were dissolved in a suitable solvent at a concentration of 1 mg/mL and diluted 200 times in methanol ($\approx$ 5 ng/mL). The diluted solutions (1μL) were delivered to the ESI source by a Dionex Ultimate 3000 RSLC chain used in FIA (Flow Injection Analysis) mode at a flow rate of 200 μL/min with a mixture of $CH_3CN/H_2O+0.1\%$ of HCO_2H (65/35). ESI conditions were as follows: capillary voltage was set at 4.5 kV; dry nitrogen was used as nebulizing gas at 0.6 bars and as drying gas set at 200°C and 7.0 L/min. ESI-MS spectra were recorded at 1 Hz in the range of 50-3000 *m/z*. Calibration was performed with ESI-TOF Tuning mix from Agilent and corrected using lock masses at *m/z* 299.294457 (methyl stearate) and 1221.990638 (HP-1221). Data were processed using Bruker DataAnalysis 4.1 software. *iii)* MaSUN Platform, University of

Namur, Belgium. High-resolution ESI mass spectra (HRMS) were performed on a Bruker maXis impact Q-TOF in the positive ion mode. The analytes were dissolved in a suitable solvent at a concentration of 1 mg/mL and diluted 200 times in methanol ($\approx$ 5 ng/mL). The diluted solutions were delivered to the ESI source by a syringe pump (kdScientific) at a flow rate of 3 μL/min with a mixture of CH_3CN/H_2O with ou without 0.1% of HCO_2H (50/50). ESI conditions were as follows: capillary voltage was set at 4.5 kV; dry nitrogen was used as nebulizing gas at 0.3 bars and as drying gas set at 180°C and 6.0 L/min. ESI-MS spectra were recorded at 1 Hz in the range of 50-3000 *m/z*. Calibration was performed with ESI-TOF Tuning mix from Agilent and corrected using lock masses at *m/z* 1221.990638 (HP-1221). Data were processed using Bruker DataAnalysis 4.1 software. *iv) Cardiff University, United Kingdom.* High-resolution ESI mass spectra (HRMS) were performed on a *Waters LCT HR TOF* mass spectrometer in the positive or negative ion mode.

6.1.2. Materials and methods

Chemicals were purchased from *Sigma Aldrich*, *Acros Organics*, *TCI*, *ABCR*, *Apollo Scientific, Alfa Aesar* and *Fluorochem* and were used as received. Solvents were purchased from *Sigma Aldrich*, *Fluorochem* or *Fischer Scientific* while deuterated solvents from *Eurisotop* and *Sigma Aldrich*. Diethyl ether and THF were distilled from sodium-benzophenone-cetyl, toluene was refluxed over calcium hydride and dichloromethane (CH_2Cl_2) was refluxed over phosphorous pentoxide or were dried on a *Braun MB SPS-800* solvent purification system. Anhydrous DMF was purchased from *Acros Organics*. Hydrochloridic acid (HCl 32%) were purchased from *Fischer Scientific*. MeOH, $CHCl_3$ and acetone were purchased as reagent-grade and used without further purification. Anhydrous conditions were achieved by drying Schlenk tubes or 2-neck flasks by flaming with a heat gun under vacuum and then purging with Argon or Nitrogen. The inert atmosphere was maintained using Argon or Nitrogen-filled balloons equipped with a syringe and needle that was used to penetrate the silicon stoppers used to close the flasks' necks. Additions of liquid reagents were performed using dried plastic or glass syringes. After extraction and washing, the organic phase containing the target compound was dried using $MgSO_4$ as drying agent.

For the amino acids and peptide synthesis the three modified amino acids bearing the protected functionalities: diol, hydrazine and thiol were synthesized in the lab from Fmoc-Gly(Propargyl)-OH supplied by *Chem.Pep.* All other materials were obtained from commercial suppliers: HPLC grade acetonitrile (MeCN) and water, piperidine, ethanedithiol (EDT), trifluoroacetic acid (TFA), triisopropylsilane (TIS), N-methylpyrrolidone (NMP), dimethylformamide (DMF), glass wood, diisopropylethylamine (DIEA), *N*α-Fmoc amino acids, HATU from *Fisher Scientific*, *Sigma Aldrich, Carbosynth., Fluorochem, Acros or AGTC Bioproducts*, and Rink-amide MBHA resin

from *aapptec*.

6.2 Experimental Procedures

6.2.1 Experimental procedures for Chapter 2

6.2.1.1 Synthesis of disulfide pyridine 2-6

Scheme 6-1 Synthesis of pyridine disulfide **2-6**; a) TrtCl, THF, 50 °C, 4 h; b) MsCl, Et$_3$N, CH$_2$Cl$_2$, 0 °C to rt, 2 h; c) NaN$_3$, DMF, 70 °C, 3 h; d) TIPS acetylene, CuSO$_4$·5H$_2$O, Na ascorbate, DMF/H$_2$O (4:1), rt, 16 h; e) *i)* TFA, TIS, CH$_2$Cl$_2$, rt, 1 h, *ii)* 2,2'-dipyridyl disulfide, DIEA, CH$_2$Cl$_2$, rt, 2 h.

6.2.1.1.1 Synthesis of 2-(tritylthio)ethanol 2-9

2-(tritylthio)ethanol **2-9** has been synthesized according to the literature procedure.[1]

6.2.1.1.2 Synthesis of (2-azidoethyl)(trityl)sulfane 2-11

A solution of 2-(tritylthio)ethanol **2-9** (2.53 g, 7.89 mmol) and Et$_3$N (3.3 mL, 23.67 mmol) in dry CH$_2$Cl$_2$ (40 mL) was cooled down at 0 °C. This was followed by the dropwise addition of a solution of mesyl chloride (1.36 g, 11.8 mmol) in dry CH$_2$Cl$_2$ (20 mL). The reaction mixture was stirred at 0 °C for 30 min and at rt for 2 h. Upon completion, the reaction was quentched with H$_2$O (10 mL) and the layers were separated. The aqueous phase was extracted with CH$_2$Cl$_2$. The combined organic layers were washed with a sat. aq. solution of NH$_4$Cl and brine, dried and

concentrated under reduced pressure to give **2-10** as an orange oil.

The crude material was dissolved in dry DMF (50 mL) and NaN_3 (1.02 g, 15.78 mmol) was added. The reaction mixture was stirred at 70 °C for 3 h. H_2O (20 mL) was added and the aqueous phase was extracted with Et_2O. Organic phase was washed with brine, dried and concentrated under reduced pressure. The crude material was precipitated in MeOH to give **2-11** as a white solid (1.72 g, 85%). M.p.: 91 °C; IR (film): ν (cm⁻¹) 3054, 2173, 2102 (-N_3), 1739, 1592, 1476, 1444, 1427, 1283, 1252, 1083, 1030, 920, 769, 744, 708, 697, 677, 629, 618, 510, 468; ¹H NMR (400 MHz, $CDCl_3$) δ_H 7.45-7.42 (*m*, 6H), 7.32-7.21 (*m*, 9H), 2.92 (*t*, *J* = 7.2 Hz, 2H), 2.44 (*t*, *J* = 7.2 Hz, 2H); ¹³C NMR (100 MHz, $CDCl_3$) δ_C 144.60, 129.67, 128.15, 126.97, 67.21, 50.33, 31.32; ESI-HRMS [M + Na]⁺ calcd for $[C_{21}H_{19}N_3NaS]^+$: 368.1192, found: 368.1193.

6.2.1.1.3 Synthesis of 4-(triisopropylsilyl)-1-(2-(tritylthio)ethyl)-1H-1,2,3-triazole 2-7

2-7
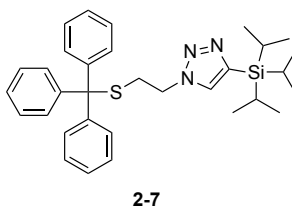
To a solution of azide **2-11** (1.03 g, 2.98 mmol) in DMF (16 mL), TIPS acetylene (1 mL, 4.47 mmol) was added, followed by the successive addition of a solution of $CuSO_4.5H_2O$ (223 mg, 0.89 mmol) in H_2O (2 mL) and a solution of sodium ascorbate (118 mg, 0.6 mmol) in H_2O (2 mL). The reaction mixture was stirred at rt for 16 h. A sat. aq. solution of Na_4EDTA was added and the aqueous phase was extracted with Et_2O. The combined organic layers were washed with brine, dried and concentrated under reduced pressure. The crude material was precipitated in pentane to give **2-7** as a white solid (1.4 g, 90%). M.p.: 106 °C; IR (film): ν (cm⁻¹) 2933, 2861, 1593, 1485, 1444, 1189, 1045, 881, 806, 755, 743, 697; ¹H NMR (400 MHz, $CDCl_3$) δ_H 7.38-7.35 (*m*, 6H), 7.28-7.18 (*m*, 10H), 3.95 (*t*, *J* = 7.2 Hz, 2H), 2.71 (*t*, *J* = 7.2 Hz, 2H), 1.34-1.27 (*m*, 3H), 1.05 (*d*, *J* = 7.6 Hz, 18H); ¹³C NMR (100 MHz, $CDCl_3$) δ_C 144.46, 141.64, 130.78, 129.66, 128.22, 127.05, 67.42, 48.57, 32.31, 18.70, 11.22; ESI-HRMS calcd for $[C_{32}H_{41}N_3SSi]^+$: 528.2858; found: 528.2863.

6.2.1.1.4 Synthesis of 2-((2-(4-(triisopropylsilyl)-1H-1,2,3-triazol-1-yl)ethyl)disulfanyl)-pyridine 2-6

2-6
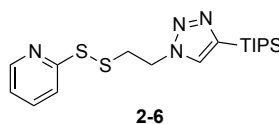
A solution of triazole **2-7** (930 mg, 1.76 mmol) in CH_2Cl_2 (10 mL) was cooled down at 0 °C. TFA

(1.36 mmol, 17.6 mmol) was added, followed by TIS (1.09 mL, 5.28 mmol). The reaction mixture was stirred at rt for 1 h. The solvent was evaporated, and the TFA was co-evaporated with toluene. The resulting crude mixture was dissolved in CH_2Cl_2 (20 mL). Then, 2,2'-dipyridyl disulfide (581 mg, 2.64 mmol) was added followed by DIEA (1.5 mL, 8.8 mmol). The reaction mixture was stirred at rt for 2 h. The solvent was evaporated under reduced pressure and the crude material was purified through silica gel column chromatography (Eluent: cyclohexane/CH_2Cl_2/EtOAc 4:2:1) to give **2-6** as a colorless oil (694 mg, 75%). IR (film): ν (cm^{-1}) 2941, 2889, 2863, 1573, 1561, 1445, 1417, 1114, 1045, 882, 759, 675, 659; ^{1}H NMR (400 MHz, CDCl$_3$) δ_H 8.46-8.44 (*m*, 1H), 7.67 (*s*, 1H), 7.64-7.57 (*m*, 2H), 7.11-7.09 (*m*, 1H), 4.72 (*t*, *J* = 6.8 Hz, 2H), 3.27 (*t*, *J* = 6.8 Hz, 2H), 1.38-1.28 (*m*, 3H), 1.07 (*d*, *J* = 7.2 Hz, 18H); ^{13}C NMR (100 MHz, CDCl$_3$) δ_C 159.00, 150.03, 141.94, 137.31, 131.18, 121.41, 120.53, 48.27, 38.51, 18.72, 11.25; ESI-HRMS calcd for [C$_{18}$H$_{31}$N$_4$S$_2$Si]$^+$: 395.1754; found: 395.1752.

6.2.1.2 Synthesis of diol 2-16
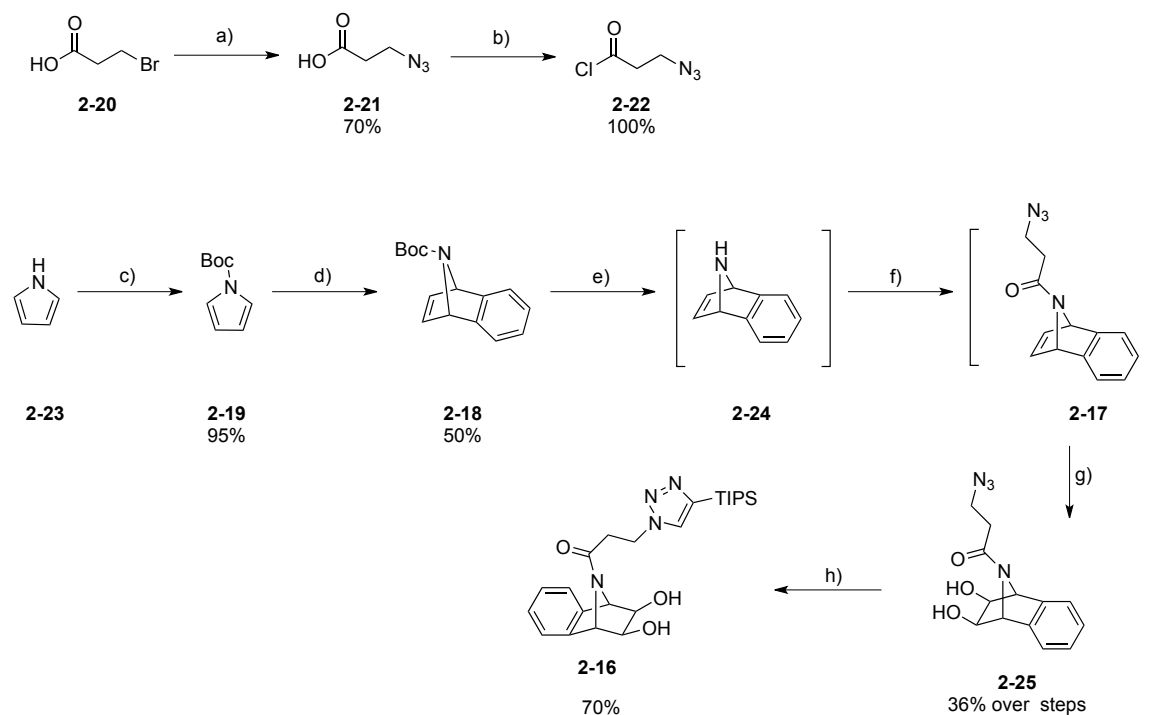
Scheme 6-2 Synthesis of diol **2-16**; a) NaN$_3$, CH$_3$CN, 85 $^{\circ}$C, 4 h; b) (COCl)$_2$, DMF, CH$_2$Cl$_2$, 0 $^{\circ}$C to rt, 20 h; c) Boc$_2$O, DMAP, CH$_3$CN, rt, 4 h; d) anthranilic acid, isoamyl nitrite, DME, 50 $^{\circ}$C, 30 min; e) AcCl, MeOH, 0 $^{\circ}$C to rt, 2 h; f) **2-22**, Et$_3$N, CH$_2$Cl$_2$, rt, 2 h; g) OsO$_4$ (4 mol%), NMO, acetone/H$_2$O (9:1), rt 16 h; (h) TIPS acetylene, CuSO$_4$ 5H$_2$O, Na ascorbate, DMF/H$_2$O (4:1), rt, 16 h.

### 6.2.1.2.1 Synthesis of 3-azidopropanoic acid 2-21

2-21
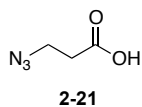
3-azidopropanoic acid **2-21** has been synthesized according to the literature procedure.[2]

6.2.1.2.2 Synthesis of 3-azidopropanoyl chloride 2-22

2-22
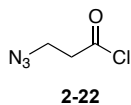
To a solution of 3-azidopropanoic acid **2-21** (500 mg, 4.34 mmol) in dry CH_2Cl_2 (6 mL), a drop of DMF was added to catalyze the reaction. This was followed by the addition of $(COCl)_2$ (0.41 mL, 4.77 mmol) at 0 °C. The reaction mixture was stirred at rt for 16 h. The volatiles were removed under reduced pressure to give **2-22** as a yellow liquid (580 mg, 100%) directly used for the next step without any further purification.

### 6.2.1.2.3 Synthesis of N-Boc-pyrrole 2-19

2-19
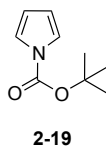
N-Boc-pyrrole **2-19** has been synthesized according to the literature procedure.[3]

6.2.1.2.4 Synthesis of 1,4-Dihydro-1,4-epiazano-naphthalene-9-carboxylic acid tert-butyl ester 2-18

2-18
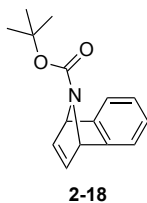
1,4-Dihydro-1,4-epiazano-naphthalene-9-carboxylic acid tert-butyl ester **2-18** has been synthesized according to the literature procedure.[4]

6.2.1.2.5 Synthesis of 3-azido-1-((1R, 2R,3S,4S)-2,3-dihydroxy-1,2,3,4-tetrahydro-1,4-epiminonaphthalen-9-yl)propan-1-one 2-25
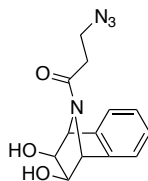
2-25

To 5 mL of absolute MeOH cooled at 0 °C, AcCl (350 μL, 4.9 mmol) was added dropwise under an argon atmosphere. The resulting solution was stirred for 5 min at 0 °C and **2-18** (200 mg, 0.82 mmol) was added. The solution was allowed to reach rt and was stirred for 2 h. H_2O (20 mL) was added and the mixture was washed with Et_2O (2 times). The aqueous phase was adjusted to pH = 10 using a 10% w/v aq. solution of K_2CO_3 and extracted with Et_2O (3 times). The final washing organic layers were combined, dried and concentrated under reduced pressure (> 400 mbar) to give **2-24** as a brown oil (117 mg.). (**2-24** was not stable enough to be purified and fully characterized). ^{1}H NMR (400 MHz, $CDCl_3$) δ_H 7.26-7.24 (*m*, 2H), 6.99-6.44 (*m*, 4H), 5.01 (*br s*, 2H), 3.97 (*br s*, 1H).

To a solution of crude **2-24** in dry CH_2Cl_2 (7 mL), Et_3N (125 μL, 0.98 mmol) was added followed by the dropwise addition of a solution of **2-22** (120 mg, 0.9 mmol) in dry CH_2Cl_2 (4 mL). The resulting solution was stirred under argon for 2 h at rt. A aq. solution of $NaHCO_3$ (0.2 M) was added and the aqueous phase was extracted with CH_2Cl_2. The organic phase was washed with brine, dried, concentrated under reduced pressure to give **2-17** as a brown oil which was directly dissolved in acetone for the following step. (**2-17** was not stable enough to be purified and fully characterized). ^{1}H NMR (400 MHz, $CDCl_3$) δ_H 7.32-7.25 (*m*, 2H), 7.09-6.94 (*m*, 4H), 5.92 (*s*, 1H), 5.56 (*s*, 1H), 3.55 (*m*, 2H), 2.48 (*m*, 2H).

To a solution of crude **2-17** (197 mg, 0.82 mmol) in a mixture of acetone/H_2O (9:1) (20 mL) were added N-methylmorpholine N-oxide (NMO; 144 mg, 1.23 mmol) and OsO_4 (8.3 mg, 0.03 mmol) in H_2O (0.5 mL). The reaction mixture was stirred at rt for 18 h. Then, a sat. aq. solution of $Na_2S_2O_5$ (10 mL) was added and the aq. phase was extracted with $CHCl_3$. The combined organic layers were dried and concentrated under reduced pressure to give a greenish oil. The crude material was purified through silica gel column chromatography (Eluent: CH_2Cl_2/MeOH 96:4) to give **2-25** as a beige solid. (81 mg, 36% over 3 steps). M.p.: 143-145 ° C; IR (film): ν (cm^{-1}) 3240, 2925, 2097, 1735, 1619, 1587, 1462, 1299, 1253, 1156, 1074, 1012, 982, 748, 585; ^{1}H NMR (400 MHz, DMSO-d_6) δ_H 7.39-7.34 (*m*, 2H), 7.20-7.17 (*m*, 2H), 5.22 (*d*, *J* = 5.6 Hz, -OH), 5.20 (*d*, *J* = 5.6 Hz, -OH), 5.18 (*s*, 1H), 5.14 (*s*, 1H), 3.70 (*t*, *J* = 5.6 Hz, 1H), 3.65 (*t*, *J* = 5.6 Hz, 1H), 3.47 (*t*, *J* = 6.4 Hz, 2H), 2.67-2.60 (*m*, 1H), 2.57-2.50 (*m*, 1H); ^{13}C NMR (100 MHz, DMSO-d_6) δ_C 167.27, 142.40, 141.98, 127.16, 127.07, 121.08, 121.03, 69.77, 69.42, 66.65, 64.28, 46.44, 32.77; ESI-HRMS [M + H]$^+$ calcd for $[C_{13}H_{15}N_4O_3]^+$: 275.1139, found: 275.1142.

6.2.1.2.6 Synthesis of 1-((1R,2R,3S,4S)-2,3-dihydroxy-1,2,3,4-tetrahydro-1,4-epiminonaph-thalen-9-yl)-3-(4-(triisopropylsilyl)-1H-1,2,3-triazol-1-yl)propan-1-one 2-16
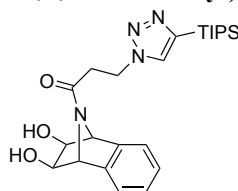

2-16

To a solution of azide **2-25** (204 mg, 0.74 mmol) in DMF (4 mL), TIPS acetylene (0.25 mL, 1.11 mmol) was added, followed by a successive addition of a solution of CuSO$_4$.5H$_2$O (55 mg, 0.22 mmol) in H$_2$O (0.5 mL) and a solution of sodium ascorbate (29 mg, 0.15 mmol) in H$_2$O (0.5 mL). The reaction mixture was stirred at rt for 16 h. A sat. aq. solution of Na$_4$EDTA was added and the aqueous phase was extracted with Et$_2$O (3 times). The combined organic layers were washed with brine, dried and concentrated under reduced pressure. The crude residue was purified through silica gel column chromatography (Eluent: CH$_2$Cl$_2$/MeOH 95:5) to give **2-16** as a colorless oil (236 mg, 70%). IR (film): ν (cm^{-1}) 3384, 2946, 2868, 1675, 1633, 1204, 1180, 1131, 801, 723; ^{1}H NMR (400 MHz, CDCl$_3$) δ_H 7.68 (*s*, 1H), 7.34-7.16 (*m*, 4H), 5.48 (*s*, 1H), 5.11 (*s*, 1H), 4.85-4.78 (*m*, 1H), 4.74-4.67 (*m*, 1H), 3.92-3.89 (*m*, 2H), 3.31-3.23 (*m*, 1H), 2.99-2.92 (*m*, 1H), 1.34-1.24 (*m*, 3H), 1.05 (*d*, *J* = 7.2 Hz, 18H); ^{13}C NMR (100 MHz, CDCl$_3$) δ_C 167.95, 141.79, 141.06, 140.55, 131.60, 128.02, 127.79, 121.44, 121.11, 70.84, 70.51, 67.68, 65.01, 45.49, 34.48, 18.65, 11.12; ESI-HRMS [M+H]$^+$ calcd for [C$_{24}$H$_{37}$N$_4$O$_3$Si]$^+$: 457.2629, found: 457.2627.

6.2.1.3 Synthesis of hydrazide 2-29
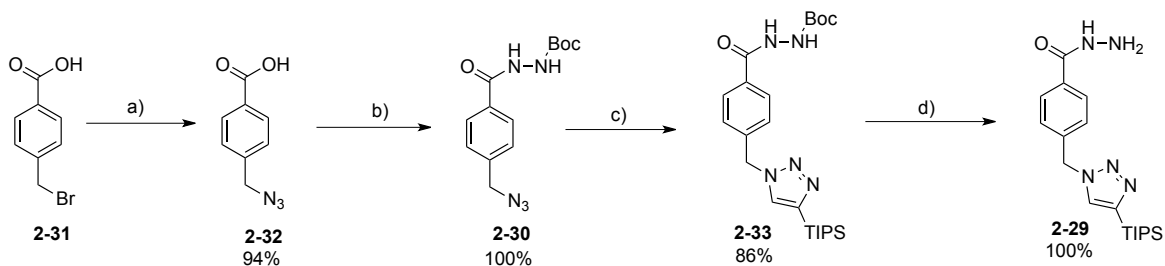
Scheme 6-3 Synthesis of hydrazide **2-29**; a) NaN$_3$, DMF, 50 °C, 15 h; b) BocNHNH$_2$, EDC.HCl, CH$_2$Cl$_2$, rt, 16 h; c) TIPS acetylene, CuSO$_4$·5H$_2$O, Na ascorbate, DMF/H$_2$O (4:1), rt, 16 h; d) TFA/CH$_2$Cl$_2$ (1:4), rt, 1 h.

6.2.1.3.1 Synthesis of 4-(azidomethyl)benzoic acid 2-32
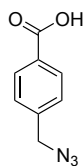

2-32

4-(azidomethyl)benzoic acid **2-32** has been synthesized according to the literature procedure.[5]

6.2.1.3.2 Synthesis of tert-butyl 2-(4-(azidomethyl)benzoyl)hydrazinecarboxylate 2-30

2-30
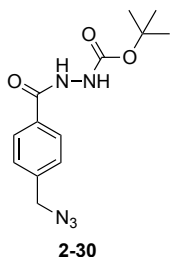
To a solution of 4-(azidomethyl)benzoic acid **2-32** (844 mg, 4.76 mmol) in CH_2Cl_2 (48 mL), $BocNHNH_2$ (661 mg, 5 mmol) was added followed by EDC.HCl (1 g, 5.24 mmol). The reaction mixture was stirred at rt for 16 h. Upon completion of the reaction, CH_2Cl_2 (50 mL) was added and the mixture was washed with a sat. aq. solution of $NaHCO_3$ (3 × 20 mL) and brine. The organic phase was dried and concentrated under reduced pressure to give **2-30** as a white solid (1.39 g, quant.). M.p.: 156 °C; IR (film): ν (cm^{-1}) 3319, 2979, 2090, 1738, 1724, 1649, 1246, 1150, 856, 755, 578, 549, 533, 454; ^{1}H NMR (400 MHz, CDCl$_3$) δ_H 8.35 (*br s*, -NH), 7.82 (*d*, *J* = 8 Hz, 2H), 7.36 (*d*, *J* = 8 Hz, 2H), 6.81 (*br s*, 1H, -NH), 4.39 (*s*, 2H), 1.49 (*s*, 9H); ^{13}C NMR (100 MHz, CDCl$_3$) δ_C 166.43, 156.03, 139.83, 131.71, 128.30, 128.01, 82.28, 54.31, 28.27; ESI-HRMS [M+H]$^+$ calcd for [C$_{13}$H$_{18}$N$_5$O$_3$]$^+$: 292.1404; found: 292.1402.

6.2.1.3.3 Synthesis of tert-butyl 2-(4-((4-(triisopropylsilyl)-1H-1,2,3-triazol-1-yl)methyl) benzoyl) hydrazinecarboxylate 2-33

2-33
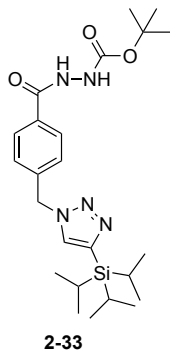
To a solution of azide **2-30** (467 mg, 1.6 mmol) in DMF (8 mL), TIPS acetylene (0.54 mL, 2.4 mmol) was added, followed by the successive addition of a solution of CuSO$_4$.5H$_2$O (120 mg, 0.48 mmol) in H$_2$O (1 mL) and a solution of sodium ascorbate (64 mg, 0.32 mmol) in H$_2$O (1 mL). The reaction mixture was stirred at rt for 16 h. A sat. aq. solution of Na$_4$EDTA was added and the aqueous phase was extracted with CH$_2$Cl$_2$ (3 times). The combined organic layers were washed with brine, dried and concentrated under reduced pressure. The crude residue was precipitated in a

mixture Et$_2$O/pentane (1:1) to give **2-33** as a white solid (756 mg, 86%). M.p.: 180 °C; IR (film): ν (cm^{-1}) 3248, 2943, 2866, 1748, 1657, 1497, 1463, 1367, 1267, 1248, 1046, 1018, 909, 883, 730, 676; ^{1}H NMR (400 MHz, CDCl$_3$) δ_H 8.31 (*br s*, -NH), 7.78 (*d, J* = 8 Hz, 2H), 7.50 (*s*, 1H), 7.21 (*d, J* = 8 Hz, 2H), 6.77 (*br s* , -NH), 5.62 (*s*, 2H), 1.48 (*s*, 9H), 1.40-1.29 (*m*, 3H), 1.07 (*d, J* = 7.6 Hz, 18H); ^{13}C NMR (125 MHz, CDCl$_3$) δ_C 166.31, 155.71, 139.60, 132.24, 130.57, 128.22, 127.98, 82.31, 53.07, 28.28, 18.70, 11.22 (one C_q missing); ESI-HRMS [M+H]$^+$ calcd for [C$_{24}$H$_{40}$N$_5$O$_3$Si]$^+$: 474.2895; found: 474.2892.

6.2.1.3.4 Synthesis of 4-((4-(triisopropylsilyl)-1H-1,2,3-triazol-1-yl)methyl)benzohydrazide 2-29
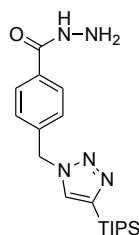

2-29

To a solution of triazole **2-33** (167 mg, 0.35 mmol) in CH$_2$Cl$_2$ (3 mL) cooled at 0 °C, TFA (0.3 mL) was added. The reaction mixture was stirred at 0 °C for 30 min and at rt for an additional hour. A sat. solution of K$_2$CO$_3$ was added and the aqueous phase was extracted with CH$_2$Cl$_2$. The combined organic layers were washed with brine, dried and concentrated under reduced pressure affording **2-29** as a colorless oil which was not purified (131 mg, quant.). IR (film): ν (cm^{-1}) 2946, 2868, 1673, 1366, 1200, 1142, 883, 799, 724, 680, 520; ^{1}H NMR (400 MHz, DMSO-*d$_6$*) δ_H 11.89 (*s*, 1H, -NH), 10.82 (*br s*, 1H, -NH), 8.39 (*s*, 1H), 7.95 (*d, J* = 8 Hz, 2H), 7.36 (*d, J* = 8 Hz, 2H), 5.76 (*s*, 2H), 1.34-1.24 (*m*, 3H), 1.04 (*d, J* = 7.2 Hz, 18H); ^{13}C NMR (100 MHz, DMSO-*d$_6$*) δ_C 165.41, 141.17, 140.17, 132.41, 130.02, 128.34, 127.82, 51.87, 18.49, 10.59; ESI-HRMS [M+H]$^+$ calcd for [C$_{19}$H$_{32}$N$_5$OSi]$^+$: 374.2370; found: 374.2371.

6.2.1.4 Synthesis of Aza-dibenzocyclooctyne 2-40

The following synthesis was performed according to the literature.[6]
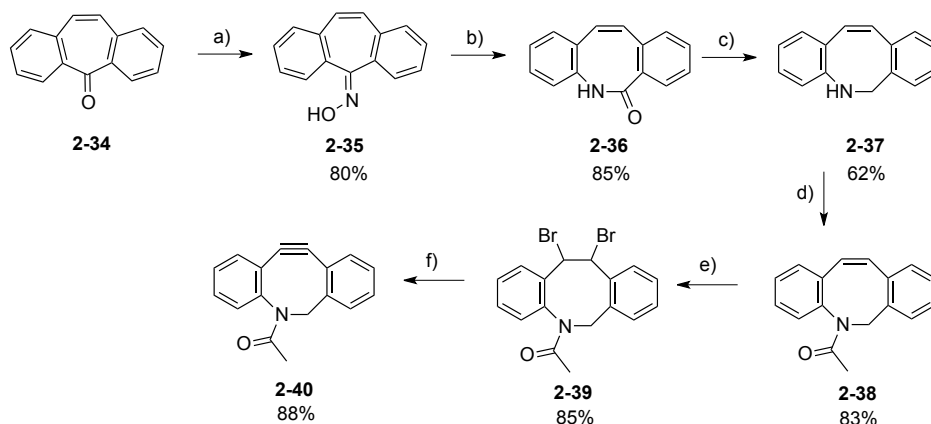
Scheme 6-4 Synthesis of ADIBO **2-40**; a) hydroxylamine.HCl, pyridine, 120 °C, 20 h; b) polyphosphoric acid, 125 °C, 1 h; c) LiAlH₄, Et₂O, 40 °C, 18 h; d) AcCl, pyridine, CH₂Cl₂, rt, 1 h; e) pyridinium tribromide, CH₂Cl₂, rt, 18 h; f) tBuOK, THF, rt, 1 h.

### 6.2.1.5.1 Synthesis of (*Z*)-5,6-dihydrodibenzo[*b,f*]azocine 2-37
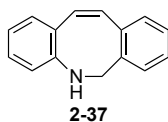
5,6-dihydrodibenzoazocine **2-37** has been synthesized according to the literature procedure.[6]

6.2.1.5.2 Synthesis of (*Z*)-1-(dibenzo[*b,f*]azocin-5(6*H*)-yl)ethanone 2-38
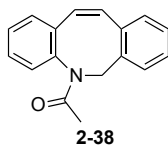
To a solution of 5,6-dihydrodibenzoazocine **2-37** (750 mg, 3.61 mmol) in CH₂Cl₂ (10 mL) were added pyridine (874 μL, 10.83 mmol) and acetyl chloride (336 μL, 4.7 mmol). The reaction mixture was stirred at rt for 1 h, diluted in CH₂Cl₂ and water. The layers were separated and the organic phase was washed with brine, dried and concentrated under reduced pressure. The crude material was purified through silica gel column chromatography (Eluent: hexane/EtOAc 1:1) to give **2-38** as a colorless oil (747 mg, 83%). IR (film): ν (cm⁻¹) 3231, 3063, 1655, 1489, 1412, 1330, 989, 921, 879, 769, 750, 648, 442; ¹H NMR (300 MHz, CDCl₃) δ_H 7.19-7.05 (*m*, 8H), 6.73 (*d*, *J* = 12 Hz, 1H), 6.53 (*d*, *J* = 12 Hz, 1H), 5.44 (*d*, *J* = 15 Hz, 1H), 4.12 (*d*, *J* = 15 Hz, 1H), 1.97 (*s*, 3H); ¹³C NMR (75 MHz, CDCl₃) δ_C 170.37, 141.44, 136.34, 136.03, 134.70, 132.79, 131.83, 130.95, 130.33, 128.52, 128.12, 127.98, 127.47, 127.39, 127.08, 54.29, 22.98; EI-HRMS calcd for [C₁₇H₁₅NO]⁺: 249.1154; found: 249.1156.

### 6.2.1.5.3 Synthesis of 1-(11,12-dibromo-11,12-dihydrodibenzo[*b,f*]azocin-5(6*H*)-yl)ethanone 2-39

2-39
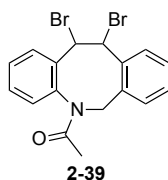
To a solution of cyclooctene **2-38** (730 mg, 2.93 mmol) in CH_2Cl_2 (4 mL) was added pyridinium tribromide (1.03 g, 3.22 mmol) at rt. The reaction mixture was stirred at rt for 18 h, diluted in CH_2Cl_2 and water. The layers were separated and the organic phase was washed with brine, dried and concentrated. The residue was passed through a short pad of silica (CH_2Cl_2) to give dibromo derivative **2-39** as a yellow solid (1.2 g, quant.). IR (film): ν (cm^{-1}) 1655, 1495, 1375, 1340, 1294, 760, 725, 661, 586; ^{1}H NMR (300 MHz, $CDCl_3$) δ_H 7.67 (*d, J* = 7.6 Hz, 1H), 7.20-6.91 (*m*, 6H), 6.82 (*d, J* = 7.6 Hz, 1H), 5.88 (*d, J* = 9.9 Hz, 1H), 5.73 (*d, J* = 14.7 Hz, 1H), 5.10 (*d, J* = 9.9 Hz, 1H), 4.10 (*d, J* = 14.7 Hz, 1H), 1.97 (*s*, 3H); ^{13}C NMR (75 MHz, $CDCl_3$) δ_C 171.20, 138.31, 137.83, 137.20, 133.04, 130.76, 130.62, 130.60, 129.71, 129.50, 129.06, 129.00, 128.73, 60.04, 55.71, 52.59, 24.19; EI-HRMS calcd for $[C_{17}H_{15}NOBr_2]^+$: 406.9520; found: 406.9503.

### 6.2.1.5.4 Synthesis of Acetyl-aza-dibenzocyclooctyne 2-40

2-40

To a suspension of tBuOK (684 mg, 6.1 mmol) in THF (10 mL) was added a solution of di-bromo derivative **2-39** (1 g, 2.44 mmol) in THF (5 mL). The reaction mixture was stirred at rt for 1 h, diluted in EtOAc, washed with an aqueous solution of HCl 5% and brine, dried, and concentrated. The crude material was purified through a plug of silica gel chromatography (Eluent: hexane/EtOAc 1:1) to give cyclooctyne **2-40** as a yellow solid (531 mg, 88%). M.p.: 115-117 °C; IR (film): ν (cm^{-1}) 3059, 2926, 1654, 1479, 1382, 1294, 1263, 752, 727, 571, 516; ^{1}H NMR (300 MHz, $CDCl_3$) δ_H 7.55 (*d, J* = 7.2 Hz, 1H), 7.24-7.10 (*m*, 7H), 5.00 (*d, J* = 15 Hz, 1H), 3.51 (*d, J* = 15 Hz, 1H), 1.97 (*s*, 3H); ^{13}C NMR (75 MHz, $CDCl_3$) δ_C 170.83, 152.39, 148.08, 132.51, 129.05, 128.42, 128.35, 128.02, 127.90, 127.17, 125.28, 123.41, 122.40, 115.08, 108.01, 55.23, 23.36; EI-HRMS calcd for $[C_{17}H_{13}NO]^+$: 247.0997; found: 247.0996.

6.2.1.5 Synthesis of *trans*-cyclooctene derivatives
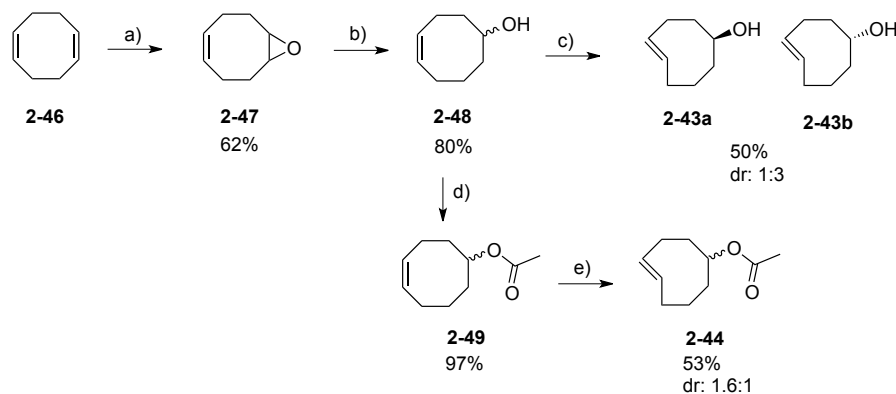
Scheme 6-5 Synthesis of *trans*-cyclooctene **2-43** and **2-44**; a) *m*-CPBA, CHCl$_3$, 0 °C to rt, 12 h; b) LiAlH$_4$, THF, 0 °C to 70 °C, 4 h; c) methyl benzoate, *hv* 254 nm, Et$_2$O/hexane (9:1), AgNO$_3$/SiO$_2$, 10 × 30 min; d) acetic anhydride, pyridine, CH$_2$Cl$_2$, 20 h, 40 °C, e) methyl benzoate, *hv* 254 nm, Et$_2$O/hexane (1:9), AgNO$_3$/SiO$_2$, 10 × 30 min.

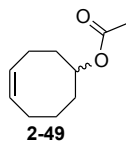## 6.2.1.5.1 Synthesis of *cis*-cyclooctenol 2-48
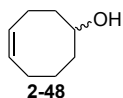
Cis-cyclooctenol **2-48** has been synthesized according to the literature.[7] ^{1}H NMR (300 MHz, CDCl$_3$) δ_H 5.77-5.50 (*m*, 2H), 3.85-3.77 (*m*, 1H), 2.35-2.23 (*m*, 1H), 2.18-2.09 (*m*, 3H), 1.99-1.80 (*m*, 2H), 1.77-1.46 (*m*, 4H); ^{13}C NMR (75 MHz, CDCl$_3$) δ_C 130.28, 129.71, 72.90, 37.87, 36.41, 25.78, 25.00, 22.89.

6.2.1.5.2 Synthesis of *trans*-cyclooctenol 2-43
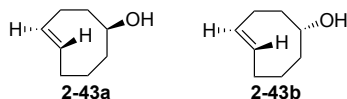
Trans-cyclooctenol **2-43** has been synthesized according to the literature (250 mg, 50% **2-43a**/ **2-43b** dr: 1:3) and the two diastereoisomers were separated through silica gel chromatography (Eluent: EtOAc/hexane 1:4).[8]

Trans-cyclooctenol **2-43 a** (minor one, 50 mg) ^{1}H NMR (300 MHz, CDCl$_3$) δ_H 5.61-5.48 (*m*, 2H), 4.01 (*dd*, *J* = 10.2 and 5.2 Hz, 1H), 2.42-2.29 (*m*, 1H), 2.24-2.13 (*m*, 2H), 2.12-2.03 (*m*, 2H), 1.90-1.72 (*m*, 3H), 1.68-1.47 (*m*, 1H), 1.29-1.20 (*m*, 1H); ^{13}C NMR (75 MHz, CDCl$_3$) 135.19, 132.90, 77.85, 44.68, 41.15, 34.43, 32.75, 31.33. *Trans*-cyclooctenol **2-43 b** (major one, 200 mg) ^{1}H NMR (300 MHz, CDCl$_3$) δ_H 5.57-5.51 (*m*, 1H), 5.38-5.32 (*m*, 1H), 3.43-3.39 (*m*, 1H), 2.33-2.21 (*m*, 3H), 1.94-1.86 (*m*, 4H), 1.65-1.52 (*m*, 3H).

6.2.1.5.3 Synthesis of cyclooctene 2-49

2-49

Cis-cyclooctene **2-49** has been synthesized according to the literature.[9] IR (film): ν (cm^{-1}) 2934, 2858, 1726 (ester), 1364, 1244, 1237, 1032, 1020, 727; ^{1}H NMR (300 MHz, CDCl$_3$) δ_H 5.73-5.57 (*m,* 2H), 4.85-4.77 (*m,* 1H), 2.39-2.26 (*m,* 1H), 2.19-2.04 (*m,* 3H), 2.00 (*s*, 3H), 1.93-1.78 (*m*, 2H), 1.74-1.66 (*m*, 1H), 1.63-1.53 (*m*, 3H).

6.2.1.5.4 Synthesis of *trans*-cyclooctene 2-44

2-44
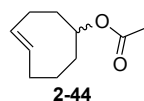
Cyclooctene **2-49** (540 mg, 4.28 mmol) and methyl benzoate (582 mg, 4.28 mmol) were added to 200 mL of solvent (Et$_2$O/hexane 1:9) in a 500 mL quartz reaction vessel. The vessel was irradiated with 254 nm light in a UV reactor. At 30 min intervals, the irradiation was stopped and the entire solution was passed through a column packed with silver nitrate (10%) impregnated silica. The solution was then transferred back into the quartz flask and the irradiation was continued. After 10 cycles, the irradiation was stopped and the silica was added to a solution of ammonium hydroxide and stirred for 5 min. Then, CH$_2$Cl$_2$ was added and the stirring was continued for another 5 min. The mixture was filtered and the organic phase was separated out, washed with brine, concentrated to give **2-44** (colorless oil, 380 mg, 53%) as a mixture of diastereoisomers (ratio 0.6:1 determined by ^{1}H NMR). As a mixture of diastereoisomers was obtained, the characterization was given as information only: IR (film): ν (cm^{-1}) 2932, 2858, 1728, 1442, 1375, 1236, 1217, 1116, 989, 952; ^{1}H NMR (300 MHz, CDCl$_3$) δ_H 5.61-5.48 (*m*, 3.2H), 4.98 (*dd, J* = 10.2, 5.2 Hz, 0.6H), 4.45-4.38 (*m*, 1H), 2.42-2.21 (*m*, 5.6H), 2.12-2.03 (*m*, 0.6H), 2.10 (*s*, 1.8H), 1.98 (*s*, 3H), 1.99-1.72 (*m*, 9.8H); ^{13}C NMR (75 MHz, CDCl$_3$) δ_C 170.54, 170.46, 135.42, 135.03, 133.18, 131.82, 80.18, 70.10, 40.99, 40.84, 38.71, 34.37, 32.63, 32.28, 31.08, 30.03, 28.28, 21.66, 21.27.
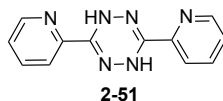
6.2.1.6 Synthesis of 3,6-dipyrid-2-yl-1,2,4,5-tetrazine 2-45

The following synthesis was performed according to the literature procedure.[10]
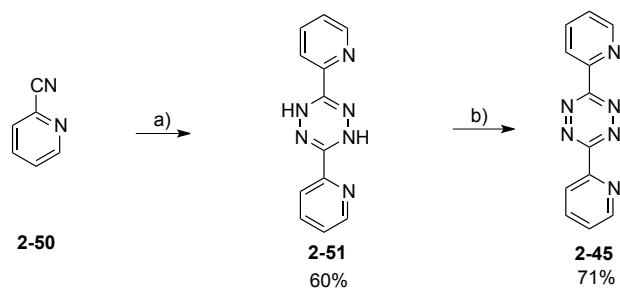
Scheme 6-6 Synthesis of dipyridyl-*s*-tetrazine **2-45**; a) hydrazine hydrate, 90 °C, 12 h; b) DDQ, toluene, 110 °C, 12 h.

6.2.1.6.1 Synthesis of 3,6-dipyrid-2-yl-1,4-dihydro-1,2,4,5-tetrazine 2-51


2-51

3,6-dipyrid-2-yl-1,4-dihydro-1,2,4,5-tetrazine **2-51** has been synthesized according to the literature.[11] ^{1}H NMR (300 MHz, DMSO-d_6) δ_H 8.99 (*s*, 2H), 8.64 (*ddd*, *J* = 7.7, 4.8, 1.2 Hz, 2H), 7.99-7.91 (*m*, 4H), 7.55-7.52 (*ddd*, *J* = 7.7, 4.7, 1.2 Hz, 2H); ^{13}C NMR (75 MHz, DMSO-d_6) δ_C 148.64, 147.24, 146.30, 137.45, 125.38, 121.05.

6.2.1.6.2 Synthesis of 3,6-dipyrid-2-yl-1,2,4,5-tetrazine 2-45

2-45
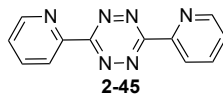
Dihydro-tetrazine **2-51** (600 mg, 2.5 mmol) and DDQ (1.13 g, 5 mmol) were dissolved in dry toluene (20 mL). The reaction mixture was stirred at 110 °C for 12 h. The solvent was removed under reduced pressure and crude residue was purified through silica gel column chromatography (solid deposit; CH$_2$Cl$_2$ to CH$_2$Cl$_2$/acetone 7:3) to give **2-45** as a red solid (420 mg, 71%) which was characterized in accordance with the literature.[12] ^{1}H NMR (300 MHz, CDCl$_3$) δ_H 8.99 (*ddd*, *J* = 4.7, 1.8, 0.9 Hz, 2H), 8.76 (*ddd*, *J* = 7.8, 1.1, 0.9 Hz, 2H), 8.03 (*td*, *J* = 7.8, 1.8 Hz, 2H), 7.60 (*ddd*, *J* = 7.8, 4.7, 1.1 Hz, 2H); ^{13}C NMR (75 MHz, CDCl$_3$) δ_C 163.95, 151.12, 150.10, 137.76, 126.81, 124.72.

6.2.1.7 Dynamic covalent chemistry
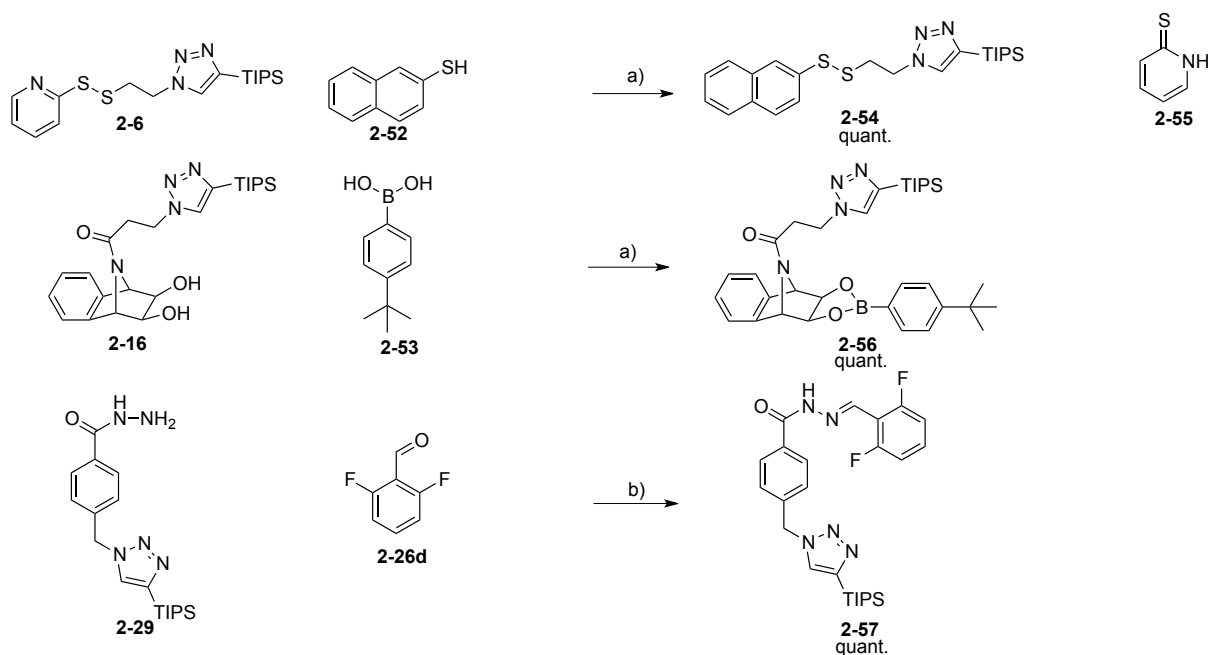
Scheme 6-7 Disulfide exchange, boronate and acyl hydrazone formation; a) THF, rt, 1 h; b) *m*-phenylenediamine, THF, rt, 1 h.

6.2.1.7.1 Synthesis of 1-(2-(naphthalen-2-yldisulfanyl)ethyl)-4-(triisopropylsilyl)-1H-1,2,3-triazole 2-54
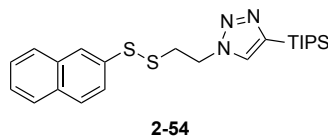
To a solution of disulfide-pyridine **2-6** (45 mg, 0.11 mmol) in THF (10 mL), 2-naphtalene thiol **2-52 (**20 mg, 0.12 mmol) was added. The reaction mixture was stirred at rt for 1 h. The solvent was evaporated under reduced pressure and the crude material was purified through silica gel chromatography plate (Eluent: EtOAc/Cyclohexane 1:3) to give **2-54** as a colorless oil (50 mg, quant.). IR (film): ν (cm^{-1}) 2941, 2889, 2863, 1461, 1189, 1132, 1096, 1046, 1017, 882, 850, 810, 674, 658, 472; ^{1}H NMR (400 MHz, CDCl$_3$) δ_H 8.02 (*s*, 1H), 7.84-7.79 (*m*, 3H), 7.66-7.62 (*m*, 1H), 7.54-7.47 (*m*, 2H), 7.38 (*s*, 1H), 4.70 (*t*, *J* = 6.8 Hz, 2H), 3.25 (*t*, *J* = 6.8 Hz, 2H), 1.38-1.22 (*m*, 3H), 1.07 (*d*, *J* = 7.6 Hz, 18H); ^{13}C NMR (100 MHz, CDCl$_3$) δ_C 141.84, 133.74, 133.54, 132.74, 131.19, 129.40, 127.97, 127.65, 127.60, 127.14, 126.72, 126.48, 48.08, 38.45, 18.70, 11.22; ESI-HRMS [M+H]$^+$ calcd for [C$_{23}$H$_{34}$N$_3$S$_2$Si]$^+$: 444.1958; found: 444.1953.

6.2.1.7.2 Synthesis of 1-((4R,9S,9aS)-2-(4-(tert-butyl)phenyl)-3a,4,9,9a-tetrahydro-4,9-epiminonaphtho[2,3-d][1,3,2]dioxaborol-10-yl)-3-(4-(triisopropylsilyl)-1H-1,2,3-triazol-1-yl)propan-1-one 2-56
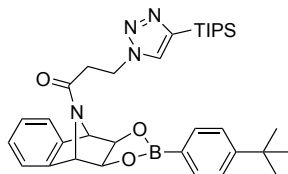
2-56

To a solution of diol **2-16** (25 mg, 0.05 mmol) in THF (5 mL), 4-tert butyl boronic acid **2-53** (11 mg, 0.06 mmol) was added. The reaction mixture was stirred at rt for 1 h. The solvent was evaporated under reduced pressure and the crude material was purified through silica gel chromatography plate (Eluent: EtOAc/Cyclohexane 2:3) to give **2-56** as a colorless oil (33 mg, quant.). IR (film): ν (cm^{-1}); 2859, 2865, 1652, 1611, 1461, 1402, 1312, 1200, 1116, 1089, 1021, 666, 643; ^{1}H NMR (400 MHz, CDCl$_3$) δ_H 7.73 (d, J = 8.4 Hz, 2H), 7.42 (d, J = 8.4 Hz, 2H), 7.42 (s, 1H), 7.35-7.21 (m, 4H), 5.66 (s, 1H), 5.17 (s, 1H), 4.66 (dd, J = 12.8, 5.4 Hz, 2H), 4.57-4.49 (m, 1H), 4.40-4.33 (m, 1H), 3.01-2.93 (m, 1H), 2.88-2.81 (m, 1H), 1.32 (s, 9H), 1.29-1.24 (m, 3H), 1.01 (d, J = 7.6 Hz, 18H); ^{13}C NMR (100 MHz, CDCl$_3$) δ_C 167.77, 155.49, 141.76, 140.66, 140.00, 135.06, 131.15, 128.50, 128.31, 125.14, 122.10, 121.62, 81.94, 81.62, 65.90, 63.55, 45.00, 35.12, 34.78, 31.29, 18.65, 11.14. ESI-HRMS [M+H]$^+$ calcd for [C$_{34}$H$_{48}$BN$_4$O$_3$Si]$^+$: 599.3590, found: 599.3581.

6.2.1.7.3 Synthesis of N'-(2,6-difluorobenzylidene)-4-((4-(triisopropylsilyl)-1H-1,2,3-triazol-1-yl)methyl)benzohydrazide 2-57

2-57

To hydrazide **2-29** (53 mg, 0.14 mmol) and *m*-phenylenediamine (8 mg, 0.07 mmol), was added a solution of 2,6-difluorobenzaldehyde **2-26d** (22 mg, 0.16 mmol) in THF (10 mL). The resulting yellow reaction mixture was stirred at rt for 1 h. The solvent was evaporated under reduced pressure and the crude residue was precipitated and washed with Et$_2$O to give **2-57** as a white solid (71 mg, quant.). M.p.: 220 °C decomposition; IR (film): ν (cm^{-1}) 3209, 2943, 2865, 1655, 1623, 1552, 1462, 1281, 1003, 785; ^{1}H NMR (400 MHz, DMSO-d_6) δ_H 11.96 (s, -NH), 8.60 (s, 1H), 8.34 (s, 1H), 7.91 (d, J = 7.6 Hz, 2H), 7.53-7.48 (m, 1H), 7.36 (d, J = 7.6 Hz, 2H), 7.21 (t, J = 8.4 Hz, 2H), 5.75 (s, 2H), 1.35-1.24 (m, 3H), 1.05 (d, J = 7.6 Hz, 18H); ^{13}C NMR (100 MHz, DMSO-d_6)

δ_C 162.59, 161.62 (*d*, J_{C-F} = 5.7 Hz), 159.09 (*d*, J_{C-F} = 5.7 Hz), 140.45, 140.34, 138.33, 132.69, 132.09, 131.92 (*t*, J_{C-F} = 9.6 Hz), 128.17, 127.55, 112.50, 112.26, 111.53 (*t*, J_{C-F} = 14.2 Hz), 51.74, 18.49, 10.59; ^{19}F (400 MHz, DMSO-*d₆*) δ_F -112.191; ESI-HRMS [M+H]$^+$ calcd for [$C_{26}H_{34}F_2N_5OSi$]$^+$: 498.2495; found: 498.2491.

6.2.1.7.4 Triorthogonal multireaction system
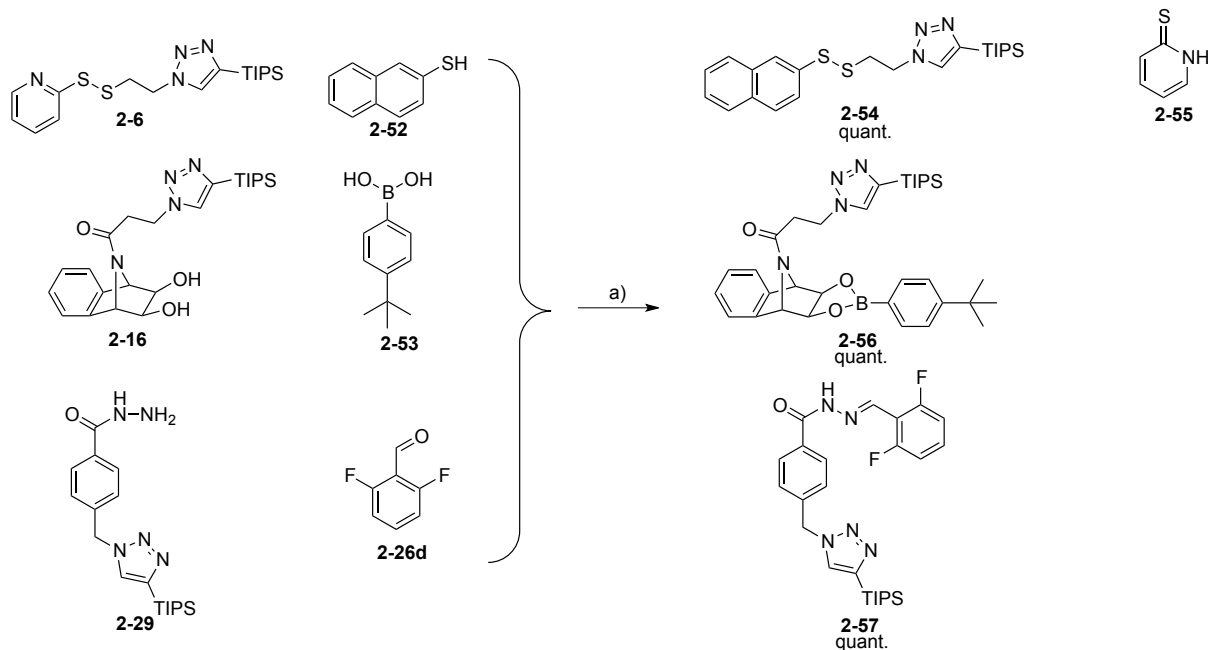
Scheme 6-8 Disulfide exchange, boronate and acyl hydrazone formation; a) *m*-phenylenediamine, THF, rt, 1 h.

In a round-bottom flask, disulfide **2-6** (20 mg, 0.05 mmol), diol **2-16** (21 mg, 0.05 mmol), hydrazide **2-29** (15 mg, 0.04 mmol), 2-naphthalenethiol **2-52** (9 mg, 0.06 mmol), 4-tert-butyl phenyl boronic acid **2-53** (9 mg, 0.06 mmol), 2,6-difluorobenzaldehyde **2-26d** (6 mg, 0.05 mmol) and *m*-phenylenediamine (2 mg, 0.02 mmol) were all dissolved in dry THF (10 mL). The reaction mixture was stirred at rt for 1 h. The solvent was evaporated under reduced pressure. The crude material was analyzed by ^{1}H NMR and MS(ESI+)-TOF (^{1}H NMR showed the quantitative formation of products **2-54**, **2-56**, **2-57**, while MS analysis showed **2-54**, **2-56**, **2-57** adducts and **2-6** and **2-16** re-formed during ionization process; see chapter 2) and was precipitated in Et$_2$O to give hydrazone **2-57** as a white solid (19 mg, quant.). The filtrate was purified through silica gel column chromatography (Eluent: cyclohexane/EtOAc 3:1) affording disulfide naphthalene **2-54** as a colorless oil (22 mg, quant.) and boronate **2-56** (partially hydrolyzed into **2-16** after the purification on silica gel).

6.2.1.8 Strain promoted azide-alkyne cycloaddition
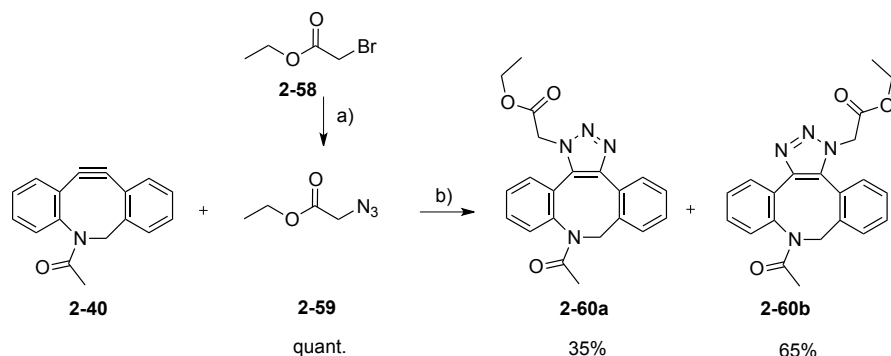
Scheme 6-9 Strain-promoted azide-alkyne cycloaddition; a) NaN$_3$, H$_2$O/acetone (1:3), 60 °C, 4 h; b) THF, rt, 1 h

6.2.1.8.1 Synthesis of ethyl 2-azidoacetate 2-59
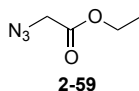
Ethyl 2-azidoacetate **2-59** has been synthesized according to the literature.[13]

6.2.1.8.2 Strain promoted azide-alkyne cycloaddition
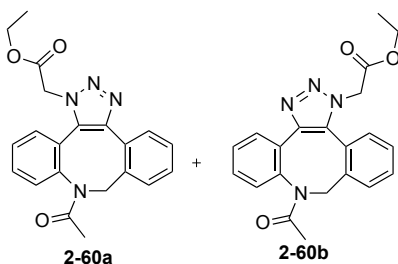
To a solution of cyclooctyne **2-40** (33 mg, 0.13 mmol) in THF (9 mL) was added a solution of azide **2-59** (27 mg, 0.2 mmol) in THF (1 mL). The reaction mixture was stirred at rt for 1 h. The solvent was removed under reduced pressure and the crude residue was purified through silica gel column chromatography (Eluent: from hexane/EtOAc 2:3 to EtOAc) to give **2-60b** as a colorless oil (regioisomer 1,3, 32 mg, 65%) and **2-60a** as a colorless oil that partially crystallized (regioisomer 1,5, 12 mg, 35%).

2-60b: IR (film): ν (cm^{-1}) 2949, 1718, 1692, 1431, 1357, 1283, 1248, 1236, 1207, 1112, 1003, 756; ^{1}H NMR (300 MHz, CDCl$_3$) δ_H 7.76-7.70 (*m*, 1H), 7.50-7.43 (*m*, 2H), 7.37-2.22 (*m*, 4H), 7.10 (*d*, *J* = 7.7 Hz, 1H), 6.14 (*d*, *J* = 16.8 Hz, 1H), 5.14 (AB*q*, Δδ$_{AB}$ = 0.13, *J* = 16.5 Hz, 2H), 4.39 (*d*, *J* = 16.8 Hz, 1H), 4.33-4.24 (*m*, 2H), 1.52 (*s*, 3H) 1.27 (*t*, *J* = 7.1 Hz, 3H); ^{13}C NMR (75 MHz, CDCl$_3$) δ_C 170.67, 166.73, 142.69, 141.01, 136.29, 135.57, 131.76, 130.85, 130.67, 130.14,

130.04, 129.88, 129.35, 127.66, 127.56, 124.18, 62.62, 51.53, 49.98, 22.50, 14.18; ESI-HRMS [M+H]$^+$ calcd for [C$_{21}$H$_{21}$N$_4$O$_3$]$^+$: 377.1614; found: 377.1604.

2-60a; As a mixture of 2 conformers (ratio: 1:0.6) was obtained the characterization is given as information only: IR (film): ν (cm^{-1}) 2924, 1747, 1660, 1655, 1373, 1213, 1020, 762, 739; ^{1}H NMR (300 MHz, CDCl$_3$) $δ_H$ 7.76-7.72 (*m*, 0.6H), 7.64-7.61 (*m*, 1H), 7.58-7.52 (*m*, 1+0.6H), 7.48-7.37 (*m*, 3+1.2H), 7.34-7.23 (*m*, 2+1.8H), 7.19-7.16 (*m*, 1H), 7.13-7.10 (*m*, 0.6H), 5.96 (*d, J* = 15.6 Hz, 1H), 5.44 (*d, J* = 18.2 Hz, 0.6H), 5.29 (*d, J* = 15.6 Hz, 0.6H), 5.28 (*d, J* = 18.2 Hz, 1H), 4.96 (*d, J* = 18.2 Hz, 0.6H), 4.84 (*d, J* = 15.6 Hz, 1H), 4.74 (*d, J* = 18.2 Hz, 1H), 4.45 (*d, J* = 15.6 Hz, 0.6H), 4.38-4.28 (*m*, 2+1.2H), 1.94 (*s*, 1.8H), 1.54 (*s*, 3H), 1.34 (*t*, 1.8H), 1.33 (*t*, 3H); ^{13}C NMR (75 MHz, CDCl$_3$, extra C peaks due to the presence of the 2 conformers) $δ_C$ 171.05, 169.35, 167.84, 166.72, 145.44, 142.41, 133.63, 133.18, 132.79, 132.54, 132.29, 132.05, 131.95, 129.42, 129.31, 129.06, 128.91, 128.80, 128.72, 128.65, 128.42, 127.61, 127.52, 127.43, 127.25, 127.18, 62.80, 62.43, 56.42, 52.93, 49.50, 49.28, 22.33, 21.28, 14.27, 14.21. ESI-HRMS [M+H]$^+$ calcd for [C$_{21}$H$_{21}$N$_4$O$_3$]$^+$: 377.1614; found: 377.1604.

6.2.1.8.3 Tetraorthogonal multireaction system
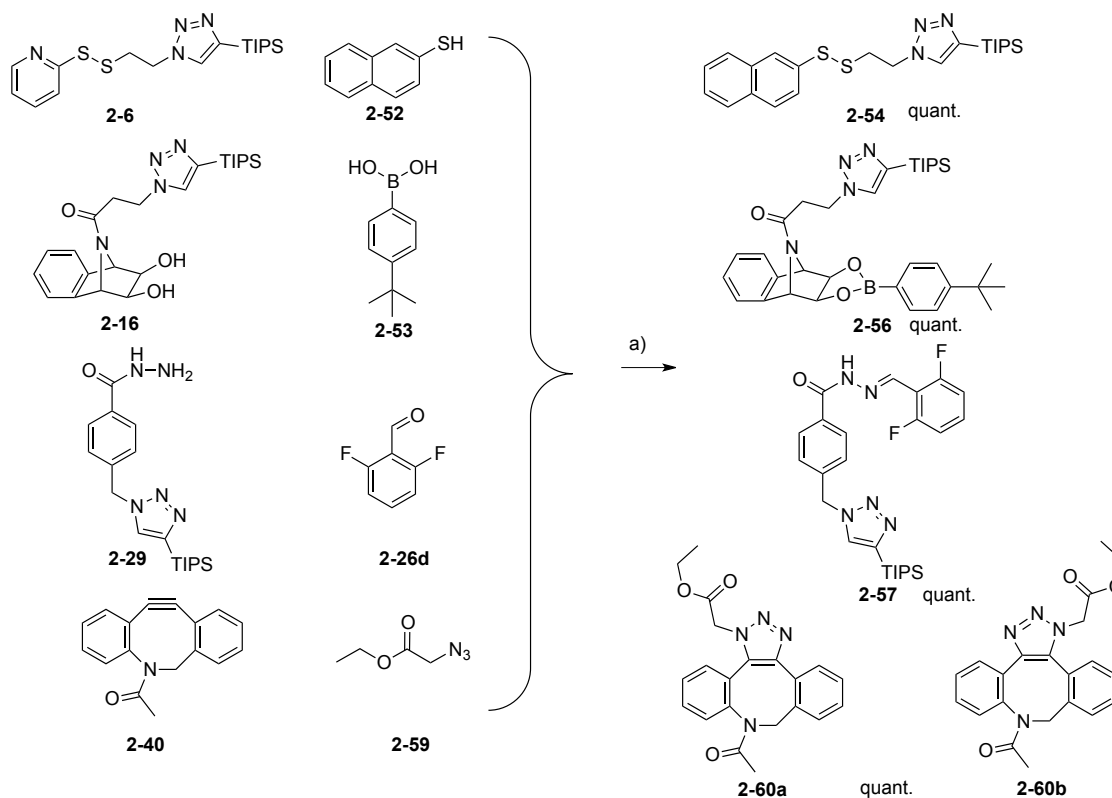
Scheme 6-10 Simultaneous disulfide interchange, boronate, acyl hydrazone formation and SPAAC; a) *m*-phenylenediamine (*m*-PDA), THF, rt, 1 h.

In a round-bottom flask, disulfide **2-6 (**12 mg, 0.03 mmol), diol **2-16** (14 mg, 0.03 mmol), hydrazide **2-29** (16 mg, 0.04 mmol) and cyclooctyne **2-40** (10 mg, 0.04 mmol) were mixed together, and the physical mixture was analyzed by ^{1}H NMR showing unreacted starting materials. Then, 2-naphthalenethiol **2-52** (7 mg, 0.04 mmol), 4-tert-butyl phenyl boronic acid **2-53** (7 mg, 0.04 mmol), 2,6-difluorobenzaldehyde **2-26d** (7 mg, 0.05 mmol), azide **2-59** (6 mg, 0.05 mmol) and *m*-phenylenediamine (2 mg, 0.02 mmol) were added and dissolved in dry THF (8 mL). The reaction mixture was stirred at rt for 1 h. The solvent was evaporated under reduced pressure. The crude material was analyzed by ^{1}H NMR and MS(ESI+)-TOF (^{1}H NMR showed the quantitative formation of products **2-54**, **2-56**, **2-57**, **2-60** while MS analysis showed **2-54**, **2-56**, **2-57, 2-60** adducts; see chapter 2) The residue was purified through silica gel column chromatography (Eluent: from cyclohexane/EtOAc 3:1 to EtOAc 100%) affording disulfide naphthalene **2-54** as a colorless oil (13 mg, quant.), hydrazone **2-57** as a white solid (20 mg, quant.), boronate **2-56** as a colorless oil (partially hydrolyzed into **2-16**), triazoles **2-60a** (5 mg, 35%) and **2-60b** (9 mg, 65%) as colorless oils.

6.2.1.9 Inverse electron demand Diels Alder
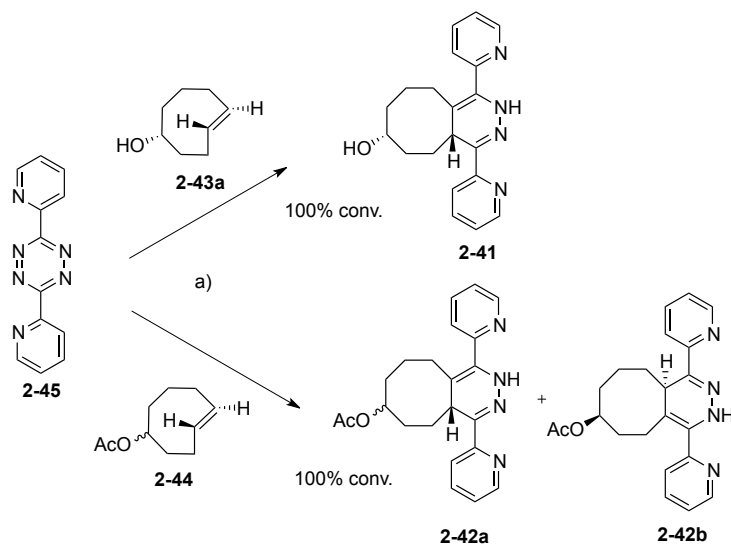
Scheme 6-6 IEDDA reaction between *trans*-cyclooctene **2-43** and **2-44** and dipyridyl *s*-tetrazine; a) THF, rt, 1 h.

6.2.1.9.1 Synthesis of 1,4-di(pyridin-2-yl)-3,5,6,7,8,9,10,10a-octahydrocycloocta[*d*]pyridazin-7-ol 2-41
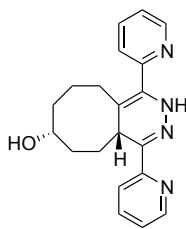
2-41

To a solution of tetrazine **2-45** (15 mg, 0.06 mmol) in THF (2 mL), was added a solution of *trans*-cyclooctenol **2-43a** (8 mg, 0.06 mmol) in THF (1 mL). The reaction mixture was stirred at rt for 1 h. Evaporation of the solvent afforded **2-41** as a yellow oil (20 mg, 100% conv.) in accordance with the literature.[14] As non pure product was obtained (tends to oxidize into pyridazine), the characterization was given as information only: IR (film): ν (cm^{-1}) 3346 (-OH), 2926, 1587, 1566, 1466, 1431, 1265, 1036, 787, 731, 700, 661; ^{1}H NMR (300 MHz, CDCl$_3$) δ_H 8.99 (*s*, 1H, -*NH*), 8.62 (*ddd*, *J* = 4.8, 1.7, 0.9 Hz, 1H), 8.58 (*ddd*, *J* = 4.8, 1.7, 0.9 Hz, 1H), 8.09 (*ddd*, *J* = 7.8, 1.1, 0.9 Hz, 1H), 7.74 (*td*, *J* = 7.8 Hz, 1.7 Hz, 1H), 7.66 (*td*, *J* = 7.8 Hz, 1.7 Hz, 1H), 7.59 (*ddd*, *J* = 7.8, 1.1, 0.9 Hz, 1H), 7.26 (*ddd*, *J* = 7.8, 4.8, 1.1 Hz, 1H), 7.20 (*ddd*, *J* = 7.8, 4.8, 1.1 Hz, 1H), 4.33 (*dd*, *J* = 10.7, 6.8 Hz, 1H), 4.07 (*dq*, *J* = 10.7, 3.8 Hz, 1H), 2.97 (*dt*, *J* = 13.5, 3.6 Hz, 1H), 2.20-2.15 (*m*, 2H), 2.03-1.39 (*m*, 7H). EI-HRMS calcd for [C$_{20}$H$_{22}$N$_4$O]$^+$: 334.1794; found: 334.1790.

6.2.1.9.2 Synthesis of 1,4-di(pyridin-2-yl)-3,5,6,7,8,9,10,10a-octahydrocycloocta[*d*]pyridazin-7-yl acetate 2-42
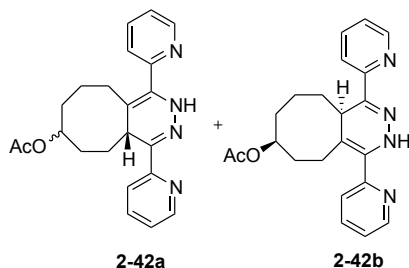
2-42a   **2-42b**

Dipyridyl *s*-tetrazine **2-45** (7 mg, 0.03 mmol) was dissolved in THF (1 mL). Then, a solution of *trans*-cyclooctene **2-44** (mixture of diastereoisomers, 5 mg, 0.03 mmol) in THF (2 mL) was added. The reaction mixture was stirred at rt for 1 h. The solvent was removed under reduced pressure and the crude residue was analyzed by ^{1}H NMR showing 100% conversion of the starting materials into **2-42** as a mixture of isomers (8 mg, 100% conv.). See ^{1}H NMR below and in appendix. IR (film): ν (cm^{-1}) 3053, 2930, 2860, 1724, 1587, 1568, 1473, 1431, 1381, 1240, 1030, 993, 793, 727, 700, 610; EI-HRMS calcd for [C$_{22}$H$_{24}$N$_4$O$_2$]$^+$: 376.1899; found: 374.1678 (oxidation into pyridazine).

Figure 6-1 ^{1}H NMR of tetrazine (bottom), *trans*-cyclooctene (middle), and crude material of tetrazine ligation product showing full conversion of the reaction (top) in CDCl$_3$.

6.2.1.9.3 Pentaorthogonal multireaction system

Scheme 6-13 Simultaneous disulfide interchange, boronate, acyl hydrazone formation, SPAAC and IEDDA; a) *m*-phenylene diamine (*m*-PDA), THF, rt, 1 h.
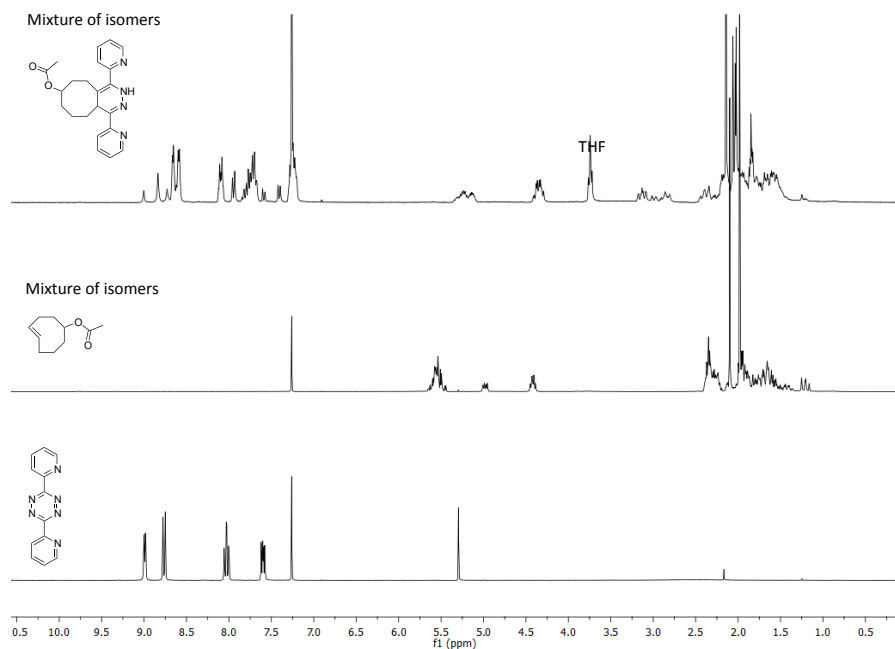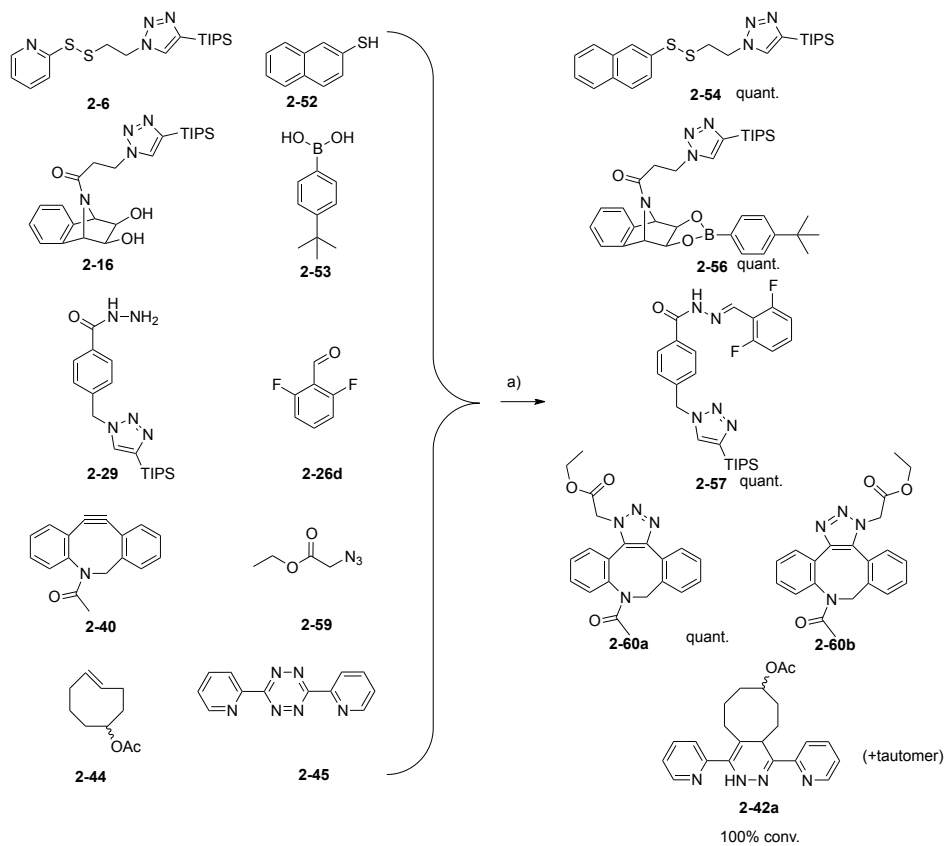
In a round-bottom flask, disulfide **2-6 (**10 mg, 0.03 mmol), diol **2-16** (10 mg, 0.02 mmol), hydrazide **2-29** (10 mg, 0.03 mmol), cyclooctyne **2-40** (10 mg, 0.04 mmol) and *trans*-cyclooctene **2-44** (7 mg, 0.04 mmol) were mixed together, and the physical mixture was analyzed by ^{1}H NMR showing unreacted starting materials. Then, 2-naphthalenethiol **2-52** (10 mg, 0.06 mmol), 4-tert-butyl phenyl boronic acid **2-53** (7 mg, 0.04 mmol), 2,6-difluorobenzaldehyde **2-26d** (8 mg, 0.05 mmol), azide **2-59** (7 mg, 0.05 mmol), *s*-tetrazine **2-45** (12 mg, 0.05 mmol) and *m*-phenylenediamine (1 mg, 0.01 mmol) were simultaneously added and dissolved in dry THF (10 mL). The reaction mixture was stirred at rt for 1 h. The solvent was evaporated under reduced pressure. The crude material was analyzed by ^{1}H NMR and MS(ESI+)-TOF; see chapter 2) The residue was purified through silica gel column chromatography (Eluent: cyclohexane/EtOAc 3:1 to EtOAc 100%) affording disulfide naphthalene **2-54** as a colorless oil (11 mg, quant.), hydrazone **2-57** as a white solid (13 mg, quant.), boronate **2-56** as a colorless oil partially hydrolyzed into **2-16**, triazoles **2-60a** (5 mg, 35%) and **2-60b** (10 mg, 65%) as colorless oil and tetrazine ligation product **2-42** (16 mg, 100% conv.) as a mixture of isomers.

6.2.2 Experimental procedures for Chapter 3

6.2.2.1 Syntheses of amino acids
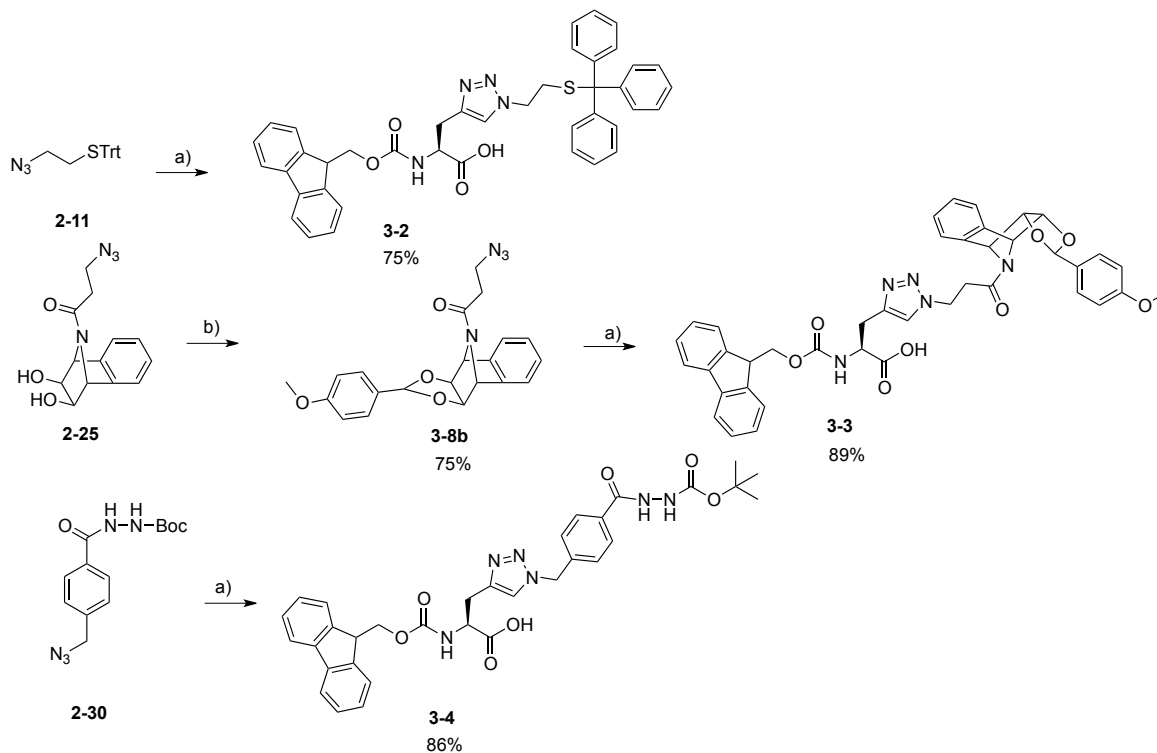
Scheme 6-14 Synthesis of modified amino acids; a) Fmoc-Gly(Propargyl)-OH, $CuSO_4.5H_2O$, Na ascorbate, DMF/H_2O (4 :1), rt, 3 h; b) anisaldehyde dimethylacetal, $pTSA.H_2O$, THF, rt, 6 h.

6.2.2.1.1 Synthesis of (S)-2-((((9H-fluoren-9-yl)methoxy)carbonyl)amino)-3-(1-(2-(tritylthio)ethyl) -1H-1,2,3-triazol-4-yl)propanoic acid 3-2

3-2

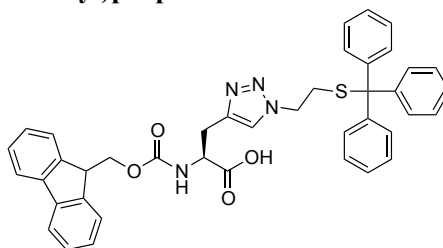To a solution of Fmoc-Gly(Propargyl)-OH (905 mg, 2.70 mmol) and azide **2-11** (1.02 g, 2.97 mmol) in DMF (40 mL), were successively added a solution of $CuSO_4.5H_2O$ (202 mg, 0.81 mmol) in H_2O (5 mL) and a solution of sodium ascorbate (107 mg, 0.54 mmol) in H_2O (5 mL). The reaction mixture was stirred at rt for 3 h. The solvents were removed under reduced pressure. The residue was partitioned between CH_2Cl_2 and a sat. aq. solution of Na_4EDTA and the layers were separated. The aqueous phase was extracted with CH_2Cl_2 and EtOAc, and the combined organic layers were washed with brine, dried and concentrated under reduced pressure. The crude material was precipitated into Et_2O to remove the excess of **2-11** affording **3-2** as a yellow solid (1.4 g, 75%). (**3-2** traps solvents, compound very difficult to dry) M.p.: 127 °C; IR (film): ν (cm^{-1}) 2970, 1715, 1621, 1488, 1443, 1365, 1275, 1049, 738, 699, 674, 620, 542, 505; ^{1}H NMR (400 MHz, DMF-d_7) δ_H 7.91 (*d*, *J* = 7.6 Hz, 2H), 7.74 (*s*, 1H), 7.66 (*d*, *J* = 7.6 Hz, 2H), 7.43-7.15 (*m*, 19H), 4.37-3.96 (*m*, 6H), 3.42-3.33 (*m*, 1H), 3.20-3.15 (*m*, 1H), 2.69 (m, 2H); ^{13}C NMR (100 MHz, DMF-d_7) δ_C 157.10, 145.65, 145.41, 145.31, 142.17, 130.47, 129.23, 128.72, 128.26, 127.97, 126.59, 124.09, 121.10, 67.95, 67.26, 56.60, 49.42, 48.17, 32.95, 27.70 (COOH missing); ESI-HRMS [M+H]$^+$ calcd for [$C_{41}H_{37}N_4O_4S$]$^+$: 681.2530, found: 681.2532.

6.2.2.1.2 Synthesis of 3-azido-1-((3aR,4R,9S,9aS)-2-(4-methoxyphenyl)-3a,4,9,9a-tetrahydro-4,9-epiminonaphtho[2,3-d][1,3]dioxol-10-yl)propan-1-one 3-8b
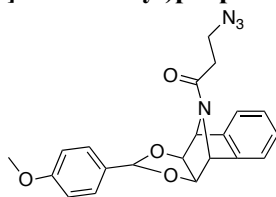
3-8b

To a solution of diol **2-25** (21 mg, 0.08 mmol) in THF (4 mL), anisaldehyde dimethylacetal (42 mg, 0.23 mmol) and *p*-toluene sulfonic acid (1.5 mg, 0.008 mmol) were successively added. The reaction mixture was stirred at rt for 6 h. A sat. aq. solution of $NaHCO_3$ was added. The aqueous phase was extracted with EtOAc and the organic phase was washed with brine, dried and concentrated under reduced pressure. The crude material was purified through silica gel column

chromatography (Eluent: P.E./EtOAc/Et$_3$N 74:24:2) to give **3-8b** as a colorless oil (22 mg, 75%).
IR (film): ν (cm^{-1}) 2936, 2095, 1646, 1519, 1440, 1253, 1171, 1067, 1032, 998, 825, 816, 757,
662 ; ^{1}H NMR (400 MHz, (CD$_3$)$_2$CO) δ_H 7.50-7.41 (*m*, 4H), 7.28-7.24 (*m*, 2H), 6.94 (*d*, *J* = Hz,
2H), 5.81 (*s*, 1H), 5.65 (*s*, 1H), 5.44 (*s*, 1H), 4.40 (*dd*, *J* = 14.8, 6 Hz, 2H), 3.81 (*s*, 3H), 3.60-3.54
(*m*, 1H), 3.47-3.41 (*m*, 1H), 2.71-2.63 (*m*, 1H), 2.60-2.54 (*m*, 1H); ^{13}C NMR (100 MHz,
(CD$_3$)$_2$CO) δ_C 167.83, 161.77, 142.56, 142.46, 129.43, 129.20, 128.50, 128.32, 122.76, 122.57,
114.28, 108.33, 82.47, 82.36, 64.67, 62.52, 55.58, 47.42, 33.90; ESI-HRMS [M+H]$^+$ calcd for
[C$_{21}$H$_{21}$N$_4$O$_4$]$^+$: 393.1557; found: 393.1553.

6.2.2.1.3 Synthesis of (2S)-2-((((9H-fluoren-9-yl)methoxy)carbonyl)amino)-3-(1-(3-((3aR,9aS)-2-(4-methoxyphenyl)-3a,4,9,9a-tetrahydro-4,9-epiminonaphtho[2,3-d][1,3]dioxol-10-yl)-3-oxopropyl)-1H-1,2,3-triazol-4-yl)propanoic acid 3-3
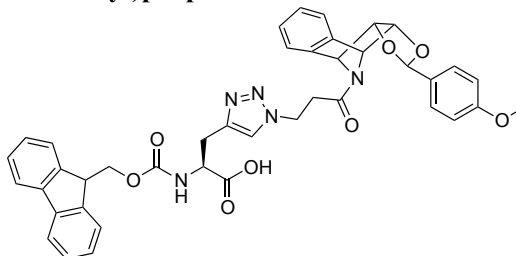
3-3

To a solution of Fmoc-Gly(Propargyl)-OH (1.81 g, 5.4 mmol) and azide **3-8b** (2.19 g, 5.58 mmol)
in DMF (50 mL), were successively added a solution of CuSO$_4$.5H$_2$O (404 mg, 1.62 mmol) in
H$_2$O (6 mL) and a solution of sodium ascorbate (214 mg, 1.08 mmol) in H$_2$O (6 mL). The reaction
mixture was stirred at rt for 3 h. Solvents were evaporated under reduced pressure and the crude
mixture was partitioned between a sat. aq. solution of Na$_4$EDTA and EtOAc. The layers were
separated and the aqueous phase was extracted with EtOAc. The combined organic layers were
washed with brine, dried and concentrated under reduced pressure. The residue was precipitated in
Et$_2$O to give **3-3** (mixture of diastereoisomers which was not separated since a single product is
obtained after the protecting group removal under resin cleavage conditions, proved from the
synthesis of **3-9**) as a white solid. (3.5 g, 89%). M.p.: 100-106 °C; IR (film): ν (cm^{-1}) 2935, 1713,
1644, 1448, 1248, 1067, 1030, 758, 740, 661; ^{1}H NMR (400 MHz, CD$_3$OD) δ_H 7.77 (*d*, *J* = 7.6 Hz,
2H), 7.63-7.54 (*m*, 3H), 7.36-7.15 (*m*, 10H), 6.90 (*m*, 2H), 5.75 and 5.74 (*two s*, 1H), 5.59 and
5.58 (*two s*, 1H), 5.21 and 5.15 (*two s*, 1H), 4.63-4.11 (*m*, 8H), 3.78 and 3.77 (*two s*, 3H), 3.23-3-
17 (*m*, 1H), 3.08-2.93 (*m*, 2H), 2.86-2.76 (*m*, 1H); ^{13}C NMR (100 MHz, CD$_3$OD) δ_C 174.39,
168.80, 162.26, 158.31, 145.27, 145.21, 142.55, 141.80, 141.61, 129.30, 129.22, 129.11, 128.95,
128.81, 128.19, 126.32, 124.76, 122.92, 120.94, 114.72, 108.72, 82.73, 82.67, 67.98, 65.54, 65.47,
63.40, 55.79, 54.99, 54.94, 49.85, 46.84, 46.79, 35.21, 28.77 (extra peaks in ^{1}H and ^{13}C NMR are
due to the mixture of diasteroisomers). ESI-HRMS [M+H]$^+$ calcd for [C$_{41}$H$_{38}$N$_5$O$_8$]$^+$: 728.2715,

found: 728.2713.

6.2.2.1.4 Synthesis of (2S)-2-((((9H-fluoren-9-yl)methoxy)carbonyl)amino)-3-(1-(3-((2R,3S)-2,3-dihydroxy-1,2,3,4-tetrahydro-1,4-epiminonaphthalen-9-yl)-3-oxopropyl)-1H-1,2,3-triazol-4-yl)propanoic acid 3-9

3-9
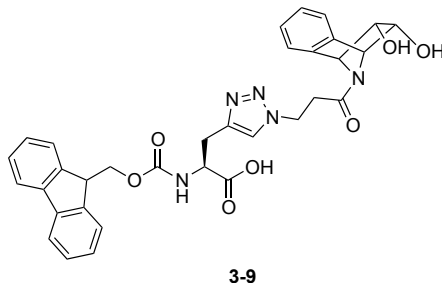
A solution of amino acid **3-3** (25 mg, 0.03 mmol) in a mixture TFA/TIS/water (95:2.5:2.5) (5 mL) was stirred at rt for 2 h. The solvents were evaporated and the crude residue was precipitated and washed with Et$_2$O to give **3-9** as a white solid. (21 mg, quant.) M.p.: 140 °C; IR (film): v (cm^{-1}) 3284, 1706, 1622, 1447, 1220, 1062, 757, 739, 662, 541; ^{1}H NMR (400 MHz, CD$_3$OD) δ_H 7.78 (*d*, *J* = 7.2 Hz, 2H), 7.68-7.54 (*m*, 3H), 7.37 (*t*, *J* = 7.2 Hz, 2H), 7.30-7.24 (*m*, 4H), 7.18-7.15 (*m*, 2H), 5.28 (*s*, 1H), 5.03 (*s*, 1H), 4.67-4.60 (*m*, 2H), 4.48-4.43 (*m*, 1H), 4.29 (*t*, *J* = 7.2 Hz, 2H), 4.20-4.15 (*m*, 1H), 3.81-3.75 (*m*, 2H), 3.23-2.88 (*m*, 4H); ^{13}C NMR (100 MHz, CD$_3$OD) δ_C 174.46, 168.94, 158.35, 145.26, 145.20, 142.65, 142.54, 142.29, 128.84, 128.80, 128.71, 128.19, 126.29, 124.92, 122.13, 120.92, 71.57, 71.41, 68.80, 68.00, 66.27, 55.04, 49.63, 47.14, 35.18, 28.72; ESI-HRMS [M+H]$^+$ calcd for [C$_{33}$H$_{32}$N$_5$O$_7$]$^+$: 610.2296 ; found: 610.2289.

6.2.2.1.5 Synthesis of (S)-2-((((9H-fluoren-9-yl)methoxy)carbonyl)amino)-3-(1-(4-(2-(tert-butoxycarbonyl)hydrazinecarbonyl)benzyl)-1H-1,2,3-triazol-4-yl)propanoic acid 3-4
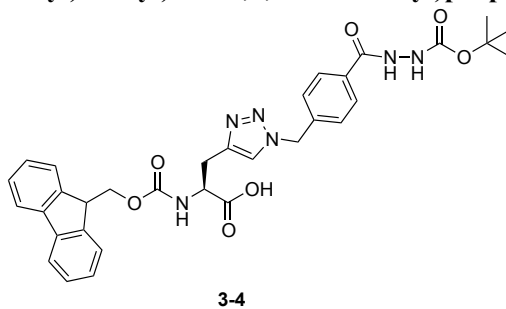

3-4

To a solution of Fmoc-Gly(Propargyl)-OH (905 mg, 2.70 mmol) and azide **2-30** (1.02 g, 2.97 mmol) in DMF (40 mL), were successively added a solution of CuSO$_4$.5H$_2$O (202 mg, 0.81 mmol) in H$_2$O (5 mL) and a solution of sodium ascorbate (107 mg, 0.54 mmol) in H$_2$O (5 mL). The reaction mixture was stirred at rt for 3 h. The solvents were evaporated under reduced pressure. The residue was partitioned between CH$_2$Cl$_2$ and a sat. aq. solution of Na$_4$EDTA. The layers were separated and the aqueous phase was extracted with CH$_2$Cl$_2$. The combined organic

layers were washed with brine, dried and concentrated under reduced pressure. The crude material was precipitated into Et_2O to remove the excess of **2-30** affording **3-4** as a colorless solid (1.45 g, 86%). M.p.: 110-114 °C; IR (film): ν (cm^{-1}) 3320, 2978, 1708, 1528, 1449, 1249, 1156, 1046, 760, 739, 620, 539; ^{1}H NMR (400 MHz, CD$_3$OD) δ_H 7.80-7.76 (*m*, 5H), 7.60 (*t*, *J* = 8.4 Hz, 2H), 7.37 (*t*, *J* = 7.6 Hz, 2H), 7.30-7.25 (*m*, 4H), 5.59 (*s*, 2H), 4.49-4.48 (*m*, 1H), 4.32-4.22 (*m*, 2H), 4.16 (*t*, *J* = 7.2 Hz, 1H), 3.34-3.30 (*m*, 1H), 3.12-3.04 (*m*, 1H), 1.49 (*s*, 9H); ^{13}C NMR (100 MHz, CD$_3$OD) δ_C 174.39, 169.1, 158.34, 157.87, 145.13, 142.52, 142.47, 140.95, 133.74, 129.16, 128.80, 128.79, 128.15, 126.21, 124.67, 120.88, 81.93, 68.00, 55.12, 54.22, 48.79, 28.95, 28.51; ESI-HRMS [M+H]$^+$ calcd for [C$_{33}$H$_{35}$N$_6$O$_7$]$^+$: 627.2562, found: 627.2564.

6.2.2.2 Peptide Synthesis and characterization

Peptide was synthesized on Rink-amide MBHA resin (0.11 mmol, 0.48 mmol/g).

The synthesis was performed on a *Focus XC automated peptide synthesizer (model P/N 300530, aapptec)* under nitrogen atmosphere. Coupling reactions were carried out using *N*-Fmoc amino acids (0.26 M; 5 equiv.) in NMP, HATU (0.3 M, 4.5 equiv.) in DMF and DIPEA (2 M, 12 equiv.) in NMP at rt for 25 min. Simple coupling was performed for most of the amino acids except the three alanines (residues 3, 10 and 17) preceding the modified amino acids for which double coupling was carried out. *N*-Fmoc deprotection was carried out at rt in three stages using piperidine/DMF (1:4, 3 × 6 mL) for 3 × 4 min. After each reaction the resin was washed with DMF (4 times). At the end of the synthesis, the peptide was acetylated in two stages in presence of Ac$_2$O/pyridine/NMP (1:2:2, 2 × 6 mL) at rt for 2 × 15 min. The resin was washed 6 times with CH$_2$Cl$_2$. The peptide was deprotected and cleaved from the resin using the cocktail cleavage TFA/water/EDT/TIS (94:2.5:2.5:1, 10 mL for 200 mg). After 2 h at rt, the sample was then filtered through glass wool, the solvent was evaporated and the crude material was precipitated in cold Et$_2$O. After centrifugation, the ether was decanted and this washing was repeated 3 times.

Analysis and purification: The analytical HPLC column used was a *Agilent ZORBAX StableBond C8* (5 μm, 4.6 x 150 mm) column. The analysis was performed at 60 °C. The preparative column used was a *Varian Pursuit XRs C18* (5 μm, 21.2 x 250 mm) column. Gradient elution was applied from 0 to 60% buffer B in 12 min; 60 to 100% buffer B in 15 min; 100% for 1 min and 100% to 0% in 1 min (buffer A: H$_2$O; buffer B: MeCN) with a flow of 1.5 mL/min for the analytical and 21 mL/min for the preparative.

6.2.2.2.1 Synthesis of Ac-(QLAX(thiol)QLA QLAX(hydrazide)QLA QLAX(diol)QLA)-NH₂ 3-11
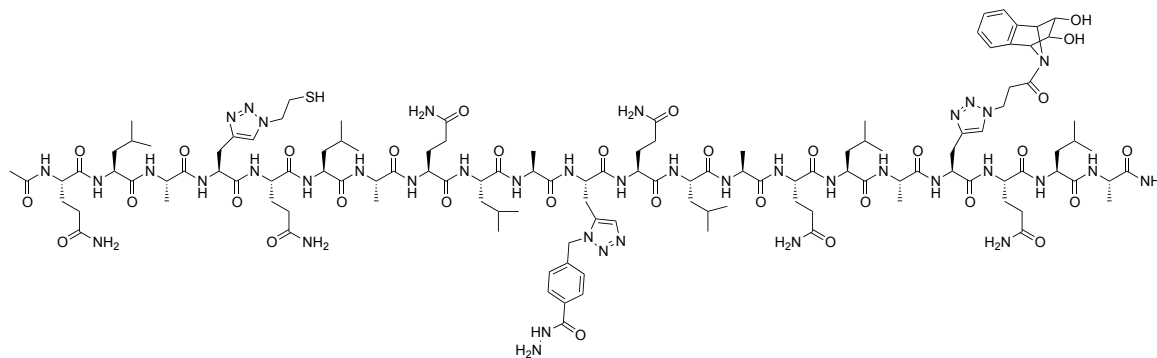
Chemical Formula: $C_{124}H_{192}N_{40}O_{32}S$
Exact Mass: 2785.43

The peptide was synthesized according the general procedure. The crude material was used for the next step without any further purification. ESI-MS(Q-Tof) showed M^{4+}, M^{3+}, M^{2+}, after deconvolution of multicharged ions, monoisotopic mass found: 2785.4569.
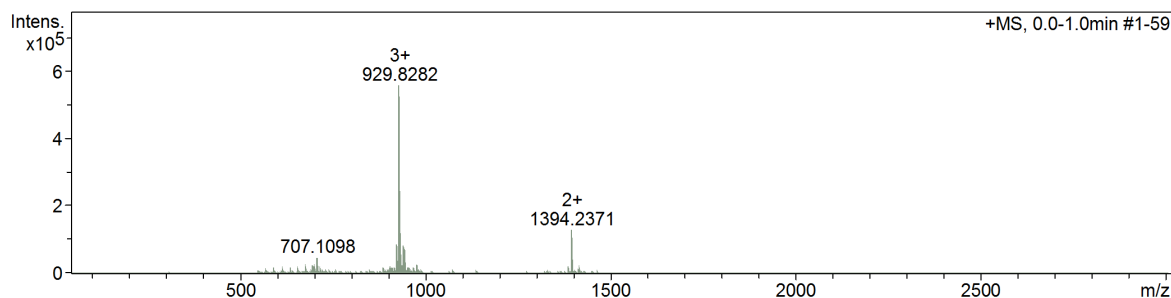
Component	Molecular Mass	Molecule	Absolute Abundance	Relative Abundance	
A	2785.4569	2787.2302	Mr	460021	100.00

6.2.2.2.2 Synthesis of Ac-(QLAX(disulfide)QLAQLAX(hydrazide)QLAQLAX(diol)QLA)-NH₂ 3-1
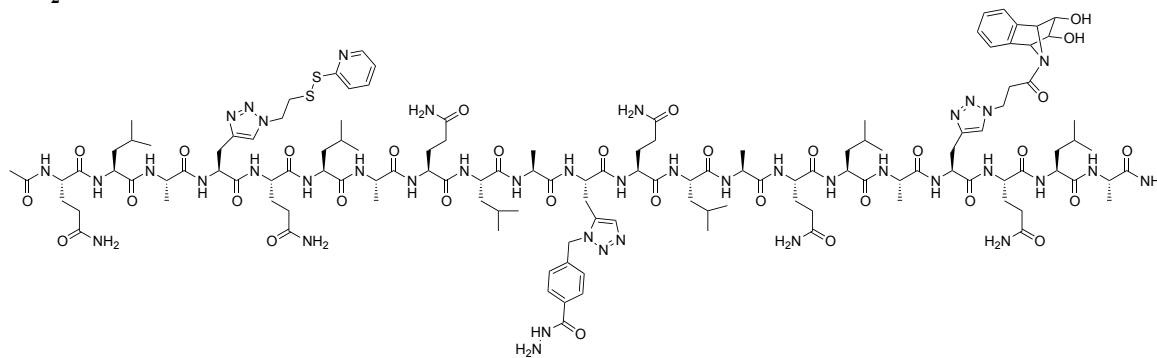
Chemical Formula: $C_{129}H_{195}N_{41}O_{32}S_2$
Exact Mass: 2894.43

To a solution of Ac-(QLAX(thiol)QLA QLAX(hydrazide)QLA QLAX(diol)QLA)-NH₂ **3-11**

(0.1 mmol) and 2,2'-dipyridine disulfide (76 mg, 0.33 mmol) in dry DMF (2 mL), DIEA (85 mg, 0.66 mmol) was added. The reaction mixture was stirred for 1 h and poured in cold Et$_2$O and the product precipitated. After centrifugation, the ether was decanted and this washing was repeated 3 times. The crude peptide was purified by preparative HPLC.

HPLC (60 °C): R$_t$ = 16.04 min. ESI-MS(Q-Tof) showed M^{4+}, M^{3+}, M^{2+}, after deconvolution of multicharged ions, monoisotopic mass found: 2894.4401.
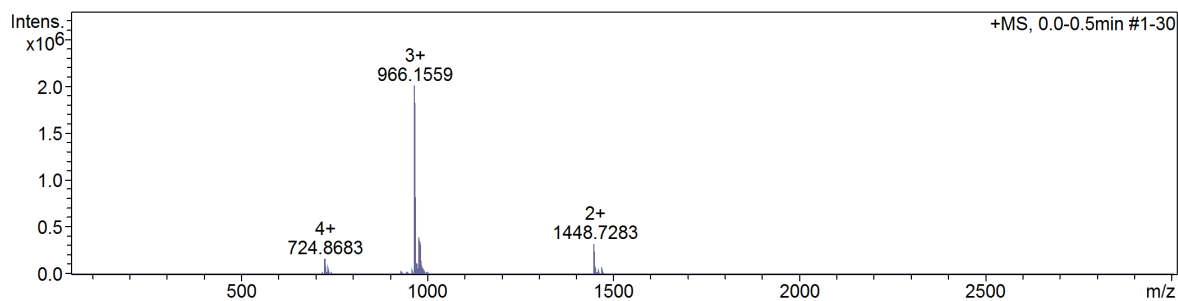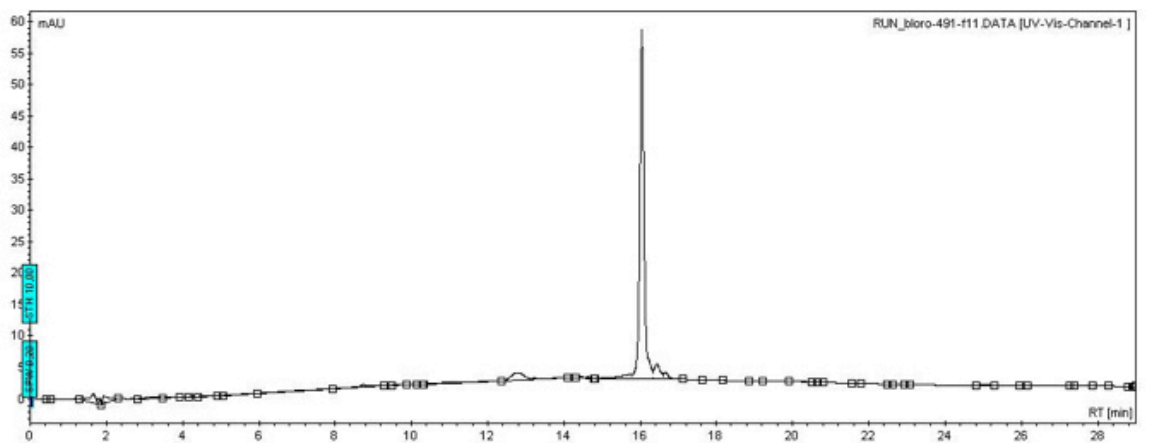
Component	Molecular Mass	Molecule	Absolute Abundance	Relative Abundance
A	2894.4401	2896.2907 Mr	1586171	100.00

6.2.2.3 Colored emitters syntheses

6.2.2.3.1 Synthesis of blue chromophore 3-12 (B-NDI)

Scheme 6-15 Synthesis of B-NDI **3-12**; a) H$_2$, Pd(OH)$_2$/C, MeOH, rt, 20 h; b) Cs$_2$CO$_3$, [Pd(PPh$_3$)$_4$], toluene, reflux, 12 h; c) **3-17**, DIEA, dioxane, 101 °C, 2 h; d) TFA, 73 °C, 24 h; e) NEt$_3$, benzoic acid, DMF, 110 °C, 6 h; f) iPrNH$_2$, 110 °C, 48 h; g) *i)* Hg(ClO$_4$)$_2$, MeOH/CH$_2$Cl$_2$ (1:5), 30 min, rt, *ii)* H$_2$S, rt, 10 min.

6.2.2.3.1.1 Synthesis of 1-(azidomethyl)-3,5-bis(2-(2-(2-methoxyethoxy)ethoxy)ethoxy) benzene 3-16

Azide **3-16** has been synthesized according to the literature procedure.[15]

6.2.2.3.1.2 Synthesis of (3,5-bis(2-(2-(2-methoxyethoxy)ethoxy)ethoxy)phenyl)methanamine 3-17

A solution of azide **3-16** (0.50 g, 1.09 mmol) and Pd(OH)$_2$ on carbon (20%, 0.30 g) in MeOH (25 mL) was stirred at 20 °C. Hydrogen was bubbled through the solution for 30 min and the reaction mixture was kept under hydrogen for 20 h. The resulting mixture was filtered through celite and the volatiles were removed under reduced pressure to give **3-17** as a colorless oil (0.47 g, 100%). The compound was characterized in accordance with the literature.[16] ^{1}H NMR (400 MHz, CDCl$_3$): δ_H 6.47 (*d*, *J* = 2.0 Hz, 2H), 6.37-6.32 (*m*, 1H), 4.08 (*t*, *J* = 4.8 Hz, 4H), 3.81 (*t*, *J* = 4.8 Hz, 4H), 3.77 (*s*, 2H), 3.74-3.59 (*m*, 12H), 3.56-3.49 (*m*, 4H), 3.35 (*s*, 6H), 2.18 (*br. s*, -*NH₂*); ESI-HRMS [M+H]$^+$ calcd for [C$_{21}$H$_{38}$NO$_8$]$^+$: 432.2592; found: 432.2591.

6.2.2.3.1.3 Synthesis of 4'-(tert-butylthio)biphenyl-4-amine 3-22

3-22
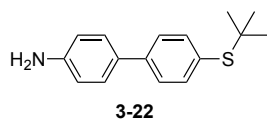
A solution of **3-21** (0.51 g, 2.07 mmol), **3-20** (0.50 g, 2.28 mmol), Cs$_2$CO$_3$ (0.68 g, 2.07 mmol) and [Pd(PPh$_3$)$_4$] (0.48 g, 0.41 mmol) in toluene (10 mL) was stirred at reflux for 12 h under argon. The volatiles were removed under reduced pressure. The crude residue was purified through silica gel column chromatography (Eluent: Et$_2$O) to afford **3-22** as a beige solid (0.40 g, 75%). M.p.: 135-137 °C. IR (film): ν (cm^{-1}) 3394, 3312, 3208, 3039, 2968, 2958, 2921, 2896, 2859, 1628, 1604, 1589, 1525, 1498, 1481, 1457, 1435, 1397, 1365, 1294, 1275, 1204, 1167, 1145, 1109, 1095, 1024, 1011, 1001, 948, 933, 844, 815, 762, 740, 712, 691, 666, 610, 579, 562, 509, 476. ^{1}H NMR (500 MHz, CDCl$_3$): δ_H 7.55 (*d*, *J* = 8.0 Hz, 2H), 7.50 (*d*, *J* = 8.0 Hz, 2H), 7.43 (*d*, *J* = 8.0 Hz, 2H), 6.77 (*d*, *J* = 8.0 Hz, 2H), 3.89 (*br. s*, -NH$_2$), 1.31 (*s*, 9H); ^{13}C NMR (125 MHz, CDCl$_3$): δ_C one C_q peak missing, 145.9, 141.52, 137.92, 130.39, 128.07, 126.38, 115.63, 46.07, 31.08; ESI-HRMS [M+H]$^+$ calcd for [C$_{16}$H$_{20}$NS]$^+$: 258.1311; found: 258.1312.

6.2.2.3.1.4 Synthesis of diethyl 4,8-diethoxy-1,3-dioxo-1,3-dihydrobenzo[*de*]isochromene-6,7-dicarboxylate 3-15

3-15
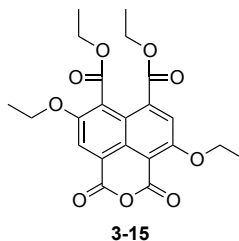
Diethyl 4,8-diethoxy-1,3-dioxo-1,3-dihydrobenzo[*de*]isochromene-6,7-dicarboxylate **3-15** has been synthesized according to the literature procedure.[17]

6.2.2.3.1.5 Synthesis of 2-(3,5-bis(2-(2-(2-methoxyethoxy)ethoxy)ethoxy)benzyl)-4,8-diethoxy-1,3-dioxo-2,3-dihydro-1H-benzo[de]isoquinoline-6,7-dicarboxylate 3-18
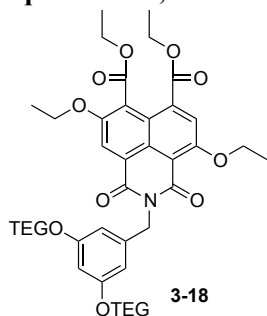

To a solution of **3-17** (1.10 g, 2.56 mmol) and DIEA (0.33 g, 2.56 mmol) in dioxane (30 mL) was added **3-15** (1.00 g, 2.32 mmol) and the reaction mixture was stirred at 101 °C for 2 h. The volatiles were removed under reduced pressure. The crude residue was purified through silica gel column chromatography (Eluent: from EtOAc to EtOAc/EtOH 10:1) to give **3-18** as a yellow solid (1.80 g, 92%). M.p.: 57-58 °C. IR (film): ν (cm^{-1}) 2981, 2874, 2822, 1739, 1723, 1699, 1655, 1616, 1582, 1504, 1475, 1436, 1408, 1387, 1373, 1350, 1326, 1310, 1298, 1283, 1226, 1208, 1182, 1135, 1124, 1105, 1079s, 1023, 971, 954, 928, 900, 881, 864, 855, 842, 826, 813, 795, 778, 768, 753, 735, 721, 691, 677, 654, 635, 619, 591, 528, 474. ^{1}H NMR (400 MHz, CDCl$_3$): δ_H 8.43 (*s*, 1H), 7.72 (*s*, 1H), 6.62 (s, 2H), 6.36 (*s*, 1H), 5.27 (*s*, 2H), 4.43-4.38 (*m*, 6H), 4.30 (*q*, *J* = 6.9 Hz, 2H), 4.06 (*t*, *J* = 4.8 Hz, 4H), 3.80 (*t*, *J* = 4.8 Hz, 4H), 3.72-3.68 (*m*, 4H), 3.67-3.62 (*m*, 8H), 3.55-3.52 (*m*, 4H), 3.37 (*s*, 6H), 1.60 (*t*, *J* = 6.9 Hz, 3H), 1.48-1.39 (*m*, 9H); ^{13}C NMR (100 MHz, CDCl$_3$): δ_C 167.31, 166.67, 163.02, 161.29, 159.89, 159.77, 154.37, 139.29, 136.50, 126.25, 124.47, 123.10, 122.08, 119.78, 119.18, 109.09, 107.28, 100.52, 71.96, 70.81, 70.67, 70.60, 69.71, 67.43, 66.12, 65.98, 62.38, 61.73, 59.08, 43.59, 14.90, 14.17; ESI-HRMS [M+H]$^{+}$ calcd for [C$_{43}$H$_{58}$NO$_{16}$]$^{+}$: 844.3750; found: 844.3745.

6.2.2.3.1.6 Synthesis of 7-(3,5-bis(2-(2-(2-methoxyethoxy)ethoxy)ethoxy)benzyl)-4,9-diethoxy-1H-isochromeno[6,5,4-def]isoquinoline-1,3,6,8(7H)-tetraone 3-19
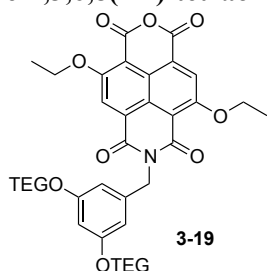
A solution of **3-18** (1.00 g, 1.18 mmol) in TFA (15 mL) was stirred at 73 °C for 24 h. The volatiles were removed under reduced pressure. The crude residue was purified through silica gel column chromatography (Eluent: EtOAc) to give **3-19** as a yellow solid (0.82 g, 91%). M.p.: 59 - 61 °C. IR (film): ν (cm^{-1}) 3081, 2986, 2923, 2897, 2871, 1782, 1731, 1705, 1664, 1610, 1591, 1576,

1499, 1474, 1441, 1417, 1378, 1358, 1343, 1319, 1301, 1253, 1235, 1199, 1177, 1162, 1122, 1105, 1068, 1016, 994, 967, 922, 916, 898, 868, 845, 825, 785, 764, 738, 724, 694, 679, 657, 631, 619, 559, 548, 514, 472; ^{1}H NMR (270 MHz, CDCl$_3$): δ_H 8.50 (*s*, 1H), 8.45 (*s*, 1H), 6.63 (*d*, *J* = 2.2 Hz, 2H), 6.37 (*dd*, *J* = 2.2, 2.2 Hz, 1H), 5.28 (*s*, 2H), 4.55 (*q*, *J* = 7.0 Hz, 2H), 4.51 (*q*, *J* = 7.0 Hz, 2H), 4.07 (*t*, *J* = 4.9 Hz, 4H), 3.81 (*t*, *J* = 4.9 Hz, 4H), 3.732-3.60 (*m*, 12H), 3.56-3.50 (*m*, 4H), 3.36 (*s*, 6H), 1.66 (*t*, *J* = 7.0 Hz, 3H), 1.65 (*t*, *J* = 7.0 Hz, 3H); ^{13}C NMR (68 MHz, CDCl$_3$): δ_C 162.03, 161.27, 160.47, 160.11, 159.99, 159.87, 155.27, 138.76, 128.49, 125.77, 123.71, 123.41, 121.46, 119.90, 112.09, 107.56, 106.90, 100.59, 71.98, 70.83, 70.70, 70.62, 69.73, 67.45, 66.76, 66.68, 59.10, 43.88, 14.80, 14.75; ESI-HRMS [M+H]$^+$ calcd for [C$_{39}$H$_{48}$NO$_{15}$]$^+$: 770.3018; found: 770.3010.

6.2.2.3.1.7 Synthesis of 2-(3,5-bis(2-(2-(2-methoxyethoxy)ethoxy)ethoxy)benzyl)-7-(4'-(tert-butylthio)biphenyl-4-yl)-4,9-diethoxybenzo[lmn][3,8]phenanthroline-1,3,6,8(2H,7H)-tetraone 3-23
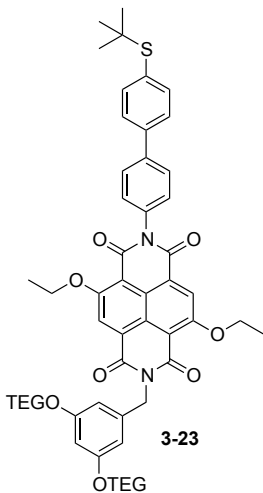
To a solution of **3-22** (0.10 g, 0.39 mmol), Et$_3$N (22.0 mg, 0.22 mmol) and benzoic acid (26.0 mg, 0.22 mmol) in DMF (3 mL) was added **3-19** (0.28 g, 0.36 mmol) and the reaction mixture was stirred at 110 °C for 6 h. The volatiles were removed under reduced pressure. The crude residue was purified through silica gel column chromatography (Eluent: EtOAc/EtOH 10:1) to give **3-23** as a yellow solid (0.26 g, 72%). M.p.: 57-59 °C. IR (film): ν (cm^{-1}) 2921, 2872, 1775, 1701, 1661, 1595, 1575, 1517, 1497, 1480, 1443, 1379, 1358, 1321, 1290, 1252, 1210, 1171, 1105, 1068, 1030, 1007, 945, 925, 870, 844, 820, 804, 790, 781, 769, 761, 747, 731, 705, 681, 660, 643, 631, 589, 571, 524, 505; ^{1}H NMR (270 MHz, CDCl$_3$): δ_H 8.50 (*s*, 2H), 7.77 (*d*, *J* = 8.3 Hz, 2H), 7.66-7.54 (*m*, 4H), 7.41 (*d*, *J* = 8.4 Hz, 2H), 6.65 (*d*, *J* = 2.0 Hz, 2H), 6.38 (*dd*, *J* = 2.1, 2.1 Hz, 1H), 5.31 (*s*, 2H), 4.57-4.44 (*m*, 4H), 4.08 (*t*, *J* = 4.7 Hz, 4H), 3.81 (*t*, *J* = 4.6 Hz, 4H), 3.73-3.60 (*m*, 12H), 3.57-3.51 (*m*, 4H), 3.37 (*s*, 6H), 1.66 (*t*, *J* = 6.9 Hz, 3H), 1.60 (*t*, *J* = 6.9 Hz, 3H), 1.34 (*s*, 9H); ^{13}C NMR (68 MHz, CDCl$_3$): δ_C 162.77, 162.40, 161.44, 160.86, 160.50, 160.22, 160.02,

141.21, 140.85, 139.05, 137.94, 134.64, 132.32, 129.23, 128.39, 127.45, 123.92, 123.79, 119.98, 111.07, 110.83, 107.58, 100.56, 72.03, 70.88, 70.75, 70.67, 69.70, 67.50, 66.72, 66.48, 59.15, 46.28, 43.88, 31.15, 14.91; ESI-HRMS $[M+H]^+$ calcd for $[C_{55}H_{65}N_2O_{14}S]^+$: 1009.4151; found: 1009.4141.
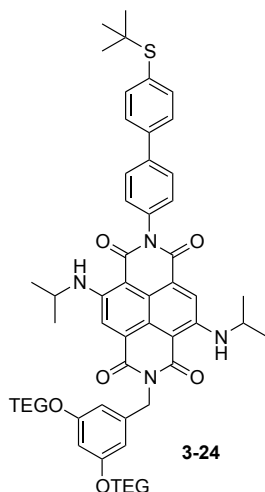
6.2.2.3.1.8 Synthesis of 2-(3,5-bis(2-(2-(2-methoxyethoxy)ethoxy)ethoxy)benzyl)-7-(4'-(tert-butylthio)biphenyl-4-yl)-4,9-bis(isopropylamino)benzo[lmn][3,8]phenanthroline-1,3,6,8(2H,7H)-tetraone 3-24

3-24

A solution of **3-23** (130 mg, 0.13 mmol) in iPrNH$_2$ (5 mL) was stirred at 110 °C for 48 h in a thick walled sealed tube. The reaction mixture was cooled down to 20 °C and volatiles were removed under reduced pressure. The crude residue was purified through silica gel column chromatography (Eluent: EtOAc) to give **3-24** as a blue solid (121 mg, 91%). M.p.: 158-161 °C. IR (film): ν (cm^{-1}) 3280, 2969, 2921, 2875, 1683, 1633, 1611, 1580, 1521, 1482, 1465, 1456, 1444, 1389, 1363, 1309, 1256, 1218, 1166, 1157, 1104, 1027, 1007, 944, 891, 842, 821, 805, 790, 765, 757, 749, 732, 706, 670, 628, 596, 568, 528, 507, 470; ^{1}H NMR (400 MHz, CDCl$_3$): δ_H 9.33 (*d*, *J* = 7.8 Hz, -N*H*), 9.26 (*d*, *J* = 7.8 Hz, -N*H*), 8.21 (*s*, 1H), 8.20 (*s*, 1H), 7.79 (*d*, *J* = 8.5 Hz, 2H), 7.62 (*dd*, *J* = 10.5 and 8.0 Hz, 4H), 7.42 (*d*, *J* = 8.2 Hz, 2H), 6.63 (*d*, *J* = 1.6 Hz, 2H), 6.39 (*br.s*, 1H), 5.31 (*s*, 2H), 4.14-4.05 (*m*, 6H), 3.82 (*t*, *J* = 4.5 Hz, 4H), 3.73-3.60 (*m*, 12H), 3.55-3.52 (*m*, 4H), 3.37 (*s*, 6H), 1.41 (*d*, *J* = 6.2 Hz, 6H), 1.37-1.32 (*m*, 12H); ^{13}C NMR (125 MHz, CD$_2$Cl$_2$): δ_C 166.79, 166.24, 163.46, 163.13, 160.41, 148.87, 148.70, 141.15, 141.00, 140.18, 138.23, 135.88, 132.89, 129.78, 128.36, 127.68, 126.42, 126.27, 121.71, 121.64, 119.10, 118.89, 107.18, 101.99, 101.81, 99.99, 72.30, 71.13, 70.91, 70.83, 70.00, 67.88, 59.0, 46.40, 44.66, 43.75, 31.22, 23.32, 23.22; ESI-HRMS $[M+Na]^+$ calcd for $[C_{57}H_{70}N_4O_{12}SNa]^+$: 1057.4603; found: 1057.4587.

6.2.2.3.1.9 **Synthesis** **of** **2-(3,5-bis(2-(2-(2-methoxyethoxy)ethoxy)ethoxy)benzyl)-4,9-bis(isopropylamino)-7-(4'-mercaptobiphenyl-4-yl)benzo[lmn][3,8]phenanthroline-1,3,6,8(2H,7H)-tetraone 3-12**
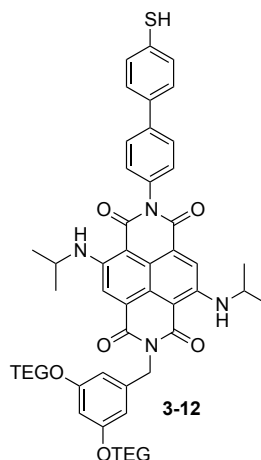

A solution of Hg(ClO$_4$)$_2$ (132 mg, 0.26 mmol) in MeOH (1 mL) was added under stirring to the solution of **3-24** (90.0 mg, 0.09 mmol) in CH$_2$Cl$_2$ (5 mL). The reaction mixture was stirred for 30 min. under argon. Freshly prepared H$_2$S was bubbled into the solution for 10 min and a black precipitate of HgS appeared. The reaction mixture was filtered through celite and washed with CH$_2$Cl$_2$. The organic solution was washed with water (2 × 50 mL), 5% NaHCO$_3$ (50 mL), and water (50 mL) and dried over MgSO$_4$. The solvent was removed under reduced pressure. The blue solid residue was purified through silica gel column chromatography (Eluent: EtOAc) to give **3-12** as a blue solid (61.0 mg, 72%). M.p.: 211-216 °C. IR (film): ν (cm^{-1}) 3279, 2970, 2923, 2875, 2566, 1683, 1632, 1581, 1523, 1483, 1465, 1444, 1389, 1367, 1308, 1256, 1222, 1200, 1168, 1104, 1081, 1028, 1005, 947, 892, 867, 841, 814, 802, 789, 765, 757, 747, 732, 705, 671, 630, 594, 568, 558, 535, 510, 471; ^{1}H NMR (400 MHz, CDCl$_3$): δ_H 9.28 (*br s*, -N*H*), 8.21 (*s*, 1H), 8.20 (*s*, 1H), 7.76 (*d*, *J* = 8.8 Hz, 2H), 7.53 (*d*, *J* = 8.0 Hz, 2H), 7.40 (*d*, *J* = 8.8 Hz, 2H), 7.38 (*d*, *J* = 8.8 Hz, 2H), 6.63 (*d*, *J* = 2 Hz, 2H), 6.39 (*br.s*, 1H), 5.31 (*s*, 2H), 4.11-4.05 (*m*, 6H), 3.82 (*t*, *J* = 4.7 Hz, 4H), 3.73-3.60 (*m*, 12H), 3.55-3.50 (*m*, 4H), 3.37 (*s*, 6H), 1.41 (*d*, *J* = 6.2 Hz, 6H), 1.35 (*d*, *J* = 6.4 Hz, 6H); ^{13}C NMR (100 MHz, CDCl$_3$): δ_C 166.61, 165.89, 163.37, 162.96, 160.03, 148.64, 148.34, 141.09, 139.35, 138.04, 134.75, 130.52, 129.88, 129.13, 128.16, 128.76, 126.08, 126.00, 121.53, 121.42, 119.02, 118.95, 107.20, 101.88, 101.52, 100.31, 72.01, 70.86, 70.72, 70.65, 69.78, 67.46, 59.12, 44.38, 43.54, 23.24, 22.12; ESI-HRMS [M+Na]$^+$ calcd for [C$_{53}$H$_{62}$N$_4$O$_{12}$SNa]$^+$: 1001.3977; found: 1001.3960; UV/Vis (DMF) λ_{max}, nm (ε, L mol^{-1} cm^{-1}): 612 (23500), 584 (14500), 362 (15900), 345 (14700), 281 (71255). Fluorescence (DMF) λ_{max}, nm: 641. Quantum Yield = 33% (determined from N,N'-di(2,6-diisopropylphenyl)-1,6,7,12-tetraphenoxyperylene-3,4 :9,10-tetracarboxylic acid bisimide (0.96 in CHCl$_3$)).[18]

The quantum yields were calculated using the following equation:

$$QY_X = QY_S \times (A_S I_X / A_X I_S) \times (n_x/n_s)^2$$

Where *QY* is the fluorescence quantum yield, *A* is the absorbance at the excitation wavelength, *I* is the integrated area of fluorescence emission, and n is the refractive index of the solvent used. Subscripts s and x refer to the standard and to the unknown, respectively.

6.2.2.3.2 Synthesis of red chromophore 3-13 (R-PDI)
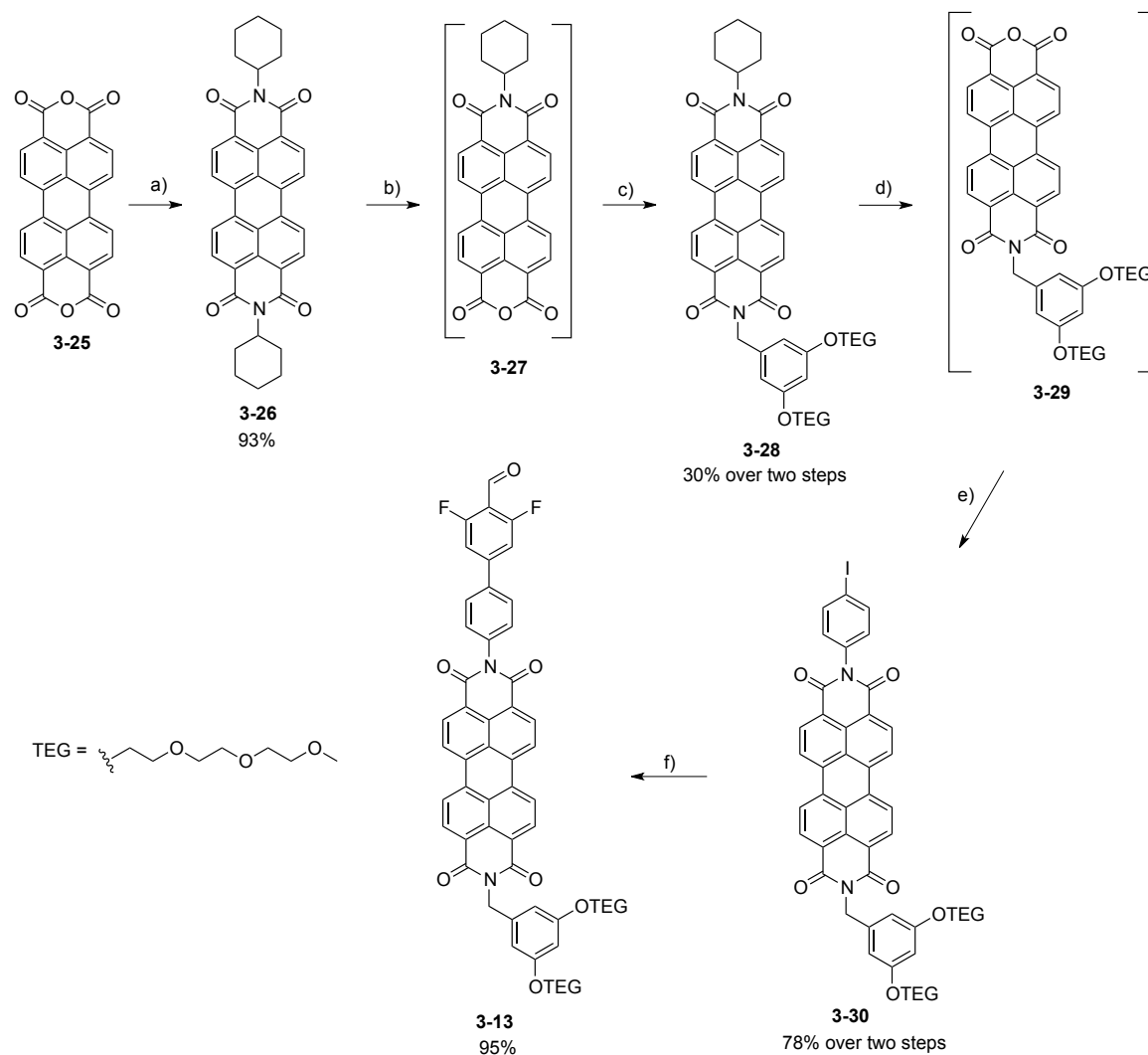
Scheme 6-16 Synthesis of R-PDI **3-13**; a) cyclohexylamine, 140 °C, 15 h; b) *i)* KOH, iPrOH/H$_2$O (6:1), 80 °C, 3 h, *ii)* AcOH, rt, 15 min; c) **3-16**, imidazole, toluene/DMF (6:1), 110 °C, 16 h; d) *i)* KOH, iPrOH/H$_2$O (6:1), 80 °C, 3 h, *ii)* AcOH, rt, 15 min; e) iodo-aniline, imidazole, toluene/DMF (6:1), 110 °C, 16 h; f) 2,6-difluoro-4-formylphenylboronic acid, K$_2$CO$_3$, [Pd(PPh$_3$)$_4$], dioxane/H$_2$O (7:1).

6.2.2.3.2.1 Synthesis of *N,N'*-dicyclohexyl-perylene-3,4,9,10- tetracarboxylic acid bisimide 3-26

3-26
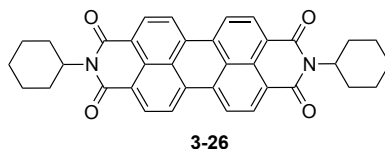
N,N'-dicyclohexyl-perylene-3,4,9,10- tetracarboxylic acid bisimide **3-26** has been synthesized according to the literature procedure.[19]

6.2.2.3.2.2 Synthesis of *N*-(Cyclohexyl)-3,4,9,10-perylenetetracarboxylic acid-3,4- anhydride-9,10-imide 3-27

3-27
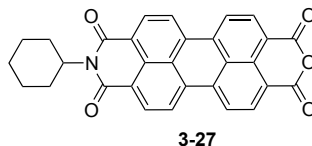
To a solution of **3-26** (1.21 g, 2.18 mmol) in H_2O/iPrOH (1:6) (82 mL), was added KOH pellets (6.11 g, 109 mmol). The reaction mixture was stirred at 85 °C for 3 h. The mixture was poured under stirring into AcOH (120 mL) was stirred at rt for 15 min. The product was extracted with CH_2Cl_2 and washed with H_2O. The organic phase was washed with brine and the solvents were evaporated under reduced pressure to give **3-27** as purple insoluble solid. The crude material was used for the next step without any further purification and characterization due to its very poor solubility.

6.2.2.3.2.3 Synthesis of *N-N'*-(Cyclohexyl)-(3,5-di(monomethyl ether triethylene glycol)-benzyl)-perylene-3,4,9,10- tetracarboxylic acid bisimide 3-28
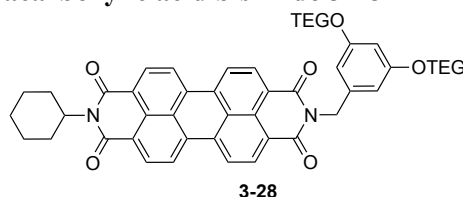

3-28

To the crude material **3-27** (421 mg) and imidazole (787 mg, 11.57 mmol) dispersed in toluene (45 mL), was added **3-17** (576 mg, 1.33 mmol) in DMF (7.8 mL). The resulting mixture was stirred at 110 °C for 16 h. The solvents were evaporated and the residue was partitioned between CH_2Cl_2 and an aqueous solution of HCl (1M). The organic phase was dried with $MgSO_4$ and filtrated to remove the unreacted starting material. The solvent was evaporated and the crude material was purified through silica gel column chromatography (Eluent: CH_2Cl_2 / EtOH 25:1) to give **3-28** as a dark purple solid (200 mg, 30% over 2 steps). M.p. > 250 °C. IR (film): ν (cm^{-1}) 2873, 1693, 1649, 1593, 1339, 1171, 1115, 809, 747.^{1}H NMR (400 MHz, CDCl$_3$): δ_H 8.44 (*d, J =* 8 Hz, 2H), 8.31 (*d, J =* 8 Hz, 2H), 8.19 (*d, J =* 8 Hz, 2H), 8.12 (*d, J =* 8 Hz, 2H), 6.68 (*d, J =* 2 Hz, 2H), 6.39 (*t, J =* 2 Hz, 1H), 5.25 (*s*, 2H), 5.08-5.01 (*m*, 1H), 4.09 (*t, J =* 4.8 Hz, 4H), 3.82 (*t, J*

= 4.8 Hz, 4H), 3.71-3.69 (*m*, 4H), 3.65-3.60 (*m*, 8H), 3.53-3.50 (*m*, 4H), 3.34 (*s*, 6H), 2.63-2-54 (*m*, 2H), 1.97-1.75 (*m*, 5H), 1.55-1.37 (*m*, 3H). ^{13}C NMR (100 MHz, CDCl$_3$): δ_C 163.44, 162.70, 160.00, 139.20, 133.88, 133.38, 130.86, 130.78, 128.78, 128.60, 125.49, 125.40, 123.77, 122.70, 122.57, 122.47, 107.87, 100.81, 71.97, 70.84, 70.70, 70.61, 69.76, 67.52, 59.09, 54.24, 43.66, 29.20, 26.70, 25.60.
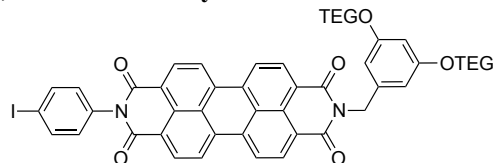
6.2.2.3.2.4 Synthesis of *N-N'*-(4-iodophenyl)-(3,5-di(monomethyl ether triethylene glycol)-benzyl)-perylene-3,4,9,10- tetracarboxylic acid bisimide 3-30


3-30

To a solution of **3-28** (48 mg, 0.05 mmol) in a mixture of H$_2$O/iPrOH (1:6) (3.5 mL), was added KOH pellets (152 mg, 2.7 mmol). The reaction mixture was stirred at 85 °C for 3 h and poured into AcOH (10 mL). The resulting mixture was stirred at rt for 15 min. The product was extracted with CH$_2$Cl$_2$ and washed with H$_2$O. The organic phase was washed with brine and the solvents were evaporated under reduced pressure to give **3-29** as a dark purple solid (45 mg, quant.). The product was used without any further purification. IR (film): ν (cm^{-1}) 2877, 1690, 1652, 1593, 1577, 1337, 1201, 1170, 1121, 1067, 810, 748. ^{1}H NMR (CDCl$_3$, 400 MHz): δ_H 8.69 (*d, J* = 8 Hz, 4H), 8.63 (*d, J* = 7.2 Hz, 4H), 6.69 (*d, J* = 2 Hz, 2H), 6.39 (*t, J* = 2 Hz, 1H), 5.32 (*s*, 2H), 4.08 (*t, J* = 4.8 Hz, 4H), 3.81 (*t, J* = 4.8 Hz, 4H), 3.74-3.69 (*m*, 4H), 3.67-3.62 (*m*, 8H), 3.56-3.52 (*m*, 4H), 3.35 (*s*, 6H).

To the crude material of monoanhydride **3-29** (46 mg, 0.06 mmol), imidazole (50 mg, 0.74 mmol) and 4-iodoaniline were dispersed in toluene (3.5 mL) and DMF (0.5 mL). The reaction mixture was stirred at 110 °C for 16 h. The solvents were evaporated under reduced pressure and the residue was partitioned between CH$_2$Cl$_2$ and an aqueous solution of HCl (1M). The aqueous phase was extracted with CH$_2$Cl$_2$ and the combined organic phases were dried and evaporated under reduced pressure. The crude mixture was purified through silica gel preparative plate (Eluent: CH$_2$Cl$_2$/EtOH 25:1) to remove the excess of 4-iodoaniline and afford **3-30** as a red solid (45 mg, 78% over two steps). M.p. > 250 °C. IR (film): ν (cm^{-1}) 2873, 1698, 1653, 1593, 1579, 1366, 1172, 1124, 1103, 1068, 850, 842, 809, 747, 513. ^{1}H NMR (400 MHz, CDCl$_3$): δ_H 8.42 (*d, J* = 8 Hz, 2H), 8.11 (*d, J* = 8 Hz, 2H), 8.03 (*d, J* = 8 Hz, 2H), 7.92 (*d, J* = 8.8 Hz, 2H), 7.88 (*d, J* = 8 Hz, 2H), 7.25 (*d, J* = 8.8 Hz, 2H), 6.64 (*d, J* = 1.6 Hz, 2H), 6.40 (*t, J* = 1.6 Hz, 1H), 5.19 (*s*, 2H), 4.09 (*t, J* = 4.8 Hz, 4H), 3.82 (*t, J* = 4.8 Hz, 4H), 3.71-3.69 (*m*, 4H), 3.65-3.60 (*m*, 8H), 3.51-3.49 (*m*, 4H), 3.33 (*s*, 6H). ^{13}C NMR (100 MHz, CDCl$_3$): δ_C 163.00, 162.63, 160.01, 139.08, 138.76,

134.91, 134.13 133.50, 131.33, 130.88, 130.78, 129.20, 128.40, 125.61, 125.31, 122.96, 122.77, 122.47, 107.82, 100.72, 94.91, 71.97, 70.83, 70.68, 70.59, 69.75, 67.51, 59.10, 43.77 (one Car missing possibly due overlapping). ESI-HRMS [M+H]$^+$ calcd for [C$_{51}$H$_{48}$IN$_2$O$_{12}$]$^+$: 1007.2246, found: 1007.2235.

6.2.2.3.2.5 Synthesis of *N-N'*-(3,5-difluoro-(1,1'-biphenyl)-4-carbaldehyde)-(3,5-di(monomethyl ether triethylene glycol)-benzyl)-perylene-3,4,9,10- tetracarboxylic acid bisimide 3-13

3-13
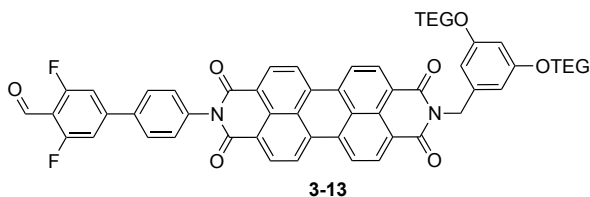
In a Schlenk tube, **3-30** (39 mg, 0.04 mmol) and K$_2$CO$_3$ (20 mg, 0.14 mmol) were dissolved in dioxane (3.5 mL) and water (0.5 mL). After degassing the solution, 3,5-difluoro-4-formylphenylboronic acid (11 mg, 0.058 mmol) and [Pd(PPh$_3$)$_4$] (4.5 mg, 0.004 mmol) were added. The reaction mixture was stirred at 80 °C for 20 h. Then, it was poured in CH$_2$Cl$_2$ and washed with H$_2$O. The organic phase was washed with brine, dried and concentrated under reduced pressure. The crude material was precipitated and in a mixture AcOEt/Et$_2$O (1:2) to remove the catalyst and the excess of boronic acid to give **3-13** as a red solid (38 mg, 95%). M.p. > 250 °C. IR (film): ν (cm^{-1}) 2875, 1696, 1660, 1634, 1595, 1365, 1339, 1248, 1173, 1126, 1103, 810. ^{1}H NMR (400 MHz, CDCl$_3$): δ_H 10.40 (*s*, 1H), 8.70 (*d*, *J* = 8 Hz, 2H), 8.59 (*d*, *J* = 8 Hz, 2H), 8.54 (*d*, *J* = 8 Hz, 2H), 8.49 (*d*, *J* = 8 Hz, 2H), 7.81 (*d*, *J* = 8.4 Hz, 2H), 7.57 (*d*, *J* = 8.4 Hz, 2H), 7.32-7.26 (*m*, 2H), 6.67 (*d*, *J* = 2 Hz, 2H), 6.40 (*br s*, 1H), 5.31 (*s*, 2H), 4.09 (*t*, *J* = 4.4 Hz, 4 H), 3.81 (*t, J* = 4.8 Hz, 4H), 3.71-3.69 (*m*, 4H), 3.65-3.60 (*m*, 8H), 3.54-3.49 (*m*, 4H), 3.35 (*s*, 6H). ^{13}C NMR not obtained due to the poor solubility of **3-13**. ESI-HRMS [M+Na]$^+$ calcd for [C$_{58}$H$_{50}$F$_2$N$_2$NaO$_{13}$]$^+$: 1043.3173, found: 1043.3167. UV/Vis (DMF) λ$_{max}$, nm (ε, L mol^{-1} cm^{-1}): 527 (85500), 491 (54500), 460 (20300), 288 (36600). Fluorescence (DMF) λ$_{max}$, nm: 540, 579. Quantum Yield = 0.04 (determined from *N,N'*-di(2,6-diisopropylphenyl)-1,6,7,12-tetraphenoxyperylene- 3,4 :9,10-tetracarboxylic acid bisimide (0.96 in CHCl$_3$)).[18]

6.2.2.3.3 Synthesis of yellow chromophore 3-14 (Y-Py)
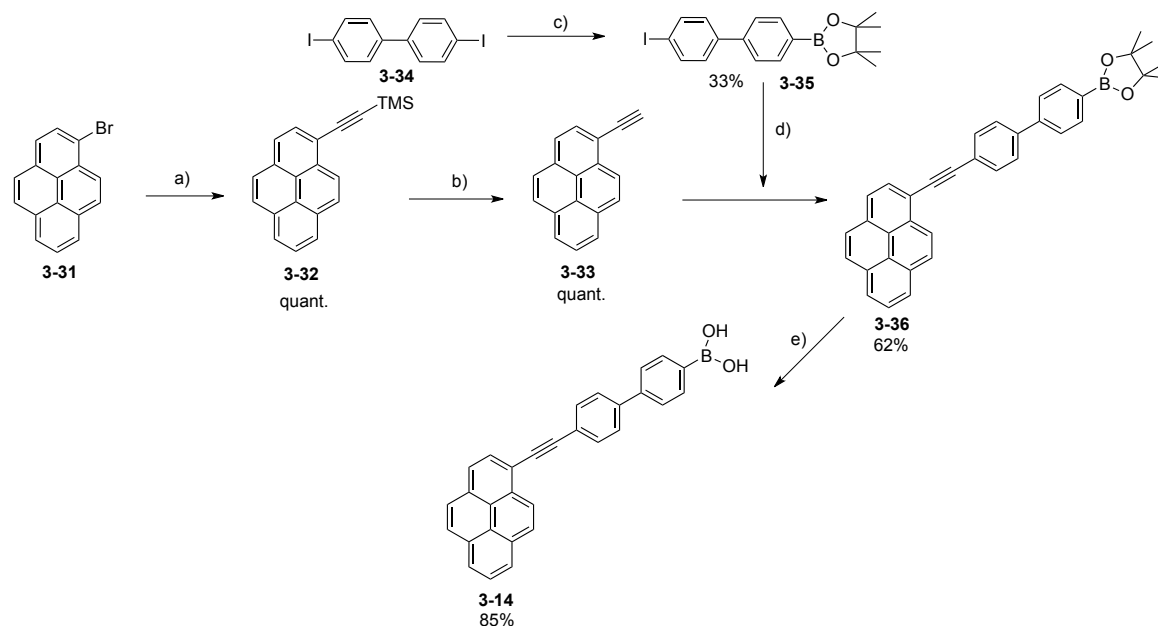
Scheme 6-17 Synthesis of Y-Py **3-14**; a) TMS-acetylene, [Pd(PPh₃)₂Cl₂], CuI, NEt₃, 70 °C, 20 h; b) K₂CO₃, MeOH/THF (1:1), rt, 20 h; c) KOAc, B₂Pin₂, [PdCl₂(dppf)], DMSO, 80 °C, 20 h d) [Pd(PPh₃)₂Cl₂], CuI, NEt₃, THF, 40 °C, 6 h; e) HCl (aq, 2M)/THF (1:2), rt, 40 h.

6.2.2.3.3.1 Synthesis of trimethyl(pyren-1-ylethynyl)silane 3-32
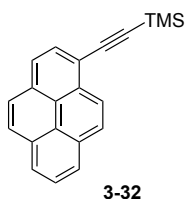
To a degassed solution of 1-bromopyrene **3-31** (505 mg, 1.8 mmol) in dry Et₃N (60 mL), were successively added [Pd(PPh₃)₂Cl₂] (126 mg, 0.18 mmol), CuI (126 mg, 0.18 mmol) and TMS-acetylene (1.26 mL, 8.98 mmol). The reaction mixture was stirred at 70 °C for 20 h. The solvent was evaporated under reduced pressure and the crude material was purified through silica gel column chromatography (Eluent: cyclohexane) to give **3-32** as a yellow oil (536 mg, quant.). IR (film): ν (cm⁻¹) 3041, 2957, 2898, 2149, 1738, 1600, 1582, 1487, 1407, 1365, 1248, 1184, 895, 836, 821, 756, 715, 633. ¹H NMR (400 MHz, CDCl₃) δ 8.57 (*d*, *J* = 9.2 Hz, 1H), 8.23-8.14 (*m*, 4H), 8.08 (*d*, *J* = 8.4 Hz, 2H), 8.04-8.01 (*m*, 2H), 0.42 (*s*, 9H); ¹³C NMR (100 MHz, CDCl₃) δ 132.39, 131.51, 131.33, 131.16, 130.06, 128.53, 128.36, 127.36, 126.34, 125.80, 125.71, 125.68, 124.51, 124.39, 117.74, 104.22, 100.36, 0.35 (one C_Ar missing possibly due to overlapping).

6.2.2.3.3.2 Synthesis of 1-ethynylpyrene 3-33

3-33
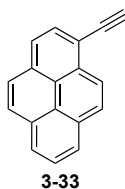
To a solution of **3-32** (512 mg, 1.72 mmol) in THF/MeOH (1:1) (20 mL), was added K_2CO_3 (1.42 g, 10.3 mmol). The suspension was stirred at rt for 20 h. H_2O was added and the aqueous phase was extracted with CH_2Cl_2. The organic phase was washed with brine, dried and concentrated under reduced pressure to give **3-33** as brown crystals (387 mg, quant.). M.p.: 105 °C. IR (film): ν (cm^{-1}) 3296, 3034, 2970, 2094, 1888, 1738, 1602, 1582, 1433, 1365, 1229, 1217, 1184, 965, 847, 836, 714, 641, 592. ^{1}H NMR (400 MHz, CDCl$_3$) δ 8.59 (*d*, *J* = 8.8 Hz, 1H), 8.23-8.16 (*m*, 4H), 8.09 (*d*, *J* = 9.2 Hz, 2H), 8.05-8.01 (*m*, 2H), 3.64 (*s*, 1H); ^{13}C NMR (100 MHz, CDCl$_3$) δ 132.60, 131.71, 131.28, 131.09, 130.27, 128.67, 128.52, 127.29, 126.40, 125.85, 125.80, 125.42, 124.49, 124.45, 124.30, 116.61, 82.74 (one C_{Ar} missing possibly due to overlapping). ESI-HRMS [M+H]$^+$ calcd for [C$_{18}$H$_{11}$]$^+$: 227.0854, found: 227.0855.

6.2.2.3.3.3 Synthesis of 2-(4'-iodo-[1,1'-biphenyl]-4-yl)-4,4,5,5-tetramethyl-1,3,2-dioxaborolane 3-35

3-35
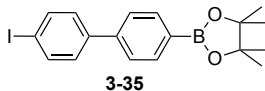
To a suspension of 4,4'-diiodo biphenyl (1 g, 2.46 mmol), KOAc (725 mg, 7.39 mmol) in DMSO (30 mL), were added B$_2$Pin$_2$ (687 mg, 2.71 mmol) and [PdCl$_2$(dppf)] (100 mg, 0.12 mmol). The reaction mixture was stirred at 80 °C for 20 h under argon. H_2O was added and the aqueous phase was extracted with CH_2Cl_2. The organic phase was washed with brine, dried and concentrated under reduced pressure. The crude residue was purified by silica gel column chromatography (Eluent: pentane to pentane/CH$_2$Cl$_2$ 1:1) to give **3-35** as a white solid (330 mg, 33%). M. p.: 143 °C. IR (film): ν (cm^{-1}) 2978, 1607, 1399, 1362, 1324, 1301, 1145, 1094, 999, 859, 810, 743, 672, 656; ^{1}H NMR (400 MHz, CDCl$_3$) δ 7.88 (*d*, *J* = 8 Hz, 2H), 7.76 (*d*, *J* = 8 Hz, 2H), 7.56 (*d*, *J* = 8 Hz, 2H), 7.35 (*d*, *J* = 8 Hz, 2H), 1.37 (*s*, 12H); ^{13}C NMR (100 MHz, CDCl$_3$) δ 142.79, 140.63, 138, 135.51, 129.18, 126.29, 93.56, 84.03, 25.02 (C$_{Ar-B}$ not observed); ESI-HRMS [M+H]$^+$ calcd for [C$_{18}$H$_{20}$BIO$_2$]$^+$: 406.0677, found: 406.0676.

6.2.2.3.3.4 Synthesis of 4,4,5,5-tetramethyl-2-(4'-(pyren-1-ylethynyl)-[1,1'-biphenyl]-4-yl)-1,3,2-dioxaborolane 3-36

3-36
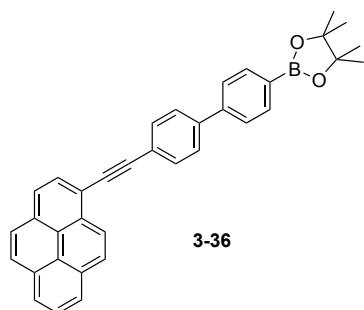
To a solution of 1-ethynylpyrene **3-33** (166 mg, 0.74 mmol) and 2-(4'-iodo-[1,1'-biphenyl]-4-yl)-4,4,5,5-tetramethyl-1,3,2-dioxaborolane **3-35** (388 mg, 0.96 mmol) in THF (8 mL), was added Et$_3$N (0.52 mL, 3.7 mmol). The solution was degassed under argon and CuI (28 mg, 0.15 mmol) and [Pd(PPh$_3$)$_2$Cl$_2$] (52 mg, 0.07 mmol) were successively added. The reaction mixture was stirred at 40 °C for 6 h under argon. H$_2$O was added and the aqueous phase was extracted with CH$_2$Cl$_2$. The organic phase was washed with brine, dried and concentrated under reduced pressure. The crude residue was precipitated in Et$_2$O. The filtrate was purified through silica gel column chromatography (Eluent: cyclohexane/EtOAc 9:1) to give an orange oil which was precipitated in MeOH affording **3-36** as an orange solid (230 mg, 62%). M. p.: 135 °C. IR (film): ν (cm^{-1}) 2970, 1738, 1607, 1527, 1435, 1360, 1229, 1217, 1142, 1092, 844, 819, 716, 656, 527; ^{1}H NMR (500 MHz, CDCl$_3$) δ 8.69 (*d, J* = 8.5 Hz, 1H), 8.25-8.20 (*m*, 4H), 8.15-8.04 (*m*, 4H), 7.93 (*d, J* = 8.5 Hz, 2H), 7.80 (*d, J* = 8.5 Hz, 2H), 7.71-7.67 (*m*, 4H), 1.39 (*s*, 12H); ^{13}C NMR (125 MHz, CDCl$_3$) δ 143.11, 141.01, 135.53, 132.27, 132.07, 131.44, 131.42, 131.25, 129.78, 128.52, 128.33, 127.42, 127.39, 126.48, 126.40, 125.81, 125.74, 125.72, 124.71, 124.66, 124.50, 122.89, 117.95, 95.21, 89.69, 84.04, 25.05 (C$_{Ar-B}$ not observed and one C$_{Ar}$ missing due to overlapping). ESI-HRMS [M+H]$^+$ calcd for [C$_{36}$H$_{30}$BO$_2$]$^+$: 505.2333, found: 505.2339.

6.2.2.3.3.5 Synthesis of (4'-(pyren-1-ylethynyl)-[1,1'-biphenyl]-4-yl)boronic acid 3-14

3-14
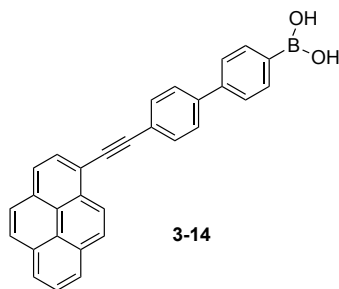
To a solution of **3-36** (44 mg, 0.087 mmol) in THF (15 mL) was added an aqueous solution of HCl (2 M, 7.5 mL). The reaction mixture was stirred at rt for 40 h. Water was added and the aqueous phase was extracted with CH$_2$Cl$_2$. The organic phase was dried and concentrated. The crude

residue was precipitated in a small amount of CHCl$_3$ to give **3-14** as a yellow solid. (31 mg, 85%). M. p.: 250 °C. IR (film): ν (cm^{-1}) 3627, 3211, 1602, 1527, 1416, 1379, 1334, 1132, 1002, 968, 847, 819, 716, 641, 613, 509; ^{1}H NMR (500 MHz, DMSO-d_6) δ 8.67 (*d*, *J* = 8.5 Hz, 1H), 8.40-8.22 (*m*, 8H), 8.15-8.10 (*m*, 3H), 7.93 (*d*, *J* = 7.5 Hz, 2H), 7.87 (*br s*, 3H), 7.75 (*d*, *J* = 7.5 Hz, 2H); ^{13}C NMR (125 MHz, DMSO-d_6) δ 140.50, 140.38, 134.91, 132.18, 131.12, 131.03, 130.81, 130.54, 129.67, 128.95, 128.47, 127.28, 127.07, 126.83, 126.08, 126.04, 125.68, 125.01, 124.89, 123.69, 123.42, 121.57, 116.73, 95.22, 89.15 (C$_{Ar-B}$ not observed); ^{11}B NMR (125 MHz, DMSO-d_6) δ 29.47; ESI-HRMS [M+H]$^+$ calcd for [C$_{30}$H$_{20}$BO$_2$]$^+$: 423.1552, found: 423.1556. UV/Vis (DMF) λ$_{max}$, nm (ε, L mol^{-1} cm^{-1}): 398 (44600), 375 (44200), 309 (36900), 286 (32300). Fluorescence (DMF) λ$_{max}$, nm: 408, 430. Quantum Yield = 0.68 (determined from quinine hemisulfate salt monohydrate (0.546 in 0.5 M H$_2$SO$_4$)).[20]

6.2.2.4 Chromophore assembly – Synthesis of peptide 3-37
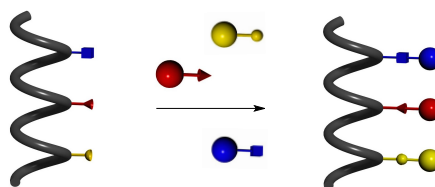
Ac-(QLAX(disulfide)QLA QLAX(hydrazide)QLA QLAX(diol)QLA)-NH$_2$ **3-1** (5.1 mg, 1.76.10^{-3} mmol), B-NDI **3-12** (5 mg, 5.28.10^{-3} mmol), R-PDI **3-13** (5.4 mg, 5.28.10^{-3} mmol), Y-pyrene **3-14** (2.2 mg, 5.28.10^{-3} mmol), *m*-phenylenediamine (0.1 mg, 8.8.10^{-4} mmol) were dissolved in anhydrous DMF (2 mL) and stirred at rt for 4 h. The mixture was poured in Et$_2$O to precipitate. After centrifugation, the ether was decanted and this washing was repeated 3 times to remove the DMF. The crude material was purified using gel permeation chromatography (GPC) with Bio-Rad Bio-Beads S-X1 Beads (operating range 600 – 14000 g.mol-1) as stationary phase with anhydrous DMF as eluent. The product was precipitated in cold Et$_2$O to give **3-37** as a purple solid.

HRMS [M+Na]$^+$ calcd for [C$_{265}$H$_{315}$BN$_{46}$O$_{56}$F$_2$NaS$_2$]$^+$: 5173.2261, found: 5173.2615. UV/Vis (DMF) λ$_{max}$, nm (ε, L mol^{-1} cm^{-1}): 612 (23500), 527 (58200), 495 (43700), 460 (19300), 398 (46300), 376 (54000); due to the high hygroscopy of peptide, molar extinction coefficients were obtained by normalizing the absorbance of the peptide and the arithmetic sum of dyes on B-NDI unit (612 nm). Fluorescence emission (DMF, 3 μM, exc 398 nm) λ$_{max}$, nm: 440, 641; (DMF, 3 μM, exc 527 nm) λ$_{max}$, nm: 538, 579, 641; (DMF, 3 μM, exc 612 nm) λ$_{max}$, nm: 641. Fluorescence excitation (DMF, 3 μM, emis 540 nm) λ$_{max}$, nm: 529, 491, 462, 399, 378; (DMF, 3 μM, emis 640 nm) λ$_{max}$, nm: 613, 529, 493, 462, 398, 363, 352.

6.2.2.5 Circular Dichroism Spectroscopy of 3-1

A stock solution of the peptide **3-1** dissolved in $H_2O/MeCN$ (1:1) was prepared. (C = 102 μM). A series of peptide solutions (51 μM) were then prepared by dissolving the stock solution in H_2O and/or TFE (0% TFE , 10% TFE (v/v_{final}) , 20% TFE, 50% TFE). Each solution was scanned between 190 and 250 nm, and the absorption spectra were corrected by subtraction of the spectra of the blank.

Figure 6-2 Circular Dichroism analysis of peptide **3-1** in CH_3CN/H_2O (1:1) dissolved in water and/or TFE (51 μM)

The estimations of the percentage values for the secondary structure elements α-helix, β-sheet and random coil was carried out via Dichroweb service (http://dichroweb.cryst.bbk.ac.uk) using the CONTINLL algorithm.[21] The determined values for the shown CD-spectra are given in Table 6-1.

Table 6-1 Content of secondary structure elements determined by CONTINLL

Peptide **3-1**/Conditions	% α-helix	% β-sheet	% random coil
0% TFE	87	1	12
10% TFE	89	1	10
20% TFE	89	1	10
50% TFE	87	1	12

6.2.2.6 Circular Dichroism Spectroscopy of 3-37

A stock solution of peptide **3-37** (102 μM) was prepared in TFE. A series of peptide solutions (34 μM) were then prepared by dissolving the stock solution in water and/or TFE **(100% TFE, 50/50**

TFE/H$_2$O (v/v$_{final}$) , 33/66% TFE/H$_2$O). Each solution was scanned between 190 and 700 nm, and the absorption spectra were corrected by subtraction of the spectra of the blank. The CD spectrum has been smoothed using Fast Fourier Transform (FFT) filter.
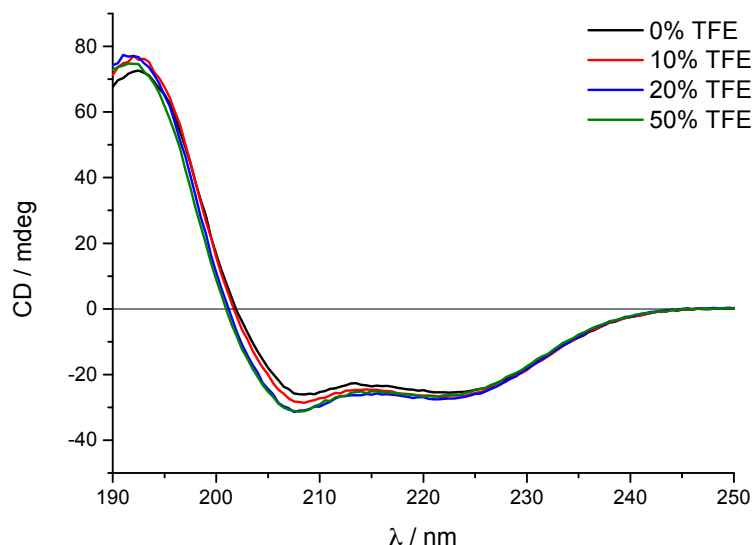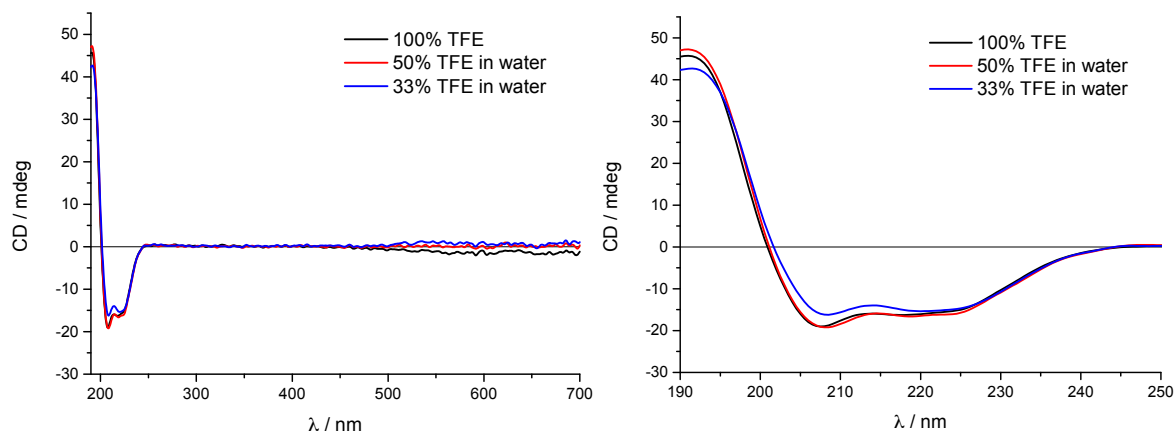

Figure 6-3 a) Circular Dichroism analysis of peptide **3-37** (34 µM) in water and/or TFE b) Zoom between 190 and 250 nm.

The calculations of the percentage values for the secondary structure elements α-helix, β-sheet and random coil were carried out via Dichroweb service (http://dichroweb.cryst.bbk.ac.uk) using the CONTINLL algorithm.[21] The determined values for the shown CD-spectra are given in Table 6-2.

Table 6-2 Content of secondary structure elements determined by CONTINLL

Peptide **3-37** /Conditions	% α-helix	% β-sheet	% random coil
100% TFE	78	4	18
50% TFE in water	82	2	16
33% TFE in water	78	4	18

6.2.3 Experimental procedures for Chapter 4

6.2.3.1 Synthesis of Y-Per 4-1
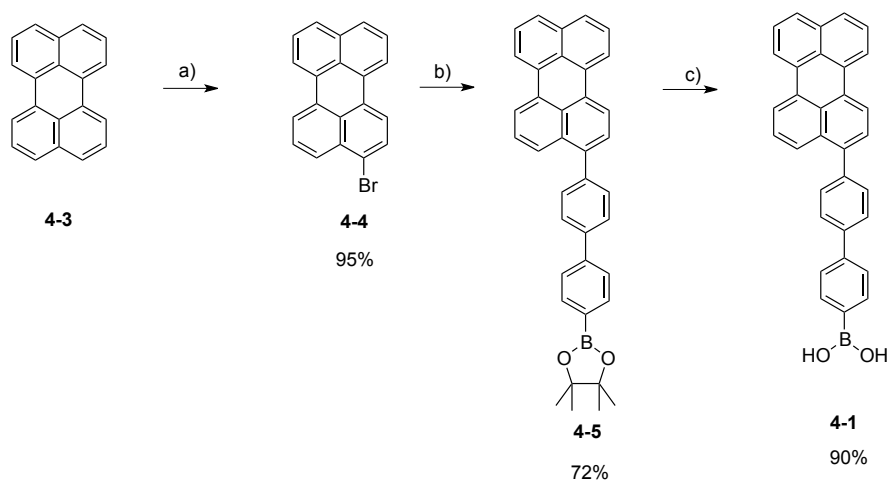
Scheme 6-18 Synthesis of Y-Per **4-1**; a) NBS, THF, rt, 24 h; b) 4,4'-biphenyldiboronic acid bis(pinacol)ester, K_2CO_3, [Pd(PPh$_3$)$_4$], dioxane/H$_2$O (6:1), 85 °C, 3 h; c) *i)* NaIO$_4$, THF/H$_2$O (4 :1), rt, 1 h 30, *ii)* HCl (1M), rt, 20 h.

6.2.3.1.1 Synthesis of 3-bromoperylene 4-4

3-bromoperylene **4-4** has been synthesized according to the literature.[22]

6.2.3.1.2 Synthesis of 4,4,5,5-tetramethyl-2-(4'-(perylen-3-yl)-[1,1'-biphenyl]-4-yl)-1,3,2-dioxaborolane 4-5
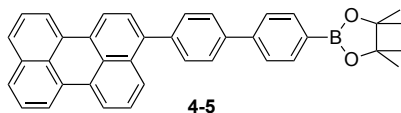
To a degassed solution of 3-bromoperylene **4-4** (88 mg, 0.26 mmol) and K_2CO_3 (144 mg, 1.04 mmol) in dioxane/H$_2$O (6:1) (14 mL) were successively added 4,4'-biphenyldiboronic acid bis(pinacol)ester (321 mg, 0.79 mmol) and [Pd(PPh$_3$)$_4$] (30 mg, 0.03 mmol). The reaction mixture was stirred at 85 °C for 3 h. H$_2$O was added and the aqueous phase was extracted with CH$_2$Cl$_2$. The organic phase was washed with brine, dried and concentrated under reduced pressure. The residue was precipitated and washed with MeOH to remove the excess of bis-boronic ester and the solid was purified by recycling GPC on a *JAI LC-9160NEXT* using GPC columns *JAIGEL-2HH, 2.5HH* and *3HH* (Eluent: CHCl$_3$) to afford **4-5** as a yellow solid (100 mg, 72%). M.p.> 250 °C; IR (neat): ν (cm^{-1}) 2975, 1607, 1389, 1362, 1147, 1093, 862, 820, 769, 656; ^{1}H NMR (300 MHz, CDCl$_3$): δ_H 8.26-8.20 (*m*, 4H), 7.95 (*d*, *J* = 8.3 Hz, 2H), 7.85 (*d*, *J* = 8.5 Hz, 1H), 7.77 (*d*, *J* = 8.3

Hz, 2H), 7.71 (*t*, *J* = 8.3 Hz, 4H), 7.61 (*d*, *J* = 8.3 Hz, 2H), 7.52-7.42 (*m*, 4H), 1.39 (*s*, 12H); ^{13}C NMR (75 MHz, CDCl$_3$): δ_C 143.56, 140.22, 140.13, 139.63, 135.51, 134.84, 133.06, 131.58, 131.55, 131.37, 130.89, 130.55, 129.25, 128.80, 127.96, 127.95, 127.90, 127.34, 126.78, 126.73, 126.56, 126.21, 120.55, 120.51, 120.30, 120.10, 84.01, 25.04 (2C$_{Ar}$ missing possibly due to overlapping); ESI-HRMS [M+H]$^+$ calcd for [C$_{38}$H$_{31}$BO$_2$]$^+$: 531.2496, found: 531.2476.

6.2.3.1.3 Synthesis of (4'-(perylen-3-yl)-[1,1'-biphenyl]-4-yl)boronic acid 4-1
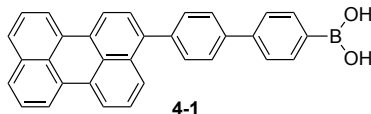
A solution of boronic ester **4-5** (32 mg, 0.06 mmol) and NaIO$_4$ (77 mg, 0.36 mmol) in THF/H$_2$O (6 mL/1.5 mL) was stirred at rt for 2 h. An aq. solution of HCl (1 M) (1.5 mL) was added and the reaction was stirred at rt for 20 h. H$_2$O was added and the aq. phase was extracted with CH$_2$Cl$_2$. The organic phase was washed with brine, dried and concentrated under reduced pressure. The residue was precipitated with a minimum of CHCl$_3$ to give **4-1** as a yellow solid (24 mg, 90%). M.p.> 250 °C; IR (neat): ν (cm^{-1}) 3344, 1603, 1524, 1494, 1387, 1344, 1119, 1044, 1020, 1003, 822, 812, 769, 733, 647, 607, 583, 533; ^{1}H NMR (300 MHz, DMSO-*d$_6$*): δ_H 8.44-8.38 (*m*, 3H), 8.15-8.11 (*m*, 2H), 7.94 (*d*, *J* = 8 Hz, 2H), 7.87 (*d*, *J* = 8 Hz, 2H), 7.78 (*d*, *J* = 8 Hz, 2H), 7.78-7.74 (*m*, 3H), 7.68-7.50 (*m*, 5H); ^{13}C NMR (125 MHz, DMSO-*d$_6$*): δ_C 141.53, 141.08, 139.31, 139.14, 138.92, 134.90, 134.78, 134.31, 132.20, 130.90, 130.57, 130.39, 130.27, 130.09, 128.38, 128.06, 128.03, 127.91, 127.83, 127.17, 127.01, 126.91, 125.67, 125.54, 121.00, 120.99, 120.77, 120.54; ESI-HRMS [M+H]$^+$ calcd for [C$_{32}$H$_{22}$BO$_2$]$^+$: 449.1713, found: 449.1678. UV/Vis (DMF) λ_{max}, nm (ε, L mol^{-1} cm^{-1}): 449 (34700), 424 (28700). Fluorescence (DMF) λ_{max}, nm: 470, 496. Quantum Yield = 70% determined in DMF using perylene as standard (QY=94% in cyclohexane).[23]

6.2.3.2 Synthesis of R-PDI 4-2

Scheme 6-19 Synthesis of new R-PDI **4-2**; a) BnBr, K₂CO₃, EtOH, reflux, 3 h; b) NaH, TEG-OTs, THF, reflux, 20 h; c) H₂, Pd/C, MeOH, rt, 20 h; d) *i)* PDA, Et₃N, iPrOH/H₂O, 120 °C, 10 d, *ii)* 5% HCl (aq), 120 °C, 10 min; e) 4-bromo-2,6-diisopropylaniline, propionic acid, MW irr, 140 °C, 7 h; f) 3,5-difluoro-4-formylphenyl boronic acid, K₂CO₃, [Pd(PPh₃)₄], dioxane/H₂O, 80 °C, 20 h.

6.2.3.2.1 Synthesis of 2-(dibenzylamino)propane-1,3-diol 4-8

2-(dibenzylamino)propane-1,3-diol **4-8** has been synthesized according to the literature.[24]

6.2.3.2.2 Synthesis of *N,N*-dibenzyl-2,5,8,11,15,16,19,24-octaoxapentacosan-13-amine 4-9

Compound **4-9** has been synthesized according to the literature.[25]

6.2.3.2.3 Synthesis of 2,5,8,11,15,16,19,24-octaoxapentacosan-13-amine 4-10 (bis-TEG-amine)


4-10
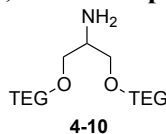
Bis-TEG-amine **4-10** has been synthesized according to the literature.[25]

6.2.3.2.4 Synthesis of *N*-(bis-TEG-amine)- perylene-3,4,9,10- tetracarboxylic acid monoimide monoanhydride 4-11

4-11
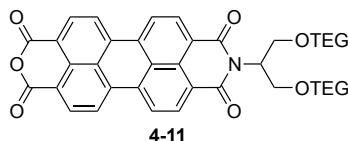
To a mixture of perylenedianhydride (624 mg, 1.58 mmol) and bis-TEG-amine **4-10** (600 mg, 1.56 mmol) in *i*PrOH/water (1:1, 60 mL), triethylamine (2.85 g, 20.28 mmol) was added, and the reaction was heated for 10 d at 110 °C. The reaction mixture was treated with excess 5% HCl at 120 °C for 10 min and cooled to room temperature. The reaction mixture was extracted with CH_2Cl_2 and the organic phases were combined and evaporated under reduced pressure to afford a red waxy solid (1.13 g). The crude material was not purified due to the low solubility of the compound however a small amount was filtrated through silica gel pad (Eluent: CH_2Cl_2/acetone 1:1) to characterize **4-11**. IR (film): ν (cm^{-1}) 2870, 1766, 1653, 1591, 1575, 1317, 1101, 1028, 810, 748, 736; ^{1}H NMR (300 MHz, CDCl$_3$) δ_H 8.63-8.45 (*m*, 8H), 5.74-65 (*m*, 1H), 4.21 (*dd*, *J* = 10.6, 7.9 Hz, 2H), 3.96 (*dd*, *J* = 10.6, 5.7 Hz, 2H), 3.78-3.40 (*m*, 24H), 3.31 (*s*, 6H); ^{13}C NMR not obtained due to the low solubility of the compound. ESI-HRMS [M+Na]$^+$ calcd for [$C_{41}H_{43}NO_{13}Na$]+: 780.2632; found: 780.2633.

6.2.3.2.5 Synthesis of *N,N'*-2-(4-bromo-2,6-diisopropylphenyl)-(bis-PEG-amine)-perylene-3,4,9,10- tetracarboxylic acid bisimide 4-12

4-12
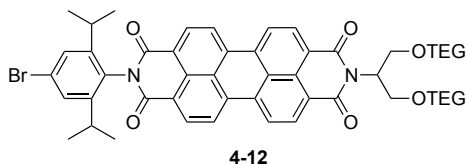
In a microwave reactor, crude monoanhydride **4-11** (92 mg) and 4-bromo 2,6-disopropylaniline (250 mg, 0.97 mmol) were suspended in propionic acid (3 mL). The mixture was stirring at 140 °C for 7 h under microwave irradiations. The solvent was evaporated under reduced pressure. The crude material was precipitated in diethyl ether, filtered-off and the filtrate was purified by column chromatography on silica gel (CH_2Cl_2 to CH_2Cl_2/EtOH 97:3) affording bromo derivative **4-12** as a red oil (46 mg, 38% over two steps). IR (film): ν (cm^{-1}) 2966, 2868, 1695, 1657, 1591, 1576, 1339, 1252, 1099, 842, 808, 746; ^{1}H NMR (300 MHz, CDCl$_3$) δ_H 8.75 (*d*, *J* = 8 Hz, 2H), 8.61 (*d*, *J* = 8

Hz, 2H), 8.59-8.52 (*m*, 4H), 7.46 (*s*, 2H), 5.77-5.62 (*m*, 1H), 4.19 (*dd*, *J* = 10.5, 7.9 Hz, 2H), 3.93 (*dd*, *J* = 10.5, 5.8 Hz, 2H), 3.77-3.40 (*m*, 24H), 3.33 (*s*, 6H), 2.82-2.68 (*m*, 2H), 1.18 (*d*, *J* = 6.8 Hz, 12H). ^{13}C NMR (75 MHz, CDCl$_3$) δ_C 163.85, 163.47, 148.29, 135.28, 134.34, 132.30, 131.55, 130.23, 129.92, 129.59, 127.81, 126.79, 126.35, 124.20, 123.70, 123.39, 123.17, 123.06, 71.99, 70.63, 70.58, 70.44, 69.33, 59.13, 52.25, 29.46, 23.96 (two CH$_2$ missing probably due to overlapping). ESI-HRMS [M+Na]+ calcd for [C$_{53}$H$_{59}$BrN$_2$O$_{12}$Na]$^+$: 1017.3149; found: 1017.3145.

6.2.3.2.6 Synthesis of *N-N'*-(3,5-difluoro-3',5'-diisopropyl-(1,1'-biphenyl)-4-carbaldehyde)-(bis-PEG-amine)-perylene-3,4,9,10- tetracarboxylic acid bisimide 4-2

4-2
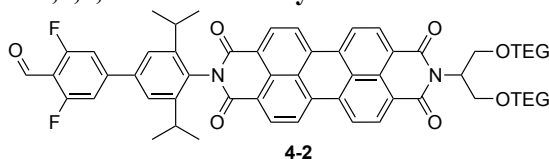
Bromo derivative **4-12** (15 mg, 0.02 mmol) and K$_2$CO$_3$ (8 mg, 0.06 mmol) under N$_2$ were dissolved in dioxane (3.5 mL) and H$_2$O (0.5 mL). The solution was deoxygenated and the boronic acid (6 mg, 0.03 mmol) and [Pd(PPh$_3$)$_4$] (2 mg, 0.002 mmol) were quickly added. The reaction mixture was stirred at 80 °C for 20 h. The reaction was diluted in CH$_2$Cl$_2$ and washed with HCl 5% (aq). The layers were separated and the aqueous phase was extracted with CH$_2$Cl$_2$. The combined organic phases were washed with brine, dried with MgSO$_4$ and concentrated under reduced pressure. The crude residue was purified by recycling GPC on a *JAI LC-9160NEXT* using GPC columns *JAIGEL-2HH, 2.5HH* and *3HH* (Eluent: CHCl$_3$) to remove the excess of boronic acid affording aldehyde **4-2** as a red oil (14 mg, 90%). IR (film): ν (cm^{-1}) 2872, 1697, 1661, 1628, 1593, 1433, 1404, 1342, 1252, 1196, 1109, 1040, 837, 810, 748, 403; ^{1}H NMR (600 MHz, CDCl$_3$) δ_H 10.41 (*s*, 1H), 8.78 (*d*, *J* = 8.0 Hz, 2H), 8.67 (*d*, *J* = 8.0 Hz, 2H), 8.71-8.63 (*m*, 4H), 7.53 (*s*, 2H), 7.30 (*d*, *J* = 9.8 Hz, 2H), 5.76-5.71 (*m*, 1H), 4.20 (*dd*, *J* = 10.5, 7.8 Hz, 2H), 3.96 (*dd*, *J* = 10.6, 5.8 Hz, 2H), 3.77 – 3.41 (*m*, 24H), 3.33 (*s*, 6H), 2.85-2.91 (*m*, 2H), 1.25 (*d*, *J* = 6.8 Hz, 12H). ^{13}C NMR (150 MHz, CDCl$_3$) δ_C 184.31, 164.40 (*d*, *J* = 6.5 Hz), 163.94, 163.61, 162.66 (*d*, *J* = 6.5 Hz), 150.24 (*t*, *J* = 11 Hz), 147.34, 139.01, 135.56, 134.51, 132.57, 132.35, 131.68, 130.39, 129.78, 128.56, 127.04, 126.59, 124.00, 123.54, 123.31, 123.27, 123.17, 112.95 (*t*, *J* = 11 Hz), 111.25 (*dd*, *J* = 21 and 3 Hz), 72.10, 70.73, 70.67, 70.64, 70.57, 69.44, 59.12, 52.49, 29.61, 24.11 (one CH$_2$ missing probably due to overlapping). ESI-HRMS [M+Na]$^+$ calcd for [C$_{60}$H$_{62}$F$_2$N$_2$O$_{13}$Na]$^+$: 1079.4117; found: 1079.4116. UV/Vis (DMF) λ_{max}, nm (ε, L mol^{-1} cm^{-1}): 528 (77200), 492 (48000), 461 (18000), 290 (32000). Fluorescence (DMF) λ_{max}, nm: 540, 581. Quantum Yield = 94% determined in DMF using Rhodamine 6G as standard (QY=94% in EtOH).[26]

6.2.3.3 Cyclic voltammetry

Cyclic voltammetry experiments were carried out at room temperature in nitrogen-purged dry DMF with a Model 800 potentiostat (CH Instruments). The working electrode consisted of a glassy carbon electrode (3 mm diameter), the counter electrode was a Pt spiral and a Ag wire was used as quasi-reference electrode (AgQRE). Working electrode and quasi-reference electrodes were polished on a felt pad with 0.05 or 0.3 μm alumina suspension and sonicated in deionized water for 1 minute before each experiment; the Pt wire was flame-cleaned. Tetraethylammonium hexafluorophosphate (TEAPF$_6$) is added to the solution as supporting electrolytes at concentrations typically 100 times higher than the electroactive analyte. Ferrocene (sublimed at reduced pressure) is used as an internal reference ($E_{Fc+/Fc}$ in DMF).
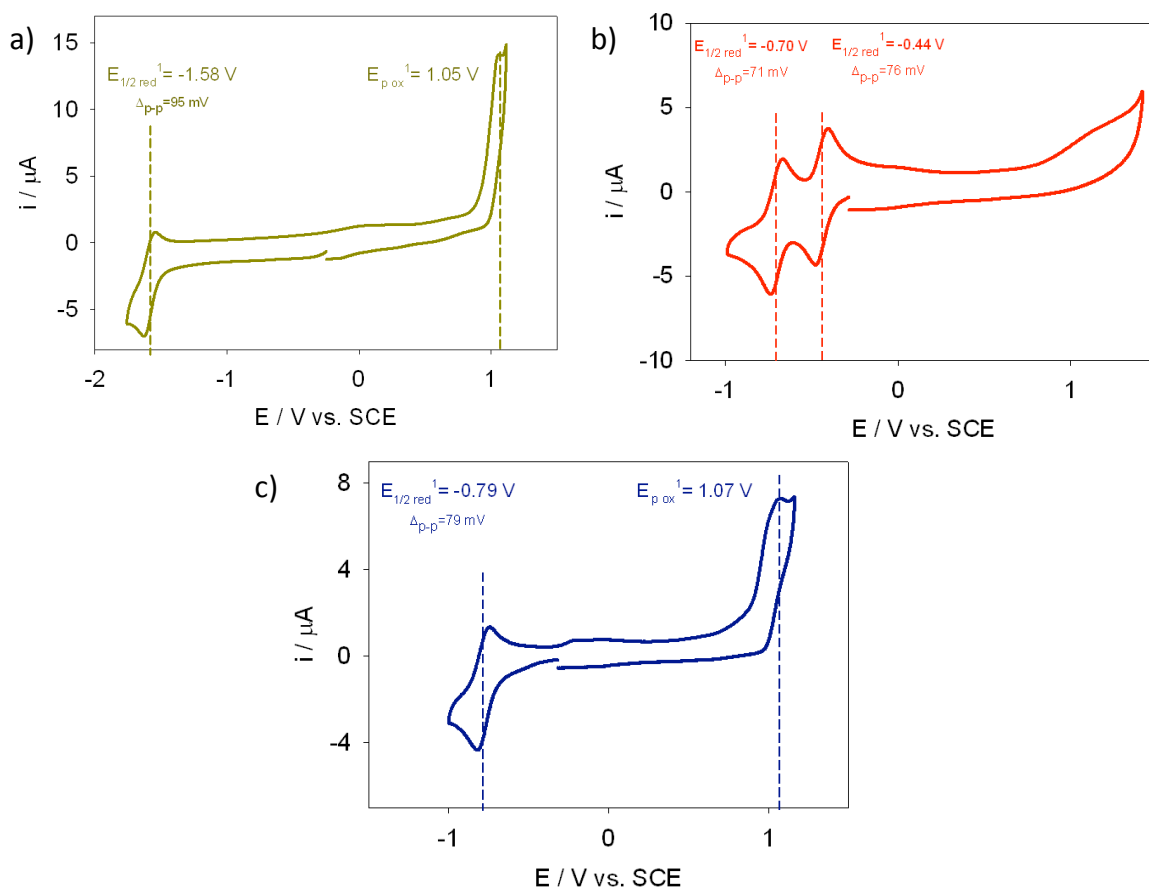

Figure 6-4 Cyclic voltammograms of a) Y-Per **4-5** (0.51 mM), scan rate 0.05 V/s; b) R-PDI **4-2** (5.0 mM), scan rate 0.05 V/s; c) B-NDI **3-24** (0.64 mM), scan rate 0.03 V/s in DMF at rt with Ferrocene as internal reference; $E_{Fc+/Fc}$=0.46 V vs. SCE.

Table 6-3 Halfwave potentials determined in DMF (in V vs. SCE)

Entry	Dyes	E_{ox}	$E_{red\ 1}$	E_{red2}
1	Y-Per **4-5**	1.05*	-1.58	nd
2	R-PDI **4-2**	nd	-0.44	-0.70
3	B-NDI **3-24**	1.07*	-0.79	nd

* Peak potentials (irreversible process)

HOMO and LUMO energies were calculated from the first formal redox potentials (half-wave potentials) using equations:

$$E_{HOMO} = -(5.1\ eV + E^l_{ox}\ vs.\ Fc^+/Fc)$$

$$E_{LUMO} = -(5.1\ eV + E^l_{red}\ vs.\ Fc^+/Fc)$$

In the cases where oxidation or reduction waves were not detected by means of cyclic voltammetry, HOMO or LUMO levels are calculated using the optical gap ΔE_{opt}, considering the maxima of the maxima of the lowest energy absorption band recorded in the same solvent, following equation:

$$\Delta E_{opt} = 1240\ /\ \lambda_{max}\ (nm).$$

6.2.3.4 Peptidic syntheses

General procedure: Peptides were synthesized on Rink-amide MBHA resin (0.11 mmol, 0.48 mmol/g). The synthesis was performed on a *Focus XC automated peptide synthesizer (model P/N 300530, aapptec)* under nitrogen atmosphere. Coupling reactions were carried out using *N*-Fmoc amino acids (0.26 M; 5 equiv.) in NMP, HATU (0.3 M, 4.5 equiv.) in DMF and DIPEA (2 M, 12 equiv.) in NMP at rt for 25 min. Simple coupling was performed for most of the amino acids except for the three alanines (residues 3, 10 and 17) preceding the modified amino acids for which double coupling was carried out. *N*-Fmoc deprotection was carried out at rt in three stages using piperidine/DMF (1:4, 3 × 6 mL) for 3 × 4 min. After each reaction the resin was washed with DMF (4 times). At the end of the synthesis, the peptide was acetylated in two stages in the presence of Ac₂O/pyridine/NMP (1:2:2, 2 × 6 mL) at rt for 2 × 15 min. The resin was washed 6 times with CH₂Cl₂. The peptide was deprotected and cleaved from the resin using the cocktail cleavage TFA/water/EDT/TIS (94:2.5:2.5:1, 10 mL for 200 mg). After 2 h at rt, the sample was then filtered through glass wool, the solvent was evaporated and the crude material was precipitated in cold Et₂O. After centrifugation, the ether was decanted and this washing was repeated 3 times.

To a solution of crude peptide (0.1 mmol) and 2,2'-dipyridine disulfide (76 mg, 0.33 mmol) in dry DMF (2 mL), DIEA (85 mg, 0.66 mmol) was added. The reaction mixture was stirred for 1 h and

poured in cold Et_2O and the product precipitated. After centrifugation, the ether was decanted and this washing was repeated 3 times. The crude peptide was purified by preparative RP-HPLC.

Analysis and purification: The analytical HPLC column used was an *Agilent Zorbax SB-C₃* (5 µm, 4.6 × 150 mm) column. The analysis was performed at 25 °C using H_2O/CH_3CN (conditions 1) as mobile phase or H_2O+0.1%TFA / CH_3CN+0.1%TFA applying the following elution gradient (Table 6-4).

Table 6-4 Elution gradients 1 (without TFA) and 2 (with TFA) applied for HPLC analysis.

Time / s	% H_2O	% CH_3CN	Flow / mL/min
0	95	5	1
5	65	35	1
30	0	100	1
36	0	100	1
35	95	5	1

Time / s	% H_2O+0.1%TFA	% CH_3CN+0.1%TFA	Flow / mL/min
0	95	5	1
5	65	35	1
29	0	100	1
30	0	100	1
31	95	5	1

The purification by RP-HPLC was performed using *Agilent Zorbax PrepHT 300SB-C₃* (7 µm, 21.2 × 150 mm) column. The purification was performed at 25 °C using H_2O/CH_3CN as mobile phase applying the following elution gradient (concentration for injection: 10 mg/mL) (Table 6-5).

Table 6-5 Elution gradient applied for HPLC purification.

Time / s	% H_2O	% CH_3CN	Flow / mL/min
0	95	5	10
5	65	35	10
26	30	70	10
27	0	100	10
28	0	100	10
29	95	5	10

6.2.3.4.1 Synthesis of peptide Ac-QLA-X(disulfide)-QLAQLAQLA-X(hydrazide)-QLAQLA QLA-X(diol)-QLA-NH₂ 4-17

Chemical Formula: $C_{157}H_{243}N_{49}O_{40}S_2$
Exact Mass: 3518.79
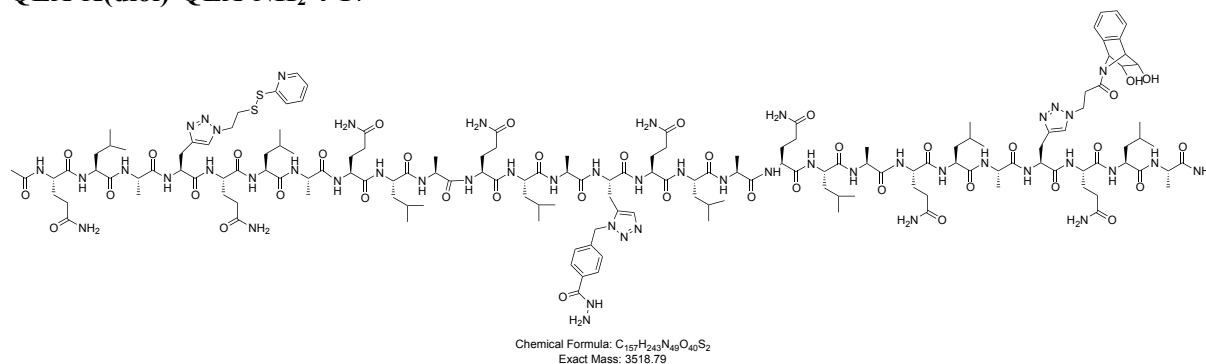
The peptide was synthesized according to the general procedure.

HPLC (25 °C): R_t = 15.6 min (gradient 1). ESI-MS(Q-Tof) showed $[M+4H]^{4+}$, $[M+3H]^{3+}$, $[M+2H]^{2+}$, after deconvolution of multicharged ions, monoisotopic mass found: 3518.79.

Figure 6-5 HPLC chromatogram of crude peptide **4-17.**

Figure 6-6 HPLC chromatogram of purified peptide **4-17**.
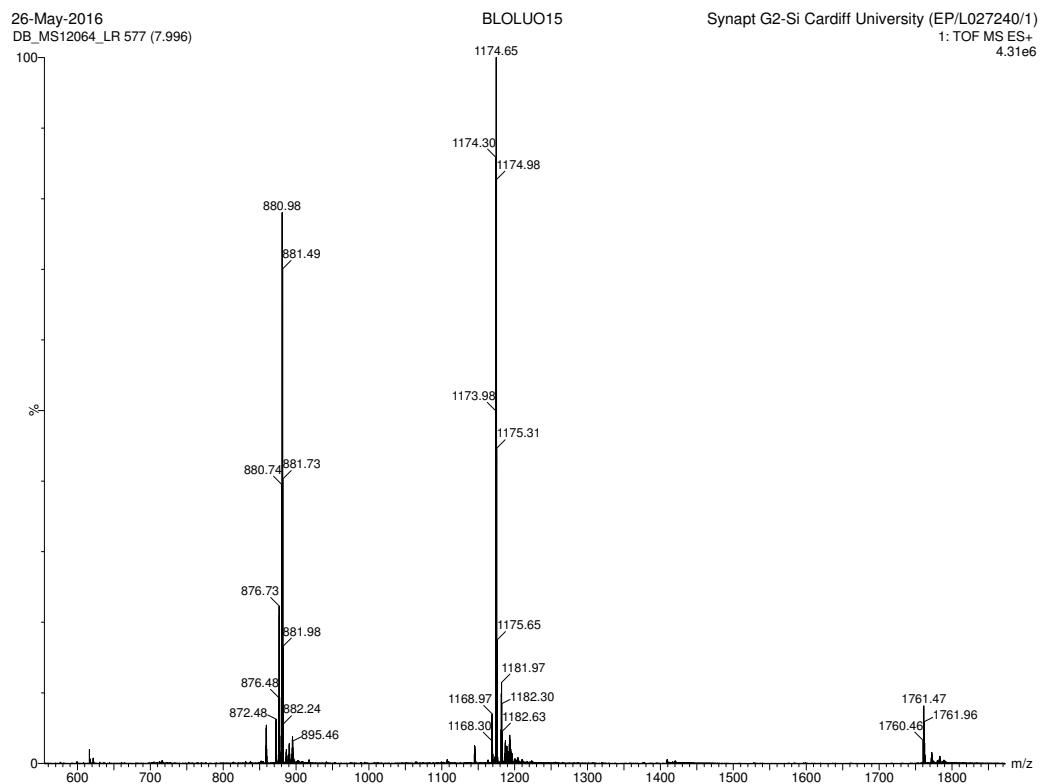
Figure 6-7 ESI-MS(Q-Tof) analysis of purified peptide **4-17.**

6.2.3.4.2 Synthesis of peptide Ac-QLA-X(disulfide)-QLAQLAQLAQLAQ-X(hydrazide)-QLAQLAQLAQLAQ-X(diol)-QLA-NH₂ 4-18
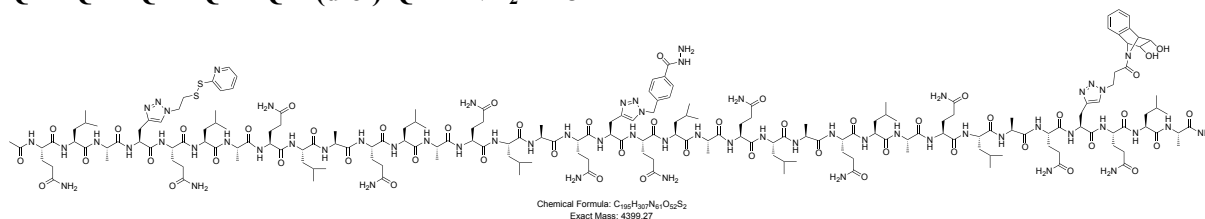
The peptide was synthesized according to the general procedure.

HPLC (25 °C): R_t = 15.9 min (gradient 1). ESI-MS(Q-Tof) showed showed $[M+5H]^{5+}$, $[M+4H]^{4+}$, $[M+3H]^{3+}$, after deconvolution of multicharged ions, monoisotopic mass found: 4399.27.

237
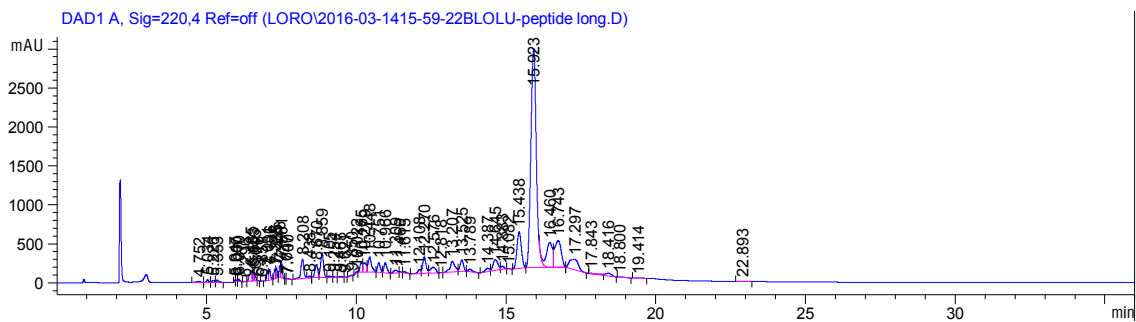
Figure 6-8 HPLC chromatogram of crude peptide **4-18**.
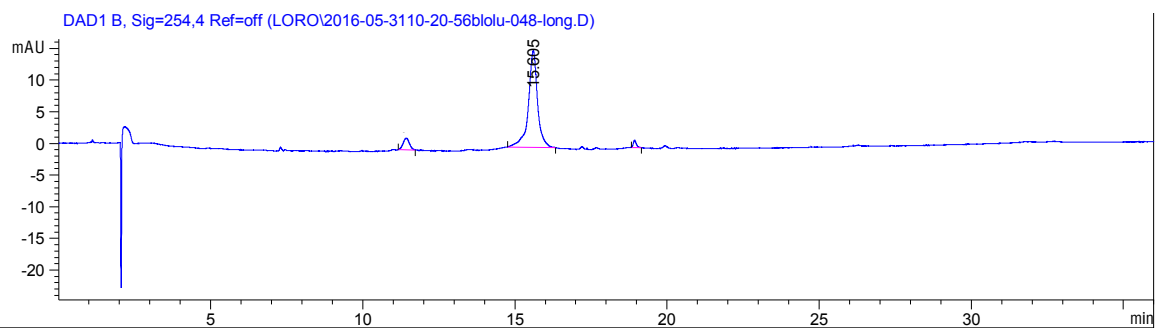
Figure 6-9 HPLC chromatogram of purified peptide **4-18**
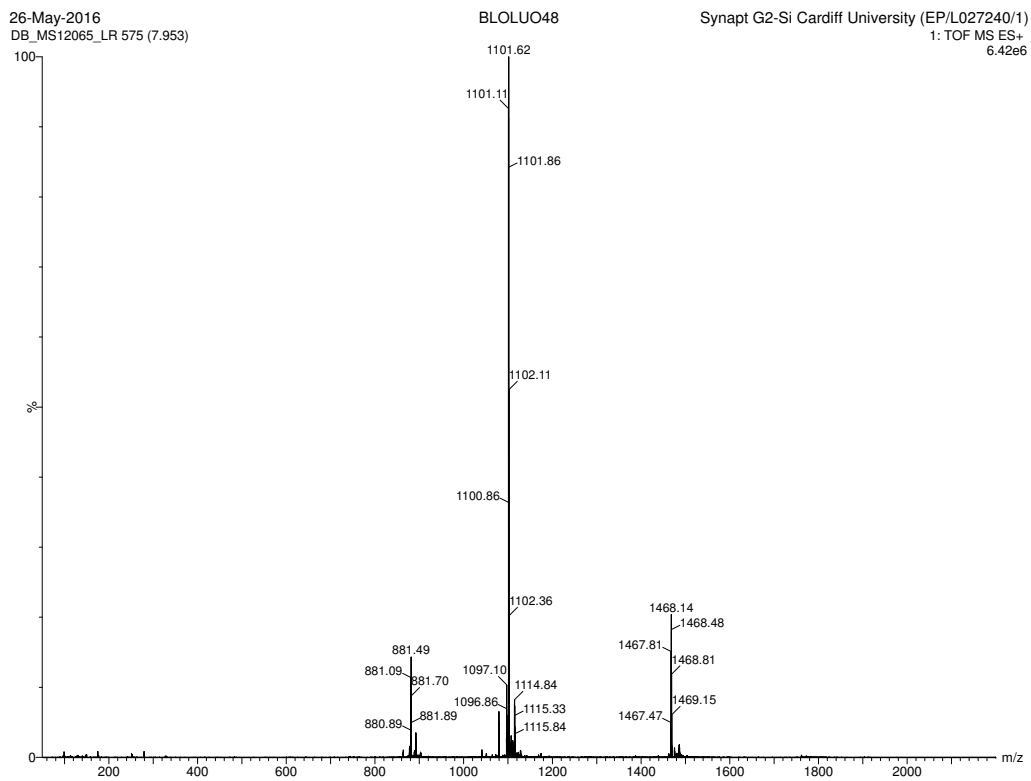
Figure 6-10 ESI-MS(Q-Tof) analysis of purified peptide **4-18.**

6.2.3.4.3 Synthesis of peptide Ac-QLA-X(disulfide)-QLAQLA-X(diol)-QLAQLA-X(hydrazide)-QLA-NH₂ 4-22

Chemical Formula: $C_{129}H_{195}N_{41}O_{32}S_2$
Exact Mass: 2894.4333
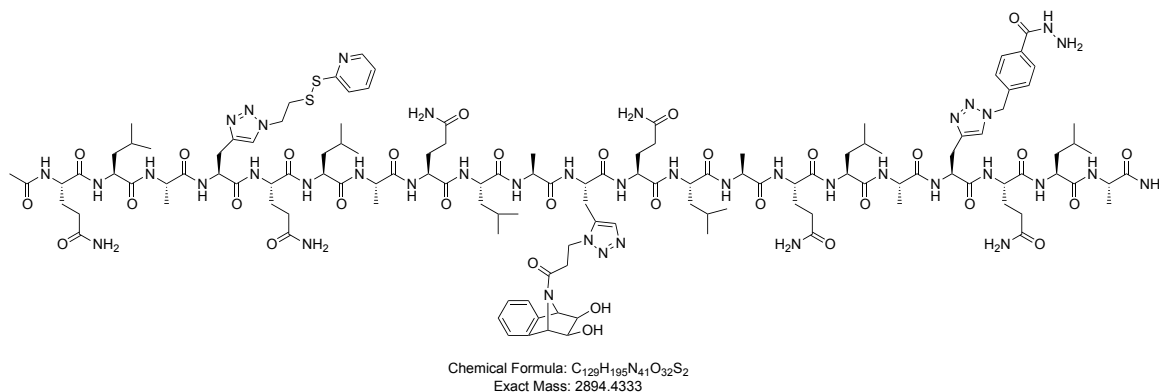
The peptide was synthesized according to the general procedure.

HPLC (25 °C): R_t = 16.2 min (gradient 1). ESI-MS(Q-Tof) showed showed $[M+4H]^{4+}$, $[M+3H]^{3+}$, $[M+2H]^{2+}$, after deconvolution of multicharged ions, monoisotopic mass found: 2894.4401.
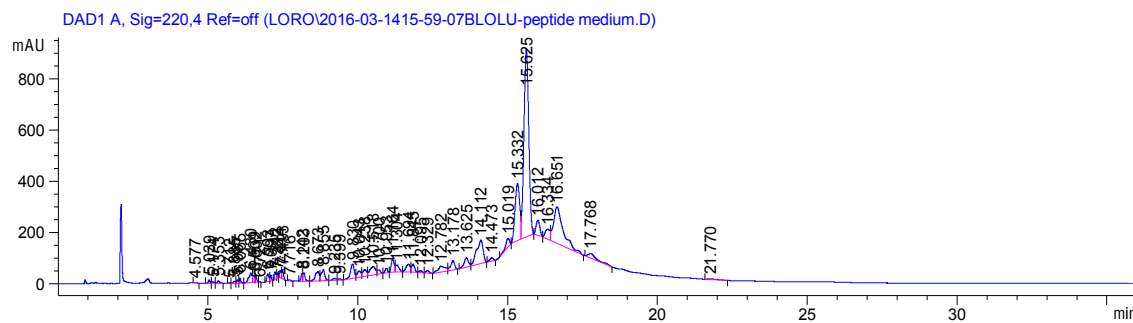

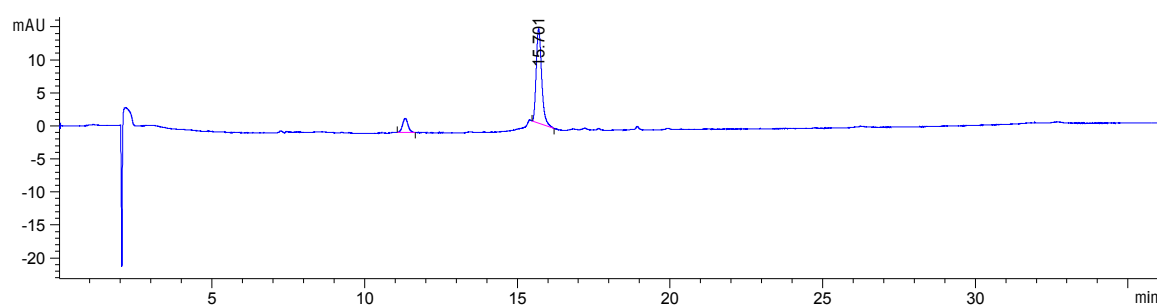**Figure 6-11** HPLC chromatogram of crude peptide **4-22.**

Figure 6-12 HPLC chromatogram of purified peptide **4-22**.
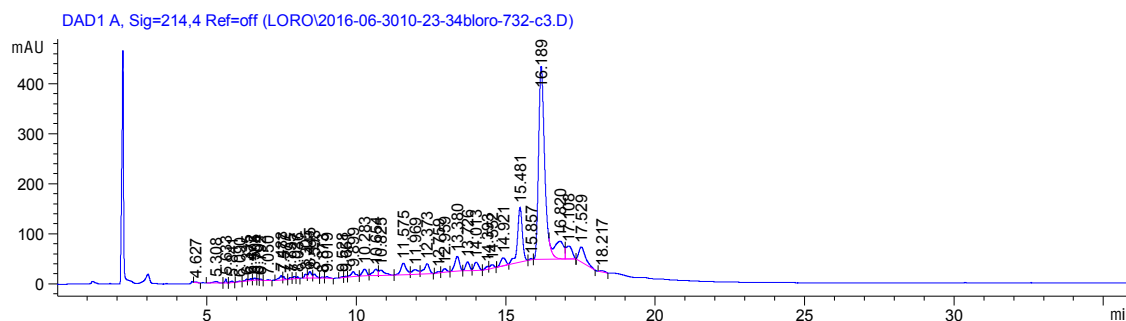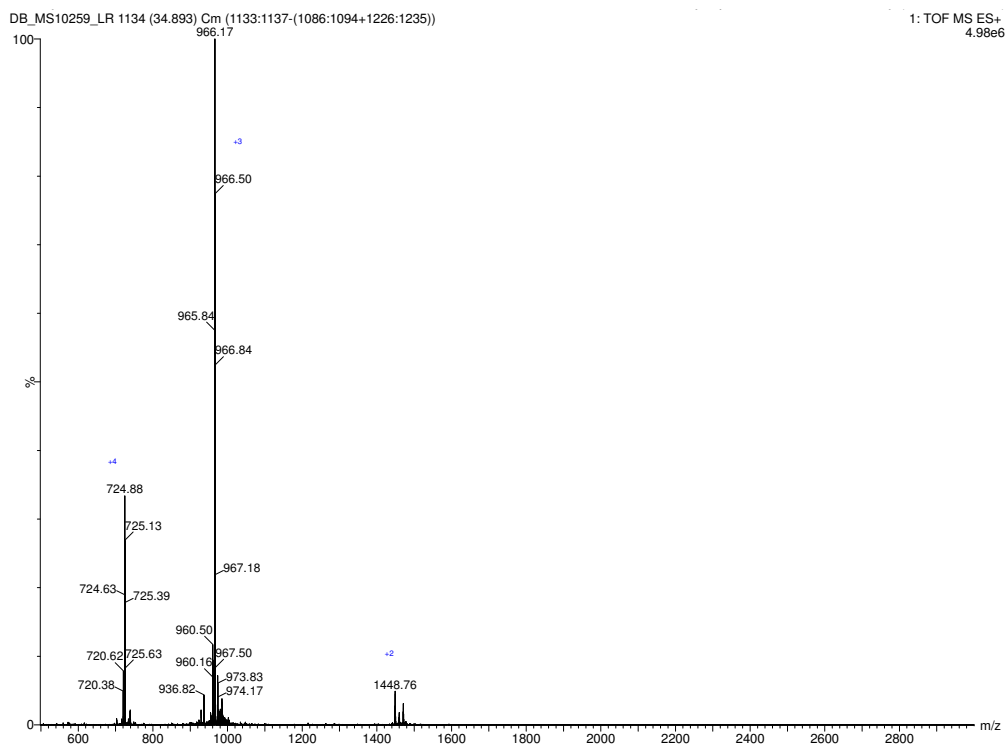
Figure 6-13 ESI-MS(Q-Tof) analysis of pure peptide **4-22.**

6.2.3.4.4 Synthesis of catechol amino acid 4-24
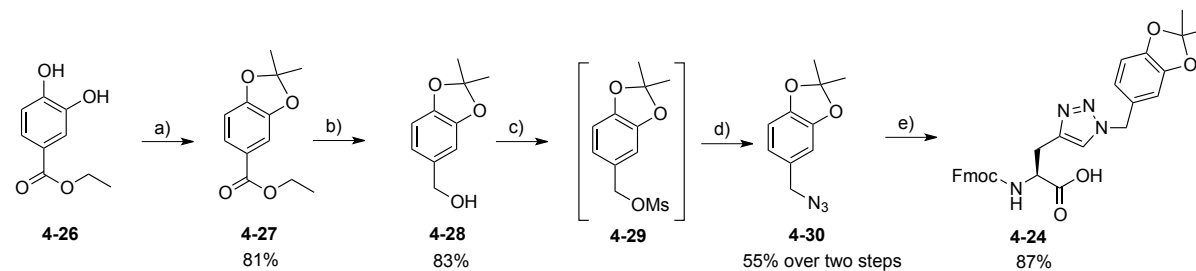
Scheme 6-20 Synthesis of amino acid **4-24;** a) acetone, PCl$_3$, benzene, rt, 16 h; b) LiAlH$_4$, THF, 0 °C to rt, 3 h; c) MsCl, NEt$_3$, CH$_2$Cl$_2$, 0 °C to rt, 1 h; d) NaN$_3$, DMF, rt, 16 h; e) Fmoc-Gly(Propargyl)-OH, CuSO$_4$·5H$_2$O, Na ascorbate, DMF/H$_2$O 4:1, rt, 16 h.

6.2.3.4.4.1 Synthesis of ethyl 2,2-dimethylbenzo[*d*][1,3]dioxole-5-carboxylate 4-27

4-27
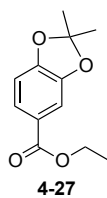
Compound **4-27** has been synthesized according to the literature.[27]

6.2.3.4.4.2 Synthesis of (2,2-dimethylbenzo[*d*][1,3]dioxol-5-yl)methanol 4-28

4-28
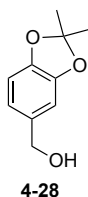
Compound **4-28** has been synthesized according to the literature.[28]

6.2.3.4.4.3 Synthesis of 5-(azidomethyl)-2,2-dimethylbenzo[*d*][1,3]dioxole 4-30

4-30
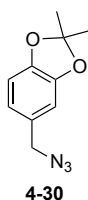
To a solution of alcohol **4-28** (1.4 g, 7.77 mmol) in CH_2Cl_2 (40 mL), NEt_3 (3.2 mL, 23.3 mmol) and a solution of mesyl chloride (0.9 mL, 11.6 mmol) in CH_2Cl_2 (6 mL) were successively added at 0 °C. The reaction mixture was stirred at rt for 1 h. A saturated solution of $NaHCO_3$ was added, the layers were separated and the aqueous phase was extracted with CH_2Cl_2. The combined organic layers were washed with a sat. solution of NH_4Cl and brine, dried and concentrated under reduced pressure. The crude material was dissolved in DMF (50 mL) and sodium azide was added (1.01 g, 15.5 mmol). The reaction mixture was stirred at rt for 16 h. Water was added and the aqueous mixture was extracted with Et_2O (3 times). The combined organic layers were washed with brine, dried and concentrated under reduced pressure. The crude material was purified through silica gel column chromatography (Eluent: P.E./EtOAc 95:5 to 9:1) to afford azide **4-30** as a colorless oil (876 mg, 55%). IR (film): ν (cm^{-1}) 2992, 2093, 1497, 1447, 1377, 1234, 982, 837; ^{1}H NMR (300 MHz, $CDCl_3$): δ_H 6.76-6.70 (*m*, 3H), 4.22 (*s*, 2H), 1.69 (*s*, 6H); ^{13}C NMR (75 MHz, $CDCl_3$): δ_C 148.00, 147.68, 128.50, 121.54, 118.50, 108.73, 108.30, 55.02, 26.00. EI-HRMS [M]$^+$ calcd for $[C_{10}H_{12}O_3]^+$: 205.0851, found: 205.0850.

6.2.3.4.4.4 Synthesis of (*S*)-2-((((9*H*-fluoren-9-yl)methoxy)carbonyl)amino)-3-(1-((2,2-dimethylbenzo[*d*][1,3]dioxol-5-yl)methyl)-1*H*-1,2,3-triazol-4-yl)propanoic acid 4-24

4-24
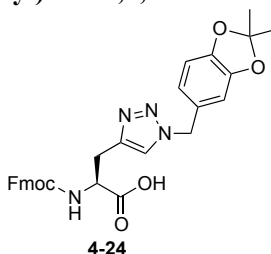
To a solution of Fmoc-Gly(Propargyl)-OH (1.22 g, 3.65 mmol) and azide **4-30** (825 mg, 4.02 mmol) in DMF (40 mL), were successively added a solution of CuSO$_4$.5H$_2$O (273 mg, 1.09 mmol) in H$_2$O (5 mL) and a solution of sodium ascorbate (144 mg, 0.73 mmol) in H$_2$O (1 mL). The reaction mixture was stirred at rt for 16 h. The solvents were removed under reduced pressure. The residue was partitioned between a mixture of EtOAc/THF and a sat. aq. solution of Na$_4$EDTA and the layers were separated. The aqueous phase was extracted with EtOAc/THF, and the combined organic layers were washed with brine, dried and concentrated under reduced pressure. The crude material was precipitated into Et$_2$O, centrifugated and washed 3 times with Et$_2$O to remove the excess of **4-30** affording **4-24** as a colorless solid (1.9 g, 87%). M.p.: 130-135 °C; IR (film): ν (cm^{-1}) 3319, 3066, 2988, 2939, 1710, 1610, 1497, 1447, 1250, 1049, 980, 758, 738; ^{1}H NMR (300 MHz, CD$_3$OD): δ_H 7.77 (*d*, *J* = 7.5 Hz, 2H), 7.63 (*s*, 1H), 7.57 (*t*, *J* = 6 Hz, 2H), 7.36 (*t*, *J* = 7.5 Hz, 2H), 7.26 (*t*, *J* = 7.4 Hz, 2H), 6.70-6.57 (*m*, 3H), 5.34 (*s*, 2H), 4.32-4.13 (*m*, 4H), 3.31-3.27 (*m*, 1H), 3.14-3.06 (*m*, 1H), 1.51 (*s*, 6H); ^{13}C NMR (75 MHz, CD$_3$OD) δ_C 158.06, 149.24, 148.99, 145.62, 145.35, 142.56, 129.63, 128.76, 128.18, 126.29, 124.19, 122.42, 120.92, 119.55, 109.18, 109.14, 67.85, 56.77, 54.74, 48.32, 29.74, 25.83 (COOH missing); ESI-HRMS [M+H]$^+$ calcd for [C$_{30}$H$_{29}$N$_4$O$_6$]$^+$: 541.2087, found: 541.2087.

6.2.3.4.5 Synthesis of peptide Ac-QLA-X(disulfide)-QLAQLA-X(catechol)-QLAQLA-X(hydrazide)-QLA-NH$_2$ 4-40
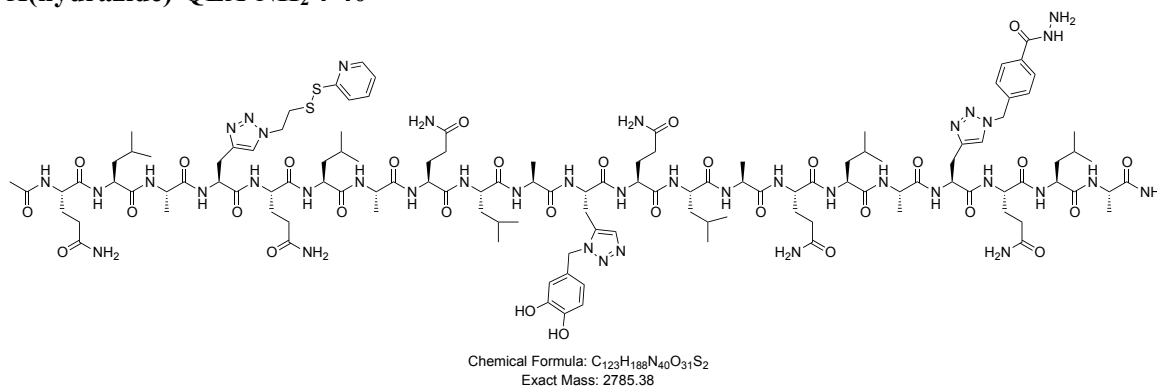
Chemical Formula: C$_{123}$H$_{188}$N$_{40}$O$_{31}$S$_2$
Exact Mass: 2785.38

The peptide was synthesized according to the general procedure. The analytical HPLC were performed with 0.1% of TFA. HPLC (25 °C): R$_t$ = 14.9 min (gradient 2). ESI-MS(Q-Tof) showed [M+3H]$^{3+}$, [M+2H]$^{2+}$, after deconvolution of multicharged ions, monoisotopic mass found: 2785.38.
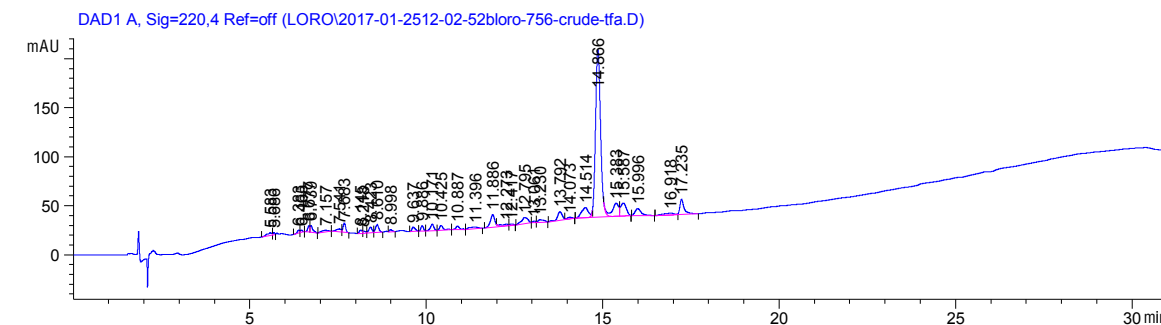
Figure 6-14 HPLC chromatogram of crude peptide **4-40.**
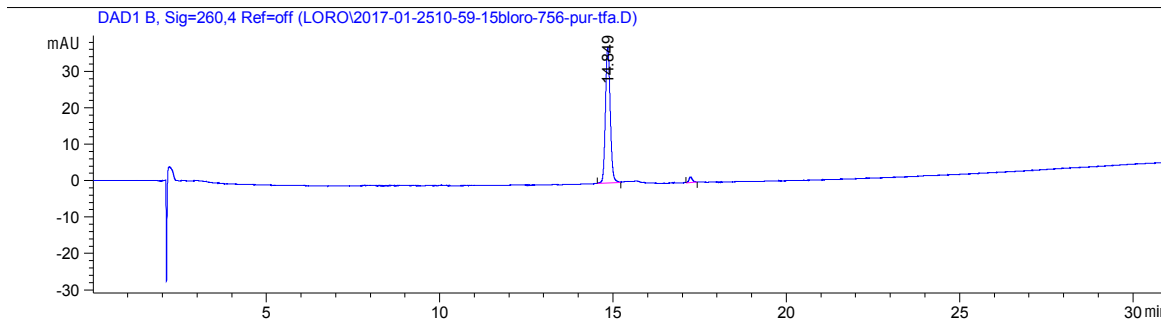
Figure 6-15 HPLC chromatogram of purified peptide **4-40.**

Figure 6-16 ESI-MS(Q-Tof) analysis of purified peptide **4-40**.

243

6.2.3.4.6 Synthesis of catechol amino acid 4-37

Scheme 6-21 Synthesis of amino acid **4-25;** a) acetone, PCl₃, benzene, rt, 1 h; b) I₂, Ag₂SO₄, EtOH, rt, 2 h; c) Propargyl alcohol, NEt₃, CuI, [Pd(PPh₃)₂Cl₂], -10 °C to rt, 17 h; d) H₂, Pd/C 10% wt, MeOH, rt, 18 h; d) MsCl, NEt₃, CH₂Cl₂, 0 °C to rt, 1 h; d) NaN₃, DMF, rt, 16 h; e) Fmoc-Gly(Propargyl)-OH, CuSO₄·5H₂O, Na ascorbate, DMF/H₂O 4:1, rt, 16 h.

6.2.3.4.6.1 Synthesis of 2,2-dimethylbenzo[*d*][1,3]dioxole 4-32

4-32

2,2-dimethylbenzo[*d*][1,3]dioxole **4-32** has been synthesized according to the literature.[29]

6.2.3.3.6.2 Synthesis of 5-iodo-2,2-dimethylbenzo[*d*][1,3]dioxole 4-33

4-33
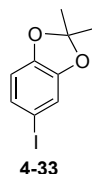
5-iodo-2,2-dimethylbenzo[*d*][1,3]dioxole **4-33** has been synthesized according to the literature.[30]

6.2.3.4.6.3 Synthesis of 3-(2,2-dimethylbenzo[*d*][1,3]dioxol-5-yl)prop-2-yn-1-ol 4-34

4-34
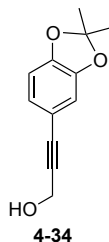
Iodoketal **4-33** (1.6 g, 5.8 mmol) was dissolved in dry THF (8 mL) and NEt$_3$ (2.3 mL) and degassed with N$_2$ under sonications for 20 min. [Pd(PPh$_3$)$_2$Cl$_2$] (203 mg, 0.29 mmol) and CuI (110 mg, 0.58 mmol) were added and the reaction mixture was stirred at rt for 5 min under N$_2$. Then, the mixture was cooled at -10 °C and propargyl alcohol (0.5 mL, 8.7 mmol) was added. The reaction was stirred at rt for 17 h. EtOAc was added and the mixture was filtered through celite. The filtrate was concentrated under reduced pressure and purified through silica pad (Eluent: EtOAc/P.E. 1:4) to afford **4-34** as an orange oil (1.14 g, 96%). IR (film): ν (cm^{-1}) 3362, 2988, 2934, 2859, 1492, 1440, 1377, 1236, 1182, 1020, 982, 833, 810; ^{1}H NMR (300 MHz, CDCl$_3$): δ_H 6.91 (*dd*, *J* = 8.0, 1.6 Hz, 1H), 6.78 (*d*, *J* = 1.6 Hz, 1H), 6.5 (*d*, *J* = 8.0 Hz, 1H), 4.46 (*d*, *J* = 5.9 Hz, 2H), 1.80 (*t*, *J* = 5.9 Hz, 1H, -OH), 1.67 (*s*, 6H); ^{13}C NMR (75 MHz, CDCl$_3$): δ_C 148.08, 147.34, 136.02, 118.71, 115.16, 111.64, 108.41, 86.00, 85.37, 51.82, 25.95. EI-HRMS [M]$^+$ calcd for [C$_{12}$H$_{12}$O$_3$]$^+$: 204.0786, found: 204.0788.

6.2.3.4.6.4 Synthesis of 3-(2,2-dimethylbenzo[*d*][1,3]dioxol-5-yl)propan-1-ol 4-35

4-35
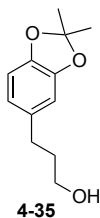
To a solution of **4-34** (740 mg, 3.6 mmol) in MeOH (36 mL) under N$_2$, was added Pd/C 10% wt (383 mg). Three cycles of vacuum/H$_2$ were performed and the reaction mixture was stirred at rt for 18 h under H$_2$ atmosphere. The mixture was filtrated-off through celite and the filter cake was washed with CH$_2$Cl$_2$. The filtrate was concentrated under reduced pressure to afford **4-35** as a greenish oil (650 mg, 87%). The product was used for the next step without further purification and was characterized in accordance with the literature.[31] IR (film): ν (cm^{-1}) 3348, 2990, 2937, 2862, 1494, 1444, 1375, 1252, 1233, 1157, 1055, 980, 837; ^{1}H NMR (CDCl$_3$, 300 MHz): δ_H 6.65-6.58 (*m*, 3H), 3.67 (*t*, *J* = 6.4 Hz, 2H), 2.61 (*t*, *J* = 7.6 Hz, 2H), 1.89-1.79 (*m*, 2H), 1.66 (*s*, 6H); ^{13}C NMR (CDCl$_3$, 75 MHz): δ_C 147.37, 145.45, 134.90, 120.40, 117.49, 108.62, 107.89, 62.13, 34.41, 31.78, 25.78; EI-HRMS [M]$^+$ calcd for [C$_{12}$H$_{16}$O$_3$]$^+$: 208.1092, found: 208.1099.

6.2.3.4.6.4 Synthesis of 5-(3-azidopropyl)-2,2-dimethylbenzo[*d*][1,3]dioxole 4-37

4-37
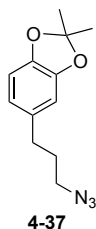
To a solution of **4-35** (570 g, 2.74 mmol) in CH_2Cl_2 (25 mL), NEt_3 (1.1 mL, 8.32 mmol) and a solution of mesyl chloride (0.32 mL, 4.1 mmol) in CH_2Cl_2 (5 mL) were added at 0 °C. The reaction mixture was stirred at rt for 1 h. A saturated solution of $NaHCO_3$ was added, the layers were separated and the aqueous phase was extracted with CH_2Cl_2. The combined organic layers were washed with brine, dried ($MgSO_4$) and concentrated under reduced pressure to afford **4-36** as an orange oil. The crude material was dissolved in dry DMF (12 mL) and sodium azide (356 mg, 5.48 mmol) was added. The reaction mixture was stirred at rt for 16 h. Water was added and the aqueous mixture was extracted with Et_2O (3 times). The combined organic layers were washed with brine, dried and concentrated under reduced pressure. The crude material was purified through silica gel column chromatography (Eluent: P.E to P.E/EtOAc 8:2) to afford **4-37** as a colorless oil (490 mg, 77% over two steps). IR (film): v (cm^{-1}) 2991, 2936, 2861, 2093, 1493, 1445, 1375, 1250, 1231, 1156, 978, 835; ^{1}H NMR (300 MHz, CDCl$_3$): δ_H 6.66-6.55 (*m*, 3H), 3.27 (*t*, *J* = 6.8 Hz, 2H), 2.61 (*t*, *J* = 7.5 Hz, 2H), 1.91-1.81 (*m*, 2H), 1.66 (*s*, 6H); ^{13}C NMR (75 MHz, CDCl$_3$): δ_C 148.22, 147.66, 134.06, 120.73, 117.81, 108.74, 108.15, 50.69, 32.63, 30.80, 25.98; EI-HRMS [M]$^+$ calcd for [C$_{12}$H$_{15}$N$_3$O$_2$]$^+$: 233.1164, found: 233.1172.

6.2.3.4.6.5 Synthesis of (*S*)-2-(((((9*H*-fluoren-9-yl)methoxy)carbonyl)amino)-3-(1-(3-(2,2-dimethylbenzo[*d*][1,3]dioxol-5-yl)propyl)-1*H*-1,2,3-triazol-4-yl)propanoic acid 4-25

4-25
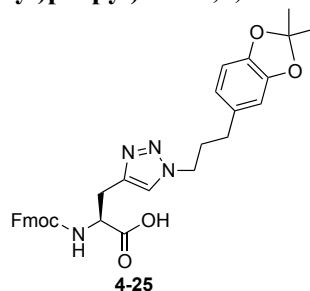
To a solution of Fmoc-Gly(Propargyl)-OH (625 mg, 1.87 mmol) and azide **4-37** (480 mg, 2.05 mmol) in DMF (20 mL), were successively added a solution of CuSO$_4$.5H$_2$O (135 mg, 0.54 mmol) in H$_2$O (3 mL) and a solution of sodium ascorbate (74 mg, 0.37 mmol) in H$_2$O (2 mL). The reaction mixture was stirred at rt for 16 h. The solvents were removed under reduced pressure. The residue was partitioned between a mixture of EtOAc and a sat. aq. solution of Na$_4$EDTA and

the layers were separated. The aqueous phase was extracted with EtOAc, and the combined organic layers were washed with brine, dried and concentrated under reduced pressure. The crude material was precipitated into Et$_2$O, centrifugated and washed 3 times with Et$_2$O to remove the excess of **4-37** affording **4-25** as a colorless solid (1 g, 94%). M.p.: 170-175 °C; IR (film): ν (cm^{-1}) 3361, 2988, 2933, 2858, 1493, 1440, 1377, 1237, 1182, 1020, 982, 833, 810, 783, 615, 509; ^{1}H NMR (300 MHz, CD$_3$OD): δ_H 7.73 (*d, J* = 7.5 Hz, 2H), 7.62 (*s*, 1H), 7.54 (*d, J* = 7.2 Hz, 2H), 7.33 (*t, J* = 7.5 Hz, 2H), 7.23 (*t, J* = 7.4 Hz, 2H), 6.55-6.48 (*m*, 3H), 4.34-4.08 (*m*, 6H), 3.34-3.30 (*m*, 1H), 3.18-3.08 (*m*, 1H), 2.40 (*t, J* = 7.7 Hz, 2H), 2.14-1.99 (*m*, 2H), 1.56 (*s*, 6H); ^{13}C NMR (75 MHz, CD$_3$OD) δ_C 158.03, 148.92, 147.16, 145.25, 142.52, 135.04, 128.75, 128.15, 126.25, 126.14, 124.42, 121.80, 120.90, 118.68, 109.57, 108.89, 67.76, 56.96, 54.80, 50.58, 48.32, 33.15, 29.74, 25.90 (COOH missing); ESI-HRMS [M+H]$^+$ calcd for [C$_{32}$H$_{33}$N$_4$O$_6$]$^+$: 569.2400, found: 569.2411.

6.2.3.4.7 Synthesis of peptide Ac-QLA-X(disulfide)-QLAQLA-X(catechol)-QLAQLA-X(hydrazide)-QLA-NH$_2$ 4-41
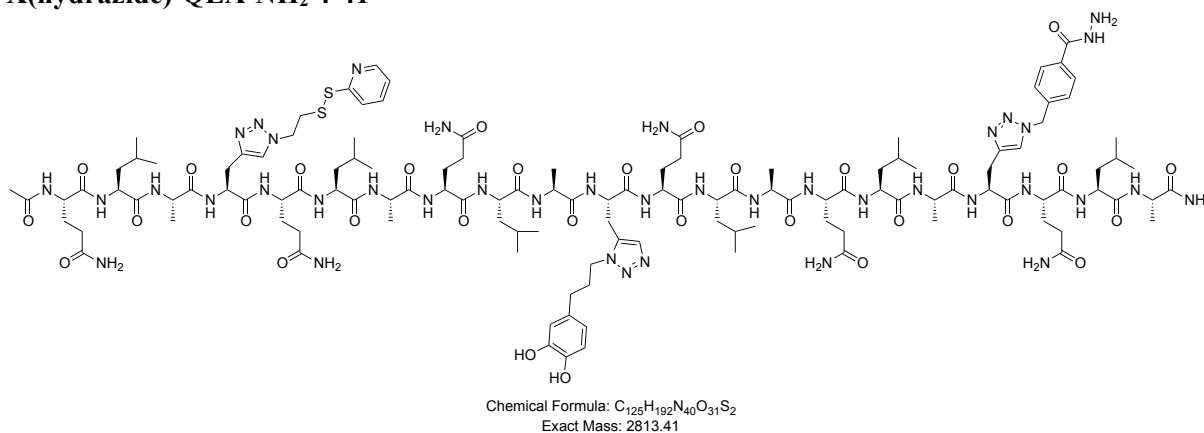
Chemical Formula: C$_{125}$H$_{192}$N$_{40}$O$_{31}$S$_2$
Exact Mass: 2813.41

The peptide was synthesized according to the general procedure. The analytical HPLC were performed without TFA. HPLC (25 °C): R$_t$ = 16.3 min (gradient 1). ESI-MS(Q-Tof) showed [M+3H]$^{3+}$, [M+2H]$^{2+}$, after deconvolution of multicharged ions, monoisotopic mass found: 2813.41.
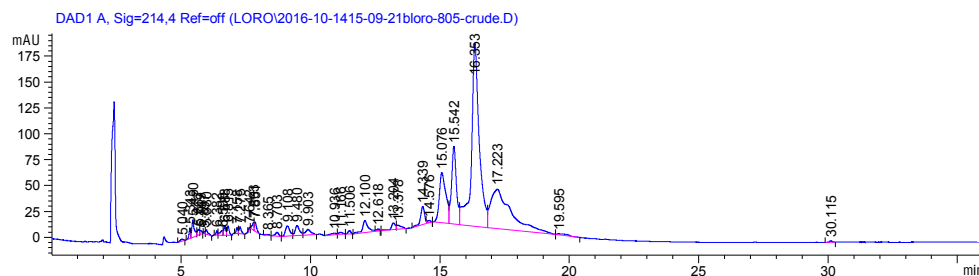
Figure 6-17 HPLC chromatogram of crude peptide **4-41**.
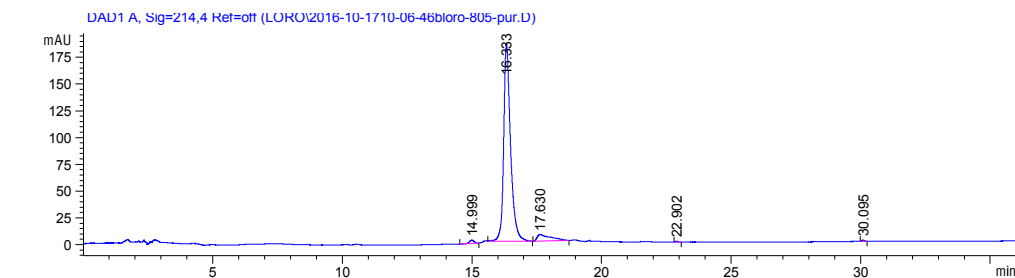
Figure 6-18 HPLC chromatogram of purified peptide **4-41**.
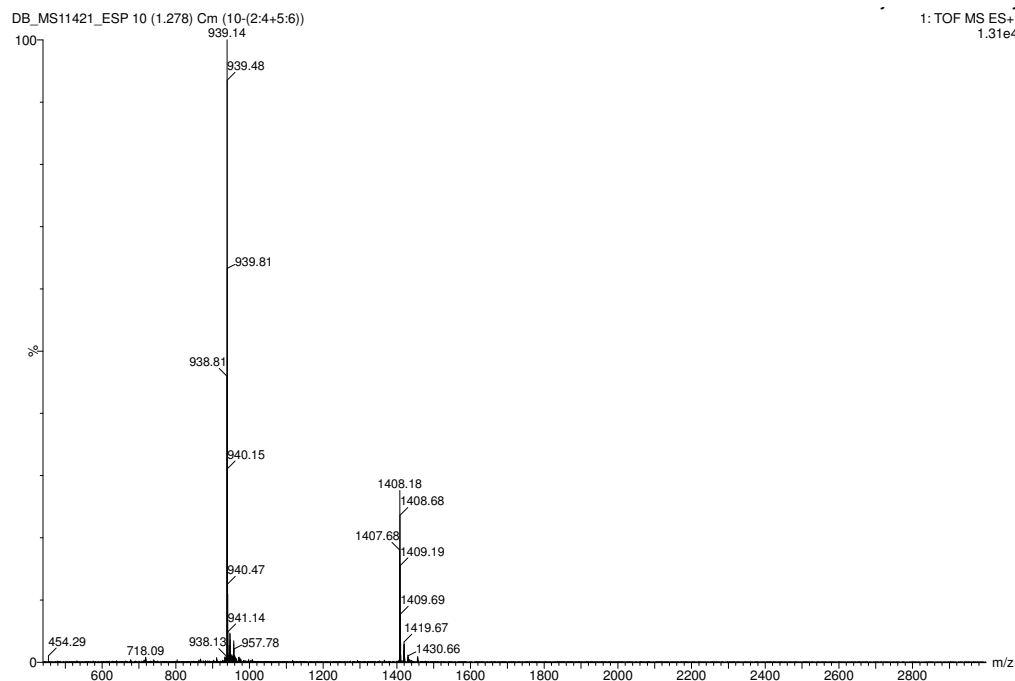
Figure 6-19 ESI-MS(Q-Tof) analysis of purified peptide **4-41.**

6.2.3.5 Chromophore assembly on peptidic scaffold
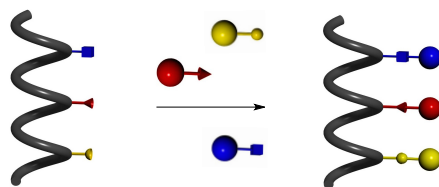
General Procedure: Peptidic scaffold (1 equiv), R-PDI (3 equiv), B-NDI (3 equiv), Y-Per (3 equiv), *m*-PDA (0.5 equiv) were dissolved in anhydrous DMF or DMA (C = 0.5 mM) and stirred at rt for 4 h. The mixture was poured in Et$_2$O and centrifuged.

For the purification of peptide **4-13**, the crude material was purified using gel permeation chromatography (GPC) with Bio-Rad Bio-Beads S-X1 Beads (operating range 600 – 14000 g.mol-

1) as stationary phase with anhydrous DMF as eluent. The product was precipitated in cold Et$_2$O to give **4-13** as brown solid. While for the other peptides **4-14, 4-19, 4-20, 4-23, 4-42** and **4-43,** the precipitate obtained after centrifugation was simply washed two times with Et$_2$O and 3 times with dry THF by sonication and centrifugation to give the colored peptide as pure material. The MALDI-Tof analyses were performed from DMF solutions (matrix: α-cynao-hydroxycinnamic acid).

Peptide **4-13**: MALDI-Tof LRMS [M+Na]$^+$ calcd for [C$_{267}$H$_{317}$BN$_{46}$O$_{56}$F$_2$NaS$_2$]$^+$: 5199.3, found: 5199.3; [M(-boronate) + Na]$^+$ calcd for [C$_{235}$H$_{300}$N$_{46}$O$_{56}$F$_2$NaS$_2$]$^+$: 4787.1, found: 4787.1; [M(-boronate-disulfide) + Na]$^+$ calcd for [C$_{182}$H$_{240}$N$_{42}$O$_{44}$F$_2$NaS]$^+$: 3810.7, found: 3810.7. UV/Vis (DMF) λ_{max}, nm (ε, L mol^{-1} cm^{-1}): 428 (41100), 455 (54000), 493 (42300), 529 (54000), 612 (23500); due to the high hygroscopy of peptide, molar extinction coefficients were obtained by normalizing the absorbance of the peptide and the arithmetic sum of dyes on B-NDI unit (612 nm). Fluorescence emission (DMF, exc 423 nm) λ_{max}, nm: 471, 498, 534, 641; (DMF, exc 495 nm) λ_{max}, nm: 538, 580, 641; (DMF, exc 609 nm) λ_{max}, nm: 641. Fluorescence excitation (DMF, emis 640 nm) λ_{max}, nm: 347, 364, 428, 453, 492, 529, 613.

Peptide **4-14**: MALDI-Tof LRMS [M+Na]$^+$ calcd for [C$_{269}$H$_{329}$BN$_{46}$O$_{56}$F$_2$NaS$_2$]$^+$: 5235.4, found: 5235.4; [M(-boronate) + Na]$^+$ calcd for [C$_{237}$H$_{312}$N$_{46}$O$_{56}$F$_2$NaS$_2$]$^+$: 4823.2, found: 4823.3. UV/Vis (DMF) λ_{max}, nm (ε, L mol^{-1} cm^{-1}): 427 (39300), 454 (49000), 492 (36700), 528 (49000), 612 (23500). Fluorescence emission (DMF, exc 423 nm) λ_{max}, nm: 473, 499; (DMF, exc 495 nm) λ_{max}, nm: 540, 581, 640; (DMF, exc 609 nm) λ_{max}, nm: 642. Fluorescence excitation (DMF, emis 640 nm) λ_{max}, nm: 462, 492, 528, 614.

Peptide **4-19**: MALDI-Tof LRMS [M+Na]$^+$ calcd for [C$_{297}$H$_{377}$BN$_{54}$O$_{64}$F$_2$NaS$_2$]$^+$: 5859.7, not found; [M(-boronate) + Na]$^+$ calcd for [C$_{265}$H$_{360}$N$_{54}$O$_{64}$F$_2$NaS$_2$]$^+$: 5447.6, found: 5447.7; [M(-boronate-disulfide) + Na]$^+$ calcd for [C$_{212}$H$_{300}$N$_{50}$O$_{52}$F$_2$NaS]$^+$: 4471.2, found: 4471.2. UV/Vis (DMF) λ_{max}, nm (ε, L mol^{-1} cm^{-1}): 429 (39400), 457 (49900), 492 (54600), 529 (69500), 612 (23900). Fluorescence emission (DMF, exc 423 nm) λ_{max}, nm: 474, 497, 641; (DMF, exc 495 nm) λ_{max}, nm: 540, 581, 641; (DMF, exc 609 nm) λ_{max}, nm: 642. Fluorescence excitation (DMF, emis 640 nm) λ_{max}, nm: 345, 362, 461, 492, 528, 614.

Peptide **4-20**: MALDI-Tof LRMS [M+Na]$^+$ calcd for [C$_{335}$H$_{441}$BN$_{66}$O$_{76}$F$_2$NaS$_2$]$^+$: 6740.2, not found; [M(-boronate) + Na]$^+$ calcd for [C$_{303}$H$_{424}$N$_{66}$O$_{76}$F$_2$NaS$_2$]$^+$: 6328.1, found: 6328.1; UV/Vis

(DMF) λ_{max}, nm (ε, L mol^{-1} cm^{-1}): 428 (34700), 456 (44100), 492 (33800), 528 (45000), 612 (23520). Fluorescence emission (DMF, exc 423 nm) λ_{max}, nm: 473, 498, 641; (DMF, exc 495 nm) λ_{max}, nm: 540, 580, 641; (DMF, exc 609 nm) λ_{max}, nm: 641. Fluorescence excitation (DMF, emis 640 nm) λ_{max}, nm: 345, 362, 461, 492, 528, 614.

Peptide **4-23**: MALDI-Tof LRMS [M+Na]$^+$ calcd for [C$_{269}$H$_{329}$BN$_{46}$O$_{56}$F$_2$NaS$_2$]$^+$: 5235.4, found: 5235.4; [M(-boronate) + Na]$^+$ calcd for [C$_{237}$H$_{312}$N$_{46}$O$_{56}$F$_2$NaS$_2$]$^+$: 4823.2, found: 4823.3; [M(-disulfide) + Na]$^+$ calcd for [C$_{216}$H$_{269}$BN$_{42}$O$_{44}$F$_2$NaS]$^+$: 4259.0, found: 4259.0; [M(-boronate-disulfide) + Na]$^+$ calcd for [C$_{184}$H$_{252}$N$_{42}$O$_{44}$F$_2$NaS]$^+$: 3846.8, found: 3846.8. UV/Vis (DMF) λ_{max}, nm (ε, L mol^{-1} cm^{-1}): 429 (31300), 456 (46000), 492 (45900), 528 (71400), 612 (23700). Fluorescence emission (DMF, exc 423 nm) λ_{max}, nm: 473, 499, 536, 641; (DMF, exc 495 nm) λ_{max}, nm: 539, 580, 641; (DMF, exc 609 nm) λ_{max}, nm: 642. Fluorescence excitation (DMF, emis 640 nm) λ_{max}, nm: 345, 361, 430, 459, 491, 528, 612. UV/Vis (DMA) λ_{max}, nm (ε, L mol^{-1} cm^{-1}): 428 (30000), 455 (47100), 491 (58750), 528 (96700), 612 (23900). Fluorescence emission (DMA, exc 423 nm) λ_{max}, nm: 471, 498, 534, 641; (DMA, exc 495 nm) λ_{max}, nm: 538, 580, 641; (DMA, exc 609 nm) λ_{max}, nm: 641. Fluorescence excitation (DMA, emis 640 nm) λ_{max}, nm: 345, 360, 430, 458, 491, 527, 612.

Peptide **4-42**: MALDI-Tof LRMS [M+Na]$^+$ calcd for [C$_{263}$H$_{322}$BN$_{45}$O$_{55}$F$_2$NaS$_2$]$^+$: 5126.3, not found; [M(-boronate) + Na]$^+$ calcd for [C$_{231}$H$_{305}$N$_{45}$O$_{55}$F$_2$NaS$_2$]$^+$: 4714.2, found: 4714.2; [M(-boronate-disulfide) + Na]$^+$ calcd for [C$_{178}$H$_{245}$N$_{41}$O$_{43}$F$_2$NaS]$^+$: 3737.8, found: 3737.8. UV/Vis (DMF) λ_{max}, nm (ε, L mol^{-1} cm^{-1}): 429 (32850), 456 (49770), 492 (52440), 528 (81590), 612 (23520). Fluorescence emission (DMF, exc 423 nm) λ_{max}, nm: 471, 498, 534, 641; (DMF, exc 495 nm) λ_{max}, nm: 538, 580, 641; (DMF, exc 609 nm) λ_{max}, nm: 641. Fluorescence excitation (DMF, emis 640 nm) λ_{max}, nm: 346, 360, 429, 462, 488, 528, 614.

Peptide **4-43**: MALDI-Tof LRMS [M+Na]$^+$ calcd for [C$_{265}$H$_{326}$BN$_{45}$O$_{55}$F$_2$NaS$_2$]$^+$: 5154.4, not found; [M(-boronate) + Na]$^+$ calcd for [C$_{233}$H$_{309}$N$_{45}$O$_{55}$F$_2$NaS$_2$]$^+$: 4742.2, found: 4742.2; [M(-boronate-disulfide) + Na]$^+$ calcd for [C$_{180}$H$_{249}$N$_{41}$O$_{43}$F$_2$NaS]$^+$: 3765.8, found: 3765.8. UV/Vis (DMF) λ_{max}, nm (ε, L mol^{-1} cm^{-1}): 429 (28700), 456 (42600), 492 (49300), 528 (74100), 612 (23900). Fluorescence emission (DMF, exc 423 nm) λ_{max}, nm: 473, 496, 534, 641; (DMF, exc 495 nm) λ_{max}, nm: 539, 580, 642; (DMF, exc 609 nm) λ_{max}, nm: 642. Fluorescence excitation (DMF, emis 640 nm) λ_{max}, nm: 345, 361, 429, 462, 491, 528, 615.

6.2.4 Experimental procedures for Chapter 5

6.2.4.1 ADIBO and TCO-emitter synthesis

6.2.4.1.1 Synthesis of ADIBO-amine 5-19

The following synthesis was performed following the literature.[32] However, the characterization of **5-7**, **5-8** and **5-9** being not mentioned in the paper, it was decided to report those three steps. Moreover, slight modification of the reported protocol was done, so the synthesis of **5-10** is described as well.
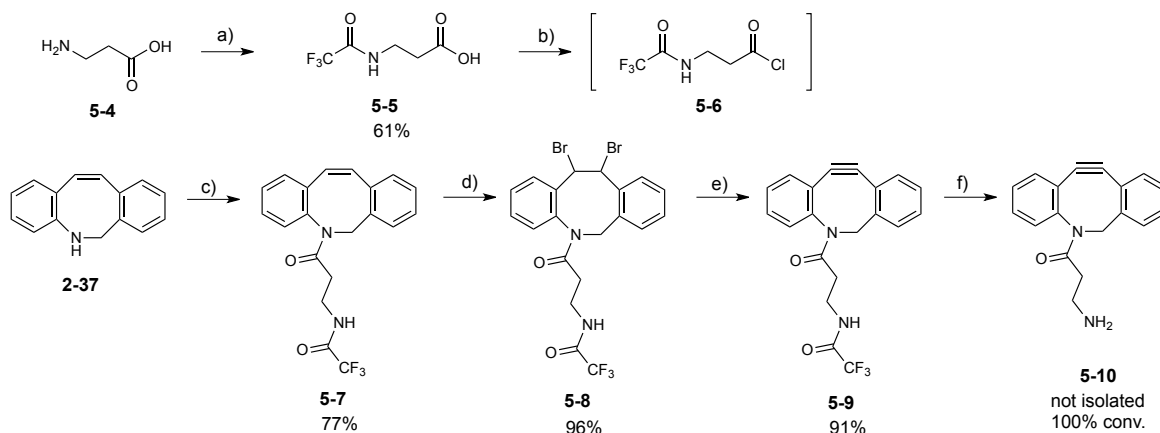
Scheme 6-22 Synthesis of ADIBO-amine **5-10**; a) ethyltrifluoroacetate, NEt$_3$, MeOH, rt, 24 h; b) oxalyl chloride, DMF (cat), CH$_2$Cl$_2$, rt, 2 h; c) **5-6**, pyridine, CH$_2$Cl$_2$, rt, 1 h; d) pyridinium tribromide, CH$_2$Cl$_2$, rt, 18 h; e) *t*BuOK, THF, rt, 1 h; f) K$_2$CO$_3$, MeOH/H$_2$O, rt, 18 h.

6.2.4.1.1.1 Synthesis of *N*-(3-(Dibenzo[b,f]azocin-5(6H)-yl)-6-oxopropyl)trifluoroacetamide 5-7

5-7
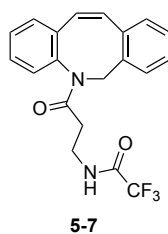
To a solution of 5,6-dihydrodibenzoazocine **2-43** (658 mg, 3.35 mmol) in CH$_2$Cl$_2$ (10 mL), pyridine (435 µL, 5.34 mmol) and a solution of acyl chloride **5-6** (3.92 mmol) in CH$_2$Cl$_2$ (9 mL) were successively added. The reaction mixture was stirred at rt for 2 h, diluted in CH$_2$Cl$_2$ and water. The layers were separated, the aqueous phase was extracted with CH$_2$Cl$_2$ and the combined organic phases were washed with brine, dried and concentrated under reduced pressure. The crude material was purified through silica gel column chromatography (Eluent: hexane/EtOAc 2:3) to give **5-7** as an orange oil (1.25 g, 77%). IR (film): ν (cm^{-1}) 3298, 3047, 3018, 2916, 1595, 1570, 1491, 1450, 1331, 1269, 1103, 800, 742, 617, 449; ^{1}H NMR (300 MHz, CDCl$_3$) δ_H 7.4 (*br s*, -NH),

7.30-7.24 (*m*, 4H), 7.20-7.12 (*m*, 4H), 6.78 (*d*, *J* = 13 Hz, 1H), 6.56 (*d*, *J* = 13 Hz, 1H), 5.54 (*d*, *J* = 15 Hz, 1H), 4.29 (*d*, *J* = 15 Hz, 1H), 3.52-3.43 (*m,* 2H), 2.33-2.23 (*m*, 1H), 2.06-1.97 (*m*, 1H); ^{13}C NMR (75 MHz, CDCl$_3$) δ_C 171.05, 157.32, 139.93, 136.38, 135.53, 134.18, 133.00, 132.32, 131.15, 130.08, 128.96, 128.68, 127.99, 127.63, 127.30, 126.99, 54.54, 35.62, 33.71.

6.2.4.1.1.2 Synthesis of *N*-(3-Trifluoroacetamidopropanoyl)-11,12-dibromo-11,12-dihydro-dibenzo[b,f]azocine 5-8

5-8
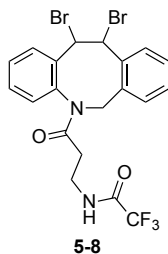
To a solution of dibenzocyclooctene **5-7** (1 g, 2.67 mmol) in CH$_2$Cl$_2$ (10 mL) pyridinium tribromide (1.03 g, 3.22 mmol) was added at rt. The reaction mixture was stirred at rt for 18 h, diluted in CH$_2$Cl$_2$ and washed with HCl 5%. The layers were separated and the organic phase was washed with brine, dried and concentrated. The remaining oil was purified through silica gel column chromatography (Eluent: EtOAc/P.E. 2:3) to give **5-8** as a white solid (1.37 g, 96%). M.p.: 160 °C decomposition; IR (film): ν (cm^{-1}) 3298, 3078, 1717, 1651, 1647, 1558, 1495, 1398, 1202, 1177, 1157, 762, 727, 663; ^{1}H NMR (300 MHz, CDCl$_3$) δ_H 7.72 (*d*, *J* = 7.4 Hz, 1H), 7.60 (*br s*, - NH), 7.28-6.89 (*m*, 7H), 5.85 (*d*, *J* = 10 Hz, 1H), 5.82 (*d*, *J* = 15 Hz, 1H), 5.16 (*d*, *J* = 10 Hz, 1H), 4.20 (*d*, *J* = 15 Hz, 1H), 3.72-3.52 (*m,* 2H), 2.65 (*ddd*, *J* = 17.3, 6.7 and 3.4 Hz, 1H), 2.38 (*ddd*, *J* = 17.3, 8.3 and 3.7 Hz, 1H); ^{13}C NMR (75 MHz, CDCl$_3$) δ_C 172.22, 138.12, 137.12, 136.27, 132.26, 131.14, 130.94, 130.48, 130.06, 129.88, 129.34, 129.26, 128.81, 60.06, 55.45, 52.47, 35.71, 34.84 (one C$_{Amide}$ not observed).

6.2.4.1.1.3 Synthesis of *N*-(3-Trifluoroacetamidopropanoyl)-5,6-dihydro-11,12-didehydro-dibenzo[b,f]azocine 5-9

5-9
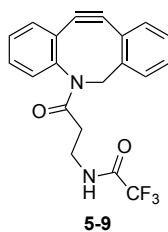
To a suspension of *t*BuOK (365 mg, 3.26 mmol) in THF (2.5 mL), a solution of dibromo derivative **5-8** (348 mg, 0.65 mmol) in THF (3.5 mL) was added. The reaction mixture was stirred

at rt for 30 min, diluted in EtOAc, washed with an aqueous solution of HCl 5% and brine, dried, and concentrated. **5-9** was used without any further purification as a colorless oil (220 mg, 91%). IR (film): ν (cm^{-1}) 3287, 3071, 2930, 1717, 1647, 1549, 1435, 1400, 1204, 1152, 762, 752, 737, 729, 519; ^{1}H NMR (300 MHz, CDCl$_3$) δ_H 7.66 (*d*, *J* = 7.2 Hz, 1H), 7.44-7.28 (*m*, 7H), 7.17 (*br s*, -NH), 5.14 (*d*, *J* = 14 Hz, 1H), 3.72 (*d*, *J* = 14 Hz, 1H), 3.52-3.45 (*m,* 1H), 3.31-3.21 (*m*, 1H), 2.53 (*ddd*, *J* = 17, 8.4, 3.9 Hz, 1H), 1.97 (*ddd*, *J* = 17, 6.9, 3.4 Hz, 1H); ^{13}C NMR (75 MHz, CDCl$_3$) δ_C 171.72, 156.78, 150.70, 147.80, 132.07, 129.05, 128.81, 128.74, 128.49, 128.07, 127.47, 125.87, 122.86, 122.79, 115.12, 107.42, 55.74, 35.70, 34.05.

6.2.4.1.1.4 Synthesis of *N*-(3-Aminopropionyl)-5,6-dihydro-11,12-didehydrodibenzo[b,f]-azocine (ADIBO-amine) 5-10

5-10
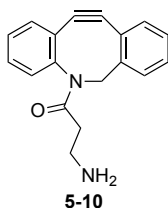
To a solution of cyclooctyne **5-9** (47 mg, 0.13 mmol) in MeOH (1.5 mL), a solution of K$_2$CO$_3$ (35 mg, 0.25 mmol) in H$_2$O (0.7 mL) was added. The reaction mixture was stirred at rt for 16 h. Solvents were removed under reduced pressure, the residue was re-dissolved in CH$_2$Cl$_2$/EtOAc (1:4), then washed with water and brine. The organic phase was dried and concentrated under reduced pressure. The crude material was used without any further purification and was directly used for the next step (unstable). ^{1}H NMR, ^{13}C NMR of the crude material were obtained in accordance with the literature.[32]

6.2.4.1.2 Synthesis of ADIBO-perylene 5-1
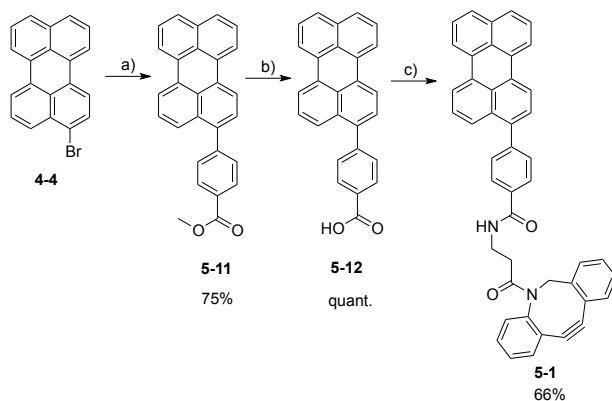
Scheme 6-23 Synthesis of ADIBO-perylene **5-1**; a) 4-Methoxycarbonylphenylboronic acid, [Pd(PPh$_3$)$_4$], K$_2$CO$_3$, dioxane/H$_2$O (7:1), 80 °C, 16 h; b) NaOH 2M (aq), THF/EtOH, rt, 20 h; c) ADIBO-amine **5-10**, EDC.HCl, DMAP, CH$_2$Cl$_2$, rt, 20 h.

6.2.4.1.2.1 Synthesis of methyl 4-(perylen-3-yl)benzoate 5-11

5-11
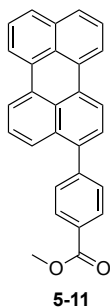
Bromo-perylene **4-4** (66 mg, 0.2 mmol) and K_2CO_3 (110 mg, 0.8 mmol) were suspended in dioxane (10 mL) and H_2O (1.5 mL). The mixture was degassed with nitrogen under sonication for 20 min. $[Pd(PPh_3)_4]$ (23 mg, 0.02 mmol) and 4-methyl ester phenyl boronic acid (72 mg, 0.4 mmol) were simultaneously added. The reaction mixture was stirred at 80 °C for 16 h. Water was added and the mixture was extracted with CH_2Cl_2 (3 times). The organic phase was washed with brine, dried and concentrated. The crude material was purified through silica gel short column chromatography (Eluent: CH_2Cl_2/P.E. (3:7) to (1:1)) to give methyl ester **5-11** as a yellow solid (58 mg, 75%). M.p.: 210-211 °C; IR (film): ν (cm^{-1}) 3044, 2959, 2922, 2851, 1717, 1608, 1497, 1389, 1287, 1103, 866, 806, 763, 706, 598; ^{1}H NMR (300 MHz, CDCl$_3$): δ_H 8.21-8.16 (*m*, 6H), 7.69 (*d*, *J* = 8.1 Hz, 3H), 7.59 (*d*, *J* = 8.1 Hz, 2H), 7.48 (*t*, *J* = 7.8 Hz, 2H), 7.41 (*t*, *J* = 8.1 Hz, 2H), 3.99 (*s*, 3H); ^{13}C NMR (75 MHz, CDCl$_3$): δ_C 167.16, 145.71, 138.82, 134.79, 132.73, 131.65, 131.42, 131.36, 131.13, 130.23, 130.15, 129.85, 129.20, 128.72, 128.17, 128.09, 127.88, 126.94, 126.79, 126.77, 125.72, 120.64, 120.60, 120.49, 119.95, 52.37. ESI-HRMS [M+H]$^+$ calcd for [$C_{28}H_{19}O_2$]$^+$: 387.1385, found: 387.1378.

6.2.4.1.2.2 Synthesis of 4-(perylen-3-yl)benzoic acid 5-12

5-12
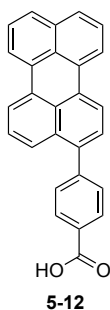
To a solution of methyl-(4-perylene)benzoate ester **5-11** (44 mg, 0.113 mmol) in EtOH (4 mL) and THF (3 mL), a solution of NaOH (2 M, aq) (2.5 mL) was added. The reaction mixture was stirred at rt for 20 h. HCl 5% (aq) was added and the aqueous phase was extracted with CH_2Cl_2/THF mixture. The organic phase was washed with brine, dried, and concentrated to afford **5-12** as a

yellow solid (42 mg, quant.). M.p.> 250 °C; IR (film): ν (cm^{-1}) 3342, 3048, 2985, 2939, 1601, 1497, 1412, 1312, 1049, 980, 866, 839, 821, 804, 772, 758, 739, 424, 209; ^{1}H NMR (300 MHz, DMSO- d_6): δ_H 8.44-8.38 (*m*, 4H), 8.11 (*d*, *J* = 8.2 Hz, 2H), 7.82 (*d*, *J* = 8.2 Hz, 2H), 7.71-7.63 (*m*, 3H), 7.56 (*t*, *J* = 8.1 Hz, 3H), 7.48 (*d*, *J* = 7.8 Hz, 1H); ^{13}C NMR (75 MHz, DMSO-d_6): δ_C 144.27, 138.40, 134.34, 132.01, 130.99, 130.61, 130.52, 130.28, 130.20, 129.97, 129.70, 128.37, 128.29, 128.22, 128.10, 127.85, 127.85, 127.45, 127.10, 125.34, 121.19, 121.13, 121.04, 120.54 (COOH not observed). The mass of the compound was not obtained due to its low solubility in volatile solvents.

6.2.4.1.2.3 Synthesis of Aza-dibenzocyclooctyne-perylene (ADIBO-Per) 5-1

5-1
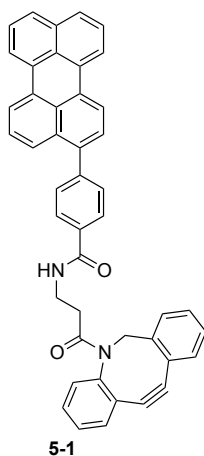
4-(perylen-3-yl)benzoic acid **5-12** (23 mg, 0.06 mmol), EDC.HCl (13 mg, 0.07 mmol), DMAP (0.7 mg, 0.01 mmol) were suspended in a solution of amine-cyclooctyne **5-10** (0.12 mmol) in CH$_2$Cl$_2$ (10 mL). The reaction mixture was stirred at rt for 20 h to give a clear solution. Water was added and the two layers were separated. The aqueous phase was extracted with CH$_2$Cl$_2$. The combined organic phases were washed with brine, dried and concentrated. The residue was purified through silica gel column chromatography (Eluent: P.E./EtOAc 1:4 to EtOAc) to afford perylene-cyclooctyne **5-1** as a yellow solid (25 mg, 66%). M.p. 130-132 °C; IR (film): ν (cm^{-1}) 3327, 3049, 2924, 2864, 1715, 1638, 1529, 1387, 1287, 1188, 1107, 1016, 827, 808, 763, 727, 543, 410; ^{1}H NMR (300 MHz, CDCl$_3$): δ_H 8.27-8.22 (*m,* 4H), 7.75-7.69 (*m*, 4H), 7.64 (*d*, *J* = 8.2 Hz, 2H), 7.53-7.22 (*m*, 13H), 6.82 (*t*, *J* = 6 Hz, 1H, -NH), 5.19 (*d*, *J* = 13.9 Hz, 1H), 3.73 (*d*, *J* = 13.9 Hz, 1H), 3.61-3.51 (*m,* 2H), 2.61 (*ddd*, *J* = 16.5, 7, 4.1 Hz, 1H), 2.12 (*ddd*, *J* = 16.5, 7, 4.1 Hz, 1H); ^{13}C NMR (75 MHz, CDCl$_3$): δ_C 172.48, 167.01, 151.07, 148.07, 143.88, 138.96, 134.77, 133.58, 132.80, 132.30, 131.61, 131.36, 131.23, 131.15, 130.11, 129.16, 128.73, 128.71, 128.61, 128.40, 128.09, 128.04, 127.93, 127.81, 127.43, 127.14, 126.85, 126.76, 125.79, 125.76, 123.09, 122.63, 120.59, 120.57, 120.41, 119.96, 114.88, 107.91, 55.64, 35.74, 35.10 (C$_{Ar}$ missing due to

overlapping). ESI-HRMS [M+H]$^+$ calcd for [C$_{45}$H$_{31}$N$_2$O$_2$]$^+$: 631.2386, found: 631.2402. UV/Vis (DMF) λ_{max}, nm (ε, L mol^{-1} cm^{-1}): 450 (45000), 424 (37000). Fluorescence emission (DMF, exc 423 nm) λ_{max}, nm: 470, 496; Quantum Yield = 96% (determined from perylene (QY=94% in cyclohexane)).[23]

6.2.4.1.3 Synthesis of ADIBO-ethynylpyrene 5-2
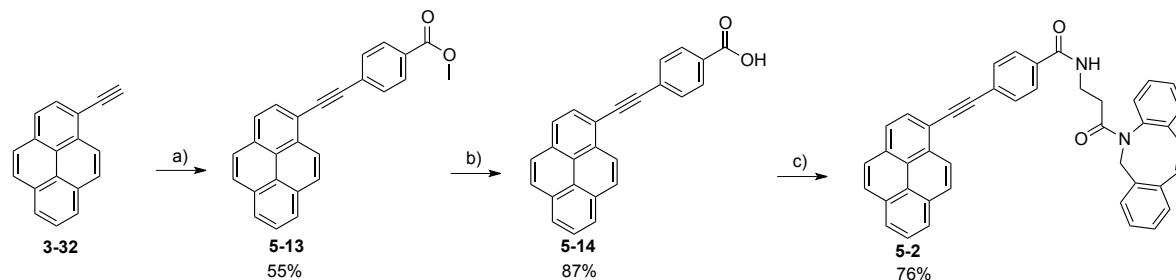
Scheme 6-24 Synthesis of ADIBO-ethynylpyrene **5-2**; a) methyl-4-bromo-benzoate, [Pd(PPh$_3$)$_2$Cl$_2$], CuI, NEt$_3$, THF, 40 °C, 16 h; b) NaOH 2M (aq), THF/EtOH, rt, 3 h; c) ADIBO-amine **5-10**, EDC.HCl, DMAP, CH$_2$Cl$_2$, rt, 20 h.

6.2.4.1.3.1 Synthesis of methyl 4-(pyren-1-ylethynyl)benzoate 5-13
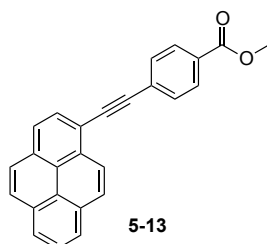
Ethynyl pyrene **3-32** (159 mg, 0.70 mmol) and methyl 4-bromobenzoate (227 mg, 1.05 mmol) were dissolved in dry THF (9 mL). Triethylamine (0.49 mL, 3.50 mmol) was added and the solution was degassed with nitrogen under sonications for 15 min. CuI (27 mg, 0.14 mmol) and [Pd(PPh$_3$)$_2$Cl$_2$] (49 mg, 0.07 mmol) were simultaneously added. The reaction mixture was stirred at 50 °C for 16 h. The solvents were evaporated. The crude residue was purified through silica gel column chromatography (Eluent: CH$_2$Cl$_2$/P.E. 3:7 to 1:1) to afford **5-13** as a yellow solid (140 mg, 55%). The compound was characterized in agreement with the literature.[33] ^{1}H NMR (300 MHz, CDCl$_3$) δ_H 8.64 (d, J = 9.1 Hz, 1H), 8.26-8.19 (m, 4H), 8.15-8.02 (m, 6H), 7.77 (d, J = 9.4 Hz, 2H), 3.97 (s, 3H); ^{13}C NMR (75 MHz, CDCl$_3$) δ_C 166.75, 132.19, 131.76, 131.69, 131.35, 131.15, 129.89, 129.79, 129.63, 128.72, 128.60, 128.37, 127.37, 126.47, 125.96, 125.92, 125.48, 124.70, 124.59, 124.39, 117.18, 94.45, 91.85, 52.44.

6.2.4.1.3.2 Synthesis of 4-(pyren-1-ylethynyl)benzoic acid 5-14

5-14
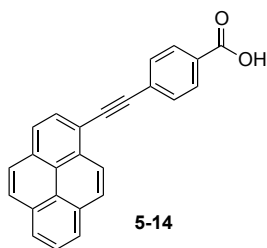
To a suspension of methyl ester **5-13** (108 mg, 0.3 mmol) in EtOH/THF (6 mL/5 mL), NaOH 2 M (aq) (5 mL) was added. The reaction mixture was stirred at rt for 18 h. HCl 5% (aq) was added until pH 3 and the mixture was extracted with CH_2Cl_2/THF mixture (3 times). The combined organic layers were washed with brine, dried and concentrated to give **5-14** as a yellow solid (90 mg, 87%). The compound was characterized in agreement with the literature.[33] ^{1}H NMR (300 MHz, DMSO-d_6) δ_H 13.26 (*br s*, 1H, -COOH), 8.64 (*d*, *J* = 9.1 Hz, 1H), 8.43-8-36 (*m*, 3H), 8.34-8.22 (*m*, 4H), 8.15 (*t*, *J* = 7.7 Hz, 1H), 8.06 (*d*, *J* = 8.3 Hz, 2H), 7.90 (*d*, *J* = 8.3 Hz, 2H); ^{13}C NMR (75 MHz, DMSO-d_6) δ_C 166.82, 131.77, 131.40, 131.34, 130.81, 130.71, 130.52, 129.91, 129.74, 129.17, 128.76, 127.31, 126.94, 126.80, 126.24, 125.07, 124.82, 123.67, 123.39, 116.13, 94.52, 91.01 (one C_{Ar} missing due to overlapping).

6.2.4.1.3.3 Synthesis of Aza-dibenzocyclooctyne-ethynyl-pyrene (ADIBO-Py) 5-2

5-2
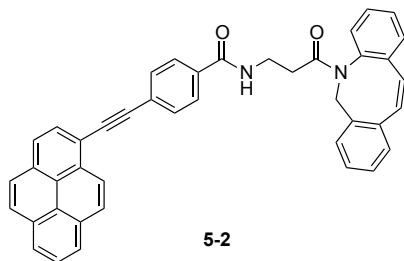
Ethynylpyrene **5-14** (27 mg, 0.08 mmol), EDC.HCl (16.5 mg, 0.09 mmol), DMAP (1 mg, 0.01 mmol) were dissolved in a solution of amine **5-10** (0.09 mmol) in CH_2Cl_2 (6 mL). The reaction mixture was stirred at rt for 20 h. H_2O was added and the layers were separated. The aqueous phase was extracted with CH_2Cl_2 (2 times). The combined organic phases were washed with brine, dried and concentrated. The crude material was purified through silica gel column chromatography (Eluent: EtOAc/hexane 1:1 to EtOAc) to give ADIBO-Py **5-2** as a yellow oil (36 mg, 76%). IR (film): ν (cm^{-1}) 3331, 2980, 2926, 2870, 1647, 1541, 1493, 1406, 1302, 847, 766, 735, 716; ^{1}H NMR (300 MHz, CDCl$_3$) δ_H 8.67 (*d*, *J* = 9.1 Hz, 1H), 8.27-8-21 (*m*, 4H), 8.17-8.02 (*m*, 4H), 7.75-7.68 (*m*, 3H), 7.60-7.56 (*m*, 2H), 7.47-7.32 (*m*, 6H), 7.24-7.21 (*m*, 1H), 6.78 (*t*, *J* = 6.0 Hz, 1H, -*NH*), 5.20 (*d*, *J* = 13.9 Hz, 1H), 3.73 (*d*, *J* = 13.9 Hz, 1H), 3.59-3.49 (*m*, 2H), 2.58 (*ddd*, *J* = 16.5, 7.0, 4.5 Hz, 1H), 2.12 (*dt*, *J* = 16.5, 7.0, 4.0 Hz, 1H); ^{13}C NMR (75 MHz, CDCl$_3$)

δ_C 171.91, 166.48, 140.40, 136.19, 135.58, 134.62, 134.04, 132.61, 132.16, 131.80, 131.68, 131.56, 131.37, 131.18, 130.35, 129.88, 128.88, 128.69, 128.52, 128.10, 127.58, 127.39, 127.28, 127.22, 126.74, 126.46, 125.93, 125.87, 125.56, 124.71, 124.62, 124.43, 117.37, 94.52, 91.05, 54.82, 35.79, 34.60 (one C_{Ar} missing due to overlapping). ESI-MS calcd for $[C_{43}H_{31}N_2O_2]^+$: 607.2386; found: 607.2383. UV/Vis (DMF) λ_{max}, nm (ε, L mol^{-1} cm^{-1}): 395 (39000), 371 (39600). Fluorescence emission (DMF, exc 423 nm) λ_{max}, nm: 426; Quantum Yield = 48% (determined from quinine hemisulfate (QY=54.6% in 0.5 M H_2SO_4)).[20]

6.2.4.1.4 Synthesis of TCO-cyanine 5-3
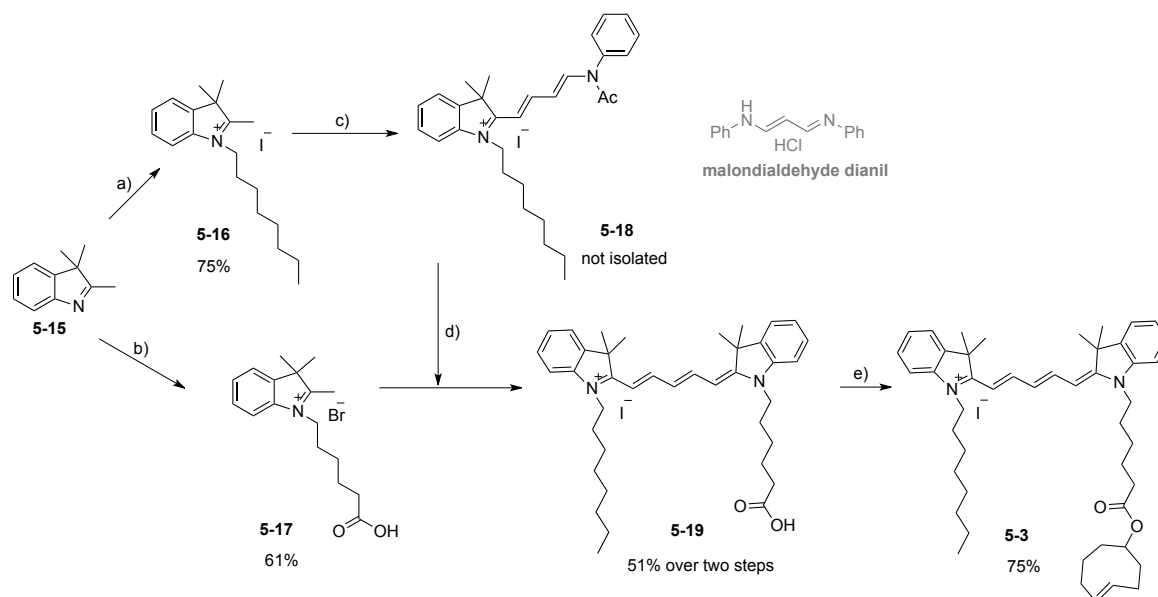
Scheme 6-25 Synthesis of TCO-cyanine **5-3**; a) 1-iodooctane, 145 °C, 3 h; b) 6-bromohexanoic acid, o-dichlorobenzene, 120 °C, 24 h; c) malondialdehyde dianil HCl, Ac$_2$O, 140 °C, 2 h; d) NaOAc, EtOH, 90 °C, 3 h; e) *trans*-cyclooctenol **2-43**, EDC.HCl, DMAP, CH$_2$Cl$_2$, rt, 20 h.

6.2.4.1.4.1 Syntheses of 5-16, 5-17 and 5-19
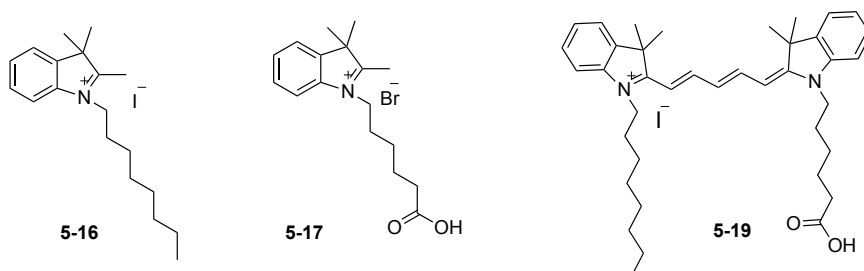
5-16, 5-17, 5-19 have been synthesized according to the literature.[34]

6.2.4.1.4.2 Synthesis of TCO-cyanine 5-3

5-3
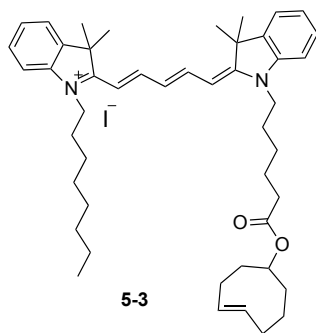
To unsymmetrical cyanine **5-19** (38 mg, 0.05 mmol) and EDC.HCl (15 mg, 0.08 mmol), a solution of *trans*-cyclooctenol **2-43** (15 mg, 0.12 mmol) in CH_2Cl_2 (1.5 mL) was added. Subsequently, another solution of DMAP (0.7 mg, 0.01 mmol) in CH_2Cl_2 (0.5 mL) was added. The reaction mixture was stirred at rt for 24 h protected from the light. The mixture was diluted in CH_2Cl_2, washed with water and brine, dried and concentrated. The residue was purified through silica gel column chromatography (Eluent: CH_2Cl_2 to CH_2Cl_2/MeOH 95:5) to give a blue oil which was precipitated in hexane to afford cyanine-TCO **5-3** as a blue sticky solid (storage at -20 °C) (33 mg, 75%). IR (film): ν (cm^{-1}) 3298, 2927, 2858, 1654, 1452, 1384, 1334, 1130, 1097, 1018, 926; ^{1}H NMR (300 MHz, CD$_3$OD): δ_H 8.27 (*t*, *J* = 13.2 Hz, 2H), 7.50 (*d*, *J* = 7.3 Hz, 2H), 7.44-7.36 (*m*, 2H), 7.30-7.24 (*m*, 4H), 6.65 (*t*, *J* = 12.4 Hz, 1H), 6.30 (*d*, *J* = 13.6 Hz, 2H), 5.63-5.36 (*m*, 2H), 4.41-4.36 (*m*, 1H), 4.11 (*t*, *J* = 7.2 Hz, 4H), 2.35-2.28 (*m*, 4H), 2.27 (*t*, *J* = 7.3 Hz, 2H), 1.97-1.76 (*m*, 10H), 1.74 (*s*, 12H), 1.69-1.57 (*m*, 6H), 1.51-1.23 (*m*, 12H), 0.91-0.86 (*m*, 3H); ^{13}C NMR (75 MHz, CD$_3$OD) δ_C 174.79, 174.70, 174.55, 155.46, 143.57, 142.69, 142.65, 136.14, 136.00, 133.84, 133.52, 129.76, 126.67, 126.30, 126.23, 112.11, 112.07, 104.43, 81.50, 78.29, 50.60, 50.56, 44.92, 44.75, 41.87, 41.79, 39.59, 35.35, 35.18, 35.11, 33.67, 33.50, 32.88, 32.40, 32.07, 30.39, 30.28, 28.47, 28.19, 27.99, 27.95, 27.84, 27.28, 25.69, 23.69, 14.45 (extra C due to mixture of diastereoisomers). ESI-HRMS [M-I]$^+$ calcd for [$C_{47}H_{65}N_2O_2$]$^+$: 689.5046, found: 689.5046.

6.2.4.1.5 Tetrazine ligation with TCO-cyanine 5-3

Scheme 6-26 Tetrazine ligation with cyanine dye; a) THF, rt, 1 h

To TCO-cyanine **5-3** (8 mg, 0.011 mmol), a solution of dipyridyl-tetrazine **2-52** (5.2 mg, 0.022 mmol) in THF (2 mL) was added. The reaction mixture was stirred at rt for 1 h. The solvent was removed under reduced pressure. The crude ^{1}H NMR showed the full conversion of cyanine-TCO into tetrazine ligation product (Figure 6-20). The crude material was purified through silica gel preparative plate (Eluent: CH$_2$Cl$_2$/MeOH 95:5) to remove the excess of tetrazine **2-52** affording **5-20** as mixture of isomers. IR (film): ν (cm^{-1}) 3366, 2924, 2855, 1722, 1575, 1477, 1446, 1373, 1331, 1215, 1128, 1085, 1041, 1015, 922, 787, 746, 708, 553; ESI-HRMS [M-I]$^+$ calcd for [C$_{59}$H$_{73}$N$_6$O$_2$]$^+$: 897.5795, found: 897.5825.

Figure 6-20 ^{1}H NMR of TCO-cyanine **5-3** (bottom), crude material showing full conversion into product and excess of tetrazine (middle), tetrazine ligation product **5-20** (top) in MeOD-d_4

6.2.4.1.6 Cyclic voltammetry

The experiments were carried out according to the procedure described in *Section 6.2.3.3* in CH_2Cl_2 using ferrocene (Fc^+/Fc) as internal reference and $TBAPF_6$ (0.1 M) as supporting electrolyte.
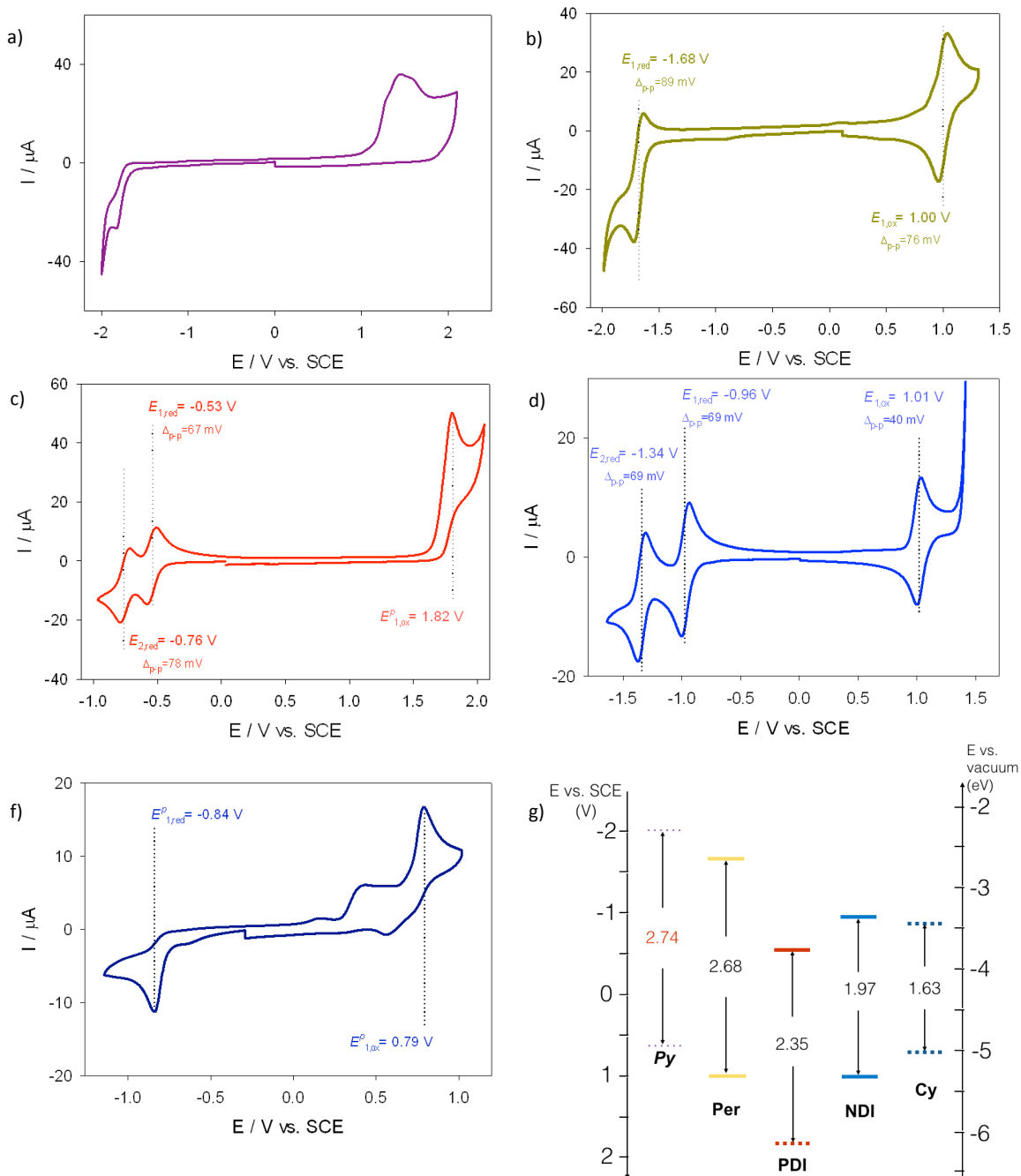
Figure 6-21 Cyclic voltammograms of a) Py-ADIBO **5-2** (1.12 mM, 0.05 V/s); b) Y-Per **4-5** (0.98 mM, 0.2 V/s); c) R-PDI **4-2** (1.35 mM, 0.05 V/s); d) B-NDI **3-24** (0.96 mM, 0.05 V/s); e) B-Cy **5-19** (0.87 mM, 0.05 V/s) in CH_2Cl_2. $TBAPF_6$ (ca. 0.1 M) was added as a supporting electrolyte; ferrocene was used as internal reference (Fc^+/Fc=0.46 V vs. SCE). f) Comparison between the redox potentials (solid lines corresponding to halfwave potentials; dashed lines to peak potentials).

6.2.4.2 Synthesis of modified amino acids

6.2.4.2.1 Synthesis of (*S*)-2-((((9*H*-fluoren-9-yl)methoxy)carbonyl)amino)-6-azidohexanoic acid 5-21
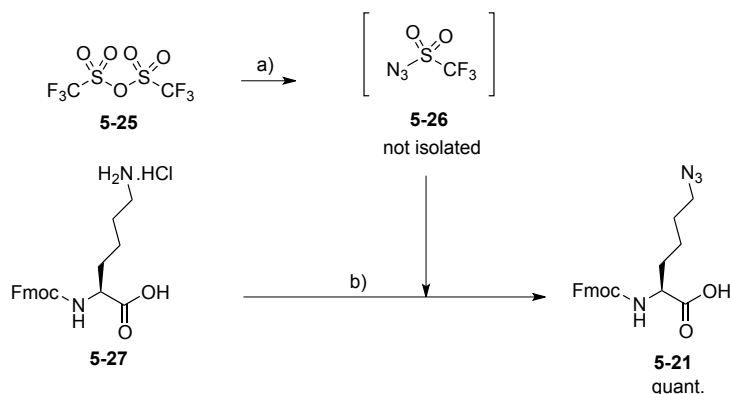
Scheme 6-27 Synthesis of Fmoc-Nle(N$_3$)-OH **5-21**; a) NaN$_3$, H$_2$O/CH$_2$Cl$_2$, rt, 2 h; b) NaHCO$_3$, CuSO$_4$.5H$_2$O, H$_2$O/MeOH (1:2), rt, 18 h.

Sodium azide (1.45 g, 22.3 mmol) was dissolved in H$_2$O (4.3 mL) and CH$_2$Cl$_2$ (7.2 mL). Triflic anhydride **5-25** (0.73 mL, 4.46 mmol) was slowly added. The reaction mixture was stirred at rt for 2 h. The layers were separated and the aqueous phase was extracted with a minimum of CH$_2$Cl$_2$ (15 mL). The combined organic layers were washed with saturated aqueous solution of NaHCO$_3$, brine and used directly for the next step. Fmoc-Lys-OH.HCl **5-27** (901 mg, 2.23 mmol), NaHCO$_3$ (1.87 g, 22.3 mmol) and CuSO$_4$.5H$_2$O (5.5 mg, 0.02 mmol) were dissolved in H$_2$O (8 mL) and CH$_3$OH (16 mL). Triflic azide **5-26** (4.46 mmol) in CH$_2$Cl$_2$ (15 mL) was added and the mixture was stirred at rt for 18 h. The organic solvents were removed under reduced pressure and the remaining solution was acidified at pH 2 with HCl 10%. The aqueous phase was extracted with EtOAc (3 times). The organic phase was washed with brine, dried and concentrated. The crude residue was purified through silica gel column chromatography (Eluent: CH$_2$Cl$_2$/MeOH 9:1) to afford **5-21** as a white solid in accordance with the literature (880 mg, quant.).[35] IR (film): ν (cm^{-1}) 3387, 3279, 2095 (-N$_3$), 1743, 1662, 1520, 1355, 1261, 1225, 1188, 1150, 1042, 754, 735, 608, 540, 494, 426; ^{1}H NMR (300 MHz, CD$_3$OD): δ_H 7.79 (*d*, *J* = 7.5 Hz, 2H), 7.68-7.65 (*m*, 2H), 7.39 (*t*, *J* = 7.5 Hz, 2H), 7.31 (*t*, *J* = 7.5 Hz, 2H), 4.36-4.19 (*m*, 4H), 3.30-3.26 (*m*, 2H), 1.95-1.31 (*m*, 6H); ^{13}C NMR (75 MHz, CD$_3$OD): δ_C 145.34, 145.18, 142.58, 128.77, 128.16, 126.26, 120.91, 67.92, 52.22, 32.10, 29.44, 24.27 (CH$_2$ missing due to overlapping). ESI-HRMS calcd for [C$_{21}$H23N$_4$O$_4$]$^+$: 395.1719; found: 395.1725.

6.2.4.2.2 Tetrazine-containing amino acids

6.2.4.2.2.1 Syntheses of R-Glu(tetrazine)-OH 5-22 and 5-23
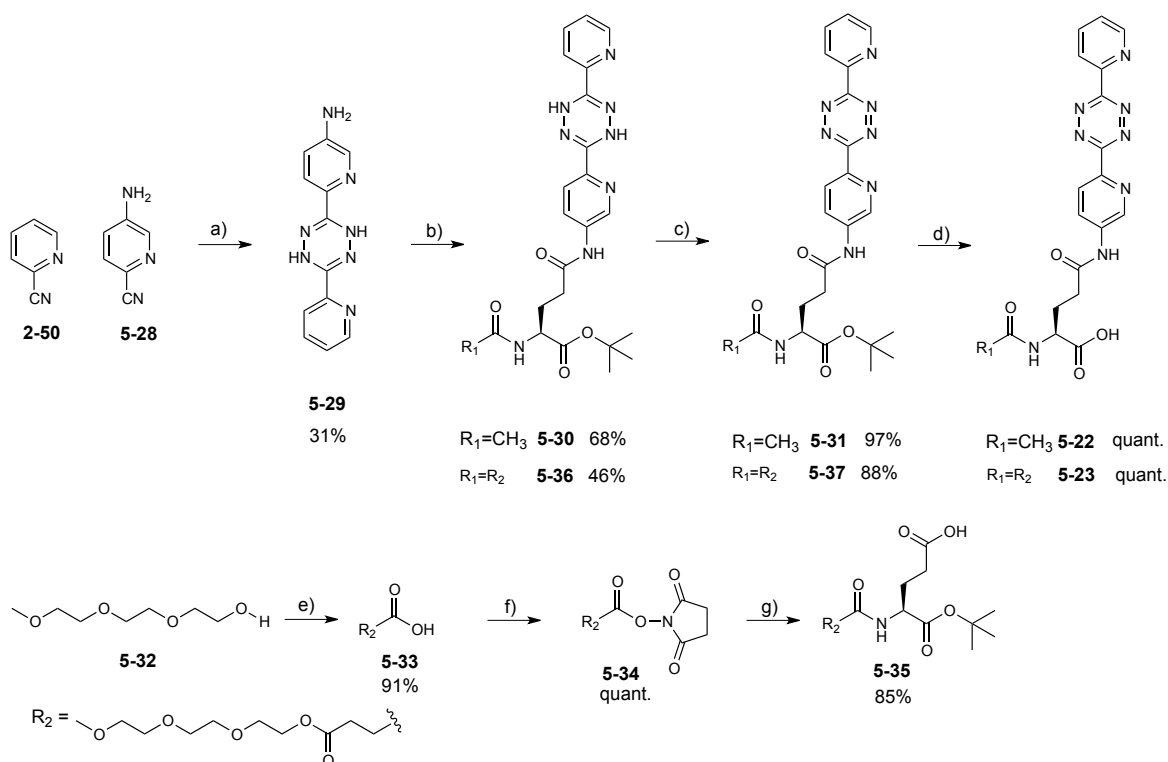
Scheme 6-28 Syntheses of tetrazine containing aa **5-22** and **5-23**; a) hydrazine hydrate, 90 °C, 12 h; b) R$_2$(CO)-Glu-O*t*Bu, EDC.HCl, DMAP, CH$_2$Cl$_2$, rt, 20 h; c) PIDA, CH$_2$Cl$_2$, rt, 1.5 h; d) TFA, CH$_2$Cl$_2$, rt, 2 h; e) succinic anhydride, DMAP, CH$_2$Cl$_2$, rt, 20 h; f) *N*-hydroxysuccinimide, EDC.HCl, DMAP, CH$_2$Cl$_2$, rt, 20 h; g) H-Glu-O*t*Bu, DIEA, DMF, rt, 16 h.

6.2.4.2.2.1.1 Synthesis of 3-(5-aminopyridin-2-yl)-6-(pyridine-2-yl)-1,4-dihydro-1,2,4,5-tetrazine 5-29
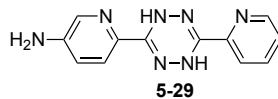
3-(5-aminopyridin-2-yl)-6-(pyridine-2-yl)-1,4-dihydro-1,2,4,5-tetrazine **5-29** has been synthesized according to the literature.[10]

6.2.4.2.2.1.2 Synthesis of Ac-L-Glu(3,6-dipyrid-2-yl-1,4-dihydro-1,2,4,5-tetrazine)-O*t*Bu 5-30

263
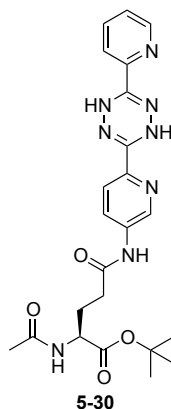
Dihydrotetrazine **5-29** (412 mg, 1.62 mmol), Ac-Glu-O*t*Bu (363 mg, 1.48 mmol), EDC.HCl (310 mg, 1.62 mmol) and DMAP (18 mg, 0.15 mmol) were suspended in CH_2Cl_2 (10 mL) and the reaction mixture was stirred at rt for 18 h. H_2O was added, the two layers were separated and the aqueous phase was extracted (2 times) with CH_2Cl_2. The combined organic layers were washed with brine, dried and concentrated. The crude material was purified through silica gel by column chromatography (Eluent: CH_2Cl_2/acetone 4:1 to 1:1) to give **5-30** as an orange solid (488 mg, 68%). M.p.: 183-187 °C; IR (film): ν (cm^{-1}) 3348, 2980, 1707, 1681, 1654, 1529, 1476, 1440, 1379, 1325, 1290, 1240, 1155, 1078, 1024, 920, 847, 748, 731, 669, 575; ^{1}H NMR (300 MHz, CDCl$_3$): δ_H 9.85 (s, 1H, -*NH*), 8.83 (d, J = 2.3 Hz, 1H), 8.57-8.53 (m, 3H), 8.20 (dd, J = 8.7, 2.3 Hz, 1H), 8.04 (d, J = 8 Hz, 1H), 8.00 (d, J = 8.7 Hz, 1H), 7.74 (td, J = 7.7, 1.7 Hz, 1H), 7.33 (ddd, J = 7.7, 4.9, 1 Hz, 1H), 6.49 (d, J = 7.8 Hz, 1H, -*NH*), 4.47 (ddd, J = 11, 7.8, 3.2 Hz, 1H), 2.50-2.45 (m, 2H), 2.32-2.23 (m, 1H), 2.10 (s, 3H), 1.93-1.83 (m, 1H), 1.46 (s, 9H); ^{13}C NMR (75 MHz, CDCl$_3$) δ_C 171.85, 171.27, 171.01, 148.43, 147.65, 146.91, 146.66, 142.43, 139.60, 136.83, 136.79, 127.19, 124.97, 121.67, 121.35, 83.69, 52.37, 34.38, 30.93, 28.08, 23.54. ESI-MS calcd for $[C_{23}H_{29}N_8O_4]^+$: 481.2312; found: 481.2324.

6.2.4.2.2.1.3 Synthesis of Ac-L-Glu(3,6-dipyrid-2-yl-1,2,4,5-tetrazine)-O*t*Bu 5-31

5-31
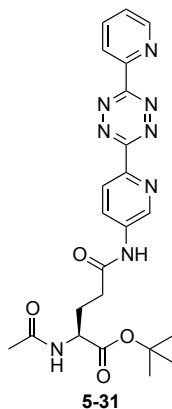
To a suspension of Ac-Glu(dihydro-1,2,4,5-tetrazine)-O*t*Bu **5-30** (207 mg, 0.43 mmol) in CH_2Cl_2 (5 mL), phenyliodine (II) diacetate (PIDA) (208 mg, 0.65 mmol) was added. The reaction was stirred at rt for 1h30 (until a pink limpid solution was obtained). The solvent was removed under reduced pressure and the crude material was purified through silica gel by column chromatography (Eluent: CH_2Cl_2 to CH_2Cl_2/MeOH 95:5) to give **5-31** as a pink solid (200 mg, 97%). M.p.: 168-170 °C; IR (film): ν (cm^{-1}) 3292, 3057, 2980, 1730, 1654, 1526, 1394, 1367, 1254, 1153, 1128, 920, 883, 783, 590; ^{1}H NMR (300 MHz, CDCl$_3$): δ_H 10.28 (s, 1H, -*NH*), 8.99 (d, J = 2.2 Hz, 1H), 8.94 (d, J = 4.2 Hz, 1H), 8.71 (d, J = 7.9 Hz, 1H), 8.68 (d, J = 8.6 Hz, 1H), 8.54 (dd, J = 8.6, 2.2 Hz, 1H), 7.98 (td, J = 7.9, 1.6 Hz, 1H), 7.55 (ddd, J = 7.9, 4.2, 1.6 Hz, 1H), 6.85 (d, J = 6.9 Hz,

1H, *-NH*), 4.47 (*ddd*, *J* = 10.1, 7.9, 3.7 Hz, 1H), 2.50-2.45 (*t*, *J* = 6.8 Hz, 2H), 2.30-2.24 (*m*, 1H), 2.04 (*s*, 3H), 1.99-1.81 (*m*, 1H), 1.41 (*s*, 9H); ^{13}C NMR (75 MHz, CDCl$_3$) δ_C 172.01, 171.59, 171.01, 163.55, 163.37, 150.98, 150.11, 144.04, 142.14, 138.69, 137.71, 126.99, 126.69, 125.31, 124.47, 83.17, 52.51, 34.09, 29.49, 28.02, 23.33. ESI-MS calcd for $[C_{23}H_{27}N_8O_4]^+$: 479.2155; found: 479.2136.

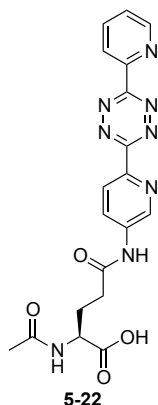### 6.2.4.2.2.1.4 Synthesis of Ac-L-Glu(3,6-dipyrid-2-yl-1,2,4,5-tetrazine)-OH 5-22

5-22

To a suspension of Ac-Glu(tetrazine)-OtBu **5-31** (63 mg, 0.13 mmol) in CH$_2$Cl$_2$ (1.5 mL) was added TFA (1.5 mL). The reaction mixture was stirred at rt for 2 h. The solvents were removed under a flow of air and the crude material was precipitated in Et$_2$O affording Ac-Glu(tetrazine)-OH **5-22** as a red solid. (55 mg, quant.) IR (film): ν (cm^{-1}) 3254, 3065, 3057, 2980, 1699, 1583, 1539, 1392, 1367, 1226, 1124, 920, 590; ^{1}H NMR (300 MHz, DMSO-*d$_6$*): δ_H 10.62 (*s*, 1H, *-NH*), 9.02 (*s*, 1H), 8.92 (*d*, *J* = 4.1 Hz, 1H), 8.61 (*d*, *J* = 8.6 Hz, 1H), 8.59 (*d*, *J* = 7.6 Hz, 1H), 8.40 (*dd*, *J* = 8.6, 2.1 Hz, 1H), 8.25 (*d*, *J* = 7.7 Hz, 1H, *-NH*), 8.15 (*td*, *J* = 7.6, 1.3 Hz, 1H), 7.73 (*dd*, *J* = 7.6, 4.1 Hz, 1H), 4.29-4.21 (*m*, 1H), 2.54-2.45 (*m*, 2H), 2.14-2.08 (*m*, 1H), 1.92-1.81 (*m*, 1H), 1.87 (*s*, 3H); ^{13}C NMR (75 MHz, DMSO-*d$_6$*) δ_C 173.62, 171.63, 169.57, 163.01, 162.79, 150.54, 150.06, 143.74, 141.23, 138.61, 138.13, 126.78, 126.25, 125.04, 124.32, 51.41, 32.81, 26.52, 22.49. ESI-MS calcd $[C_{19}H_{19}N_8O_4]^+$: 423.1529; found: 423.1523.

6.2.4.2.2.1.5 Synthesis of 12-oxo-2,5,8,11-tetraoxapentadecan-15-oic acid (PEG-acid) 5-33

5-33
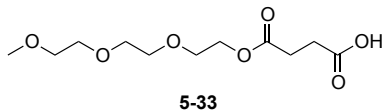
PEG-acid **5-33** has been synthesized according to the literature.[36]

6.2.4.2.2.1.6 Synthesis of 2,5-dioxopyrrolidin-1-yl (2-(2-(2-methoxyethoxy)ethoxy)ethyl) succinate 5-34

5-34
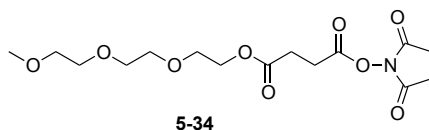
To a solution of TEG-acid **5-33** (800 g, 3.03 mmol) in CH_2Cl_2 (15 mL), *N*-hydroxysuccinimide (366 mg, 3.18 mmol), EDC.HCl (639 mg, 3.33 mmol) and DMAP (37 mg, 0.3 mmol) were added. The reaction mixture was stirred at rt for 20 h. H_2O was added, the layers were separated and the aqueous phase was extracted with CH_2Cl_2. The combined organic phases were washed with brine, dried over MgSO4 and concentrated under reduced pressure to afford **5-34** as a colorless oil (1.1 g, quant.). IR (film): ν (cm^{-1}) 2934, 2880, 1708, 1204, 1088, 1070, 849, 816, 650; ^{1}H NMR (300 MHz, CDCl$_3$): δ_H 4.26 (*t, J* = 4.7 Hz, 2H), 3.71-3.61 (*m*, 8H), 3.55-3.52 (*m*, 2H), 3.36 (*s*, 3H), 2.94 (*t, J* = 7 Hz, 2H), 2.83 (*s*, 4H), 2.76 (*t, J* = 7 Hz, 2H); ^{13}C NMR (100 MHz, CDCl$_3$): δ_H 171.13, 169.02, 167.82, 72.04, 70.69, 69.06, 64.34, 59.18, 28.78, 26.38, 25.68 (CH$_2$ missing due to overlapping).

6.2.4.2.2.1.7 Synthesis of 5-oxo-2-(12-oxo-2,5,8,11-tetraoxapentadecan)-L-Glu-O*t*Bu 5-35

5-35
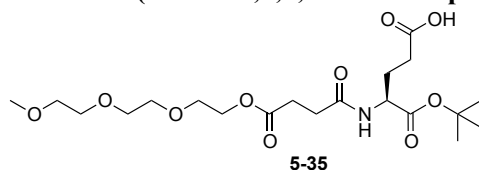
To a solution of NHS-ester **5-34** (542 mg, 1.5 mmol) in DMF (10 mL), H-Glu-O*t*Bu (303 mg, 1.5 mmol) and DIEA (388 mg, 3 mmol) were successively added. The reaction mixture was stirred at rt for 16 h. HCl 5% (aq) was added and the aqueous phase was extracted with CH_2Cl_2 (3 times). The combined organic layers were washed with brine, dried and concentrated under reduced pressure. The crude residue was purified through a short silica gel column chromatography (Eluent: CH_2Cl_2 to CH_2Cl_2/MeOH 95:5) to afford **5-35** as a colorless oil (674 mg, 85%). IR (film): ν (cm^{-1}) 3327, 2934, 1718, 1647, 1541, 1368, 1213, 1153, 1093, 845, 652; ^{1}H NMR (300 MHz, CDCl$_3$): δ_H 6.59 (*d, J* = 7.8 Hz, 1H, -*NH*), 4.51-4.46 (*m*, 1H), 4.28-4.17 (*m*, 2H), 3.70-3.62 (*m*, 8H), 3.56-3.54 (*m*, 2H), 3.37 (*s*, 3H), 2.77-2.48 (*m*, 4H), 2.42-2.32 (*m*, 2H), 2.20-2.15 (*m*, 1H), 1.96-1.89 (*m*, 1H), 1.45 (*s*, 9H); ^{13}C NMR (100 MHz, CDCl$_3$) δ_C 172.95, 171.85, 171.10, 82.64, 71.96, 70.60, 70.59, 70.51, 69.11, 63.94, 59.07, 52.39, 30.92, 30.33, 29.55, 28.06, 27.76.

6.2.4.2.2.1.8 Synthesis of 5-oxo-2-(12-oxo-2,5,8,11-tetraoxapentadecan)-L-Glu(3,6-dipyrid-2-yl-1,4-dihydro-1,2,4,5-tetrazine)-O*t*Bu 5-36

5-36
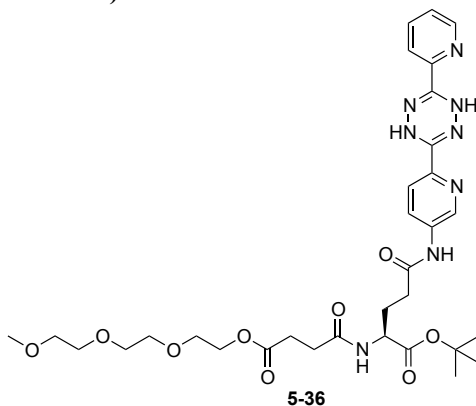
5-35 (613 mg, 1.3 mmol), 3-(5-aminopyridin-2-yl)-6-(pyridine-2-yl)-1,4-dihydro-1,2,4,5-tetrazine **5-29** (380 mg, 1.5 mmol), EDC.HCl (288 mg, 1.5 mmol) and DMAP (18 mg, 0.15 mmol) were dissolved in CH_2Cl_2 (15 mL). The reaction mixture was stirred at rt for 16 h. Water and CH_2Cl_2 were added, the layers were separated and the aqueous phase was extracted with CH_2Cl_2. Organic layers were combined, washed with brine, dried and concentrated. The crude residue was purified through silica gel column chromatography (Eluent: CH_2Cl_2/acetone 4:1 to 1:1) to afford **5-36** as an orange oil (450 mg, 46%). The product was directly used for the next step (unstable). IR (film): ν (cm^{-1}) 3310, 2932, 2890, 1734, 1541, 1395, 1234, 1153, 1105, 848, 669; ^1H NMR (400 MHz, CD_2Cl_2): 9.44 (*s*, 1H, -*NH*), 8.77 (*dd*, *J* = 2.4, 0.6 Hz, 1H), 8.57 (*ddd*, *J* = 4.9, 1.8, 1.0 Hz, 1H), 8.46 (*d*, *J* = 1.8 Hz, 2H), 8.19 (*dd*, *J* = 8.7, 2.4 Hz, 1H), 8.03 (*dt*, *J* = 7.9, 1.0 Hz, 1H), 7.98 (*dd*, *J* = 8.7, 0.6 Hz, 1H), 7.77 (*td*, *J* = 7.9, 1.8 Hz, 1H), 7.37 (*ddd*, *J* = 7.9, 4.9, 1.0 Hz, 1H), 6.58 (*d*, *J* = 8 Hz, 1H, -*NH*), 4.53-4.47 (*m*, 1H), 4.22-4.19 (*m*, 2H), 3.67-3.57 (*m*, 8H), 3.50-3.48 (*m*, 2H), 3.31 (*s,* 3H), 2.85-2.77 (*m*, 1H), 2.67-2.54 (*m*, 3H), 2.47-2.40 (*m*, 2H), 2.32-2.27 (*m*, 1H), 1.93-1.87 (*m,* 1H), 1.45 (*s*, 9H); ^{13}C NMR (100 MHz, CD_2Cl_2) δ_C 173.27, 172.75, 171.64, 171.21, 148.77, 147.95, 147.01, 146.74, 142.45, 139.70, 137.42, 137.18, 127.31, 125.28, 121.75, 121.48, 83.11, 72.21, 70.90, 70.76, 69.33, 64.26, 58.97, 52.49, 33.99, 31.27, 30.12, 29.79, 28.05 (one CH_2 missing due to overlapping); ESI-MS calcd for $[C_{32}H_{45}N_8O_9]^+$: 685.3310; found: 685.3283.

6.2.4.2.2.1.9 Synthesis of 5-oxo-2-(12-oxo-2,5,8,11-tetraoxapentadecan)-L-Glu(3,6-dipyrid-2-yl-1,2,4,5-tetrazine)-O*t*Bu 5-37

5-37
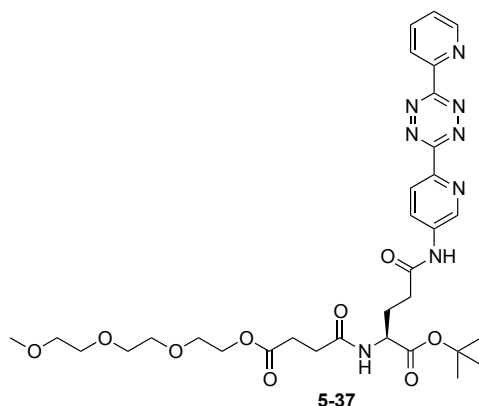
To a solution of PEG-Glu(dihydro-1,2,4,5-tetrazine)-O*t*Bu **5-36** (240 mg, 0.35 mmol) in CH$_2$Cl$_2$ (4 mL), phenyliodine (II) diacetate (PIDA) (170 mg, 0.52 mmol) was added. The reaction mixture was stirred at rt for 1h30. The crude material was purified through silica gel column chromatography (Eluent: CH$_2$Cl$_2$ to CH$_2$Cl$_2$/MeOH 95:5) to afford **5-37** as a pink oil (210 mg, 88%). IR (film): ν (cm^{-1}) 3296, 3098, 3057, 2933, 1730, 1652, 1526, 1394, 1367, 1252, 1152, 1128, 922, 590; ^{1}H NMR (300 MHz, CDCl$_3$): 9.79 (*s*, 1H, -*NH*), 9.02 (*d*, *J* = 2.2 Hz, 1H), 8.98 (*d*, *J* = 4.5 Hz, 1H), 8.73 (*d*, *J* = 8.7 Hz, 1H), 8.73 (*d*, *J* = 7.7 Hz, 1H), 8.60 (*dd*, *J* = 8.7, 2.2 Hz, 1H), 7.98 (*t*, *J* = 7.7 Hz, 1H), 7.55 (*dd*, *J* = 7.7, 4.5 Hz, 1H), 6.64 (*d*, *J* = 8 Hz, 1H, -*NH*), 4.58-4.50 (*m*, 1H), 4.24 (*t$_{app}$*, 2H), 3.71-3.62 (*m*, 8H), 3.56-3.51 (*m*, 2H), 3.34 (*s*, 3H), 2.92-2.82 (*m*, 1H), 2.69-2.51 (*m*, 5H), 2.39-2.31 (*m*, 1H), 1.98-1.90 (*m*, 1H), 1.46 (*s*, 9H); ^{13}C NMR (100 MHz, CDCl$_3$) δ_C 173.17, 172.47, 171.97, 170.98, 163.66, 163.52, 151.09, 150.35, 144.32, 142.30, 138.55, 137.60, 126.87, 126.58, 125.29, 124.46, 83.21, 71.98, 70.66, 70.65, 69.13, 64.04, 59.11, 52.19, 33.88, 31.09, 29.94, 29.56, 28.09 (one CH$_2$ missing due to overlapping); ESI-MS calcd for [C$_{32}$H$_{43}$N$_8$O$_9$]$^+$: 683.3184; found: 683.3153.

6.2.4.2.2.1.10 Synthesis of 5-oxo-2-(12-oxo-2,5,8,11-tetraoxapentadecan)-L-Glu(3,6-dipyrid-2-yl-1,2,4,5-tetrazine)-OH 5-23
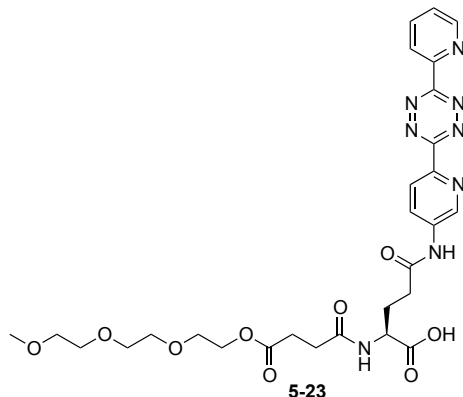

5-23

To a solution of PEG-Glu(tetrazine)-O*t*Bu **5-37** (210 mg, 0.31 mmol) in CH_2Cl_2 (2 mL) was added TFA (2 mL). The reaction mixture was stirred at rt for 2 h. The solvents were removed under a flow of air and the crude material was precipitated in Et_2O affording PEG-Glu(tetrazine)-OH **5-23** as a red sticky solid. (195 mg, quant.). The compound was directly used for the SPPS (unstable). IR (film): ν (cm^{-1}) 3283, 3080, 2901, 1734, 1647, 1541, 1386, 1367, 1130, 1092, 927, 779, 704, 586; ^{1}H NMR (300 MHz, CD$_3$OD): 9.07 (*d, J* = 2.3 Hz, 1H), 8.91 (*d, J* = 4.5 Hz, 1H), 8.85 (*d, J* = 7.7 Hz, 1H), 8.80 (*d, J* = 8.7 Hz, 1H), 8.51 (*dd, J* = 8.7, 2.3 Hz, 1H), 8.28 (*t, J* = 7.7 Hz, 1H), 7.55 (*dd, J* = 7.7, 4.5 Hz, 1H), 4.52 (*dd, J* = 9.2, 4.8 Hz, 1H), 4.20 (*t$_{app}$*, 2H), 3.69-3.60 (*m*, 8H), 3.54-3.51 (*m*, 2H), 3.34 (*s,* 3H), 2.69-2.53 (*m*, 6H), 2.40-2.29 (*m*, 1H), 2.12-2.02 (*m*, 1H); ^{13}C NMR (75 MHz, CD$_3$OD) δ_C 174.77, 174.41, 174.25, 173.71, 164.03, 163.82, 150.39, 149.88, 144.19, 141.91, 141.40, 140.63, 128.90, 128.83, 126.55, 126.03, 72.88, 70.45, 71.31, 69.99, 64.99, 59.06, 52.93, 33.96, 31.21, 30.84, 28.05 (one CH_2 missing due to overlapping); ESI-MS calcd for $[C_{28}H_{35}N_8O_9]^+$: 627.2527; found: 627.2554.

6.2.4.2.2.2 Synthesis of H-Gly-tetrazine.TFA 5-24

5-29   **5-38**   **5-39**   **5-24**
                  68%   97%   quant.

Scheme 6-29 Synthesis of H-Gly-tetrazine **5-24**; a) Boc-Gly-OH, EDC.HCl, DMAP, CH_2Cl_2, rt, 20 h; b) PIDA, CH_2Cl_2, rt, 16 h; c) TFA, CH_2Cl_2, rt, 1 h.

6.2.4.2.2.2.1 Synthesis of Boc-Gly-dihydrotetrazine 5-38

5-38

To Boc-Gly-OH (143 mg, 0.82 mmol), EDC.HCl (157 mg, 0.82 mmol), 3-(5-aminopyridin-2-yl)-6-(pyridine-2-yl)-1,4-dihydro-1,2,4,5-tetrazine **5-29** (207 mg, 0.82 mmol), DMAP (10 mg, 0.08 mmol), CH_2Cl_2 (10 mL) was added. The reaction mixture was stirred at rt for 20 h. H_2O and CH_2Cl_2 were added and the layers were separated. The aqueous phase was extracted (2 times) with

CH_2Cl_2. The solvent was evaporated under reduced pressure. The residue was suspended in CH_2Cl_2 (5 mL) and Et_2O was added. The precipitate was filtrated and washed with Et_2O to give **5-38** as an orange solid (227 mg, 68%). The product was characterized in accordance with the literature.[37]

6.2.4.2.2.2.2 Synthesis of Boc-Gly-tetrazine 5-39

5-39

Boc-Gly-dihydrotetrazine **5-38** (200 mg, 0.5 mmol) was suspended in CH_2Cl_2 (15 mL) and PIDA (241 mg, 0.75 mmol) was added. The reaction mixture was stirred at rt for 16 h. The suspension was poured in Et_2O. The precipitate was filtrated and washed with Et_2O and purified through silica gel column chromatography (Eluent: CH_2Cl_2 to CH_2Cl_2/MeOH 92:8) to afford **5-39** as a pink solid (193 mg, 97%). The product was characterized in accordance with the literature.[37]

6.2.4.2.2.2.3 Synthesis of H-Gly-tetrazine.TFA 5-24

5-24

Boc-Gly-tetrazine **5-39** (20 mg, 0.05 mmol) was suspended in CH_2Cl_2 (2 mL) and TFA was added (200 µL). The reaction mixture was stirred at rt for 1 h. The volatiles were removed under a flow of N_2, the residue was precipitated with Et_2O and dried under vacuum affording **5-24** (20 mg, quant.). The material was directly used in the step without further purification.

6.2.4.3 Syntheses of tritopic peptidic scaffolds

6.2.4.3.1 Synthesis of peptide Ac-QLA-X(disulfide)-QLAQLA-Nle(N₃)-QLAQLA-X(hydrazide)-QLA-NH₂ 5-42

Chemical Formula: $C_{117}H_{186}N_{40}O_{29}S_2$
Exact Mass: 2679.3751

270

The peptide was synthesized according to the general procedure except for the cleavage step. The peptide was deprotected and cleaved from the resin using the cocktail cleavage TFA/water/TIS (95:2.5:2.5, 10 mL for 200 mg) for 1.5 h. The analytical HPLC were performed with 0.1% of TFA. HPLC (25 °C): R_t = 17 min (gradient 2). ESI-MS(Q-Tof) showed $[M+3H]^{3+}$, $[M+2Na]^{2+}$ after deconvolution of multicharged ions, monoisotopic mass found: 2679.37.
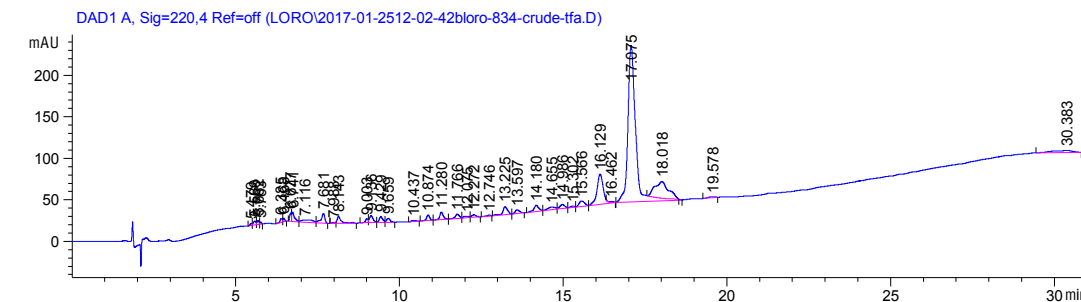

Figure 6-22 HPLC chromatogram of crude peptide **5-42**.
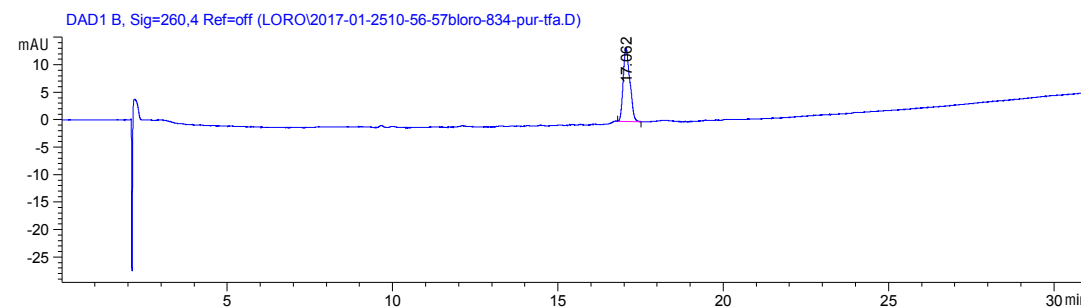
Figure 6-23 HPLC chromatogram of purified peptide **5-42.**
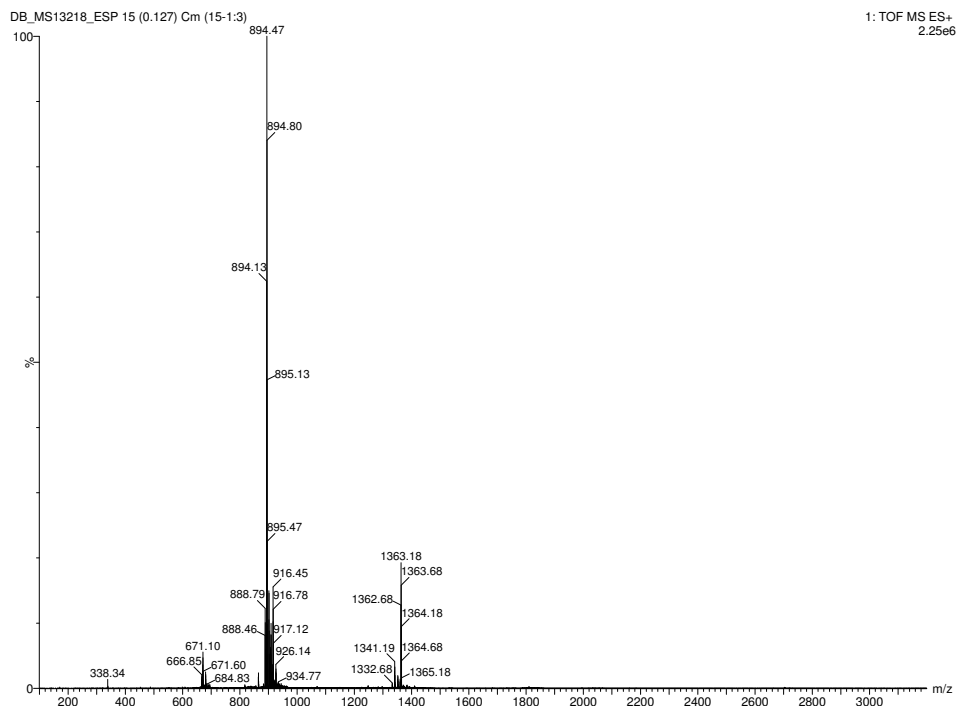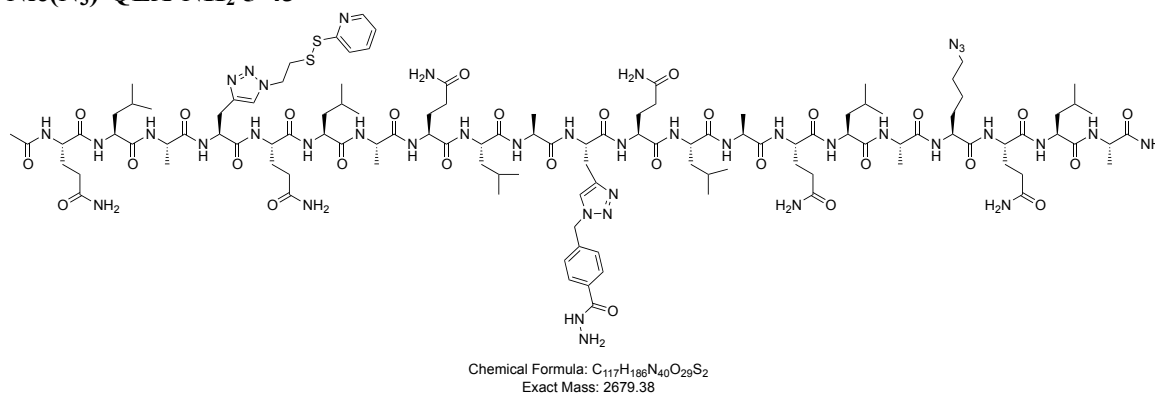

Figure 6-24 ESI-MS(Q-Tof) analysis of purified peptide **5-42**.

271

6.2.4.3.2 Synthesis of peptide Ac-QLA-X(disulfide)-QLAQLA-X(hydrazide)-QLAQLA-Nle(N₃)-QLA-NH₂ 5-43

Chemical Formula: C₁₁₇H₁₈₆N₄₀O₂₉S₂
Exact Mass: 2679.38

The peptide was synthesized according to the general procedure except for the cleavage step. The peptide was deprotected and cleaved from the resin using the cocktail cleavage TFA/water/TIS (95:2.5:2.5, 10 mL for 200 mg) for 1.5 h. The analytical HPLC were performed with 0.1% of TFA. HPLC (25 °C): R_t = 18.2 min (gradient 2). ESI-MS(Q-Tof) showed $[M+3H]^{3+}$, $[M+2H]^{2+}$; after deconvolution of multicharged ions, monoisotopic mass found: 2679.37.
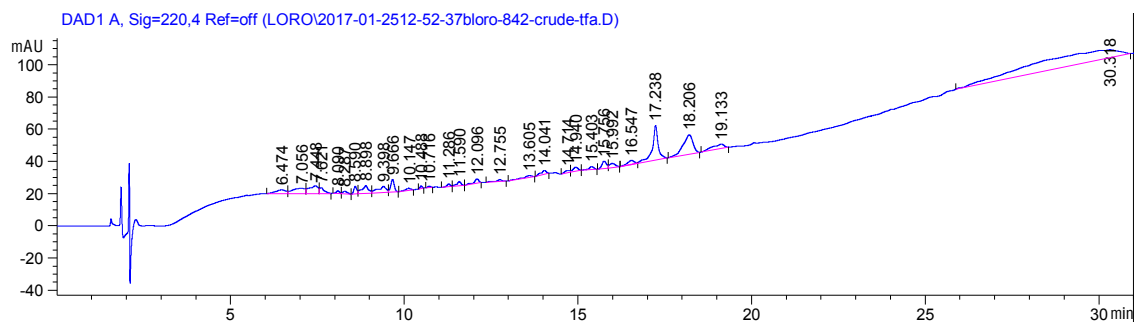

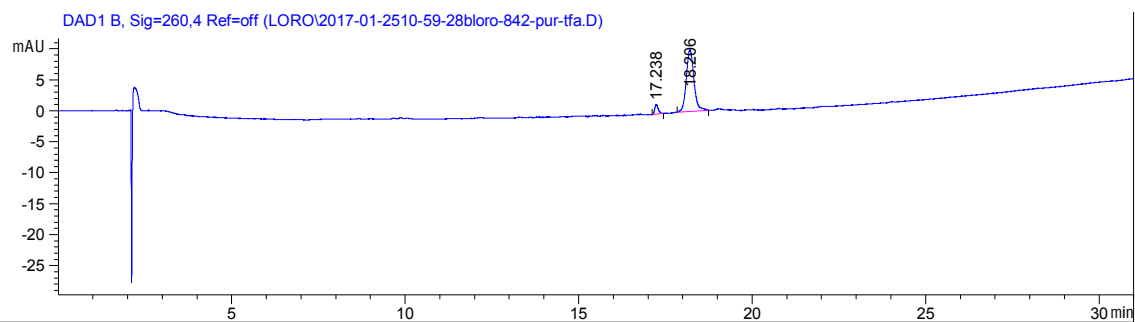**Figure 6-25** HPLC chromatogram of crude peptide **5-43**.

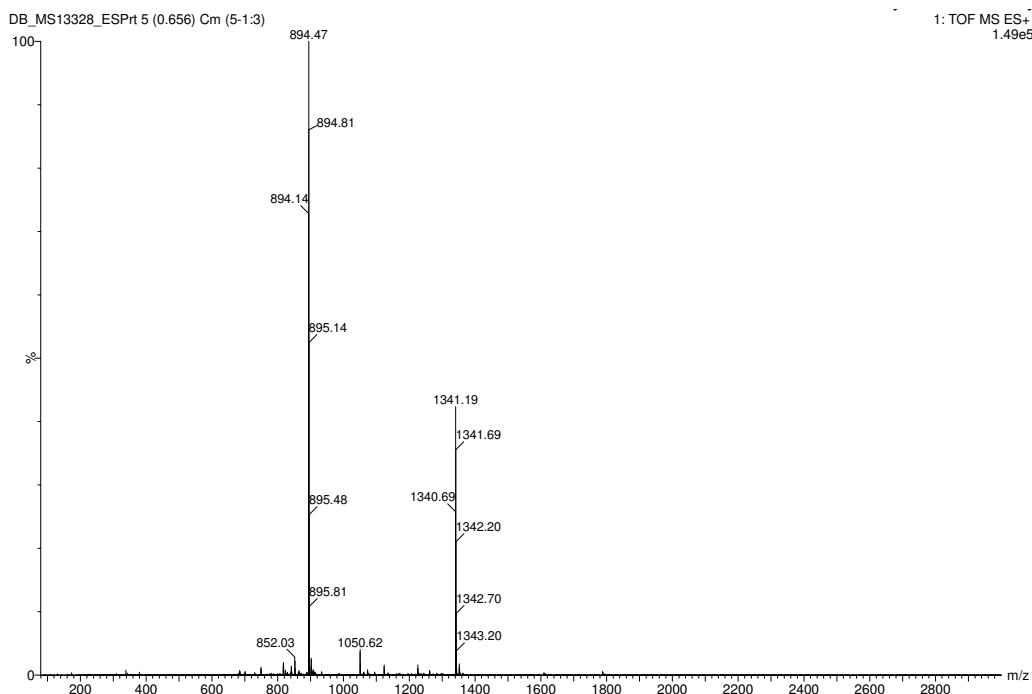**Figure 6-26** HPLC chromatogram of purified peptide **5-43**.

272

Figure 6-27 ESI-MS(Q-Tof) analysis of purified peptide **5-43**.

6.2.4.3.3 Synthesis of peptide 5-47

Chemical Formula: $C_{36}H_{39}N_{15}O_6S_2$
Exact Mass: 841.26
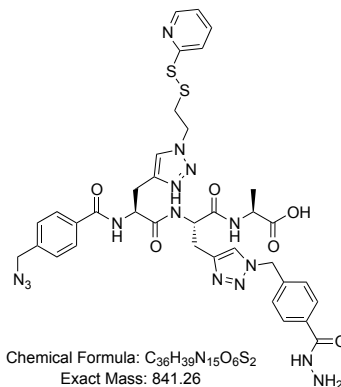
The general procedure was slightly modified for the synthesis of peptide **5-47**: the peptide was synthesized on Fmoc-Ala Wang resin (0.12 mmol, 0.6 mmol/g). Couplings with aa were carried out using *N*-Fmoc amino acids (0.26 M; 5 equiv.) in NMP, HATU (0.3 M, 4.5 equiv.) in DMF and DIPEA (2 M, 12 equiv.) in NMP at rt for 1 h, while Fmoc deprotection steps were performed according to the general procedure. Coupling with **2-32** was performed as the aa couplings but stirred for 1h30. The peptide was deprotected and cleaved from the resin using the cocktail cleavage TFA/water/TIS (95:2.5:2.5, 10 mL for 200 mg) for 2 h. The disulfide exchange was performed according to the general procedure and the crude material was not purified by RP-HPLC. HPLC (25 °C): R_t = 13.87 min (gradient 3). ESI-MS(Q-Tof) showed $[M+2H]^{2+}$, $[M+H]^+$; after deconvolution of multicharged ions, monoisotopic mass found: 841.27.
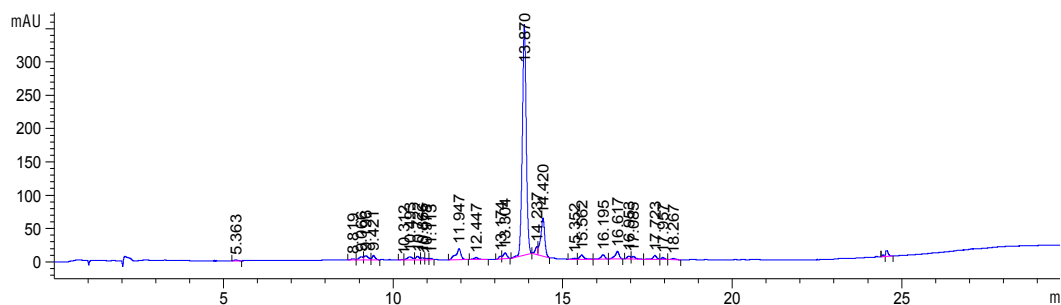
Figure 6-28 HPLC chromatogram of crude peptide **5-47**.

Table 6-6 Elution gradients 3 applied for HPLC analysis.

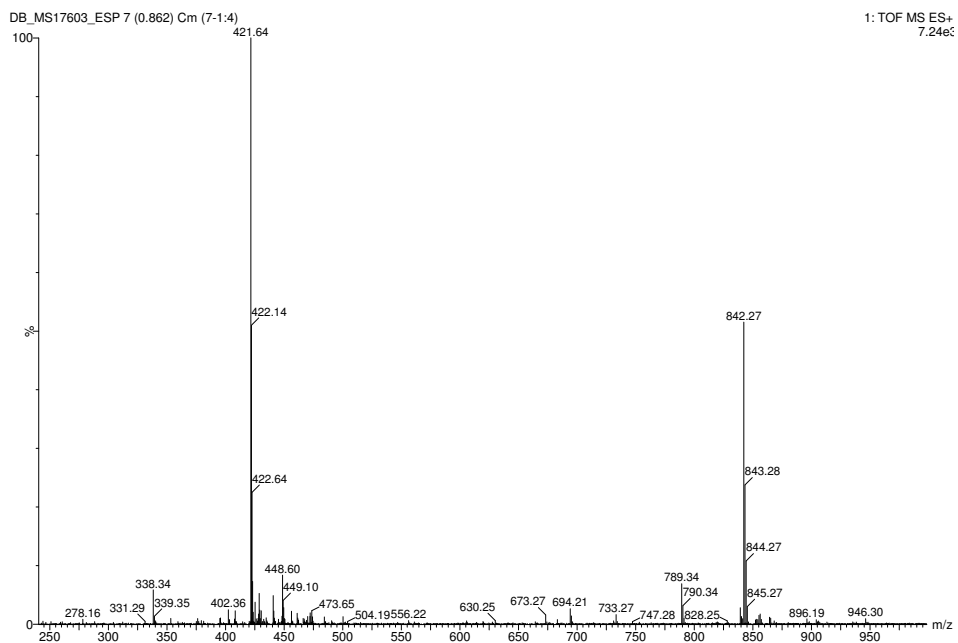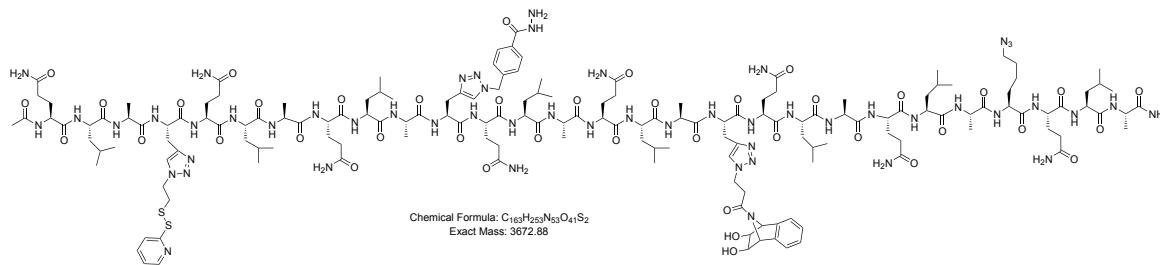| Time / s	% H$_2$O (+0.1%TFA)	% CH$_3$CN (+0.1%TFA)	Flow / mL/min
0	95	5	1
5	80	20	1
20	50	50	1
25	0	100	1
29	0	100	1
30	95	5	1

Figure 6-29 ESI-MS(Q-Tof) analysis of peptide **5-47**.

6.2.4.4 Syntheses of tetratopic peptidic scaffolds

6.2.4.4.1 Synthesis of peptide Ac-QLA-X(disulfide)-QLAQLA-X(hydrazide)-QLAQLA-X(diol)-QLAQLA-Nle(N$_3$)-QLA-NH$_2$ 5-50

The peptide was synthesized according to the general procedure except for the cleavage step. The peptide was deprotected and cleaved from the resin using the cocktail cleavage TFA/water/TIS (95:2.5:2.5, 10 mL for 200 mg) for 2 h. HPLC (25 °C) (gradient 1): R_t possibly 17.24 min; Preparative RP-HPLC: hydrophobic peptide possibly stacks on C_3 column.
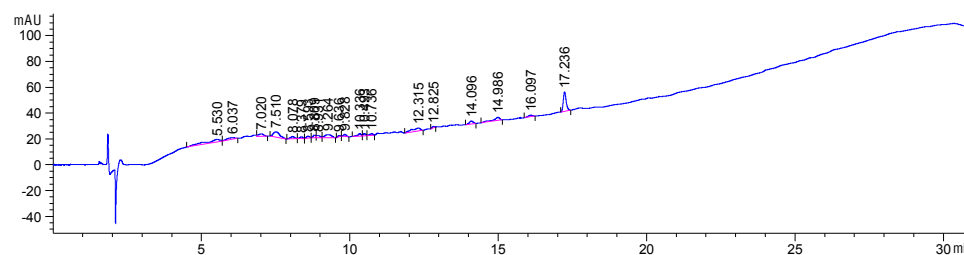

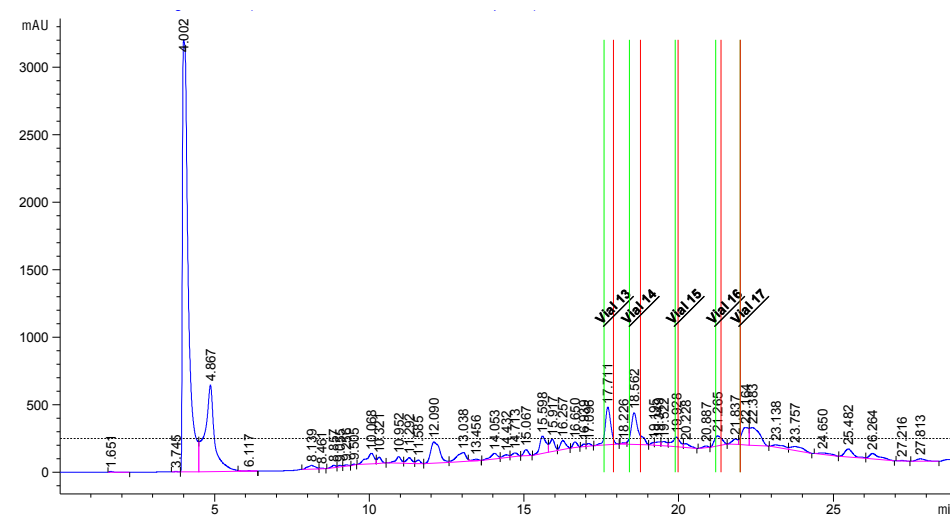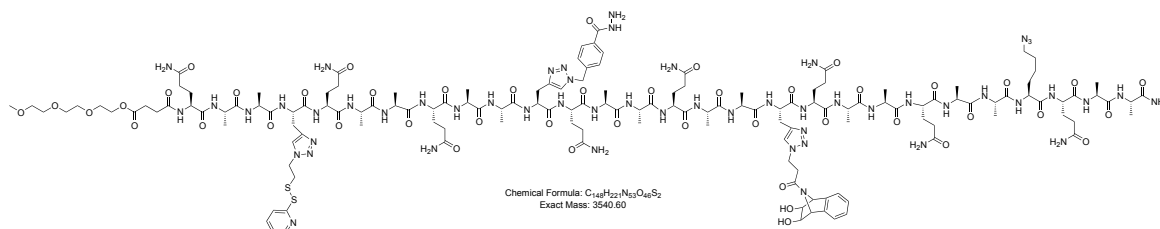**Figure 6-30** HPLC chromatogram of crude peptide **5-50.**

Figure 6-31 Preparative HPLC chromatogram of crude peptide **5-50.**

6.2.4.4.2 Synthesis of peptide PEG-QAA-X(disulfide)-QAAQAA-X(hydrazide)-QAAQAA-X(diol)-QAAQAA-Nle(N₃)-QAA-NH₂ 5-52

275

The peptide was synthesized according to the general procedure; however, the acetylation step was replaced by a last coupling with PEG-acid **5-**⟨⟩ he coupling was perforr⟨⟩ n double coupling (2 × 25 min). The peptide was deprotected an⟨⟩ aved from the resin usir⟨⟩ e cocktail cleavage TFA/water/TIS (95:2.5:2.5, 10 mL for 200 m⟨⟩ r 1.5 h.

HPLC (25 °C): R_t = 10.9 min (gradient 4). E⟨⟩ S(Q-Tof) showed M^{4+}: ⟨⟩ l, M^{3+}: 1181.2, M^{2+}: 1771.3, after deconvolution of multicharged i⟨⟩ monoisotopic mass foun⟨⟩ 40.6.

Table 6-7 Elution gradient 4 applied for HPLC analysis.

Time / s	% H$_2$O	% CH$_3$CN	Flow / mL/min
0	95	5	1
30	0	100	1
31	95	5	1

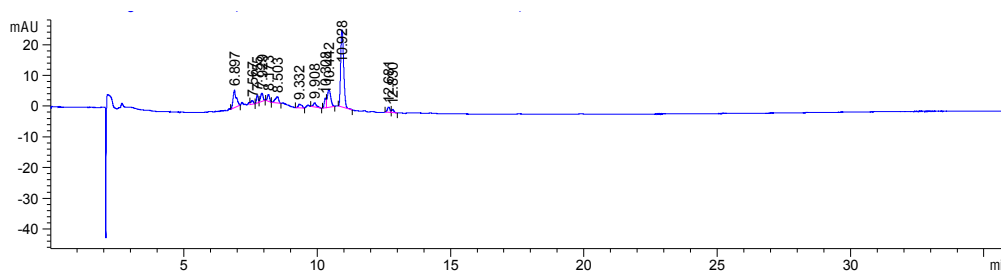**Figure 6-32** HPLC chromatogram of crude peptide **5-52.**
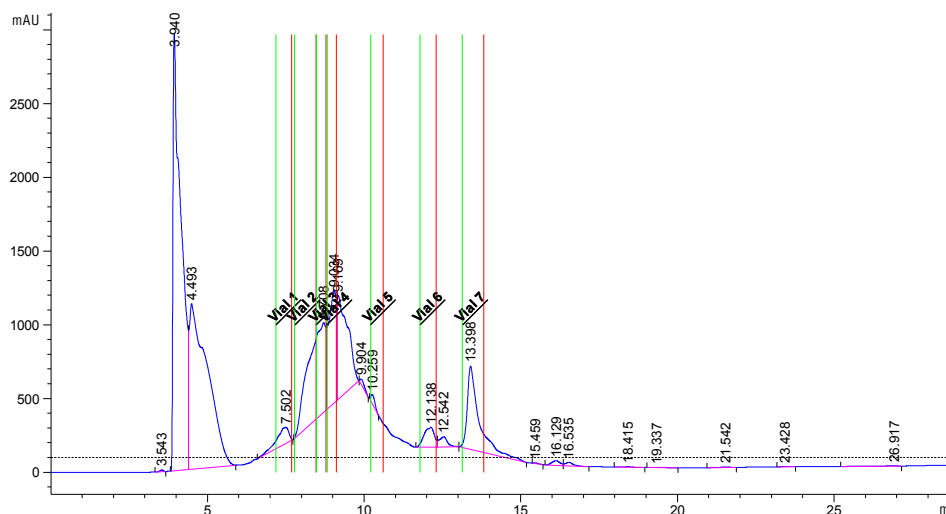
Figure 6-33 Preparative HPLC chromatogram of crude peptide **5-52.**

Figure 6-34 ESI-MS(Q-Tof) analysis of purified peptide **5-52**.

6.2.4.4.3 Synthesis of peptide 5-54

Chemical Formula: $C_{81}H_{83}N_{19}O_{13}S$
Exact Mass: 1561.61

The general procedure was modified for the synthesis of peptide **5-54**: the peptide was synthesized on H-Ala 2-Cl Trt resin (0.12 mmol, 0.6 mmol/g). Couplings with aa were carried out using *N*-Fmoc amino acids (0.26 M; 5 equiv.) in NMP, HATU (0.3 M, 4.5 equiv.) in DMF and DIPEA (2 M, 12 equiv.) in NMP at rt for 1 h, while Fmoc deprotection steps were performed according to the general procedure. Coupling with **2-32** was performed as the aa couplings but stirred for 1h30. The peptide was cleaved from the resin using the cocktail cleavage AcOH/TFE/CH$_2$Cl$_2$ (1:1:8, 20 mL for 200 mg) for 30 min. HPLC (25 °C): R_t = 15.2 min (gradient 1). ESI-HRMS(Q-Tof)

showed $[M+2H]^{2+}$, $[M+H]^+$, and fragmented $[M(-Trt-Boc)+H]^+$,$[M(-Trt)+H]^+$; monoisotopic mass found: 1562.6223 (calcd for $[C_{81}H_{84}N_{19}O_{13}S]^+$ 1562.6217).
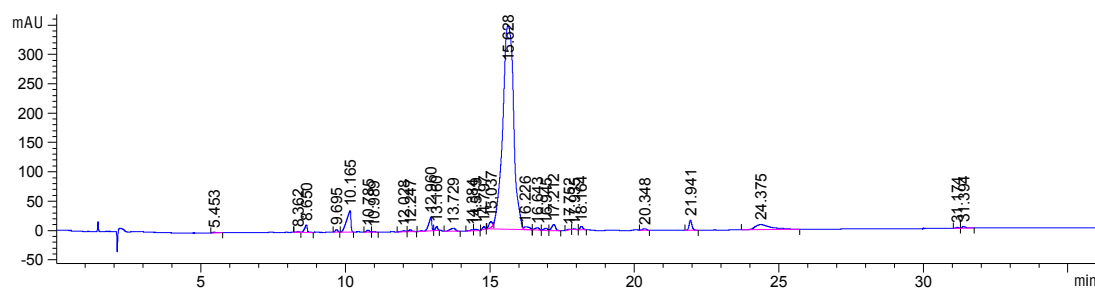
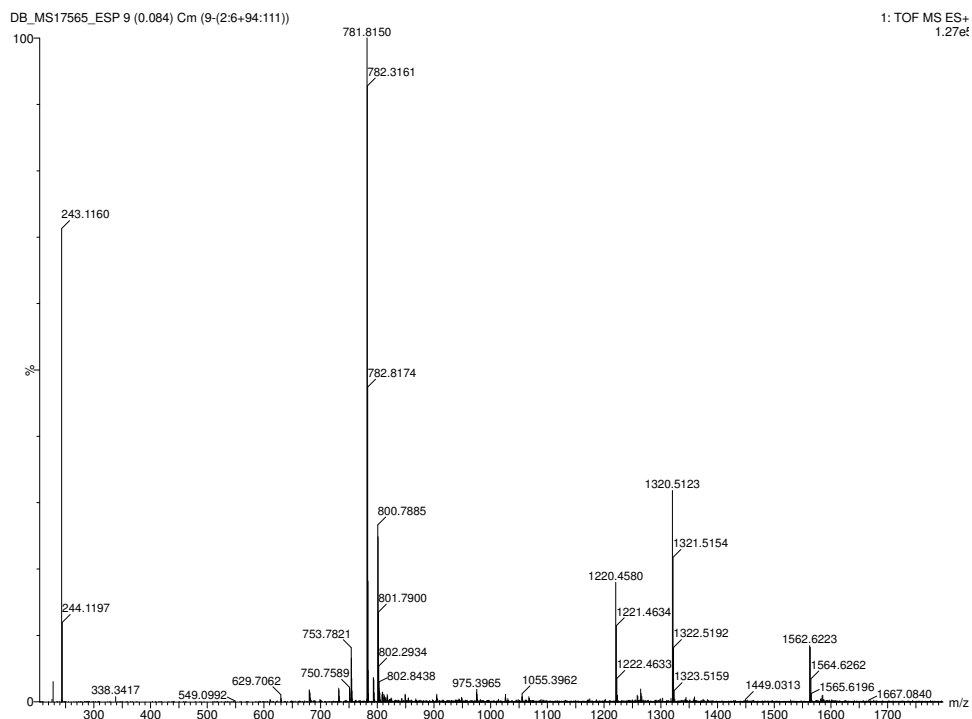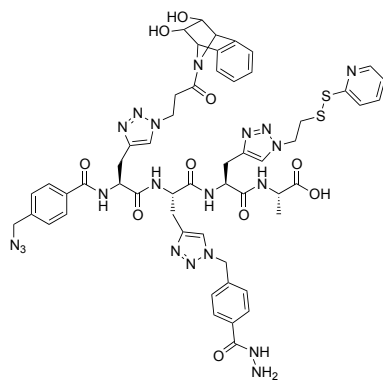

Figure 6-35 HPLC chromatogram of crude peptide **5-54.**

Figure 6-36 ESI-HRMS(Q-Tof) analysis of purified peptide **5-54**.

6.2.4.4.4 Synthesis of peptide 5-55

Chemical Formula: $C_{54}H_{58}N_{20}O_{10}S_2$
Exact Mass: 1210.41

Peptide **5-54** (5 mg, $3.2.10^{-3}$ mmol) was deprotected with TFA/water/TIS (95:2.5:2.5, 1 mL) for 2 h. The volatiles were evaporated under a flow of N_2 and the crude material was precipitated in cold Et_2O. After centrifugation, the ether was decanted and this washing was repeated 3 times. The precipitate was dried and dissolved in DMF (0.5 mL) in the presence of 2,2'-dipyridyl disulfide (2.2 mg, 1.10^{-2} mmol). Then, DIEA (4 mg, 3.10^{-2} mmol) was added and the mixture was stirred at rt for 30 min. The material was precipitated in cold Et_2O. After centrifugation, the ether was decanted and this washing was repeated 3 times. The white solid was directly used for the assembly without further purification. The analytical HPLC were performed with 0.1% of TFA. HPLC (25 °C): R_t = 9.97 min (gradient 4). ESI-HRMS(Q-Tof) showed $[M+2H]^{2+}$, $[M+H]^{+}$, $[M+Na]^{+}$; monoisotopic mass found: 1211.4160 (calcd for $[C_{54}H_{59}N_{20}O_{10}S_2]^{+}$ 1211.4164).
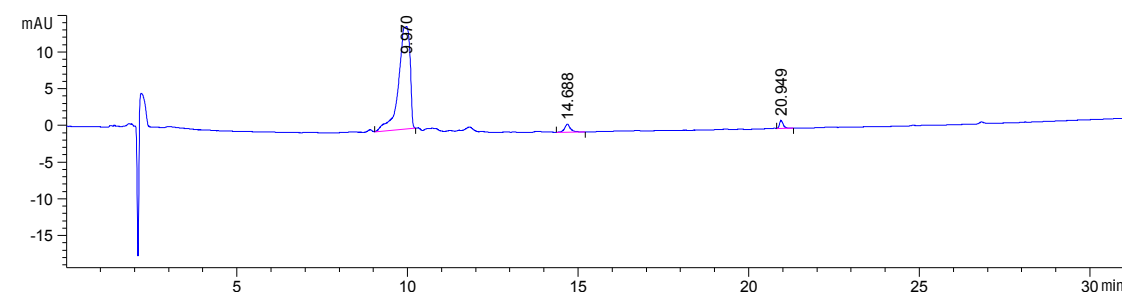

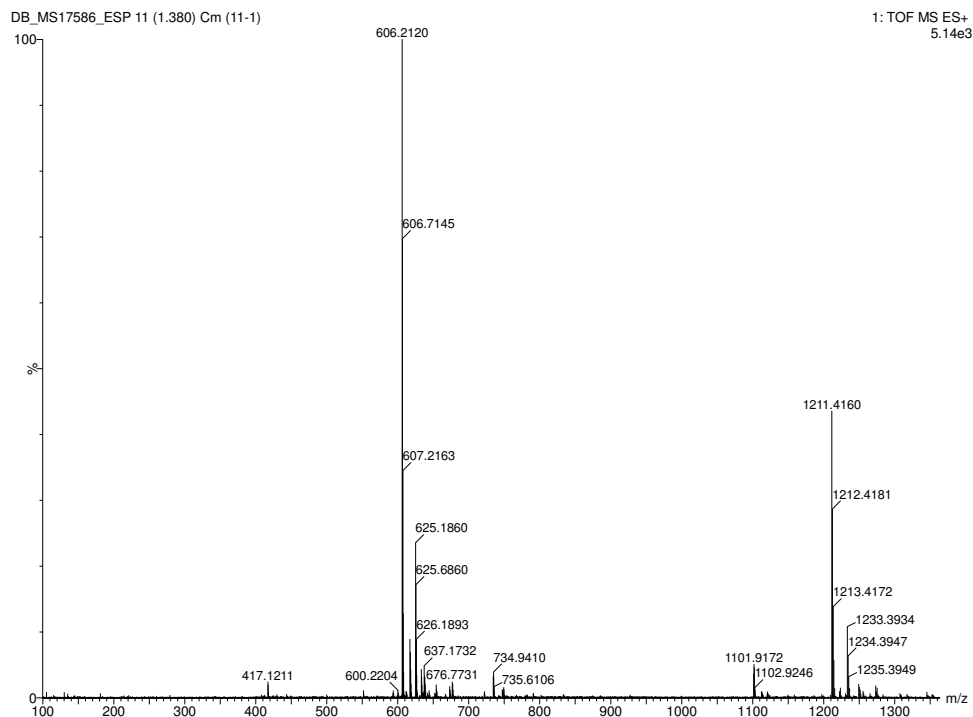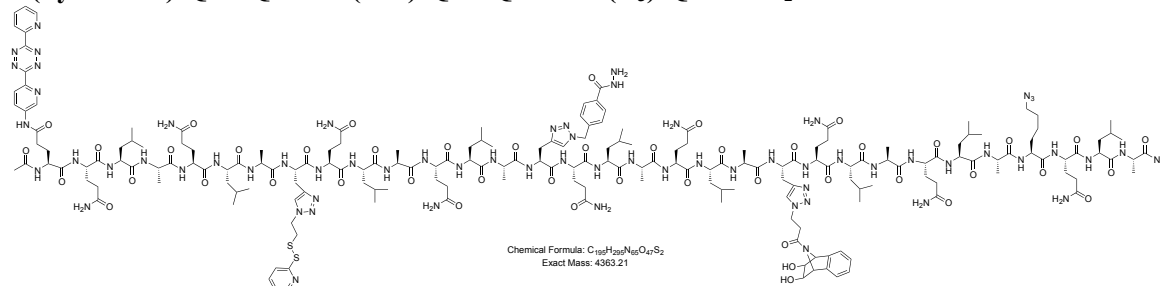**Figure 6-37** HPLC chromatogram of crude peptide **5-55.**

Figure 6-38 ESI-HRMS(Q-Tof) analysis of purified peptide **5-55**.

6.2.4.5 Syntheses of pentatopic peptides

6.2.4.5.1 Synthesis of of peptide Ac-E(tetrazine)-QLAQLA-X(disulfide)-QLAQLA-X(hydrazide)-QLAQLA- X(diol)-QLAQLA-Nle(N₃)-QLA-NH₂ 5-58

Chemical Formula: $C_{195}H_{295}N_{65}O_{47}S_2$
Exact Mass: 4363.21

The peptide was synthesized according to the general; however, the acetylation step was replaced by a last coupling with Ac-Glu(tetrazine)-OH **5-22**. The coupling was performed for 1 h. The peptide was deprotected and cleaved from the resin using the cocktail cleavage TFA/water/TIS (95:2.5:2.5, 10 mL for 200 mg) for 1.5 h.

The analytical HPLC were performed with 0.1% of TFA. HPLC (25 °C): see Figure 6-38, R_t 17.2 min? (gradient 2); hydrophobic peptide stacks on preparative C_3 column.
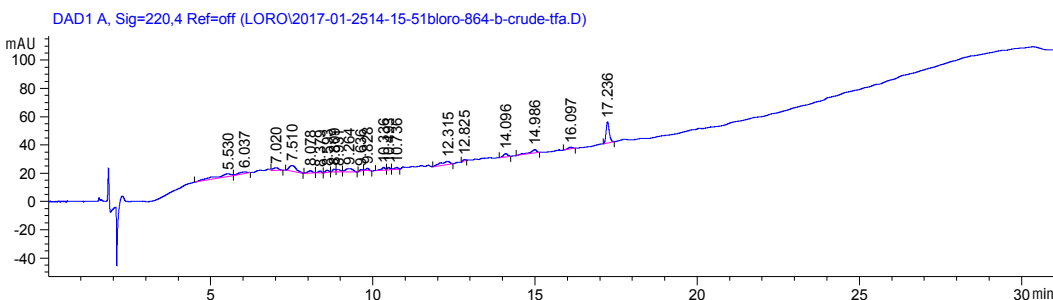

Figure 6-39 HPLC chromatogram of crude peptide **5-58**.
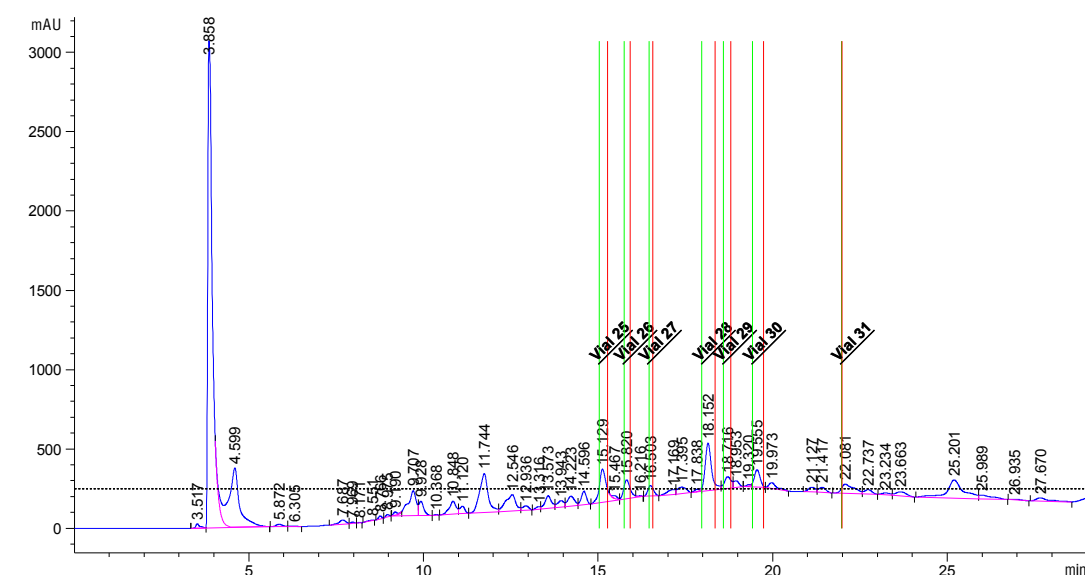
Figure 6-40 Preparative HPLC chromatogram of crude peptide **5-58.**

6.2.4.5.2 Synthesis of of peptide PEG-E(tetrazine)-QAAQAA-X(disulfide)-QAAQAA-X(hydrazide)-QAAQAA- X(diol)-QAAQAA-Nle(N₃)-QAA-NH₂ 5-60
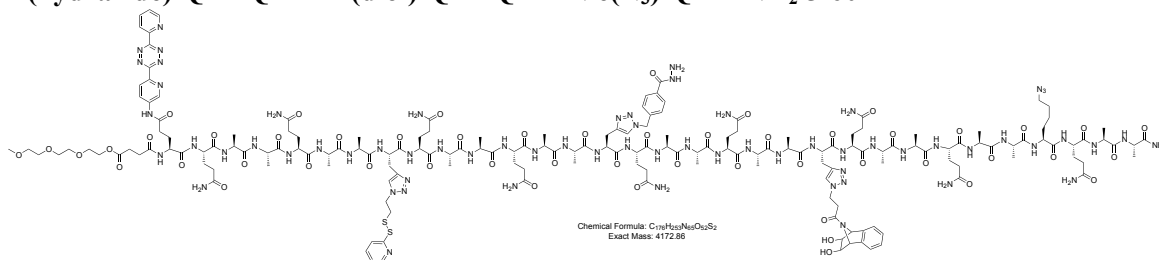
The peptide was synthesized according to the general; however, the acetylation step was replaced by a last coupling with PEG-Glu(tetrazine)-OH **5-23**. The coupling was performed for 1 h. The peptide was deprotected and cleaved from the resin using the cocktail cleavage TFA/water/TIS (95:2.5:2.5, 10 mL for 200 mg) for 1.5 h. The analytical HPLC were performed with 0.1% of TFA. HPLC (25 °C): see Figure 6-38; R_t 10.9 min? (gradient 2); Peptide possibly stacks on preparative C_3 column.
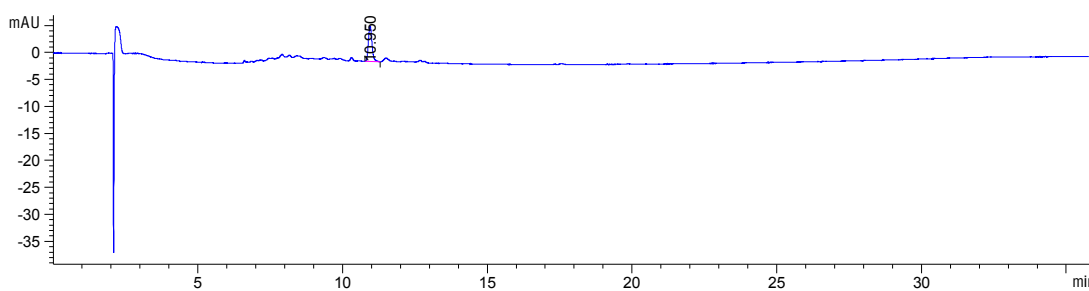
Figure 6-41 HPLC chromatogram of crude peptide **5-60.**
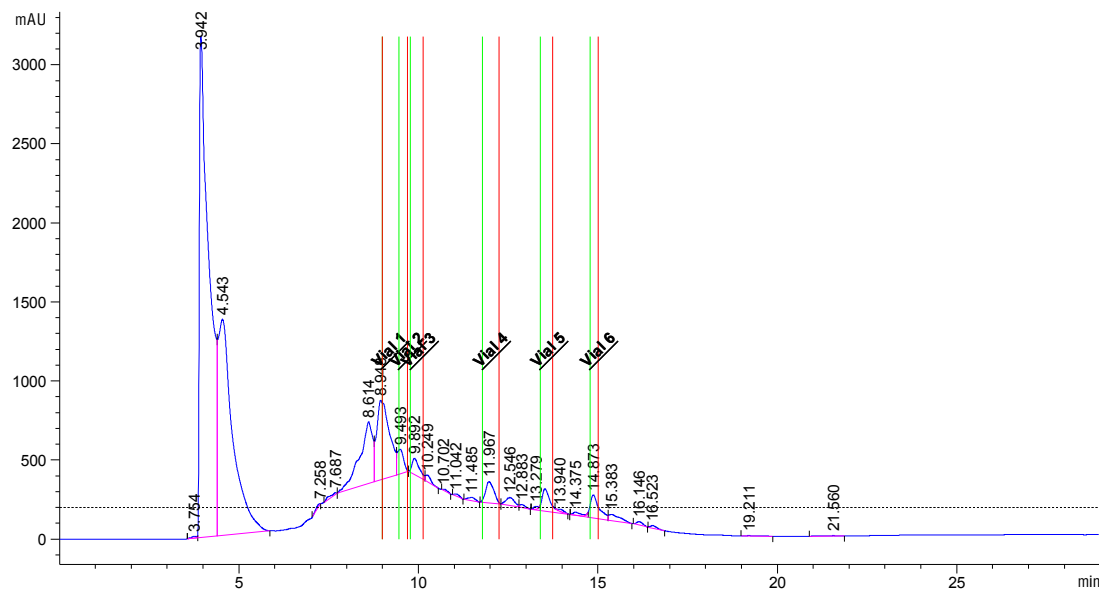
Figure 6-42 Preparative HPLC chromatogram of crude peptide **5-60.**

DB_MS170061_ESPrta 666 (10.275) Cm (664:671-(607:624+726:737))   1: TOF MS ES+
3.71e7
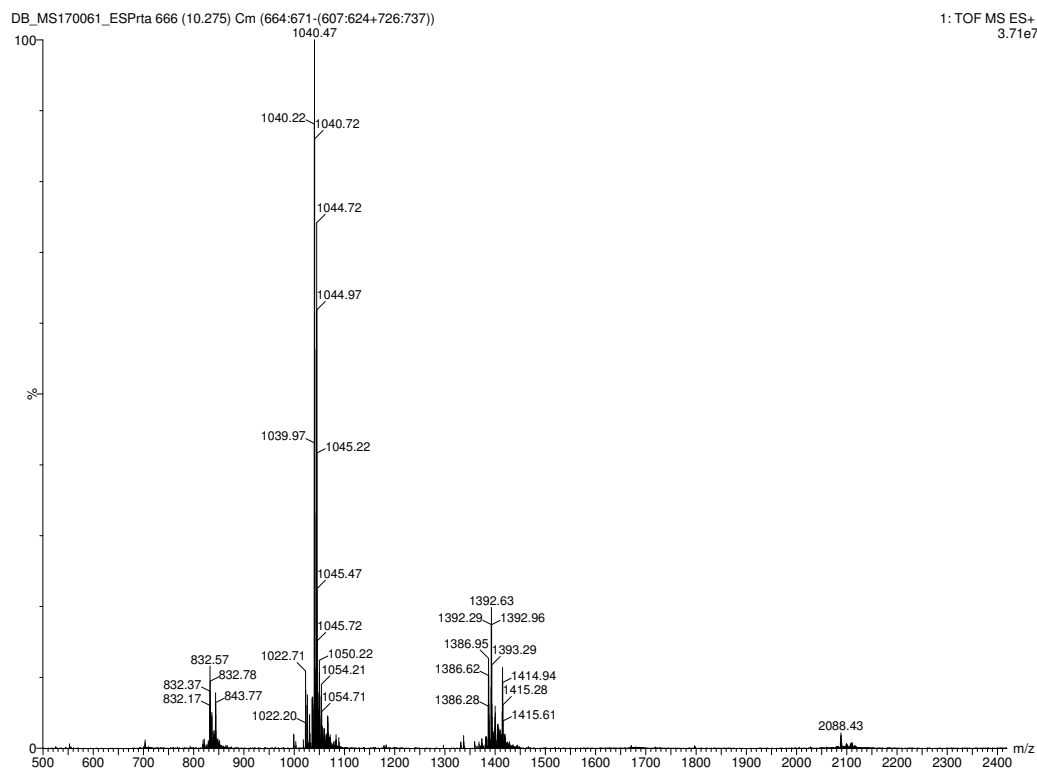
Figure 6-43 LC-ESI-MS(Q-Tof) analysis of crude peptide **5-60** showing $[(M+2)+2H]^{2+}$, $[(M+2)+3H]^{3+}$, $[(M+2)+4H]^{4+}$.

6.2.4.5.3 Synthesis of pentatopic peptide 5-63
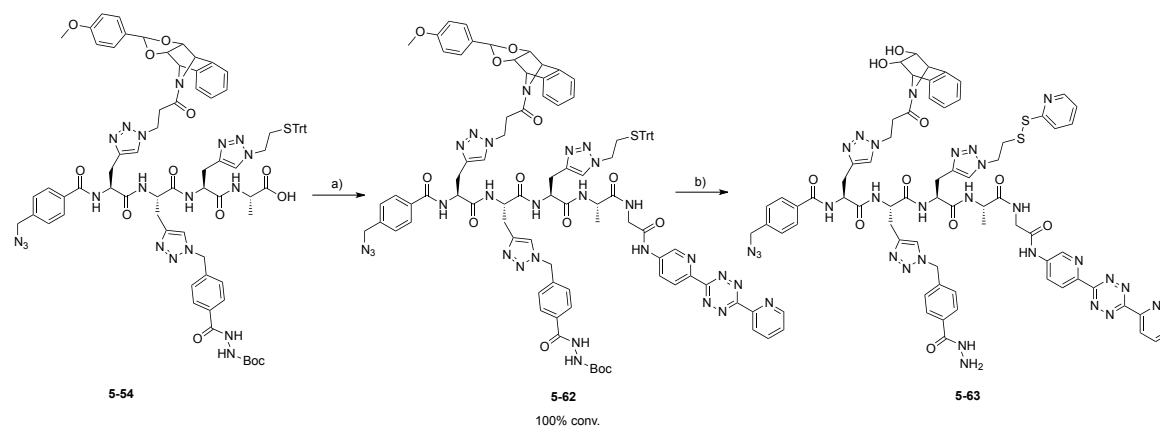
Scheme 6-30 Synthesis of pentapeptide **5-63**; a) **5-24**, HATU, DIEA, DMF/NMP, rt, 1h30; b) *i)* TFA/TIS (5 equiv) /H$_2$O, rt, 2 h; *ii)* 2,2'-dipyridyl disulfide, DIEA, DMF, 30 min.

6.2.4.5.3.1 Synthesis of peptide 5-62

Chemical Formula: $C_{95}H_{93}N_{27}O_{13}S$
Exact Mass: 1851.7167
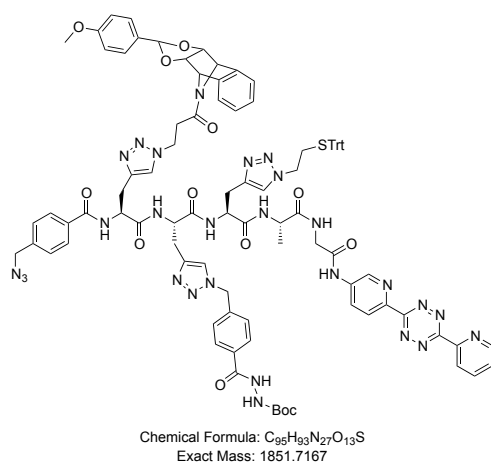
To peptide **5-54** (20 mg, 0.013 mmol) and H-Gly-tetrazine **5-24** (10.5 mg, 0.026 mmol) suspended in DMF (1 mL), solutions of HATU in DMF (0.3 M, 53 µL, 0.016 mmol) and DIEA in NMP (2 M, 65 µL, 0.13 mmol) were successively added. The reaction mixture was stirred at rt for 1h30. H_2O was added and the aqueous solution was extracted with CH_2Cl_2 (3 times). The combined organic phases were washed with brine, dried over $MgSO_4$ and concentrated. The crude residue was purified through silica gel (Eluent: CH_2Cl_2 to CH_2Cl_2/MeOH (9:1)) (33 mg, HPLC profile showed 100% conv). After evaporation of the solvents, the material was re-dissolved in H_2O/CH_3CN (1:1) was lyophilized and re-purified by RP-HPLC. HPLC (25 °C): R_t = 19.4 min (gradient 1). ESI-HRMS(Q-Tof) showed $[M+2H]^{2+}$, $[M+H]^+$, and fragmented $[M(-Trt-Boc)+2H]^{2+}$, $[M(-Trt-Boc)+H]^+$, $[M(-Trt)+H]^+$; monoisotopic mass found: 1852.7262 (calcd for $[C_{95}H_{94}N_{27}O_{13}S_1]^+$ 1852.7245).
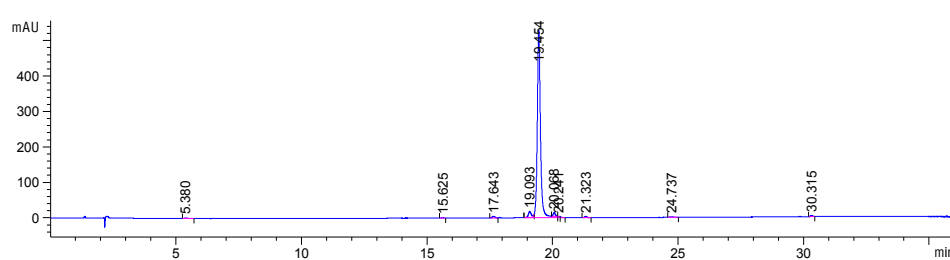

Figure 6-44 HPLC chromatogram of purified peptide **5-62.**
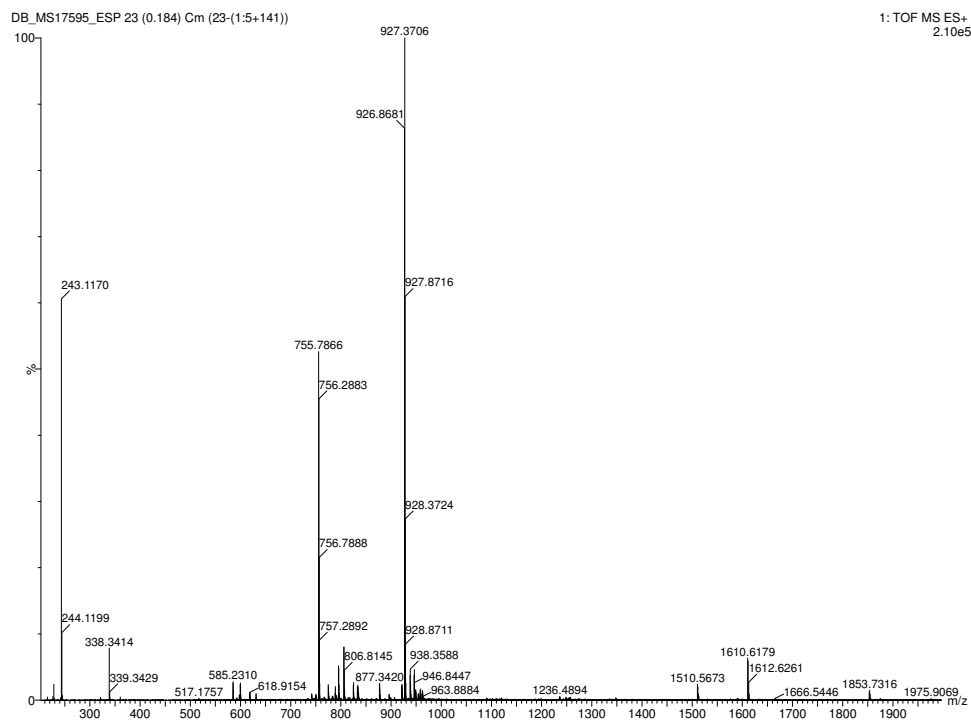
Figure 6-45 ESI-MS(Q-Tof) analysis of peptide **5-62.**

6.2.4.5.3.2 Synthesis of peptide 5-63

Chemical Formula: $C_{68}H_{68}N_{28}O_{10}S_2$
Exact Mass: 1500.5115
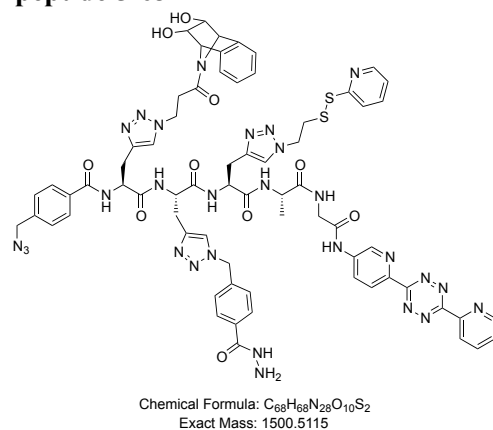
Peptide **5-62** (3.6 mg, $1.9.10^{-3}$ mmol) was dissolved with TFA/water/TIS (0.5 mL/ 2 µL ($9.7.10^{-3}$ mmol)/ 2 µL) for 2 h. The volatile were removed under a flow of N_2 and the crude material was precipitated in cold Et_2O. After centrifugation, the ether was decanted and this washing was repeated 3 times. The disulfide exchange was performed according to the general procedure (stirring for 30 min) and the material was not purified by RP-HPLC. The analytical HPLC were performed with 0.1% of TFA. HPLC (25 °C): R_t = 14.78 min (gradient 4). ESI-HRMS(Q-Tof) showed $[M+3H]^{3+}$, $[M+2H]^{2+}$, $[M+H]^+$; monoisotopic mass found: 1501.5209 (calcd for $[C_{68}H_{69}N_{28}O_{10}S_2]^+$ 1501.5193).
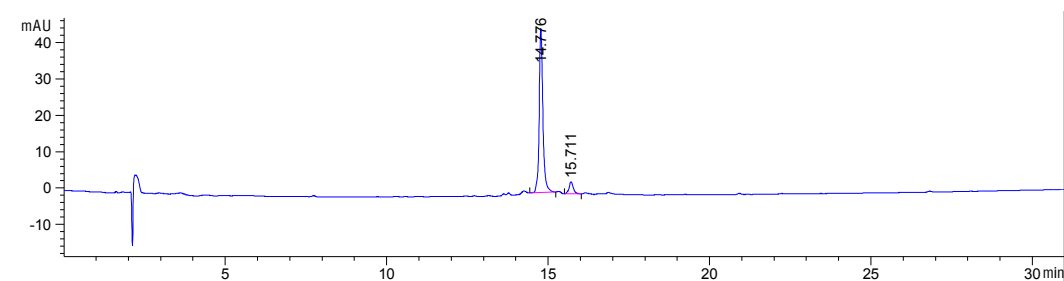
Figure 6-46 HPLC chromatogram of crude peptide **5-63.**
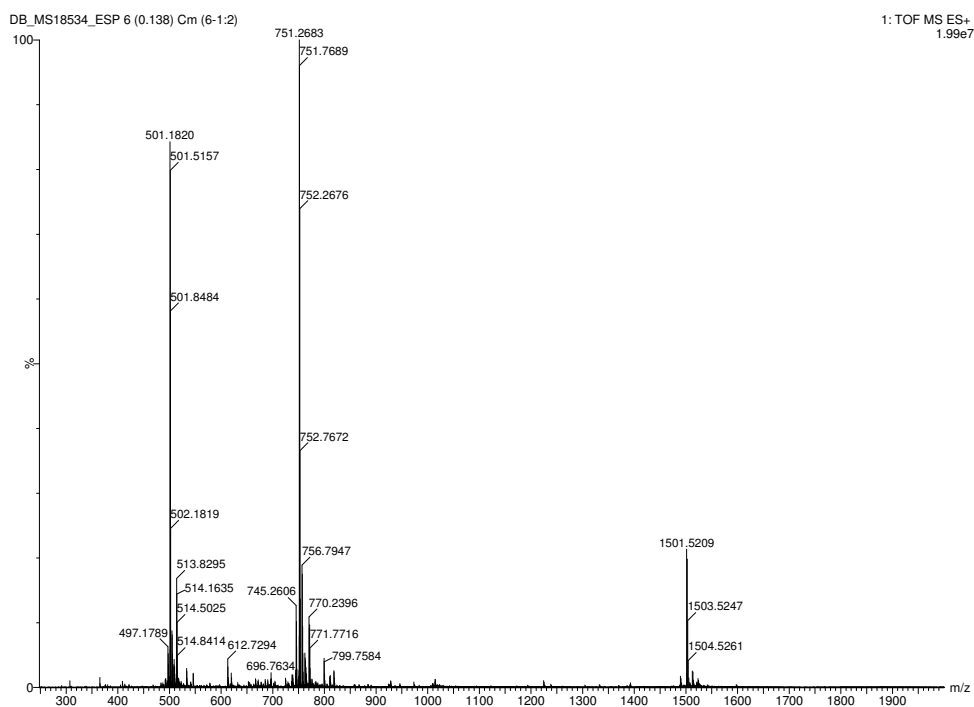
Figure 6-47 ESI-MS(Q-Tof) analysis of peptide **5-63.**

6.2.4.6 Chromophore assembly on peptidic scaffold

General Procedure: Peptidic scaffold (1 equiv), chromophoric units (3 equiv), *m*-PDA (0.5 equiv) were dissolved in anhydrous DMA (C = 0.5 mM). The time and the temperature of the reaction are specified in each case. The crude material was purified using gel permeation chromatography (GPC) with Bio-Rad Bio-Beads S-X1 Beads (operating range 600 – 14000 g.mol-1) as stationary phase with anhydrous DMA as eluent.

Peptide **5-44**: Reaction was stirred at rt for 4 h and 40 °C for two additional hours. MALDI-Tof LRMS $[M+Na]^+$ calcd for $[C_{270}H_{333}N_{47}O_{55}F_2NaS_2]^+$: 5238.4, found: 5238.4; $[M(\text{-disulfide}) + Na]^+$ calcd for $[C_{217}H_{273}N_{43}O_{43}F_2NaS]^+$: 4262.0, found: 4262.0. UV/Vis (DMA) λ_{max}, nm (ε, L mol^{-1} cm^{-1}): 425 (55200), 451 (78700), 492 (66900), 528 (110600), 612 (23600); molar extinction coefficients obtained by normalizing the absorbance of the peptide and the arithmetic sum of dyes on B-NDI unit (612 nm). Fluorescence emission (DMA, exc 423 nm) λ_{max}, nm: 468, 497, 539,

285

581, 641; (DMA, exc 495 nm) λ_{max}, nm: 540, 581, 641; (DMA, exc 609 nm) λ_{max}, nm: 642. Fluorescence excitation (DMA, emis 640 nm) λ_{max}, nm: 344, 362, 423, 451, 491, 527, 612.

Peptide **5-45**: Reaction was stirred at rt for 2 h and 40 °C for two additional hours. MALDI-Tof LRMS $[M+Na]^+$ calcd for $[C_{270}H_{333}N_{47}O_{55}F_2NaS_2]^+$: 5238.4, found: 5238.4; $[M(-triazole; N_3) + Na]^+$ calcd for $[C_{225}H_{303}N_{45}O_{53}F_2NaS_2]^+$: 4608.2, found: 4608.2; ; $[M(-triazole; N) + Na]^+$ calcd for $[C_{225}H_{303}N_{43}O_{53}F_2NaS_2]^+$: 4580.2, found: 4580.2; $[M(-disulfide) + Na]^+$ calcd for $[C_{217}H_{273}N_{43}O_{43}F_2NaS]^+$: 4262.0, found: 4262.0. UV/Vis (DMA) λ_{max}, nm (ε, L mol^{-1} cm^{-1}): 424 (40900), 452 (60800), 492 (74000), 528 (121300), 612 (23600); molar extinction coefficients obtained by normalizing the absorbance of the peptide and the arithmetic sum of dyes on B-NDI unit (612 nm). Fluorescence emission (DMA, exc 423 nm) λ_{max}, nm: 468, 497, 539, 581, 640; (DMA, exc 495 nm) λ_{max}, nm: 540, 581, 640; (DMA, exc 609 nm) λ_{max}, nm: 642. Fluorescence excitation (DMA, emis 640 nm) λ_{max}, nm: 344, 360, 423, 453, 491, 527, 613.

Peptide **5-48**: Reaction was stirred at rt for 17 h. MALDI-Tof LRMS $[M+H]^+$ calcd for $[C_{189}H_{187}F_2N_{32}O_{22}S_2]^+$: 3378.3, found: 3378.4; $[M+Na]^+$ calcd for $[C_{189}H_{186}F_2N_{32}NaO_{22}S_2]^+$: 3400.3, found: 3400.4; $[M(-PDI-H_2O) + H]^+$ calcd for $[C_{129}H_{124}N_{20}O_{19}S_2]^+$: 2320.9, found: 2320.9 (hydrolysis of acyl hydrazone and cyclization during ionization process); UV/Vis (DMA) λ_{max}, nm (ε, L mol^{-1} cm^{-1}): 424 (56500), 453 (78800), 493 (72000), 528 (116400), 612 (22100); molar extinction coefficients obtained by normalizing the absorbance of the peptide and the arithmetic sum of dyes on R-PDI unit (527 nm). Fluorescence emission (DMA, exc 423 nm) λ_{max}, nm: 468, 497, 539, 581, 640; (DMA, exc 495 nm) λ_{max}, nm: 540, 581, 640; (DMA, exc 609 nm) λ_{max}, nm: 642. Fluorescence excitation (DMA, emis 640 nm) λ_{max}, nm: 344, 360, 423, 453, 491, 527, 613.

Peptide **5-56**: Reaction stirred at rt for 2 h, 40 °C for 2 h and additional 16 h at rt. MALDI-Tof LRMS $[M+H]^+$ calcd for $[C_{237}H_{221}BF_2N_{27}O_{36}S_2]^+$: 4133.6, found: 4133.6; $[M+Na]^+$ calcd for $[C_{237}H_{220}BF_2N_{27}NaO_{36}S_2]^+$: 4155.6, found: 4155.6; $[M(-PDI-H_2O)+H]^+$ calcd for $[C_{177}H_{158}BN_{25}O_{23}S_2]^+$: 3077.1, found: 3077.1 (cyclization during ionization process); UV/Vis (DMA) λ_{max}, nm (ε, L mol^{-1} cm^{-1}): 367 (93300), 395 (81400), 424 (31200), 458 (36400), 493 (46300), 528 (63500), 612 (23800); molar extinction coefficients obtained by normalizing the absorbance of the peptide and the arithmetic sum of dyes on B-NDI unit (612 nm). Fluorescence emission (DMA, exc 398 nm) λ_{max}, nm: 412, 415, 470, 497, 539, 581, 640; (DMA, exc 423 nm) λ_{max}, nm: 468, 497, 539, 581, 640; (DMA, exc 495 nm) λ_{max}, nm: 540, 581, 640; (DMA, exc 609

nm) λ_{max}, nm: 642. Fluorescence excitation (DMA, emis 640 nm) λ_{max}, nm: 344, 360, 423, 453, 491, 527, 613.

Peptide **5-64**: Reaction stirred at rt for 2 h, 40 °C. MALDI-Tof LRMS $[M-I]^+$ calcd for $[C_{298}H_{295}BF_2N_{35}O_{38}S_2]^+$: 5084.2, found: 5082.2 ($[C_{298}H_{293}BF_2N_{35}O_{38}S_2]^+$ after oxidation of dihydropyridazine); UV/Vis (CHCl$_3$) λ_{max}, nm (ε, L mol^{-1} cm^{-1}): 368 (80000), 398 (65200), 427 (36900), 457 (50000), 492 (64200), 529 (99400), 618 (49000), 658 (83300); molar extinction coefficients obtained by normalizing the absorbance of the peptide and the arithmetic sum of dyes on Y-Py unit (396 nm). Fluorescence emission (CHCl$_3$, exc 398 nm) λ_{max}, nm: 410, 413, 471, 498, 536, 651, 672; (CHCl$_3$, exc 423 nm) λ_{max}, nm: 471, 500, 536, 578, 641, 677; (DMA, exc 495 nm) λ_{max}, nm: 536, 578, 654, 668; (CHCl$_3$, exc 570 nm) λ_{max}, nm: 651, 671; (DMA, exc 630 nm) λ_{max}, nm: 674. Fluorescence excitation (CHCl$_3$, emis 670 nm) λ_{max}, nm: 364, 397, 423, 458, 491, 527, 627, 660; Fluorescence excitation (CHCl$_3$, emis 630 nm) λ_{max}, nm: 364, 394, 458, 490, 527, 627. Fluorescence excitation (CHCl$_3$, emis 580 nm) λ_{max}, nm: 368, 392, 424, 458, 490, 527. Fluorescence excitation (CHCl$_3$, emis 465 nm) λ_{max}, nm: 373, 400, 423, 449.

Evaluation of Quenching of fluorescence within tetrad 5-56 and pentad 5-64 vs. single dyes
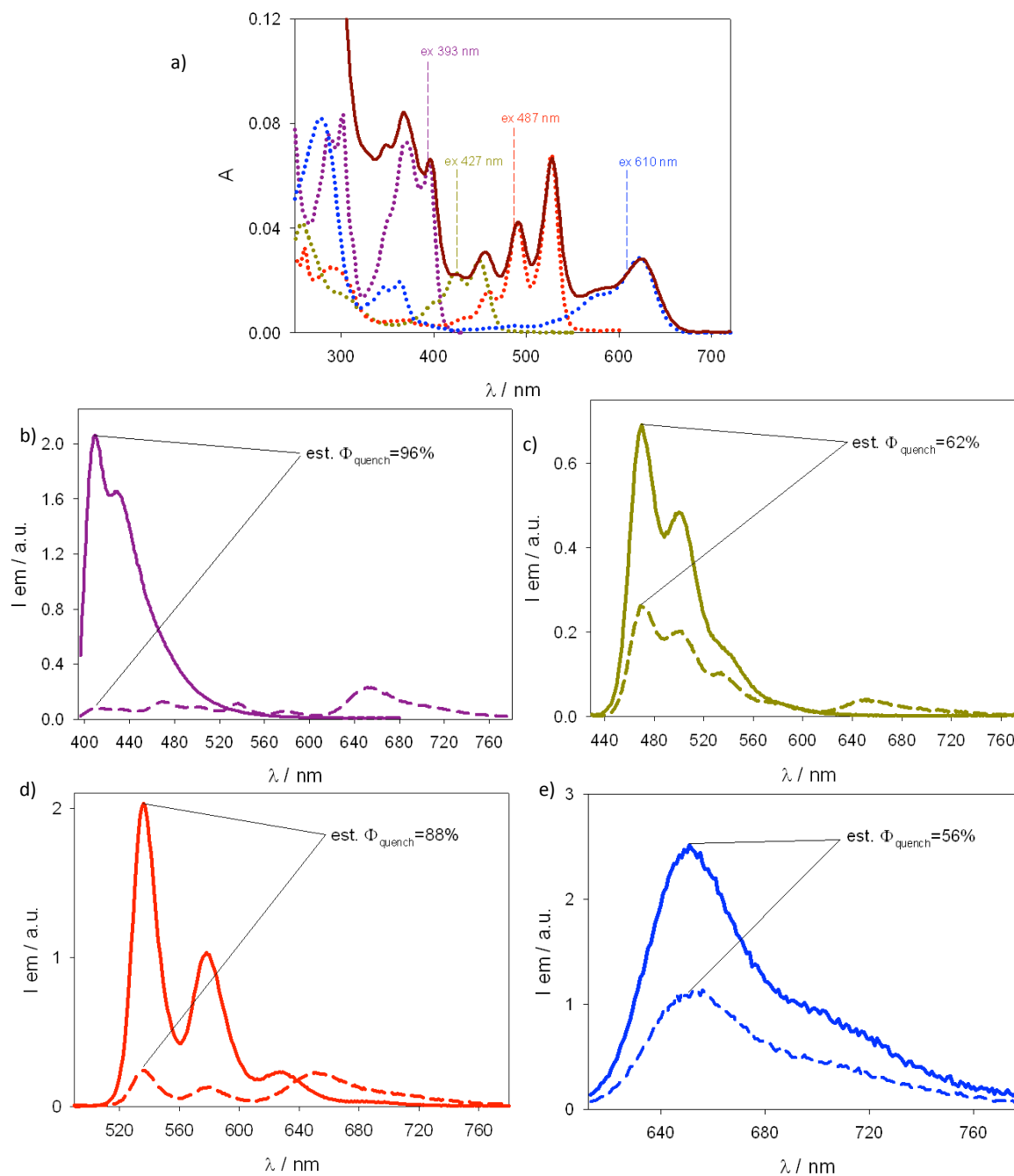
Figure 6-48 a) Absorption and emission spectra of tetrad **5-56** and free dyes (dashed line) used to evaluate the emission quenching on tetrad **5-56** (dashed lines): b) Y-Py (λ_{exc}=393 nm), c) Y-Per (λ_{exc}=427 nm), d) R-PDI (λ_{exc}=487 nm), d) B-NDI (λ_{exc}=610 nm).
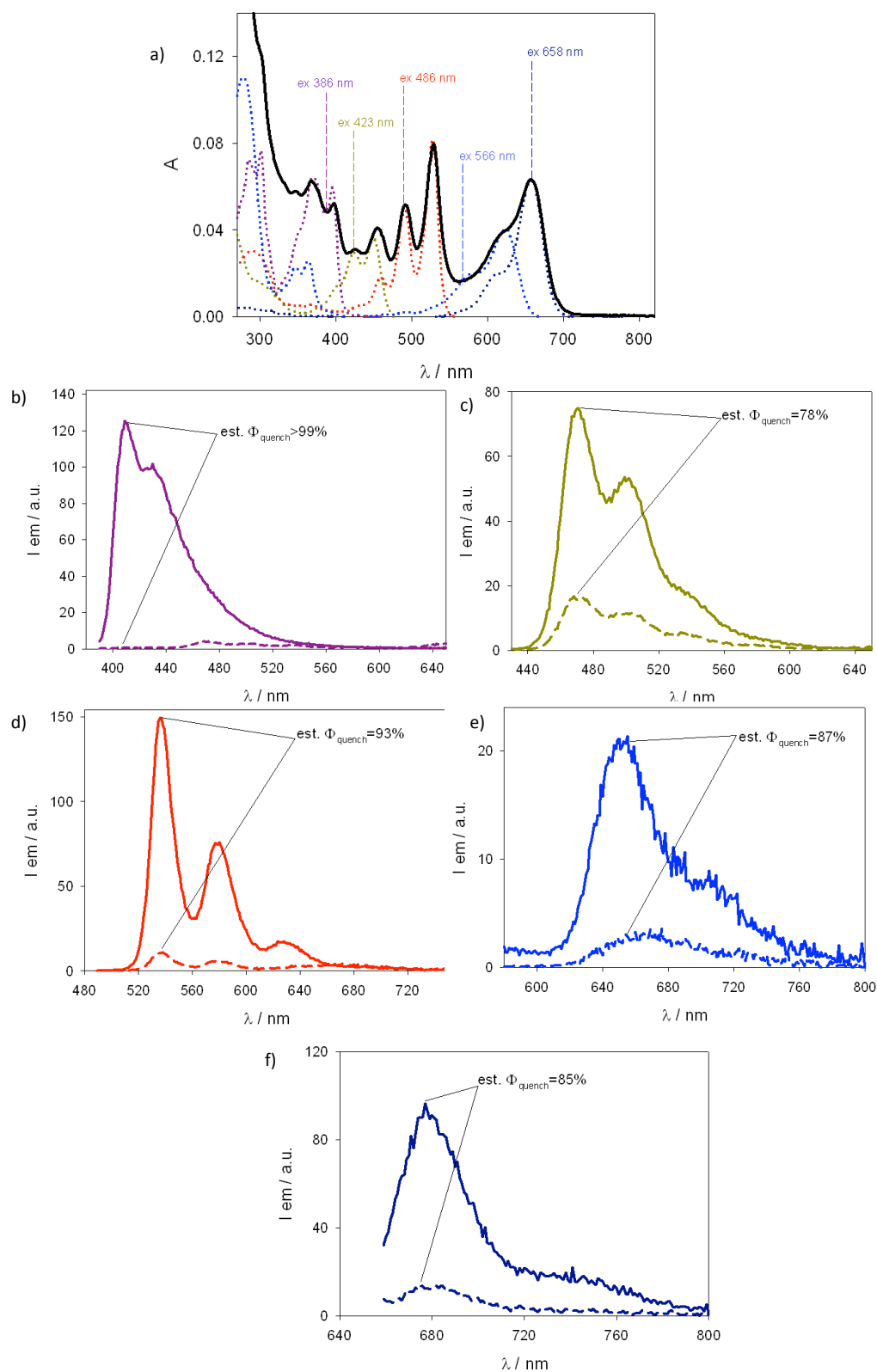
Figure 6-49 a) Absorption and emission spectra of pentad **5-64** and free dyes (dashed line) used to evaluate the emission quenching on pentad **5-64** (dashed lines): b) Y-Py (λ_{exc}=393 nm), c) Y-Per (λ_{exc}=423 nm), d) R-PDI (λ_{exc}=486 nm), d) B-NDI (λ_{exc}=566 nm), e) B-Cy (λ_{exc}=658 nm).

Evaluation of Quenching of fluorescence within pentad 5-64 vs. mixture of dyes

Figure 6-50 a) Absorption and emission spectra pentad **5-64** and mixture of free dyes (dashed line) used to evaluate the emission quenching on pentad **5-64** (dashed lines): b) Y-Py (λ_{exc}=393 nm), c) Y-Per (λ_{exc}=423 nm), d) R-PDI (λ_{exc}=485 nm), d) B-NDI (λ_{exc}=565 nm), e) B-Cy (λ_{exc}=655 nm).
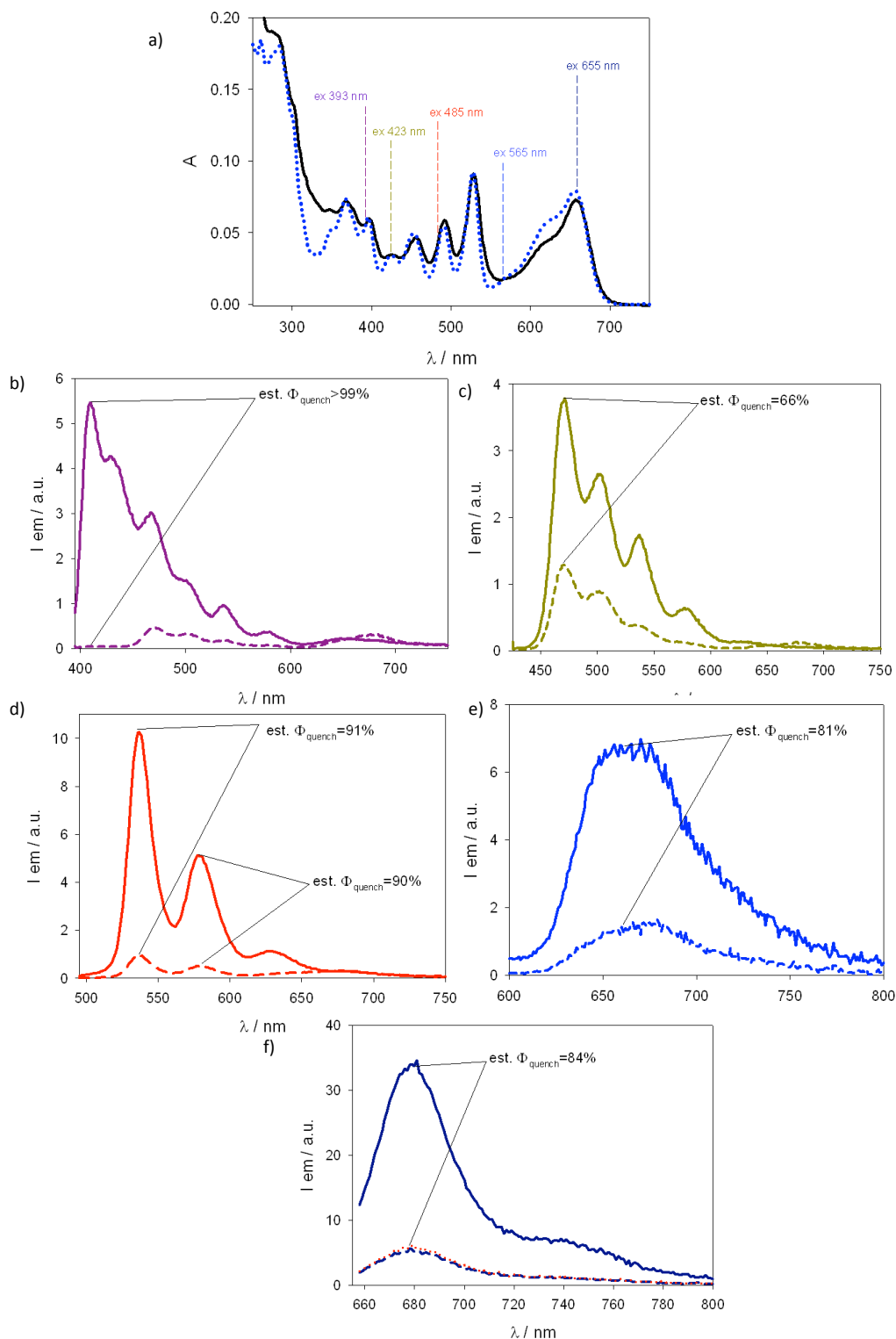
6.3 References
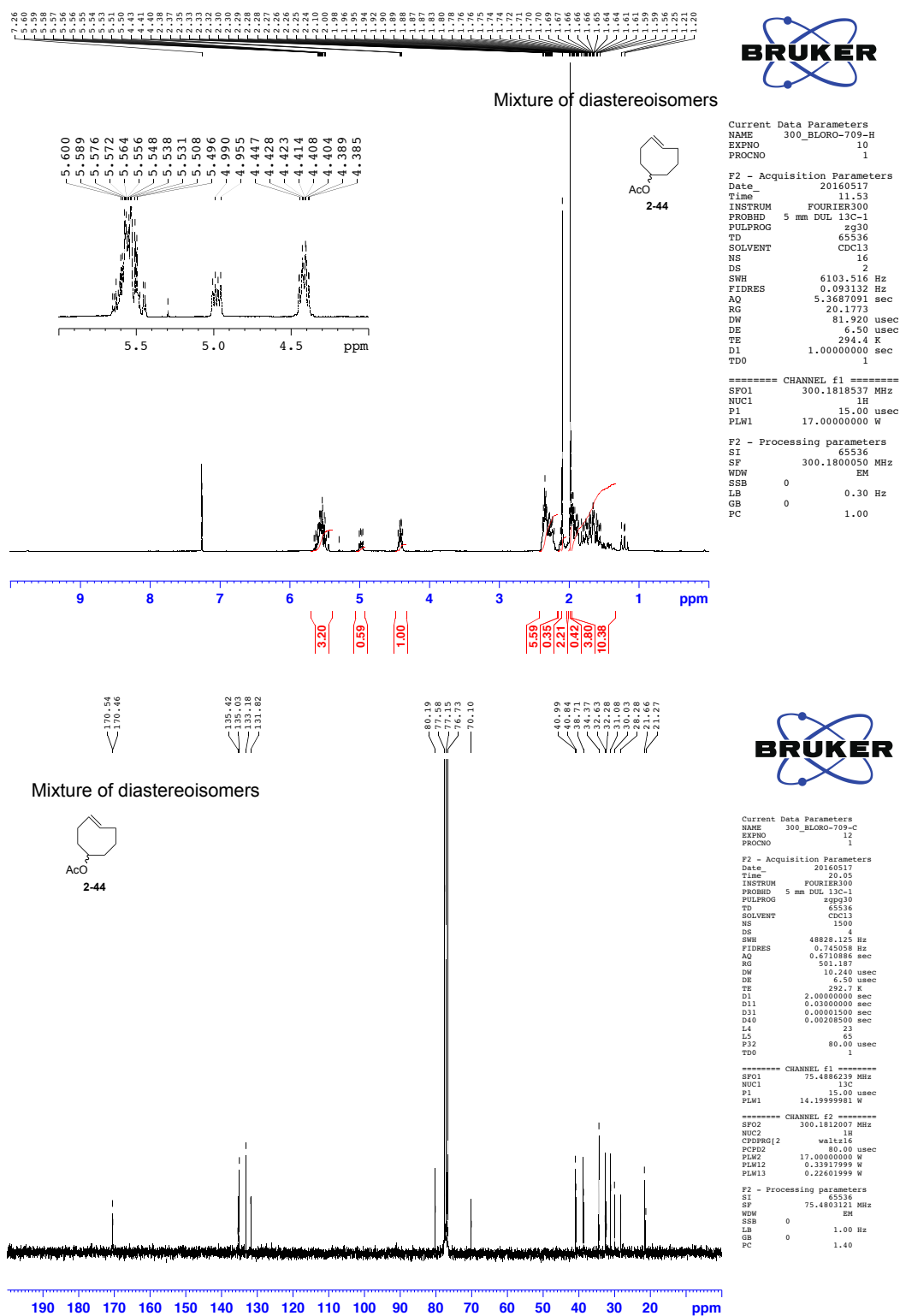
[1]   W. S. Yeo, D. H. Min, R. W. Hsieh, G. L. Greene, M. Mrksich, *Angew. Chem. Int. Ed.* **2005**, *44*, 5480-5483.

[2]   M. Di Antonio, G. Biffi, A. Mariani, E. A. Raiber, R. Rodriguez, S. Balasubramanian, *Angew. Chem. Int. Ed.* **2012**, *51*, 11073-11078.

[3]   H. Salman, Y. Abraham, S. Tal, S. Meltzman, M. Kapon, N. Tessler, S. Speiser, Y. Eichen, *Eur. J. Org. Chem.* **2005**, 2207-2212.

[4]   M. Lautens, K. Fagnou, V. Zunic, *Org. Lett.* **2002**, *4*, 3465-3468.

[5]   M. Wrobel, J. Aubé, B. König, *Beilstein J. Org. Chem.* **2012**, *8*, 1027-1036.

[6]   A. Kuzmin, A. Poloukhtine, M. A. Wolfert, V. V. Popik, *Bioconjugate Chem.* **2010**, *21*, 2076-2085.

[7]   P. G. Clark, E. N. Guidry, W. Y. Chan, W. E. Steinmetz, R. H. Grubbs, *J. Am. Chem. Soc.* **2010**, *132*, 3405-3412.

[8]   C. J. Zhang, C. Y. J. Tan, J. Ge, Z. Na, G. Y. J. Chen, M. Uttamchandani, H. Sun, S. Q. Yao, *Angew. Chem. Int. Ed.* **2013**, *52*, 14060-14064.

[9]   A. Blencowe, G. G. Qiao, *J. Am. Chem. Soc.* **2013**, *135*, 5717-5725.

[10]   M. L. Blackman, M. Royzen, J. M. Fox, *J. Am. Chem. Soc.* **2008**, *130*, 13518-13519.

[11]   M. H. Klingele, P. D. W. Boyd, B. Moubaraki, K. S. Murray, S. Brooker, *Eur. J. Inorg. Chem.* **2006**, 573-589.

[12]   R. Hoogenboom, G. Kickelbick, U. S. Schubert, *Eur. J. Org. Chem.* **2003**, 4887-4896.

[13]   S. S. Bag, S. Jana, A. Yashmeen, S. De, *Chem. Commun.* **2015**, *51*, 5242-5245.

[14]   A. Vázquez, R. Dzijak, M. Dračínský, R. Rampmaier, S. J. Siegl, M. Vrabel, *Angew. Chem. Int. Ed.* **2017**, *56*, 1334-1337.

[15]   U. Hahn, S. Engmann, C. Oelsner, C. Ehli, D. M. Guldi, T. Torres, *J. Am. Chem. Soc.* **2010**, *132*, 6392-6401.

[16]   S. Zhang, H. J. Sun, A. D. Hughes, B. Draghici, J. Lejnieks, P. Leowanawat, A. Bertin, L. Otero De Leon, O. V. Kulikov, Y. Chen, D. J. Pochan, P. A. Heiney, V. Percec, *ACS Nano* **2014**, *8*, 1554-1565.

[17]   A. A. Berezin, A. Sciutto, N. Demitri, D. Bonifazi, *Org. Lett.* **2015**, *17*, 1870-1873.

[18]   G. Seybold, G. Wagenblast, *Dyes Pigm.* **1989**, *11*, 303-317.

[19]   Z. J. Chen, L. M. Wang, G. Zou, L. Zhang, G. J. Zhang, X. F. Cai, M. S. Teng, *Dyes Pigm.* **2012**, *94*, 410-415.

[20]   A. M. Brouwer, *Pure Appl. Chem.* **2011**, *83*, 2213-2228.

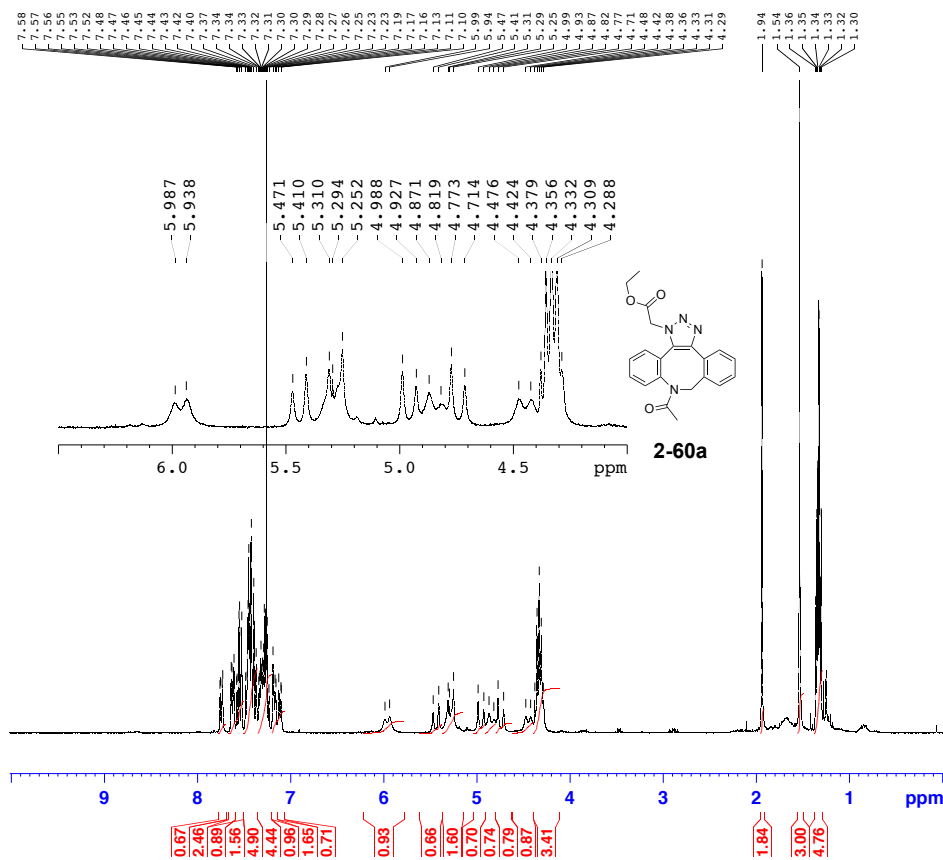[21]   S. W. Provencher, J. Glöckner, *Biochemistry* **1981**, *20*, 33-37.

[22]   É. Torres, M. N. Berberan-Santos, M. J. Brites, *Dyes Pigm.* **2015**, *112*, 298-304.

[23]   I. B. Berlman, *Handbook of fluorescence spectra of aromatic molecules*, Academic Press: New York, **1971**.

[24]   R. Kota, R. Samudrala, D. L. Mattern, *J. Org. Chem.* **2012**, *77*, 9641-9651.

[25]   M. R. Hansen, T. Schnitzler, W. Pisula, R. Graf, K. Muellen, H. W. Spiess, *Angew. Chem. Int. Ed.* **2009**, *48*, 4621-4624, S4621/4621-S4621/4628.

[26]   M. Fischer, J. Georges, *Chem. Phys. Lett.* **1996**, *260*, 115-118.

[27]   E. Seraya, Z. Luan, M. Law, A. F. Heyduk, *Inorg. Chem.* **2015**, *54*, 7571-7578.

[28]   Y. Kita, M. Arisawa, M. Gyoten, M. Nakajima, R. Hamada, H. Tohma, T. Takada, *J. Org. Chem.* **1998**, *63*, 6625-6633.

[29]   A. V. Ivanov, P. A. Svinareva, L. G. Tomilova, N. S. Zefirov, *Russ. Chem. Bull.* **2001**, *50*, 919-920.

[30]   G. Lopez-Frias, A. A. Camacho-Davila, D. Chavez-Flores, G. Zaragoza-Galan, V. H. Ramos-Sanchez, *Molecules* **2015**, *20*, 8654-8665.

[31]   V. S. Wilms, H. Bauer, C. Tonhauser, A.-M. Schilmann, M.-C. Mueller, W. Tremel, H. Frey, *Biomacromolecules* **2013**, *14*, 193-199.

[32]   Z. Cheng, D. R. Elias, N. P. Kamat, E. D. Johnston, A. Poloukhtine, V. Popik, D. A. Hammer, A. Tsourkas, *Bioconjugate Chem.* **2011**, *22*, 2021-2029.

[33]   T. Hirano, T. Osaki, S. Fujii, D. Komatsu, I. Azumaya, A. Tanatani, H. Kagechika, *Tetrahedron Lett.* **2009**, *50*, 488-491.

[34]   D. S. Pisoni, L. Todeschini, A. C. A. Borges, C. L. Petzhold, F. S. Rodembusch, L. F. Campo, *J. Org. Chem.* **2014**, *79*, 5511-5520.

[35]   a) H. Katayama, H. Hojo, T. Ohira, Y. Nakahara, *Tetrahedron Lett.* **2008**, *49*, 5492-5494; b) P. S. Ghosh, A. D. Hamilton, *J. Am. Chem. Soc.* **2012**, *134*, 13208-13211.

[36]   M. I. Montañez, Y. Hed, S. Utsel, J. Ropponen, E. Malmström, L. Wågberg, A. Hult, M. Malkoch, *Biomacromolecules* **2011**, *12*, 2114-2125.

[37]   K. Lang, L. Davis, J. Torres-Kolbus, C. Chou, A. Deiters, J. W. Chin, *Nat. Chem.* **2012**, *4*, 298-304.

Selected ^{1}H NMR, ^{13}C NMR spectra and mass analysis

The ^{1}H NMR, ^{13}C NMR spectra of the published compounds are avalaible under http://dx.doi.org/10.1002//ani.201507186.

Mixture of diastereoisomers

AcO
2-44

Current Data Parameters
NAME   300_BLORO-709-H
EXPNO   10
PROCNO   1

F2 - Acquisition Parameters
Date_   20160517
Time   11.53
INSTRUM   FOURIER300
PROBHD   5 mm DUL 13C-1
PULPROG   zg30
TD   65536
SOLVENT   CDCl3
NS   16
DS   2
SWH   6103.516 Hz
FIDRES   0.093132 Hz
AQ   5.3687091 sec
RG   20.1773
DW   81.920 usec
DE   6.50 usec
TE   294.4 K
D1   1.00000000 sec
TD0   1

======== CHANNEL f1 ========
SFO1   300.1818537 MHz
NUC1   1H
P1   15.00 usec
PLW1   17.00000000 W

F2 - Processing parameters
SI   65536
SF   300.1800050 MHz
WDW   EM
SSB   0
LB   0.30 Hz
GB   0
PC   1.00

Mixture of diastereoisomers

AcO
2-44

Current Data Parameters
NAME   300_BLORO-709-C
EXPNO   12
PROCNO   1

F2 - Acquisition Parameters
Date_   20160517
Time   20.05
INSTRUM   FOURIER300
PROBHD   5 mm DUL 13C-1
PULPROG   zgpg30
TD   65536
SOLVENT   CDCl3
NS   1500
DS   4
SWH   48828.125 Hz
FIDRES   0.745058 Hz
AQ   0.6710886 sec
RG   501.187
DW   10.240 usec
DE   6.50 usec
TE   292.7 K
D1   2.00000000 sec
D11   0.03000000 sec
D31   0.00001500 sec
D40   0.00208500 sec
L4   23
L5   65
P32   80.00 usec
TD0   1

======== CHANNEL f1 ========
SFO1   75.4886239 MHz
NUC1   13C
P1   15.00 usec
PLW1   14.19999981 W

======== CHANNEL f2 ========
SFO2   300.1812007 MHz
NUC2   1H
CPDPRG[2   waltz16
PCPD2   80.00 usec
PLW2   17.00000000 W
PLW12   0.33917999 W
PLW13   0.22601999 W

F2 - Processing parameters
SI   65536
SF   75.4803121 MHz
WDW   EM
SSB   0
LB   1.00 Hz
GB   0
PC   1.40

293

2-60a

2-60a

2-60b

2-60b

Crude material

2-41

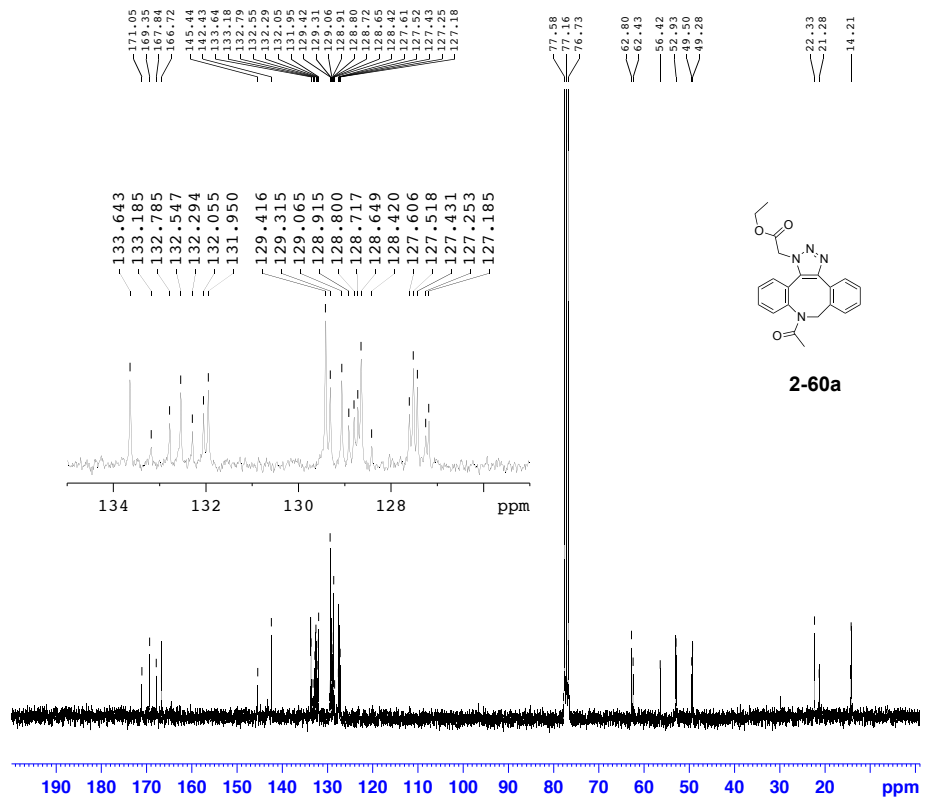Current Data Parameters
NAME   300_BLORO-697-1
EXPNO   10
PROCNO   1

F2 - Acquisition Parameters
Date_   20160429
Time   9.34
INSTRUM   FOURIER300
PROBHD   5 mm DUL 13C-1
PULPROG   zg30
TD   65536
SOLVENT   CDCl3
NS   16
DS   2
SWH   6103.516 Hz
FIDRES   0.093132 Hz
AQ   5.3687091 sec
RG   23.0977
DW   81.920 usec
DE   6.50 usec
TE   295.0 K
D1   1.00000000 sec
TD0   1

======== CHANNEL f1 ========
SFO1   300.1818537 MHz
NUC1   1H
P1   15.00 usec
PLW1   17.00000000 W

F2 - Processing parameters
SI   65536
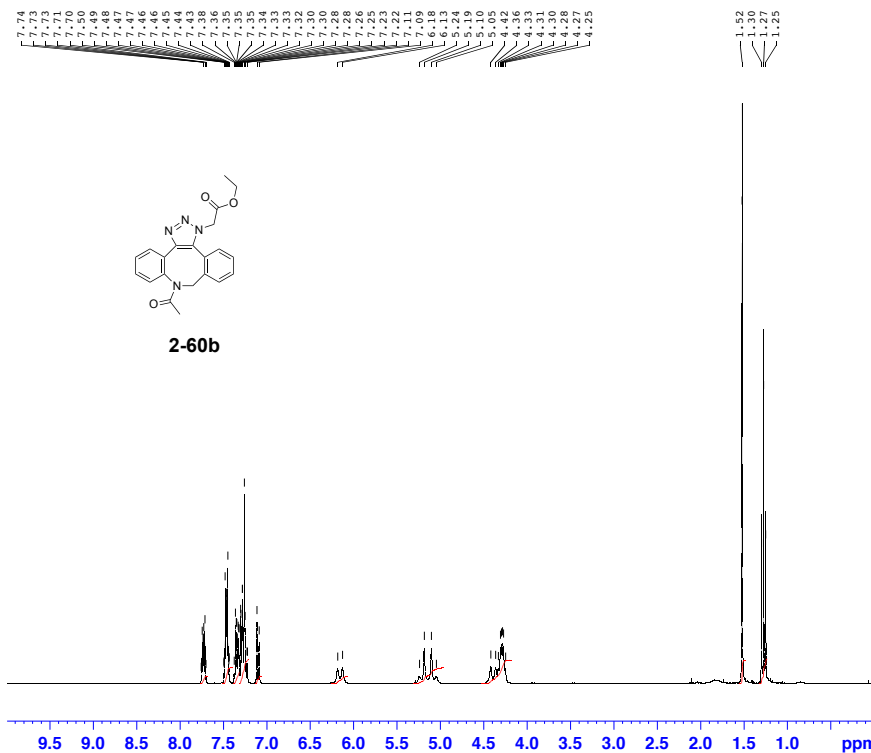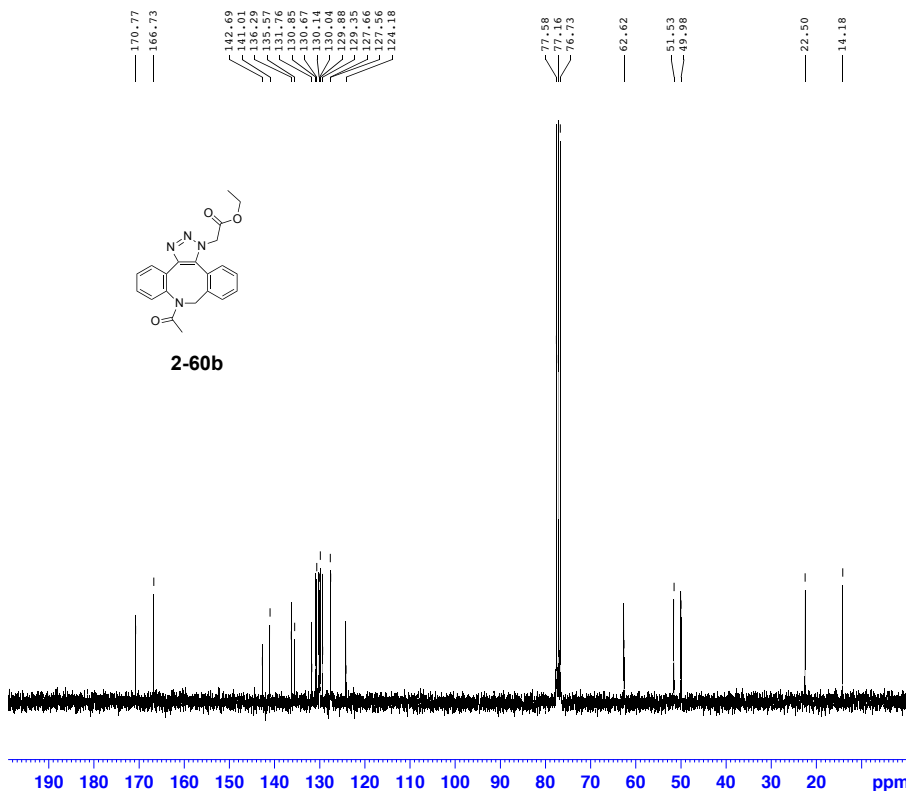SF   300.1800051 MHz
WDW   EM
SSB   0
LB   0.30 Hz
GB   0
PC   1.00

Crude material

2-42a + **2-42b**

THF

Current Data Parameters
NAME   300_BLORO-710-CRUDE
EXPNO   10
PROCNO   1

F2 - Acquisition Parameters
Date_   20160517
Time   14.48
INSTRUM   FOURIER300
PROBHD   5 mm DUL 13C-1
PULPROG   zg30
TD   65536
SOLVENT   CDCl3
NS   16
DS   2
SWH   6103.516 Hz
FIDRES   0.093132 Hz
AQ   5.3687091 sec
RG   31.623
DW   81.920 usec
DE   6.50 usec
TE   294.1 K
D1   1.00000000 sec
TD0   1

======== CHANNEL f1 ========
SFO1   300.1818537 MHz
NUC1   1H
P1   15.00 usec
PLW1   17.00000000 W

F2 - Processing parameters
SI   65536
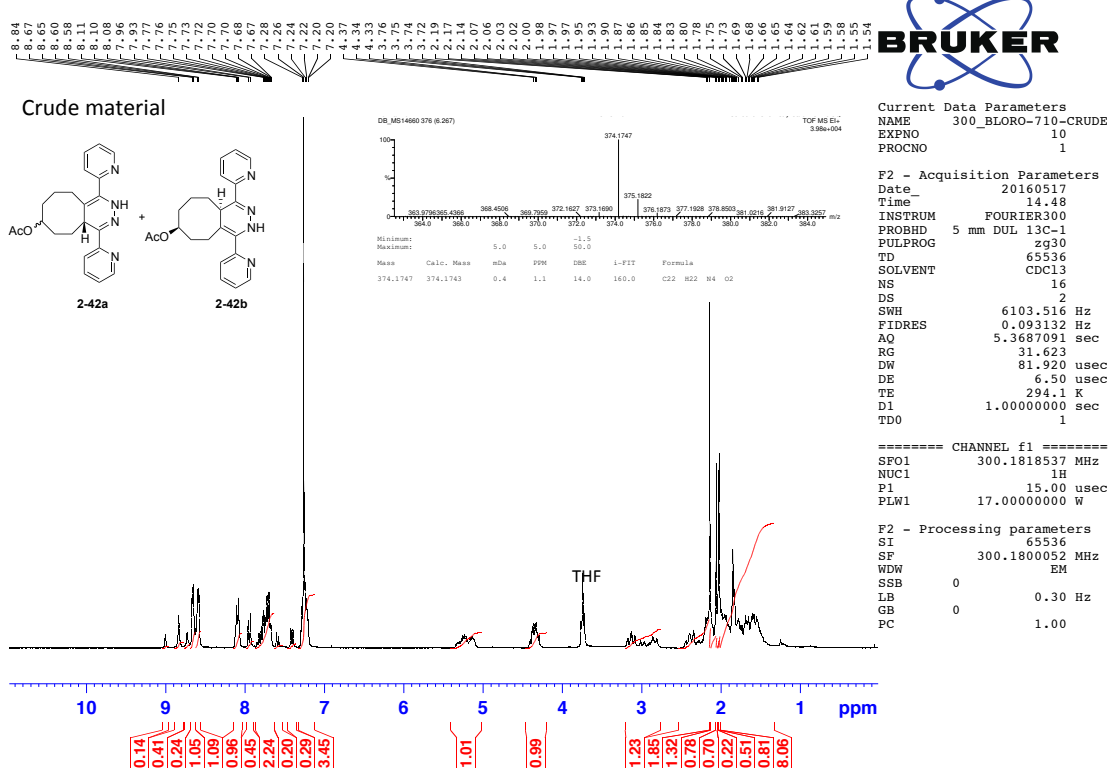SF   300.1800052 MHz
WDW   EM
SSB   0
LB   0.30 Hz
GB   0
PC   1.00

8.45
8.43
8.41
8.38
8.15
8.11
7.95
7.92
7.89
7.86
7.83
7.80
7.78
7.77
7.75
7.74
7.68
7.65
7.63
7.60
7.59
7.56
7.54
7.52
7.49

3.36

2.50

4-1

8.435
8.410
8.384
8.150
8.114
7.950
7.924
7.888
7.861
7.829
7.803
7.781
7.767
7.754
7.741
7.626
7.599
7.590
7.563
7.539
7.519

Current Data Parameters
NAME   300_BLORO-827-H
EXPNO   20
PROCNO   1

F2 - Acquisition Parameters
Date_   20161115
Time   17.40
INSTRUM   FOURIER300
PROBHD   5 mm DUL 13C-1
PULPROG   zg30
TD   65536
SOLVENT   DMSO
NS   16
DS   2
SWH   6103.516 Hz
FIDRES   0.093132 Hz
AQ   5.3687091 sec
RG   31.623
DW   81.920 usec
DE   6.50 usec
TE   293.6 K
D1   1.00000000 sec
TD0   1

======== CHANNEL f1 ========
SFO1   300.1818537 MHz
NUC1   1H
P1   15.00 usec
PLW1   17.00000000 W

F2 - Processing parameters
SI   65536
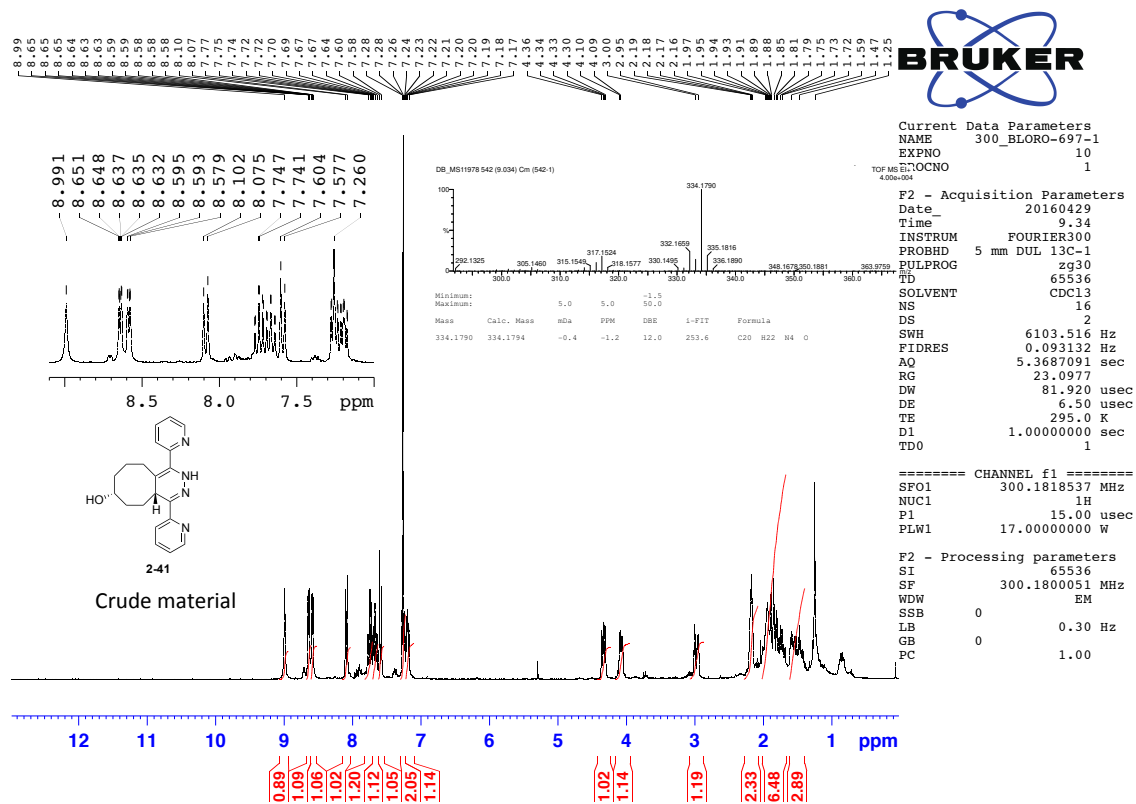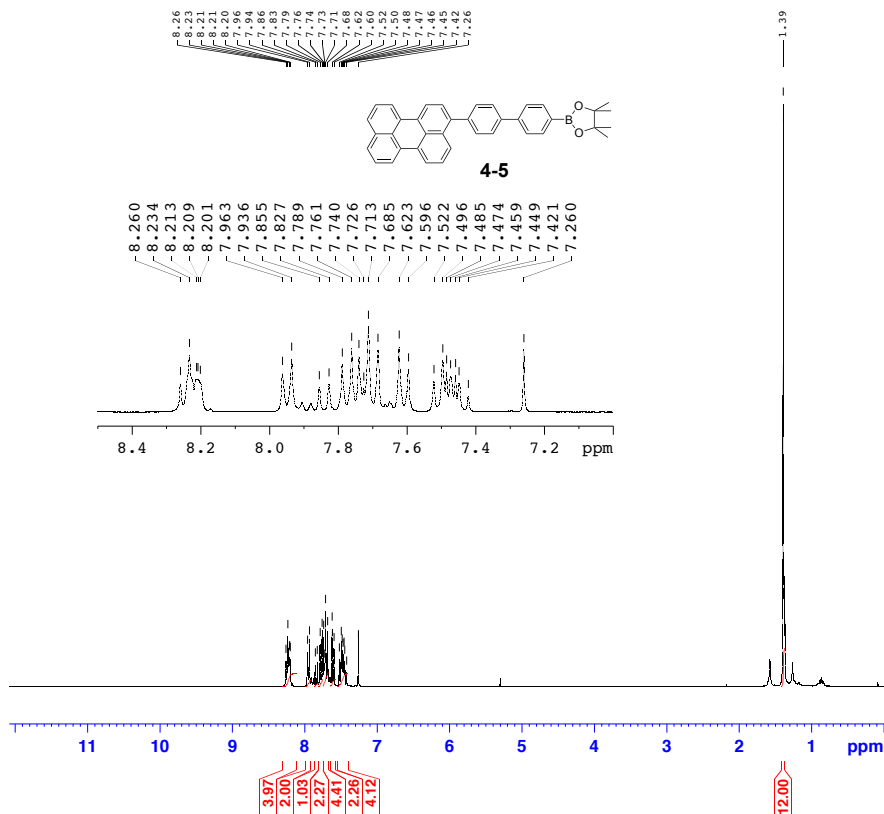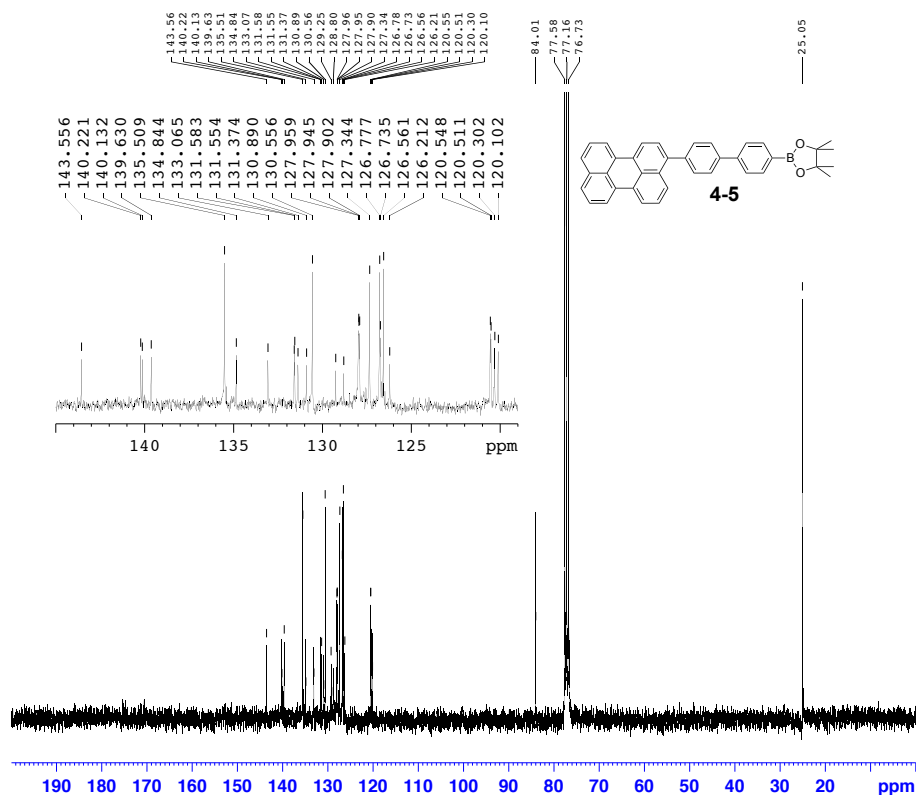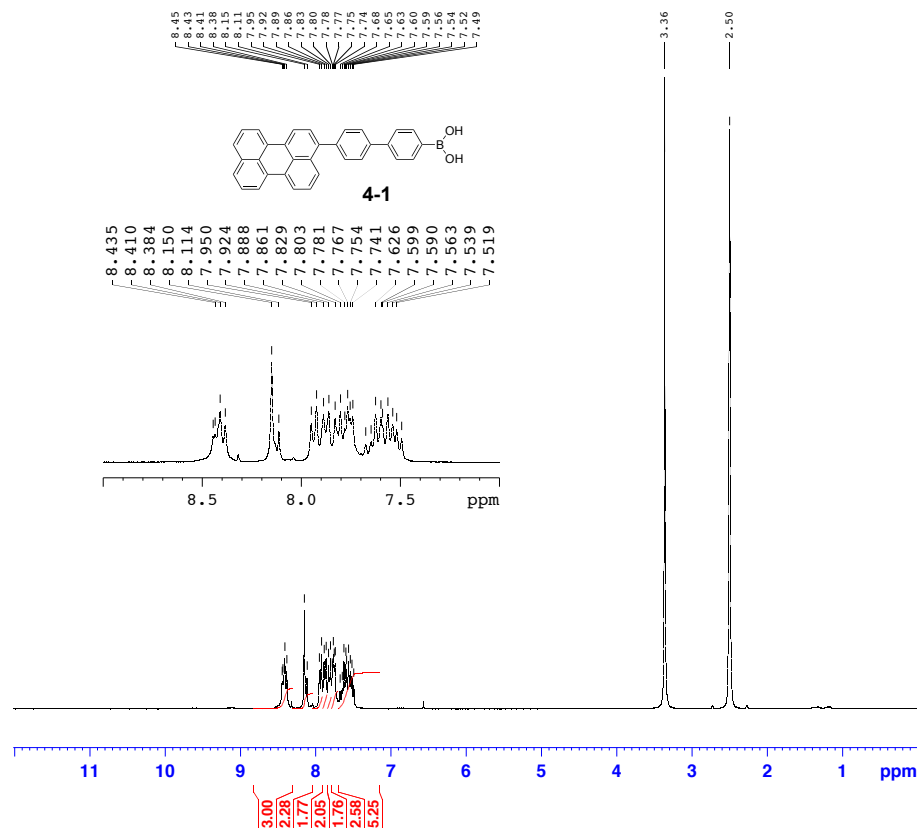SF   300.1800000 MHz
WDW   EM
SSB   0
LB   0.30 Hz
GB   0
PC   1.00

3.00 2.28 1.77 2.05 1.76 2.58 5.25

141.53
141.08
139.31
139.14
138.92
134.90
134.78
134.31
132.20
132.19
130.90
130.57
130.39
130.27
130.09
128.38
128.06
128.03
127.91
127.83
127.18
127.01
126.91
125.67
125.54
121.00
120.99
120.77
120.54

40.02
39.85
39.78
39.69
39.61
39.52
39.35
39.19
39.02

141.526
141.079
139.307
139.136
138.921
134.896
134.776
134.311
132.199
130.901
130.572
130.391
130.266
130.093
128.381
128.061
128.026
127.915
127.830
127.175
127.015
126.912
125.667
125.538
120.999
120.985
120.769

4-1

Current Data Parameters
NAME   500_BLORO-527-C
EXPNO   10
PROCNO   1

F2 - Acquisition Parameters
Date_   20161118
Time   23.10
INSTRUM   spect
PROBHD   5 mm CPPBBO BB
PULPROG   zgpg30
TD   119044
SOLVENT   DMSO
NS   5000
DS   4
SWH   31250.000 Hz
FIDRES   0.262508 Hz
AQ   1.9047040 sec
RG   187.96
DW   16.000 usec
DE   19.87 usec
TE   297.8 K
D1   1.00000000 sec
D11   0.03000000 sec
TD0   1

======== CHANNEL f1 ========
SFO1   125.7816793 MHz
NUC1   13C
P1   10.00 usec
PLW1   60.00000000 W

======== CHANNEL f2 ========
SFO2   500.1720007 MHz
NUC2   1H
CPDPRG[2   waltz64
PCPD2   80.00 usec
PLW2   13.60000038 W
PLW12   0.30599999 W
PLW13   0.15391999 W

F2 - Processing parameters
SI   131072
SF   125.7679054 MHz
WDW   EM
SSB   0
LB   1.00 Hz
GB   0
PC   1.40

4-12
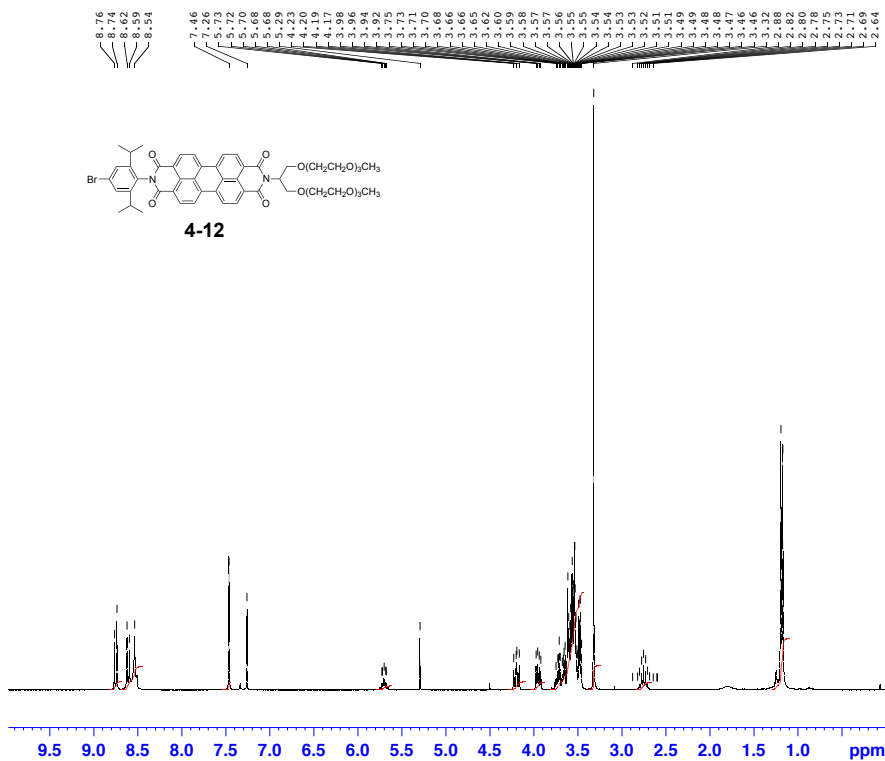
Current Data Parameters
NAME   300_BLORO-679-H
EXPNO   20
PROCNO   1

F2 - Acquisition Parameters
Date_   20160405
Time   16.58
INSTRUM   FOURIER300
PROBHD   5 mm DUL 13C-1
PULPROG   zg30
TD   65536
SOLVENT   CDCl3
NS   16
DS   2
SWH   6103.516 Hz
FIDRES   0.093132 Hz
AQ   5.3687091 sec
RG   16.8099
DW   81.920 usec
DE   6.50 usec
TE   295.5 K
D1   1.00000000 sec
TD0   1

======== CHANNEL f1 ========
SFO1   300.1818537 MHz
NUC1   1H
P1   15.00 usec
PLW1   17.00000000 W

F2 - Processing parameters
SI   65536
SF   300.1800050 MHz
WDW   EM
SSB   0
LB   0.30 Hz
GB   0
PC   1.00

2.04 5.91 1.90 1.00 2.01 2.00 24.57 6.13 1.97 13.07

4-12
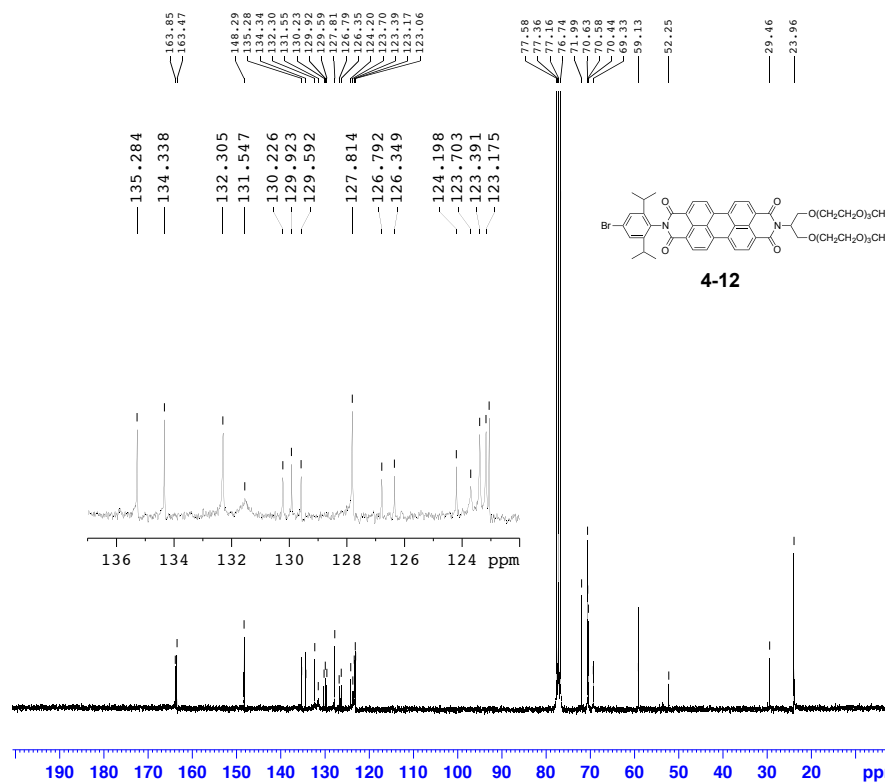
Current Data Parameters
NAME   300_BLORO-679-C
EXPNO   10
PROCNO   1

F2 - Acquisition Parameters
Date_   20160405
Time   20.06
INSTRUM   FOURIER300
PROBHD   5 mm DUL 13C-1
PULPROG   zgpg30
TD   65536
SOLVENT   CDCl3
NS   8000
DS   4
SWH   48828.125 Hz
FIDRES   0.745058 Hz
AQ   0.6710886 sec
RG   501.187
DW   10.240 usec
DE   6.50 usec
TE   295.4 K
D1   2.00000000 sec
D11   0.03000000 sec
D31   0.00001500 sec
D40   0.00208500 sec
L4   23
L5   65
P32   80.00 usec
TD0   1

======== CHANNEL f1 ========
SFO1   75.4886239 MHz
NUC1   13C
P1   15.00 usec
PLW1   14.19999981 W

======== CHANNEL f2 ========
SFO2   300.1812007 MHz
NUC2   1H
CPDPRG[2   waltz16
PCPD2   80.00 usec
PLW2   17.00000000 W
PLW12   0.33917999 W
PLW13   0.22601999 W

F2 - Processing parameters
SI   65536
SF   75.4803122 MHz
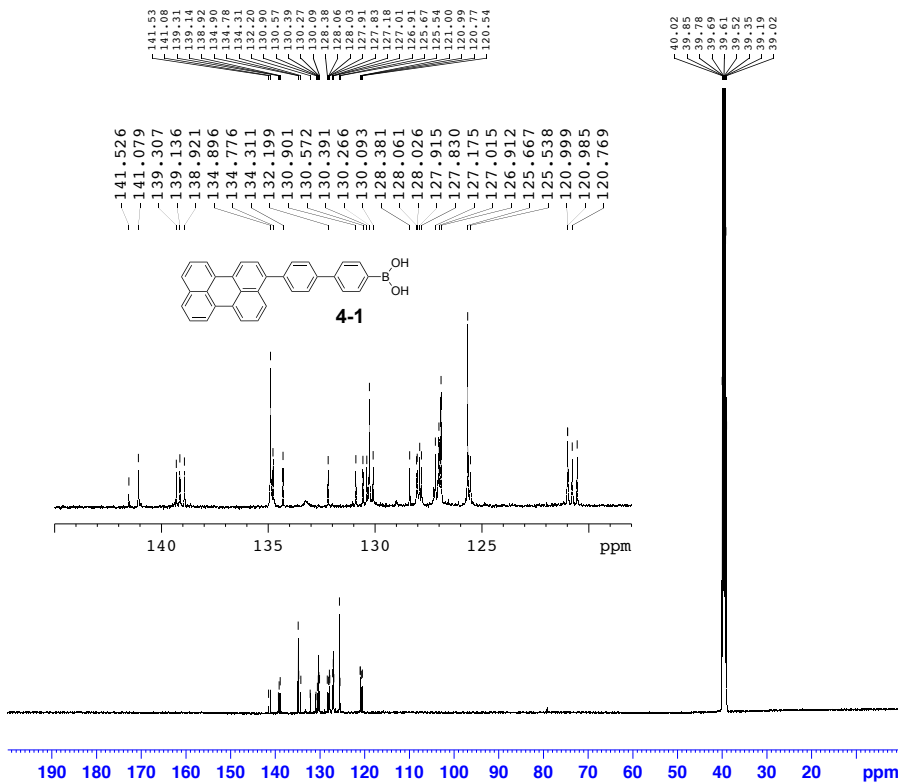WDW   EM
SSB   0
LB   1.00 Hz
GB   0
PC   1.40

4-2

4-2

4-24

4-24

DB_MS11407_ESP 68 (0.286) Cm (68-(1:10+99))

1: TOF MS ES+
4.66e5

Chemical Formula: C$_{30}$H$_{28}$N$_4$O$_6$
Exact Mass: 540.20

4-24

541.2087

542.2115

543.2139

163.0789

4-25

4-25

DB_MS11411_ESP 14 (0.073) Cm (14-(173:178+1:10))

1: TOF MS ES+
2.97e5

569.2411

570.2449

571.2464

Chemical Formula: C$_{32}$H$_{32}$N$_{4}$O$_{6}$
Exact Mass: 568.23

4-25

5-11

8.210, 8.194, 8.186, 8.175, 8.167
7.704, 7.677, 7.608, 7.581, 7.507, 7.481, 7.454, 7.445, 7.413, 7.386, 7.260

8.21, 8.19, 8.19, 8.17, 8.17, 7.70, 7.68, 7.61, 7.58, 7.51, 7.48, 7.45, 7.44, 7.41, 7.39, 7.26

3.99

1.59, 1.26

8.4 8.2 8.0 7.8 7.6 7.4 7.2 ppm

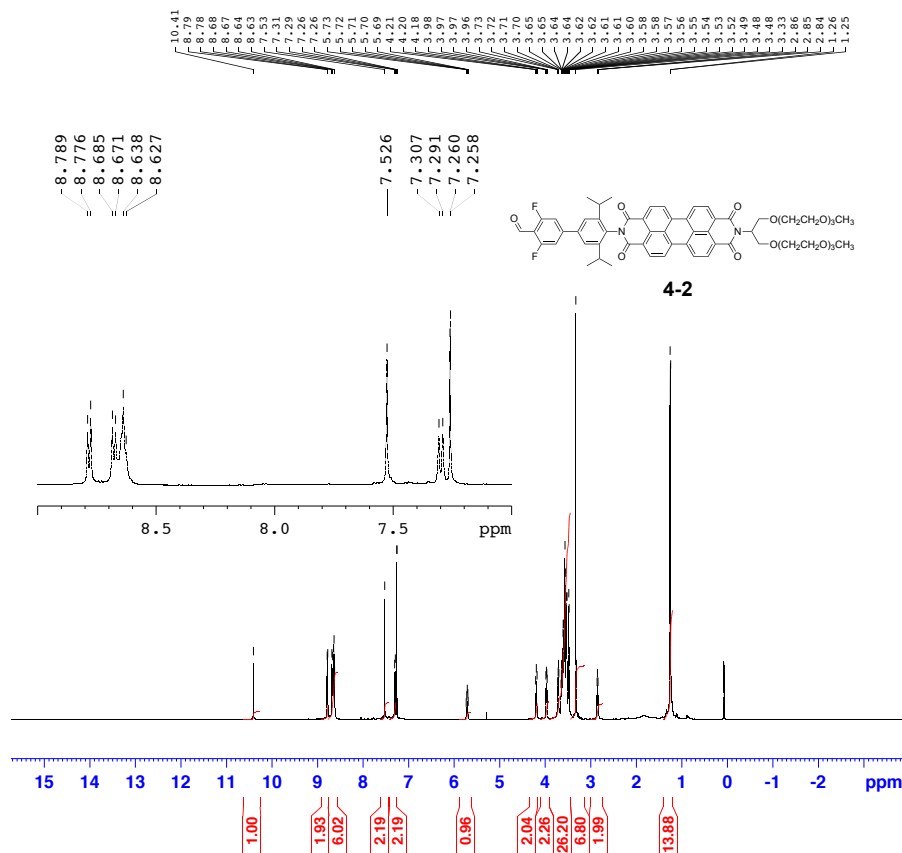Current Data Parameters
NAME   300_BLORO-816-H
EXPNO   10
PROCNO   1

F2 - Acquisition Parameters
Date_   20161103
Time   13.20
INSTRUM   FOURIER300
PROBHD   5 mm DUL 13C-1
PULPROG   zg30
TD   65536
SOLVENT   CDCl3
NS   16
DS   2
SWH   6103.516 Hz
FIDRES   0.093132 Hz
AQ   5.3687091 sec
RG   25.284
DW   81.920 usec
DE   6.50 usec
TE   292.8 K
D1   1.00000000 sec
TD0   1

======== CHANNEL f1 ========
SFO1   300.1818537 MHz
NUC1   1H
P1   15.00 usec
PLW1   17.00000000 W

F2 - Processing parameters
SI   65536
SF   300.1800048 MHz
WDW   EM
SSB   0
LB   0.30 Hz
GB   0
PC   1.00

11 10 9 8 7 6 5 4 3 2 1 ppm

5.62 2.98 2.06 1.99 2.05   3.00

5-11

167.16
145.71, 138.82, 134.79, 132.73, 131.65, 131.42, 131.36, 131.13, 130.23, 130.15, 129.85, 129.20, 128.72, 128.17, 128.09, 127.88, 126.94, 126.79, 126.77, 125.72, 125.64, 120.60, 120.49, 119.95

77.58, 77.16, 76.73

52.37

138.818
134.786, 132.726, 131.653, 131.418, 131.357, 131.129, 130.234, 130.151, 129.851, 129.203, 128.724, 128.175, 128.092, 127.882, 126.938, 126.789, 126.773, 125.721, 120.639, 120.604

135 130 125 ppm

Current Data Parameters
NAME   300_BLORO-816-C
EXPNO   12
PROCNO   1

F2 - Acquisition Parameters
Date_   20161103
Time   21.43
INSTRUM   FOURIER300
PROBHD   5 mm DUL 13C-1
PULPROG   zgpg30
TD   65536
SOLVENT   CDCl3
NS   3000
DS   4
SWH   48828.125 Hz
FIDRES   0.745058 Hz
AQ   0.6710886 sec
RG   501.187
DW   10.240 usec
DE   6.50 usec
TE   293.5 K
D1   2.00000000 sec
D11   0.03000000 sec
D31   0.00001500 sec
D40   0.00208500 sec
L4   23
L5   65
P32   80.00 usec
TD0   1

======== CHANNEL f1 ========
SFO1   75.4886239 MHz
NUC1   13C
P1   15.00 usec
PLW1   14.19999981 W

======== CHANNEL f2 ========
SFO2   300.1812007 MHz
NUC2   1H
CPDPRG[2   waltz16
PCPD2   80.00 usec
PLW2   17.00000000 W
PLW12   0.33917999 W
PLW13   0.22601999 W

F2 - Processing parameters
SI   65536
SF   75.4803119 MHz
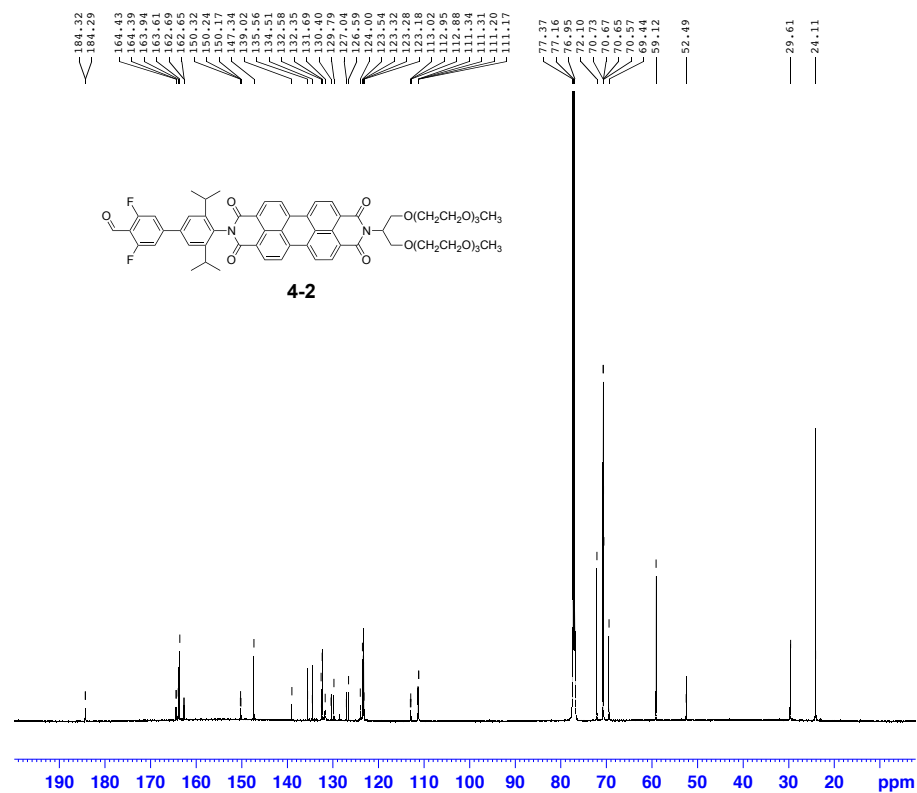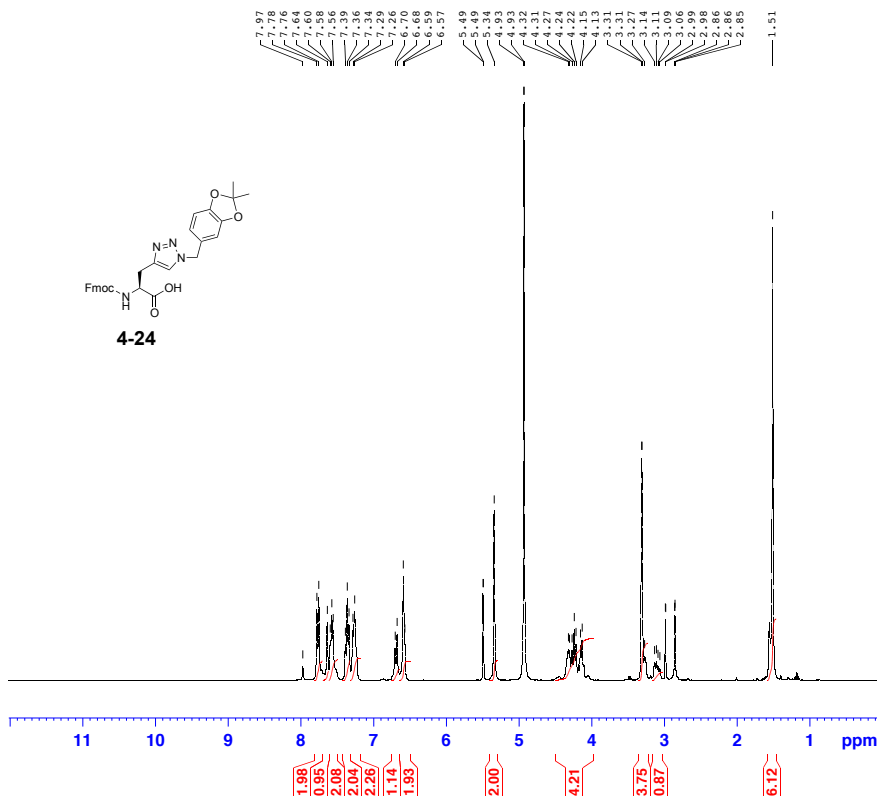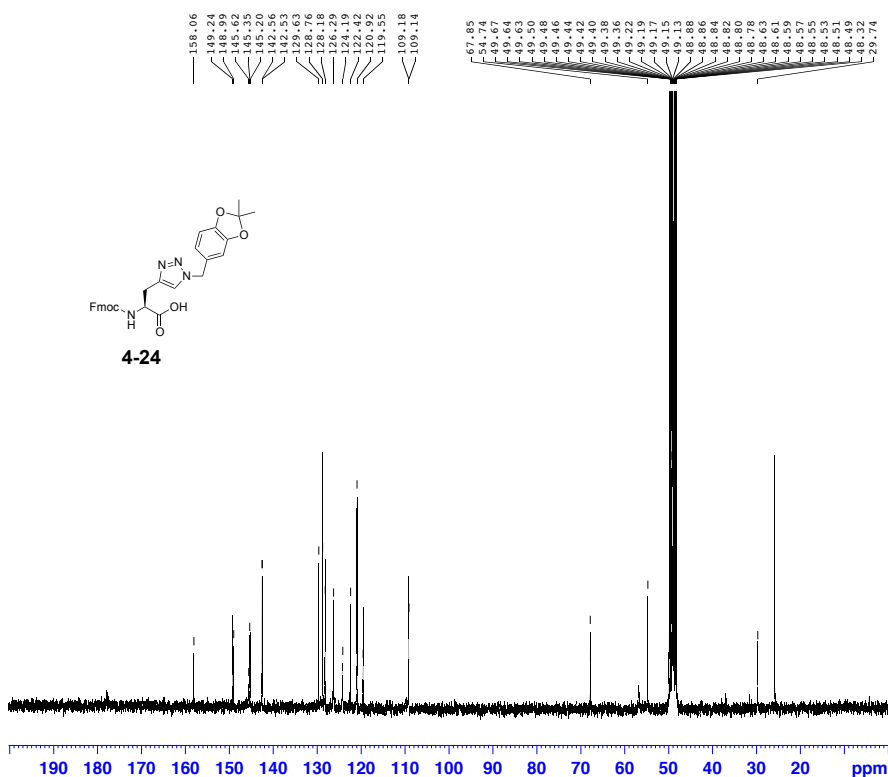WDW   EM
SSB   0
LB   1.00 Hz
GB   0
PC   1.40

190 180 170 160 150 140 130 120 110 100 90 80 70 60 50 40 30 20 ppm

5-1

5-1

5-2

5-21

Current Data Parameters
NAME   300_BLORO-844-H
EXPNO   10
PROCNO   1

F2 - Acquisition Parameters
Date_   20161209
Time   18.22
INSTRUM   FOURIER300
PROBHD   5 mm DUL 13C-1
PULPROG   zg30
TD   65536
SOLVENT   MeOD
NS   16
DS   2
SWH   6103.516 Hz
FIDRES   0.093132 Hz
AQ   5.3687091 sec
RG   22.4643
DW   81.920 usec
DE   6.50 usec
TE   295.1 K
D1   1.00000000 sec
TD0   1

======== CHANNEL f1 ========
SFO1   300.1818537 MHz
NUC1   1H
P1   15.00 usec
PLW1   17.00000000 W

F2 - Processing parameters
SI   65536
SF   300.1800065 MHz
WDW   EM
SSB   0
LB   0.30 Hz
GB   0
PC   1.00

5-21
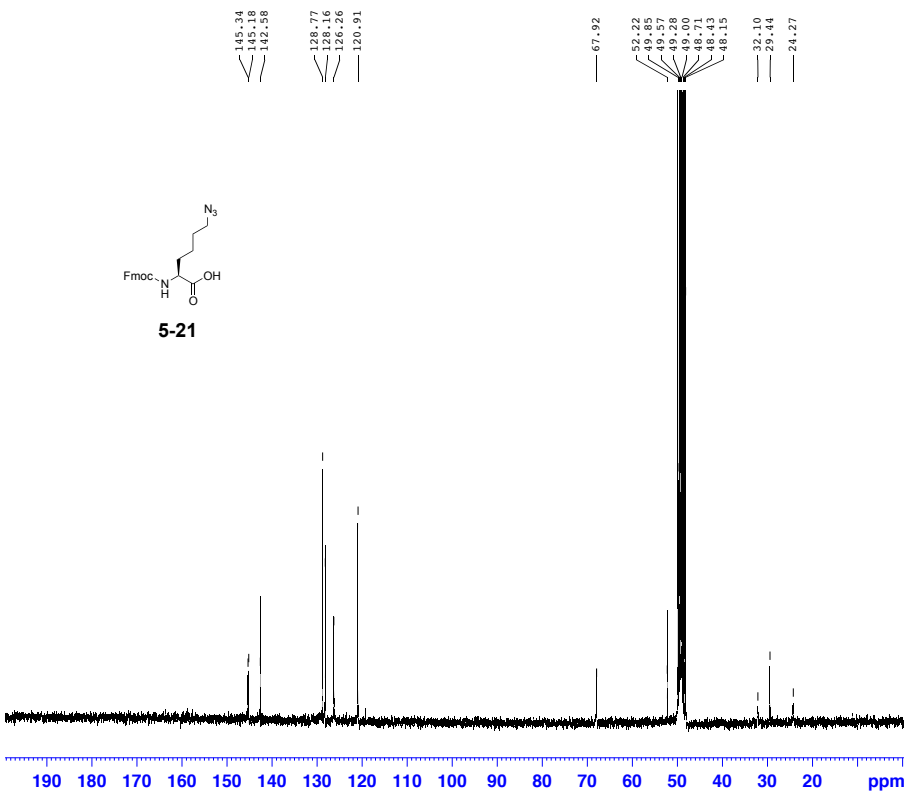
Current Data Parameters
NAME   300_BLORO-844-C
EXPNO   10
PROCNO   1

F2 - Acquisition Parameters
Date_   20161211
Time   20.07
INSTRUM   FOURIER300
PROBHD   5 mm DUL 13C-1
PULPROG   zgpg30
TD   65536
SOLVENT   MeOD
NS   7000
DS   4
SWH   48828.125 Hz
FIDRES   0.745058 Hz
AQ   0.6710886 sec
RG   501.187
DW   10.240 usec
DE   6.50 usec
TE   295.0 K
D1   2.00000000 sec
D11   0.03000000 sec
D31   0.00001500 sec
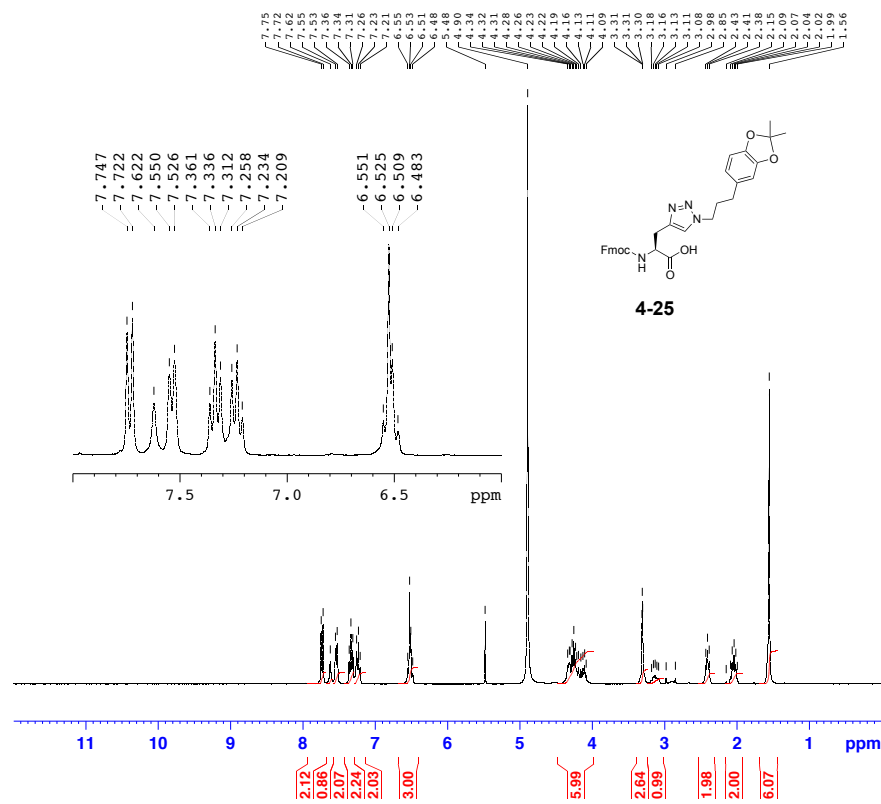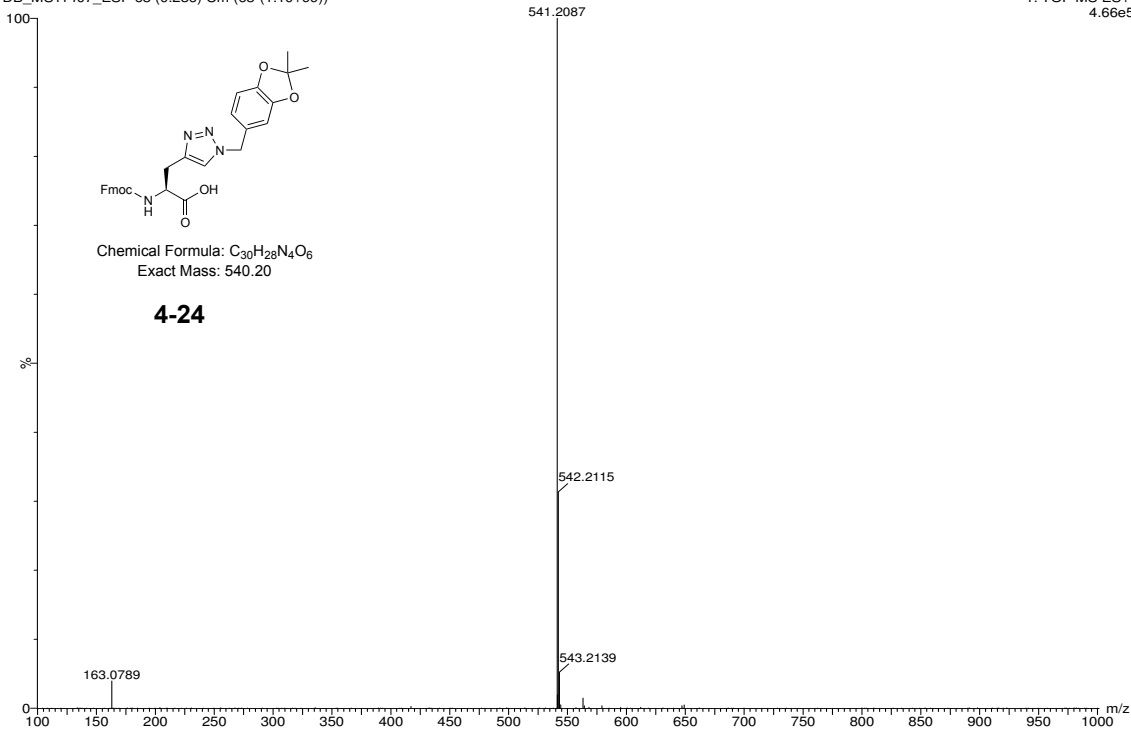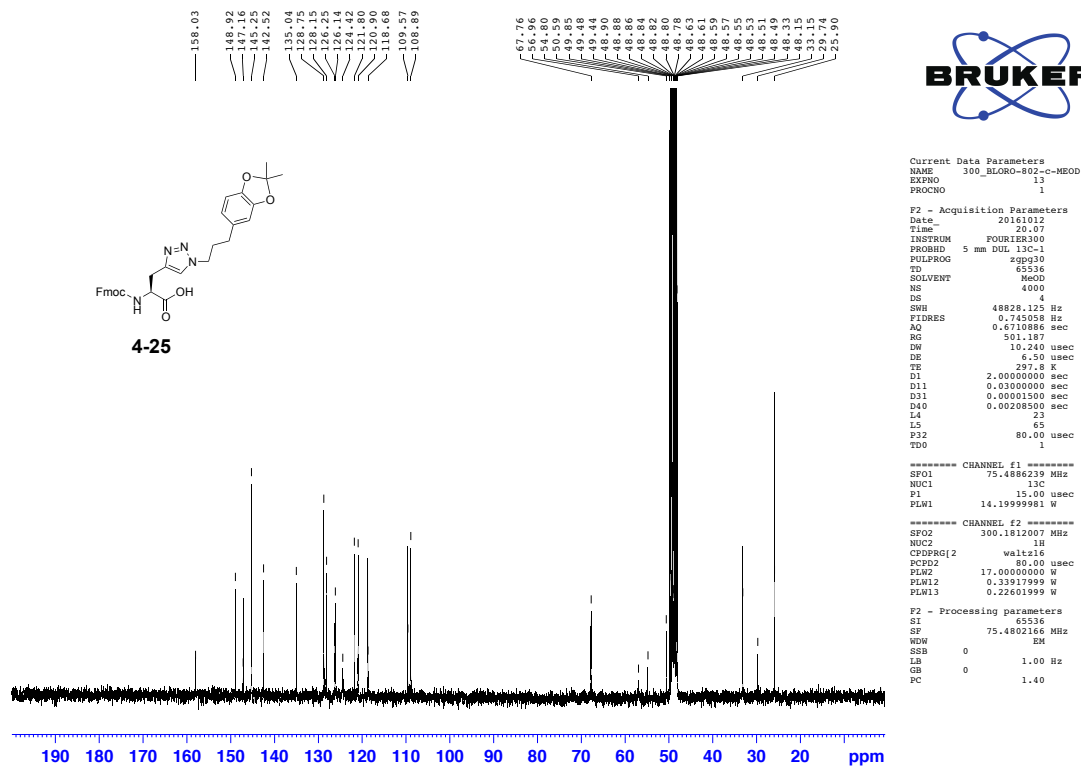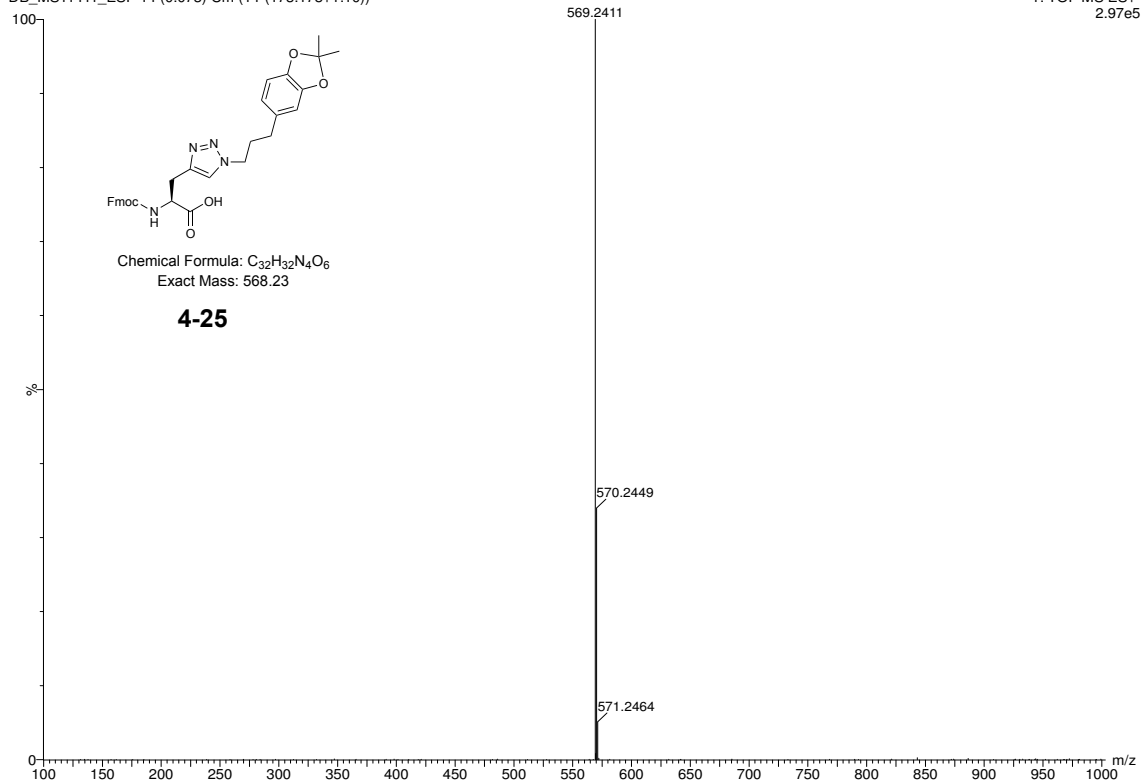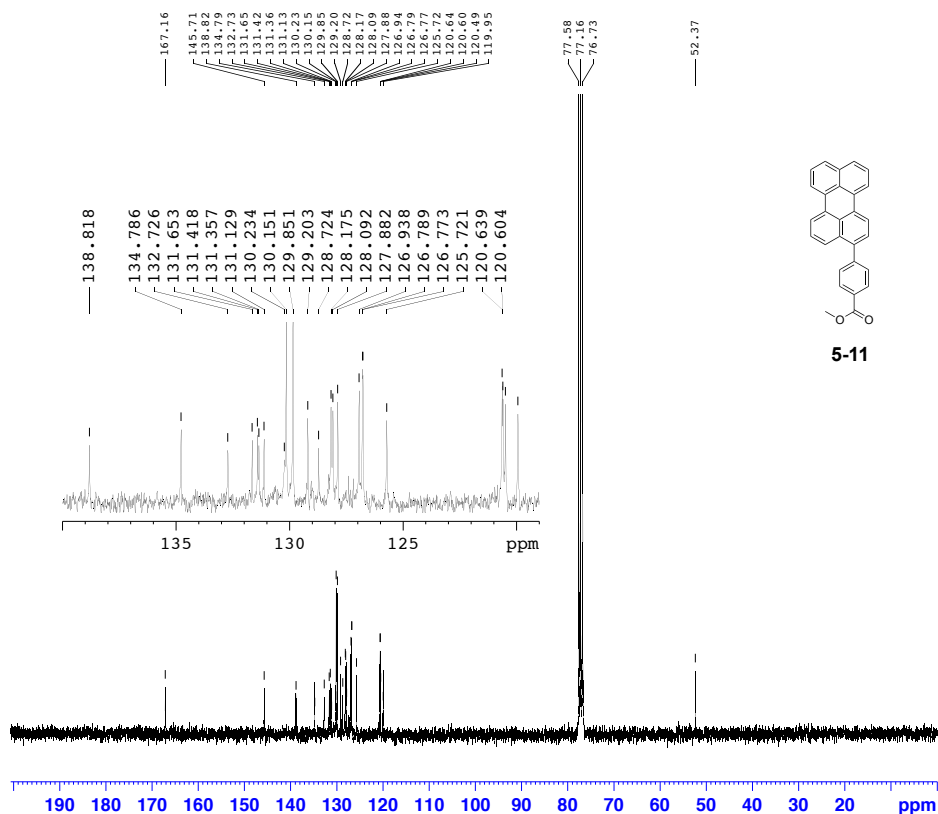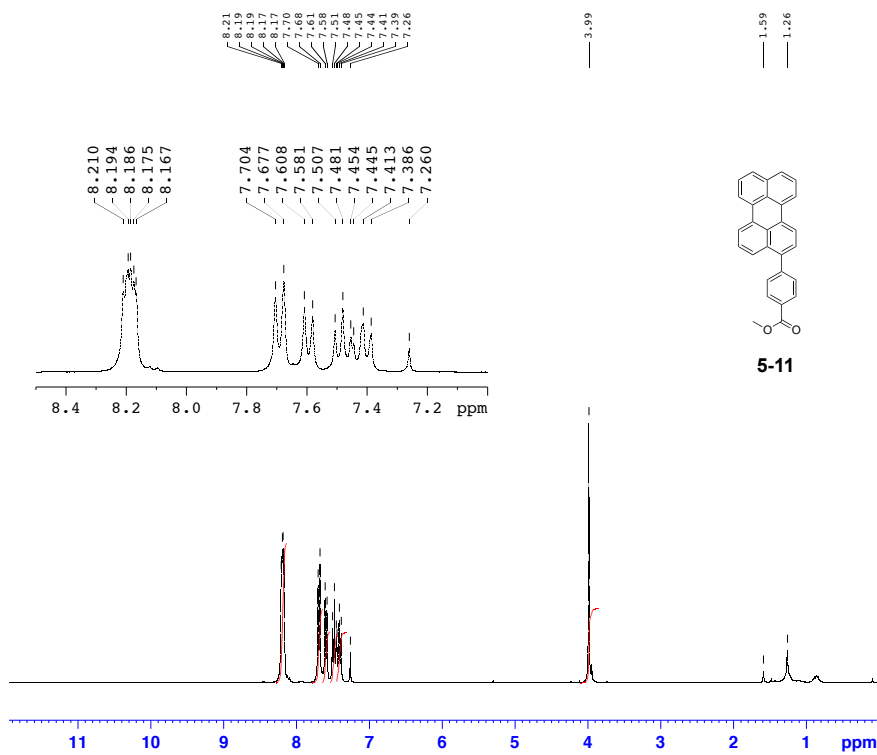D40   0.00208500 sec
L4   23
L5   65
P32   80.00 usec
TD0   1

======== CHANNEL f1 ========
SFO1   75.4886239 MHz
NUC1   13C
P1   15.00 usec
PLW1   14.19999981 W

======== CHANNEL f2 ========
SFO2   300.1812007 MHz
NUC2   1H
CPDPRG[2   waltz16
PCPD2   80.00 usec
PLW2   17.00000000 W
PLW12   0.33917999 W
PLW13   0.22601999 W

F2 - Processing parameters
SI   65536
SF   75.4802166 MHz
WDW   EM
SSB   0
LB   1.00 Hz
GB   0
PC   1.40

8.837
8.830
8.572
8.555
8.552
8.544
8.533
8.224
8.216
8.195
8.187
8.055
8.028
8.013
7.984
7.750
7.745
7.345
7.341
7.336
7.260

5-30

Current Data Parameters
NAME   300_BLORO-AC-DIHYDROTET
EXPNO   10
PROCNO   1

F2 - Acquisition Parameters
Date_   20170107
Time   14.04
INSTRUM   FOURIER300
PROBHD 5 mm DUL 13C-1
PULPROG   zg30
TD   65536
SOLVENT   CDCl3
NS   16
DS   2
SWH   6103.516 Hz
FIDRES   0.093132 Hz
AQ   5.3687091 sec
RG   31.623
DW   81.920 usec
DE   6.50 usec
TE   293.0 K
D1   1.00000000 sec
TD0   1

======== CHANNEL f1 ========
SFO1   300.1818537 MHz
NUC1   1H
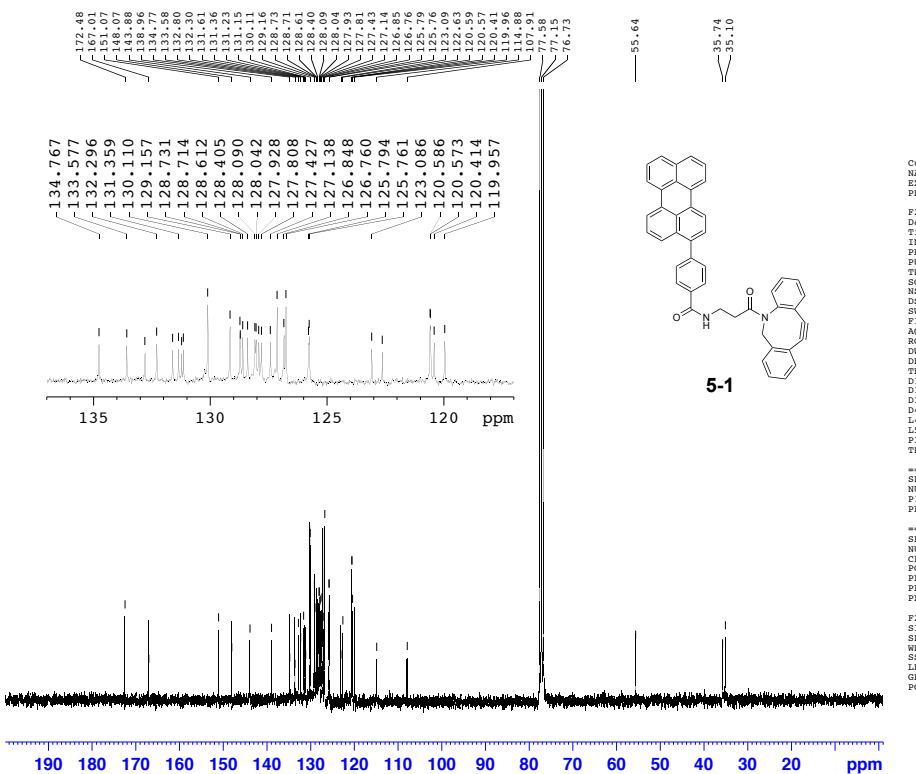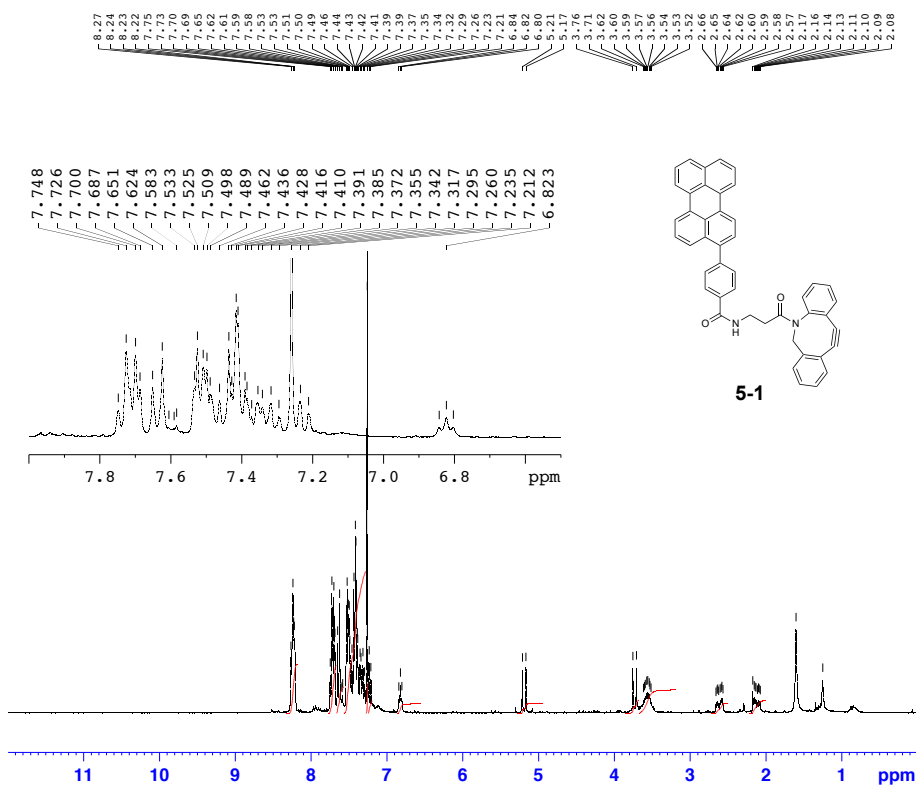P1   15.00 usec
PLW1   17.00000000 W

F2 - Processing parameters
SI   65536
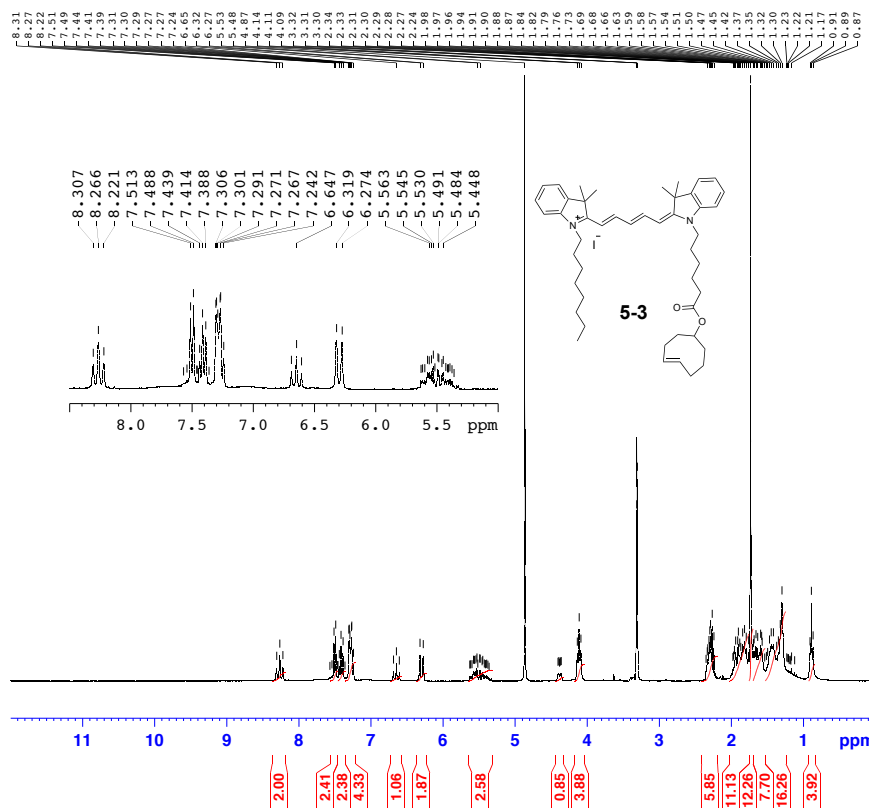SF   300.1800083 MHz
WDW   EM
SSB   0
LB   0.30 Hz
GB   0
PC   1.00

171.85
171.27
171.01
148.50
146.91
146.66
142.43
139.60
136.84
136.79
127.19
124.97
121.67
121.35
83.69
77.58
77.37
77.16
76.73
52.37
34.38
30.93
28.08
23.54

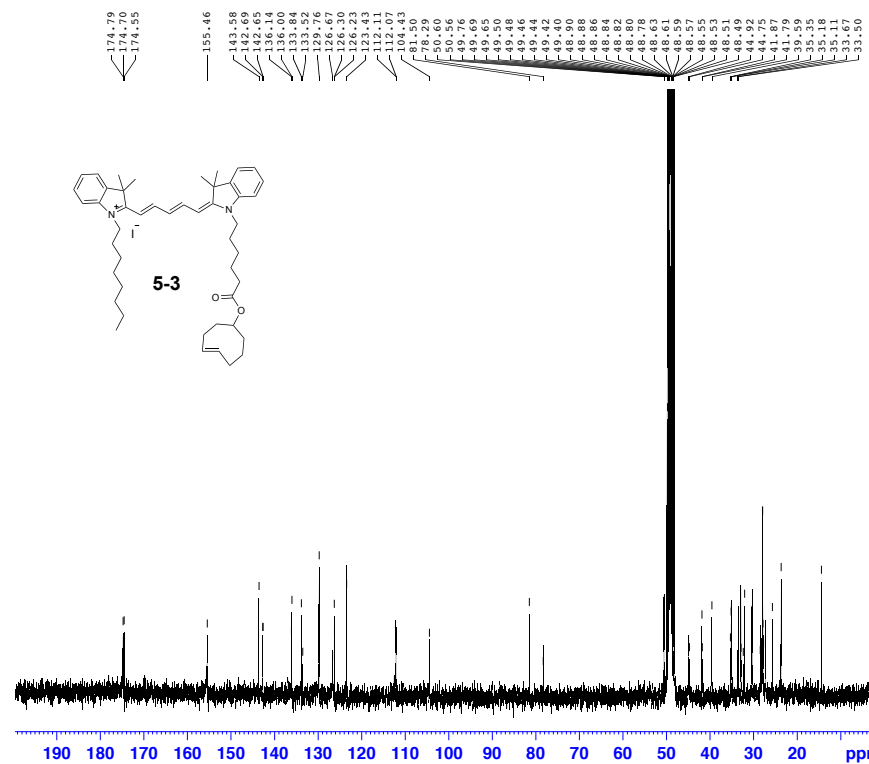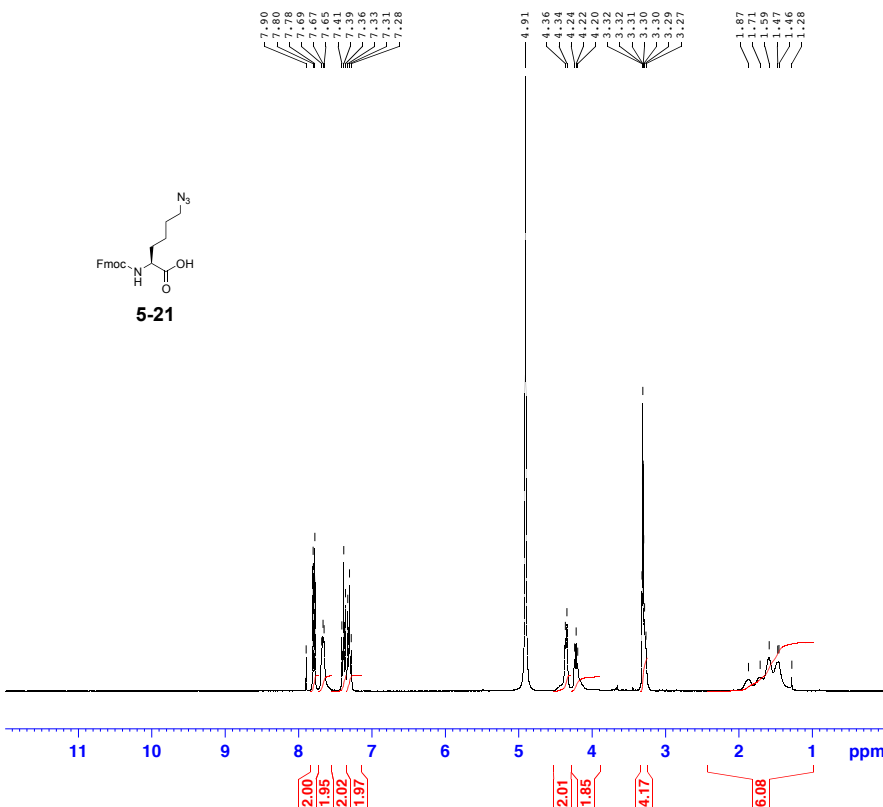**5-30**

Current Data Parameters
NAME   300_BLORO-AC-DIHYDROTET
EXPNO   11
PROCNO   1

F2 - Acquisition Parameters
Date_   20170107
Time   20.05
INSTRUM   FOURIER300
PROBHD 5 mm DUL 13C-1
PULPROG   zgpg30
TD   65536
SOLVENT   CDCl3
NS   4000
DS   4
SWH   48828.125 Hz
FIDRES   0.745058 Hz
AQ   0.6710886 sec
RG   323.887
DW   10.240 usec
DE   6.50 usec
TE   293.0 K
D1   2.00000000 sec
D11   0.03000000 sec
D31   0.00001500 sec
D40   0.00208500 sec
L4   23
L5   65
P32   80.00 usec
TD0   1

======== CHANNEL f1 ========
SFO1   75.4886239 MHz
NUC1   13C
P1   15.00 usec
PLW1   14.19999981 W

======== CHANNEL f2 ========
SFO2   300.1812007 MHz
NUC2   1H
CPDPRG[2   waltz16
PCPD2   80.00 usec
PLW2   17.00000000 W
PLW12   0.33917999 W
PLW13   0.22601999 W

F2 - Processing parameters
SI   65536
SF   75.4803136 MHz
WDW   EM
SSB   0
LB   1.00 Hz
GB   0
PC   1.40

309

10.28 9.00 8.99 8.95 8.93 8.71 8.70 8.69 8.67 8.56 8.54 8.53 8.01 7.99 7.98 7.96 7.58 7.57 7.55 7.53 7.26 6.87 6.84

5.27

4.51 4.50 4.47 4.45 4.44

2.59 2.57 2.54 2.29 2.28 2.26 2.24 2.07 2.04 1.99 1.95 1.94 1.91 1.41

8.999 8.994 8.948 8.934 8.715 8.700 8.689 8.672 8.567 8.560 8.538 8.530 7.986 7.981 7.960 7.575 7.573 7.556 7.550 7.534 7.260

5-31

Current Data Parameters
NAME   300_BLORO-AC-TET
EXPNO   10
PROCNO   1

F2 - Acquisition Parameters
Date_   20170107
Time   14.11
INSTRUM   FOURIER300
PROBHD   5 mm DUL 13C-1
PULPROG   zg30
TD   65536
SOLVENT   CDCl3
NS   16
DS   2
SWH   6103.516 Hz
FIDRES   0.093132 Hz
AQ   5.3687091 sec
RG   13.608
DW   81.920 usec
DE   6.50 usec
TE   292.9 K
D1   1.00000000 sec
TD0   1

======== CHANNEL f1 ========
SFO1   300.1818537 MHz
NUC1   1H
P1   15.00 usec
PLW1   17.00000000 W

F2 - Processing parameters
SI   65536
SF   300.1800106 MHz
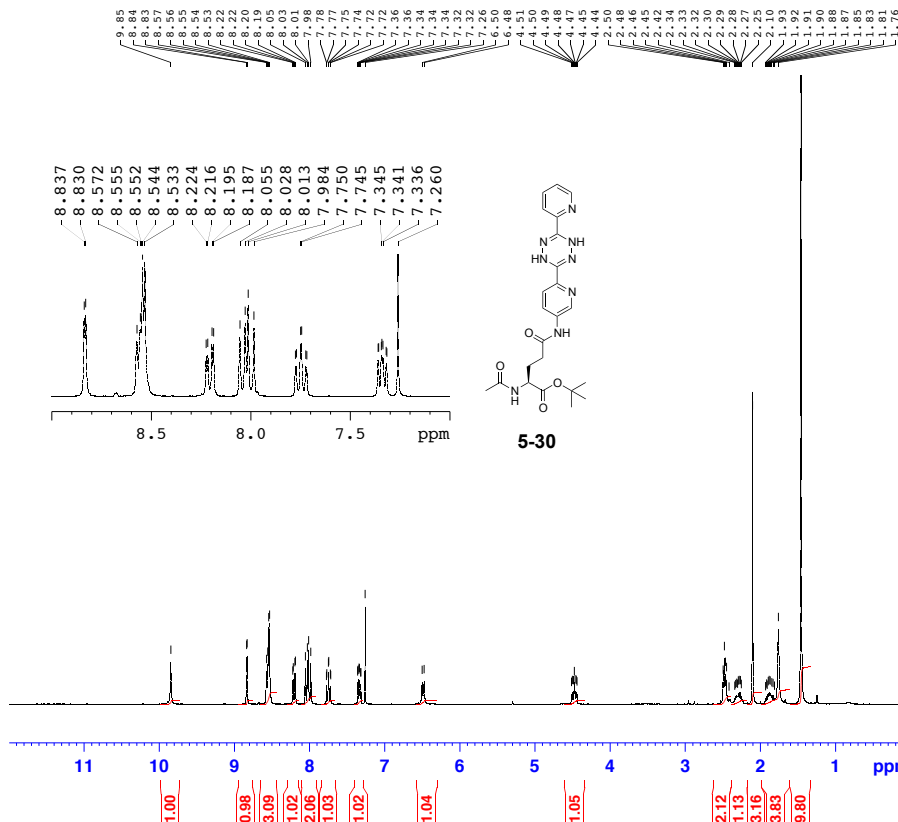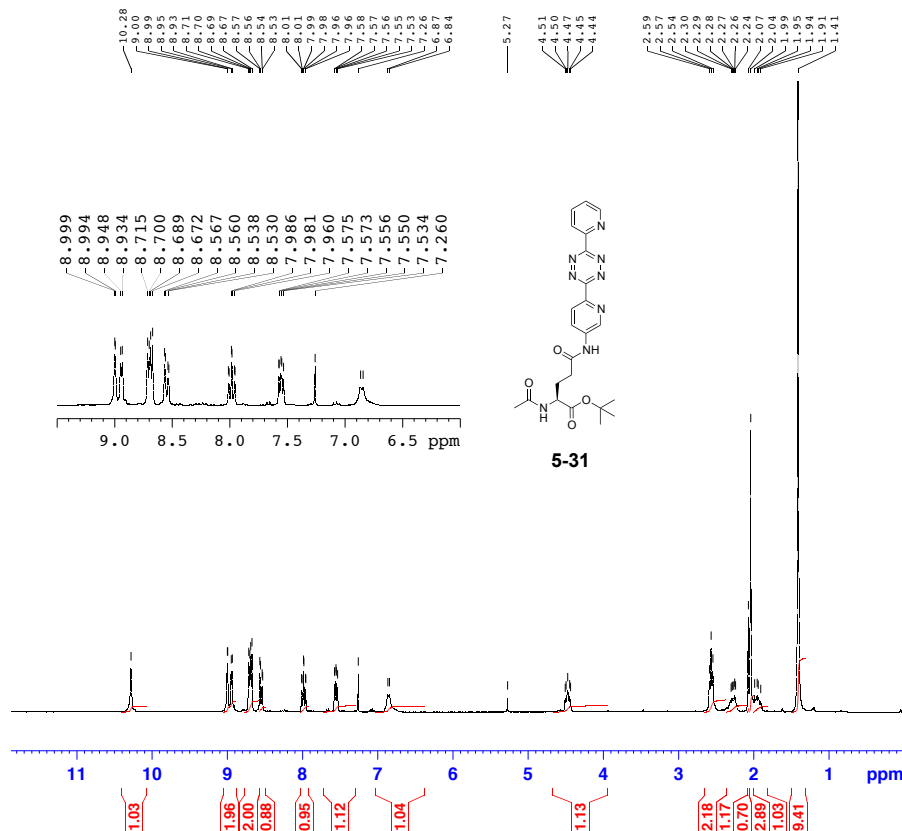WDW   EM
SSB   0
LB   0.30 Hz
GB   0
PC   1.00

172.01 171.59 171.01 163.55 163.37 150.98 150.11 144.04 142.14 138.69 137.71 126.99 126.69 125.31 124.47

83.17 77.58 77.16 76.73

52.51

34.09 29.49 28.02 23.33

5-31

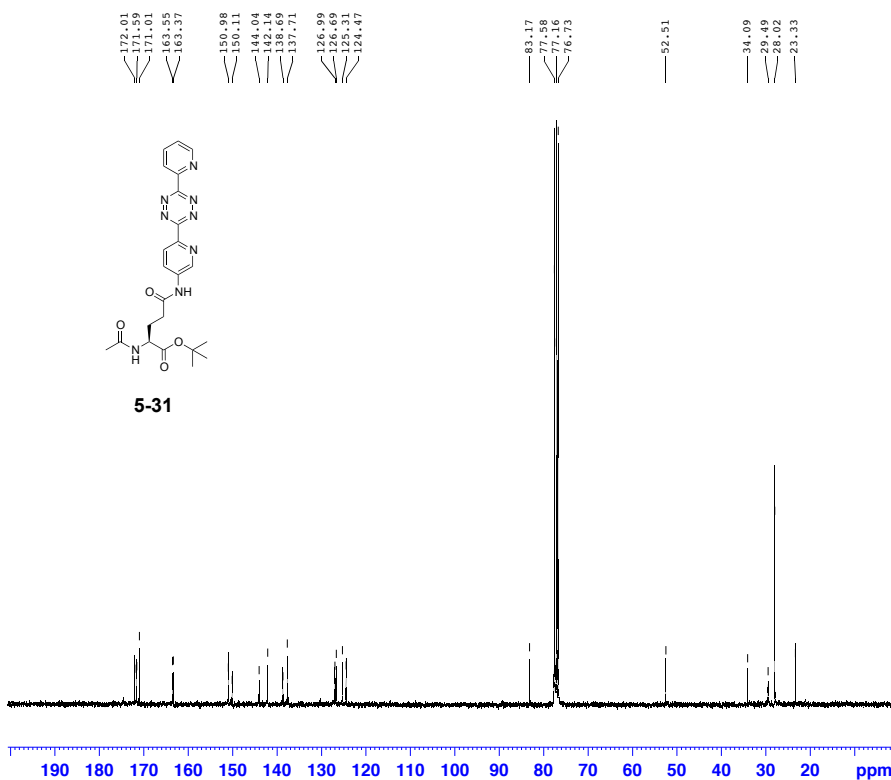Current Data Parameters
NAME   300_BLORO-AC-TET
EXPNO   11
PROCNO   1

F2 - Acquisition Parameters
Date_   20170107
Time   23.11
INSTRUM   FOURIER300
PROBHD   5 mm DUL 13C-1
PULPROG   zgpg30
TD   65536
SOLVENT   CDCl3
NS   4000
DS   4
SWH   48828.125 Hz
FIDRES   0.745058 Hz
AQ   0.6710886 sec
RG   501.187
DW   10.240 usec
DE   6.50 usec
TE   293.6 K
D1   2.00000000 sec
D11   0.03000000 sec
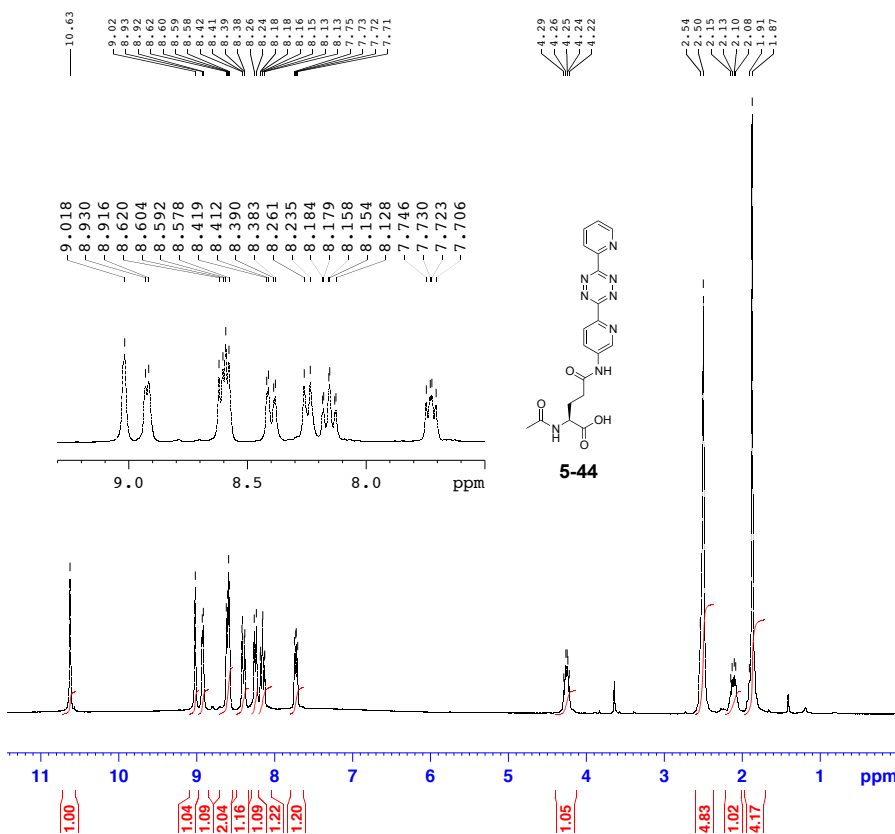D31   0.00001500 sec
D40   0.00208500 sec
L4   23
L5   65
P32   80.00 usec
TD0   1

======== CHANNEL f1 ========
SFO1   75.4886239 MHz
NUC1   13C
P1   15.00 usec
PLW1   14.19999981 W

======== CHANNEL f2 ========
SFO2   300.1812007 MHz
NUC2   1H
CPDPRG[2   waltz16
PCPD2   80.00 usec
PLW2   17.00000000 W
PLW12   0.33917999 W
PLW13   0.22601999 W

F2 - Processing parameters
SI   65536
SF   75.4803203 MHz
WDW   EM
SSB   0
LB   1.00 Hz
GB   0
PC   1.40

310

DB_MS14084_ESP 11 (1.106) Cm (11-1:4)
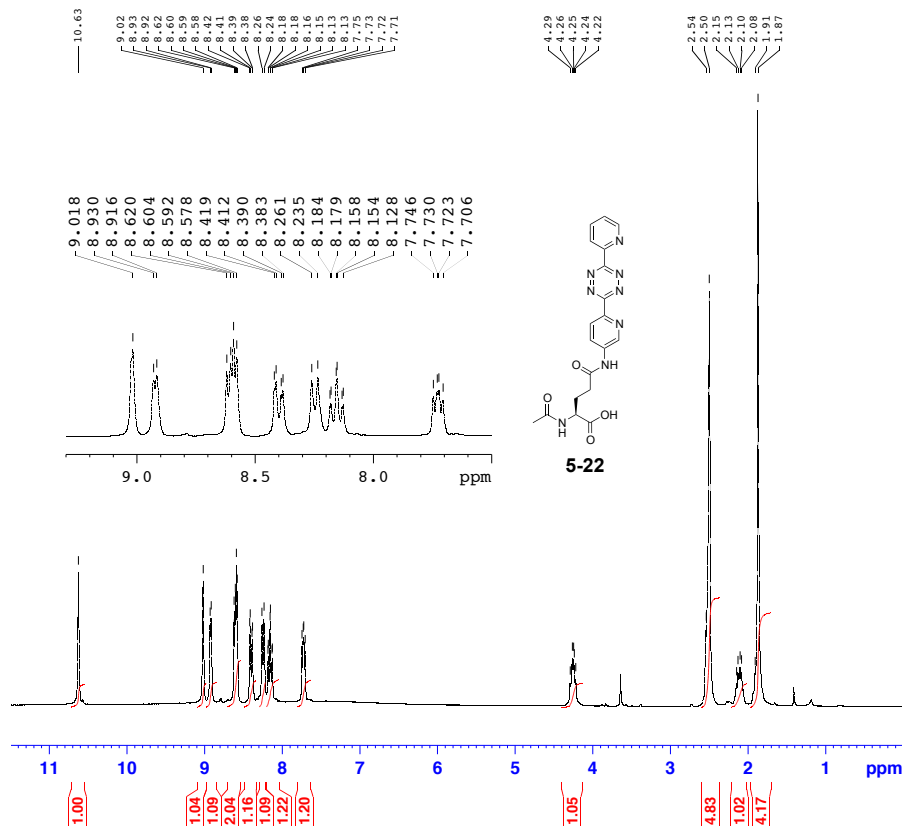
100

479.2136

%

480.2220

481.2326

467.2080

482.2368

0

220 240 260 280 300 320 340 360 380 400 420 440 460 480 500 520 540 560 580 600 m/z

Chemical Formula: C₂₃H₂₆N₈O₄
Exact Mass: 478.21

5-31

10.63

9.02
8.93
8.92
8.62
8.60
8.59
8.58
8.42
8.41
8.39
8.38
8.26
8.24
8.18
8.16
8.15
8.13
8.13
7.73
7.72
7.71

4.29
4.26
4.25
4.22

2.54
2.50
2.15
2.13
2.10
2.08
1.91
1.87

BRUKER

9.018
8.930
8.916
8.620
8.604
8.592
8.578
8.419
8.412
8.390
8.383
8.261
8.235
8.184
8.179
8.158
8.154
8.128
7.746
7.730
7.723
7.706

9.0   8.5   8.0   ppm

5-44

11   10   9   8   7   6   5   4   3   2   1   ppm

1.00

1.04
1.09
2.04
1.16
1.09
1.22
1.20

1.05

4.83
1.02
4.17

5-22

5-36

5-36

5-37

13C NMR spectrum peaks: 173.167, 172.471, 171.965, 170.981, 163.659, 163.522, 151.091, 150.345, 144.321, 142.302, 138.551, 137.600, 126.865, 126.578, 125.293, 124.459, 83.211, 77.477, 77.362, 77.159, 76.841, 71.983, 70.664, 70.647, 70.127, 69.105, 64.044, 59.105, 52.185, 33.881, 31.090, 29.935, 29.556, 28.087

5-37
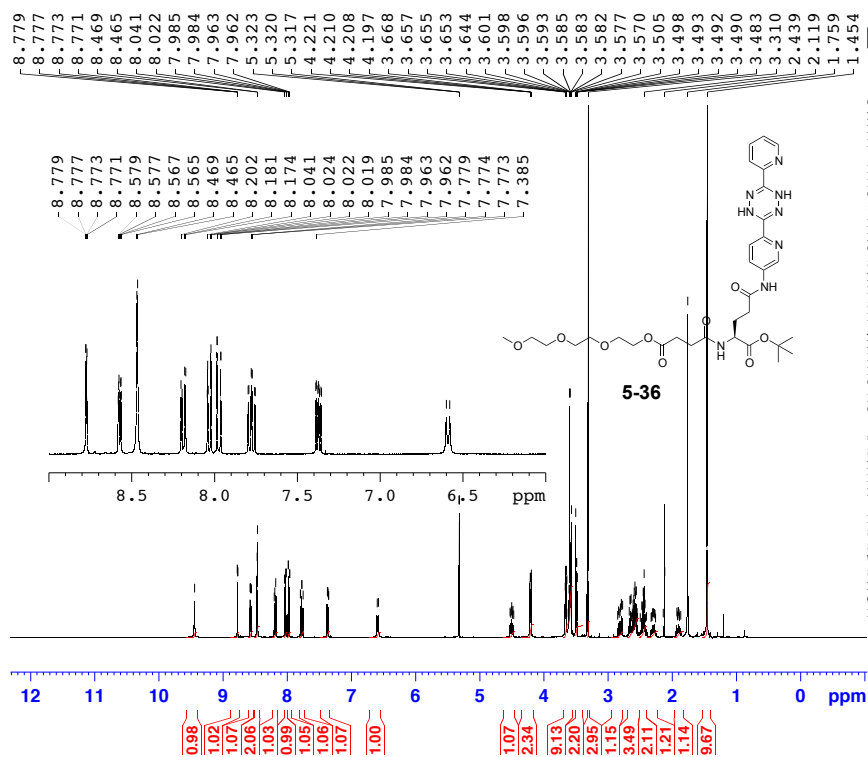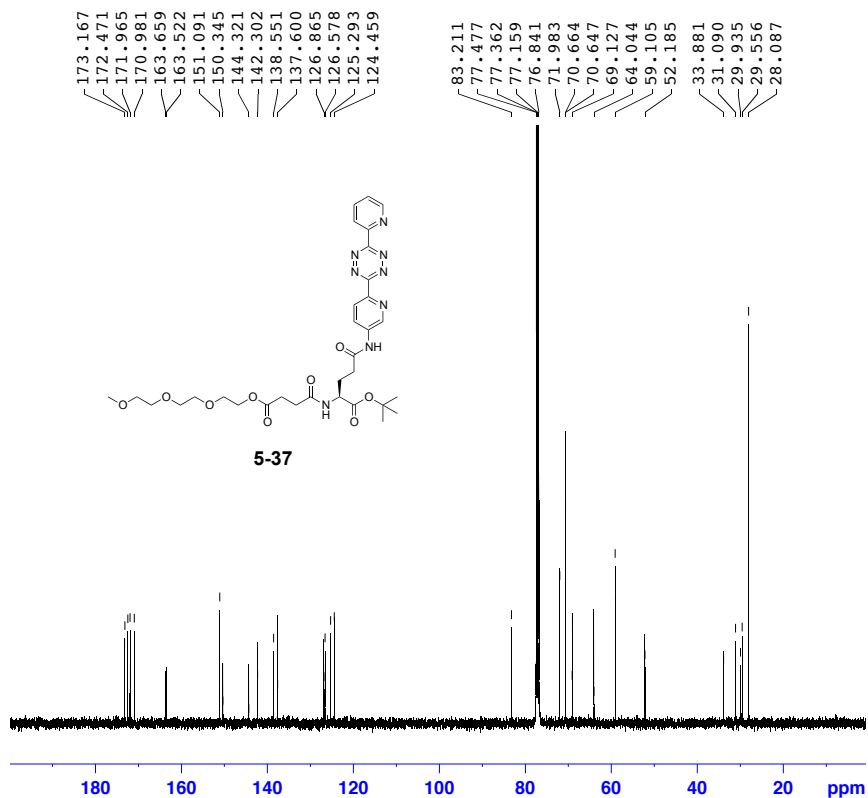
Current Data Parameters
NAME   400_BLORO-918-C
EXPNO   10
PROCNO   1

F2 - Acquisition Parameters
Date_   20170904
Time   12.57
INSTRUM   spect
PROBHD   5 mm PABBO BB/
PULPROG   zgpg30
TD   119044
SOLVENT   CDCl3
NS   1600
DS   4
SWH   25000.000 Hz
FIDRES   0.210006 Hz
AQ   2.3808801 sec
RG   208.99
DW   20.000 usec
DE   10.12 usec
TE   293.1 K
D1   1.00000000 sec
D11   0.03000000 sec
TD0   1

======== CHANNEL f1 ========
SFO1   100.6238346 MHz
NUC1   13C
P1   10.00 usec
PLW1   59.00000000 W

======== CHANNEL f2 ========
SFO2   400.1316005 MHz
NUC2   1H
CPDPRG[2   waltz64
PCPD2   90.00 usec
PLW2   14.30000019 W
PLW12   0.18729000 W
PLW13   0.09420800 W

F2 - Processing parameters
SI   131072
SF   100.6127578 MHz
WDW   EM
SSB   0
LB   1.00 Hz
GB   0
PC   1.40

DB_MS14493_ESP3 5 (0.656) Cm (5-1)

1: TOF MS ES-
9.88e

683.3184

Chemical Formula: C32H42N8O9
Exact Mass: 682.31

5-37

684.3361

705.3137

671.3199

706.3175

707.3238

539.3077
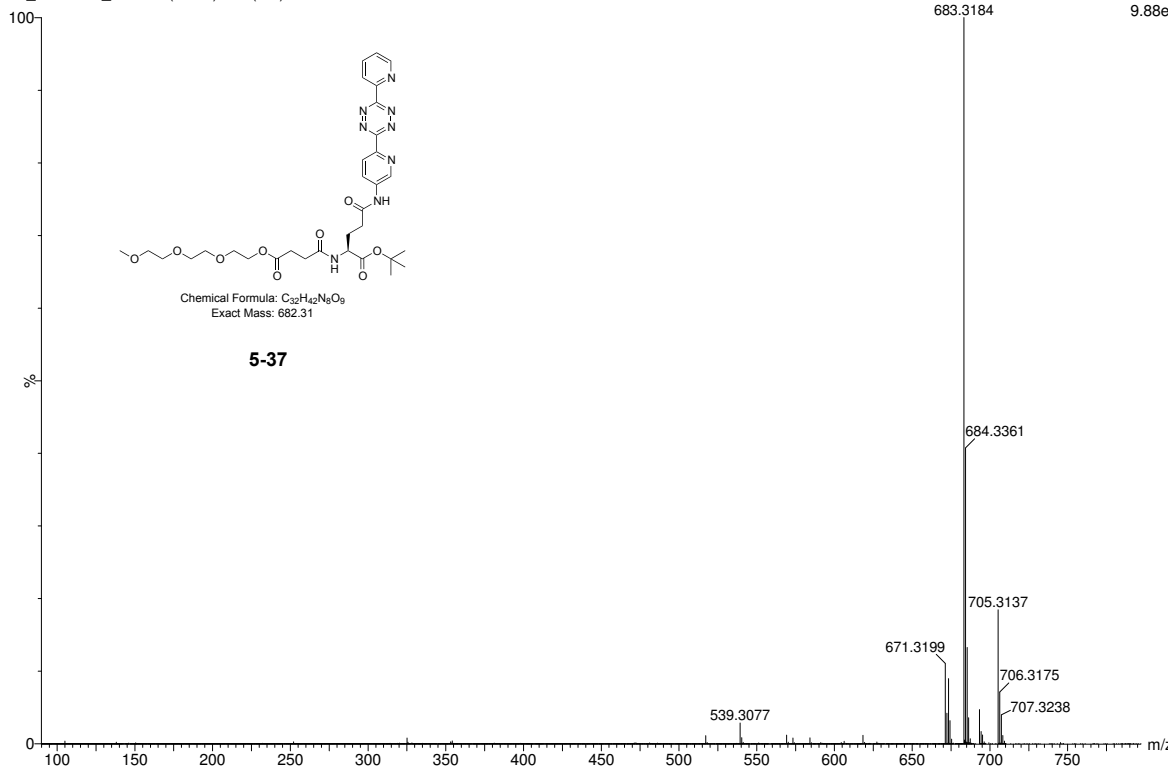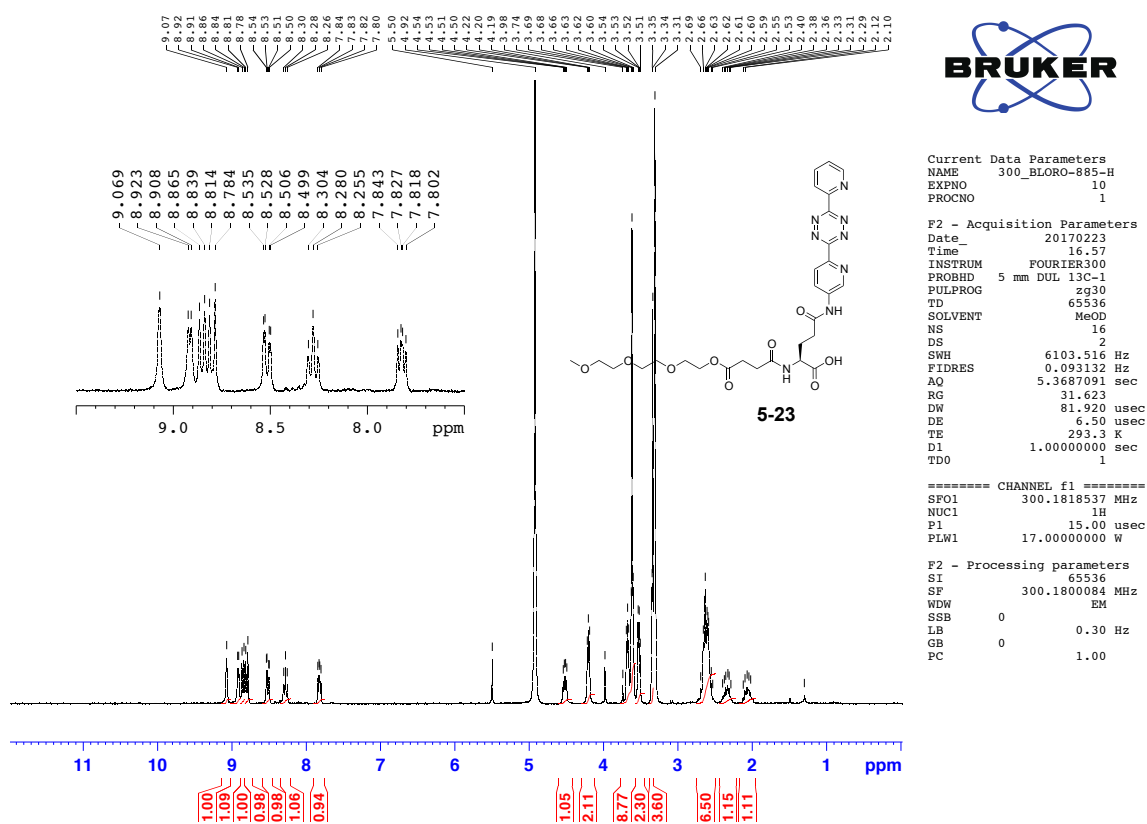
Crystallographic data

Table 1. Crystal data and structure refinement

	2-25	**3-8b**	**2-60a**
Identification code	shelxl	shelxl	shelxl
Empirical formula	$C_{13}H_{14}N_4O_3$	$C_{21}H_{20}N_4O_4$	$C_{21}H_{20}N_4O_3$
Formula weight (Da)	274.28	392.41	376.41
Temperature (K)	293	150	150
Wavelength (Å)	0.711	0.711	0.711
Crystal system	Monoclinic	Monoclinic	Monoclinic
Space group	P21/c	P 21/n	P 21/n
a (Å)	9.6443(5)	9.5206(4)	8.5453(4)
b (Å)	14.4488(7)	18.4764(7)	12.8377(5)

c (Å)	9.0841(4)	11.1089(5)	17.0979(9)
α (°)	90	90	90
β (°)	93.599(4)	105.090(5)	104.350(5)
γ (°)	90	90	90
Volume (Å^3)	1263.36(11)	1886.75(14)	1817.15(15)
Z	4	4	4
Density (g.cm^3)	1.442	1.382	1.376
F (000)	576	824	792
Absorption coefficient (mm^{-1})	0.106	0.098	0.095
Crystal size (mm^3)	0.10 x 0.30 x 0.40	0.33 x 0.38 x 0.43	0.50 x 0.32 x 0.20
θ min, max (°)	3.3, 28.0	2.9, 25.0	3.404, 29.746
Index ranges	-8: 12 ; -17: 18 ; -10: 11	-11: 10 ; -18: 21 ; -9: 13	-11 : 8 ; -12 : 17 ; -20 : 21
Reflections collected	5952	8012	8136
Independent refl.	2614, [R(int) = 0.019]	3311, [R(int) = 0.024]	4200 [R(int) = 0.0169]
Obs. Ref. [I>2.0 σ (I)]	2125	2939	-
Completeness	1.05	1.05	0.97
Refinement method	Full-matrix least-squares on F^2	Full-matrix least-squares on F^2	Full-matrix least-squares on F^2
Data / restraints / parameters	2614 / 0 / 181	3311 / 0 / 263	4200 / 0 / 255
Goodness-of-fit on F^2	1.052	1.049	1.056
Final R indices [I>2.0 σ (I)]	R1 = 0.0432, wR2 = 0.1046	R1 =0.0381, wR2 = 0.0898	R1 = 0.0449, wR2 = 0.1133
R indices (all data)	0.0554	0.0448	0.0532
Extinction coefficient	n/a	n/a	n/a

Largest diff. peak and hole (e.Å^{-3})	-0.19, 0.19	-0.21, 0.22	0.544, -0.412

Curriculum Vitae

1989   Born on January 7, in Versailles, France

2004-2007   Secondary high school at Bourg-Chevreau Sainte Anne, Segré, France
                   Scientific Baccaleuréat with honors

2007-2010   University of Angers, France
                   First class B.Sc. in chemistry, graduated with honors

2010-2012   University of Montpellier II, France
                   M.Sc. in biomolecular chemistry, graduated with honors

2012 (6 m.)   Hoffmann-La Roche, Basel, Switzerland
                   Master Thesis "β-Peptides as inhibitors of protein-protein interactions" supervised
                   by Dr. E. Kitas.

2012-2017   University of Namur, Belgium
                   Cardiff University, United Kingdom
                   Ph.D. in organic chemistry "Programming Artificial Antennas through Templated
                   Assembly of Chromophores" supervised by Prof. D. Bonifazi

Scientific communication

- Communication: L. Rocard, A. Berezin, F. De Leo, D. Bonifazi "Templated Chromophore Assembly by Dynamic Covalent Bonds", *Angew. Chem. Int. Ed.* **2015**, *54*, 15739-15743. DOI: 10.1002/anie.201507186

- Inside Cover: Templated Chromophore Assembly by Dynamic Covalent Bonds (*Angew. Chem. Int. Ed.* 52/2015), DOI: 10.1002/anie.201511090

- Full Paper: L. Rocard, D. Wragg, S. Leoni, L. Luciani, D. Bonifazi "Templated Chromophore Assembly on peptidic scaffold: structural evolution of the system" *manuscript in preparation*

- Review: O. Kulyk, L. Rocard, D. Bonifazi "Synthetic strategies tailoring colours in multichromophoric systems" *manuscript in preparation*

- Communication: L. Rocard, A. Fermi, D. Bonifazi "Chromophoric Assembly using pentaorthogonal multireaction system" *manuscript in preparation*

- Oral Presentation: "Templated chromophore assembly for mimicking natural antenna systems", 15th Annual Cardiff Chemistry Conference, School of Chemistry, United Kingdom

- Oral Presentation: "Self-Assembly of Chromophores", Symposium "Supramolecular Chemistry and Materials", University of Leuven, Belgium

- Oral Presentation: "Color Ordering via Orthogonal Covalent Bonds", "Material, Interfaces, and Nanostructures" doctoral school, University of Mons, Belgium

- Poster Presentation: "Templated Chromophore Assembly for mimicking natural antenna systems" Southampton Supramolecular Symposium, United Kingdom

- Poster Presentation: "Templated Chromophore Assembly for mimicking natural antenna systems" Speaking of Science: interdisciplinary conference, Cardiff University, United Kingdom

- Poster Presentation: "Templated Chromophore Assembly by Dynamic Covalent Bonds" European Winter School on Physical Organic Chemistry (e-WISPOC 2016), Bressanone, Italy

- Poster Presentation: "Colour ordering on a-helix peptides via orthogonal dynamic covalent bonds", 18th Sigma-Aldrich Organic Synthesis Meeting, Blankenberge, Belgium

- Poster Presentation: "Peptide scaffolds for chromophore organization through Dynamic Covalent Chemistry", Ischia Advanced School of Organic Chemistry 2014, Italy